Water-Soluble Metallocene-Containing Poly(ethylene glycol)s as Multi-Stimuli-Responsive Materials for Catalysis, Coatings and Staining

Dissertation zur Erlangung des Grades

„Doktor der Naturwissenschaften“ im Promotionsfach Chemie

am Fachbereich Chemie, Pharmazie und Geowissenschaften

der Johannes Gutenberg-Universität Mainz

Arda Alkan

geboren in Şişli (Istanbul)

Mainz, 2016

JOHANNES GUTENBERG UNIVERSITÄT MAINZ

Max-Planck-Institut für Polymerforschung

Max Planck Institute for Polymer Research

Dekan: Prof. Dr. Dirk Schneider

Prodekan: Prof. Dr. Holger Frey

1. Berichterstatter: Dr. Frederik R. Wurm

2. Berichterstatter: Prof. Dr. Holger Frey

Tag der mündlichen Prüfung: 15.06.2016

The thesis was carried out from April 2013 until May 2016 in the department of Professor Katharina Landfester and the group of Dr. Frederik Wurm at the Max Planck Institute of Polymer Research in Mainz in collaboration with the group of Professor Holger Frey at the Institute of Organic Chemistry, Johannes Gutenberg-University, Mainz.

Hiermit versichere ich gemäß § 10 Abs. 3d der Promotionsordnung vom 24.07.2007

a) Ich habe die jetzt als Dissertation vorgelegte Arbeit selbst angefertigt und alle benutzten Hilfsmittel (Literatur, Apparaturen, Material) in der Arbeit angegeben.
b) Ich habe oder hatte die jetzt als Dissertation vorgelegte Arbeit nicht als Prüfungsarbeit für eine staatliche oder andere wissenschaftliche Prüfung eingereicht.
c) Ich hatte weder die jetzt als Dissertation vorgelegte Arbeit noch Teile davon bei einer anderen Fakultät bzw. einem anderen Fachbereich als Dissertation eingereicht.

_____

Arda Alkan

Für meine Familie

"Ich habe keine besondere Begabung, sondern bin nur leidenschaftlich neugierig."

Albert Einstein

Danksagung (Acknowledgments)

Hiermit möchte ich mich bei allen Menschen bedanken, die mir beim Gelingen dieser Doktorarbeit geholfen und mich unterstützt haben. Folgenden Personen bin ich dabei besonders dankbar.

Mein besonderer Dank gilt **Dr. Frederik Wurm** für die Betreuung und Möglichkeit nach erfolgreichem Abschluss der Diplomarbeit, thematisch anknüpfend die Forschungsarbeiten fortsetzen zu können. Die häufigen Unterhaltungen und Diskussionen, nicht nur während der Arbeitszeit, sondern auch bei Freizeitaktivitäten, waren ein sehr wichtiger Aspekt, der zu neuen Ideen und zum Erfolg vieler Projekte dieser Arbeit geführt hat.

Ich danke **Prof. Dr. Katharina Landfester** für die Mitbetreuung dieser Doktorarbeit und für viele wichtige wissenschaftliche Gespräche. Darüber hinaus danke ich für die finanzielle Unterstützung, auch für die Teilnahme an nationalen und internationalen Konferenzen.

Ich möchte mich bei **Prof. Dr. Holger Frey** für die Mitbetreuung dieser Doktorarbeit und für die Möglichkeit, meine Diplom- sowie meine Doktorarbeit in seinen Laboren anzufertigen, bedanken.

Ich danke dem **Deutschen Akademischen Austauschdienst** für das Auslandssemester-Stipendium, während meines Studiums und für Kongressreisen, während meiner Promotion, wodurch ich meine Ergebnisse auf internationalen Konferenzen präsentieren konnte.

Besonders möchte ich mich bei **Dr. Adrian Natalello** für viele gemeinsame, erfolgreiche Projekte bedanken. Wir hatten wirklich sehr viel Spaß, ob im Labor oder privat – ein Freund fürs Leben.

Großer Dank gilt auch **Dr. Rebecca Klein** für unser gemeinsames Projekt (Kapitel 2.1) und der lustigen TOC Grafik, die sie gezeichnet hat. Ich bedanke mich auch sehr bei **ihr** und **Christian Schubert** für ihr Engagement bei außeruniversitären Unternehmungen. Tolle Freunde, die ich während unserer Promotionszeiten gewonnen habe.

Dr. Tobias Steinbach und **Dr. Christian Moers** danke ich für die Unterstützung im Labor und viele fachlichen Gespräche!

Ich bedanke mich sehr bei **Sarah Wald** für die Zusammenarbeit beim Einsatz der amphiphilen PfcGE-*b*-PEG Blockcopolymere als „Smart Surfactant“ (Kapitel 3.1).

Laura Thomi danke ich für die Zusammenarbeit bei der Synthese von responsiven Nanopartikeln aus Polyalkylene:VfcGE Homopolymeren.

Vielen Dank an **Elisabeth Rieger** für die Zusammenarbeit an der sequenzkontrollierten Polymerisation von Aziridinen.

Bei **Keti Piradashvili** bedanke ich mich für die praktische Einführung in die Miniemulsionspolymerisation im Labor.

Bei **Thomas Fritz**, **Matthias Worm** und **Benjamin Weber** bedanke ich mich für die Zusammenarbeit bei der Synthese und Anwendung der ruthenocenhaltigen amphiphilen Polymere als Kontrastmittel (Kapitel 2.4).

Dr. Manfred Wagner danke ich für zahlreiche Echtzeit NMR Kinetik-Messungen.

Vielen Dank an **Dr. Vadim Ksenofontov** und **Sergii I. Shylin** für die Zusammenarbeit bei der Analyse der oxidierten *hb*P[fcGE-*co*-G] Systeme mit Hilfe von Mößbauerspektroskopie.

Bei **Tassilo Gleede**, **Jan Blankenburg**, **Eduard Grune** und **Kamil Maciol** möchte ich mich für die Zusammenarbeit im Rahmen ihrer Module und bei **Christian Steinmetz** für die Zusammenarbeit im Rahmen seiner Bachelorarbeit bedanken. Es freut mich sehr, dass ihr euch für die Diplom-, Master- und Doktorarbeiten im Bereich makromolekularer Chemie entschieden habt.

Den **Doktoranden**, **Mitarbeitern** und **Alumni** danke ich für die warmherzige Aufnahme im Arbeitskreis und nette Arbeitsatmosphäre. Die gemeinsamen Aktivitäten, wie das Hüttenseminar in Grindelwald, habe ich wirklich sehr genossen und hoffe auch in Zukunft weiterhin teilnehmen zu können.

Bei **Luka Decker** bedanke ich mich für die fleißige Unterstützung im Labor.

Großer Dank gilt **Margarete Deptolla** für die Hilfe bei säulenchromatographischen Problemstellungen, **Ulrike Kemmer-Jonas** und **Angelika Manhart** für die synthetische Hilfe im Labor, **Monika Schmelzer** und **Christine Rosenauer** für GPC-Messungen, **Maria Müller** für DSC-Messungen, **Dr. Elena Berger-Nicoletti** für MALDI-ToF MS Messungen, **Christoph Sieber** für TEM-Messungen, **Dr. Johannes Liermann** für NMR-Messungen, **Ingrid Kosi** und **Ines Wollmer** für die Bestellung von Chemikalien, sowie **Heike Riegel-Allen** für ihre Hilfe bei organisatorischen Aufgaben.

Weiterhin möchte ich **all meinen Freunden** außerhalb des Instituts und der Universität für die willkommenen Ablenkungen danken.

Tiefste Dankbarkeit empfinde ich gegenüber **meinen Eltern**, die mich finanziell und moralisch unterstützt haben, sowie meiner Schwester **Merve** für die moralische Unterstützung. Meiner Verlobten **Neri** danke ich für ihre bedingungslose Unterstützung, während meines Studiums und meiner Promotion. Ohne **meine Familie** wäre diese Arbeit nicht möglich gewesen!

Table of Content

Danksagung (Acknowledgments) 1

Table of Content 5

Motivation and Objectives 7

Graphical Abstract 9

Abstract 13

Chapter 1: Introduction 15

1.1 Water-Soluble Metallocene-Containing Polymers 16

Chapter 2: Water-Soluble Multi-Stimuli-Responsive Metallocene-Containing Copolymers ... 45

2.1 Water-Soluble and Redox-Responsive Hyperbranched Polyether Copolymers Based on Ferrocenyl Glycidyl Ether 46

2.1.1 Supporting Information 63

2.2 Vinyl Ferrocenyl Glycidyl Ether: An Unprotected Orthogonal Ferrocene Monomer for Anionic and Radical Polymerization 70

2.2.1 Supporting Information 89

2.3 Triple-Stimuli Responsive Ferrocene-Containing PEGs in Water and on Surface 94

2.3.1 Supporting Information 112

2.4 PEG-Staining for Electron Microscopy with Ruthenocenyl Glycidyl Ether 120

2.4.1 Supporting Information 129

Chapter 3: Water-Soluble Ferrocene-Containing Block Copolymers 139

3.1 Amphiphilic Ferrocene-Containing PEG Block Copolymers as Micellar Carriers and Surfactants 140

3.1.1 Supporting Information 154

Chapter 4: Monomer Sequence Monitoring by Real-Time NMR Spectroscopy 157

4.1 Ferrocene-Containing Multifunctional Polyethers: Monomer Sequence Monitoring via Quantitative ^{13}C NMR Spectroscopy in Bulk 158

4.1.1 Supporting Information 178

References 187

Appendix 203
A.1 Cooperation Projects 204
A.1.1 Water-Soluble Multi-Stimuli-Responsive Metallocene-Containing Copolymers .. 206
A.1.2 Water-Soluble Ferrocene-Containing Block Copolymers 224
A.1.3 Monomer Sequence Monitoring by Real-Time NMR Spectroscopy 238
A.2 List of Publications 314
A.2.1 Journal Articles 314
A.2.2 Conference Contributions 316

Motivation and Objectives

Poly(ethylene glycol) (PEG) is applied in biology, medicine, food, health and personal care, because of its biocompatibility and water-solubility. This thesis used the "PEG–backbone" due to these properties to generate metallocene-containing multi-stimuli responsive materials that may be applied for applications going beyond those of "normal" PEG.

It is synthesized via anionic ring-opening polymerization (AROP) of ethylene oxide (EO). The copolymerization of EO and a more hydrophobic epoxide monomer leads to thermo-responsive polymers with lower critical solution temperature (LCST) behavior. Therefore, hydrophobic metallocene-containing monomers were designed for copolymerization with EO to combine thermo-responsivity with redox-responsive properties of inorganic sandwich-complexes.

In 2013, our group introduced ferrocenyl glycidyl ether (fcGE), the first ferrocene epoxide monomer. FcGE was copolymerized with EO leading to linear, water-soluble and dual-stimuli-responsive polymers. The following milestone was to synthesize an even more hydrophilic polymer with more ferrocene (mol%) incorporated. This aim was achieved by copolymerization of fcGE with glycidol leading to hyperbranched polyethers with multiple hydroxyl groups, which increased the hydrophilicity. The increased hydrophilicity is indicated by an increased cloud-point.

To introduce a third stimulus, a novel monomer had to be designed. A five step reaction to an orthogonal monomer, vinylferrocenyl glycidyl ether (VfcGE), fulfilled this objective. VfcGE could be copolymerized with EO in the AROP under the same reaction conditions as for fcGE and EO. The resulting polymers carry vinyl functionalities for post-polymerization modifications, which was used to introduce a pH-responsive group via thiol-ene addition reaction. Therefore, 3-mercaptopropionic acid and cysteamine have been used as model compounds for the introduction of a carboxylic acid and an amine groups. The triple-responsive behavior of the resulting polymers was investigated on a glass surface and in solution. VfcGE was also homopolymerized in a free radical polymerization. The multiple epoxide functionalities were utilized for redox-responsive nanoparticle formation.

PEG is a well-established polymer for biomedical applications and is used as hydrophilic segment in various self-assembled structures and other nanomaterials. Transmission electron microscopy (TEM) is often used to visualize these materials, however, PEG is typically invisible due to its low electron density. Metallocene-PEGs have high electron density and therefore, the iron center in fcGE is substituted by ruthenium, which has an approximately 69% higher electron density. Ruthenocenyl glycidyl ether (rcGE) is copolymerized with EO leading into PEG with a low amount of rc. PEG with up to 2 to 3% rcGE exhibit high water-solubility, barely different than pure PEG, whereas its electron density is much higher and thus its visualization in electron microscopy (EM) is much better.

FcGE is also a key monomer to synthesize PEG-based "smart surfactants". These can be used in miniemulsion polymerizations for stabilization. But other than usual surfactants, they can be washed off after oxidation and reused. The synthesis of a redox- and pH-responsive amphiphilic macromolecule is performed by the homo polymerization of fcGE using mPEG as macroinitiator. The resulting polymer is amphiphilic with a hydrophobic PfcGE block. But if the fc units are oxidized to the ferrocenium ion, the block copolymer will become totally water-soluble.

The copolymerization of fcGE with EO was analyzed in details by real-time ^{1}H NMR spectroscopy. The microstructure is found to be random. ^{1}H NMR analysis of copolymerizations of epoxide monomers with overlapping proton signals are hard to accomplish. This is the case for copolymerization of allyl glycidyl ether (AGE) and fcGE, which is performed in bulk. Real-time ^{13}C NMR spectroscopy in a conventional NMR tube is developed to analyze this system. The natural abundance of ^{13}C isotopes in bulk is sufficient enough to analyze the copolymerization behavior of both monomers by measuring NMR spectra within a few minutes.

Graphical Abstract

Chapter 1: Introduction

1.1 Water-Soluble Metallocene-Containing Polymers

Chapter 2: Water-Soluble Multi-Stimuli-Responsive Metallocene-Containing Copolymers

2.1 Water-Soluble and Redox-Responsive Hyperbranched Polyether Copolymers Based on Ferrocenyl Glycidyl Ether

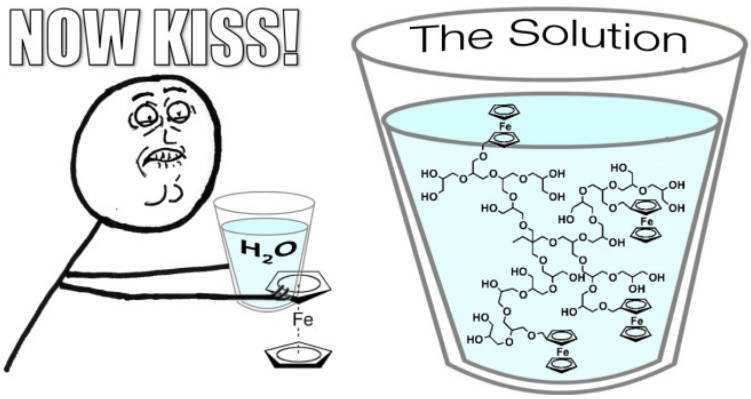

2.2 Vinyl Ferrocenyl Glycidyl Ether: an Unprotected Orthogonal Ferrocene Monomer for Anionic and Radical Polymerization

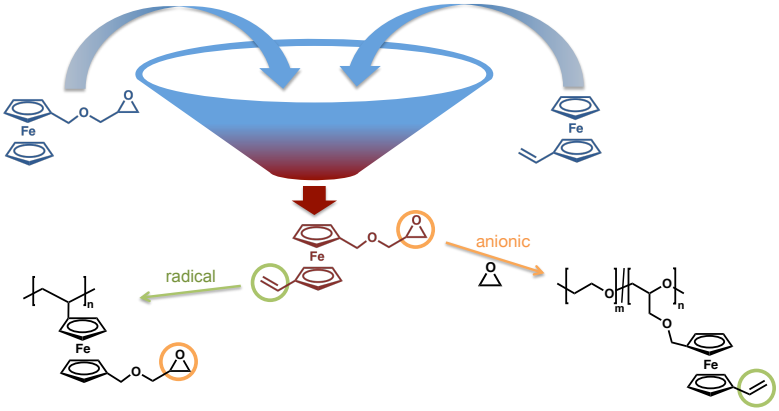

2.3 Triple-Stimuli-Responsive Ferrocene-Containing PEGs in Water and on the Surface

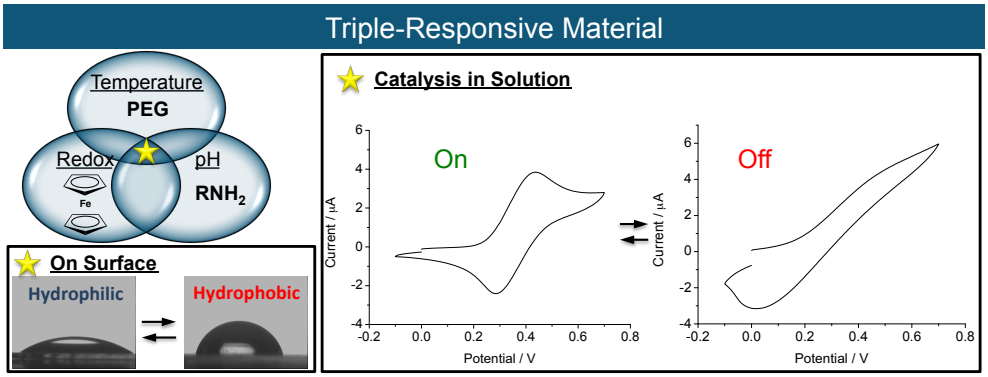

2.4 PEG-Staining for Electron Microscopy with Ruthenocenyl Glycidyl Ether

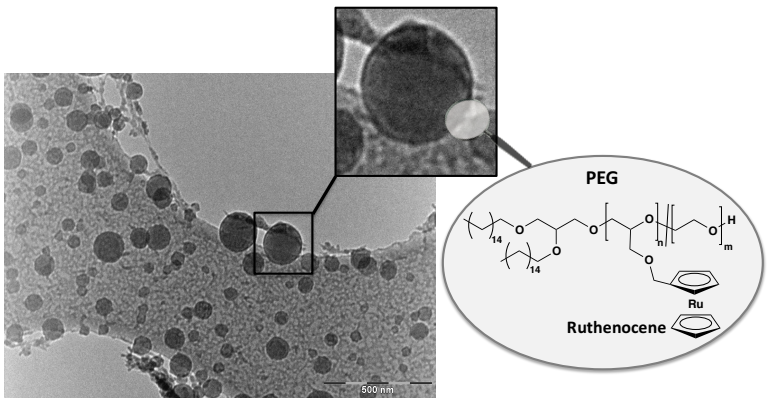

Chapter 3: Water-Soluble Ferrocene-Containing Block Copolymers

3.1 Amphiphilic Ferrocene-Containing PEG Block Copolymers as Micellar Carriers and Surfactants

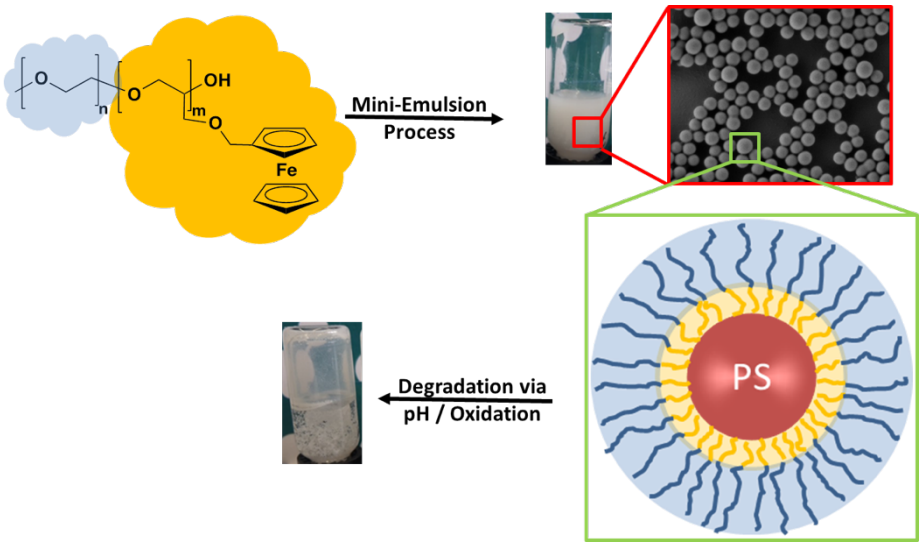

Chapter 4: Monomer Sequence Monitoring by Real-Time NMR Spectroscopy

4.1 Ferrocene-Containing Multifunctional Polyethers: Monomer Sequence Monitoring via Quantitative ^{13}C NMR Spectroscopy in Bulk

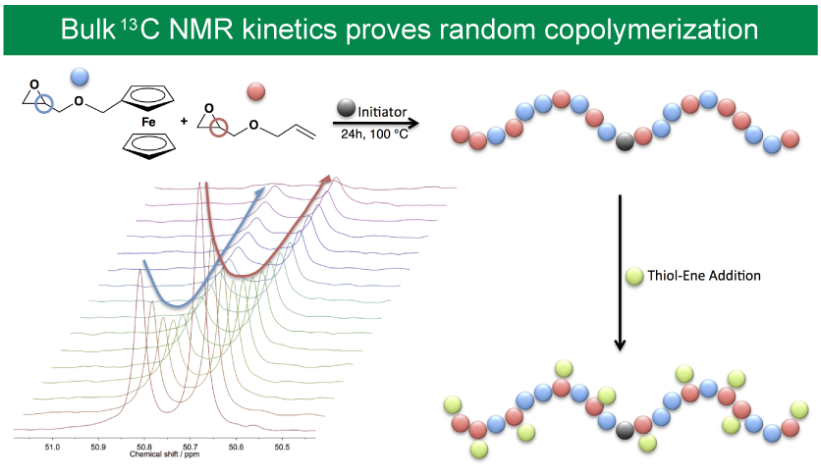

Abstract

The focus of this work is on the synthesis of novel water-soluble metallocene-containing polyethers. Linear and hyperbranched (co-)polymers and block copolymers with ferrocene or ruthenocene units have been prepared. New monomer syntheses have been developed and their polymerization behavior has been studied in detail. Further, the stimuli-responsive properties in solution and also applications on surface are presented.

Chapter 1 gives a short introduction to water-soluble metallocene-containing polymers by summarizing all synthetic routes to such structures and also clarifying the motivation and underlying idea. Not only ferrocene, but also cobaltocenium- and ruthenocene-containing polymers are discussed. If applicable, applications of these systems are shown and unexplored possible applications are mentioned.

Chapter 2 deals with the synthesis of novel water-soluble metallocene-containing polymers. The polymerization of a known ferrocene monomer (fcGE) with glycidol (G) to novel hyperbranched structures (Chapter 2.1), the synthesis and polymerization of a novel orthogonal ferrocene monomer (VfcGE; Chapter 2.2) and its functionalization to triple-stimuli-responsive materials (Chapter 2.3) as well as the synthesis and polymerization of a novel ruthenocene monomer, ruthenocenyl glycidyl ether (rcGE), is described (Chapter 2.4).

In collaboration with Dr. Rebecca Klein the copolymerization of fcGE with G to hyperbranched structures and their properties in solution were investigated (Chapter 2.1). The relation between thermo- and redox-responsivity for this material is analyzed further by Mößbauer spectroscopy.

In Chapter 2.2 the synthesis of a novel orthogonal ferrocene monomer, namely vinylferrocenyl glycidyl ether (VfcGE), and its radical and anionic polymerization is described. The radical homopolymerization leads to polyalkylene:VfcGE with multi-epoxide functions. The anionic ring-opening copolymerization (AROP) with ethylene oxide leads to water-soluble copolymers with vinyl groups for further functionalization.

The post-polymerization modification to triple-stimuli-responsive materials is described in Chapter 2.3. Material properties in solution and at the interface by covalent linkage to a glass surface have been investigated.

In Chapter 2.4 a new PEG-staining strategy for electron microscopy (EM) is described. Therefore, a novel epoxide monomer bearing ruthenocene is designed and copolymerized with ethylene oxide in a AROP. Ruthenocene was chosen for high stability reasons and also high electron density, which is necessary for high contrast in EM.

Chapter 3 presents amphiphilic ferrocene-containing block copolymer structures. In Chapter 3.1 fcGE is homopolymerized using mPEG as macroinitiator. In collaboration with Sarah Wald this block copolymer is used as smart surfactant for miniemulsion processes. Emulsions could be stabilized successfully with this amphiphilic block copolymer and destabilized by the responsive fc-containing block via pH and various oxidizing agents.

In **Chapter 4** the copolymerization behavior of two monomers in an oxy-anionic polymerization is investigated. Since it is hard to gain knowledge from the resulting copolymer, real-time NMR spectroscopy is the key method to easily analyze the microstructure of copolymers. The copolymerizations were performed in a conventional NMR tube and NMR spectra were measured during polymerization.

In collaboration with Dr. Adrian Natalello the copolymerization behavior of fcGE and AGE to multifunctional ferrocene-containing materials is determined. The polymerization war carried out in bulk at 100 °C. Under these conditions no isomerization of the allyl double bonds was observed, which was unexpected. Since the copolymerization could not be followed by ^{1}H NMR spectroscopy, because of overlapping signals of the two monomers, real-time ^{13}C NMR spectroscopy was introduced to determine the incorporation ratio. The resulting copolymer was post-modified via thiol-ene addition reaction of the allyl double bonds and a protected cysteine-derivative, namely *N*-acetyl-L-cysteine methyl ester.

Chapter 1: Introduction

1.1 Water-Soluble Metallocene-Containing Polymers

Submitted for publication.

Authors: *Arda Alkan, Frederik R. Wurm*

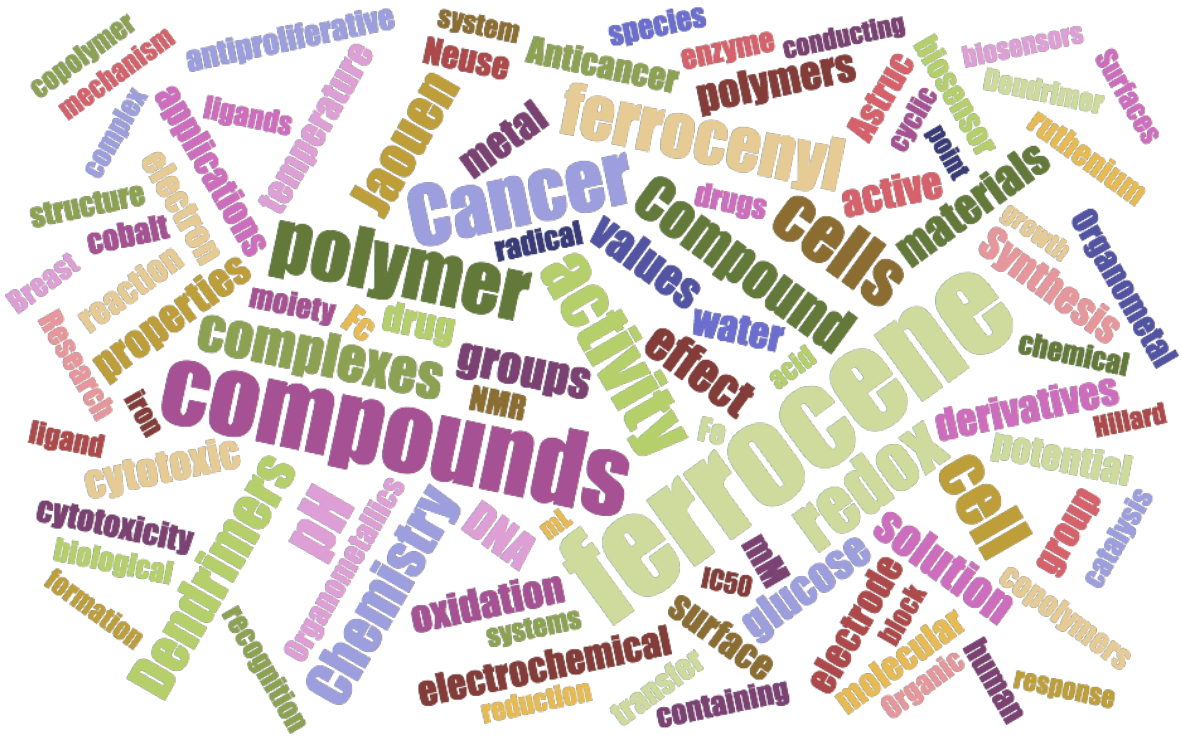

Abstract

Metallocenes are organometallic compounds with interesting chemical and physical properties. The participation in reversible redox processes with tunable oxidation and reduction potentials – depending on the metal and substituents at the cyclopentadienyl rings – is essential for many applications like catalysis or sensing. Metallocenes have been introduced in macromolecules to combine the redox-activity with polymer properties. There are many examples of such hydrophobic polymer materials, but much less water-soluble examples are found scattered in the polymer literature. However, in terms of drug delivery and other biological applications the water-solubility is inevitable. For this very reason, this review collects and discusses all synthetic routes to water-soluble metallocene containing polymers. This review focuses on ferrocene- and ruthenocene-containing neutral and cobaltocenium-containing macromolecules (i.e. symmetrical sandwich complexes). The synthetic protocols, self-assembly behavior, and other benefits of the obtained materials are discussed.

Introduction

Ferrocene (fc) is probably the most famous and best understood iron complex and belongs to the so called “sandwich” complexes, consisting of Fe(II) and two cyclopentadienyl ligands. It was discovered simultaneously in 1951 by Miller et al.[1] and Kealy and Pauson.[2] The structure was determined later by Wilkinson et al.[3] and Fischer et al.,[4] who were awarded the Nobel Prize in Chemistry in 1973. Ferrocene is a stable 18-electron complex allowing redox chemistry in organic environment. Other sandwich-complexes are known with either metal or ligand variations derived from ferrocene such as ruthenium, i.e. ruthenocene (rc). Also other ligands than cyclopentadienyl can be used; for example benzene as it is in

bis(benzene)chromium. More exotic structures have also been reported, e.g. with uranium forming a sandwich-complex with two cyclooctatetraenide ligands, i.e. uranocene ($U(COT)_2$). In addition to these symmetric structures, also unsymmetrical sandwich-complexes, particularly half-sandwich complexes like methylcyclopentadienyl manganese tricarbonyl (MMT) are known, which are often used in catalysis.[5] Catalysis is the largest field of application for sandwich complexes,[6] especially asymmetric catalysis, for example in Ziegler-Natta polymerizations.[7,8] Other applications for sandwich-complexes are based on their redox-profile, e.g. in amperometric glucose sensors, where they act as mediators between the analyte and the electrode.[9-14] They are also used as antiknock agents in gasoline to increase its octane rating,[5] or are discussed in modern cancer therapeutics.[15-17]

As a hydrophobic material with a relatively high vapor pressure (e.g. purification is achieved by sublimation), ferrocene's use is limited; polymerization of metallocene-derivatives is an attractive strategy to expand the application potency. The combination of polymer properties, such as no vapor pressure, plasticizing and the combination with other materials properties by copolymerization are just a few examples to rationalize metallocene incorporation into polymers. Today, many publications describe the synthesis of metallocene-containing polymers, which are in most cases hydrophobic materials. Several reviews and books describe such materials extensively.[18-22]

Interestingly, the number of water-soluble metallocene-containing polymers is much lower, despite the stable redox properties (also in water) and the presence of various hydrophilic polymers for mainly biomedical applications. Herein we summarize the synthesis routes and techniques to water-soluble metallocene-containing polymers. An overview about all possible synthetic strategies is given in Scheme 1. This is the first review with the focus on metallocene polymers of variable structure in water and for different aqueous applications. This review is attractive for researchers working in bio-related fields, since ferrocene and its derivatives are relevant in anticancer research. Its redox-responsive behavior makes ferrocene interesting as a component for drug-delivery systems. Also researchers working with responsive materials may benefit from water-soluble redox-responsive properties. It is

also a guideline on how to transfer hydrophobic organometallic structures or reactions into water, e.g. to avoid organic solvents and achieve green chemistry.

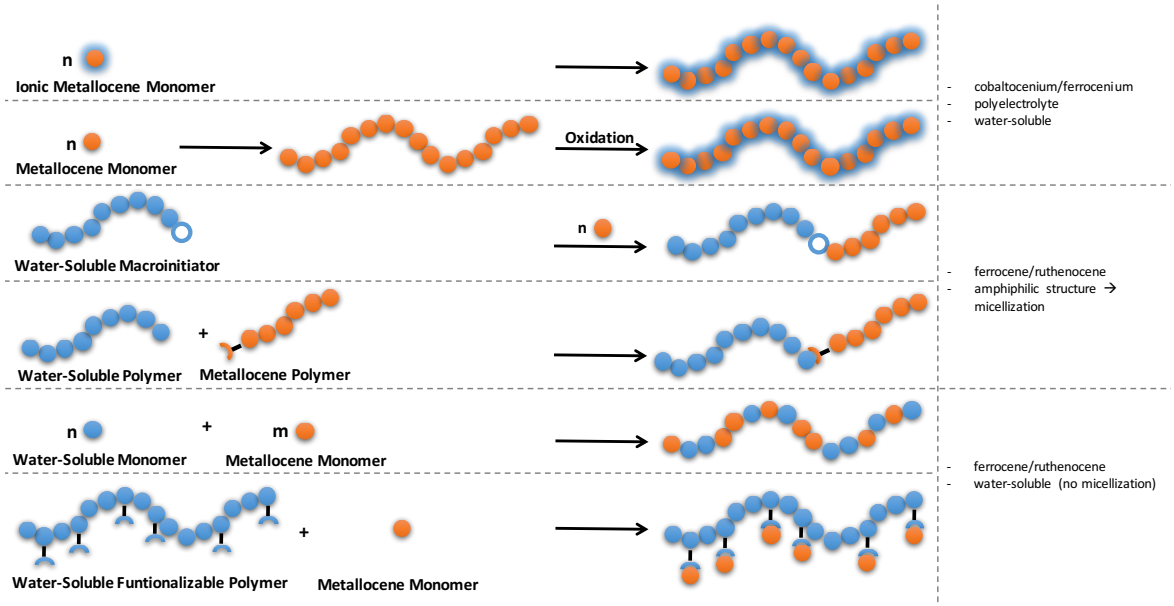

Scheme 1. General overview about synthetic strategies to metallocene-containing water-soluble polymers.

Ferrocene and its derivatives in cancer treatment: ferrocifen.

Ferrocene is a water-insoluble compound and becomes hydrophilic, when it is oxidized to the 17 electron complex, i.e. the ferrocenium ion, which is not as stable as ferrocene.[23] Especially in terms of cytotoxic ferrocenes for cancer treatment, water-solubility of the final drug-complex is necessary for targeting.[24]

A famous example of such a ferrocene-containing molecule combining the important properties of water-solubility and cytotoxicity is ferrocifen.[16,25-27] There are also other organometallics,[28-31] ferrocenium salts,[32,33] or ferrocene derivatives[34-36] with cytotoxicity and

even other examples showing antifungal properties,[37] antimalarial activity,[38,39] which have been investigated. Ferrocifen (**2**) is derived from tamoxifen (**1**), which is a chemotherapeutic agent for patients with hormone-dependent breast cancer.[40,41]

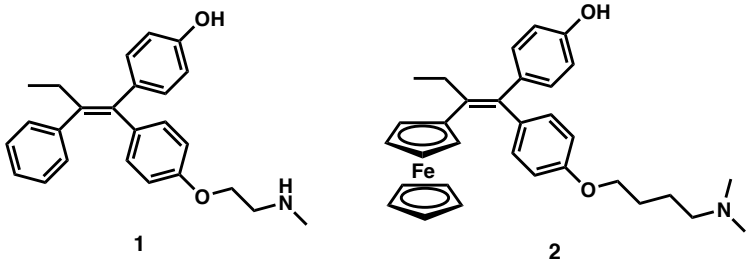

Figure 1. Structures of tamoxifen (1) and ferrocifen (2).

Jaouen and co-workers substituted the phenyl rings in established drugs with ferrocene groups and discovered different derivatives of ferrocifen.[42-46]

First ferrocene-containing water-soluble polymers: motivation and objective.

Since Ringsdorf's early studies, polymers have been regarded as drug carriers.[47-49] In 1989, Neuse et al. presented the first water-soluble polymers (poly(aspartamide)) carrying ferrocene units in the side chains, which exhibit enhanced cytotoxicity.[50-55] Neuse and coworkers studied water-soluble ferrocene-containing polymers before, when they synthesized poly(ferrocene) and oxidized it with $FeCl_3$ to a polycation.[56] They assumed that an enhanced water-solubility would lead to an enhanced cytotoxicity, since water-soluble ferrocenium salts always show at least good antiproliferative and antineoplastic behavior against human transplanted tumors.[32,57] Since the ferrocenium cation is instable in aqueous medium at physiological pH, the half-lives in the vascular circulation system is too short for effective survival *en route* to the target cells. Therefore, they had set themselves the task to

increase the hydrophilicity of ferrocene by functionalizing a polymer, which is known for high water-solubility, with ferrocene.

Neuse et al. has shown that polyaspartamide can be used as polymeric carrier for ferrocene.[50,52] Therefore, polyaspartamide is modified with poly(ethylene oxide) side chains to enhance the water-solubility. The polymer is further functionalized with ferrocene leading to water-soluble ferrocene-bearing polymers. Selected conjugates are tested for antiproliferative activity against HeLa and LNCaP human cancer cell lines. The results show IC50 values in the range of 2-20 μg Fe/mL.

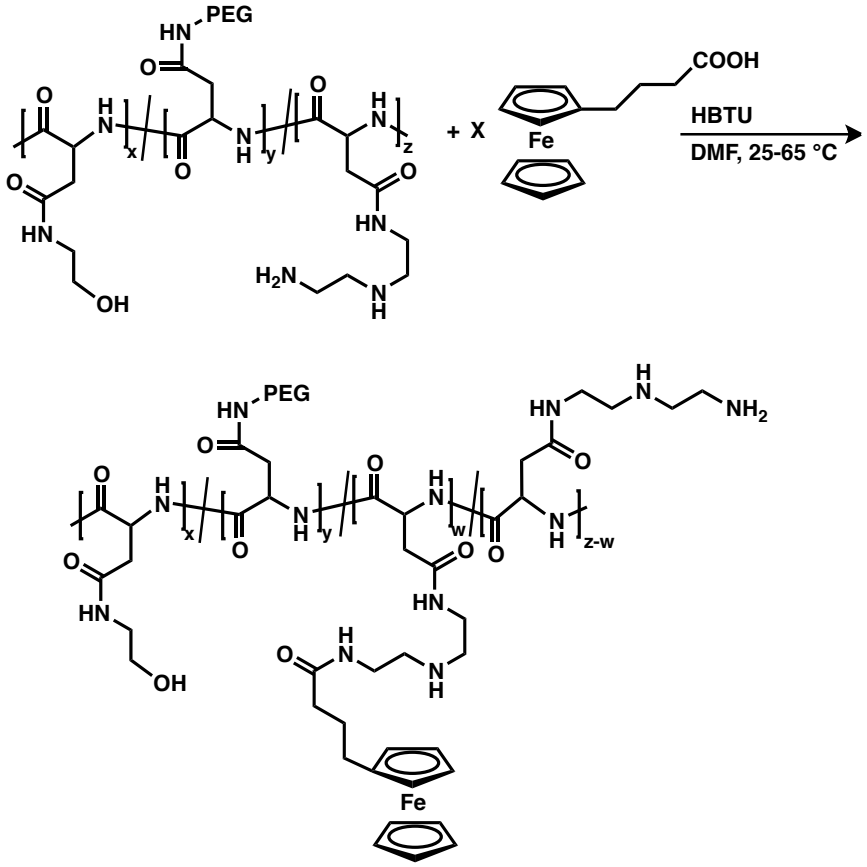

Scheme 2. Functionalization of PEG-modified polyaspartamide with ferrocene in DMF in the presence of 2-(1H-benzotriazol-1-yl)-1,1,3,3-tetramethyluronium fluorophosphate (HBTU).[50]

Another strategy to solubilize ferrocene and its derivatives in water can be achieved by the formation of inclusion complexes, e.g. with cyclodextrine; however, this strategy typically leads to an inactive ferrocene unit and, in addition the stability of these structures are concentration dependent and will not be discussed herein.[58-60]

Synthetic Routes to Water-Soluble Ferrocene-Containing Block Copolymers

The synthesis of block copolymers is the most studied approach to generate water-soluble metallocene-containing materials. The hydrophilic segment (e.g. PEG, PNIPAM, etc.) is combined with a hydrophobic block, carrying the ferrocene units.

Manners and coworkers studied the aqueous self-assembly of a poly(ferrocenyldimethylsilane)-*block*-poly[2-(*N*,*N*-dimethylamino)ethyl methacrylate] (PFS-*b*-PDMAEMA) diblock copolymer to cylindrical micelles. The synthesis is based on the anionic ring-opening polymerization (AROP) of ferrocenyldimethylsilane (FDMS), initiated by (*tert*-butyldimethylsilyloxy)-1-propyllithium. After deprotection of the silyl-protected initiator, the terminal hydroxyl group is used for the subsequent anionic polymerization of 2-(*N,N*-dimethylamino)ethyl methacrylate (DMAEMA). The resulting diblock copolymer is water-soluble under formation of cylindrical micelles, which is characteristic for the crystalline PFDMS block.[61]

Generally, when a solution of an amphiphilic PFDMS diblock copolymer with a good solvent for both blocks is added to a selective solvent for the hydrophilic segment and a poor solvent for PDMFS, these polymers readily self-assemble to form cylindrical micelles.[62] The crystallization-driven self-assembly (CDSA) has been shown to follow kinetics similar to a 'living' chain growth polymerization, when additional block copolymer (i.e. unimer) is added to the micellar solutions.[63,64] With this strategy various block copolymers have been used to

generate multicompartment micelles or more complex architectures by the addition of different unimers.[65]

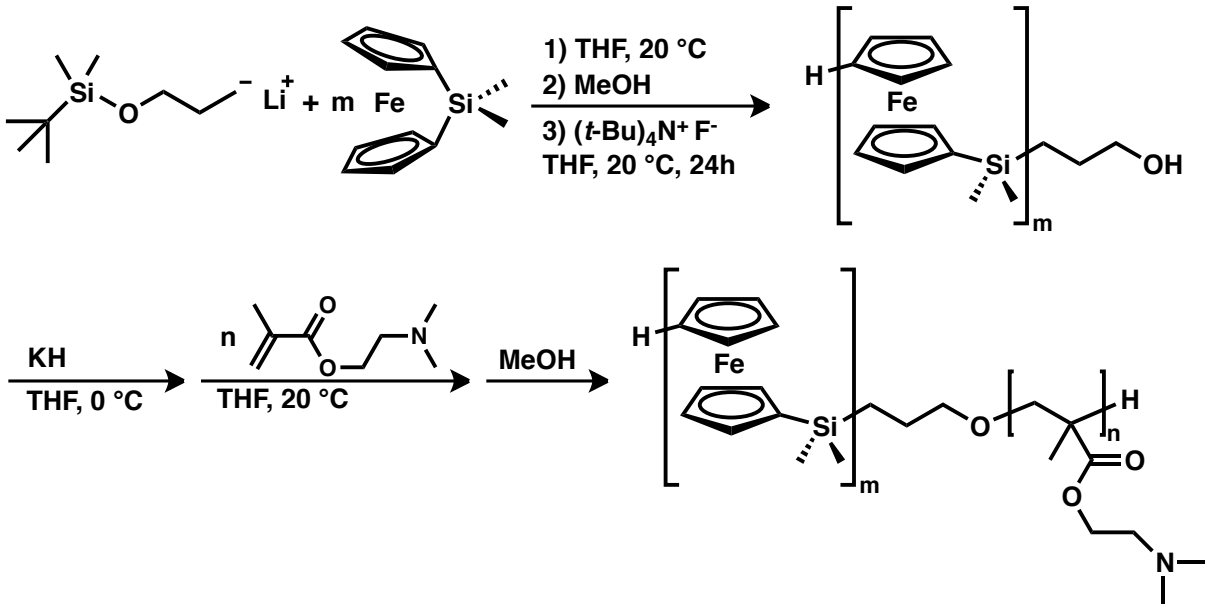

Scheme 3. Synthetic protocol of PFDMS-*b*-PDMAEMA.[61]

Gohy et al. synthesized an amphiphilic poly(ethylene oxide)-*block*-poly(ferrocenylsilane) block copolymer by the AROP of DMFS initiated by *tert*-butyldimethylsilyloxy-1-propyllithium, which was hydrolyzed after the reaction. The OH-terminated PFDMS was then reacted than with an isocyanate-functionalized terpyridine and linked to the PEG block via a bis(terpyridine)ruthenium(II) complex.[66]

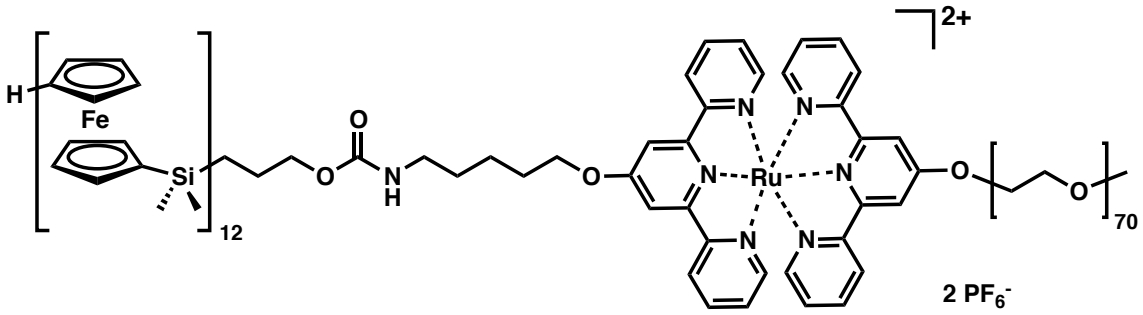

Scheme 4. Structure of PFDMS-*b*-PEG block copolymer with a bis(terpyridine)ruthenium(II) complex linkage of the two blocks.[66]

Even though the polymer does not readily dissolve in water, cylindrical micelles in water were realized after transfer from a good solvent for both blocks, which is *N*,*N*-dimethylformamide (DMF), into water.

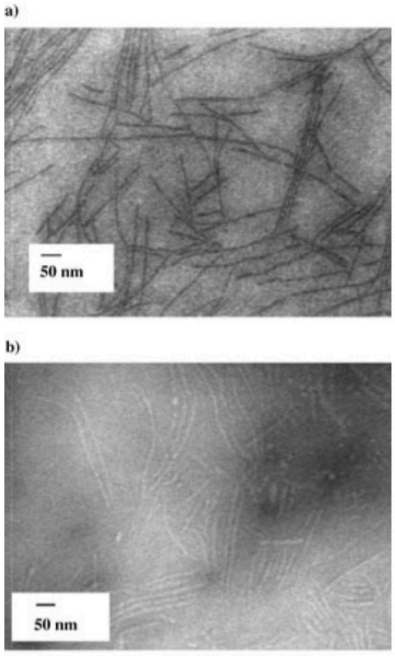

Scheme 5. TEM images for PFS_{12}-[Ru]-PEO_{70} block copolymers: a) without staining and b) with negative staining.[66]

Manners and coworkers synthesized water-soluble PFS block copolymers via the alkyne/azide click reaction.[67] Therefore, the anionic ring-opening polymerization of DMFS was terminated with an aldehyde bearing a trimethylsilyl-protected alkyne. After the removal of the silyl protective group, the Cu(I)-catalyzed alkyne/azide cycloaddition (CuAAC) was performed with different hydrophilic azide-terminated polymers. By these means PFS-*b*-PEG, PFS-*b*-poly(N-isopropylacrylamide) (PFS-*b*-PNIPAM) and PFS-*b*-poly(2-(dimethylamino)ethyl methacrylate) (PFS-*b*-PDMAEMA) block copolymers were generated and purified by dissolution/precipitation in selective solvents. The authors assume that this method should be readily applicable to other polymers prepared by living anionic polymerization.

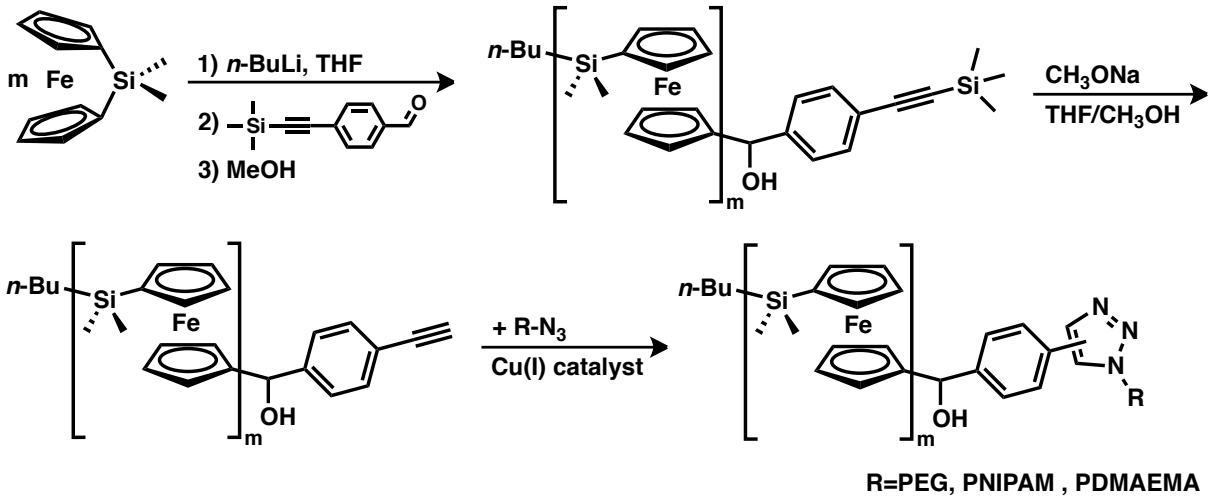

Scheme 6. Synthetic route to PFDMS-*b*-R block copolymers via CuAAC "click" chemistry (R=PEG, PNIPAM, PDMAEMA).[67]

Natalello et al. developed a full chain-growth protocol to PFS-*b*-PEG block copolymers. Epoxide termination of living PFDMS was used to switch from carbanionic to oxyanionic polymerization.[68] This was realized by capping the living PFDMS anions with 1,1-dimethylsilacyclobutane and 1,1-diphenylethylene, and subsequent termination with allyl

glycidyl ether. The generated terminal hydroxyl group was deprotonated to form a macroinitiator for polymerization of ethylene oxide leading to amphiphilic PFDMS-*b*-PEG block copolymers carrying an additional allyl bond at the block junction. These block copolymers also self-assembled into rod-like micelles in alcohol and water.

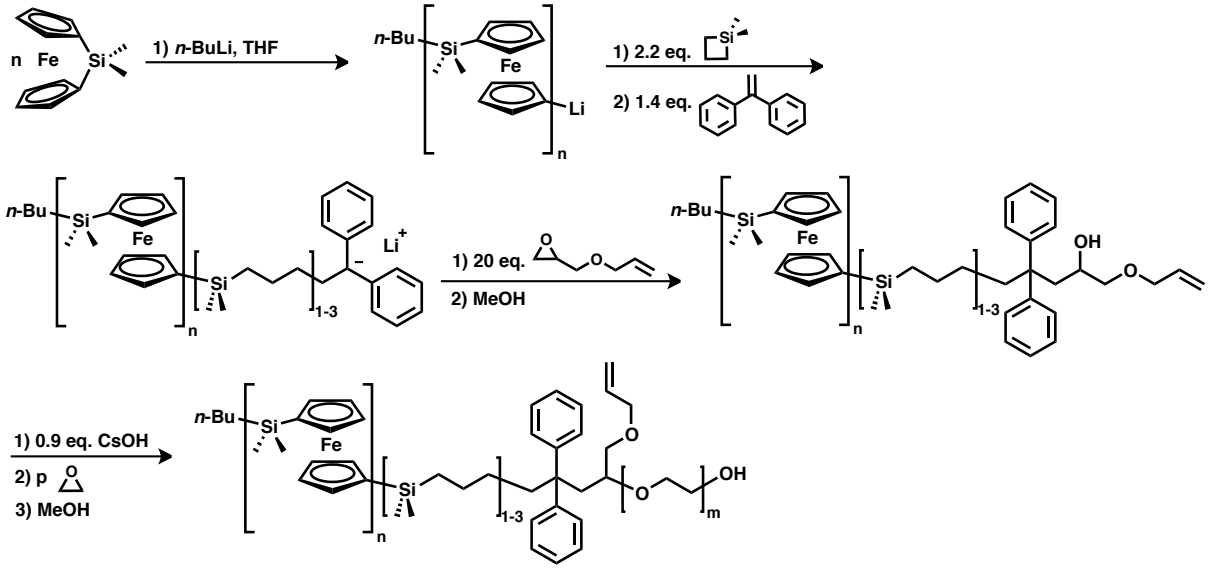

Scheme 7. Synthetic route to PFDMS-*b*-PEG block copolymers by switching from living carb- to oxyanionic polymerization.[68]

Schacher et al. prepared star-block copolymers consisting of PFDMS and PEG blocks. The ring-opening polymerization of DMFS was catalyzed by the Karstedt's catalyst, in the presence of a four-arm star-shaped PEG macroinitiator.[69] This strategy was used before by Resendes et al. to synthesize linear water-soluble PEG-*b*-PFS block copolymers.[70]

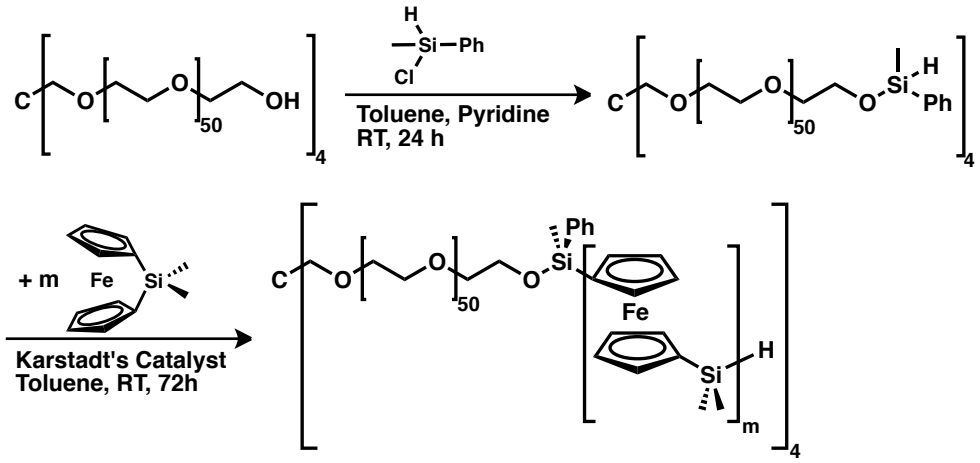

Scheme 8. Synthesis of a four-arm PEG_{50}-*b*-$PFDMS_m$ star-shaped block copolymers.[69]

The crystalline-coil PFS-*b*-PEG star-block copolymers were used to generate pH-responsive vesicles via self-assembly. A photoacid generator is encapsulated for UV-induced generation of HCl and subsequent degradation.

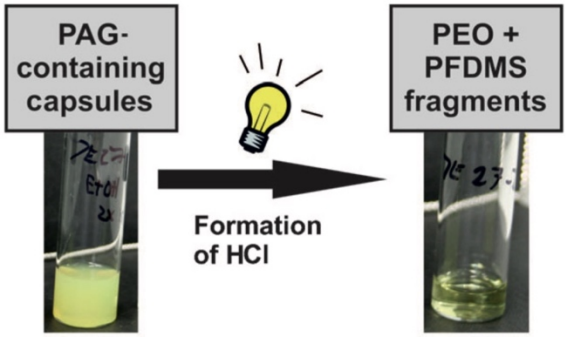

Figure 2. UV-induced degradation of PFS-*b*-PEG vesicles using a photoacid generator.[69]

Water-soluble ferrocene-containing block copolymers were also synthesized based on poly(vinylferrocene) (PVfc). Tonhauser et al. have synthesized poly(vinylferrocene) in a carb-anionic polymerization and end-capped the living chain end with benzyl glycidyl ether.[71] After termination with methanol, the generated hydroxyl group was used for the oxy-anionic polymerization of ethylene oxide. Also the benzyl-protected hydroxyl group could be

released by hydrogenation and used as a second initiating group at the chain end to form AB_2 miktoarm star copolymers with excellent water-solubility. TEM images of an aqueous solution show agglomerated micellar structures.

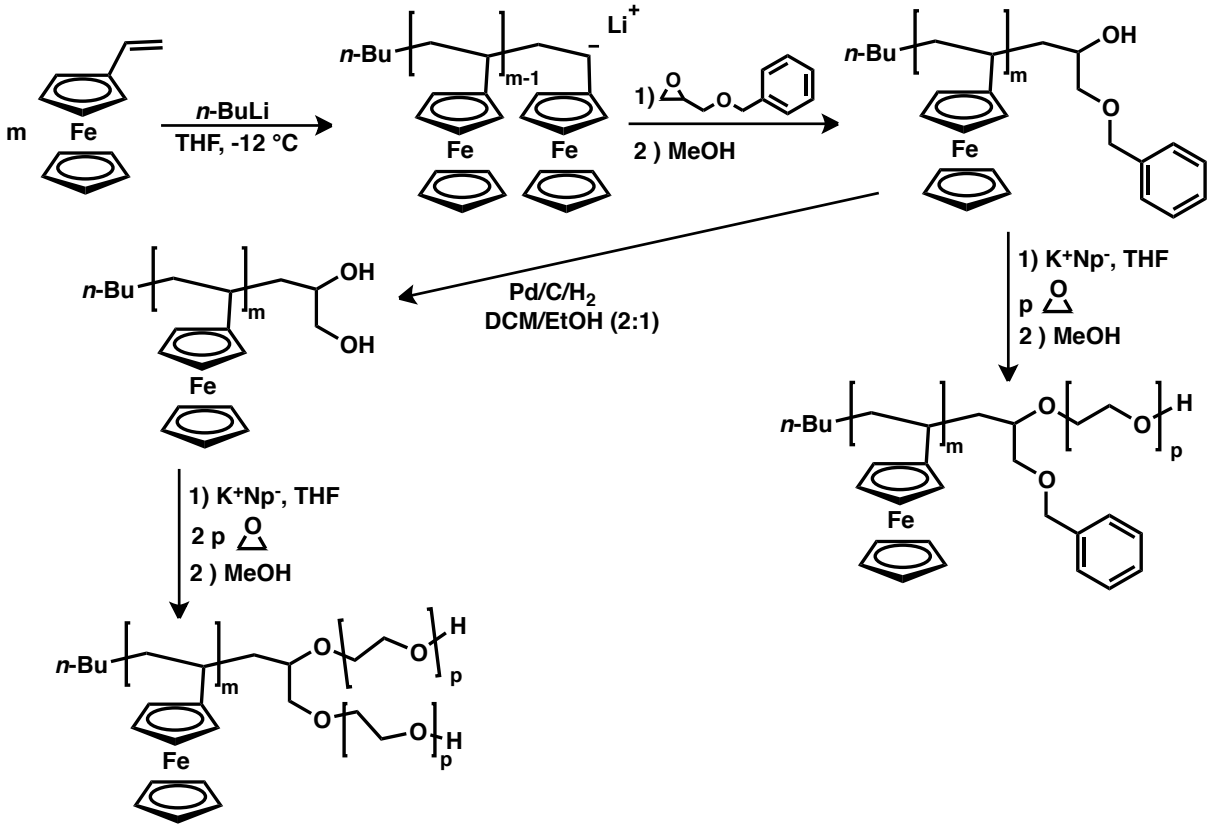

Scheme 9. Synthesis of PVfc-*b*-PEG block and AB_2 miktoarm star copolymers by switching from carb-anionic to oxy-anionic polymerization.[71]

Very recently, Zhang and co-workers have synthesized nano-assemblies of ferrocene-containing block copolymers, whereby the morphologies underwent the transition from worms-to-vesicles-to-multilayer vesicles.[72]

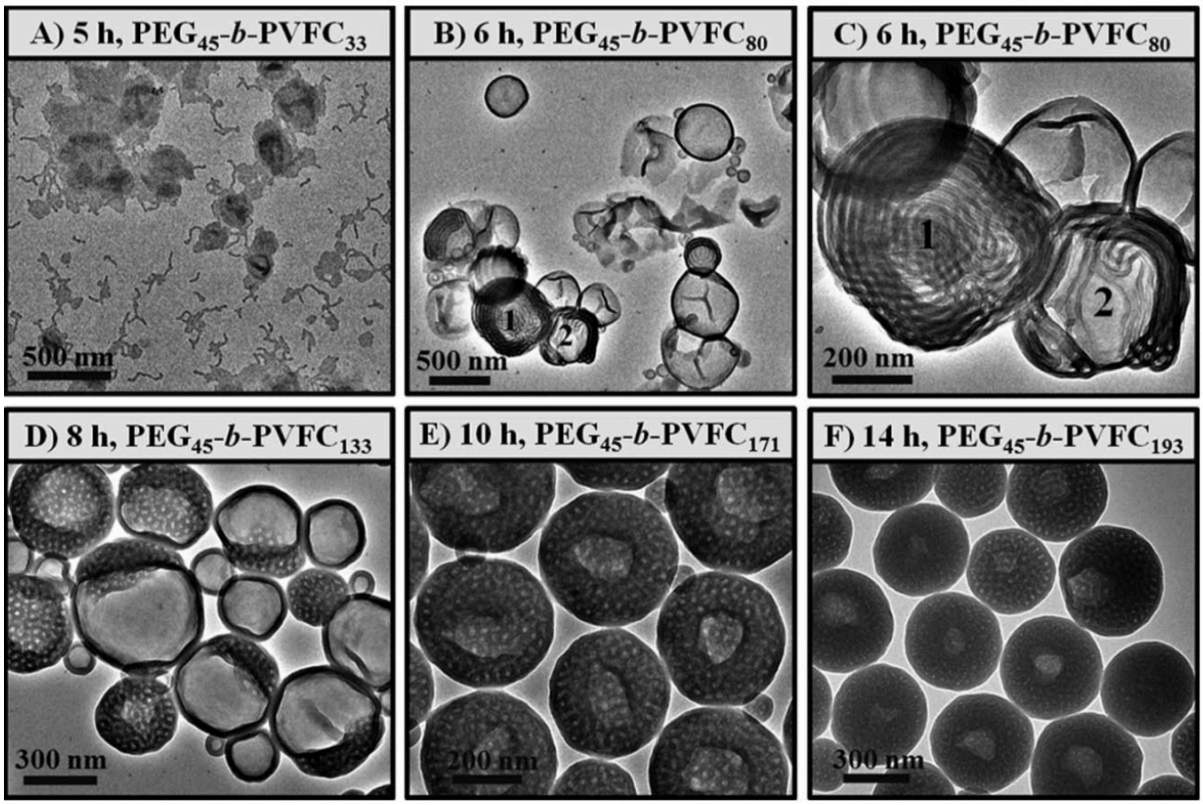

Figure 3. Different morphologies depending on PVFC block lengths.[72]

Therefore, a PEG-TTC (PEG-trithiocarbonate) macro-RAFT agent was prepared and a subsequent dispersion RAFT polymerization of 4-vinylbenzyl ferrocenecarboxylate (VFC), which was synthesized prior from ferrocenecarboxylate, was performed leading to poly(ethylene glycol)-*block*-poly(4-vinylbenzyl ferrocenecarboxylate) (PEG-*b*-PVFC). The same strategy was used before by Xiao et al. to synthesize PEG-*b*-poly(2-formal-4-vinylphenyl ferrocenecarboxylate) (PEG-*b*-FVFC).[73]

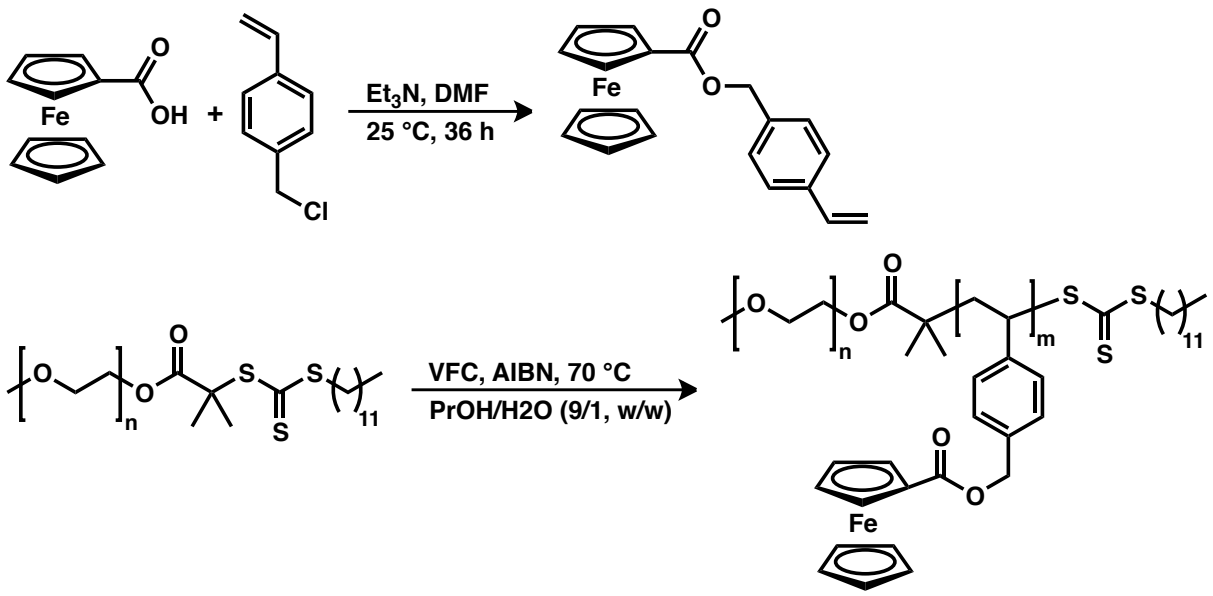

Scheme 10. Monomer synthesis: VFC, and homopolymerization using a PEG-TTC as RAFT-agent.[72]

Synthetic Routes to Water-Soluble Ferrocene-Containing Homopolymers and Statistical Copolymers

Water-soluble ferrocene-containing polymers can be achieved by post-modification of a previously synthesized polymer with functionalizable groups. For example, Hatozaki and Anson describe the labelling of poly(acrylic acid) (PAA) with ferrocenylethanol (one unit) in a esterification reaction. It was enabled to estimate the diffusion coefficient of PAA. Therefore, the fc unit was oxidized at a rotation disc electrode, and the diffusion coefficient was estimated by analysis of the rotation rate dependences of the measured currents.[74,75]

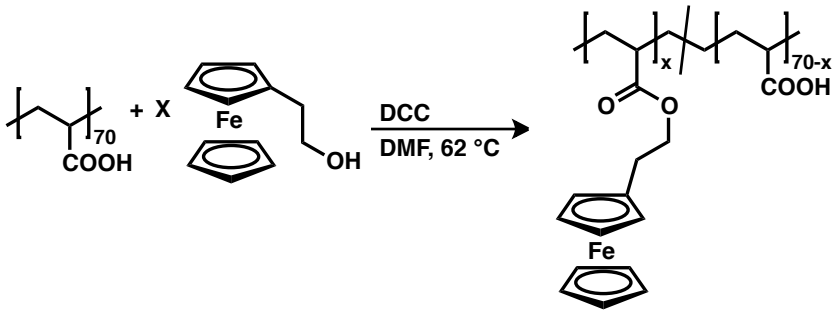

Scheme 11. PAA is labelled with ferrocenylethanol in the presence of dicyclohexylcarbodiimide (DCC) in DMF.[74]

Water-soluble PFS can also be synthesized using ionic substituents. Power-Billard et al. used ROP of a chloroalkyl side chain bearing ferrocenophane and 4-dimethylaminopyridine afterwards in a substitution reaction of the chloride leading to water-soluble PFS.[76]

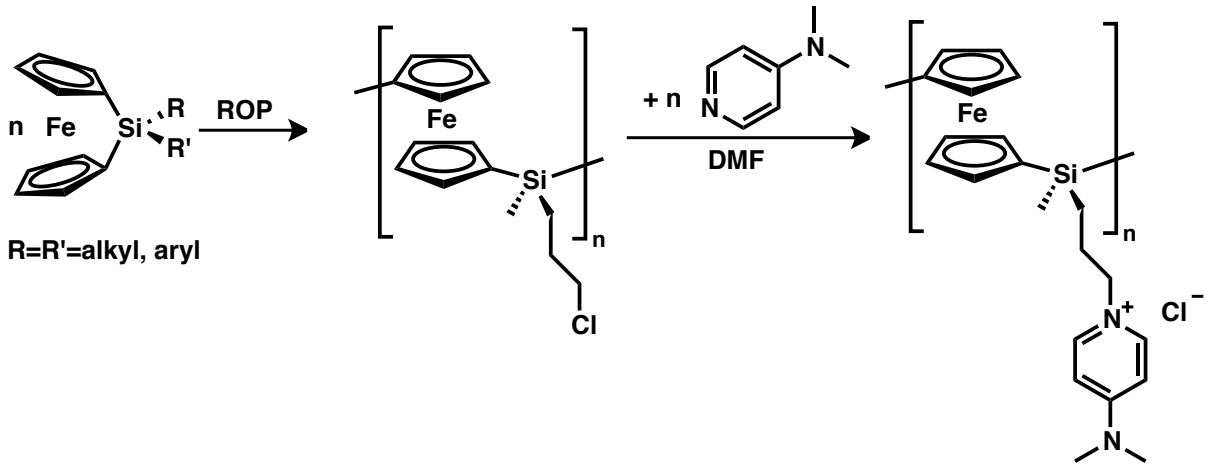

Scheme 12. ROP of ferrocenophane and substitution of chloride with dimethylaminopyridine to a water-soluble polycation structure.[76]

There are also more ionic side-chain substituted PFS, which are water-soluble. Polycations were synthesized bearing ammonium groups in there side chains,[77,78] and also polyanions were synthesized bearing carboxylates,[79] or sulfonates[80] which were than used in a layer-by-layer (LbL) deposition.[81] LbL deposition of these structures could also be used to construct

redox responsive shells on hydrophobic CdSe/ZnS quantum dots (QDs), which made the QD colloids stable in water in both reduced and oxidized forms of the fc, whereby the two states show modulated florescence changes.[82]

Watson et al. synthesized an amphiphilic ferrocene-bearing norbornene monomer with a quaternary ammonium bridge.[83] The monomer can be polymerized in a ring-opening metathesis polymerization (ROMP) using Grubbs' first generation catalyst leading to a polymer with high water-solubility. The authors claim that this strategy can be extended to include many other molecules, which contain ammonium functionalities.

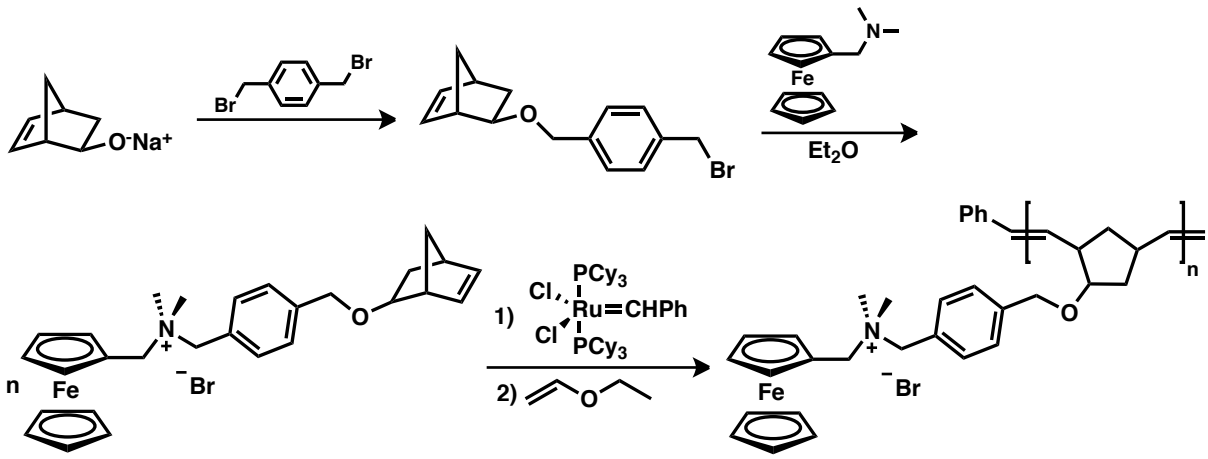

Scheme 13. Synthesis of ferrocene-bearing norbornene monomer and ROMP using Grubbs 1st generation catalyst.[83]

Le Foch et al. have synthesized water-soluble ferrocene-bearing polythiophenes with a similar strategy. They also used a cationic quaternary ammonium bridge for hydrophilicity reasons. First 3-(2-bromoethoxy)-4-methylthiophene was synthesized in a 2-step reaction and then reacted with dimethylaminomethyl ferrocene. The ionic thiophene derivative was polymerized to the desired product, which is used as transducer for electrochemical detection of DNA.[84]

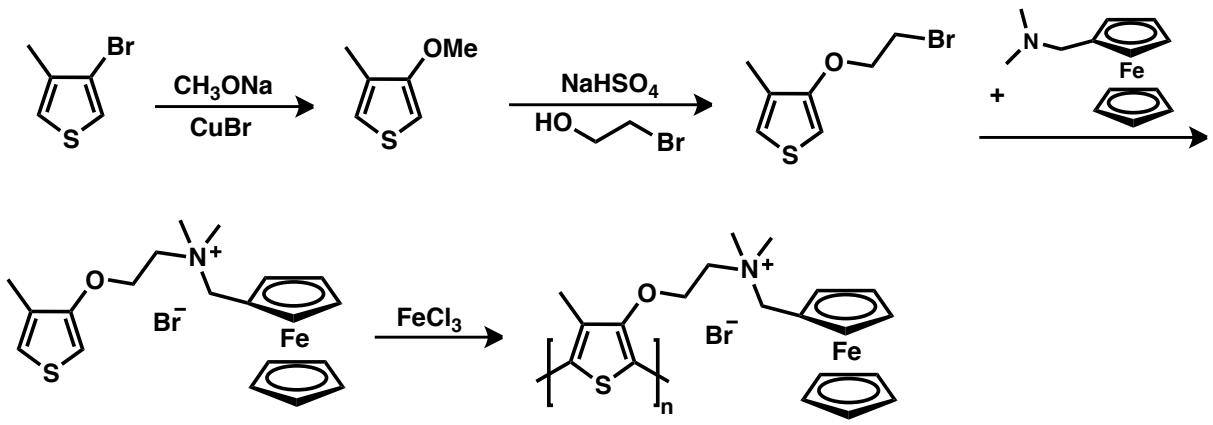

Scheme 14. Synthesis of ferrocene-bearing cationic thiophene and polymerization.[84]

In 2013, our group developed the first ferrocene epoxide monomer for the oxyanionic polymerization.[85] The monomer, ferrocenyl glycidyl ether (fcGE), is synthesized in a 3-step reaction and was homopolymerized to hydrophobic PfcGE and copolymerized with EO leading to random P(fcGE-*co*-EO) copolymers, which was proven by NMR kinetics (Figure 4).

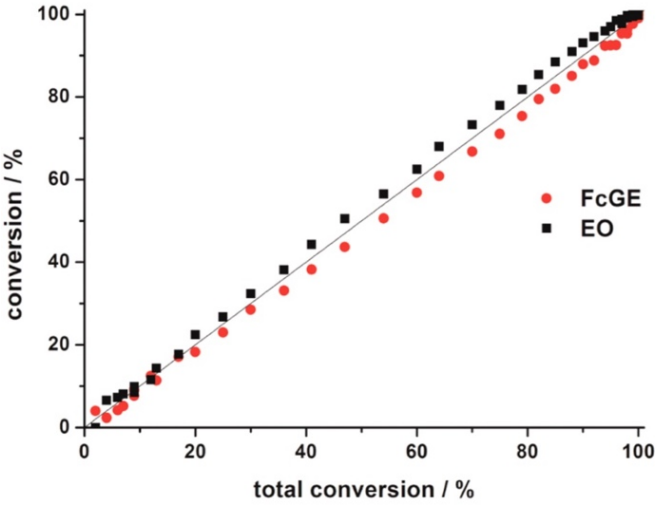

Figure 4. Random copolymerization behavior of fcGE with EO.[85]

These copolymers are water-soluble and show cloud points (LCST) depending on the fcGE comonomer content. It was also found, that low amounts of fcGE within the PEG chain did not show any cytotoxic effect, but with fc-contents above 5% the "ferrocene-PEGs" were efficient cytostatica.

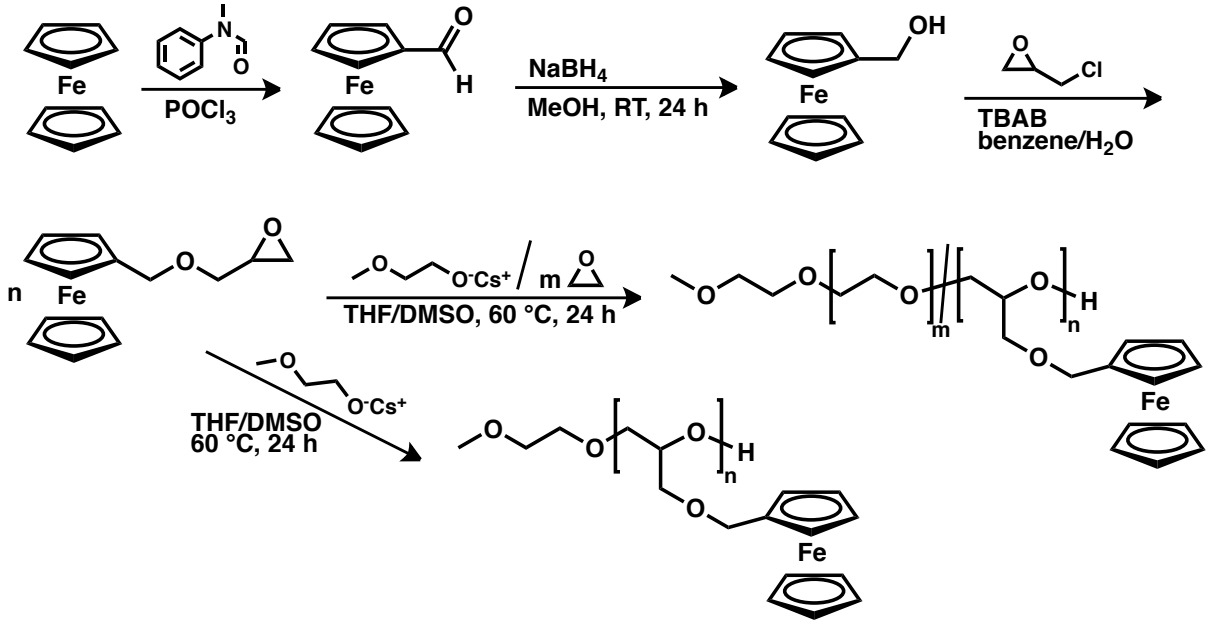

Scheme 15. Top: Synthesis of ferrocenyl methyl glycidyl ether (fcGE); bottom: anionic homo- and copolymerization of fcGE with EO.[85]

fcGE is also a key monomer to water-soluble hyperbranched copolymers with glycidol exhibiting dual-stimuli-responsive behavior. Comparing to P[EO-*co*-fcGE] copolymers, the introduction of additional hydroxyl groups (from glycidol) increased the overall water-solubility and therefore also the cloud point temperatures for a certain fc-content. The copolymerization of glycidol (G) with fcGE produces a hyperbranched poly(glycerol) bearing many fc-units with high water-solubility (*hb*P[fcGE-*co*-G]). Thus the cloud point can be raised from 7 to 49 °C for the hyperbranched structures compared to the linear P[fcGE-*co*-EO] copolymers with the same amount of fcGE.[86]

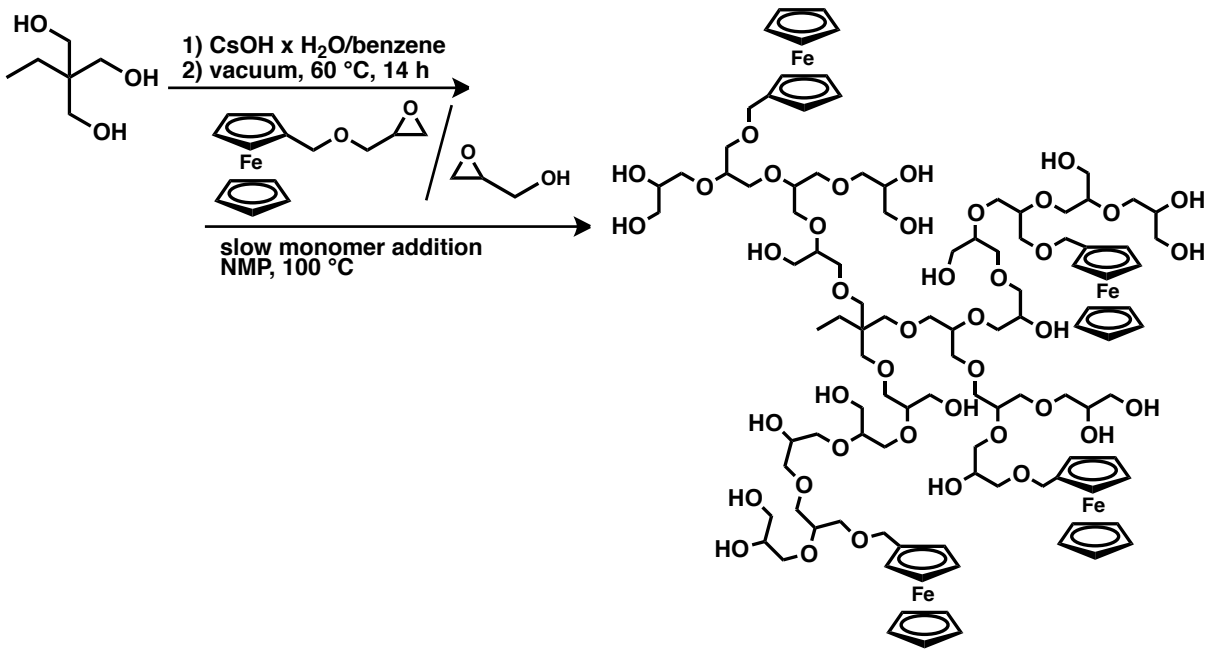

Scheme 16. Synthesis of hyperbranched copolymers from fcGE and glycidol.[86]

The hyperbranched copolymers exhibit molecular weight distributions between *Đ*=1.4-1.7, which is still rather well-defined for statistically branched polymers. However, if monodisperse structures are desired, more synthetic effort is needed to prepare, e.g. ferrocene-containing carbohydrate dendrimers. Ashton et al. synthesized carbohydrate-coated ferrocene derivatives by connecting 1,1'-dichlorocarbonylferrocene with acylated β-D-glucopyranosyl residues, which were released afterwards affording the water-soluble dendrimers. The electrochemical behavior of the dendrimers were investigated and the complex formation with β-cyclodextrin were studied for the derivatives with only one substituted cyclopentadienyl ring.[87,88]

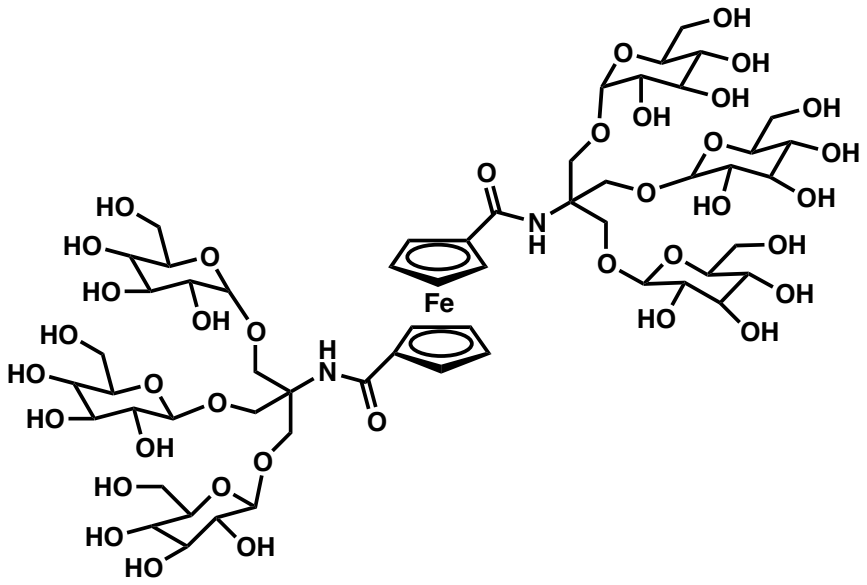

Figure 5. Structure of a dendritic carbohydrate-functionalized ferrocene.[87]

More recently, we introduced vinyl ferrocenyl glycidyl ether (VfcGE), which is one of the very few bivalent monomers that can be polymerized by two orthogonal polymerization mechanisms; for VfcGE either AROP or free radical polymerization was applied.[89] In both cases, functional fc-containing polymers are obtained, either carrying additional epoxide or vinyl pendant groups. The copolymerization of VfcGE with EO leads to water-soluble ferrocene-PEGs, similar to the abovementioned P[fcGE-*co*-EO] copolymers.[85] However, additional pendant vinyl groups at the fc-groups remain after the polymerization for post-modification reactions to further alter the solubility profile, cloud points, etc.

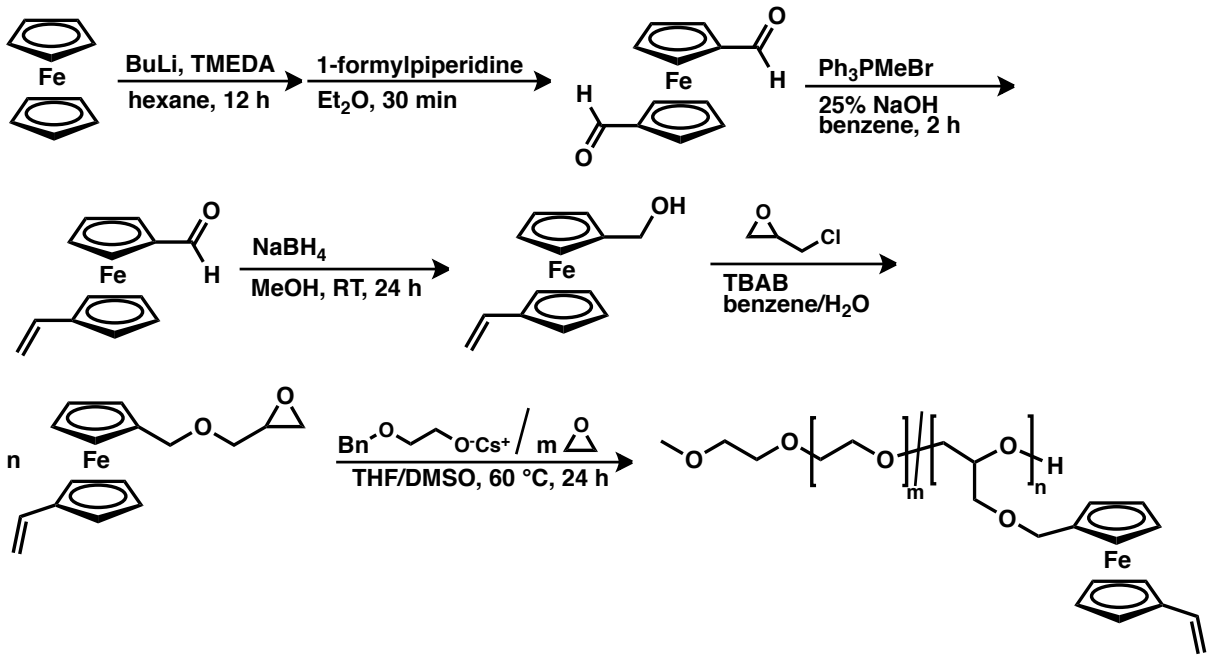

Scheme 17. Synthesis of VfcGE and its copolymerization with EO.[89]

The cloud point temperatures of P(VfcGE-*co*-EO) copolymers were varied by post-modification with thioacetic acid or cysteamine via thiol-ene addition.[90] This leads to triple-stimuli-responsive materials in aqueous solution: besides temperature and redox stimuli, the pendant carboxylic acid or amine groups introduce an additional pH trigger. The electrochemical response and catalytic activity of fc could be switched on and off via pH and temperature changes (Figure 6). Glass surfaces were also modified with this triple-stimuli-responsive material to produce smart surfaces.

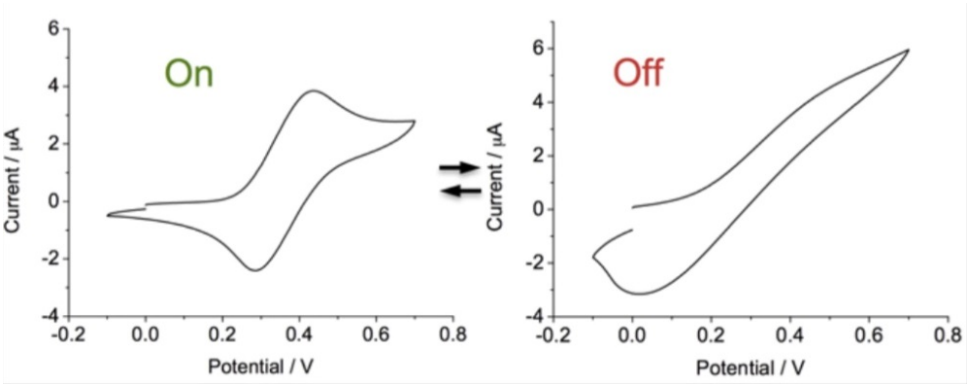

Figure 6. Cyclic voltammograms of P[VfcGE$_1$-ran-CAfcGE$_9$-co-EO$_{206}$] below and above the cloud point temperature.[90]

Synthetic Routes to Water-Soluble Cobaltocenium-Containing Polymers

Cobaltocene is a 19-electron complex and therefore unstable in air. It readily oxidizes with oxygen under release of a single electron to the cobaltocenium cation, which is isoelectronic with fc. Comparing to the ferrocenium ion, the cobaltocenium cation is more stable, since it complies with the 18-electron rule. Cobaltocenium is known to be water-soluble, because of its ionic structure. Nevertheless, reactions and modifications at the aromatic cyclopentadienyl ligands of cobaltocenium cation are challenging and rarely found in literature, in contrast to fc derivatization; in most cases substituted cp-ligands are used for the complexation of cobalt ions.[91]

Manners and co-workers synthesized a strained dicarba[2]cobaltocenophane for thermal and anionic ROP.[92] After oxidation of the resulting polymer a polycobaltocenium polyelectrolyte is obtained.[93]

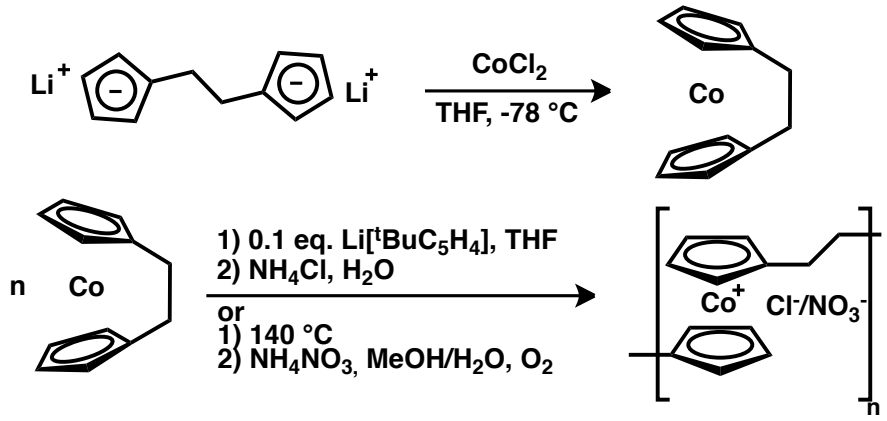

Scheme 18. Flytrap synthesis of dicarba[2]cobaltocenophane, and anionic/thermal polymerization.

Tang and coworkers designed a cobaltocenium acrylate monomer, namely 2-(methacrylolyoxy)ethyl cobaltoceniumcarboxylate hexafluorophosphate ($MAECoPF_6$), which is synthesized from cobaltocenium acyl chloride and 2-hydroxyethyl methacrylate (HEMA). The monomer is polymerized by free radical polymerization to $PMAECoPF_6$, a water-soluble polyelectrolyte. The effect of different anions on the solubility of cationic cobaltocenium-containing polymers were explored after ion-exchange processes.[94] RAFT polymerization leads to narrowly distributed $PMAECoPF_6$ homopolymers and also heterobimetallic diblock copolymers with additional fc-units, i.e. ($PMAECoPF_6$-*b*-poly(2-(methacrylolyoxy)ethyl ferrocenecarboxylate) ($PMAECoPF_6$-*b*-PMAEFc)), which self-assembled into heterogeneous spherical micelles in selective solvents.[95] Cobaltocenium-labeled polymers via atom transfer radical polymerization (ATRP),[96] side-chain cobaltocenium polymers via metathesis polymerization,[97] and side-chain cobaltocenium-containing block copolymers via post-modification,[98] and dendrimers[99] are also accessible.

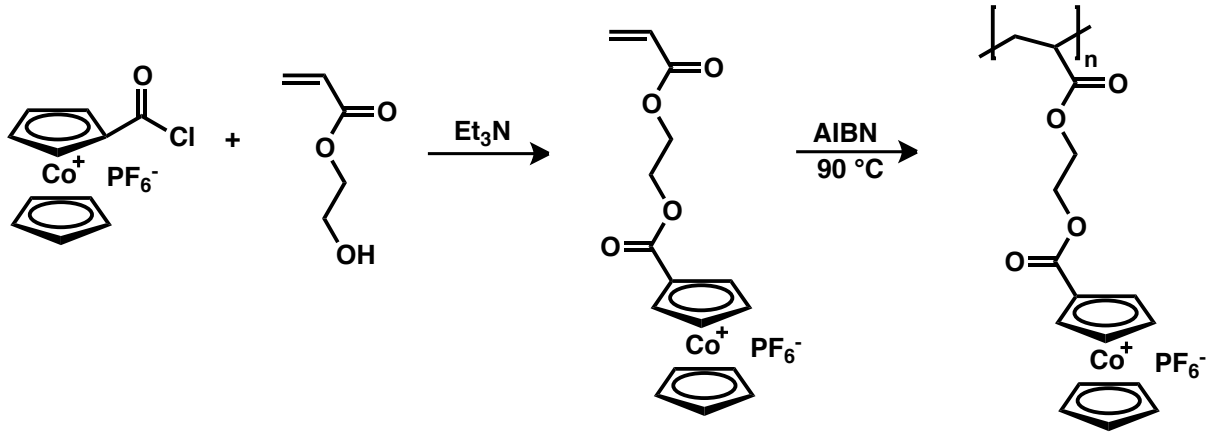

Scheme 19. Synthesis of $MAECoPF_6$ and its free radical homopolymerization.

These cobaltocenium-containing polymers were used as a precursor for versatile inorganic cobalt materials,[100] or also using heterobimetallic block copolymers with ferrocene.[101] These structures were used against multi-drug resistant bacteria, combining cobaltocenium-containing polymers with antibiotics (Figure 7).[102]

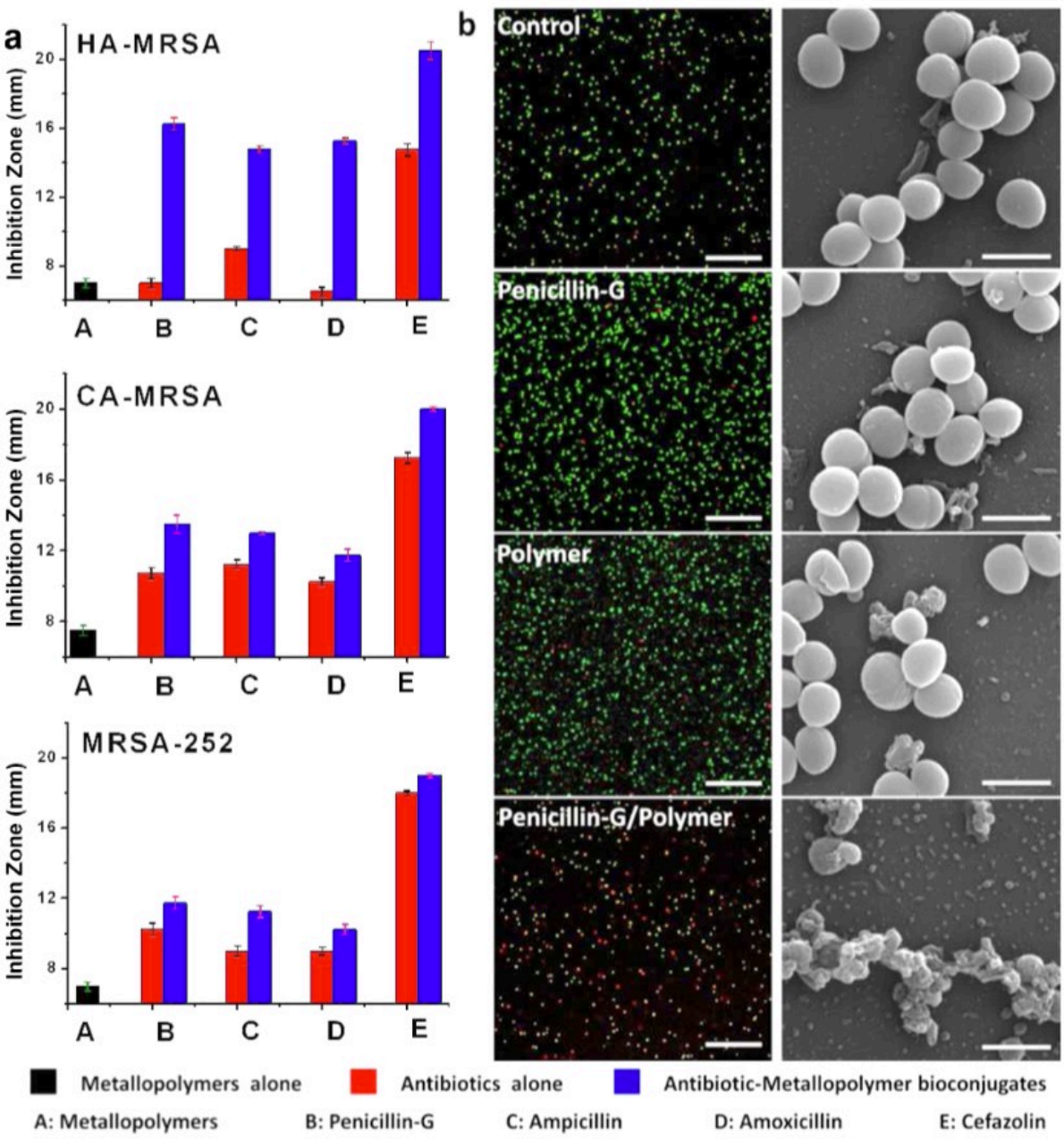

Figure 7. High activity of Antibiotic-Metallopolymer bioconjugates (compared to metallopolymers or Antibiotics alone) against multi-drug resistant bacteria – high efficiency especially for HA-MRSA cells.[102]

Gu et al. synthesized cobaltocenium-containing (block co-)polymers via ROMP.[103] A norbornene amino derivative was functionalized with cobaltocenium chlorocarbonyl. The cationic monomer could be polymerized using Grubbs' third generation catalyst to water-

soluble homopolymers as well as diblock copolymers with a ferrocenium-bearing block. The diblock copolymer synthesis was realized by sequential addition of the second ferrocenium monomer, which was synthesized in analogy to the cobaltocenium monomer. The resulting polymers were analyzed by cyclic voltammetry showing reversible redox behavior and the molecular weights were determined using Bard-Anson's electrochemical method.

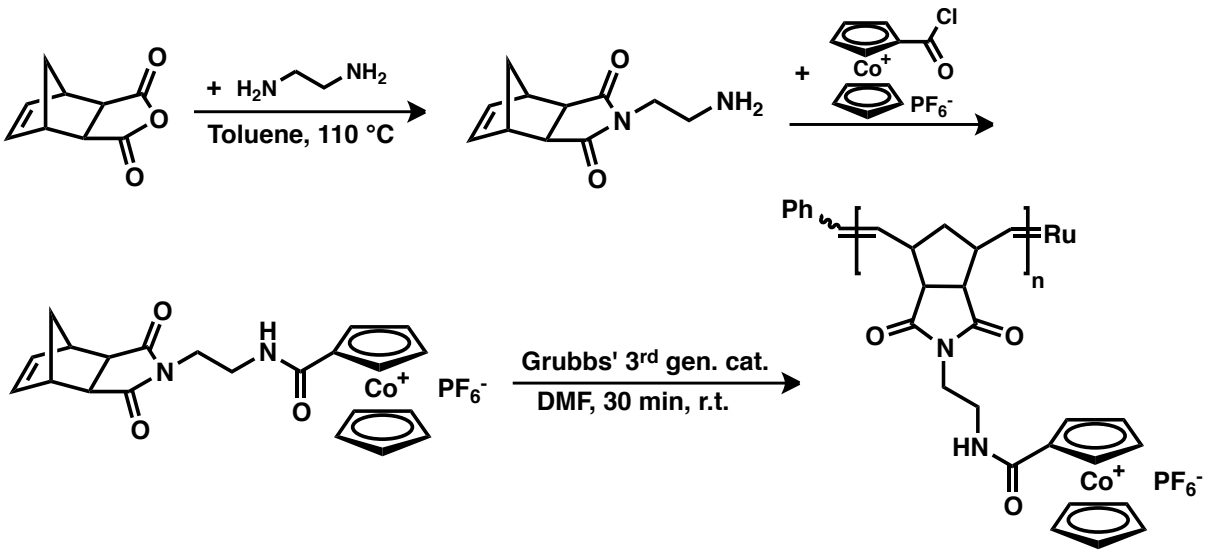

Scheme 20. Synthesis of a cobaltocenium homopolymer via ROMP.[103]

Synthetic Routes to Water-Soluble Ruthenocene-Containing Polymers

Ruthenocene as another stable 18 electron complex can be oxidized to the ruthenocenium cation, with a reversible oxidation depending on the counter ion; however, in most cases a reduction process cannot be performed.[104,105]

Tang and coworkers have introduced a ruthenocene-containing methacryl monomer, namely 2-(methacryloyloxy)ethyl ruthenocenecarboxylate

(MAERu), which was synthesized in a 4-step reaction, starting from ruthenocene (Scheme 21). It was polymerized by ATRP using PEG-Br as a macro-intiator to a PEG-*b*-PMAERu amphiphilic diblock copolymer. Another synthesis route to such water-soluble structures is a controlled radical polymerization of PEGMA using PMAERu-RAFT as a macro-RAFT agent.[106] These amphiphilic diblock copolymers can self-assemble into spherical and worm-like micelles.

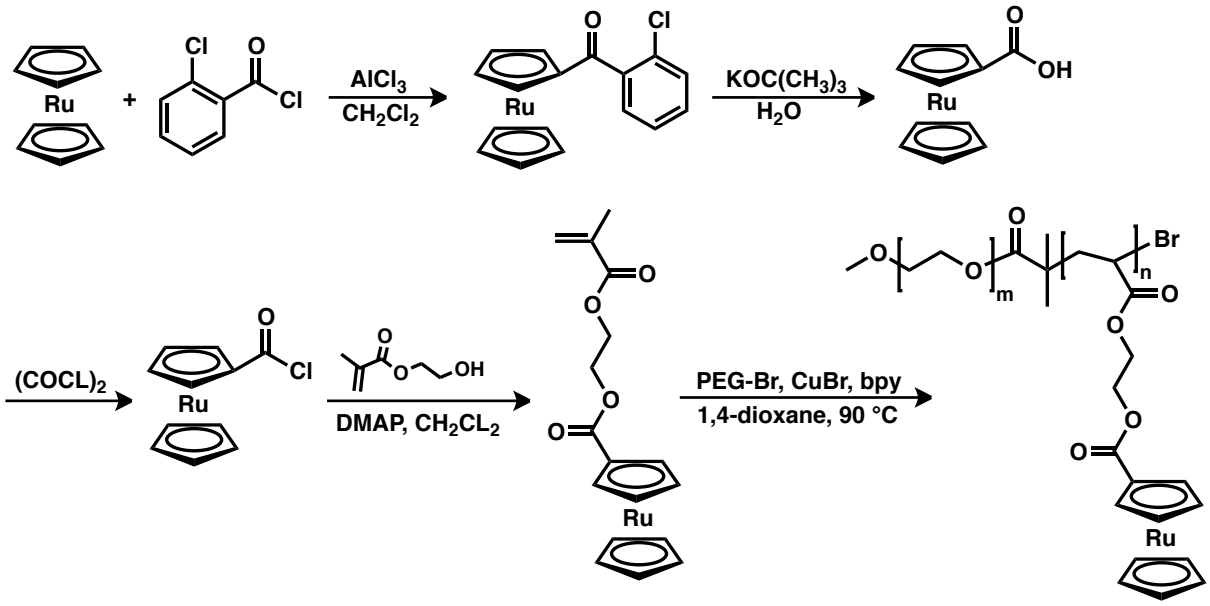

Scheme 21. Synthesis of 2-(methacryloyloxy)ethyl ruthenocenecarboxylate (MAERu) via ATRP polymerization using PEG-Br as macroinitiator.[106]

Summary and Outlook

This review sums up all important synthetic routes to water-soluble metallocene (i.e. ferrocene, cobaltocenium and ruthenocene)-containing (co-)polymers. Different approaches to generate homopolymers, random and block copolymers, star-shaped polymers or

dendrimers to bring the organometallic complexes into water-soluble macromolecules are available. Water-soluble block copolymers are in general amphiphilic, resulting in the formation of nanostructures in water, such as spherical or cylindrical micelles, with the fc-rich hydrophobic blocks building the core. Therefore, the reactivity of fc and also the ability to catalyze in such systems is lowered; the majority of the published literature studies their self-assembly and electrochemical behavior. Although there are different structures accessible via various synthetic routes, applications in areas like drug delivery, sensing, catalysis and nanotechnology are barely studied – especially in aqueous environment.

With the synthetic routes developed to date, the era of organometallic (co)polymers for future aqueous applications is still to come. With the self-assembly and copolymerization behavior understood, the basis for further research is in our hands and we can be curious to their future applications.

Chapter 2: Water-Soluble Multi-Stimuli-Responsive Metallocene-Containing Copolymers

2.1 Water-Soluble and Redox-Responsive Hyperbranched Polyether Copolymers Based on Ferrocenyl Glycidyl Ether

Published in *Polymer Chemistry,* **2015**, 6, 7112-7118. (Published by the Royal Society of Chemistry.)

Authors: *Arda Alkan,[a,b,†] Rebecca Klein,[a,b,†] Sergii I. Shylin,[d] Ulrike Kemmer-Jonas,[b] Holger Frey,[b] and Frederik R. Wurm[a,*]*

[a]Max Planck Institute for Polymer Research (MPIP), Ackermannweg 10, 55128 Mainz, Germany.

[b]Institute of Organic Chemistry, Johannes Gutenberg-University, Duesbergweg 10-14, 55128 Mainz, Germany.

[c]Graduate School Materials Science in Mainz, Staudingerweg 9, 55128 Mainz, Germany.

[d]Institute of Inorganic and Analytical Chemistry, Johannes Gutenberg University, Duesbergweg 10-14, 55128 Mainz, Germany.

† These authors contributed equally.

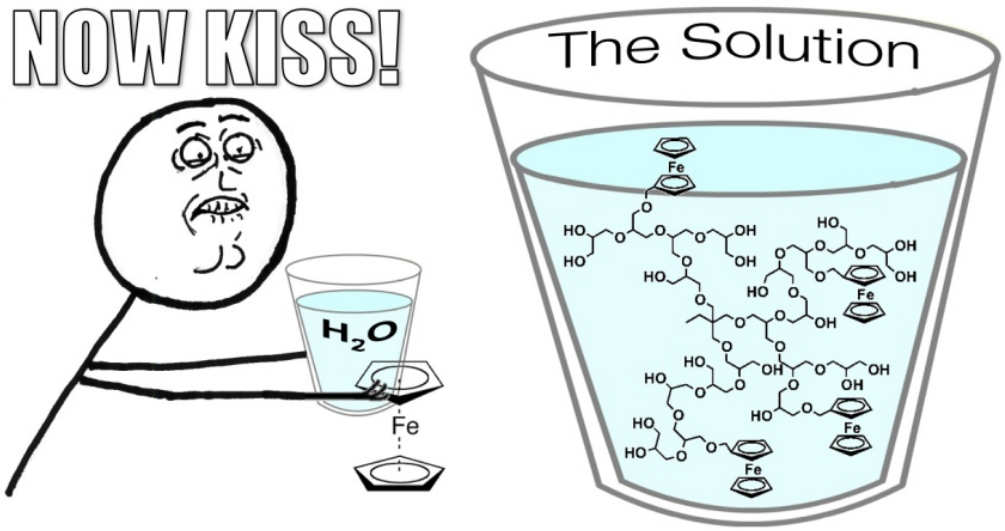

Abstract

Water-soluble copolymers of ferrocenyl glycidyl ether (fcGE) and glycidol are prepared via anionic ring-opening multibranching polymerization (ROMBP). The resulting hyperbranched materials with molecular weights (M_n) of 3 500 to 12 300 g mol^{-1} and narrow molecular weight distributions (M_w/M_n = 1.40-1.69) exhibit both temperature- as well as redox-responsive behavior, which was studied via turbidity measurements. The cloud point temperatures (T_c) were adjusted between 45 and 60 °C through variation of the fcGE comonomer content. Additionally, these T_cs can be increased by the addition of an oxidizing agent. The extent of oxidation of the materials is also quantified by Mößbauer spectroscopy and can be correlated to the change in the T_cs. Furthermore, the copolymers were investigated via ^{1}H and inverse gated (IG) ^{13}C NMR spectroscopy, size exclusion chromatography (SEC), MALDI-ToF mass spectroscopy and differential scanning calorimetry (DSC). The reversible oxidation of the fc moities is demonstrated by cyclic voltammetry.

Introduction

Organometallic polymers combine the unique properties of inorganic materials, such as redox activity with polymer properties. In such polymers, metals are often incorporated in stable 18 electron sandwich-complexes to ensure durable polymers in bulk and in solution. Metallocenes, such as ferrocene (fc), can be incorporated either in the polymer backbone or as side chains, the most prominent examples being poly(ferrocenylsilane) (PFS)[107,108] and poly(vinylferrocene) (PVfc).[109] Also organometallic acrylates have been reported.[110] Recently, our group introduced the first fc-containing epoxide monomer for oxyanionic ring-opening polymerization, i.e. ferrocenyl methyl glycidyl ether (fcGE).[85,89,111] This epoxide monomer was copolymerized with ethylene oxide (EO) to generate water-soluble, multi-stimuli responsive materials.

While there are many studies on linear ferrocene-containing polymers, branched materials with fc-units have been reported only rarely,[112] some works have focused on fc-

dendrimers.[113] In recent years hyperbranched (*hb*) polymers have found increasing attention as randomly branched analogues of dendrimers. To the best of our knowledge only very few, albeit hydrophobic ferrocene-containing hyperbranched polymers, based on hyperbranched poly(carbosilane)s (*hb*PCSs),[114,115] poly(3-ethyl-3-(hydroxymethyl)-oxetane)s (*hb*POs)[116] and poly(phenylene)s (*hb*PPs),[117] have been reported to date.

Hyperbranched polymers offer potential, e.g., for biomedicine, catalysis, membrane materials and coatings.[118-120] One benefit in comparison to the perfectly branched dendrimers is their accessibility in facile one-step syntheses even on larger scales, opening their use for industrial applications.[121] Hyperbranched polyglycerol (*hb*PG), which is synthesized via anionic ring-opening multibranching polymerization (ROMBP) of glycidol, a latent cyclic AB_2 monomer, is a highly interesting material due to its water-solubility, the flexible polyether backbone,[122,123] high functionality and excellent biocompatibility.[124,125] The synthesis of *hb*PG via slow monomer addition (SMA) enables control over molecular weights (6 000 to 24 000 g mol^{-1}), narrow molecular weight distributions ($Đ$ = 1.3 – 1.8) and high degree of branching.[126,127] Copolymerization of glycidol with (functional) glycidyl ethers[128] or the post-polymerization modification of *hb*PG allows for the synthesis of stimuli-responsive *hb*PG showing temperature-,[129-132] pH-,[133-135] or redox-responsive behavior.[136]

In this work, the copolymerization of glycidol and fcGE is introduced (Scheme 1), enabling the one-pot synthesis of multi-stimuli-responsive materials. The combination of the *hb*PG backbone with multiple hydroxyl groups provides excellent water-solubility and, in combination with the hydrophobic fc groups, temperature-dependent solubility of the copolymers in aqueous solution is achieved, even higher than for the already reported linear fc-containing poly(ethylene glycol)s P[fcGE-*co*-EO].[85] Furthermore, the iron centers in the fc units are redox-responsive and can be oxidized reversibly from Fe(II) to Fe(III) enabling to vary the hydrophilicity of the copolymers.

Scheme 1. **Synthetic AB/AB$_2$ Copolymerization Strategy for Water-Soluble *hb*P[G-*co*-fcGE] Copolymers.**

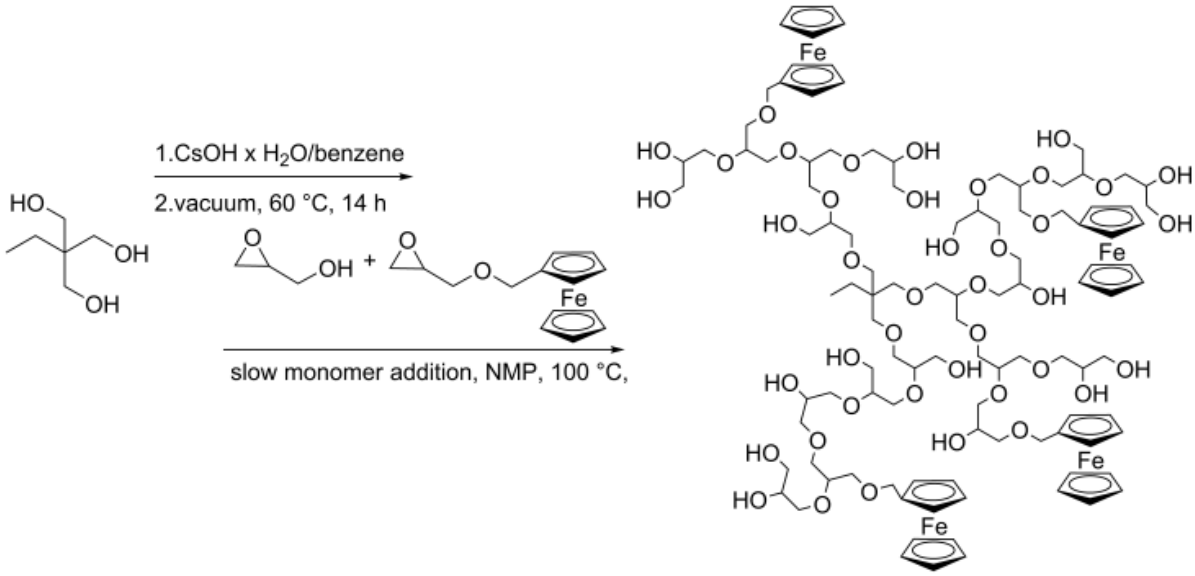

Experimental

Reagents. All solvents and reagents were purchased from Acros Organics or Sigma Aldrich and used as received, unless otherwise stated. Glycidol and *N*-methyl-2-pyrrolidone (NMP) were freshly distilled from CaH_2 prior to use. fcGE was synthesized according to the published procedures, purified via column chromatography and dried by azeotropic distillation of benzene to remove traces of water.[85]

Instrumentation. ^{1}H and ^{13}C NMR spectra were recorded at 400 and 100 MHz on a Bruker Avance II 400 NMR spectrometer. For SEC measurements in DMF (containing 0.25 g L^{-1} of LiBr), an Agilent 1100 series was used as an integrated instrument including a PSS Gral column ($10^6/10^4/10^2$ Å porosity) and a RI detector. Calibration was achieved using poly(ethylene glycol) (PEG) standards provided by PSS. DSC measurements were performed using a PerkinElmer 8500 thermal analysis system and a PerkinElmer CLN2 thermal analysis controller in the temperature range from -90 to +100 °C with heating rates of 10 K min^{-1}. MALDI-ToF MS measurements were performed using a Shimadzu Axima CFR MALDI-TOF mass spectrometer, employing dithranol (1,8,9-trishydroxy-anthracene) as a matrix.

Turbidity measurements. Cloud points were determined in deionized water (5 g L^{-1}) and observed by optical transmittance of a light beam (λ = 500 nm) through a 1 cm sample quartz cell. The measurements were performed in a Jasco V-630 photospectrometer with a Jasco ETC-717 Peltier element. The intensity of the transmitted light was recorded versus the temperature of the sample cell. The heating/cooling rate was 5 K min^{-1}, and values were recorded in 1 K steps.

Cyclic voltammetry (CV). CV measurements of the copolymer samples were carried out in a conventional three-electrode cell using a WaveDriver 20 bipotentiostat (Pine Intrument Company, USA) and deionized water as solvent for polymer solutions with 5 g L^{-1} concentration. Potassium chloride at concentrations of 0.1 M was used as supporting electrolyte. A glassy carbon disk served as working electrode. Ag/AgCl and platinum wire were used as reference and counter electrodes, respectively.

Mößbauer Spectroscopy. ^{57}Fe-Mößbauer spectra were recorded in transmission geometry with a ^{57}Co source embedded in a rhodium matrix using a conventional constant-acceleration Mößbauer spectrometer ("*Wissel*") equipped with a nitrogen gas-flow cryostat at 80 K. The absorbers were prepared by freezing aqueous solutions of samples in plastic holders. Fits of the experimental data were performed using the *Recoil* software.[137] Isomer shifts are given relatively to α-Fe at ambient temperature.

Synthesis of hyperbranched poly(glycerol-*co*-ferrocenyl glycidyl ether) (*hb*P[G-*co*-fcGE]). In a dry Schlenk flask under argon atmosphere, 1,1,1-trimethylolpropane (TMP) as initiator was suspended with cesium hydroxide monohydrate (0.3 eq) in 5 mL benzene and stirred for 30 min at 60 °C under static vacuum. Then, remaining water impurities were removed by azeotrope distillation with benzene at 60 °C for 12 h under high vacuum. The initiator salt was dissolved in 0.5 mL NMP at 100 °C. Glycidol and fcGE were dissolved in a separate flask in NMP to obtain a 50 % dilution. The monomer solution was added slowly to the initiator solution over 6 hours via a syringe pump while vigorously stirring. After complete addition, it was stirred for another 30 min and methanol (0.5 mL) was added to terminate the

polymerization. The solvents were removed under vacuum and the resulting polymer precipitated twice from methanol into cold diethyl ether, to obtain the product as brownish highly viscous liquid. Yields: 85-90 %. ^{1}H NMR (DMSO-d_6, 400 MHz): δ [ppm]: 4.80 – 4.40 (m, O*H*-groups), 4.23 (s, fc), 4.14 (s, fc), 3.76 – 3.19 (m, polyether backbone), 1.20 (br, 2H, CH_2-TMP), 0.80 (br, 2H, CH_3-TMP).

Two-step synthesis of high molecular weight hyperbranched poly(glycerol-*co*-ferrocenyl glycidyl ether) (*hb*P[G-*co*-fcGE]). A literature protocol using a macroinitiator was applied for the synthesis of high molecular weight polymers. [127] P1 (100 mg, M_n=3500 g mol^{-1}, 6.1 % fcGE) and CsOH·H_2O (19.1 mg, 0.1 eq) were dissolved in benzene and dried for 15 h under high vacuum. The macroinitiator salt was dissolved in dry NMP (0.4 mL) at 100 °C. Glycidol (338 mg) and fcGE (79 mg) were dissolved in a separate flask in NMP (0.6 mL). The monomer solution was added slowly to the initiator solution over 10 hours via a syringe pump while vigorously stirring. After complete addition, it was stirred for another 30 min and methanol (0.5 mL) was added to terminate the polymerization. The solvents were removed under vacuum and the resulting polymer precipitated twice from methanol into cold diethyl ether, to obtain the product as brownish highly viscous liquid.
Note: During prolonged drying a partly oxidation of the sample was observed.

Results and Discussion

Synthesis and Molecular Weight Determination

In order to generate copolymers of glycidol and fcGE a modified synthesis procedure had to be devised.[138] First, the trishydroxyfunctional initiator, trimethylol propane (TMP), was partly deprotonated (30 mol%) with cesium hydroxide and a mixture of glycidol and fcGE was added via slow monomer addition over 6 hours at 100 °C (Scheme 1). It is essential to use *N*-methyl-2-pyrrolidone (NMP) as a solvent. The copolymers P1-P5 were obtained as orange to brown, highly viscous liquids that were soluble in aqueous solution at room

temperature. Detailed characterization of the resulting polymers confirmed the incorporation of both monomers and

Table 1. Characterization Data for *hb*P[G-*co*-fcGE] Copolymers.

no.	sample	M_n[a] [g mol^{-1}]	M_n[b] [g mol^{-1}]	$Đ$[b]	fcGE [mol%]	DB[c]	T_g[d] [°C]	T_c[e] [°C]
P1	*hb*P[G_{37}-*co*-fcG$E_{2.4}$]	3500	1600	1.56	6.1	0.54	-22	-
P2	*hb*P[G_{36}-*co*-fcG$E_{5.0}$]	4100	2100	1.42	9.9	0.53	-17	60
P3	*hb*P[G_{67}-*co*-fcG$E_{8.2}$]	7300	2000	1.55	10.9	0.49	-15	49
P4	*hb*P[G_{46}-*co*-fcG$E_{6.3}$]	5300	1700	1.40	12.0	0.40	-24	45
P5	*hb*P[G_{140}-*co*-fcGE_{7}]	12300	6800	1.69	4.8	0.62	-24	-

[a]M_n determined from ^{1}H NMR spectroscopy in DMSO-d_6 by end-group analysis. [b]M_n determined via size exclusion chromatography in DMF vs PEG standards using the RI-signal detection, $Đ = M_w/M_n$. [c]DB determined via IG ^{13}C NMR spectroscopy (DMSO-d_6; 100 MHz) according to eq. 1. [d]Glass transition temperature (T_g) determined from differential scanning calorimetry (heating/cooling rate 10 K min^{-1}; second heating run). [e]Cloud point temperature for a 5 mg mL^{-1} solution of the copolymer in deionized water, measured with a heating rate of 5 K min^{-1}.

formation of the hyperbranched structure as discussed in the following. The ^{1}H NMR spectrum (cf. Supporting Information, Figure S1) shows the resonances of the polyether backbone (δ = 3.19 – 3.76 ppm), the hydroxyl groups (δ = 4.40 – 4.80 ppm) and the characteristic signals of the ferrocene units at δ = 4.14 and 4.23 ppm. The comparison of the integrals of the initiator

resonances (CH_3: δ = 0.80 ppm and CH_2: δ = 1.20 ppm) with the hydroxyl and ferrocene signals, respectively, allows to determine the

incorporation ratio of both monomers and the molecular weight of the polymer. The calculated molecular weights are in the range of 3 500 to 7 300 g mol^{-1} with a fcGE content of 6.1 to 12.0 % and are in agreement with the theoretical values based on the amount of

TMP initiator employed. Higher comonomer contents are certainly feasible, however, have not been targeted, since water-soluble hyperbranched polymers were in the focus of this work. The molecular weights determined via SEC are consistently lower than the NMR values (1 600 and 2 100 g mol^{-1}, cf. Figure S4). This can be attributed to the use of linear PEG standards. The hyperbranched topology, the multiple hydroxyl groups and the additional ferrocene units have an impact on the hydrodynamic volume of the polymers and therefore, a change in elution times and consequent underestimation of molecular weights, which is often observed for hyperbranched polymers.[139]

As the controlled synthesis of *hb*PG is limited to 6 000 g mol^{-1},[122] the synthesis of polymers with higher molecular weights is conducted by a two-step approach using a low molecular weight *hb*PG macroinitiator.[127] The copolymer P5 was synthesized using P1: after deprotonation (10 % of hydroxyl groups) a mixture of glycidol and 5 % fcGE was slowly added via a syringe pump. The obtained copolymer showed a strong increase in molecular weight (M_n = 12 300 g mol^{-1}) under preservation of the low molecular weight dispersity ($Đ$ = 1.69). Furthermore, the targeted fcGE content of 5 % was obtained according to NMR characterization.

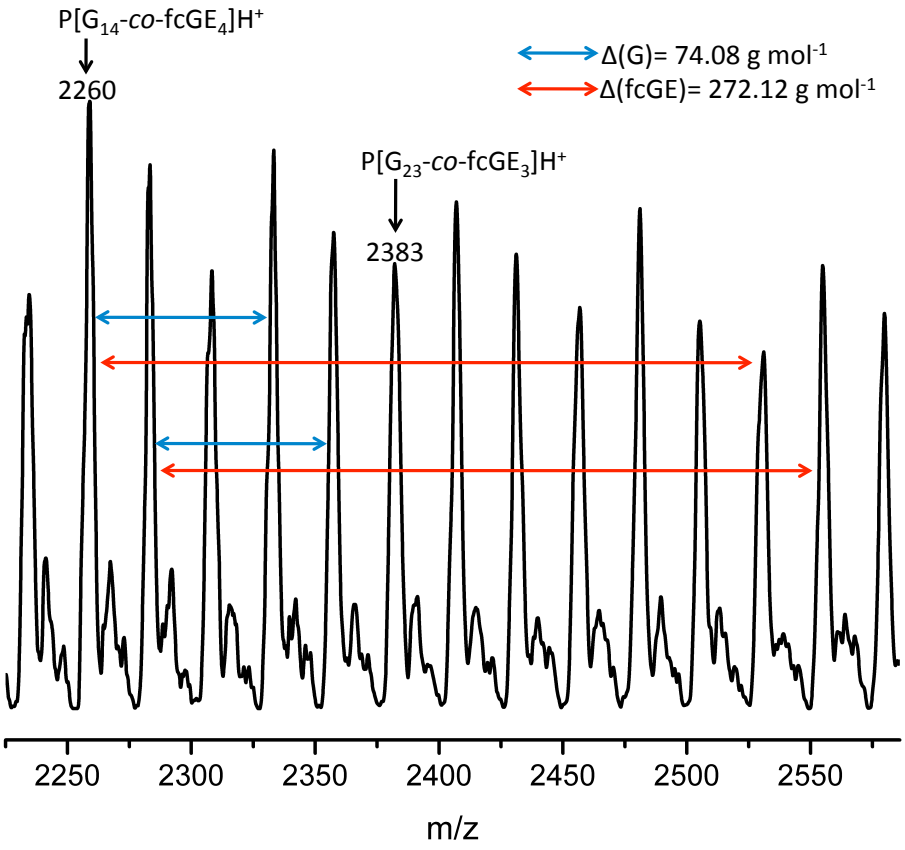

Figure 1. MALDI ToF MS of *hb*P[G_{36}-*co*-$fcGE_{5.0}$] (P2).

Matrix-assisted laser desorption/ionization time-of-flight mass spectrometry (MALDI-ToF MS) was performed to confirm incorporation of both monomers in the polymer backbone. Figure S5 shows the mass spectrum of sample P2, and Figure 1 a zoom into the spectrum: the molecular masses of glycidol (74.08 g mol^{-1}, blue) and fcGE (272.12 g mol^{-1}, red) can be assigned, evidencing successful copolymerization of both monomers. Furthermore, two signals are marked for the corresponding copolymer cationized with H^+.

Degree of Branching

The degree of branching (DB) is an important parameter of hyperbranched polymers, which is 0 for linear polymers and 1 for maximum branching. Inverse gated (IG) ^{13}C NMR spectroscopy enables the integration of ^{13}C resonances and thus calculation of the relative

abundance of the different structural units. Glycidol can be incorporated as dendritic (D), linear-1,3 ($L_{1,3}$), linear-1,4 ($L_{1,4}$) and terminal (T) unit, whereas fcGE can only be incorporated as linear (L_{fcGE}) or terminal (T_{fcGE}) unit as depicted in Figure 2. The DB was calculated using equation (1),[140,141] which is feasible for the copolymerization of glycidol with a cyclic AB monomer like fcGE.

$$DB = \frac{2D}{2D + L_{13} + L_{14} + L_{fcGE}} \quad (1)$$

The calculated DB values are summarized in Table 1 and the relative integrals of the different structural units are shown in Table S1. The DB decreases from 0.54 to 0.40 for increasing fcGE content, as expected for the copolymerization of an AB and AB_2 monomer.[128] The differentiation between L_{fcGE} and T_{fcGE} units is not possible in the NMR spectra. Therefore all incorporated fcGE units were considered as linear units for the calculation of the DB, which is realistic, considering that fcGE monomer was only used as the minority fraction. However, to determine the error of this assumption the DB was also calculated based on the assumption that all fcGE units were incorporated at the termini. In this case, the DB values are 5 to 10 % higher than the values given in Table 1, without influencing the observed trend.

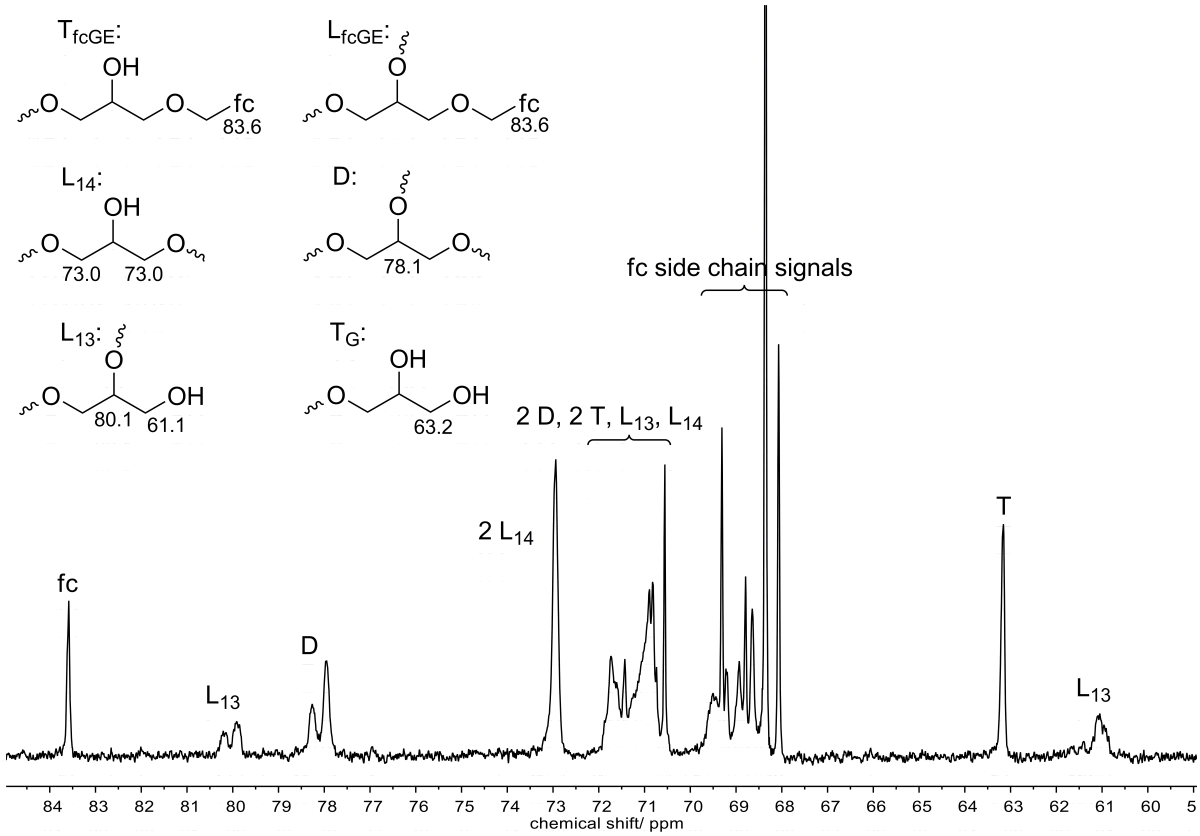

Figure 2. Inverse-Gated (IG) ^{13}C NMR spectrum (100 MHz, DMSO-d_6) of *hb*P[G_{36}-*co*-fcGE$_{5.0}$] (P2).

Thermal Properties

Differential scanning calorimetry (DSC) measurements were performed to obtain information on the thermal properties of the copolymers (Table 1). The glass transition temperature (T_g) for the *hb*PG homopolymer is detected in the range between -19 to -26 °C,[126] whereas the linear P(fcGE) homopolymer shows a T_g of -8 °C.[111] For the copolymers P1 to P3 the T_g increases with increasing fcGE content and increasing molecular weight (from -24 to -15 °C, Table 1). It is remarkable that the fc groups hardly affect the T_g of the hyperbranched polyethers in comparison to *hb*PG. Ferrocene is a sterically demanding substituent and therefore can be expected to impede bond rotation, which explains these observations. However, P4 shows the lowest T_g of all polymers although this sample exhibits

the highest fcGE content. We assume that in this case different effects like molecular weight, comonomer content and degree of branching lead to a non-linear trend of the T_gs.

Redox-Responsive Properties in Aqueous Solution

The redox-responsive properties of the copolymers have been studied by cyclovoltammetry. Applying a cyclic potential to a polymer solution, the reversible redox-activity of fc can be studied. All synthesized copolymers were analyzed via cyclic voltammetry at three different scan rates (50 mV/s, 100 mV/s and 150 mV/s, Figures 3 and S9-S11). The copolymers were dissolved in water at a concentration of 5 g L^{-1} with 0.1 M potassium chloride as a conducting salt. The reversible redox-activity of fc is visualized by plotting the cyclic potential against the measured current. The graphs show the characteristic oxidation and reduction peaks of fc. Reversibility of the electrochemical reduction is indicated by the symmetry of the measured cycles, whereas the potentials at the current maxima and minima are independent of the scan rates for all samples. Neither degradation nor consecutive reactions were detected in several consecutive measured cycles.

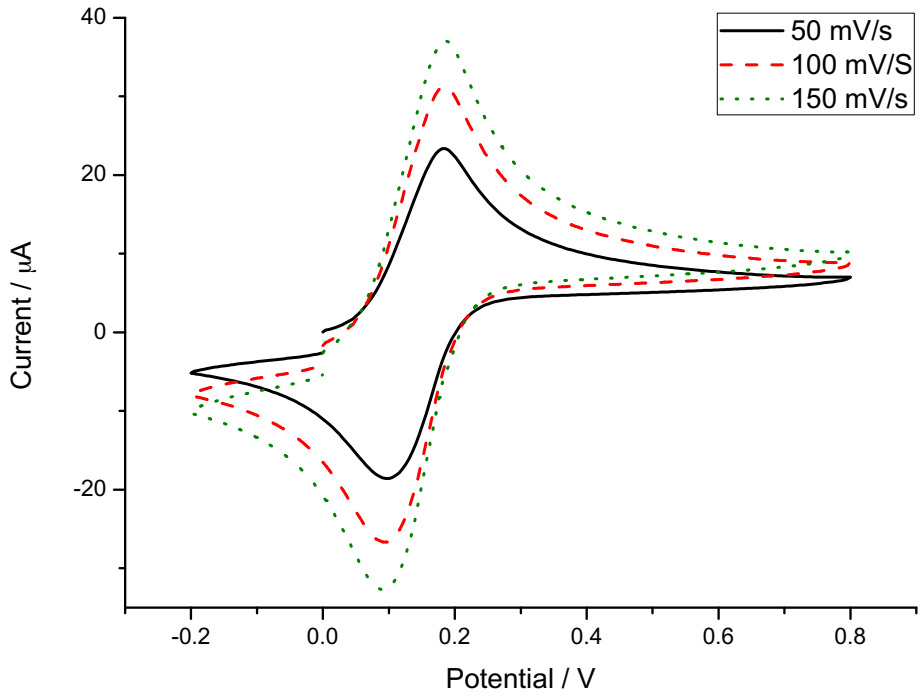

Figure 3. Cyclic voltammograms of *hb*P[G_{46}-*co*-fcG$E_{6.3}$] (P4) at different scan rates (H_2O, 5 g L^{-1} P1, 0.1 M KCl).

It has been reported that copolymers of EO and a hydrophobic comonomer exhibit lower hydrophilicity compared to PEG. Materials of this type show cloud point temperatures below 100 °C or may be insoluble in aqueous solution. In the case of fcGE, the cloud point temperatures (T_c) of the linear P[fcGE-*co*-EO] copolymers were varied from 7.2 to 82.2 °C.[85] Copolymers of glycidol and a hydrophobic comonomer show similar properties, however, due to the large number of hydroxyl groups the overall hydrophilicity is higher. The cloud point temperatures of the herein synthesized *hb*P[G-*co*-fcGE] copolymers can be varied from 45 to 60 °C. However, to obtain the same T_c in case of the *hb* polymers a higher amount of fcGE could be incorporated compared to the linear PEG-copolymers. Sample P1 and P5 with the lowest amounts of fcGE are water-soluble over the whole temperature range. The turbidity measurements of P2, P3 and P4 are shown in Figure 4. A cooling curve of P2 is also shown to demonstrate the typical low hysteresis of the copolymers. The transitions for the *hb* copolymers are not as sharp as for the linear PEG-copolymers as reported previously, certainly due to the somewhat higher dispersity of the *hb* copolymers. Especially for low molecular weights and low amounts of fc incorporated, the absolute amount of fc among the individual polymer chains varies significantly, and consequently the solubility differs strongly.

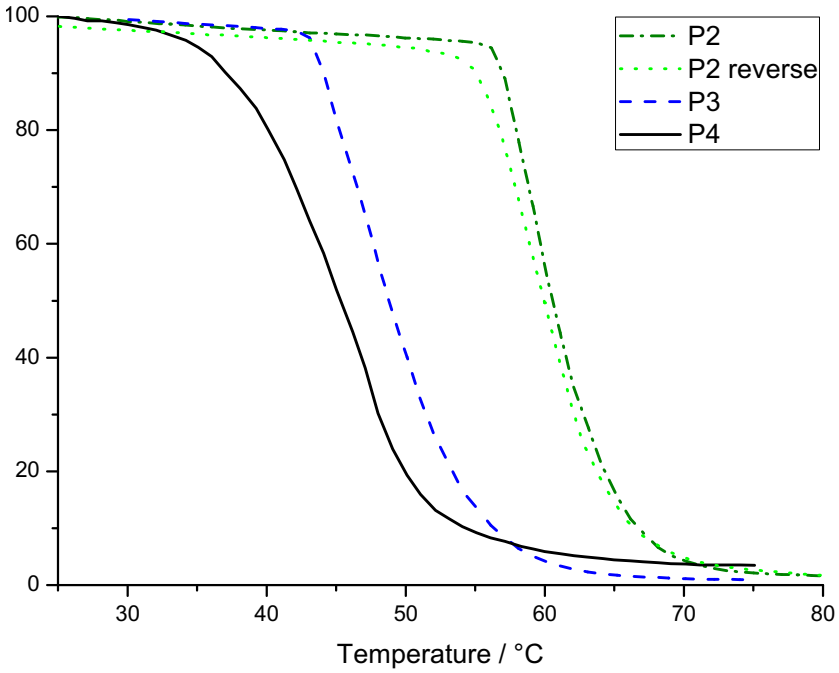

Figure 4. Turbidimetry measurements of P2, P3 and P4 with a cooling curve for P2 in water (5 g L^{-1}; heating/cooling rate 5 °C min^{-1}).

Since fc is redox-active, the hydrophilicity of the copolymer can be increased by oxidation of Fe(II) to Fe(III), and the sandwich complex becomes positively charged. Thus, the T_c of a given copolymer can be shifted to a higher temperature by partial oxidation. The T_c of P3 is compared to the partly oxidized and fully oxidized P3 (Figure 5). The partly oxidized sample shows a higher T_c (as expected), and in addition the transmittance does not reach 0 %, but remains at ca. 40 %, which indicates the presence of fully water-soluble copolymers in the mixture. The oxidized P3 is water-soluble, and the transmittance remains very high throughout the whole temperature range.

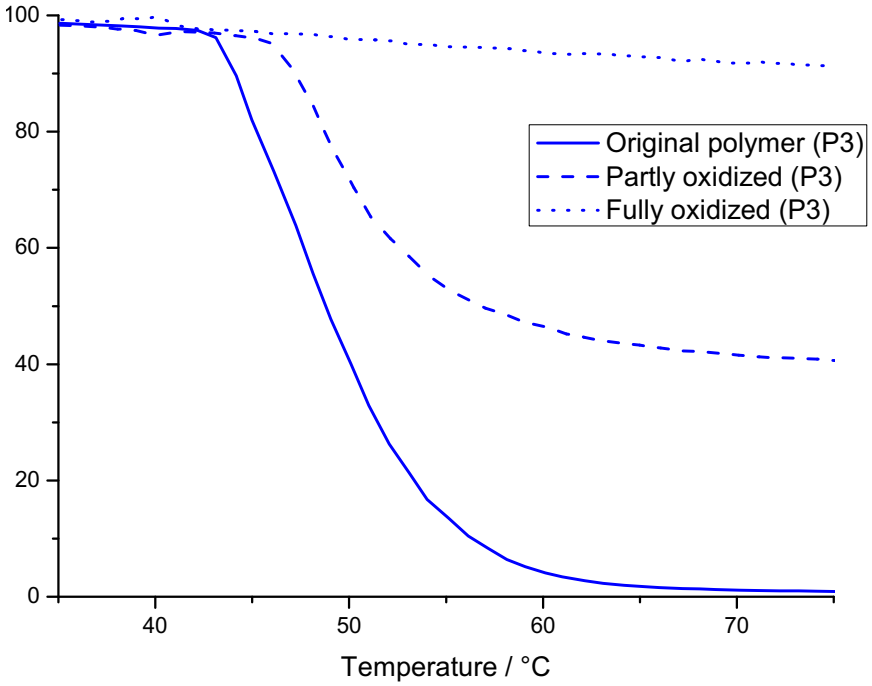

Figure 5. Turbidity measurements of P3 upon oxidation. After partly (53 % of fc units) oxidation of the starting polymer (P3, line) the cloud point temperature is lowered (P3, dashed) until finally the thermoresponsive behavior completely disappears (dotted) for 100 % oxidation (5 g L^{-1}; heating/cooling rate 5 °C min^{-1}).

Mößbauer spectroscopy has hardly been employed to characterize the degree of oxidation of redox-active dendritic polymers.[110] The influence of oxidation on the aqueous solubility of the hyperbranched copolymers was further quantified by Mößbauer spectroscopy. The copolymer P3 exhibits an original cloud point of 49 °C, after partial oxidation with silver triflate the T_c increased to 66 °C. After full oxidation of the copolymer P3 no cloud point could be detected. Quantitative analysis of the three samples (not oxidized P3, partially oxidized P3 and fully oxidized P3) via Mößbauer spectroscopy provided the ratio of ferrocenium ions to ferrocene, since ferrocene shows a doublet with a quadrupole splitting at 2.37 mm s^{-1} and ferrocenium salts show a singlet.[142] The amount of ferrocenium ions was determined to be 0 % for the non-oxidized sample P3 (Figure S6), 53±4 % for the partially oxidized (Figure 6) and 100 % for the fully oxidized (Figure S7) sample. A second-order fit was created to describe the influence of oxidation. (generated ferrocenium ions) to the copolymers´ water solubility, which is in fact only valid for P3 (Figure S8). However, a similar

correlation of the concentration of ferrocenium ions and the T_c for other copolymers is likely.

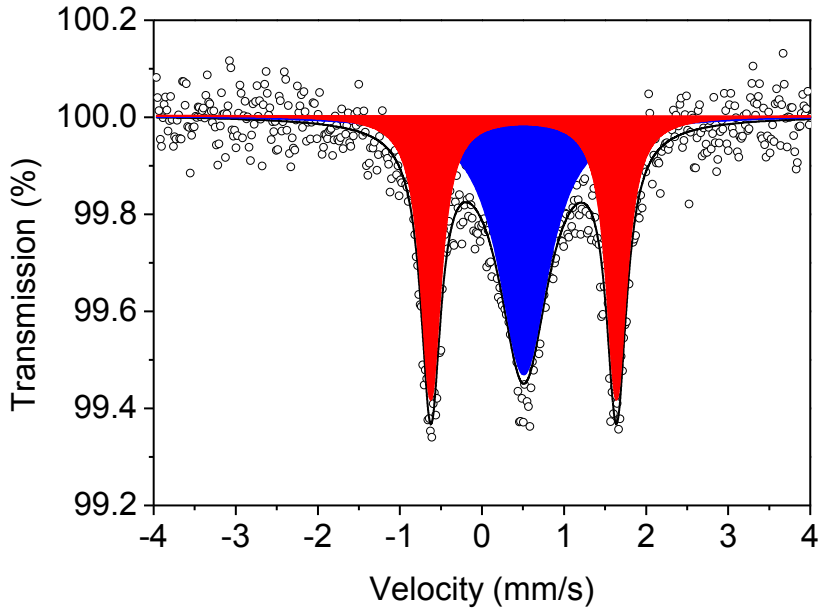

Figure 6: Mößbauer spectrum of the partially (53±4 %) oxidized copolymer P3 showing Fe(II) doublet (red) and Fe(III) singlet (blue).

Conclusions

In summary, we have introduced the first water-soluble hyperbranched polyether copolymers with redox-active ferrocene units. Capitalizing on the one-pot AB + AB_2 copolymerization under slow monomer addition conditions, the copolymerization of glycidol and fcGE via anionic ROMBP provided copolymers with molecular weights of 3 500 to 12 300 g mol^{-1} with low molecular weight dispersities ($Đ$ = 1.40 to 1.69). Detailed characterization of the polymers confirms successful copolymerization of both monomers, resulting in water-soluble hyperbranched ferrocene-containing polymers. Additionally, the polymers exhibit multi-stimuli responsive behavior. The cloud point temperature could be adjusted by variation of the fcGE comonomer content, as well as the amount of oxidized iron-centers. These materials significantly enhance the scope of ferrocene-based polymers, as they exhibit

a large number of hydroxyl groups, enabling further functionalization and an overall higher degree of hydrophilicity. The latter resulted in increased cloud point temperatures of the fc-containing PGs compared to the linear PEG analogues. Thus higher amounts of fcGE can be incorporated with lower influence on the solubility of the polymers. Mößbauer spectroscopy was used to correlate the degree of oxidation of fc with an increase of the cloud point temperatures. These findings render the novel polymers promising for a variety of purposes, e.g., as polymer therapeutics, or in detection or sensing applications.

2.1.1 Supporting Information

Additional characterization data

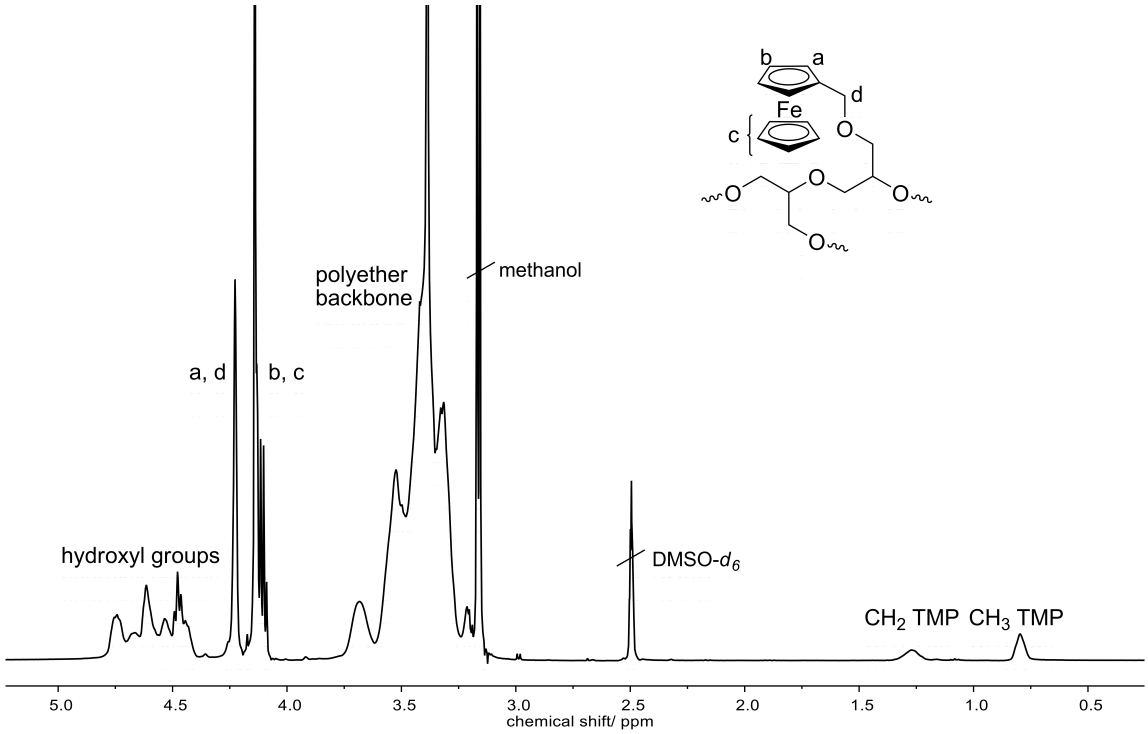

Figure S1: ^{1}H NMR (400 MHz, 298K, DMSO-d_6) of *hb*P[G_{36}-*co*-fcGE_5] (P2) with signal assignments.

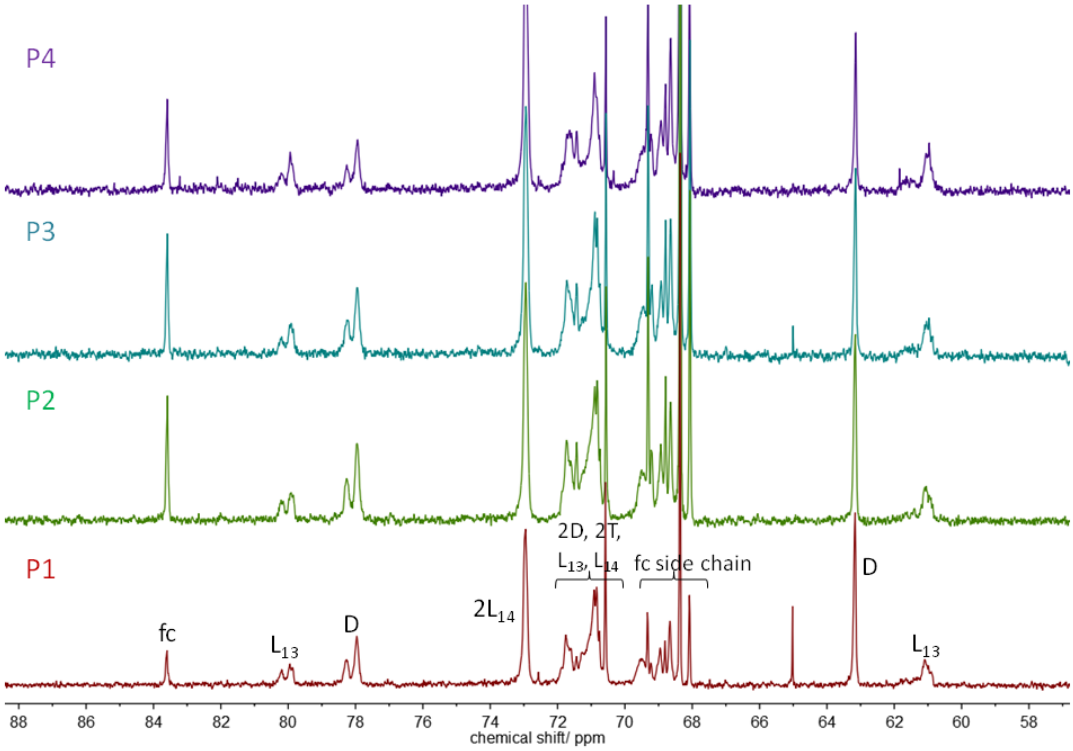

Figure S2: ^{13}C NMR (100 MHz, 298K, DMSO-d_6) of *hb*P[G-*co*-fcGE] copolymers with signal assignments.

Table S1: Relative integrals of the different repeating units determined by inverse gated (IG) ^{13}C NMR spectroscopy and used for the calculation of the degree of branching.

no.	sample	L_{13}	L_{14}	L_{fcGE}	D	T	DB
P1	*hb*P[G_{37}-*co*-fcG$E_{2.4}$]	0.12	0.26	0.06	0.25	0.31	0.54
P2	*hb*P[G_{36}-*co*-fcGE_5]	0.11	0.24	0.13	0.27	0.25	0.53
P3	*hb*P[G_{67}-*co*-fcG$E_{8.2}$]	0.12	0.28	0.13	0.25	0.22	0.49
P4	*hb*P[G_{46}-*co*-fcG$E_{6.3}$]	0.14	0.33	0.12	0.20	0.21	0.40
P5	*hb*P[G_{140}-*co*-fcGE_7]	0.12	0.23	0.06	0.33	0.26	0.62

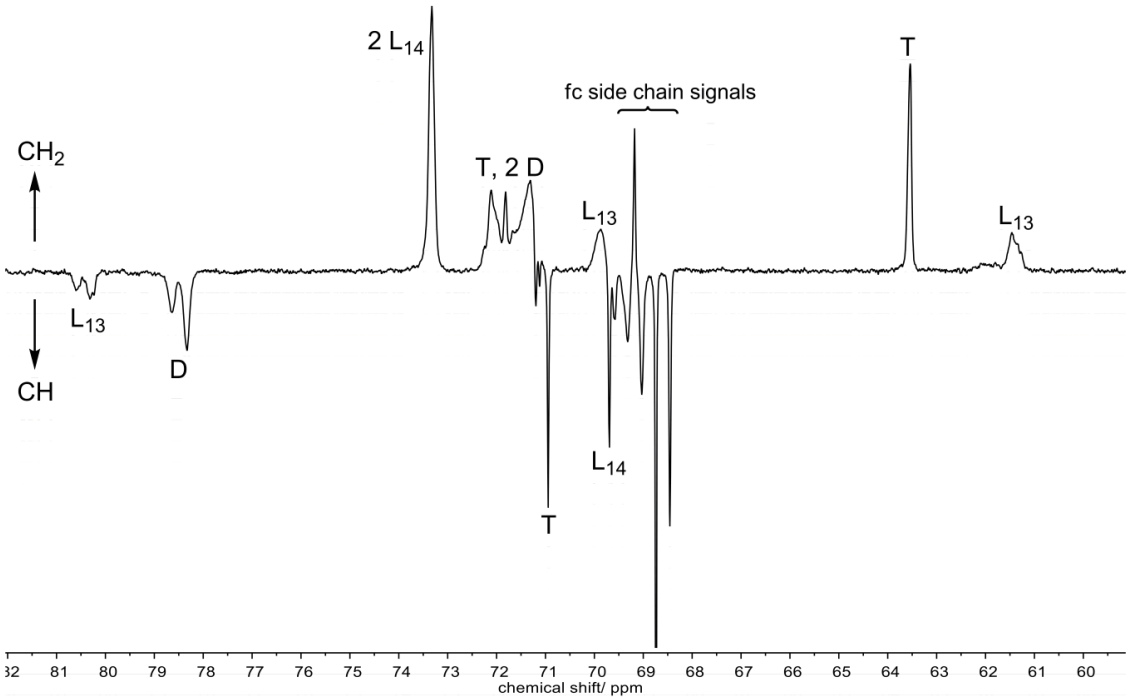

Figure S3: ^{13}C DEPT NMR (100 MHz, 298 K, DMSO-d_6) of *hb*P[G_{36}-*co*-fcGE_5] with signal assignments.

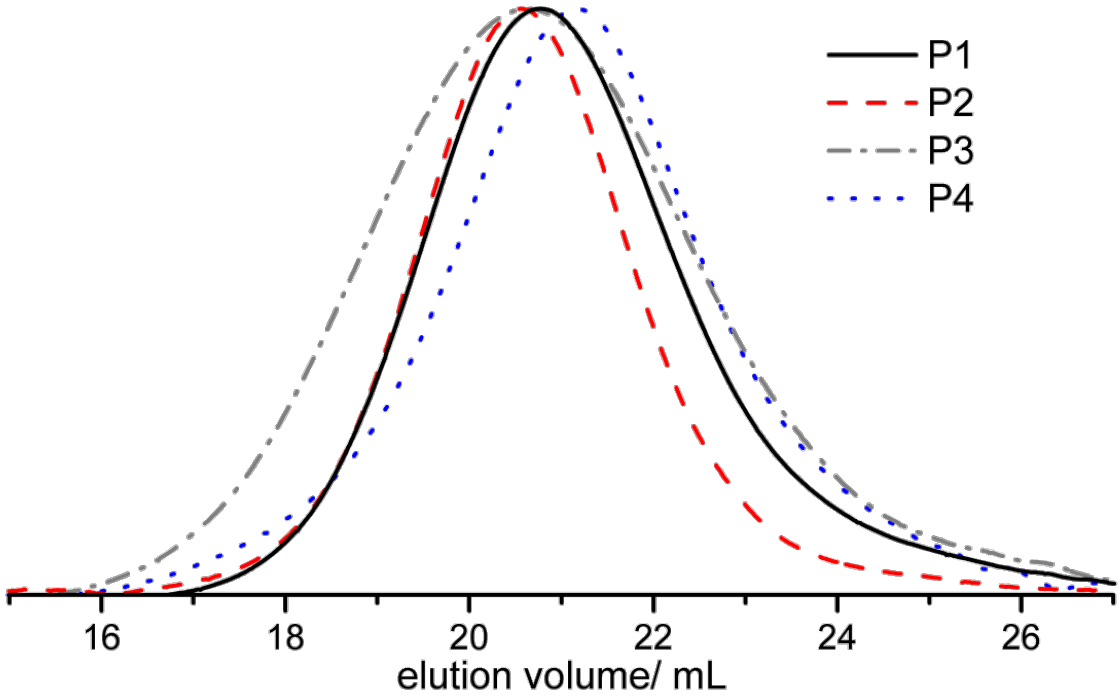

Figure S4: SEC traces (DMF, PEG standard) of *hb*P[G-*co*-fcGE] copolymers (P1, P2, P3, P4).

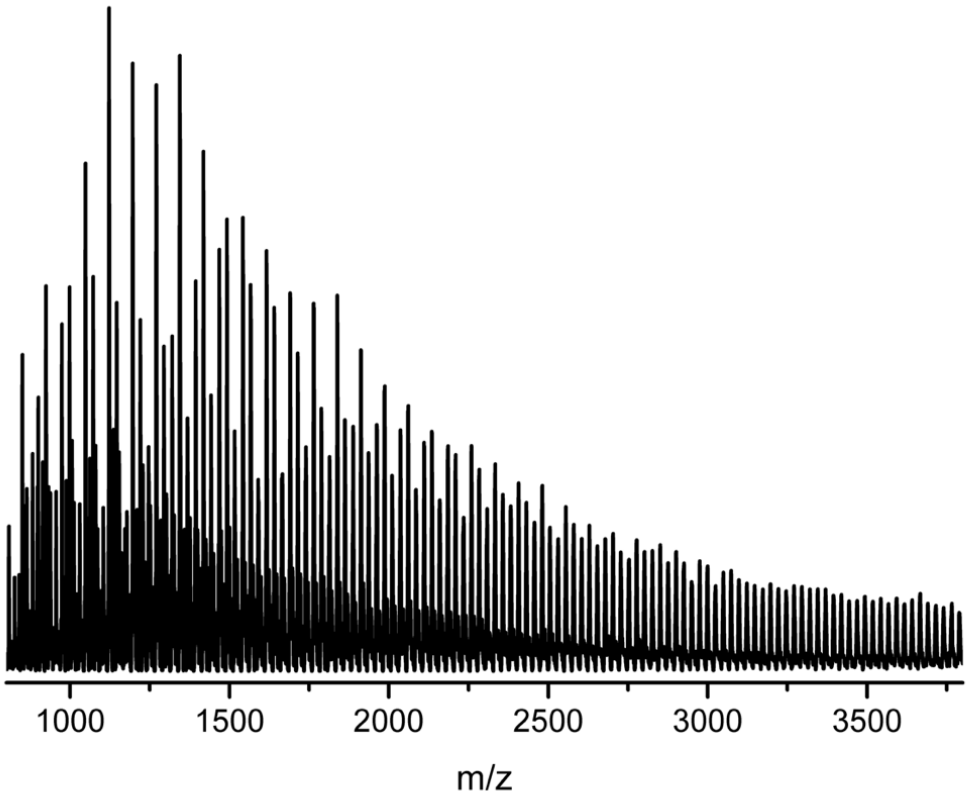

Figure S5: MALDI ToF MS of *hb*P[G_{36}-*co*-fc$GE_{5.0}$] (P2).

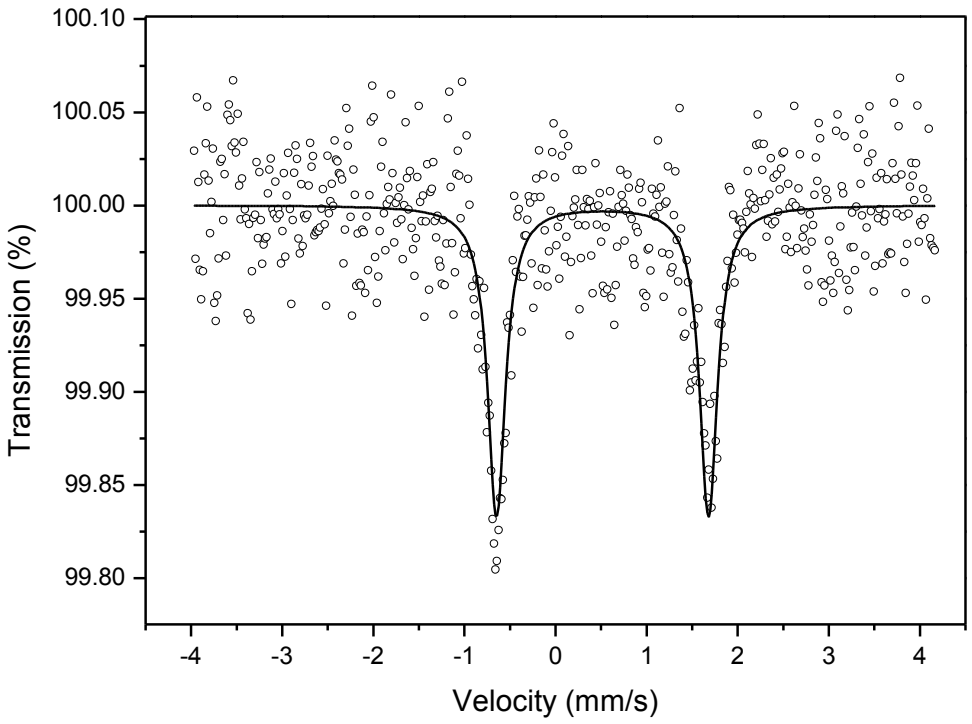

Figure S6: Mößbauer spectrum of the original (i.e. not oxidized) copolymer P3.

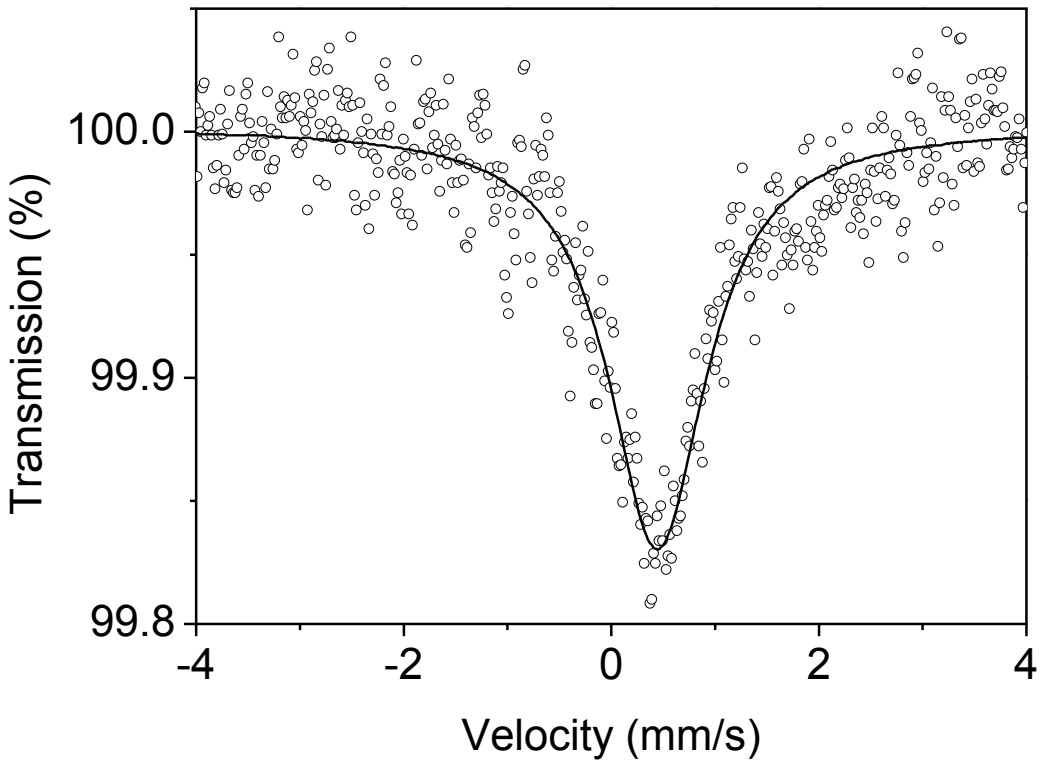

Figure S7: Mößbauer spectrum of the fully oxidized copolymer P3.

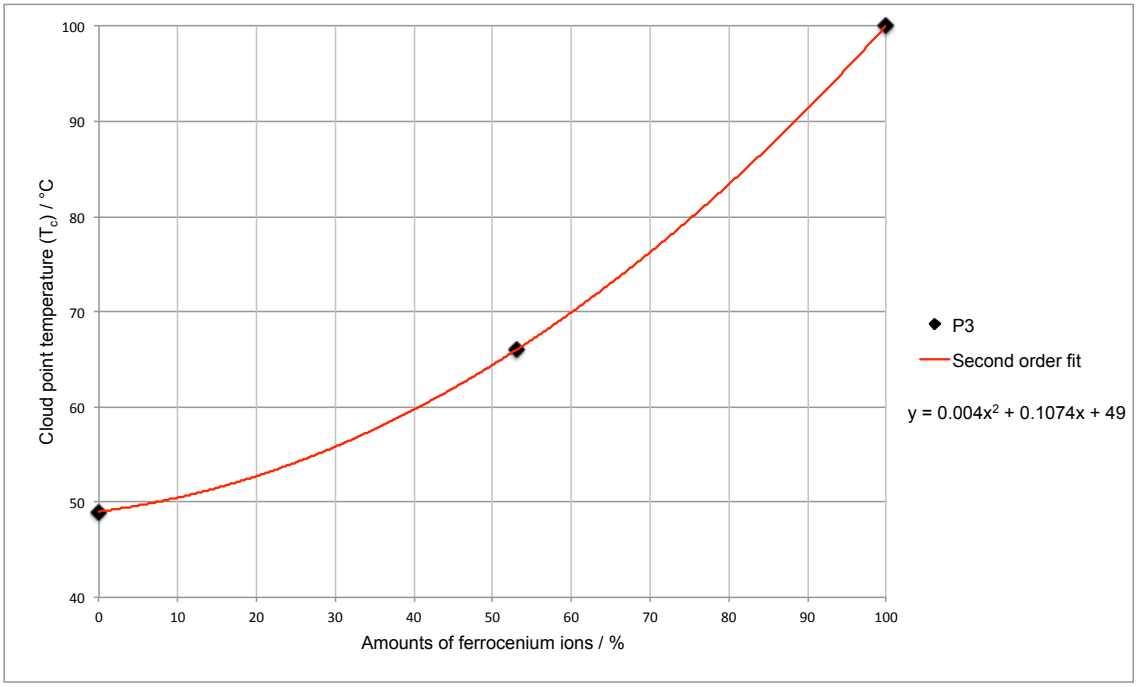

Figure S8: Cloud point temperature (T_c in °C) plotted against the degree of oxidation (amounts of ferrocenium ions in %).

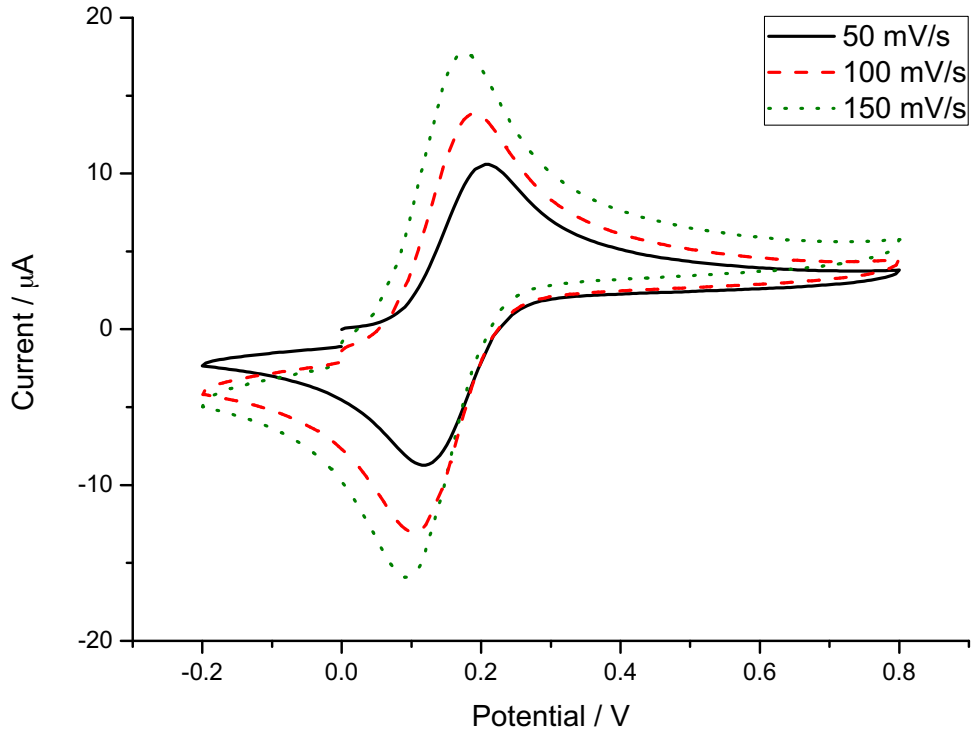

Figure S9: Cyclic voltammograms of *hb*P[G_{37}-*co*-fcG$E_{2.4}$] (P1) at different scan rates (H_2O, 5 g/L P1, 0.1 M KCl).

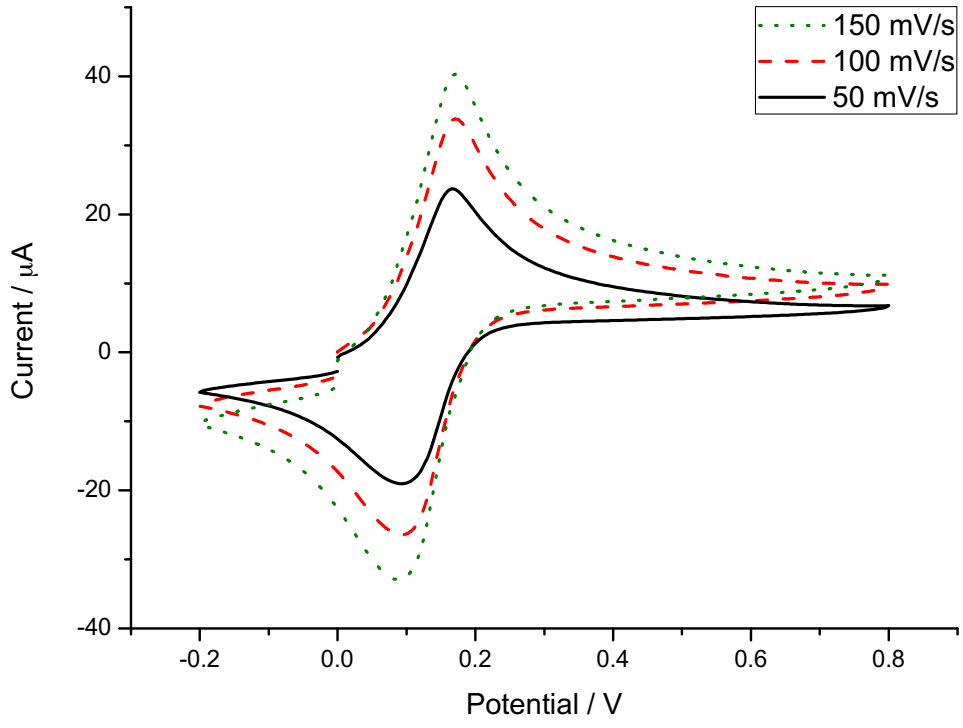

Figure S10: Cyclic voltammograms of *hb*P[G_{36}-*co*-fcGE_5] (P2) at different scan rates (H_2O, 5 g/L P1, 0.1 M KCl).

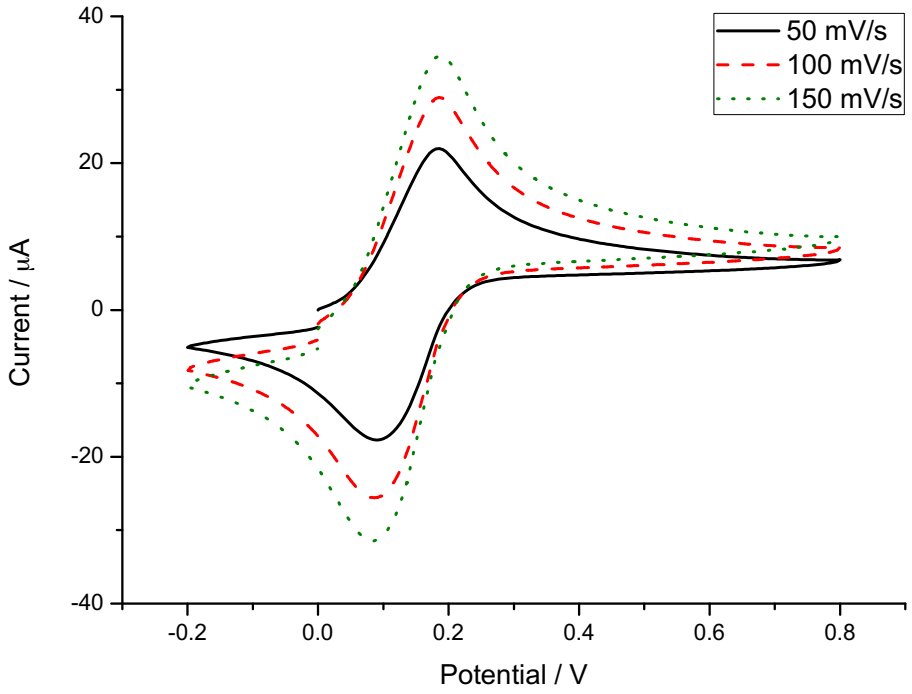

Figure S11: Cyclic voltammograms of *hb*P[G_{67}-*co*-fcG$E_{8.2}$] (P3) at different scan rates (H_2O, 5 g/L P1, 0.1 M KCl).

2.2 Vinyl Ferrocenyl Glycidyl Ether: An Unprotected Orthogonal Ferrocene Monomer for Anionic and Radical Polymerization

Published in *Polymer Chemistry* **2015**, 6, 3617–3624. (Published by the Royal Society of Chemistry.)

Authors: *Arda Alkan,*[a,b] *Laura Thomi,*[b] *Tassilo Gleede,*[a] *and Frederik R. Wurm*,*[b]

[a]Institute of Organic Chemistry, Johannes Gutenberg-Universität Mainz (JGU), Duesbergweg 10-14, 55099 Mainz, Germany.

[b]Max Planck Institute for Polymer Research (MPIP), Ackermannweg 10, 55128 Mainz, Germany.

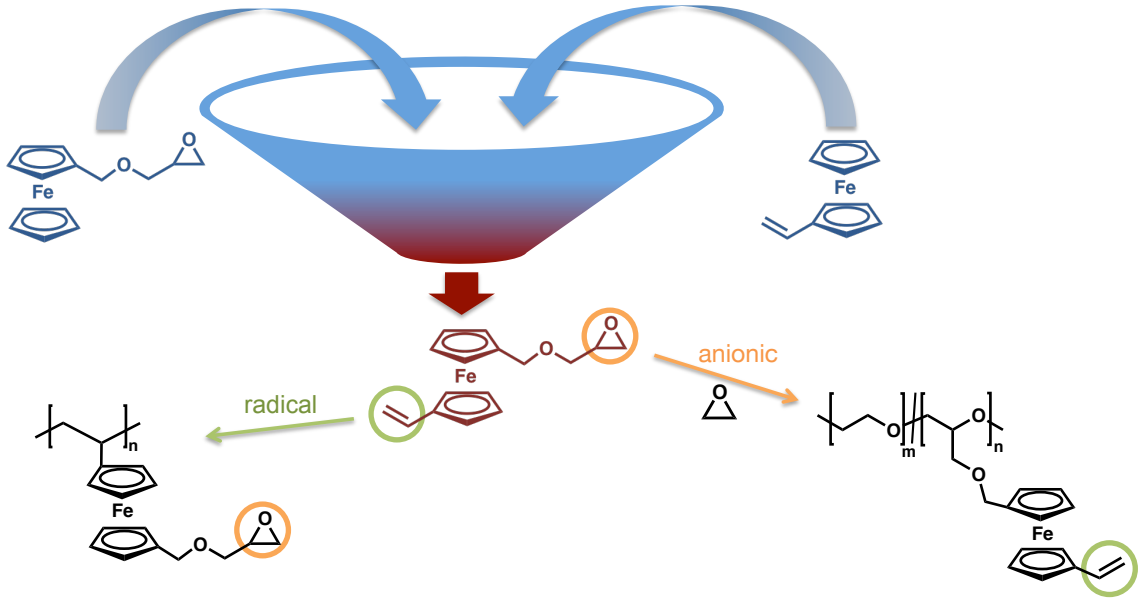

Abstract

The first orthogonal ferrocene monomer, vinyl ferrocenyl glycidyl ether (VfcGE), for both anionic and radical polymerization - without the need of a protection group - is presented. Anionic ring-opening copolymerization of VfcGE and ethylene oxide (EO) generates stimuli-responsive, multifunctional poly[(vinyl ferrocenyl glycidyl ether)-*co*-(ethylene oxide)] (P[VfcGE-*co*-EO]) copolymers (molecular weights of ca. 7,500 g/mol and low molecular weight dispersities ($Đ \leq 1.14$)). The amount of the equimolar ferrocenyl and vinyl groups are controlled by the comonomer ratio up to 15.4 mol% VfcGE. The pendant vinyl groups of P[VfcGE-*co*-EO] were post-modified with 3-mercaptopropionic acid via thiol-ene chemistry. The EO copolymers exhibit temperature-, redox-, and pH-responsive behavior in water depending on the polymers' microstructure. Free radical polymerization of VfcGE leads to polyalkylene:(vinyl ferrocenyl glycidyl ether) with pendant epoxide side chains at each ferrocene unit. The resulting polymer was used to generate redox-responsive protein nanoparticles with bovine serum albumin (BSA) by nucleophilic ring-opening of the pendant epoxides.

Introduction

Metallocene-containing polymers combine peculiar physical and chemical properties for several materials science applications. In the family of metallocenes, ferrocene (fc) is probably the most interesting compound, since it can be oxidized reversibly to the ferrocenium species (Fe(III)) and iron redox processes play an important role in living organisms. Both states exhibit high stability with ferrocene (Fe(II)) being very stable as an 18e complex. To date, fc-containing compounds are used as polyelectrolytes,[143] electroactive materials in amperometric glucose sensors[9,11,144] and catalyst[145-147] in fuel for the oxidation of soot.[148] Fc-based materials are also used in responsive elastomeric opal films,[149] for the redox responsive assembly and disassembly of nanotubes[150] and in colour-

tunable fluorescent multiblock micelles.[65] Furthermore, recently biomedical applications became an important field for the utilization of metallocene-containing materials.[16,102]

Ferrocene itself and its low molecular weight derivatives find limited application in materials science due to high crystallinity or low vapor pressure. The incorporation of fc into polymers allows usage of the organometallic properties.[151] Fc can be incorporated either as side chains or in the polymer backbone. Besides the famous main-chain polyferrocenyl silanes,[107,108,114] several examples of polymers with ferrocene-based side chains have been reported. The most popular monomer, which is known since 1955,[109] is probably vinyl ferrocene (Vfc, **1**, Figure 1) that can be polymerized via radical or anionic polymerization mechanisms. Also, (meth)acrylate-based side-chain ferrocene-containing monomers have been studied intensely.[110,152] In 2013, we introduced the first fc-containing epoxide monomer, i.e. ferrocene glycidyl ether (fcGE, **2**, Figure 1) for oxyanionic polymerization.[85] **2** was homopolymerized, but also copolymerized with ethylene oxide (EO), the latter produces water-soluble fc-containing poly(ethylene glycol)s which may find useful applications in the biomedical field or as stabilizers. From kinetic studies the anionic copolymerization of sterically demanding **2** and EO was found to be random;[85] interestingly, despite the bulky fc-side group, no gradient copolymers were generated under these conditions. More recently, we have expanded the use of **2** and synthesized multifunctional fc-containing polyethers by -again random- copolymerization with allyl glycidyl ether, which was carried out in bulk at 100 °C and monitored *in situ* via ^{13}C NMR spectroscopy.[111]

Polyfunctional, stimuli-responsive materials are a growing field in modern materials and bio-related science. Nature uses the principle of polyvalency for receptor-mediated processes, for example. In polymer science, polyvalency is typically achieved by the polymerization of a functional monomer or copolymerization of several monomers. Especially monomers with functional groups, which do not have to be protected during the polymerization, are of high interest, since protection and deprotection steps are spared. Orthogonal monomers with two different polymerizable groups are also very interesting, since they make the copolymerization of several monomers (with often unwanted copolymerization behavior) redundant. But especially monomers with two different polymerizable groups, whereas the second group acts as an unprotected functionality, are rarely found to date.[153-155] The

reported bifunctional monomers to date rely on rather simple monomer structures without additional properties.[153]

The current work presents the first orthogonal metallocene monomer carrying both an epoxide and a vinyl group, *viz*. vinyl ferrocenyl glycidyl ether (VfcGE (**3)**, Figure 1). **3** differs significantly from all other ferrocene side-chain monomers reported so far, since it is designed for both radical or anionic ring-opening (co-)polymerization[156] and the organometallic polymers carry multiple reactive groups for postpolymerization modification. Both selective anionic and radical polymerization of **3** are investigated in detail and the copolymerization with ethylene oxide to water-soluble, organometallic, and polyfunctional poly(ethylene glycol)s is presented. Subsequent postpolymerization modification of the pendant epoxide or vinyl groups was carried out. The polyethers are -in addition to their chemical polyvalency- further multi-stimuli responsive with respect to solubility in water, depending on pH, redox-potential and side-chain functionality.

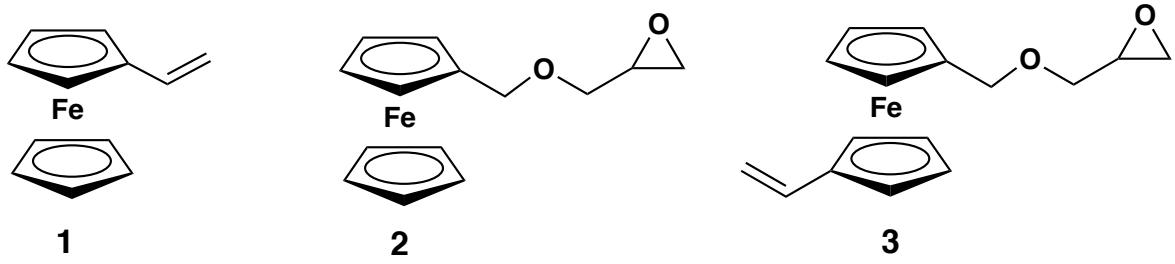

Figure 1. Side-Chain Ferrocene Monomers.

Results and discussion

Monomer and polymer synthesis

Fc-containing (co)polymers with polyether backbone as well as polyalkylene backbone are of high interest for multi stimuli-responsive materials. In this study we have developed an orthogonal ferrocene monomer (VfcGE, **3**), which can be polymerized via two different polymerization techniques: radical and anionic polymerization. VfcGE opens new possibilities to fast access to ferrocene-containing multifunctional polyethers as well as polyalkylenes

with ferrocene units bearing reactive epoxides (Scheme 1). The free radical polymerization of VfcGE leads to a polyalkylene structure whereas the anionic ring-opening polymerization leads to a polyether backbone.

Scheme 1. Synthetic Protocol for Free Radical and Anionic Copolymerization of VfcGE and EO.

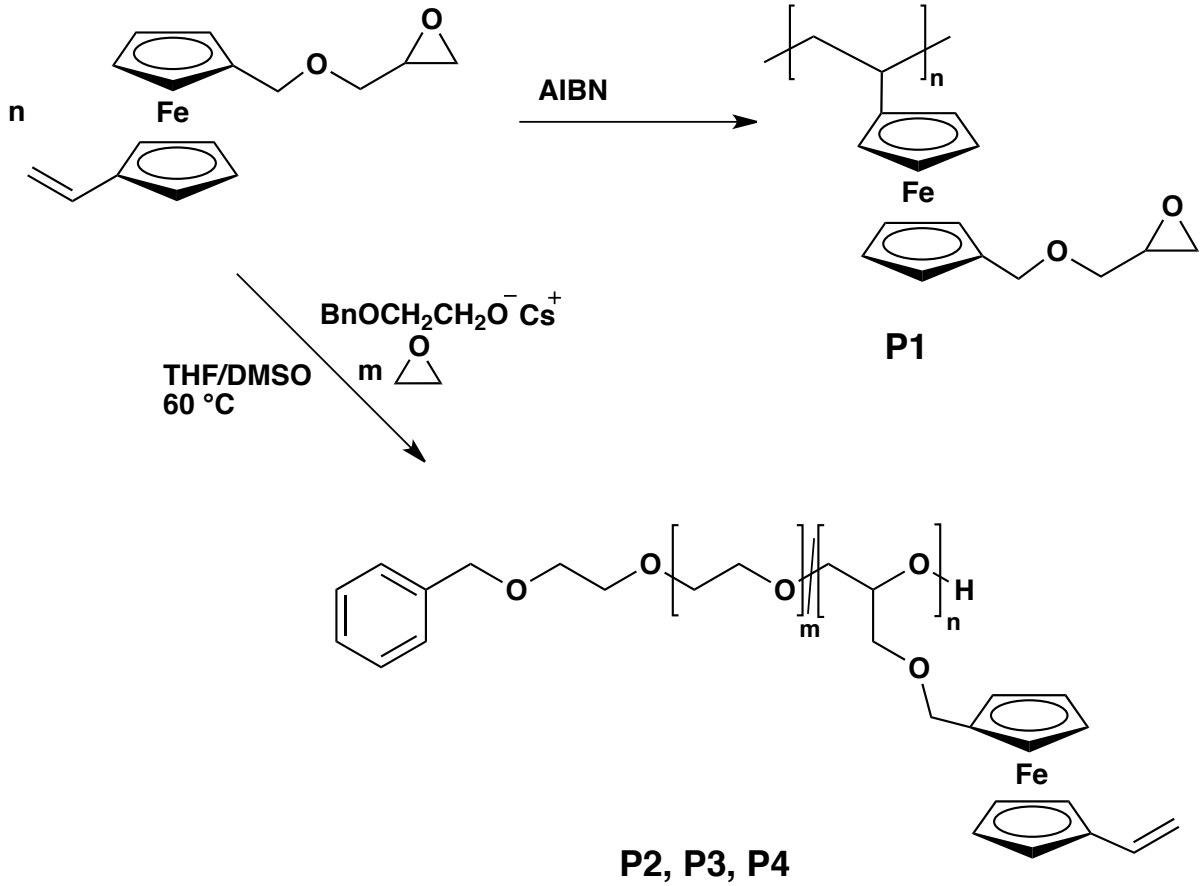

The monomer (**3**) was synthesized in a four-step protocol (Scheme 2), starting with the dilithiation of ferrocene to generate ferrocene-1,1'-dicarbaldehyde (**4**). In the second step, one of the aldehyde groups was transformed into a vinyl group by a Wittig reaction.[157] The resulting compound, 1-vinyl-1'-carboxaldehyde ferrocene (**5**), was then reduced with sodium borohydride to 1-vinyl-1'-hydroxymethyl ferrocene (**6**). **6** was then converted to vinyl ferrocenyl glycidyl ether (**3**) via a nucleophilic substitution with epichlorohydrin under phase transfer catalysis, similar to the synthetic protocols of other previously described glycidyl ethers (GEs).[158,159]

Scheme 2. Synthesis Route to the Orthogonal Monomer Vinyl Ferrocenyl Glycidyl Ether (VfcGE, 3).

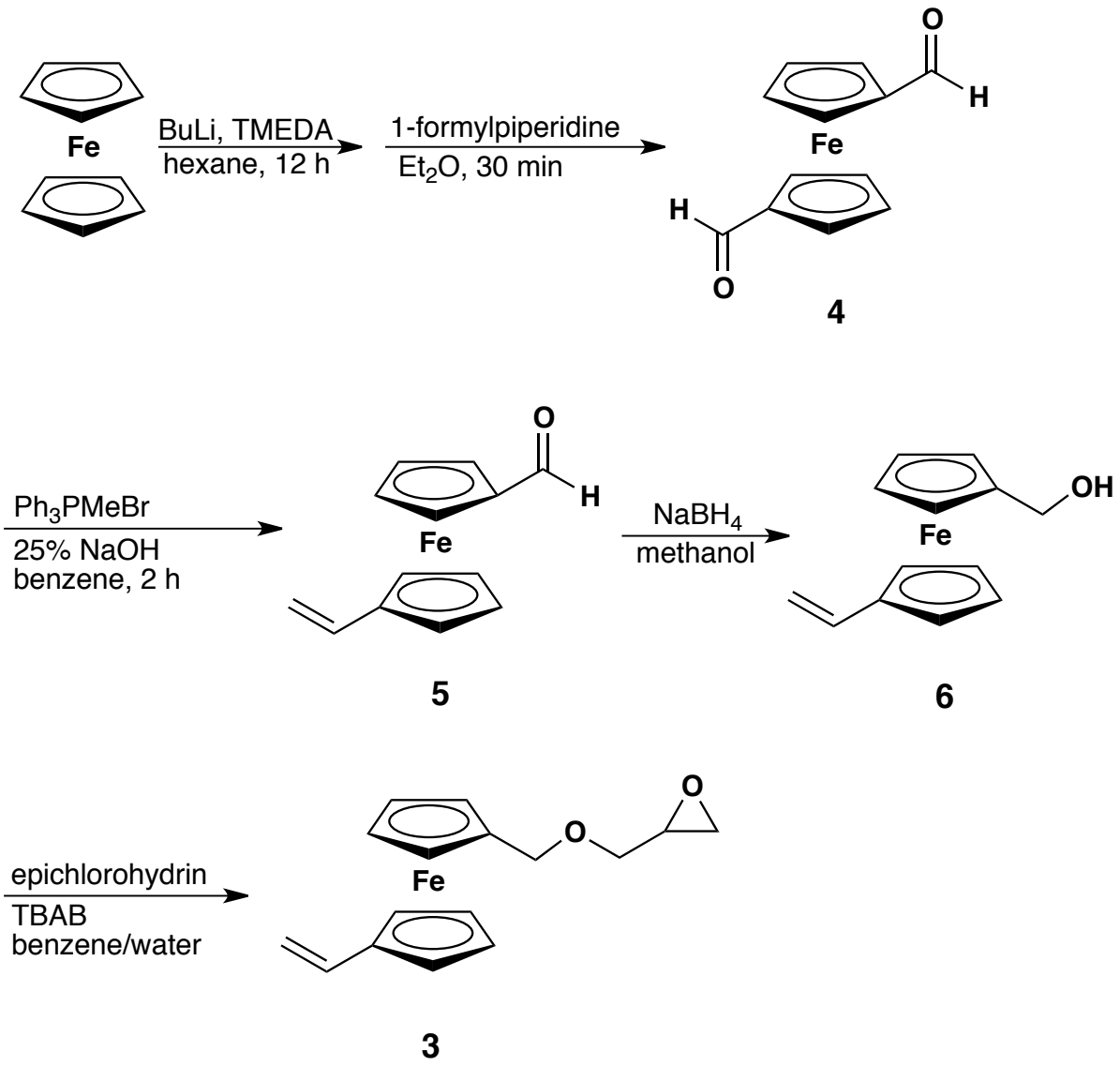

The monomer was obtained as dark orange liquid in overall good yields and purified by column chromatography. Figure 2 shows the ^{1}H NMR spectrum of **3** in benzene-d_6; ^{13}C (Figure S1), ^{13}C DEPT (Figure S2), HSQC (Figure S3), HMBC (Figure S4) and COSY (Figure S5) NMR spectra with the respective assignments can also be found in the Supplementary Information proving the signal assignments.

The free radical polymerization of **3** was carried out with 2,2'-azobis(2-methylpropionitrile) (AIBN) as the initiator in tetrahydrofuran (THF) at 80 °C with a initiator:monomer ratio is 1:60. The resulting polymer (polyalkylene:P[VfcGE], **P1**) has a monomodal molecular weight distribution with a molecular weight dispersity of $Đ$ = 1.83 (Figure 3**)**, whereas a small elution

peak for the monomer is present. The apparent molecular weight was determined to be 6,000 g/mol from size exclusion chromatography (SEC) in THF vs. polystyrene (PS) standards. The molecular weight determined from matrix-assisted laser desorption/ionization time-of-flight mass spectrometry (MALDI ToF MS) is in good agreement with the results from the SEC measurements, which is shown in Figure S6 and also confirms the repeating unit of VfcGE with a molecular weight of 298.16 g/mol.

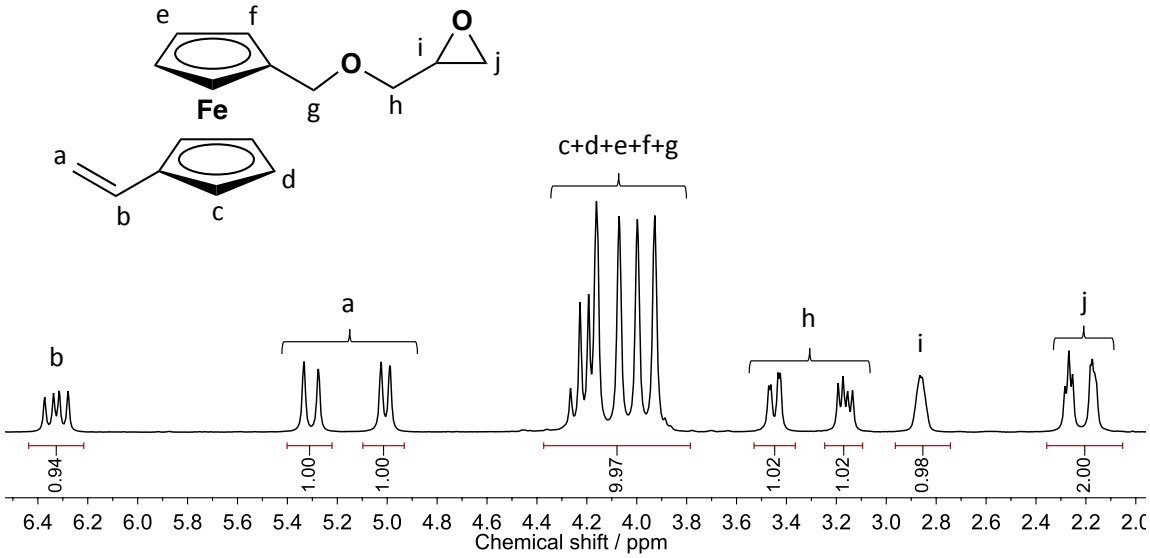

Figure 2. Detailed assignment of ^{1}H NMR resonances of vinyl ferrocenyl glycidyl ether (**3**) (benzene-d_6, 300 MHz, 298 K).

The homopolymer was also characterized by ^{1}H NMR spectroscopy. The spectrum in Figure S7 shows broad polymeric resonances and all signals can be assigned to the polyalkylene:VfcGE homopolymer. The protons of the polyethylene backbone are detected between 1.0 and 2.4 ppm. The epoxide protons can be detected in the region from 2.5 to 3.6 ppm and overlap with the aromatic ferrocene protons from 3.6 to 4.8 ppm (detailed peak assignment can be found in the Supplementary Information Figure S7).

The anionic ring-opening copolymerization of VfcGE and EO was carried out similar to previous works on EO copolymerizations.[85,160,161] The copolymerization was initiated by the cesium salt of 2-benzyloxyethanol in a mixture of THF:DMSO (ratio 100:1), whereas dimethyl sulfoxide (DMSO) increase the polarity of the solvent mixture and therefore the solvation of the cesium cation. The polymerization was allowed to proceed for 12-24 h at 60 °C to reach

complete conversion. All copolymers synthesized exhibited narrow molecular weight distributions ($Đ \leq 1.14$) and monomodal SEC traces (in dimethylformamide (DMF) vs polyethylene glycol (PEG) standards; Figure 3), which is important since side reactions at the functional double bonds are conceivable and this proves the stability of the vinyl group in the side chain under the polymerization conditions. Copolymers with a maximum of 15.4 mol% were synthesized to generate water-soluble materials.

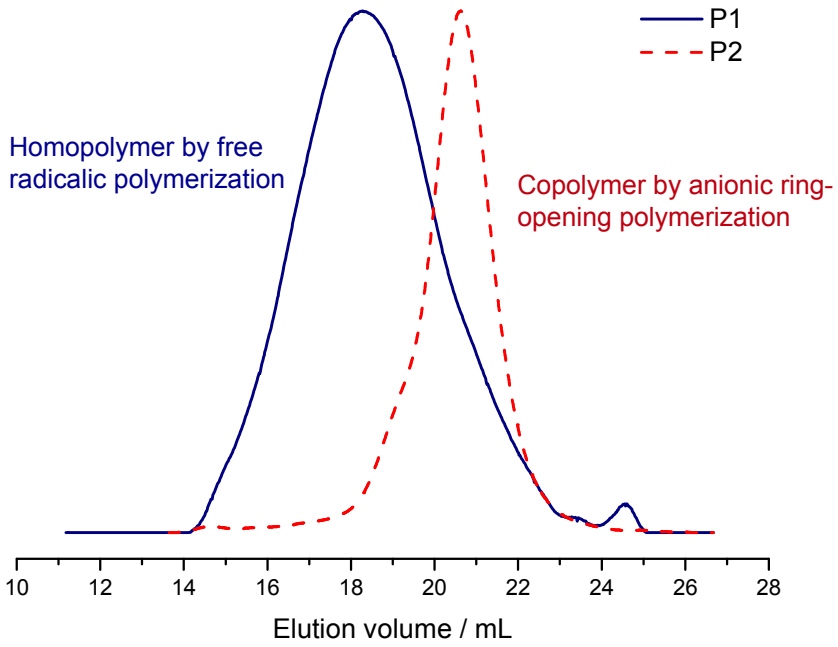

Figure 3. SEC traces of **P1** (THF, RI detection, 1 mL/min) and **P2** (DMF, RI detection, 1 mL/min).

Functionalization and Materials Properties of P[VfcGE-*co*-EO] Copolymers

The absolute molecular weights of the copolymers as well as the comonomer content from the anionic ROP can be determined by ^{1}H NMR spectroscopy (Figure S8) and are in good agreement with the theoretical values. The methylene group and aromatic resonances of the initiator (at 4.34 and 7.31 ppm) can be used as reference signals and are compared to the polyether backbone between 3.68 and 3.45 ppm and the signals of the vinyl group at 4.95-5.43 ppm and 6.27-6.47 ppm and cyclopentadienyl (cp) rings of fc at 4.02-4.29 (detailed peak assignment can be found in the Supplementary Information Figure S8). The incorporation of both comonomers was also confirmed by MALDI ToF MS (Figure S9): a linear combination of

the monomer masses of both repeating units can be detected in the spectrum and are marked with arrows.

The reaction between olefins and thiols is often used for polymer post-modification and was conducted with several vinyl-functionalized polymers before.[162] The application of the radical thiol-ene addition allows the introduction of functional groups into the organometallic polyether that would not sustain the conditions of an anionic ROP. Thus, the pendant vinyl groups of the P[VfcGE-*co*-EO] copolymers were post-modified with 3-mercaptopropionic acid and AIBN as the respective initiator at 80 °C in THF (Scheme 3) to induce an additional pH-responsive behavior into the copolymers.

Table 1. Characterization Data for Polyalkylene:VfcGE Homopolymer and P[VfcGE-*co*-EO] Copolymers.

no.	sum	VfcGE (mol%)	M_n[a] (g/mol)	M_n[b] (g/mol)	M_n[c] (g/mol)	$Đ$[c]
P1	Polyalkylene:VfcGE	100	-	-	6 000	1.83
P2	BnO[P($VfcGE_{12}$-*co*-EO_{138})]	4.8	5 800	12 300	2 200	1.09
P3	BnO[P($VfcGE_{7}$-*co*-EO_{70})]	8.8	7 100	5 200	1 700	1.11
P4	BnO[P($VfcGE_{14}$-*co*-EO_{75})]	15.4	8 400	7 500	1 800	1.14

a) Theoretical molecular weight according to initiator concentration; b) M_n determined from ^{1}H NMR by end group analysis; c) M_n determined via SEC in DMF vs. PEG (for **P2**, **P3** and **P4**) and in THF vs PS (in the case of **P1**) standards, $Đ = M_w/M_n$.

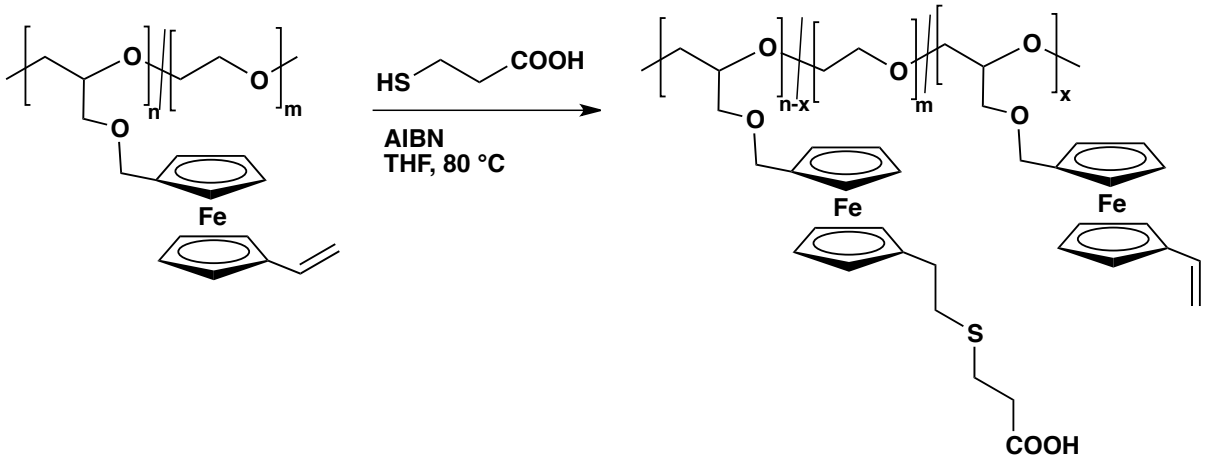

Scheme 3. Functionalization of P[VfcGE-*co*-EO] copolymer with 3-mercaptopropionic acid.

A comparison of the ^{1}H NMR spectra before and after the functionalization is depicted in Figure 4. It is noticeable that the protons of the vinyl groups, which appear in the range from 5.0 to 6.5 ppm, vanish and instead new signals for the ethylene linkage between ferrocene and the sulfur center appear at 3.0 to 2.6 ppm; less than 10% of the vinyl groups remain un-functionalized under these conditions.

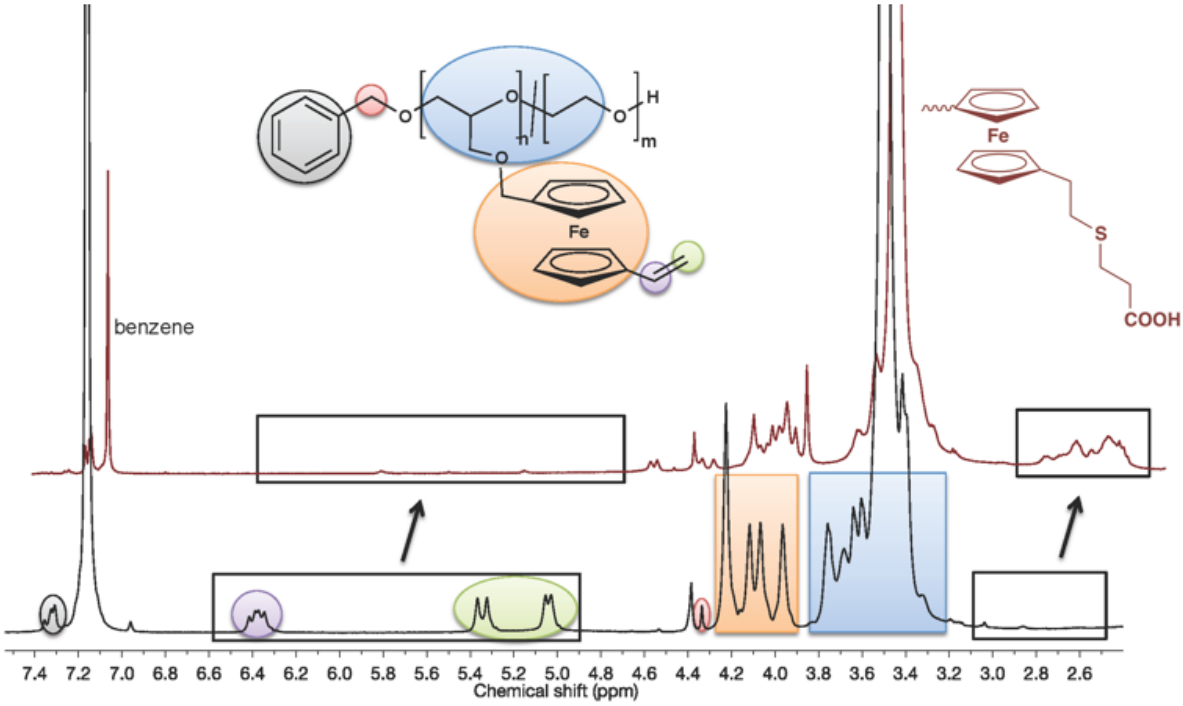

Figure 4. Functionalization of P[VfcGE-*co*-EO] (**P2**, before functionalization, bottom; and **P2'**, after functionalization, top) with 3-mercaptopropionic acid monitored by ^{1}H NMR spectroscopy (benzene-d_6, 400 MHz, 298 K).

Lower Critical Solution Temperature (LCST) Behavior

Copolymers of EO and hydrophobic comonomers exhibit a tunable thermoresponsive behavior depending on the amount and type of the comonomer. The cloud point temperature can be varied over a broad temperature range (typically over the whole range of liquid water, *viz.* 0-100 °C). The LCST can be lowered by increasing the amount of the hydrophobic comonomer or by increasing its hydrophobicity. As previously reported for poly(ferrocenyl glycidyl ether-*co*-ethylene oxide) (P[fcGE-*co*-EO]) copolymers,[85] we have also

detected thermoresponsive behavior for the P[VfcGE-*co*-EO] copolymers, as expected. The P[VfcGE-*co*-EO] copolymers with more than 15.4 mol% **3** incorporated are water-insoluble, which is the reason, why copolymers with higher VfcGE contents or even homopolymers were not synthesized. An interesting feature of these organometallic copolymers is the tunable cloud point by partial or complete oxidation of the ferrocene moieties to the ferrocenium ions as demonstrated for the P[fcGE-*co*-EO] copolymers previously.[85] Turbidity measurements of **P2** and **P3** are shown in Figure 5. **P3** with 8.8 mol% VfcGE shows a cloud point temperature of 9 °C while **P2** with only 4.8 mol% VfcGE exhibits a lower solubility limit at 37 °C. The cooling curve for **P3** is also shown in Figure 5, indicating a low hysteresis with a shifted cloud point towards lower temperatures, whereas the hysteresis is less than 1 °C.

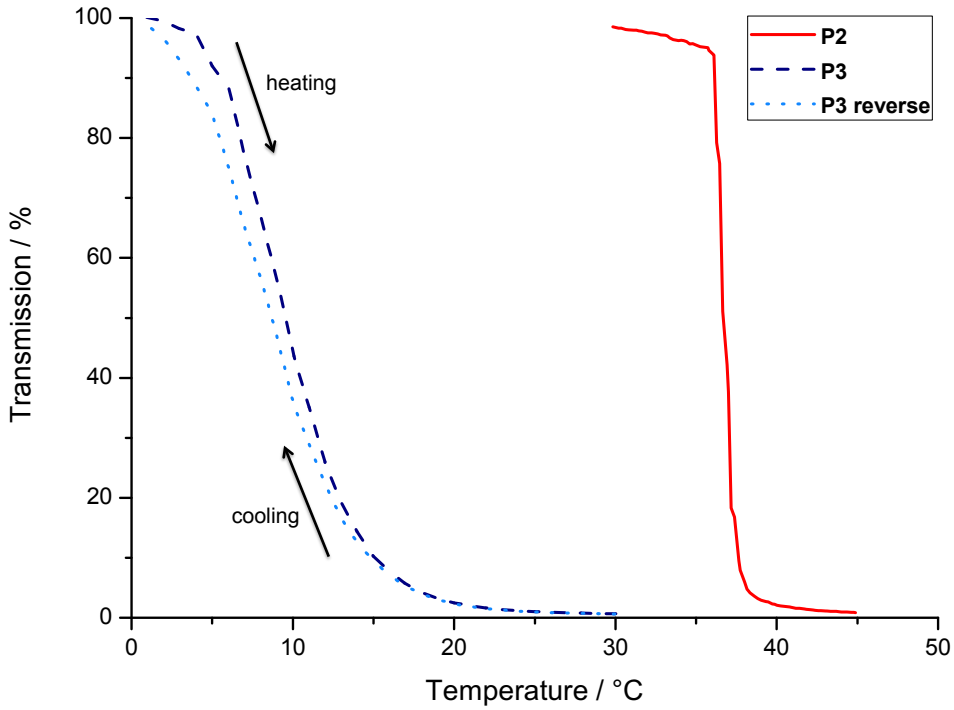

Figure 5. Turbidity measurements of **P2** and **P3** (λ = 500 nm; heat rate = 1 °C/min) and the reversed measurement for **P3** (cooling rate = 1 °C/min).

In contrast to the P[fcGE-*co*-EO] copolymers, the novel P[VfcGE-*co*-EO] allow further chemical tuning of the cloud point temperature by functionalization of the pendant vinyl groups: hydrophilic groups are introduced via thiol-ene addition as described above. The 3-

mercaptopropionic acid- functionalized copolymer (**P2'**) shows an increased cloud point temperature due to the increased hydrophilicity of the polymer. The cloud point temperature of **P2'** at pH 3 was determined to be 62 °C (Figure 6). Interestingly, the copolymer is water-soluble over the whole temperature range at pH-values higher than 3 due to (partial) deprotonation of the pendant carboxylic acid groups. Also, slow degradation of ferrocene under more acidic conditions limits the application to pH-values of ca. 3.

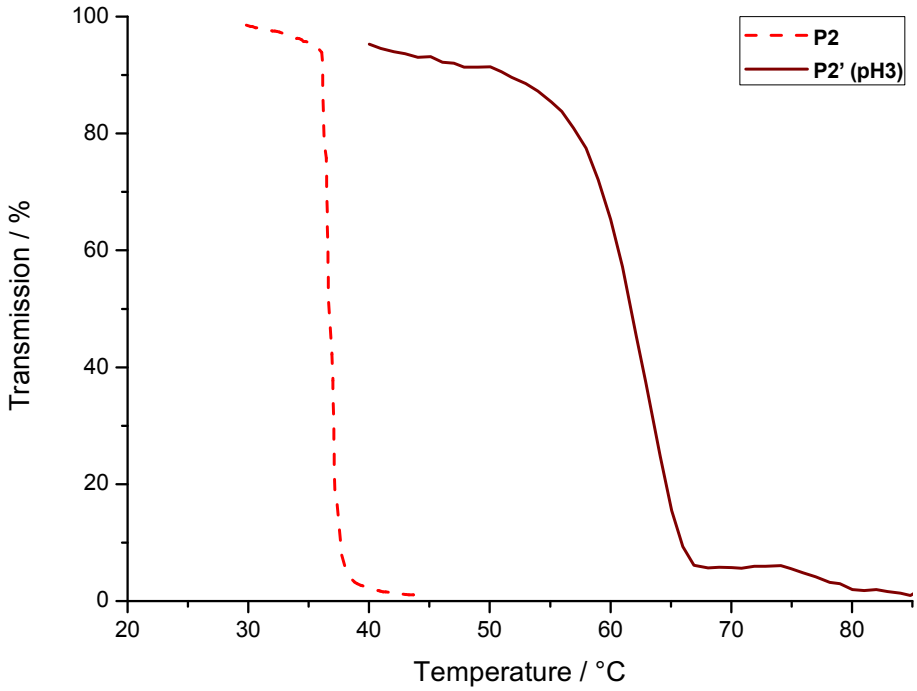

Figure 6. Comparison of the turbidity measurements of **P2** (at pH = 7) and post-modified P2 bearing carboxylic acid side chains (i.e. **P2',** at pH = 3), λ = 500 nm; heat rate = 1 °C/min.

Nanoparticle formation from Polyalkylene:VfcGE

The pendant groups of **P1** were used to generate nanoparticles by the efficient nucleophilic ring-opening of epoxides with amines.[163] In order to take advantage of the numerous epoxides attached to fc, redox-responsive nanoparticles have been synthesized. Such nanoparticular systems are interesting for delivery or self-healing applications as demonstrated previously.[164,165] The hydrophobic **P1** can be reacted in a miniemulsion

polyaddition with polyfunctional, water-soluble amines. We chose bovine serum albumin (BSA), a 66 kDa protein with 59 lysine units as an example for a biomolecule, capable of reacting with **P1** to generate potentially biodegradable and redox-responsive nanocarriers. Nanoparticles were prepared by interfacial nucleophilic addition from the protein dissolved in stable water-droplets, which were dispersed in toluene containing the ferrocene-containing polyepoxide by adapting a previously published protocol.[166] The resulting particles showed a size of ca. 309 nm from dynamic light scattering (DLS). Imaging of the nanoparticles by TEM shows spherical structures with diameters much smaller than those determined by DLS (Figure 7). This is probably caused by drying effects, as the polymer chains collapse during the process, indicating the formation of a cross-linked nanoparticle based on the protein and the ferrocene-containing cross-linker. After redispersion in water, the size of the particles decreases to 92 nm as determined by DLS, because the chains of **P1** are not soluble in water leading to shrinkage of the nanoparticles.

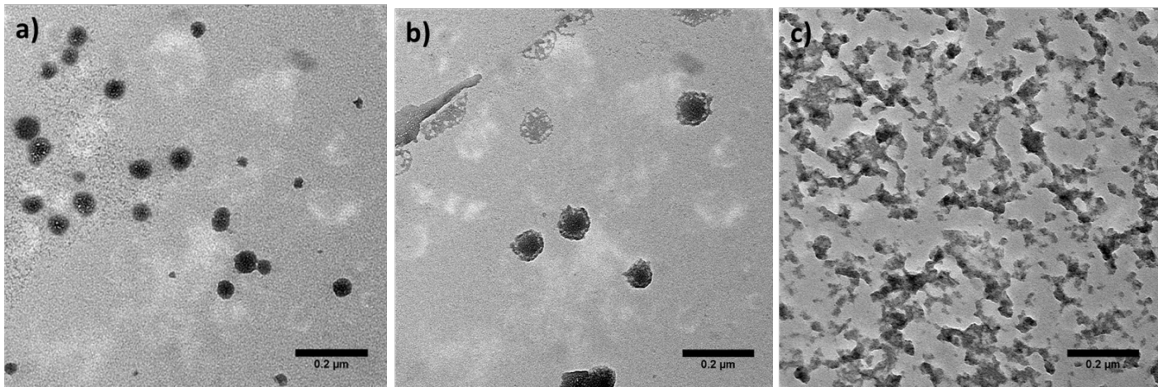

Figure 7. TEM images of cross-linked polyalkylene:VfcGE-BSA nanoparticles drop-cast from the toluene dispersion (a), drop-cast from the aqueous dispersion (b), and the formation of a gel after oxidation of the aqueous dispersion (c).

To show the redox-responsivity of these nanoparticles, the ferrocene units of **P1** were oxidized with hydrogen peroxide under slightly acidic conditions. After oxidation, no precise size determination by DLS measurements was possible due to the formation of large aggregates, probably due to electrostatic interactions. TEM imaging (see Figure 7) shows no distinct nanoparticles after oxidation, but the formation of supramolecular aggregates.[167]

This strategy could be further used for a redox-controlled gelators, which is currently under investigation in our group.

Conclusion

Both of ferrocene's cyclopentadienyl ligands have been used as handles for the attachment of polymerizable groups. The first orthogonal ferrocene monomer, namely vinyl ferrocene glycidyl ether (VfcGE), has been synthesized and polymerized via two different polymerization techniques: on the one hand the vinyl group enables the radical polymerization, and on the other the epoxide enables the living oxyanionic ring-opening polymerization. The two monomer sites polymerize selectively without any influence on the other functionality. In addition VfcGE could also serve as a novel organometallic/ redox-responsive linker molecule for many other applications.

After polymerization, however, multifunctional organometallic (co-)polymers are obtained. They can be easily post-modified without previous protection and deprotection steps. VfcGE combines two side-chain monomers, the classical vinylferrocene and the rather new ferrocenyl glycidyl ether in a novel bifunctional monomer. Radical polymerization of the vinyl group produces redox-responsive polyepoxides that have been utilized for the formation of protein nanoparticles, but may find further application in epoxy resins with additional redox potential. When the epoxide in **1** is polymerized by anionic polymerization, polyethers with pendant vinyl groups are generated. By copolymerization of **1** with ethylene oxide, water-soluble poly(ethylene glycol)-derivatives are obtained exhibiting cloud point temperatures depending on the amount and oxidation state of ferrocene within the polymer. Further tuning of the cloud point temperature was achieved by chemical functionalization of the pendant vinyl groups of the P[VfcGE-*co*-EO] copolymers: functionalization with 3-mercaptopropionic acid further introduces pH-responsibility for the cloud point temperatures. We believe that this new monomer opens various potential applications for

ferrocene-containing polymers with additional functionalities, for example for advanced sensors or the formation of biomimetic, redox-controlled nanoparticles.

Experimental

Instrumentation. ^{1}H NMR spectra (300, 400 and 500 MHz) and ^{13}C NMR spectra (75.5, and 101 MHz) were recorded using a Bruker AC300, a Bruker AMX400 and Bruker Avance 500. All spectra were referenced internally to residual proton signals of the deuterated solvent.

For size exclusion chromatography (SEC) measurements in DMF (containing 0.25 $g \cdot L^{-1}$ of lithium bromide as an additive) an Agilent 1100 Series was used as an integrated instrument, including a PSS HEMA column (106/105/104 $g \cdot mol^{-1}$), a UV detector (275 nm), and a RI detector at a flow rate of 1 $mL \cdot min^{-1}$ at 50 °C. Calibration was carried out using PEG standards provided by Polymer Standards Service.

SEC in THF was performed on an instrument consisting of a Waters 717 plus auto sampler, a TSP Spectra Series P 100 pump and a set of three PSS SDV columns (10^4/500/50 Å). Signal detection occurred by a UV (TSP Spectra System UV 2000, 254 nm), and a refractive index (Agilent 1260) detector. Calibration was carried out using PS standards provided by Polymer Standards Service.

Matrix-assisted laser desorption/ionization time-of-flight (MALDI-ToF) measurements were performed using a Shimadzu Axima CFR MALDI-TOF mass spectrometer, employing DCTB (*trans*-2-[3-(4-*tert*-butylphenyl)-2-methyl-2-propenylidene]malononitrile) as a matrix (5 $mg \cdot mL^{-1}$ in THF).

For electron microscopy measurements 3 µL sample were placed on a carbon-coated copper grid. TEM measurements were carried out on a JEOL 1400 at a voltage of 120 kV and images were taken with a GATAN Ultrascan 1000 CCD-camera.

Turbidity measurements were performed in deionized water and observed by optical transmittance of a light beam (λ = 500 nm; 50%) through a 1 cm sample quartz cell. The measurements were performed in a Jasco V-630 photospectrometer with a Jasco ETC-717 Peltier element. The intensity of the transmitted light was recorded versus the temperature

of the sample cell. The heating/cooling rate was 1 °C min^{-1}, and values were recorded every 0.1 °C.

Dynamic light scattering (DLS) were performed on diluted dispersions with a Nicomp™ 380 Submicron Particle Sizer (PSS-Nicomp) at an angle of 90° or on an ALV spectrometer consisting of a goniometer and an ALV-5004 multiple-tau full-digital correlator (320 channels) which allows measurements over an angular range from 20° to 150. A He-Ne Laser (wavelength of 632.8 nm) is used as light source.

Reagents. Solvents and reagents were purchased from Acros Organics, Sigma-Aldrich or Fluka and used as received, unless otherwise stated. Chloroform-d_1 and benzene-d_6 were purchased from Deutero GmbH. EO was freshly distilled before use. 1-vinyl-1'-carboxaldehyde (**5**) was synthesized starting from ferrocene as described in literature.[157]

Synthesis of 1-vinyl-1'-hydroxymethyl ferrocene (6). 1.85 g 1-vinyl-1'-carboxaldehyde ferrocene (**5**; 7.7 mol) were dissolved in methanol. 120 mg sodium borohydride (3.1 mmol, 0.4 eq.) were added in small portions under stirring at room temperature. The mixture was stirred until all sodium borohydride was dissolved (approx. 30 min). Distilled water was added and the reaction mixture was extracted three times with diethyl ether. The solvent was removed at reduced pressure and the product was obtained as yellow solid (1.82 g, 7.53 mmol) and was pure enough for further reactions. Yield: 98%. ^{1}H NMR (C_6D_6, 300 MHz, 298 K): δ(ppm) = 6.37-6.24 (dd, 1H, H_2C=C*H*-fc, *J* = 17.5, 10.7 Hz), 5.32-5.23 (dd, 1H, H*H*C=CH-fc, *J* = 17.5, 1.6 Hz), 5.00-4.94 (dd, 1H, *H*HC=CH-fc, *J* = 10.8, 1.5 Hz), 4.22-4.15 (d, 2H, fc-CH_2-OH, *J* = 4.1 Hz), 4.15-3.87 (m, 8H, *fc*). (Detailed peak assignment can be found in the Supplementary Information Figure S10.)

Synthesis of vinyl ferrocenyl glycidyl ether (VfcGE, 3). A mixture of a 8 mL 50% aqueous KOH solution, 0.57 mL epichlorohydrin (7.3 mmol) and 100 mg tetrabutylammonium bromide as phase transfer catalyst cooled to ca. 0 °C with an ice bath. 1.64 g (6.8 mmol) 1-vinyl-1'-hydroxymethyl ferrocene (**6**) were dissolved in benzene and added drop-wise to the reaction mixture. The mixture was rapidly stirred and allowed to warm up to room

temperature. After 24 h ice was added and the mixture extracted with diethyl ether. After washing with brine, the solvent was removed at reduced pressure. The crude product was purified by column chromatography over silica using a mixture of ethyl acetate and petroleum ether (3:7) as eluent. The pure product was obtained as a dark orange liquid. Yield: 83%. ^{1}H NMR (C_6D_6, 300 MHz, 298 K): δ(ppm) = 6.44-6.22 (dd, 1H, H_2C=C*H*-fc, *J* = 17.5, 10.7 Hz), 5.38-5.23 (d, 1H, H*H*C=CH-fc, *J* = 17.0 Hz), 5.09-4.94 (d, 1H, *H*HC=CH-fc, *J* = 10.6 Hz), 4.35-3.80 (m, 10H, *fc*-CH_2-O), 3.52-3.38 (dd, 1H, fc-CH_2OC*H*H, J = 11.4, 3.0 Hz), 3.25-3.10 (dd, 1H, fc-CH_2OCH*H, J* = 11.4, 5.9 Hz), 2.92-2.80 (m, 1H, epoxide C*H*), 2.32-2.12 (m, 2H, epoxide CH_2). (Detailed peak assignment in Figure 2; for additional characterization data, see Supporting Information Figure S1 (^{13}C), S2 (^{13}C{H} DEPT), S3 (HSQC), S4 (HMBC) and S5 (COSY).)

General procedure for the copolymerization of VfcGE and EO (P2, P3, P4): P[EO-*co*-VfcGE]. 17.6 mg (0.116 mmol) 2-(benzyloxy)ethanol and 17.5 mg (0.104 mmol, 0.9 eq.) of cesium hydroxide monohydrate were placed in a 100 mL Schlenk flask and suspended in 10 mL of benzene. The mixture was stirred at 60 °C under an argon atmosphere for 1 h and evacuated at 60 °C (10^{-2} mbar) for 12 h to remove benzene and water (as an azeotrope with benzene) to generate the corresponding cesium alkoxide. Subsequently, approx. 20 mL of dry THF were cryo-transferred into the Schlenk flask. 0.5 mL (11.0 mmol) EO was cryo-transferred to a graduated ampule and then cryo-transferred into the reaction flask containing the initiator in THF. Then 170 mg (0.580 mmol; for a composition of 1:19) of the second comonomer, VfcGE (**3**), was added via syringe in a 50 wt% solution in anhydrous DMSO. The reaction mixture was heated up to 60 °C and stirred for 12-24 h before the living chain ends were terminated with methanol. The copolymer solution was dried *in vacuo* and precipitated into cold diethyl ether. The copolymer was obtained as an orange to dark orange viscous material, the color strongly depending on fc content. Yields: 70-90%. ^{1}H NMR (C_6D_6, 400 MHz, 298 K): δ(ppm) = 7.31 (m, 5H, aromatic protons of initiator), 6.47-6.28 (dd, H_2C=C*H*-fc), 5.41-4.96 (m, H_2C=CH-fc), 4.33 (s, 2H, aliphatic signals of initiator), 4.29-3.91 (m, *fc*-CH_2-O), 3.85-3.10 (residual protons: PEO backbone, fc-CH_2-O-CH_2-backbone).

Procedure for the free radical polymerization of VfcGE: Polyalkylene:VfcGE (P1). 100 mg VfcGE (**3**) and 1,2 mg azobis(isobutyronitrile) (AIBN) were dissolved in 2 mL THF. After three-pump-thaw cycles (to remove any oxygen from the system) the reaction mixture was heated to 80 °C and stirred for 12 h. The reaction mixture was flushed with air and precipitated into cold methanol. The polymer was obtained as a yellow highly viscous liquid. Yield: 90%. ^{1}H NMR (C_6D_6, 400 MHz, 298 K): δ(ppm) = 5.0-3.5 (m, br, 11H, fc-*H*, fc-C*H*$_2$-O-C*H*H-), 3.5-3.25 (m, br, 1H, -O-CH*H*-epoxide), 3.25-3.00 (m, br, 1H, C*H* of epoxide), 2.90-2.70 (m, br, 1H, C*H*$_2$ of epoxide), 2.70-2.45 (m, br, 1H, C*H*$_2$ of epoxide), 2.45-1.00 (m, br, 3H, polyalkylene backbone).

Polymer modification via thiol-ene addition. 100 mg of the respective copolymer were dissolved in 5 mL THF and a 20-fold molar excess (156 mg) of 3-mercaptopropionic acid and 13.9 mg (0.75 eq.) of AIBN with respect to the absolute number of vinyl groups, were added. After three freeze-pump-thaw cycles (to remove any oxygen from the system) the reaction mixture was heated to 80 °C and stirred for 12 h. The reaction mixture was dialyzed against methanol, using benzoylated tubings (MWCO 1,000 g/mol) over a period of 24 h. Yield: 95%. ^{1}H NMR (C_6D_6, 400 MHz, 298 K): δ(ppm) = 7.31 (m, 5H, aromatic protons of initiator), 4.33 (s, 2H, aliphatic signals of initiator), 4.29-3.91 (m, *fc*-C*H*$_2$-O), 3.85-3.10 (residual protons: PEO backbone, fc-CH$_2$-O-C*H*$_2$-backbone), 3.00-2.55 (m, fc-C*H*$_2$-C*H*$_2$-S).

Polymer nanoparticle formation via nucleophilic ring-opening of the pendant epoxides of P1 with amino-groups of BSA. 25 mg bovine serum albumin (BSA) and 3.8 mg sodium chloride were dissolved in 0.25 g Milli-Q water. Separately, 17.9 mg polyglycerin-polyricinoleate (PGPR) as surfactant were dissolved in 4.2 g toluene by treatment in an ultrasound bath at 60 °C for 20 minutes and added drop-wise to the aqueous solution. After stirring for one hour at room temperature, the resulting macroemulsion was subjected to ultrasonication using a Branson W450-D sonifier with a 1/8 inch tip at 69% amplitude for 3 minutes (20 seconds pulse, 10 seconds pause) under ice-cooling. Separately, 5.4 mg PGPR

and 6.8 mg of **P1** were dissolved in 2.8 g toluene and added dropwise to the obtained emulsion. The reaction was carried out for 24 h at room temperature. The resulting dispersion was filtered to remove any aggregates. For purification the dispersion was centrifuged at 1163 rcf for 20 minutes. After removing the supernatant, the particles were redispersed in an equivalent amount of fresh toluene. Centrifugation and redispersion steps were repeated once. For redispersion in water, 5 g of an aqueous solution of cetyltrimethylammonium chloride (CTMACl) (1 wt%) were added dropwise to 1 g of the nanoparticle dispersion. After toluene evaporation the aqueous dispersion was dialyzed against Milli-Q water for 24 h to remove an excess of surfactant. For oxidation, 1 mL aqueous dispersion was mixed with 2.5 µL 35% H_2O_2 solution and 6 µL 0.1 M HCl. The nanoparticle dispersion was characterized by DLS and TEM at every step.

2.2.1 Supporting Information

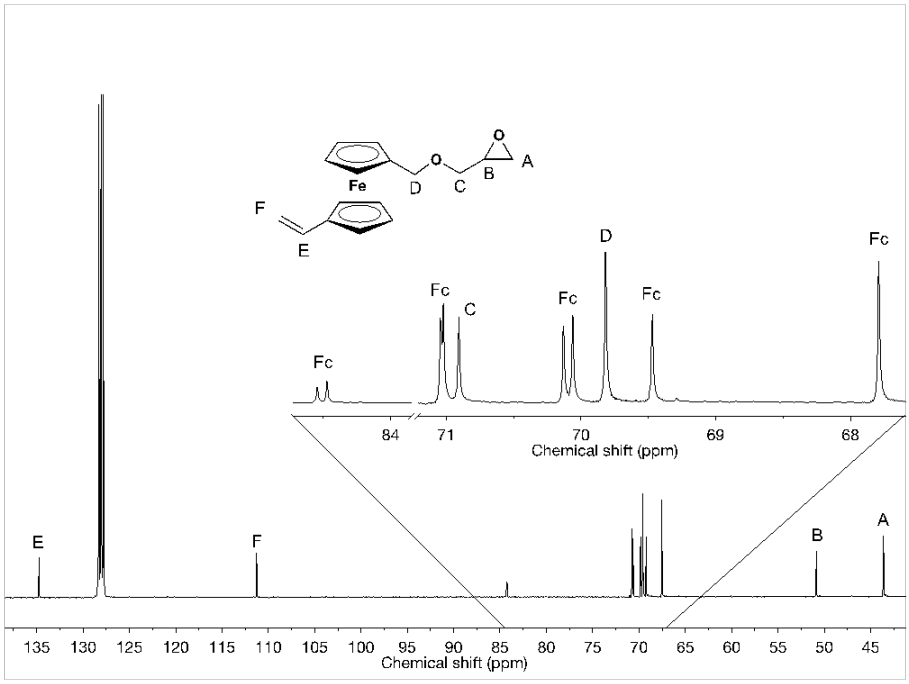

Figure S1. $^{13}C\{H\}$ NMR (101 MHz, C_6D_6, 298 K) of VfcGE.

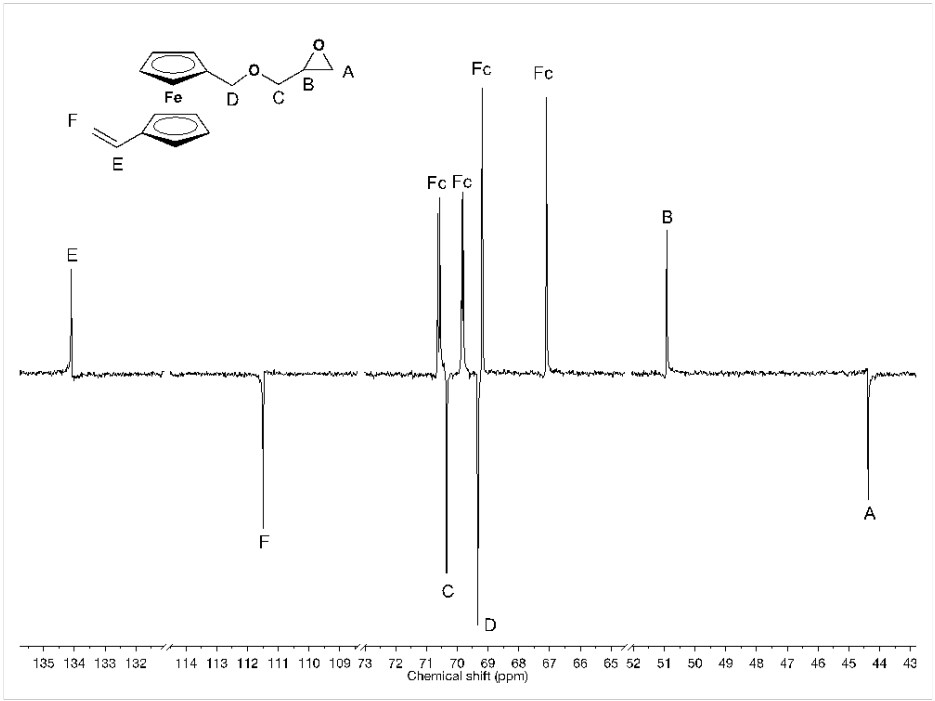

Figure S2. $^{13}C\{H\}$ DEPT NMR (101 MHz, $CDCl_3$, 298 K) of VfcGE.

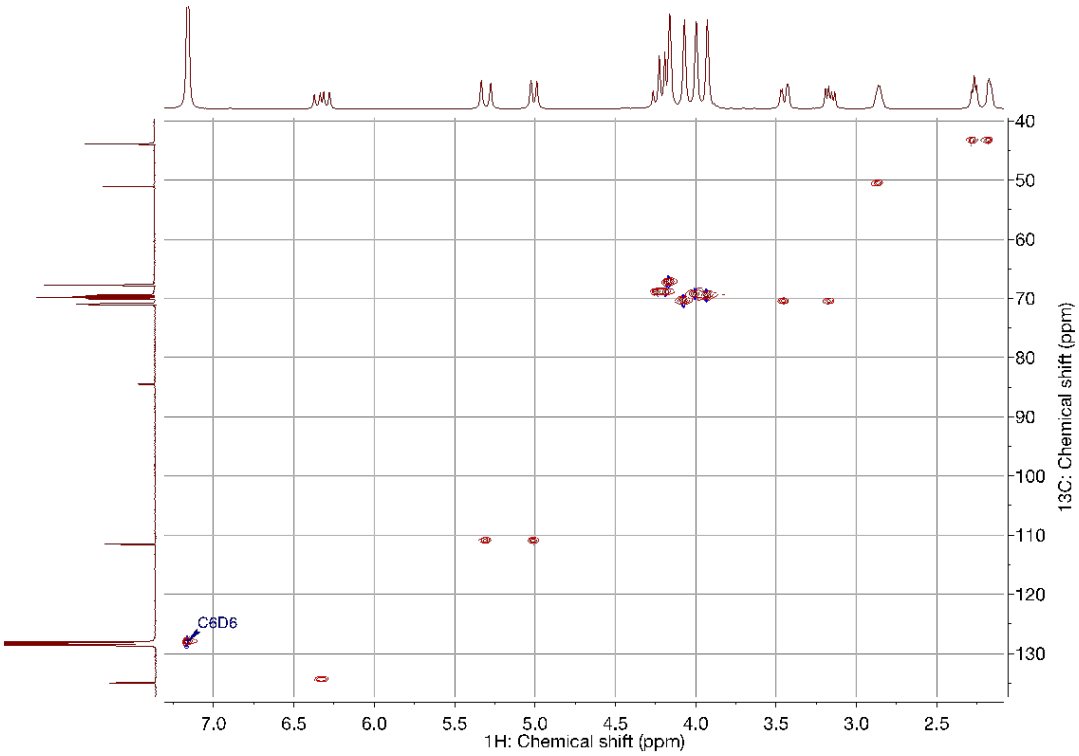

Figure S3. HSQC NMR (400 MHz, C_6D_6, 298 K) of VfcGE.

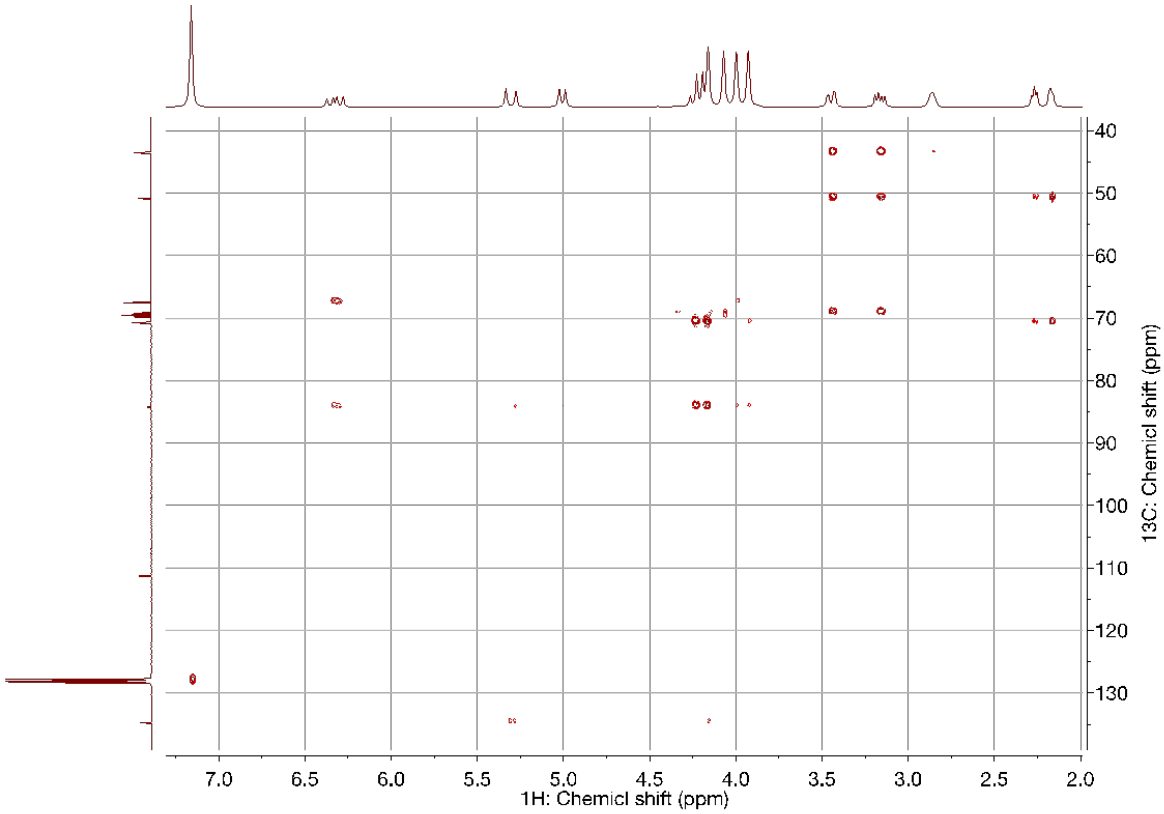

Figure S4. HMBC NMR (400 MHz, C_6D_6, 298 K) of VfcGE.

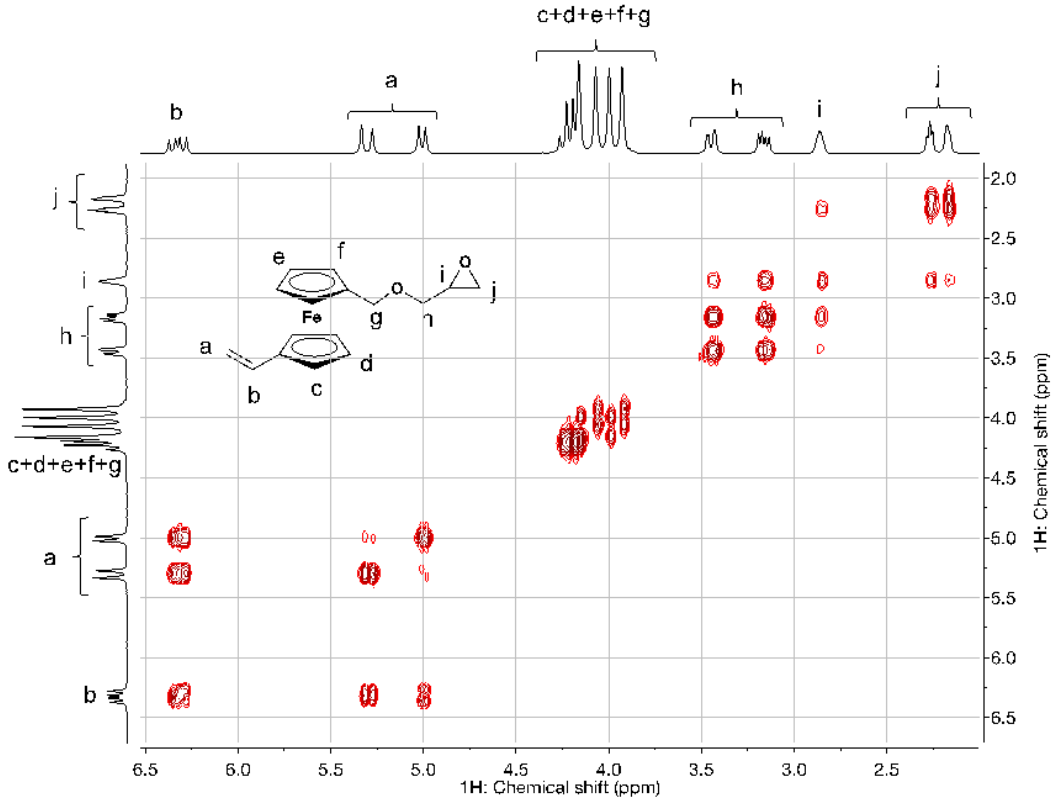

Figure S5. COSY NMR (400 MHz, C_6D_6, 298 K) of VfcGE.

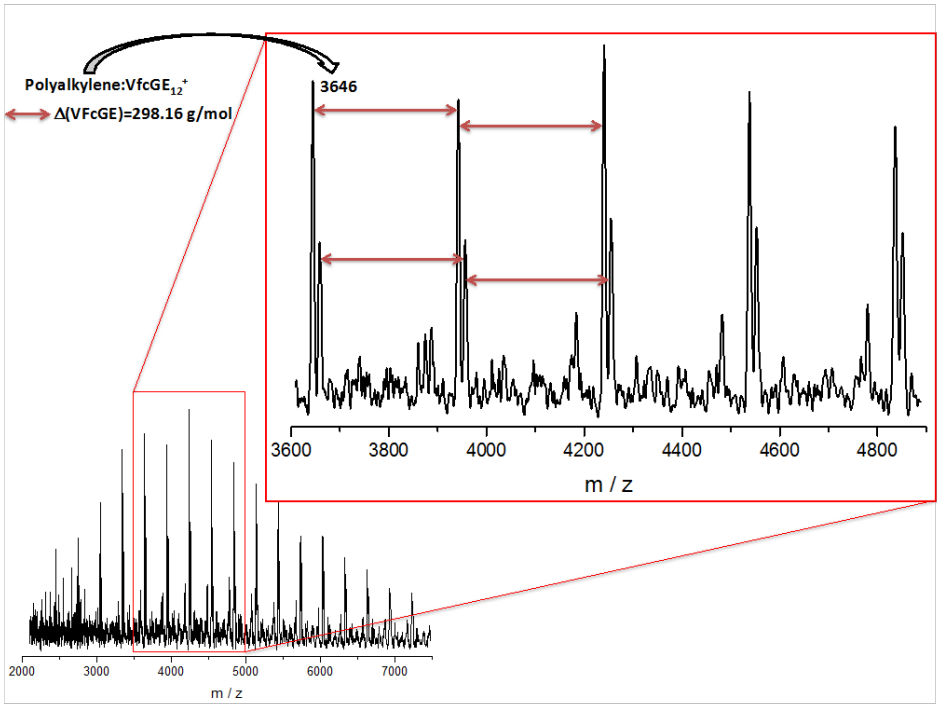

Figure S6. MALDI ToF mass spectrum of polyalkylene:VfcGE (**P1**) prepared by free radical polymerization.

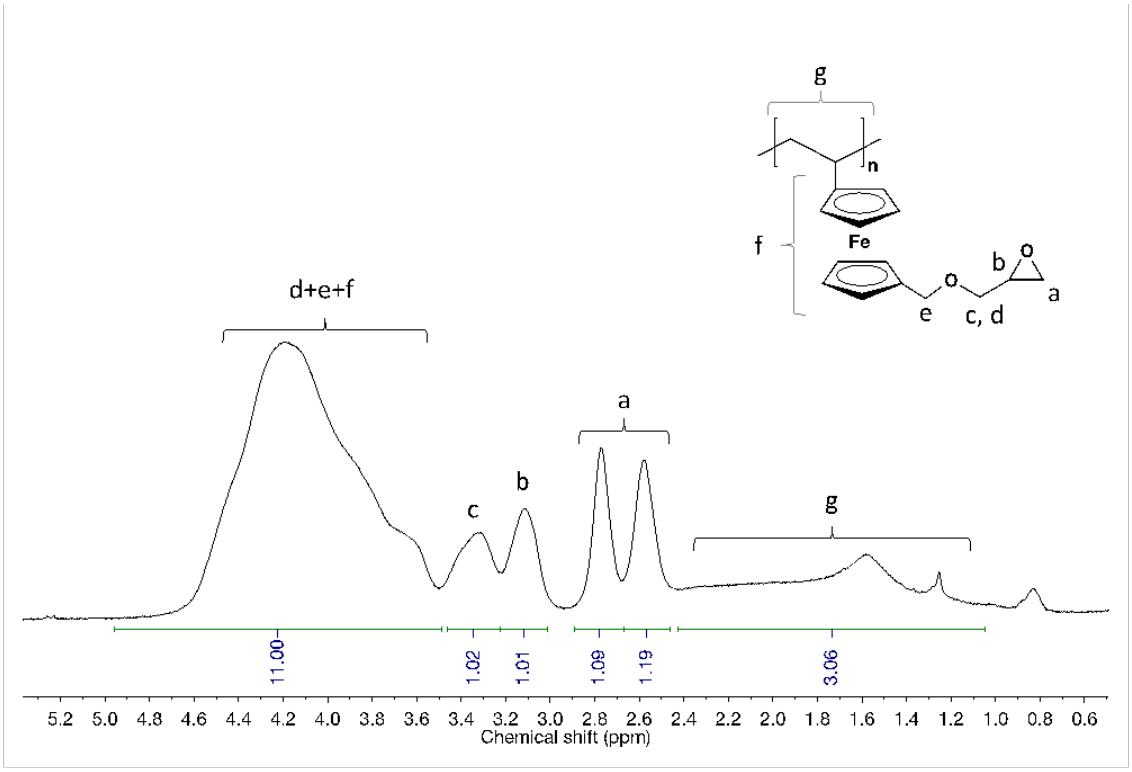

Figure S7. ^{1}H NMR (400 MHz, C_6D_6, 298 K): Peak assignment of polyalkylene:VfcGE (**P1)**.

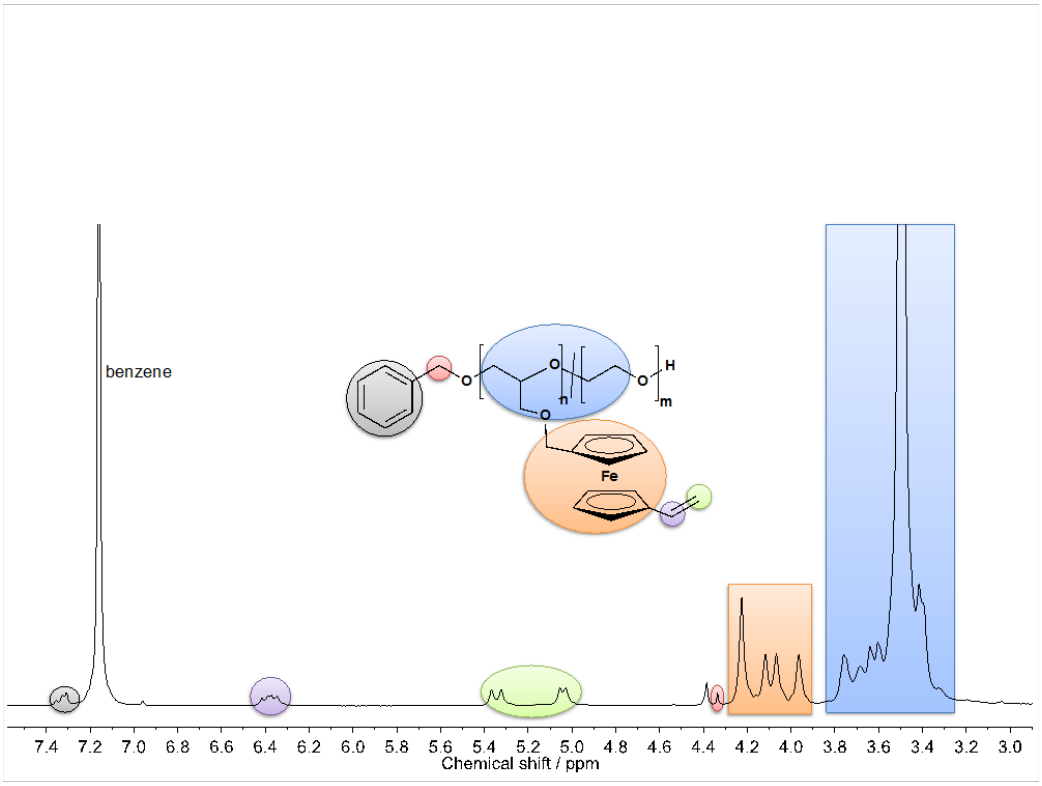

Figure S8. ^{1}H NMR (400 MHz, C_6D_6, 298 K): Peak assignment of P[EO-*co*-VfcGE] (**P2)**.

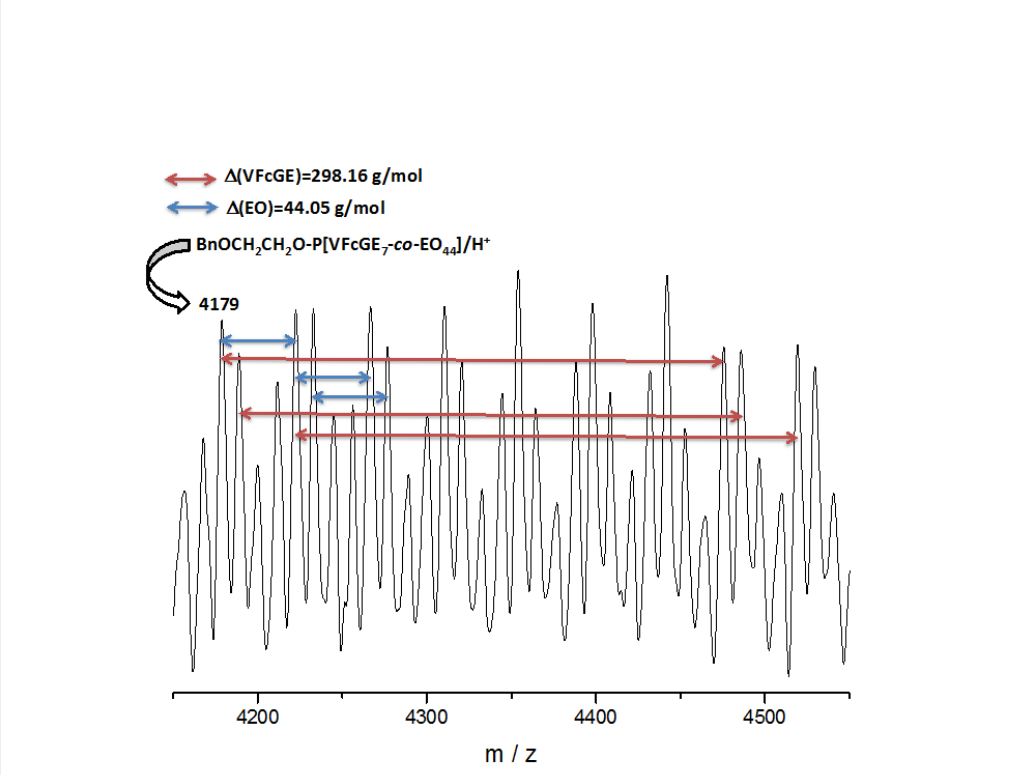

Figure S9. Zoom into the MALDI ToF mass spectrum of P[EO-*co*-VfcGE] (**P3**).

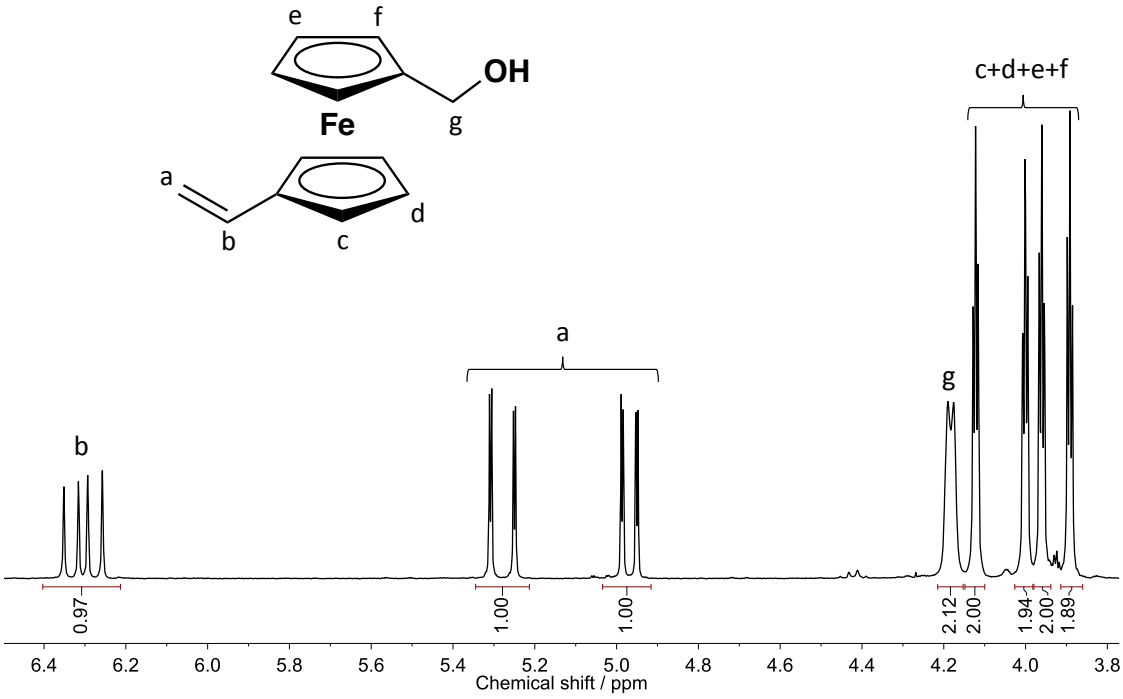

Figure S10. ^{1}H NMR (400 MHz, $CDCl_3$, 298 K) of 1-vinyl-1'-hydroxymethyl ferrocene (**6**).

2.3 Triple-Stimuli Responsive Ferrocene-Containing PEGs in Water and on Surface

Published in *ACS Appl. Mater. Interfaces* **2015**, 7, 26137-26144. (Published by the American Chemical Society.)

Authors: *Arda Alkan, Christian Steinmetz, Katharina Landfester, and Frederik R. Wurm*

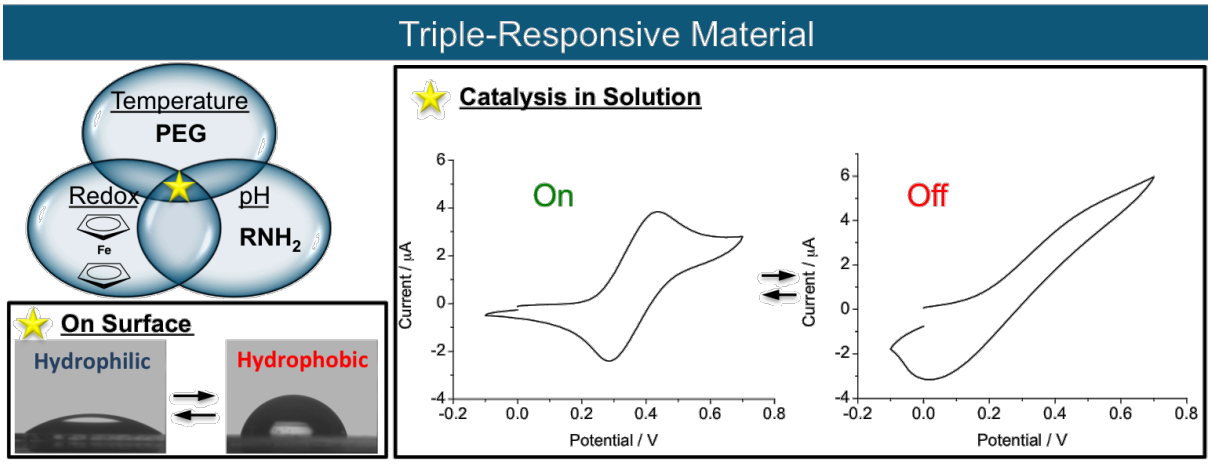

Abstract

Triple-stimuli responsive PEG-based materials are prepared by living anionic ring-opening copolymerization of ethylene oxide and vinyl ferrocenyl glycidyl ether and subsequent thiol-ene postpolymerization modification with cysteamine. The hydrophilicity of these materials can be tuned by three stimuli: i) temperature (depending on the comonomer ratio), ii) oxidation-state of iron centers in the ferrocene-moieties, iii) pH-value (through amino groups), both in aqueous solution and at the interface after covalent attachment to a glass surface. In such materials, the cloud point temperatures can be varied over a broad temperature range in solution by changing oxidation-state and/or pH. On surface, the contact angle increases with increasing pH, temperature and after oxidation, making these smart surfaces interesting for catalytic applications. Also, their redox-response can be switched by temperature and pH, making this material useful for catalysis and electrochemistry applications. Exemplarily, the temperature-dependent catalysis of the chemiluminescence of luminol (a typical blood analysis tool in forensics) was investigated with these polymers.

Introduction

Smart materials are compounds, which can change their properties depending on the environment.[168] Stimuli-responsive polymers, for example, can change their shape,[169] color,[111,170] conductivity,[171] or solubility[85,172] responding to an external stimulus like light,[173,174] a change in temperature,[175,176] or pH value.[177,178] Another interesting feature is redox-responsivity, which is far less studied than the other stimuli, but can be implemented via i) cleavable disulfide bridges[179] or by ii) reversible redox behavior of metallocene sandwich complexes, mostly ferrocene (fc), which can be oxidized reversibly to the hydrophilic ferrocenium cation.[109-17]

Polyethers, derived from ethylene oxide (EO) and hydrophobic comonomers exhibit thermal response in water over a broad temperature range, depending on the structure of the

comonomer and the molar fraction incorporated into the backbone.[85,158,160,180-20] Much more attention, however, was drawn to poly(*N*-isopropylacrylamide) (PNIPAM) that is available by radical polymerization and exhibits a lower critical solution temperature (LCST) near body temperature around 31-33 °C.[181,182] The LCST of PNIPAM can be affected by a few degrees,[183] while PEG copolymers allow a broad variation of the LCST from 0-100 °C (at 1 bar) depending on the copolymer composition.[180]

Besides the temperature-response, additional stimuli-responsive moieties can be built in a single polymer,[184] resulting in multi-stimuli responsive materials. A straightforward handle is to introduce carboxylates or amines that are responsive to changes in the pH value. Recently, Roberts and coworkers utilized a copolymer of NIPAM and acrylic acid for reversible control of electrochemical properties in water: the conductivity of an aqueous copolymer solution was measured at different temperatures, therefore cyclic voltammetry measurements were performed below and above the LCST.[171] The same polymer was also used as a pH buffer, whereas the pH value of the system is programmable via the temperature.[185] These dual-stimuli responsive copolymers show promising properties, combining pH and temperature responsiveness and build the basis for future all-rounder polymers combining several stimuli in one material. Materials combining the three different stimuli responsive triggers light, pH and temperature[186-188] or light, redox and temperature[189] are known to date. To the best of our knowledge, no material has been reported to date, which combines temperature, pH and redox responsiveness – especially both in solution and on surface.

Herein, ferrocene-containing polyethers are presented as the first triple-responsive organometallic materials, that combine i) thermo-, ii) pH-, and iii) redox-responsive behavior (Scheme 1).[190]

Scheme 1. Triple-stimuli responsive behavior of fc-containing polyethers after functionalization with cysteamine *in solution* and *on surface*.

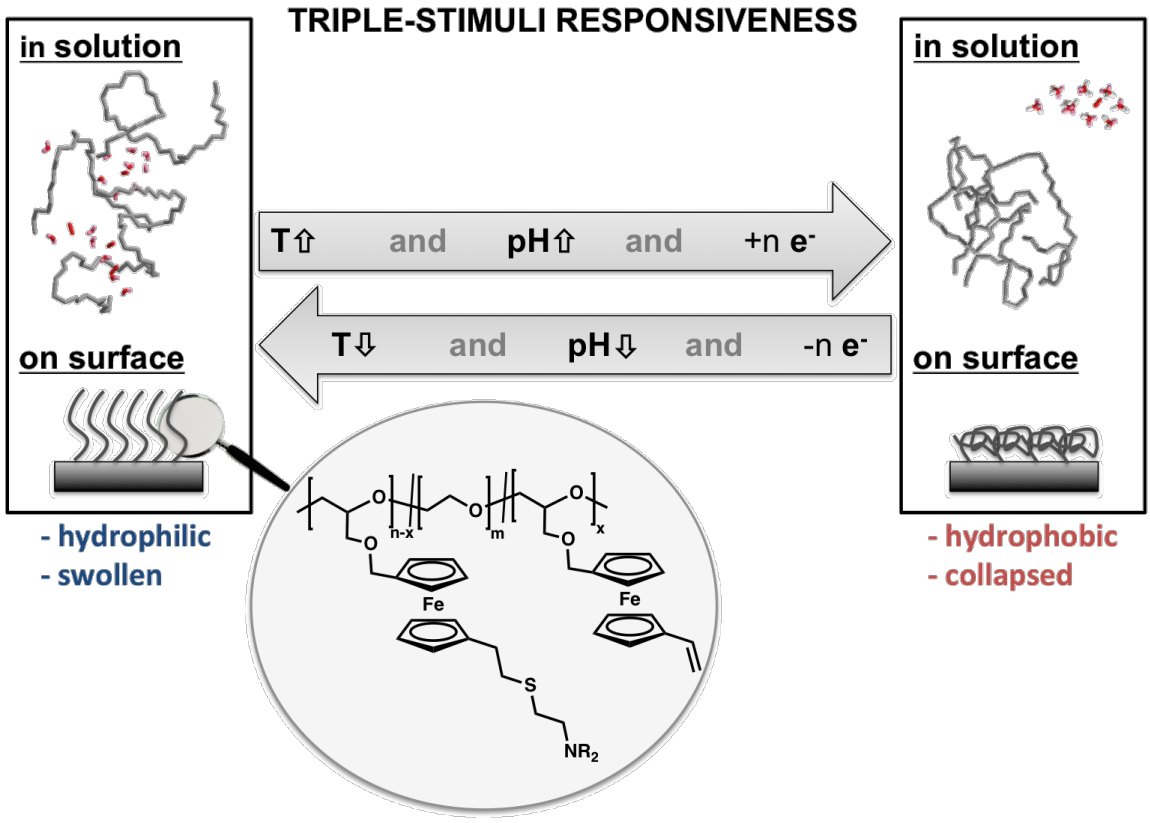

The copolymers (P[EO_x-*co*-$VfcGE_y$]) are prepared by anionic copolymerization of vinyl ferrocenyl glycidyl ether (VfcGE) and ethylene oxide (Scheme S1). The ferrocene units introduce both reversible redox-response (due to Fe(II)-Fe(III) redox pair) and temperature-response (due to the hydrophobicity of the VfcGE units) into the polymer. The pendant double bounds of the ferrocene units of P[EO-*co*-VfcGE] copolymers were post-modified via thiol-ene addition with cysteamine to introduce amine functionalities and thus an additional pH-response (Scheme 1 and Scheme S1). The post-modified copolymers carry, in addition to the hydrophobic fc-groups, also hydrophilic amino groups and thus exhibit higher cloud point temperatures (T_c) in aqueous solution compared to the non-functionalized P[EO-*co*-VfcGE]. Besides this stimuli-responsive behavior in water, the polymers were covalently fixed to benzophenone-modified glass surfaces by radical coupling. On surface, the same material allowed to control the hydrophilicity of the polymer layer by adjusting the pH-, temperature- or oxidation state.

Since ferrocene is used widely, e.g. in electrochemistry,[191] batteries,[192] sensing,[13,193,194] biology,[195,196] and catalysis,[197-200] many fields may benefit from such unique multi-stimuli responsive materials. For example, these new materials could be useful in catalysts or sensors, which operate within a defined temperature range depending on pH and oxidation state of fc or in a defined pH range depending on the temperature and oxidations state of fc.

Experimental Section

Instrumentation. ^{1}H NMR spectra (400 MHz) and ^{13}C NMR spectra (75.5 MHz) were recorded using a Bruker AMX400. All spectra were referenced internally to residual proton signals of the deuterated solvent. For SEC measurements in DMF (containing 0.25 g·L^{-1} of lithium bromide as an additive) an Agilent 1100 Series was used as an integrated instrument, including a PSS HEMA column (106/105/104 g·mol^{-1}), a UV detector (275 nm), and a RI detector at a flow rate of 1 mL·min^{-1} at 50 °C. Calibration was carried out using PEO standards provided by Polymer Standards Service. Cyclic voltammetry (CV) was carried out in a conventional three electrode cell using a WaveDriver 20 bipotentiostat (Pine Instrument Company, USA) and deionized water as solvent for polymer solutions with 5 g·L^{-1} concentration. No supporting electrolyte was used. A glassy carbon disk served as working electrode. Ag/AgCl and platinum wire were used as reference and counter electrodes, respectively. Turbidity measurements were performed in deionized water and observed by optical transmittance of a light beam (λ=500 nm; 50%) through a copolymer solution in water (5 mg/mL) in a quartz cuvette (1 cm). The transmission at the beginning of the measurement, when the copolymer is totally water-soluble, is normalized and set to 100%. The measurements were performed in a Jasco V-630 photospectrometer with a Jasco ETC-717 Peltier element. The intensity of the transmitted light was recorded versus the temperature of the sample cell. The heating rate was 1 °C·min^{-1}, and values were recorded every 0.1 °C. The luminol experiments were performed at the same spectrometer, detecting only the emission intensity at 450 nm.

Reagents. Solvents and reagents were purchased from Acros Organics, TCI or Sigma-Aldrich and used as received, unless otherwise stated. Chloroform-*d* and benzene-d_6 were purchased from Deutero GmbH. VfcGE was synthesized according to the published procedures.[89] VfcGE was dried by azeotropic distillation of benzene to remove traces of water. The general procedure for the copolymerization of VfcGE and EO to P[EO_{206}-*co*-$VfcGE_{10}$] copolymers (M_n(SEC) = 2 200 g·mol^{-1}; $Đ$=1.09; M_n(NMR)=12 300 g·mol^{-1}) is described in literature.[89] 4-(3'-chlorodimethylsilyl(propyoxybenzophenone) was synthesized according to literature.[89]

Polymer Modification via Thiol-Ene Addition. 100 mg of the P[EO_{206}-*co*-$VfcGE_{10}$] copolymer were dissolved in 5 mL THF and a 20-fold molar excess (138 mg; 1.79 mmol) of cysteamine and 0.75 eq. (13.9 mg; 0.0846 mmol) of AIBN with respect to the number of vinyl groups, were added. After three freeze-pump-thaw cycles (to remove any oxygen from the system) the reaction mixture was heated to 75 °C and stirred for 12 h. The reaction mixture was then precipitated into diethyl ether. Yield: 95%. ^{1}H NMR ($CDCl_3$, 400 MHz, 298 K): δ(ppm)=7.31 (m, 5H, aromatic protons of initiator), 4.33 (s, 2H, aliphatic signals of initiator), 4.29-3.91 (m, *fc*-C*H*$_2$-O), 3.85-3.10 (residual protons: PEO backbone, fc-CH_2-O-C*H*$_2$-backbone), 3.00-2.55 (m, fc-C*H*$_2$-C*H*$_2$-S-C*H*$_2$-C*H*$_2$-).

Chemiluminescence of Luminol. 0.2 g Luminol was suspended in 20 mL deionized water and a 2.5 M sodium hydroxide solution was added drop-wise until luminol was fully dissolved. 2 mL of the luminol solution were transferred to a 1 cm quartz cuvette. 2 mg copolymer was dissolved in 0.2 mL hydrogen peroxide solution (30%). This oxidizing solution was injected via syringe to the cuvette and the chemiluminescence intensity at 450 nm was recorded.

Surface Functionalization. For covalent attachment of the copolymers, glass surfaces were purified via UV-ozone surface treatment and were functionalized with 4-(3'-chlorodimethylsilyl(propyoxybenzophenone), which was synthesized according to literature (Scheme S3).[201] A clean glass surface is wetted with a dry solution of 4-(3'-chlorodimethylsilyl(propyoxybenzophenone) in toluene with catalytic amounts of

triethylamine and was left standing over night under an argon atmosphere. After washing, the triple stimuli-responsive copolymers were than spin-coated from a toluene solution on the functionalized surfaces and dried at reduced pressure. The samples were irradiated with a UV-A/B lamp for 4 hours to link the polymers to the surface (Scheme 2). The height profiles of the modified glass surfaces were analyzed with a contact profilometer (see Results and Discussion).

Results and Discussion

Functionalization of P[VfcGE-*co*-EO] Copolymers to Multi Stimuli-Responsive Copolymers

Our group recently introduced the first ferrocene-containing epoxide monomer, namely ferrocenyl glycidyl ether (fcGE) and we were able to show that copolymers with ethylene oxide (EO) show adjustable cloud point temperatures depending on the molar ratio between fcGE and EO.[85] Very recently, we presented a bifunctional monomer, namely VfcGE, that produces polyfunctional poly(vinyl ferrocenyl glycidyl ether-*co*-ethylene oxide) copolymers (P[VfcGE-*co*-EO]), also exhibiting thermo- and redox-responsive behavior.[89] Herein, the pendant vinyl groups were further functionalized with amines to introduce pH responsiveness as an additional, third stimulus (Scheme 1 and Scheme S1) and to attach such polymers to surfaces via radical crosslinking (*see below*).

Thiol-ene addition is often used for polymer post-modification reactions, since high conversions can be achieved.[162,202] This technique was used to modify the pendant vinyl groups in the P[VfcGE-*co*-EO] copolymers to introduce pendant amines. Amines have to be inserted in a post-polymerization reaction as they would not sustain the conditions of an anionic polymerization.

The vinyl groups in P[$VfcGE_{10}$-*co*-EO_{206}] (M_n(NMR)=12 300 g·mol^{-1}) were successfully post-modified via radical thiol-ene addition with cysteamine using azobisisobutyronitrile (AIBN) as the initiator at 80 °C in THF. The ^{1}H NMR spectra of the P[VfcGE-*co*-EO] copolymers prior to and after functionalization with cysteamine are compared in Figure S1: the resonances for

the vinyl groups (between 6.5 and 5.0 ppm) are reduced after the reaction, whereas the new signals for cysteamine and the ethylene bridge between the fc unit and sulfur center appear (between 3.2 and 2.5 ppm). The degree of functionalization was calculated to be 90-95% under these conditions, i.e. 9 amine groups per polymer are available after functionalization, i.e P[VfcGE$_1$-*ran*-CAfcGE$_9$-*co*-EO$_{206}$] (the "CA" indicates the repeating units modified with cysteamine).

pH-Control of Cloud Point Temperatures

After modification of the fc-containing PEG-copolymers with cysteamine, the toolbox for the variation of the cloud point temperature is enlarged: not only the comonomer:EO ratio determines the cloud point temperature, but in addition, the same composition exhibits tunable cloud points depending on the pH-values due to protonation/deprotonation of the pendant amines. The cloud point temperatures of the amino-modified P[VfcGE$_1$-*ran*-CAfcGE$_9$-*co*-EO$_{206}$] were measured at different pH-values in order to prove the additional pH responsiveness of the copolymer (Figure S2). The temperature-dependent transmission of a light beam (500 nm) through a copolymer solution in water (5 mg/mL) is measured. When reaching the cloud point temperature, the copolymer precipitates and the transmission of the light beam drops to a lower transmission value of around 5 to 10%. The cloud point temperatures can be shifted from 30 °C (pH=12.0), over 36 °C (pH=8.5), to 61 °C (pH=7.0). At lower pH values the polymer becomes too hydrophilic and is soluble over the whole temperature range.

Temperature Switch of the Redox-Activity (at a certain pH)

The temperature-dependent solubility of the fc-containing copolymers in water is utilized as a switch for the redox-activity: if the polymer is soluble in water, a redox-response of fc can be measured by cyclic voltammetry ("switch on" = below the cloud point); if the polymer is

precipitated, no redox-response can be obtained from ferrocene ("switch off" = above the cloud point). Cyclic voltammograms were recorded by applying a cyclic potential in water without adding conducting salt (Figure 1, at constant pH=8.5, T_c=36 °C), since the amine functionalities are partially protonated in water and generate enough ions to measure the conductivity.

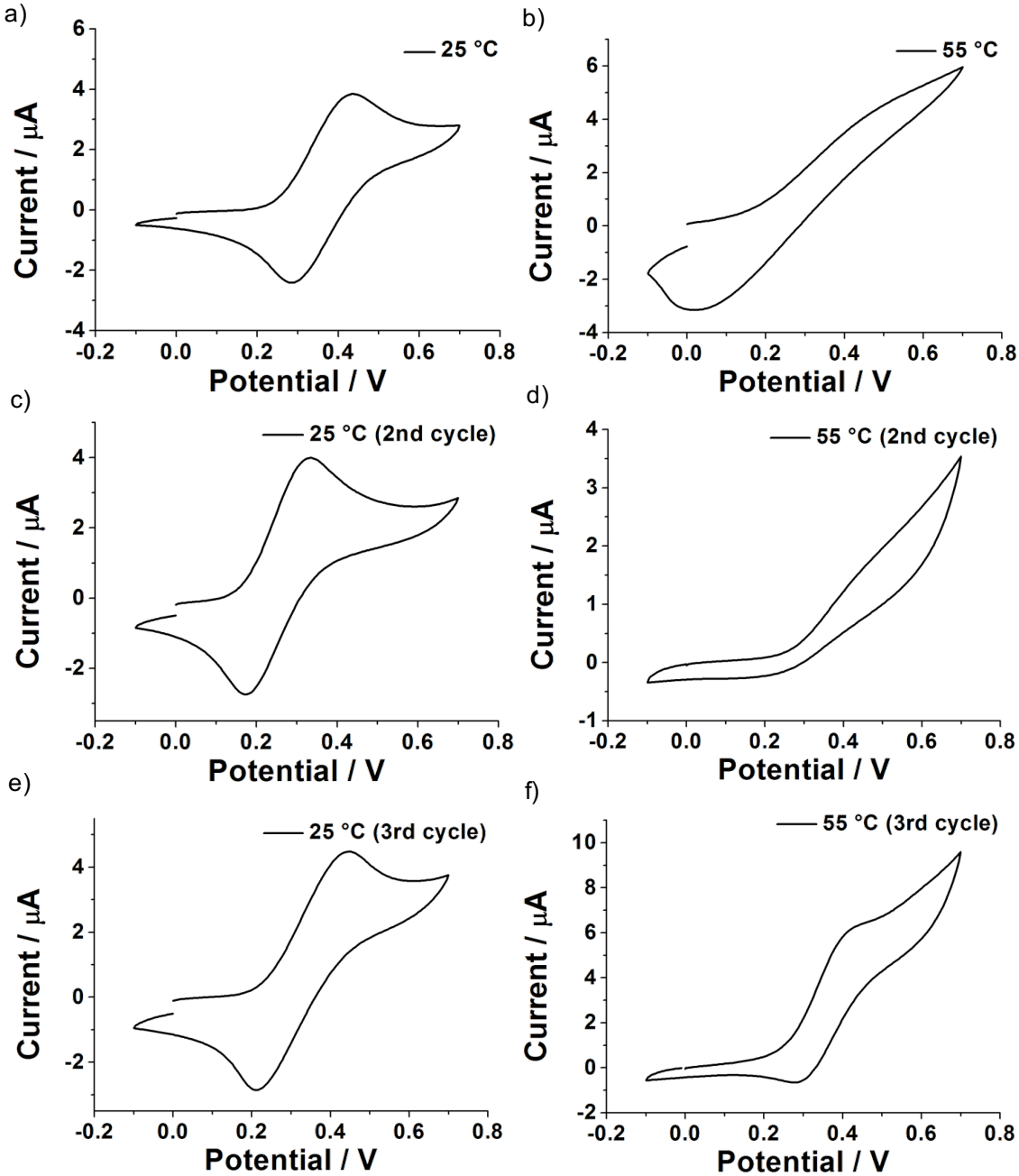

Figure 1. Cyclic voltammograms of P[VfcGE$_1$-*ran*-CAfcGE$_9$-*co*-EO$_{206}$] copolymer below the cloud point temperature (T_c) at 25 °C (Figure 1 a, c and e) and above the T_c at 55 °C (Figure 1 b, d and f) at pH=8.5 (three cycles).

The cyclic voltammogram below the cloud point temperature at 25 °C shows an oxidation and reduction signal of the fc moieties (a), as the polymer is fully soluble. The voltammogram is symmetrical, which indicates the reversibility of the oxidation process. This demonstrates the high redox-activity of fc in the polyether side-chains as well as the stability under these conditions. Above the cloud point temperature at 55 °C the polymer forms bigger aggregates and precipitates, so that no oxidizing and reducing signals can be observed for the fc units (b). The reversibility of the "on" and "off" states were proven by three cycles. The temperature was lowered again and a cyclic voltammogram of the totally dissolved polymer was recorded at 25 °C (c) with the response of fc. After heating to 55 °C, the redox-response disappears again (d). This procedure was repeated for another cycle, which is shown in e) and f) with no detectable difference.

Temperature-Dependent Catalysis of Luminol's Chemiluminescence

This temperature dependent redox-activity of the copolymer is utilized for the temperature dependent catalysis of luminol's (3-aminophthalhydrazide) chemiluminescence (Figure 2 and Scheme S2). Luminol is used by forensic investigators to detect traces of blood, particularly iron(II), which is fixed in hemoglobin. For this test, luminol is dissolved in water under basic conditions (pH ca. 10) and then reacts with an appropriate oxidizing agent. The oxidation of luminol proceeds under emission of a distinct chemiluminescence. The chemiluminescence intensity is typically rather low, if no catalyst is added. However, even in the presence of only traces of Fe acting as catalyst, e.g. from blood, a very strong chemiluminescence is detectable.[203] Herein this sensitive chemiluminescence of luminol is used to demonstrate the usage of the P[VfcGE$_1$-*ran*-CAfcGE$_{13}$-*co*-EO$_{75}$] copolymer as a temperature-dependent catalyst. The polymeric catalyst (P[VfcGE$_1$-*ran*-CAfcGE$_{13}$-*co*-EO$_{75}$]) is dissolved in water with hydrogen peroxide and added to luminol. The cloud point temperature of the polymer under those conditions is ca. 25 °C. The intensity of the emitted light is detected at two different temperatures over time: at 21 °C (below the T_c) the detected chemiluminescence is about

five times higher as compared to the same experiment at 28 °C, which lies above the T_c (Figure 2 and S3).

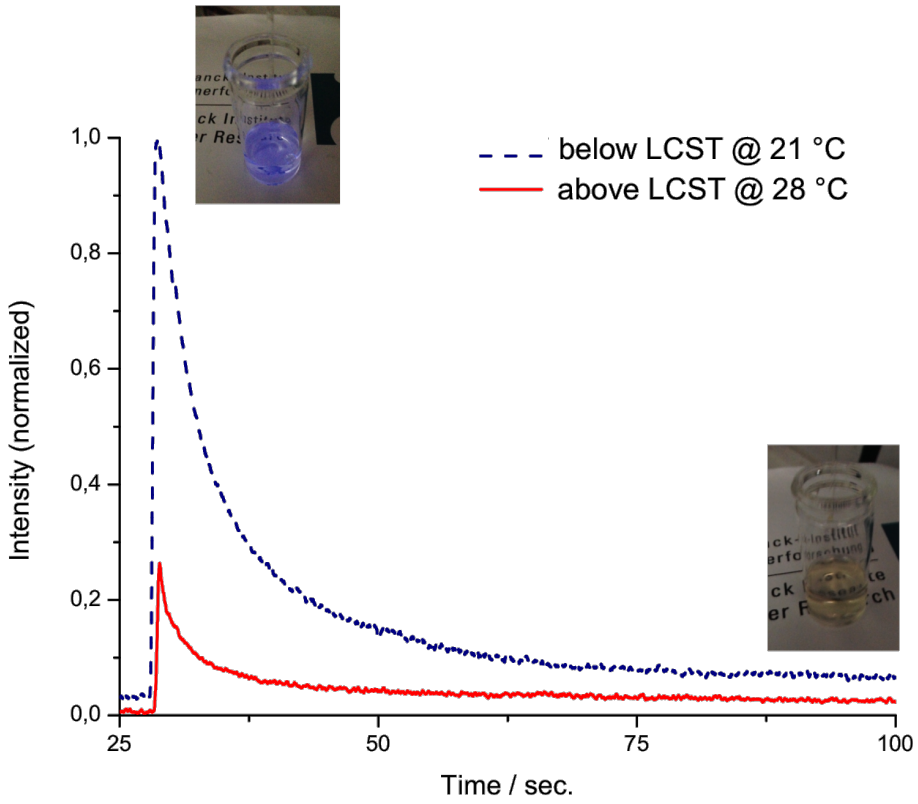

Figure 2. Chemiluminescence of luminol after the addition hydrogen peroxide in the presence of the functionalized copolymer at 21 °C (below T_c) and 28 °C (above T_c).

As the polymer is completely dissolved below the T_c, it can catalyze the reaction as expected for an Fe(II) species ("switch on"). If the temperature is increased above the copolymer's cloud point temperature, a strong decrease of both the chemiluminescence intensity and half-life time is detected, since the polymeric catalyst is "switched off", i.e. precipitated, proving that the efficiency of the catalytic properties of the iron(II) centers are strongly influenced by the solubility of the copolymer.

pH Switch of the Redox-Activity (at a Certain Temperature)

P[VfcGE$_1$-*ran*-CAfcGE$_{13}$-*co*-EO$_{75}$] was utilized to switch ferrocene's redox-activity by the variation of the pH value at a certain temperature. The aqueous solution of P[VfcGE$_1$-*ran*-CAfcGE$_{13}$-*co*-EO$_{75}$] was analyzed by cyclic voltammetry at three different pH values (pH 6, 7 and 8 at constant temperature of 25 °C). The cyclic voltammogram of the copolymer solution at pH 6, at which the copolymer is completely soluble, since the amine groups are partially protonated, shows a clear redox-response of ferrocene and a reversible oxidation of fc to ferrocenium ("switch on", Figure 3).

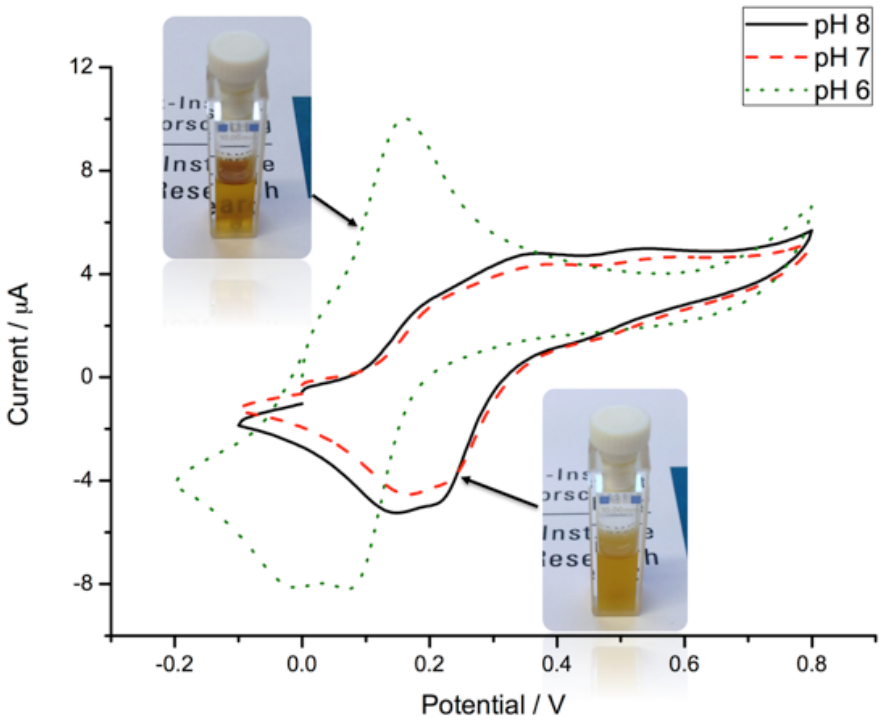

Figure 3. Cyclic voltammogram of cysteamine-functionalized P[VfcGE$_1$-*ran*-CAfcGE$_{13}$-*co*-EO$_{75}$] copolymer at 25 °C at three different pH values, whereas only below pH 6 the copolymer is totally water-soluble and precipitates above pH 7.

It is also noticeable that, the reduction peak splits in two signals, leading to the conclusion, that consecutive reactions occur at the iron centers, causing partial decomposition at this pH.[204] In the cyclic voltammograms at pH 7 and 8 the oxidation signal is strongly decreased

("switch off") and instead an uneven, flattened curve is measured. The reduction peak is comparable to the one, measured at pH 6, but the measured negative current is much lower. The reason for appearance of such a reduction peak is that low amounts of copolymers with oxidized ferrocenium species are still present and dissolved in the polymer solution. With increasing amount of ferrocenium species (fc^+) the polymer become more hydrophilic and finally totally water-soluble as a polycation. This pH-dependent switching of the redox-activity in a physiological relevant regime might be of potential use for future nanoparticular drug delivery or diagnostic vehicles, which is currently under investigation in our group.

On Surface Stimuli-Response

The triple stimuli-responsive copolymers are covalently linked to a glass surface to generate multi stimuli-responsive polymer films and to enable pH- and temperature-dependent electrocatalysis reactions *on surface*.

To allow covalent binding of the copolymers, glass surfaces were functionalized with 4-(3'-chlorodimethylsilyl(propyoxybenzophenone) (Scheme S3) and the triple stimuli-responsive copolymers were than spin-coated on the functionalized surfaces. The samples were irradiated with a UV-A/B lamp to link the polymers to the surface (Scheme 2).[201] The height profiles of the modified glass surfaces were analyzed with a contact profilometer (Figure S4; Topographic pictures of two glass surfaces modified with polymer P[VfcGE$_1$-*ran*-CAfcGE$_6$-*co*-EO$_{115}$] are shown in Figure S5). The film thicknesses of covalently bound P[VfcGE$_1$-*ran*-CAfcGE$_6$-*co*-EO$_{115}$] were determined to be 20.1±3.3 nm (surface 1, Figure S4a) and 19.3±2.9 nm (surface 2 , Figure S4b), respectively, with homogenous roughness of less than 16%.

Scheme 2. Schematic representation of polymer film formation (Covalent linkage of P[VfcGE$_1$-*ran*-CAfcGE$_9$-*co*-EO$_{206}$] to the modified glass surface).

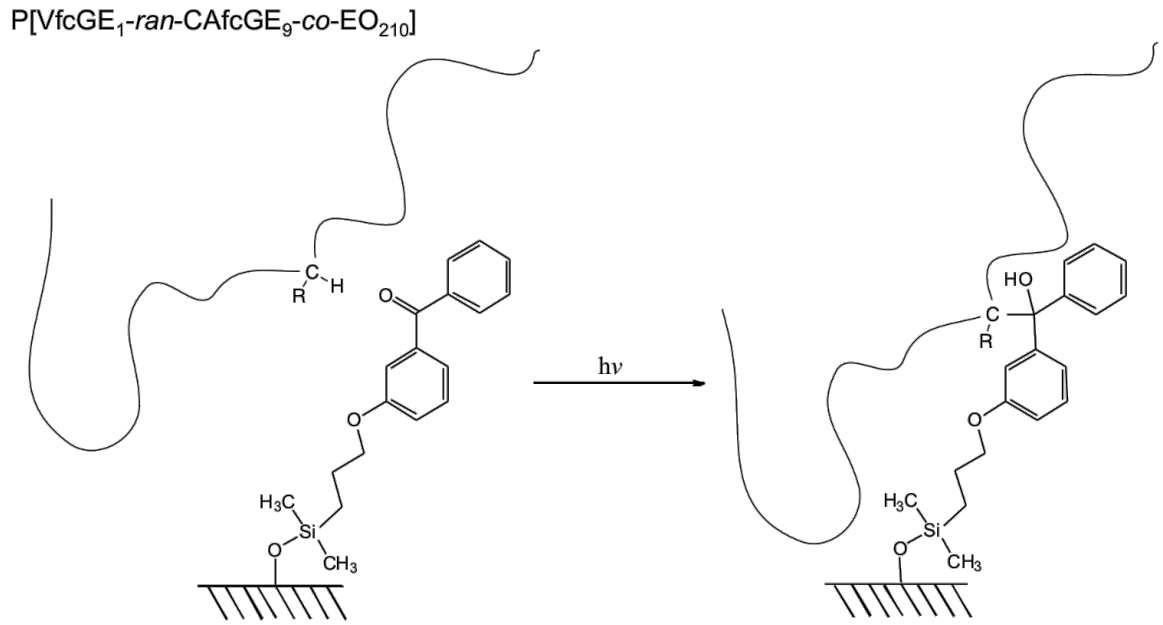

The copolymer P[VfcGE$_1$-*ran*-CAVfcGE$_6$-*co*-EO$_{115}$] exhibited a cloud point at 33 °C at pH 7.0 in solution. After surface-attachment the stimuli-responsive behavior of the polymer films were analyzed by contact angle measurements, which were performed at various temperatures, pH-values and after oxidation/ reduction (Fe(II) or Fe(III)).

Temperature-Dependent Contact Angle Measurements

The polymer-modified glass surfaces were placed on a furnace and after equilibration 3 µL of water was dropped on the sample; the contact angles were determined in the temperature range from 10 to 70 °C (Figure 4a). Two reference samples were also measured, which were not modified after the UV-ozone treatment. For the reference surfaces the determined contact angles follow the Eötvös rule, which, briefly explained, describes the almost linear decay of the surface tension of a liquid on a surface with increasing temperature.[205] For the polymer modified surfaces this behavior is superimposed with the change in hydrophilicity over temperature (T_c), i.e. the contact angles (ϑ) stay rather constant (up to 30-40 °C), which

indicates that the Eötvös rule is leveled by the temperature responsive polymer that becomes more and more hydrophobic. However, above temperatures of 40 °C the contact angles increase significantly from initially ϑ=51-54° (up to 40 °C) to ϑ=76-81° (at 70 °C, also compare Figure 4d, which shows a picture of the reference glass surface (taken during contact angle measurements with a water droplet at 70 °C and Figure 4e, where surface 1 at 70 °C shows a more hydrophobic surface).

pH-Dependent Contact Angle Measurements

The pH-dependency of the polymer-modified surfaces were measured at constant temperature (20 °C) applying 3 µL of an aqueous solution at a certain pH-value (pH=5, 7 and 9) and compared to the control surface (Figure 4b). Both polymer-modified surfaces show higher contact angles, thus become hydrophobic, with increasing pH-values (Figure 4b): At pH 5.0 and 7.0 the amine groups are partially protonated, which increases the hydrophilicity of the polymer on the glass surfaces, resulting in contact angles of ϑ=47-50° (pH=5) similar to the reference. At pH=7.0 both polymer-modified surfaces show a slight increase in the contact angle to the same degree as the reference (ϑ=50-55°), however at pH=9.0 with the ammonium groups being deprotonated, a strong increase of the contact angles of up to ϑ=75° for the polymer-modified surfaces is observed, which indicates a more hydrophobic surface, whereas the reference remains rather unchanged (ϑ=42°).

Oxidation-Dependent Contact Angle Measurements

The film thicknesses of covalently bound P[VfcGE$_7$-*co*-EO$_{115}$] were determined to be 35.8±6.7 nm (surface 1) and 48.3±5.3 nm (surface 2). The redox-activity of P[VfcGE$_7$-*co*-EO$_{115}$] @ surface 1 and 2 were analyzed by reversible oxidation of the surfaces prior to the contact angle measurements (Figure 4c). The contact angles of the polymer-modified surfaces before oxidation (at 20 °C) were determined to be similar to the reference surface (ϑ>50°).

Treating the polymer film with an aqueous hydrogen peroxide solution oxidizes ferrocene to the hydrophilic ferrocenium cation [Fe(II) → Fe(III)] resulting in a reduction of the contact angle to $\vartheta \approx 40°$. For subsequent reduction, the samples were treated with sodium ascorbate to reduce the ferrocenium cation back to the uncharged ferrocene with again an increase of the contact angle to the starting value of $\vartheta > 50°$.

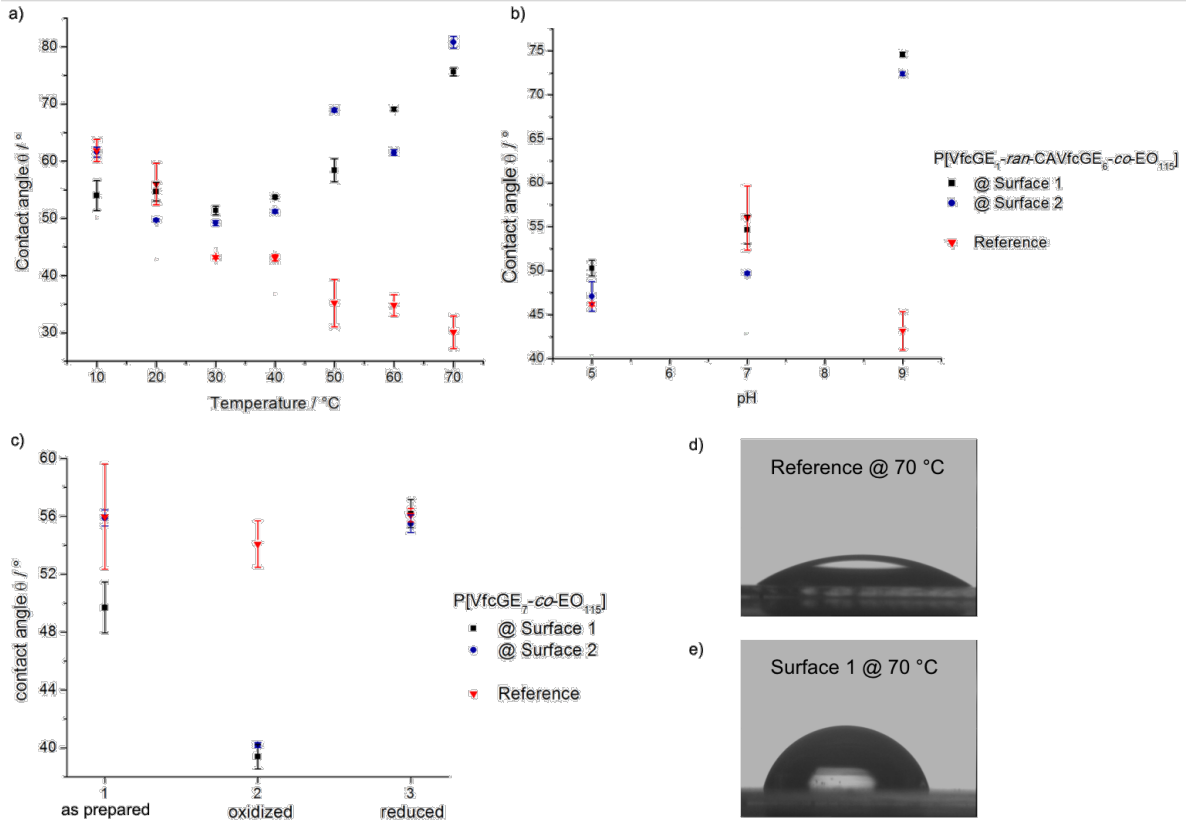

Figure 4. Contact angles of polymer-modified glass surfaces (black squares and blue circles; compared to the unmodified glass surface as a reference, red triangles) at different condition: a) P[VfcGE$_1$-*ran*-CAVfcGE$_6$-*co*-EO$_{115}$]-modified glass surface: temperature-dependency; b) P[VfcGE$_1$-*ran*-CAVfcGE$_6$-*co*-EO$_{115}$]-modified glass surface: pH-dependency; c) P[VfcGE$_7$-*co*-EO$_{115}$]-modified glass surface: oxidation-state dependency; d) picture of a water droplet on the glass reference sample at 70 °C; e) picture of a water droplet on surface 1 at 70 °C.

Conclusion

In summary, we have synthesized the first triple-stimuli responsive organometallic polymer exhibiting pH-, temperature-, and redox-response. These PEG-based copolymers are composed of a randomly distributed amino-functionalized ferrocene-comonomer within an ethylene oxide chain, that undergo phase transitions in solution or after covalent modification of glass surfaces. For the first time, thermo- and pH-responsive behavior is combined with the redox-activity of ferrocene, resulting in a temperature- and pH-dependent control of the redox activity of the system ("on and off" switch of the redox-active state).

By variation of the pH-value, a single copolymer exhibits different cloud point temperatures from 30 °C up to 61 °C. In addition, this pH-dependent cloud point can be utilized to control the redox response of the polymer solutions: at a certain pH, redox activity can be switched by temperature variation: above the cloud point, the polymer is agglomerated and the fc-species cannot be detected by cyclic voltammetry. As soon as the temperature decreases below the cloud point, a strong redox signal can be recorded. This tool allows us to use these materials also as temperature-dependent catalyst. We chose the chemiluminescent oxidation of luminol as an example: only if the polymer is below its cloud point temperature (LCST), i.e. dissolved, a strong chemiluminescence is detectable. A much weaker chemiluminescence is detectable above the cloud point temperature of the copolymer. After covalent attachment to glass surfaces, this temperature-response allow to switch from hydrophilic surfaces at low temperature to hydrophobic surfaces at temperatures above 40 °C.

In addition to temperature, the redox-activity can be controlled by the variation of the pH (at a constant temperature). This allows developing pH-sensors based on ferrocene's redox activity. Polymer films can also be switched from hydrophilic (at low pH) to hydrophobic (at high pH). Herein, we adjusted the pH switch to occur in physiological relevant regime between pH 6 and 7 (switched off below pH 7, switched on above pH 7), which may be interesting for future drug delivery or diagnostic carriers as the intracellular pH-value is with

a pH of 6-6.5 in many cells slightly lower than the extracellular environment, if specific cell targeting to e.g. tumor cells is achieved, for example.

We are currently working on drug delivery systems with selective and triple triggered release. Also, these triple-responsive materials could find use in electrochemical reactions, in which fc act as catalyst. Therefore, it could also serve as mediator in sensors, which operate at certain temperatures and pH regions.

2.3.1 Supporting Information

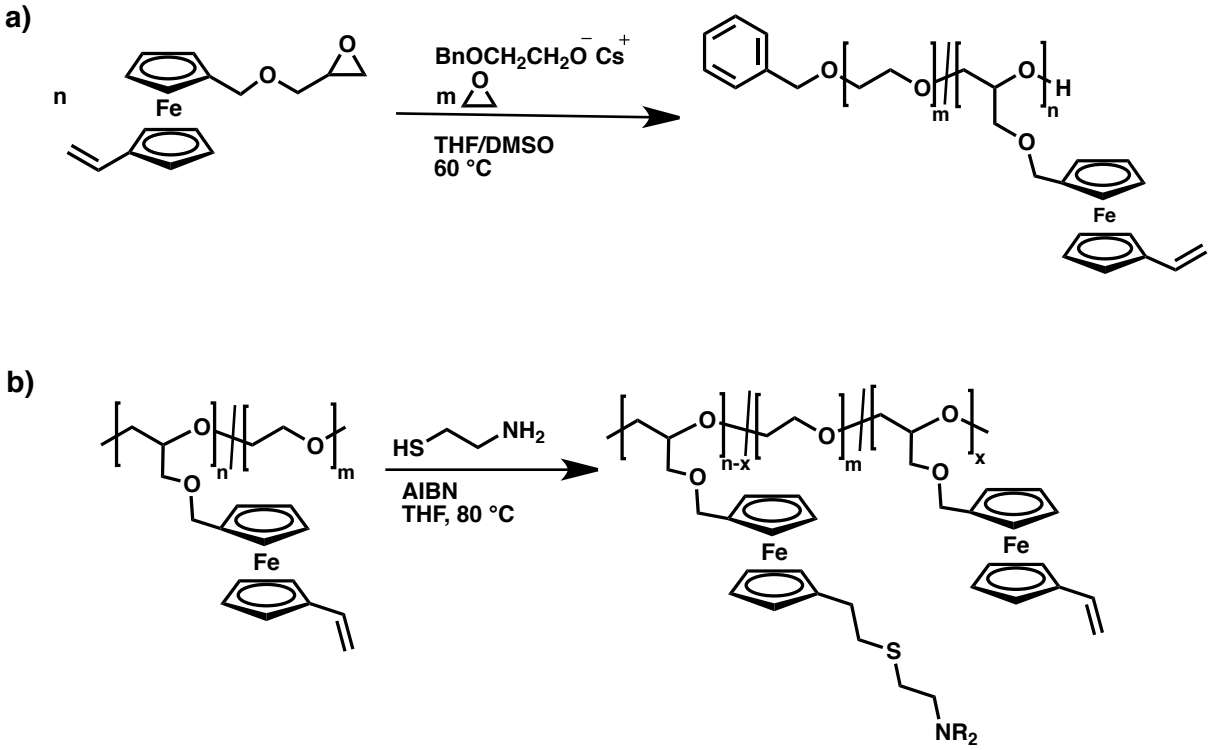

Scheme S1. Synthetic strategy of P[VfcGE$_1$-*ran*-CAfcGE$_9$-*co*-EO$_{206}$]. a) Anionic ring-opening copolymerization of EO and VfcGE. b) Thiol-ene addtition of cysteamine with available vinyl groups in P[VfcGE$_{10}$-*co*-EO$_{206}$].

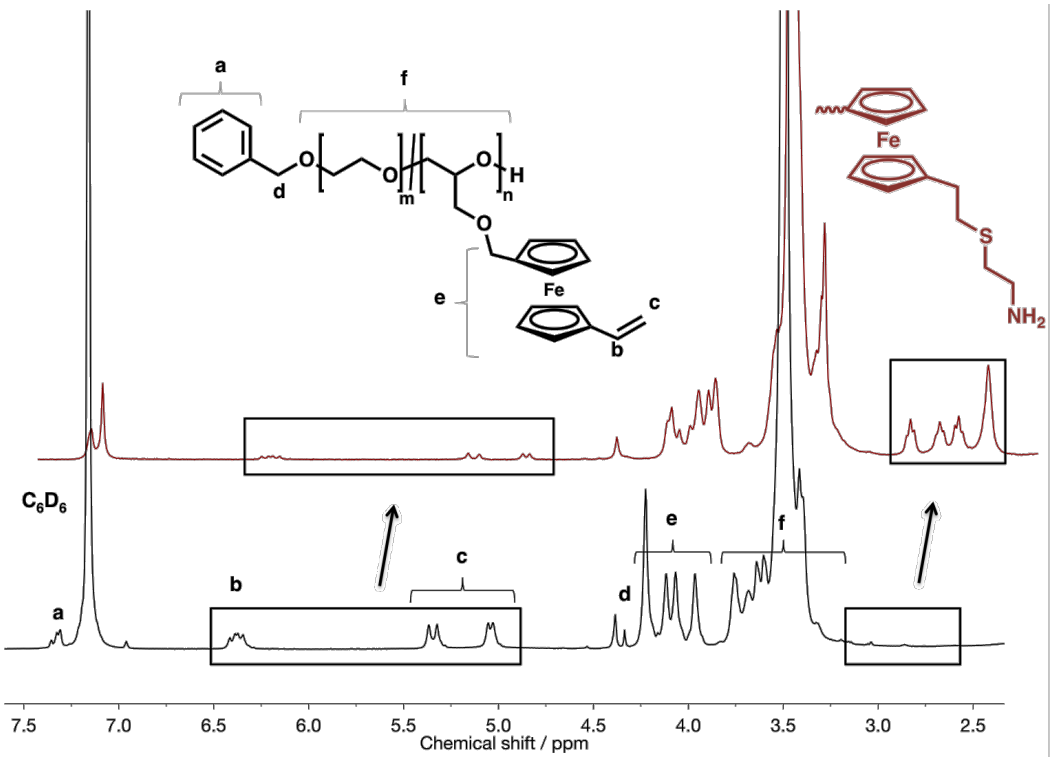

Figure S1. Functionalization of P[VFcGE$_{10}$-*co*-EO$_{206}$] copolymer with cysteamine followed by ^{1}H NMR (C_6D_6, 400 MHz, 298 K).

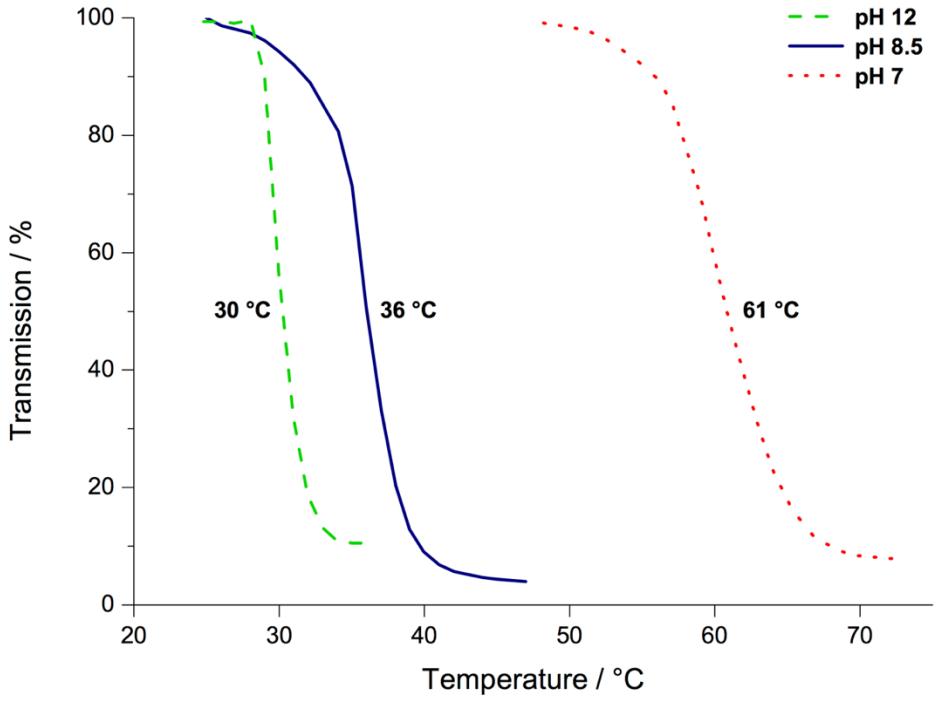

Figure S2. Turbidity measurements (heating curves) of P[VFcGE$_1$-*ran*-CAfcGE$_9$-*co*-EO$_{206}$] copolymer (λ=500 nm; heat rate=1 °C/min) at three different pH values (pH 12.0, 8.5 and 7.0).

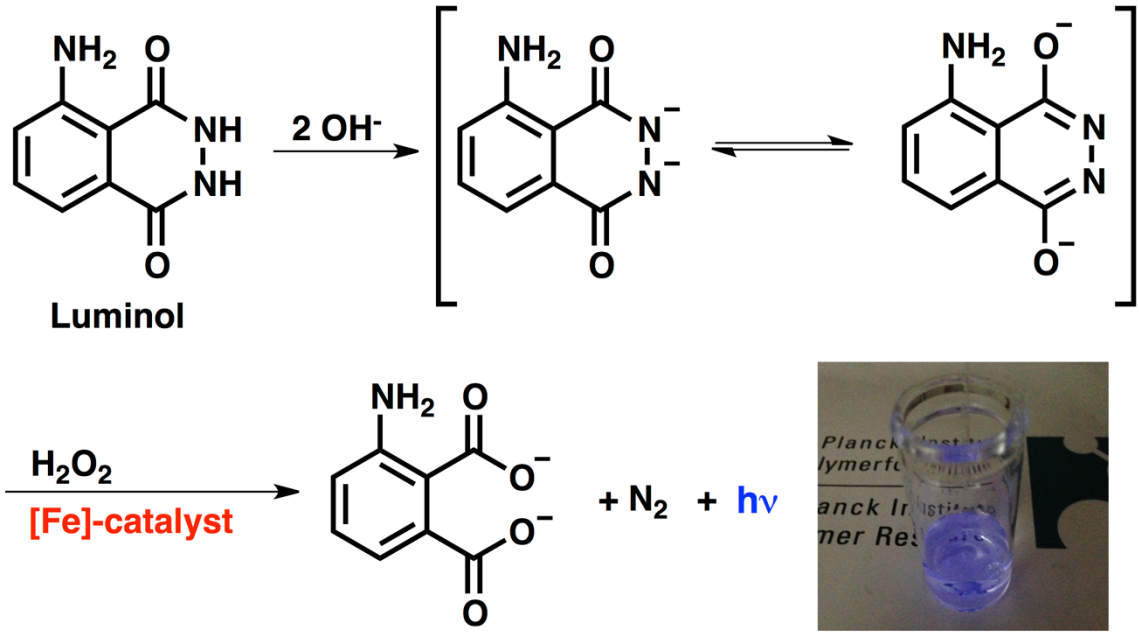

Scheme S2. The chemiluminescence of luminol under basic conditions using hydrogen peroxide as oxidizing agent and iron (Fe) as catalyst. The photo shows the color of the chemiluminescence of the polymer solution below the T_c.

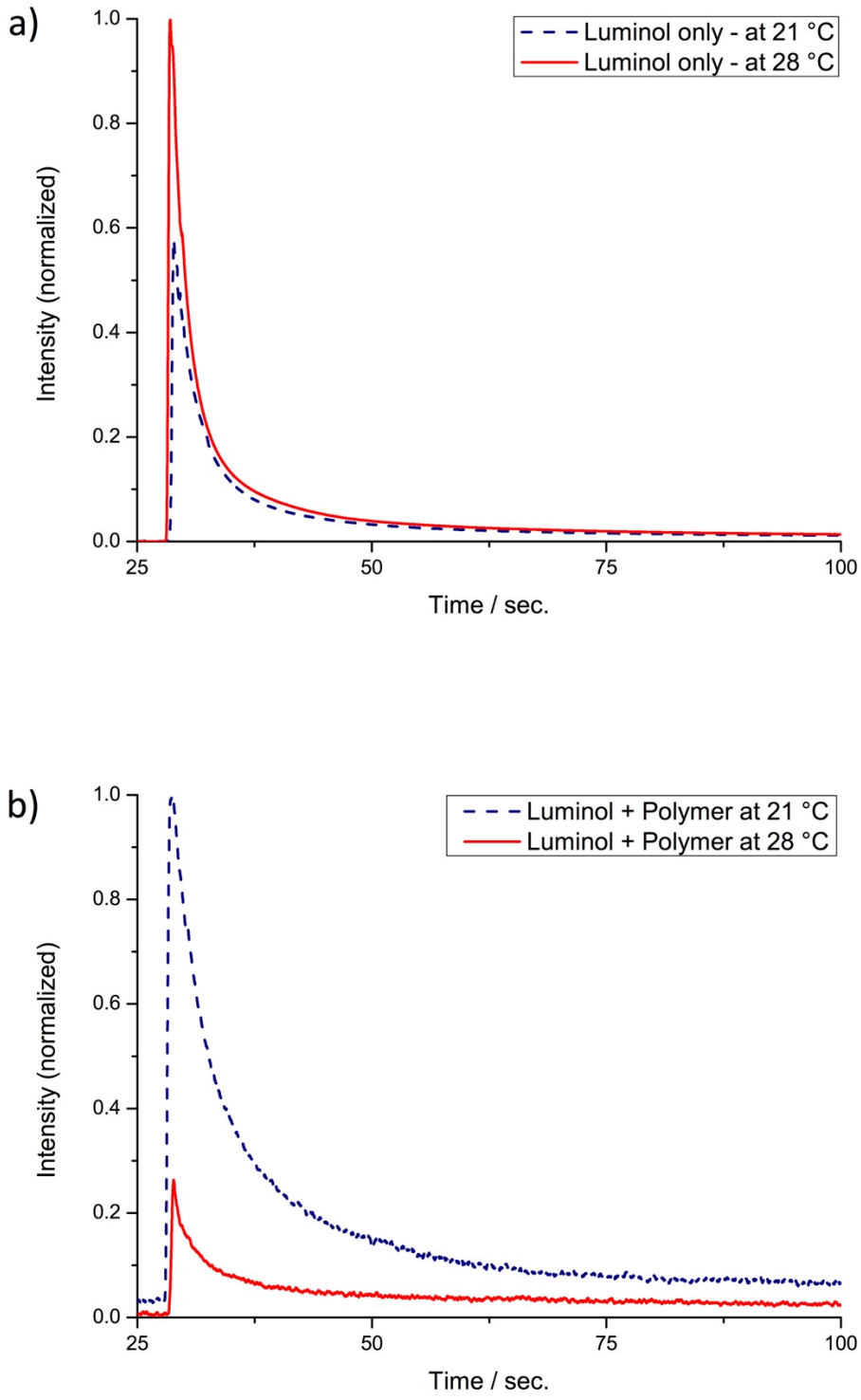

Figure S3. Comparing the chemiluminescence of luminol with and without P[VfcGE$_1$-*ran*-CAfcGE$_{13}$-*co*-EO$_{75}$] as catalyst. a) Chemiluminescence of luminol after the addition of hydrogen peroxide at 21 °C and 28 °C. b) Chemiluminescence of luminol after the addition hydrogen peroxide in the presence of the functionalized copolymer at 21 °C (below T_c) and 28 °C (above T_c).

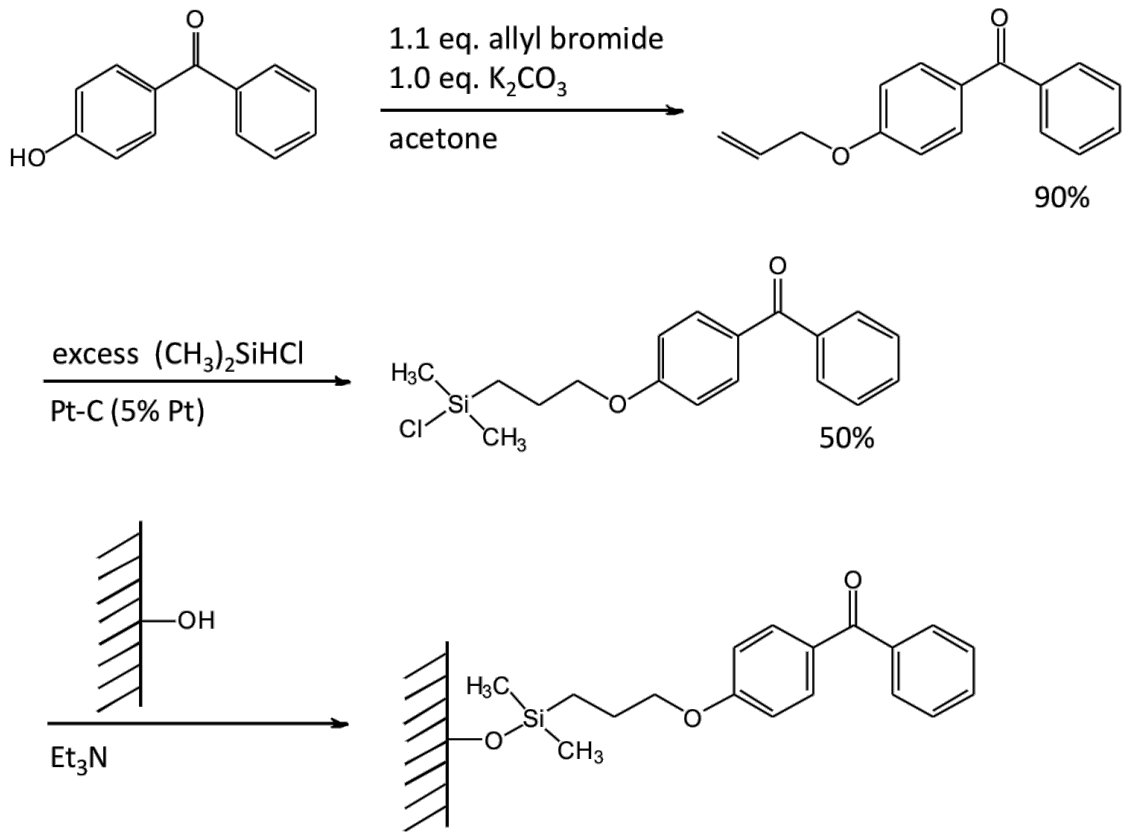

Scheme S3. Synthesis of 4-(3'-chlorodimethylsilyl(propyoxybenzophenone) and functionalization of glass surfaces.

The thicknesses of the polymer films (Figure S4) were analyzed by scratching the polymer film off the surface with a cannula. The vertical scratch, which is seen in the middle of the pictures (Figure S5), enables the thickness measurement of the polymer film.

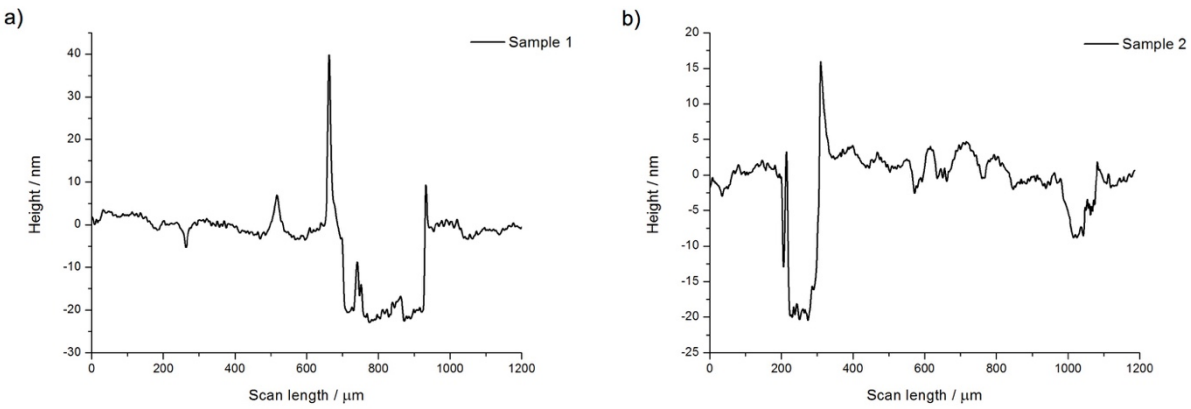

Figure S4. Height profiles of polymer modified glass surfaces: a) Sample 1 and b) Sample 2.

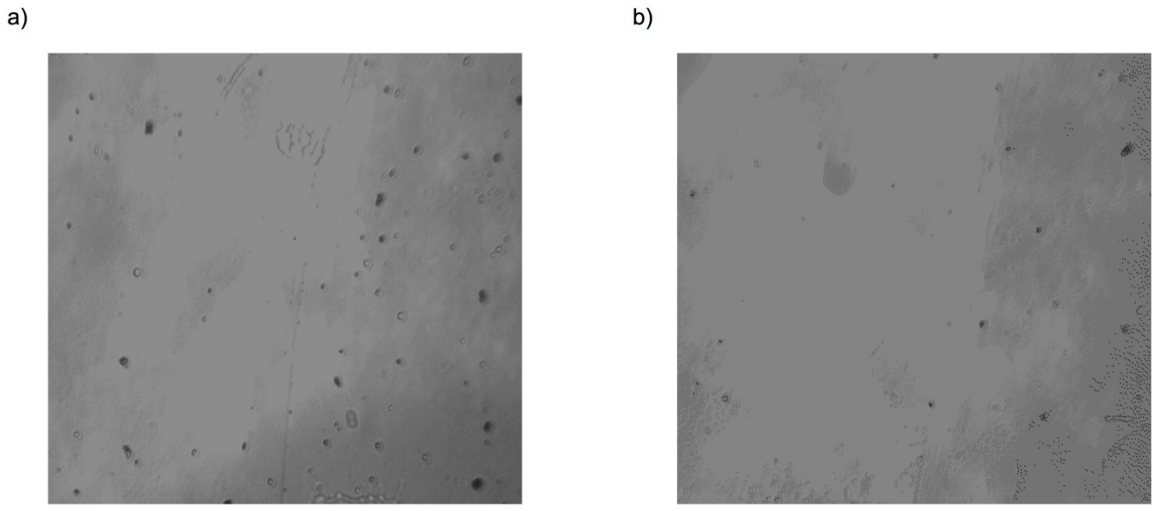

Figure S5. Topographic pictures of polymer modified glass surfaces: a) Sample 1 and b) Sample 2.

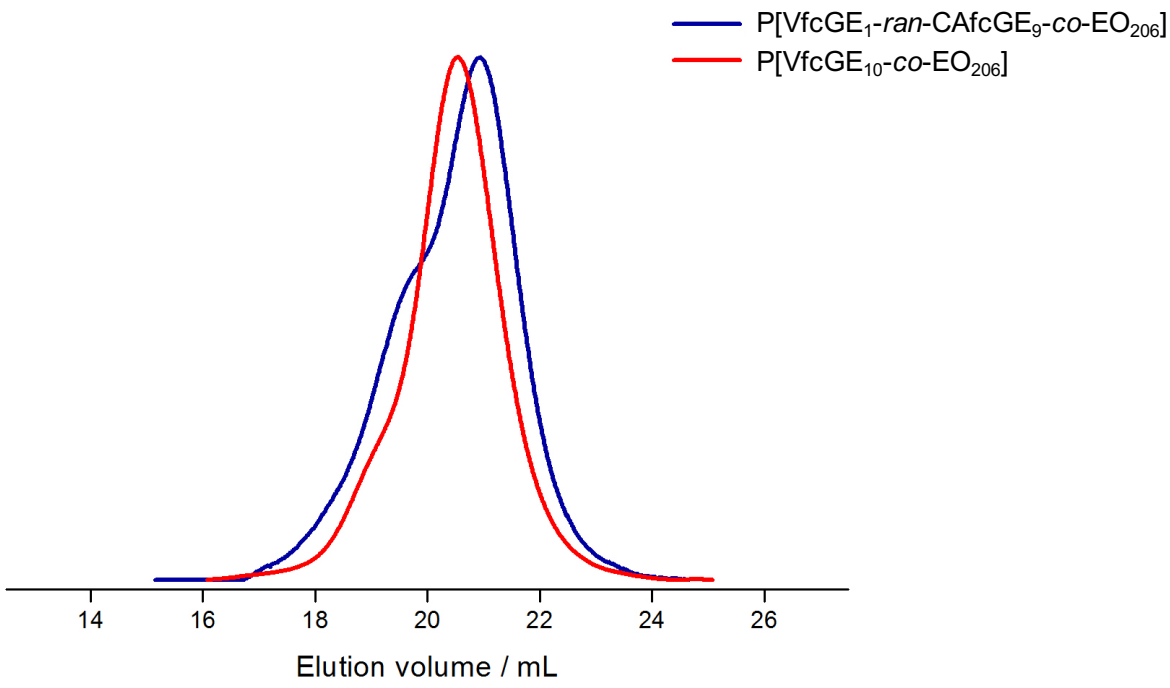

Figure S6. SEC traces of P[VFcGE$_{10}$-*co*-EO$_{206}$] (red) and after functionalization with cysteamine P[VfcGE$_1$-*ran*-CAfcGE$_9$-*co*-EO$_{206}$] (blue) (DMF, RI detection, 1 mL min^{-1}).

Table S1. Polymer Characterization.

no.	sum	VfcGE[a] / %	M_n[a] / g/mol	M_n[b] / g/mol	$Đ$	T_c / °C (@pH 7)
1	$BnOCH_2O$-P[VFcGE$_{10}$-*co*-EO$_{206}$]	4.8	12300	2200	1.09	37
1'	P[VFcGE$_1$-*ran*-CAVfcGE$_9$-*co*-EO$_{206}$]	-	13000	-	-	61
2	$BnOCH_2O$-P[VFcGE$_{14}$-*co*-EO$_{75}$]	15.4	7500	1800	1.14	-
2'	P[VFcGE$_1$-*ran*-CAVfcGE$_{13}$-*co*-EO$_{75}$]	-	8500	-	-	-
3	$Ph(CH_2O)_2$-P[VFcGE$_7$-*co*-EO$_{115}$]	5.5	7200	3000	1.07	33
3'	P[VFcGE$_1$-*ran*-CAVfcGE$_6$-*co*-EO$_{115}$]	-	7700	-	-	63

a) Determined from ^{1}H NMR; b) Determined via SEC in DMF vs. PEG.

Table S2. Temperature Dependent Contact Angle Measurements of Sample 1 and 2 and References 1 and 2.

Temperature / °C		**10**	**20**	**30**	**40**	**50**	**60**	**70**
Sample 1	θ / °	54.0	54.7	51.4	53.7	58.4	69.1	75.6
	Δθ / °	2.6	1.7	0.8	0.2	2.0	0.3	0.7
Sample 2	θ / °	61.6	49.7	49.2	51.2	68.9	61.5	80.8
	Δθ / °	0.9	0.2	0.5	0.3	0.3	0.5	1.0
Reference	θ / °	61.9	56.0	43.2	43.1	35.2	34.8	30.1
	Δθ / °	2.0	3.6	0.3	0.5	4.1	1.9	2.8

Table S3. pH Dependent Contact Angle Measurements of Sample 1 and 2 and References 1 and 2.

pH		**5.0**	**7.0**	**9.0**
Sample 1	θ / °	50.3	54.7	74.6
	Δθ / °	0.9	1.7	0.3
Sample 2	θ / °	47.1	49.7	72.4
	Δθ / °	1.7	0.2	0.2
Reference 2	θ / °	46.2	56.0	43.2
	Δθ / °	0.2	3.6	2.2

2.4 PEG-Staining for Electron Microscopy with Ruthenocenyl Glycidyl Ether

Manuscript in preparation.

Authors: *Arda Alkan,[+] Thomas Fritz,[‡] Matthias Worm,[§] and Frederik R. Wurm*[*,+]*

[+]Max Planck Institute for Polymer Research (MPIP), Ackermannweg 10, 55128 Mainz, Germany.

[‡]Institute of Pharmacy and Biochemistry, Johannes Gutenberg-University, Staudingerweg 5, 55128 Mainz, Germany.

[§] Institute of Organic Chemistry, Johannes Gutenberg University, Duesbergweg 10-14, 55128 Mainz, Germany.

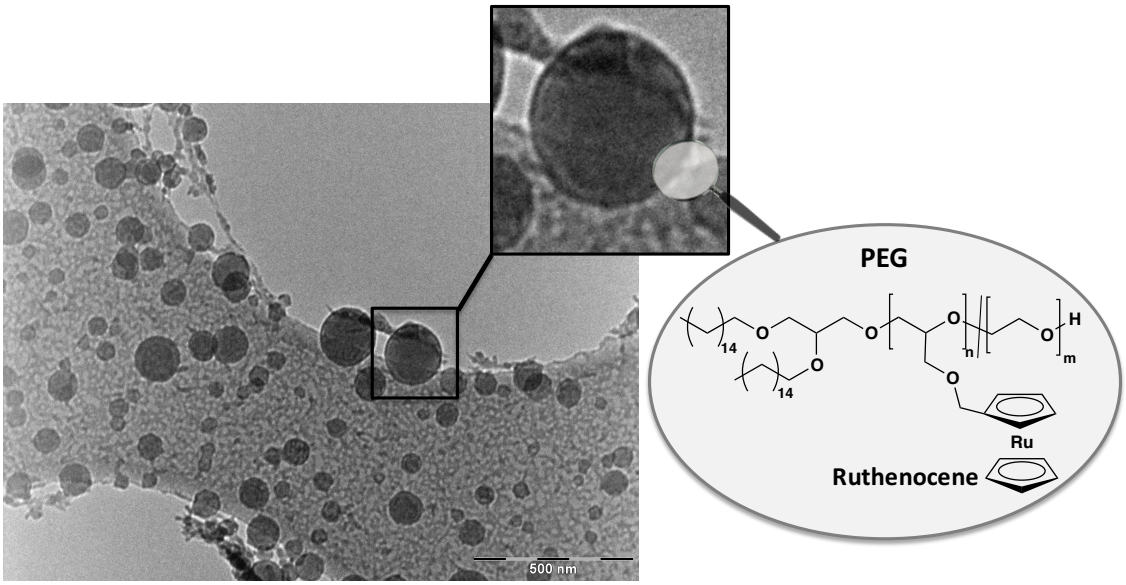

Abstract

Amphiphilic polymers were prepared using a lipophilic alkyl-macroinitiator for the anionic ring-opening copolymerization of ethylene oxide and ruthenocenyl glycidyl ether, rcGE - an epoxide monomer bearing ruthenocene. The incorporation of low amounts (1 to 2.5%) of a heavy metal such as ruthenium by copolymerization with rcGE into a poly(ethylene glycol) (PEG) backbone retains the properties of PEG, but increased contrast in TEM. The hydrophilicity of the ruthenocene-functionalized PEGs was not changed significantly, which led to readily water-soluble amphiphilic structures. These amphiphilic polymers were used in the synthesis of liposomes, which were then analyzed by cryo-TEM, expecting to yield a much higher contrast compared to ruthenocene-free systems. The heavy ruthenocene-loaded polymers were shown to reveal a much higher electron density and therefore should show a higher mass-thickness contrast.

Introduction

Drug carriers (such as nanoparticles and liposomes) or biological specimens are visualized by cryogenic transmission electron microscopy (cryo-TEM) to ensure pictures from the materials with the original shape in the preferable environment.[206-208] Chemical fixation, metal shadowing and negative staining are excellent methods, but they all rely on changing the specimen in order to make it more suitable for observation.[209,210] Therefore, low contrast is often a problem for materials with low electron density in EM.

Poly(ethylene glycol) (PEG) is one of the most often used polymers in biological applications and medicine, especially for drug delivery systems. It is today's standard for covalent bioconjugation i.e. PEGylation of proteins and several PEGylated drugs are commercialized. PEG is known for its "stealth" behavior, resulting in prolonged blood circulation times and

low immungeneity. [211,212] The stability and circulation times of liposomal nanoparticles are also increased by PEGylation, i.e. “stealth liposomes”, [213] and as such systems have emerged as powerful platforms for drug delivery, they are still under intense investigation. [214]

The visualization of nanocarriers in aqueous media is typically achieved by cryo-EM as the best method for the conservation of the original shape excluding drying artefacts. A challenge for cryo-EM is the staining of low-contrast samples and especially if the polymer, e.g. PEG should be visualized, only contrast images are obtained as PEG has a low electron density and in addition is highly hydrated in water further reducing the contrast.

Herein, we present the synthesis of covalently stained model PEGs, which can be used to visualize nanocarriers via TEM. These PEGs are copolymers of ethylene oxide and ruthenocenyl glycidyl ether (rcGE). Ruthenocene itself is an organometallic sandwich-complex, consisting of a ruthenium center and two cyclopentadienyl ligands. Due to the high molecular weight (high Z) metal ion, it provides many electrons and therefore a high mass-thickness contrast in EM.

These copolymers exhibit high water solubility and were incorporated into the membrane of liposomes to increase the contrast for cryo-EM. A schematic illustration of this liposomes is shown in Scheme 1. This general imaging protocol could be applied to any other structure (micelles, nanoparticles etc.) with PEG as the hydrophilic segment. Key is the synthesis of a novel monomer that can be copolymerized with ethylene oxide, i.e. rcGE to generate ruthenocene-loaded PEGs, i.e. poly(ethylene oxide-*co*-ruthenocenyl glycidyl ether) copolymers (rcGE content from 1 to 2.5%).

Scheme 1. Schematic illustration of liposomes with amphiphilic rc-containing polymers.

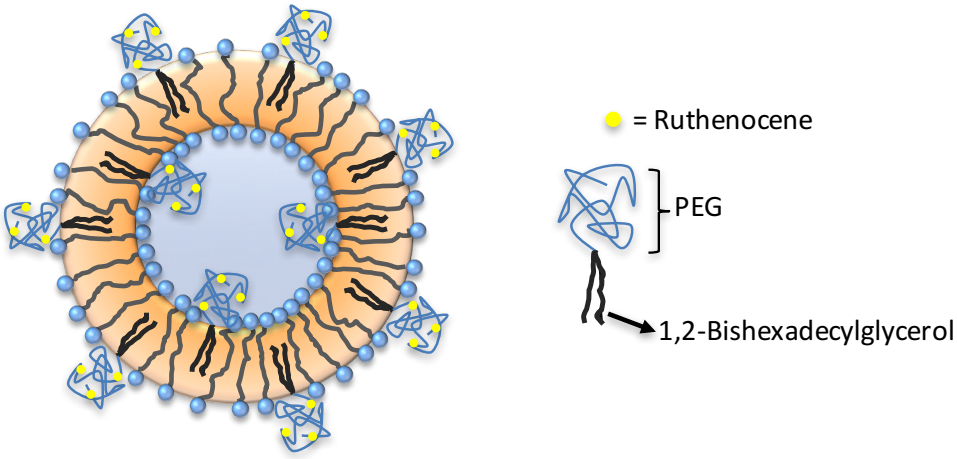

Results and Discussion

The monomer (**1**) was synthesized in a three-step protocol starting from ruthenocene (rc), which is shown in Scheme X. In the first step, rc is deprotonated with a mixture of *tert*-butyllithium (*t*-BuLi) and potassium *tert*-butoxide (*t*-BuOK), the so-called Schlosser's base. The intermediate ruthenocene carboxaldehyde is obtained after adding dimethylformamide (DMF) to the carbanion.[215] In the second step, ruthenocene carboxaldehyde (**2**) is reduced with lithium aluminiumhydride (LAH) to generate ruthenocenylmethanol (**3**).[216] Ruthenocenyl glycidyl ether (**1**), is then obtained after deprotonation of the alcohol with potassium hydride and reaction with epibromohydrin, similar to the previously described glycidyl ethers, which are synthesized in a phase transfer catalysis reaction. [85,89] The monomer was obtained as a light yellow liquid in an overall yield of about 68% after purification via column chromatography.

Scheme 2. Synthetic strategy to ruthenocenyl glycidyl ether (rcGE).

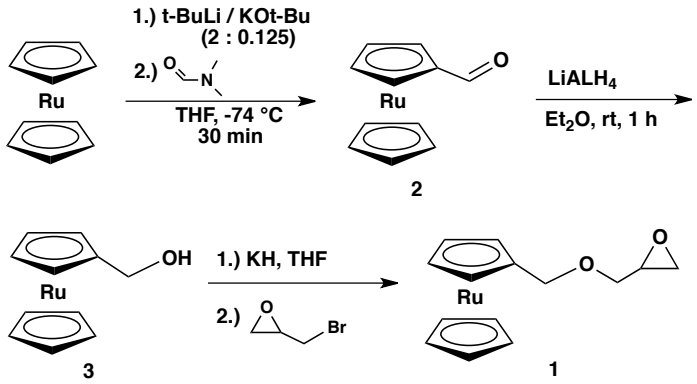

Figure 1 shows the ^{1}H NMR spectrum of **1** in chloroform-d_1; ^{13}C (Fig. S1), ^{13}C DEPT (Fig. S2), HSQC (Fig. S3), HMBC (Fig. S4) and COSY (Fig. S5) NMR spectra with the respective assignments can be found in the SI proving the signal assignments.

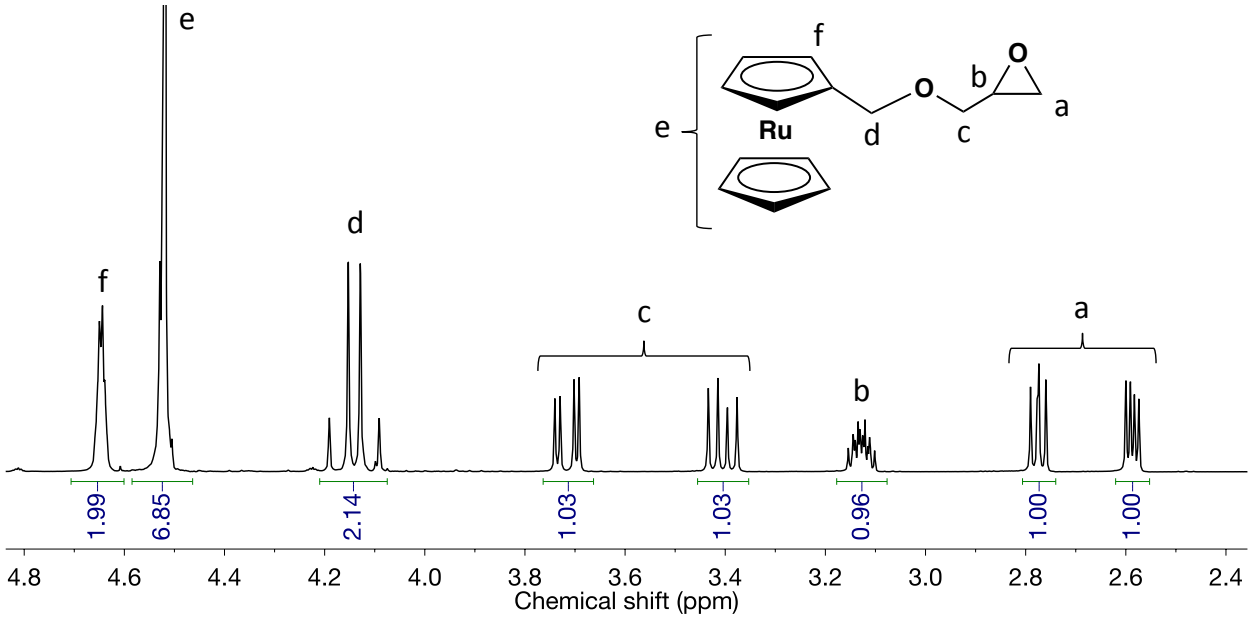

Figure 1. ^{1}H NMR spectrum of rcGE (**1**) (300 MHz, chloroform-d_1).

The copolymerization of rcGE and EO was performed similar to the synthesis of P[EO-*co*-fcGE] copolymers.[85] The initiator is formed by deprotonation of 1,2-bishexadecylglycerol with cesium hydroxide monohydrate. The cesium alkoxide was than used to initiate the copolymerization of rcGE and EO in a THF/DMSO mixture leading to 1,2-bis-*n*-hexadecyl

glyceryl ether initiated P[rcGE-*co*-EO] copolymers. Molecular weights were calculated by endgroup ananlysis from ^{1}H NMR by comparing the integrals of the initiator and the polymer backbone. Molecular weights from 5600 to 6300 g mol^{-1} were synthesized. The molar fraction of rcGE was varied from 1 to 2.5% (**A1** and **A2**). The narrow dispersities ($Đ=M_w/M_n$) range from 1.10 to 1.15 and are listed in Table X, which are determined by size exclusion chromatography. Molecular weights, which are determined via SEC, are slightly underestimated compared to molecular weights determined from ^{1}H NMR spectroscopy.

Scheme 3. Copolymerization of rcGE and EO with 1,2-bishexadecylglycerol as initiator.

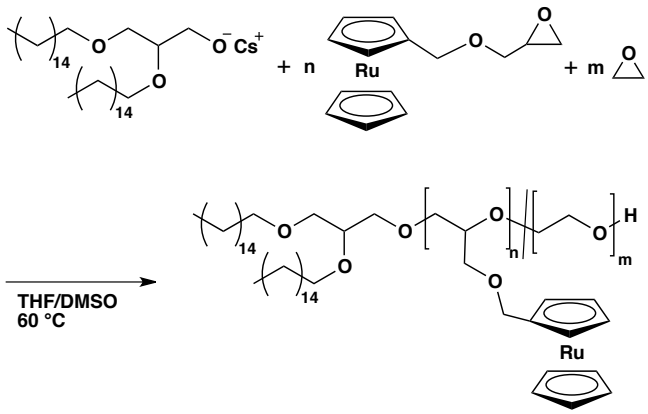

Table 1. Characterization Data for Amphiphilic Polymers with (**A1** and **A2**) and without rcGE (**A3**).

code	formula	rcGE (mol%)	M_n [a]	M_n [b]	$Đ$ [b]
A1	1,2-Bishexadecylglycerol P[EO_{121}-*co*-$rcGE_{1.2}$]	1.0	6 300	1 600	1.10
A2	1,2-Bishexadecylglycerol P[EO_{97}-*co*-$rcGE_{2.5}$]	2.5	5 600	2 000	1.10
A3	1,2-Bishexadecylglycerol PEO_{62}	-	3 300	2 200	1.05

a) M_n and molar ratio of fcGE (mol%) determined from ^{1}H NMR; b) M_n determined via SEC in DMF vs PEG standards, $Đ=M_w/M_n$. R is the aliphatic initiator.

Liposomes were prepared by the dual centrifugation (DC)[217] process in an adopted protocol from earlier work.[218] Cholesterol, egg phosphatidylcholine and the respective amphiphile were combined at a molar ratio of 45:50:5. Therefore, the amphiphilic rc-containing PEG (1,2-bishexadecylglycerol P[EO-*co*-rcGE]) samples **A1** and **A2** as well as the rc-free PEG sample **A3** were utilized for comparison. Ceramic beads and Dulbecco's Phosphate Buffered

Saline were added before subjecting to DC at 2500 RPM. The samples were purified afterwards by removing the residual non-aggregated molecules *via* gravity-flow gel filtration chromatography.

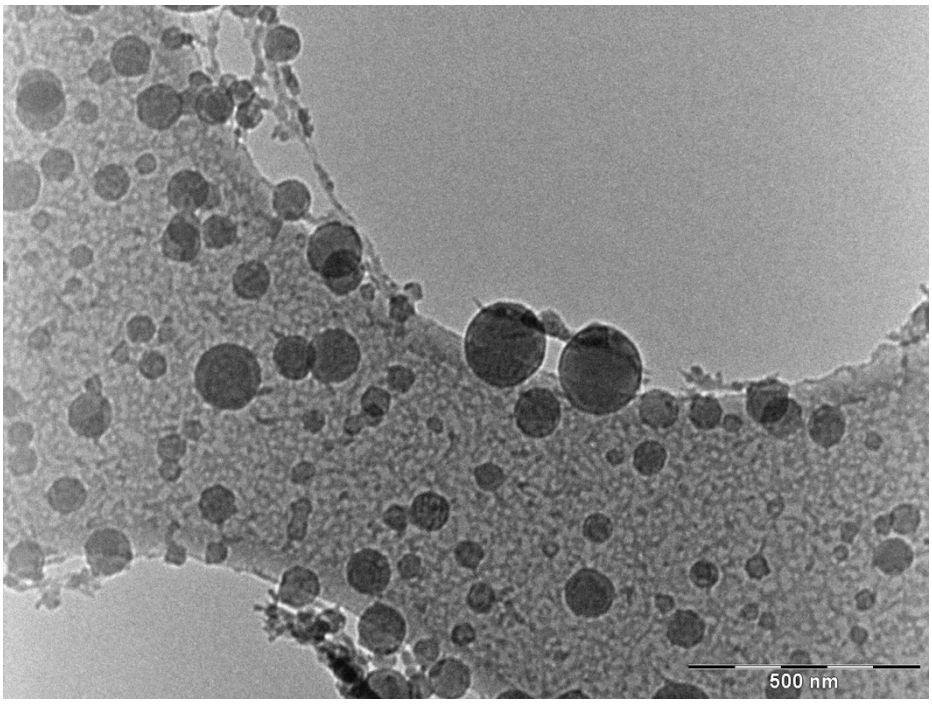

Figure 2. Cryo-TEM image showing P[EO_{97}-*co*-rcG$E_{2.5}$] (**A2**) functionalized liposomes with high contrast.

Liposome samples from polymers **A2** and **A3** were mixed just before starting cryo-TEM analysis. The 1,2-bishexadecylglycerol P[EO_{97}-*co*-rcG$E_{2.5}$] functionalized liposomes show a much higher contrast compared to those without rc functionalized PEG in literature,[219,220] even though the liposomes from **A3** without rc could not be detected in the same cryo-TEM images. The visible liposomes appear on the grid, which also influence the overall contrast. This could also be the reason for the absence of rc-free liposomes. The molar fraction of rcGE is with 2.5% very low and therefore does not change the properties of PEG. It should be mentioned at this point, that this is an assumption due to the good water-solubility of the resulting polymers. P[EO_{97}-*co*-rcG$E_{2.5}$] is still hydrophilic, shows good water-solubility and do no agglomerate as it is proven in the cryo-EM pictures. The appearance of the liposomes is

very smooth and uniform. The membranes of the liposomes have a very sharp contrast and are clearly visible.

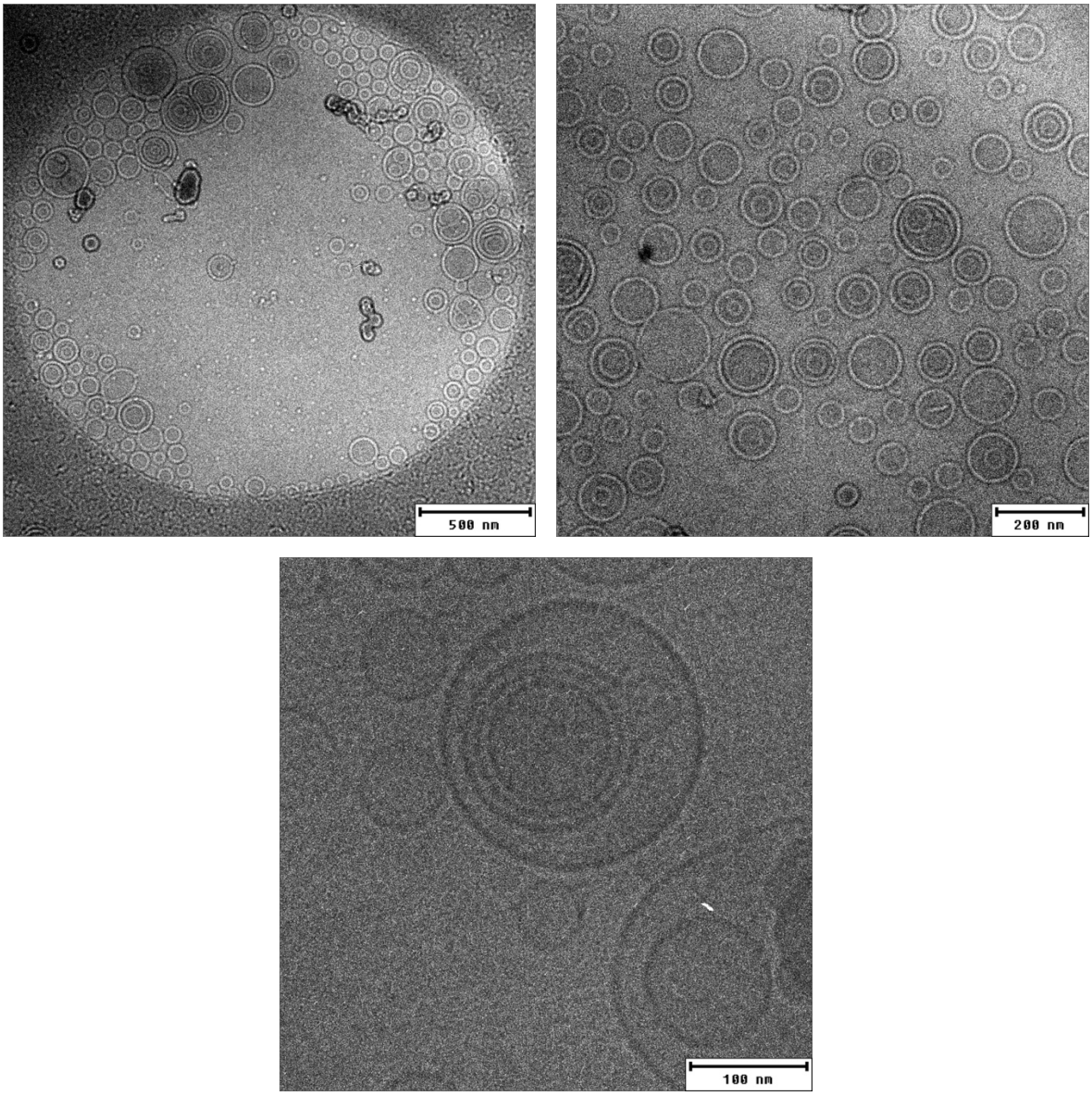

Figure 3. Cryo-TEM images as reference showing PEO_{62} (**A3**) functionalized liposomes with low contrast.

The reference cryo-EM pictures show liposomes with PEO_{62} (**A3**), which is not functionalized with rc and appear with less contrast than in Figure 2 for rc-functionalized sample. They are still good visible in this case, which is an exception and can also be found in literature.[217] There are a lot of examples in literature, where it was hard to make PEG visible in cryo-EM

pictures. This covalent-staining strategy with rc is the solution for this problem and will also find usage in different PEGylated systems other than liposomes.

Conclusion

Amphiphilic polymers with a hydrophilic PEG block, containing covalently linked rc (up ro 2.5mol%) — without significantly lowering PEGs hydrophilicity, were prepared. These amphiphilic polymers were used in the synthesis of liposomes via DC. The liposomes were then analyzed by cryo-TEM, showing a much higher contrast compared to ruthenocene-free systems, even though the liposomes without rc and therefore with a lower contrast could not be detected. This experiment has to be repeated, since a cryo-TEM image showing both rc-containing and rc-free PEG functionalized liposomes would be a solid evidence.

2.4.1 Supporting Information

Experimental Section

Instrumentation. ^{1}H NMR spectra (300, 400 MHz) and ^{13}C NMR spectra (75.5 MHz) were recorded using a Bruker AC300 and a Bruker AMX400. All spectra were referenced internally to residual proton signals of the deuterated solvent. For SEC measurements in DMF (containing 0.25 g·L^{-1} of lithium bromide as an additive) an Agilent 1100 Series was used as an integrated instrument, including a PSS HEMA column (106/105/104 g·mol^{-1}), a UV detector (275 nm), and a RI detector at a flow rate of 1 mL·min^{-1} at 50 °C. Calibration was carried out using PEO standards provided by Polymer Standards Service. Cryo-TEM micrographs were recorded on a Tecnai 12 BioTwin cryo transmission electron microscope, FEI, USA at 120 kV.

Reagents. Solvents and reagents were purchased from Acros Organics, Sigma-Aldrich or Fluka and used as received, unless otherwise stated. Chloroform-d_1 and benzene-d_6 were purchased from Deutero GmbH. Ruthenocenylmethanol (X) was synthesized starting from ruthenocene (rc) according to literature procedures. [215,216]

3-Benzyl-1,2-bishexadecylglycerol **(1)***.* In a 1000mL three-necked round-bottom flask equipped with a reflux condenser and a mechanical stirrer, 1-benzyl-*rac*-glycerol (5.0 g, 27.4 mmol) and sodium hydride (2.6 g, 109.7 mmol) were dissolved in dry THF (400 mL) under argon. 1-Bromohexadecane (33.5 g, 109.7 mmol) was added via syringe and the reaction mixture was stirred at reflux for 6 d. The solvent was evaporated under reduced pressure and the resulting residue was dissolved in a 1/1-mixture of diethyl ether/water (500 mL). After stirring for 16 h, the aqueous phase was neutralized via addition of diluted sulfuric acid (1 mol/L) and the organic phase was separated. The aqueous solution was extracted three times with diethyl ether and the combined organic layers were dried over sodium sulfate and filtrated. The solvent was removed at reduced pressure and excess 1-bromohexadecane was removed in high vacuum at elevated temperatures. The pure product (10.1 g, 16.0 mmol, 58 %) was obtained after column chromatography (eluent: petrol ether/ diethyl ether

30:1) over silica. ^{1}H NMR (400 MHz, $CDCl_3$): δ [ppm] 7.40–7.23 (m, 5H, CH_{Ar}), 4.56 (s, 2H, ArCH_2), 3.65–3.37 (m, 9H, CH_2-CH_2-O, CH-CH_2-O and CH_2-C*H-O*), 1.66–1.48 (m, 4H, CH_2-CH_2-O), 1.43–1.15 (m, 52H, CH_2), 0.88 (t, 6H, J_{AB} = 6.3 Hz, CH_3-CH_2).

1,2-Bishexadecylglycerol **(5)**. 3-Benzyl-1,2-bishexadecylglycerol **(4)** (10.1 g, 16.0 mmol) was dissolved in DCM (200mL) and stirred with 10wt%-palladium on activated charcoal (505 mg) under hydrogen atmosphere for 3 d. The residue was subsequently filtrated through Celite and the filter cake was washed with DCM. After evaporation of the solvent, the pure product was afforded as colorless crystals in quantitative yield. ^{1}H NMR (400 MHz, $CDCl_3$): δ [ppm] 3.78–3.36 (m, 9H, CH_2-CH_2-O, CH-CH_2-O and CH_2-C*H-O*), 1.63–1.49 (m, 4H, CH_2-CH_2-O), 1.40–1.17 (m, 52H, CH_2), 0.88 (t, 6H, J_{AB} = 6.6 Hz, CH_3-CH_2).

1,2-Bishexadecylglycerol PEG **(6)**. 1,2-Bishexadecylglycerol **(5)** (200 mg, 0.371 mmol) was dissolved in benzene (10 mL) and stirred in a dry Schlenk flask under slightly reduced pressure at 60 °C for 15 min keeping the stopcock closed. Moisture was removed by azeotropic distillation of benzene and subsequent drying at 70 °C in high vacuum for 16 h. After cooling to RT, dry THF (15 mL) was cryo-transferred into the Schlenk flask and potassium naphthalenide in THF (0.37 mL, 0.18 mmol, c = 0.5 mol•L^{-1}, prepared from potassium (235 mg, 6.0 mmol) and naphthalene (770 mg, 6.0 mmol) in dry THF (12 mL) in a glovebox under argon) was added via syringe. Generated hydrogen was removed in vacuum and ethylene oxide (1.11 mL, 22.3 mmol) were cryo-transferred via a graduated ampule into the initiator solution. The reaction was proceeded at 40 °C for 3 h and subsequently continued at 60 °C for 3 d. The polymerization was quenched with methanol (2 mL) and the polymer was precipitation in cold diethyl ether. After removing all volatiles in vacuum, the pure polymer was obtained. (Yield: 82 %) ^{1}H NMR (400 MHz, DMSO-d_6): δ [ppm] 3.70–3.20 (m, 250H, CH_2-O and CH_2-C*H-O*), 1.50–1.38 (m, 4H, CH_2-CH_2-O), 1.34–1.10 (m, 52H, CH_2), 0.84 (t, 6H, J_{AB} = 6.4 Hz, CH_3-CH_2).

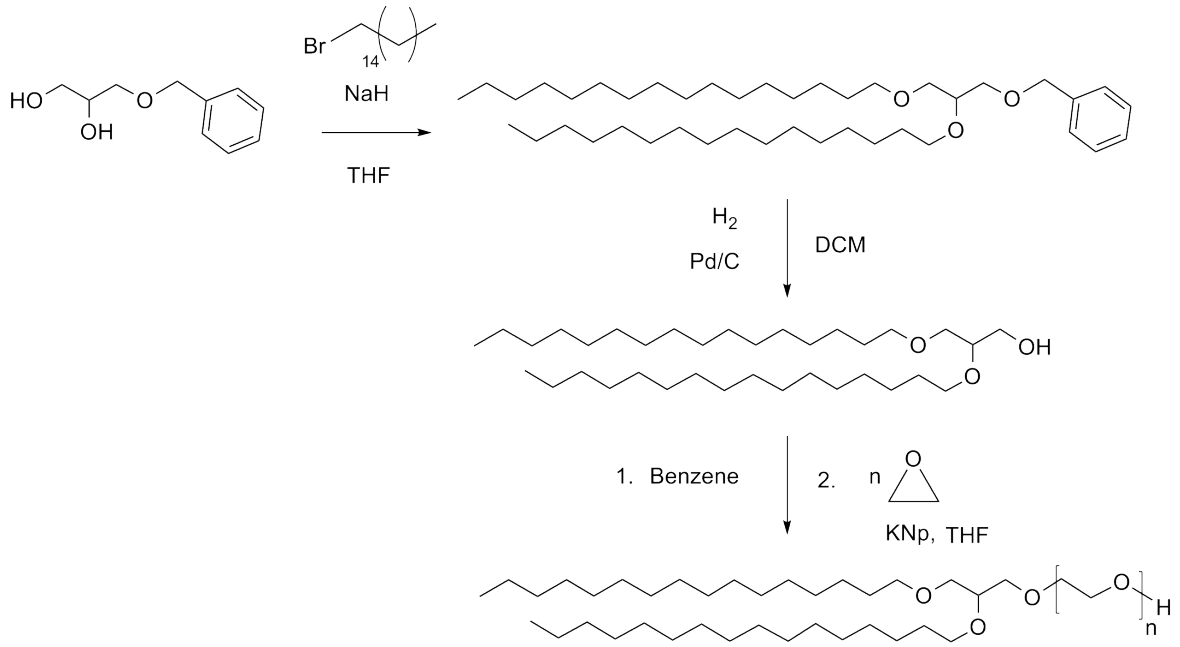

Scheme 1. Synthesis of 1,2-bishexadecylglycerol PEGs

Synthesis of ruthenocenyl glycidyl ether (rcGE, ***1****).* 3.10 g ruthenocenylmethanol (11.9 mmol) was dissolved in 200 mL dry THF. 480 mg potassium hydride (11.9 mmol; 1 eq.) was than suspended in this solution and vigorously stirred (since potassium ruthenocenylmethanolate precipitates in THF) for 1 h. The suspension was cooled down to 0 °C and 4.88 g epibromohydrin (35.6 mmol; 3 eq.) is added dropwise. The solution was stirred for another 2 h at 0 °C and then stirred overnight at room temperature. Distilled water was added and the reaction mixture was extracted three times with diethyl ether. The solvent was removed at reduced pressure and the crude product was purified by column chromatography over silica using a mixture of ethyl acetate and petroleum ether (2:8) as eluent. The pure product was obtained as a light yellow liquid. Yield: 92%. ^{1}H NMR ($CDCl_3$, 400 MHz, 298 K): δ (ppm) = 4.69-4.62 (m, 2H, cp: -C*H*-CR-C*H*-), 4.57-4.49 (m, 7H, residual rc protons), 4.21-4.08 (dd, 2H, rc-CH_2-O-, *J* = 11.4 Hz), 3.77-3.67 (dd, 1H, -O-C*H*H-epoxide, *J* = 11.4, 3.1 Hz), 3.46-3.36 (dd, 1H, -O-CH*H*-epoxide, *J* = 11.4, 5.8 Hz), 3.18-3.09 (m, 1H, epoxide C*H*), 2.82-2.74 (dd, 1H, epoxide C*H*H, *J* = 5.0, 4.1 Hz), 2.63-2.56 (dd, 1H, epoxide CH*H, J* = 5.0, 2.7 Hz).

General Procedure for the copolymerization of rcGE and EO: 1,2-bishexadecylglycerol P(EO-co-rcGE). The initiator, 287.4 mg (0.5317 mmol) 1,2-bishexadecylglycerol, and 80.4 mg (0.4787 mmol, 0.9 eq.) cesium hydroxide monohydrate were placed in a 100 mL Schlenk flask and suspended in 10 mL benzene. The mixture was stirred at 60 °C under an argon atmosphere for 1 h and evacuated at 40 °C (10^{-2} mbar) for 12 h to remove benzene and the water formed (as an azeotrope with benzene) to generate the corresponding cesium alkoxide. Subsequently, approx. 20 mL dry THF were cryo-transferred into the Schlenk flask. 1.4 mL (31 mmol) EO was cryo-transferred to a graduated ampule and then cryo-transferred into the reaction flask containing the initiator in THF. Then 337.4 mg (1.519 mmol) rcGE was added via syringe in a 50 wt% solution in anhydrous DMSO. The reaction mixture was heated up to 60 °C and stirred for 24 h before the living chain ends were terminated with methanol and the copolymer was precipitated in cold diethyl ether to get rid of unreacted rcGE. The copolymer was obtained as a light yellow solid. Yields: 86-93%. ^{1}H NMR ($CDCl_3$, 300 MHz): δ (ppm) = 4.64-4.59 (br, 2H, cp (*2*, *5*)), 4.53-4.46 (br, 7H, cp (*3*, *4*)-Ru-*cp*), 4.11-4.04 (s, 2H, rc-C*H*$_2$-O), 3.90-3.82 (t, 1H, C*H* (glycerol)), 3.80-3.31 (br, C*H*$_2$-O and CH$_2$-C*H*$_2$-*O*), 1.59-1.47 (m, 4H, H$_3$C-(CH$_2$)$_{13}$-C*H*$_2$-CH$_2$-O-), 1.34-1.19 (br, 52H, H$_3$C-(C*H*$_2$)$_{14}$-CH$_2$-), 0.90-0.82 (t, 6H, *H*$_3$C).

Liposome synthesis. Liposomes were prepared via dual centrifugation[217] in an adopted protocol from earlier work.[218] Ethanolic stock solutions of cholesterol, egg phosphatidylcholine (EPC, kind gift from Lipoid GmbH, Ludwigshafen, Germany) and the respective amphiphile **A1**, **A2** or **A3** were combined in a PCR vial at a molar ratio of 45:50:5 to a total amount of 8.4 µmol, dried in vacuum and stored at -20°C until usage. For formulation, 70 mg ceramic beads (SiLiBeads ZY 0.3-0.4 mm, kindly provided from Sigmund Lindner, Warmesteinach, Germany) and 9.3 µL Dulbecco's Phosphate Buffered Saline (DPBS, ThermoFisher, Waltham, MA, USA) were added before subjecting to 20 min. dual centrifugation (DC) at 2500 RPM. Then, 28 µL DPBS were added and the sample subjected to two 2 min. DC runs, between which the sample was reoriented by 180° in the sample holder. To remove residual, non-aggregated molecules, 10 µL of the resulting liposomes were purified *via* gravity-flow gel filtration chromatography on a custom-made Sepharose 2B-CL column.

Additional NMR characterization data for rcGE (**1**):

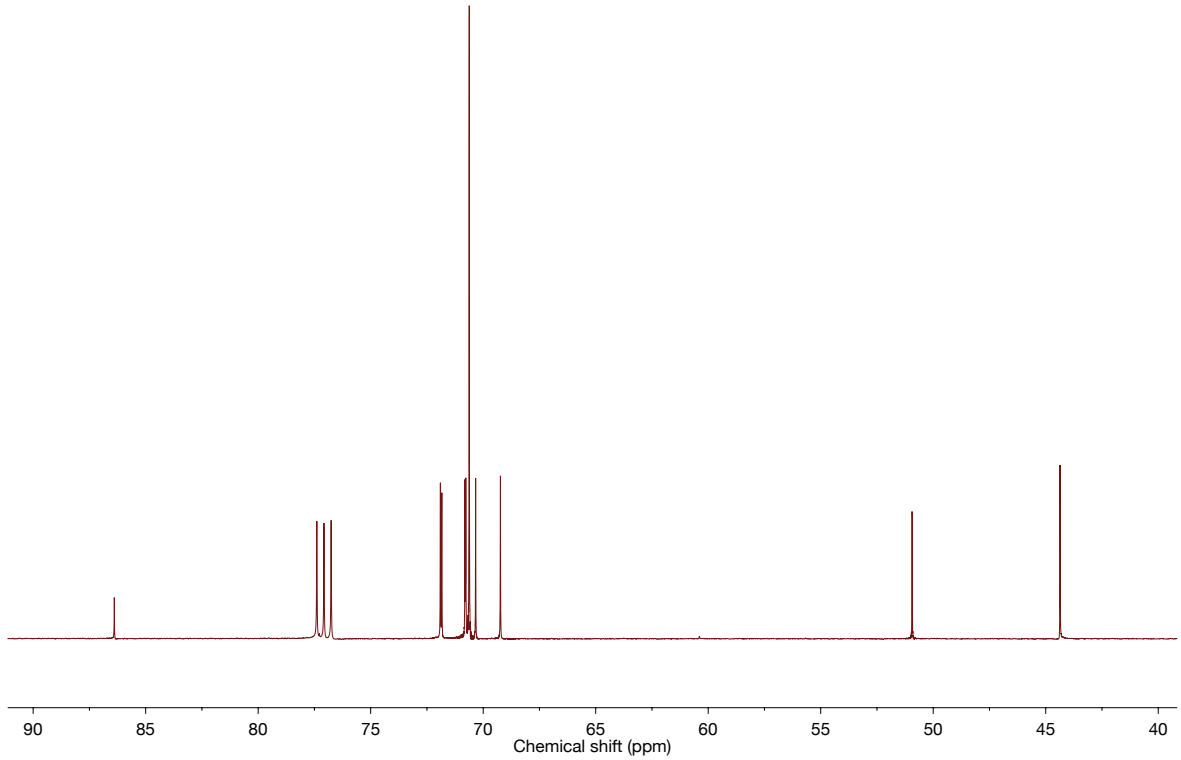

Figure S1. $^{13}C\{H\}$ NMR of rcGE (101 MHz, $CDCl_3$).

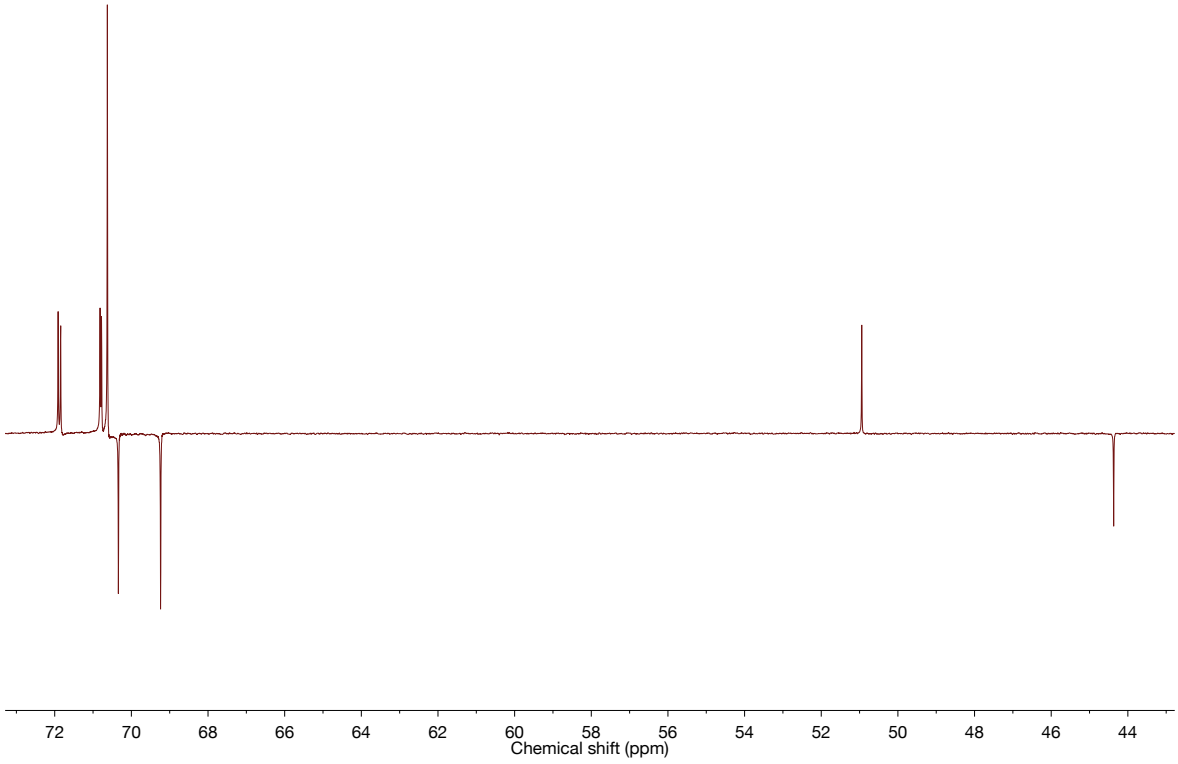

Figure S2. $^{13}C\{H\}$ DEPT NMR (101 MHz, $CDCl_3$) of rcGE.

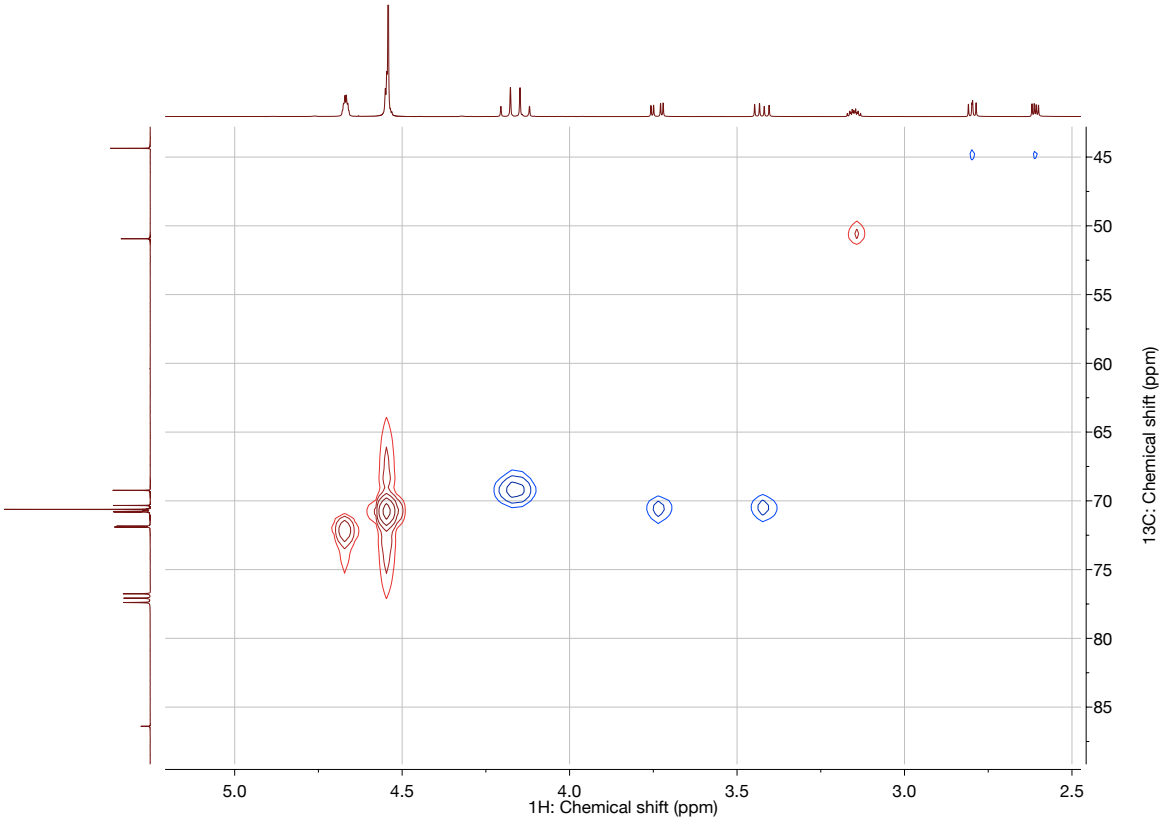

Figure S3. HSQC NMR (400, 101 MHz, $CDCl_3$) of rcGE.

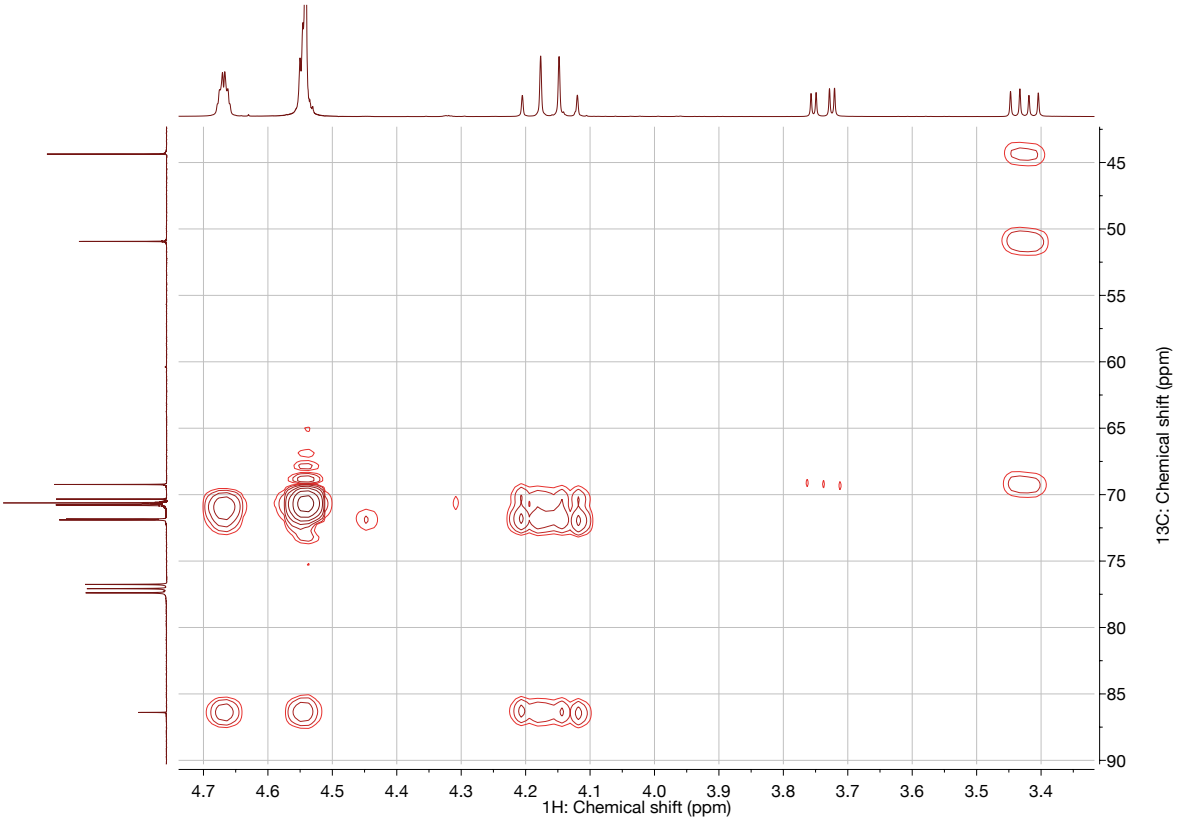

Figure S4. HMBC NMR (101 MHz, $CDCl_3$) of rcGE.

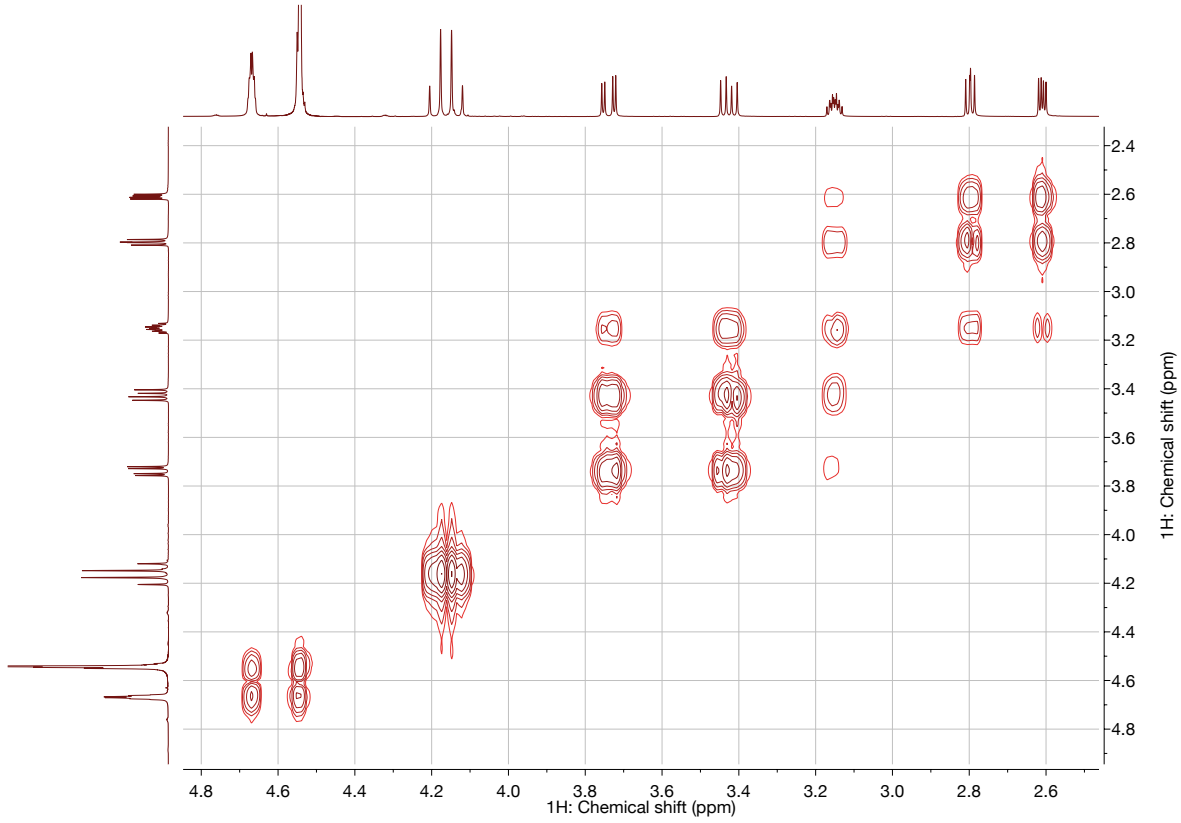

Figure S5. COSY NMR (400 MHz, $CDCl_3$) of rcGE.

Chapter 3: Water-Soluble Ferrocene-Containing Block Copolymers

3.1 Amphiphilic Ferrocene-Containing PEG Block Copolymers as Micellar Carriers and Surfactants

Manuscript in preparation.

Authors: *Arda Alkan,[+,‡] Sarah Wald,[+,‡] and Frederik R. Wurm*[*,+]*

‡ These authors contributed equally.

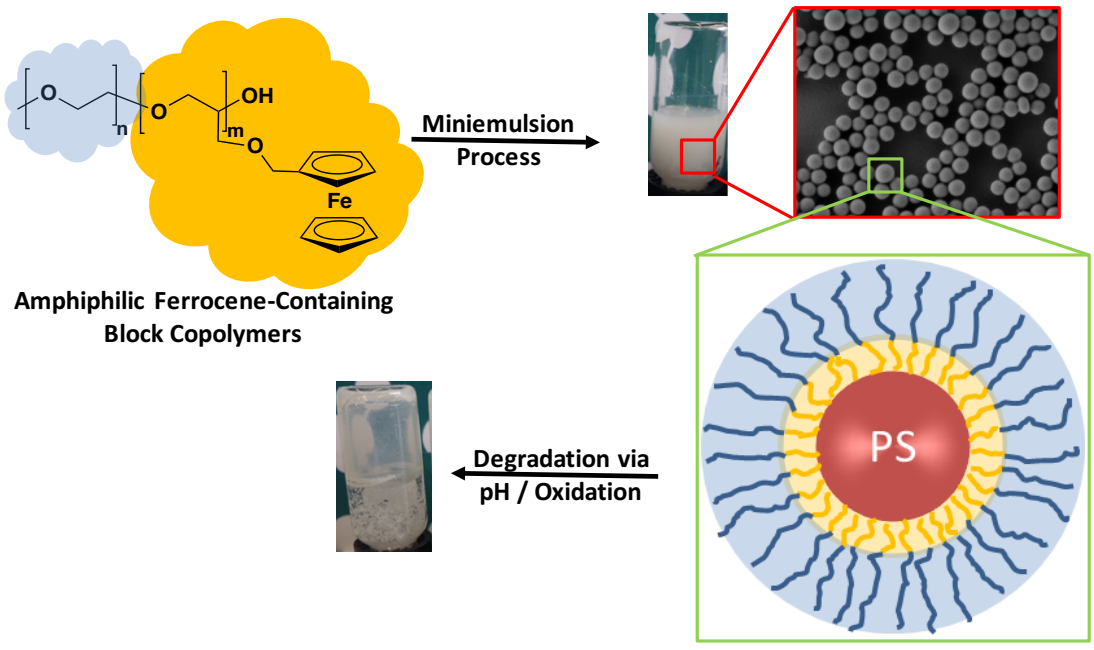

Abstract

Water-soluble block copolymers consisting of a poly(ethylene glycol) (PEG) block and a poly(ferrocenyl glycidyl ether) (PfcGE) block were prepared via anionic ring-opening polymerization (AROP) of fcGE using commercially available PEG monomethyl ether as macroinitiator. The resulting block copolymers with molecular weights (M_n) of 3600 to 8600 g mol^{-1} and narrow molecular weight distributions (M_w/M_n = 1.04-1.10), show a very good water-solubility. The block copolymers were investigated via ^1H and DOSY NMR spectroscopy, size exclusion chromatography (SEC) and MALDI-ToF mass spectroscopy. Furthermore, the block copolymers were used as redox-responsive surfactants in the oil-in-water miniemulsion polymerization and the miniemulsion process in combination with solvent evaporation to stabilize poly(styrene) (PS) nanoparticles. Destabilization studies were performed in acidic media and under oxidative conditions, generating ferrocenium species, which are hydrophilic and convert the amphiphilic block copolymer into a totally water-soluble macromolecule.

Introduction

Surfactants are used as cleaning agents, in cosmetics, food, plant or oil production as well as in paper, paint or textile industry, because of their ability to modify the interfacial properties by changing the surface or interfacial tension and self-assemble into micelles or other nanostructures. Surfactants including pH-, T-, light- or redox-active groups are of interest to spread their applications in the field of separation methods,[221] foam formation[222] and to reduce surfactant waste and usage or process costs.[223] Surfactants based on redox-responsive molecules like ferrocene, viologens and *N*-alkylated nicotin acids were studied.[224] The results proved that *N*-alkylated nicotinic acid derivatives do not show a reversible redox behavior in water, whereas redox reactions using ferrocene and viologen surfactants

showed reversibility and drastic solubility changes.[224] Most studied redox-active surfactants are based on ferrocene, because it is chemically stable over a wide range of solution conditions with simple control of the oxidation state in aqueous solution.[225] These low molecular weight surfactants have been synthesized with a lot of different modifications.[226] They varied in the number and length of alkyl chains, single chained[225,227-230] or double-chained,[231-235] included non-ionic,[235-240] cationic,[225,228-234,241-244] or anionic[227,235,245] (head) group as well as double bonds[224] for further polymerization, which leads in changes of the self-assemble in aqueous media.

Different water-soluble ferrocene-containing polymers have been synthesized in various ways, which is reviewed in Chapter 1.1. In 2013, we have synthesized linear fc-containing copolymers by the copolymerization of fcGE and ethylene oxide (EO),[85] and later hyperbranched copolymers by the copolymerization of fcGE and glycidol (G).[86] Block copolymers have been synthesized in the past, mainly consisting of a poly(vinyl ferrocene) (PVfc) or poly(ferrocenyl silane) (PFS) and a water-soluble block, often PEG. PVfc-based block copolymers are used to generate redox-sensitive porous multicompartment vesicles to release guest molecules after a redox-trigger.[246] Self-assembly into spherical or ribbon-like micelles were researched with poly(styrene)-*b*-poly(ferrocenylsilane) block copolymers including different alkyl groups. Amorphous diblock copolymers ended up in spherical micelles with an oxidized PFS core and a PS corona, whereas block copolymers with semicristalline PFS segments formed ribbon-like micelles. After reduction neutral chains were generated back without significant chain scission.[170] Also in colloid science, such ferrocenyl-based amphiphilic block copolymers are only used as nanocarrier material. For example, redox-responsive nanocapsules composed of an PVfc-based shell and an hydrophobic liquid core including hydrophobic payloads were generated by the miniemulsion approach in combination with solvent evaporation. The formed nanocapsules can release the incorporated payload after oxidation of the ferrocene blocks by introducing polar domains in the shell, which also leads in shell morphology changes.[165]

The current work describes the first block copolymers based on the monomer fcGE. PEG monomethyl ether is used as macroinitiator for the anionic ring-opening polymerization of fcGE.[85] The block copolymers prepared herein are readily soluble in water under the formation of micelles with a hydrophobic PfcGE core. The block copolymer can be transferred into a fully water-soluble block copolymer after oxidation with an oxidizing agent or under acidic conditions. Furthermore, we employ this redox-responsive behavior, to generate redox-sensitive polystyrene nanoparticles stabilized with the amphiphilic block copolymers is shown in Scheme 1. The nanoparticles are synthesized by the free radical polymerization in direct miniemulsion[164,247] or the miniemulsion approach in combination with solvent evaporation by investigating the influence of the nanoparticle sizes by changing the surfactants concentration.[247] The nanoparticle dispersions were stable over a long period of time and "on-demand" destabilization was achieved by a pH- or redox-trigger leading to flocculation or film formation.

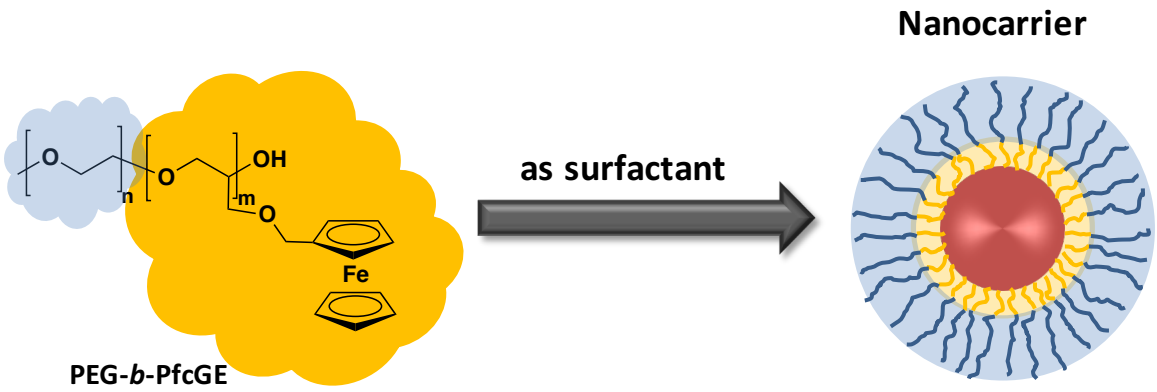

Scheme 1. mPEG-*b*-PfcGE block copolymers as redox-active surfactants for nanocarriers.

Results and Discussion

The anionic ring-opening polymerization of fcGE was achieved by the cesium alkoxide of mPEG (with n=44 or 113 in Scheme 2 respectively) acting as a macroinitiator. The initiator was generated by the reaction of mPEG with cesium hydroxide. It was then used to initiate the polymerization of fcGE in bulk leading to mPEG-*b*-PfcGE block copolymers (Scheme 2).

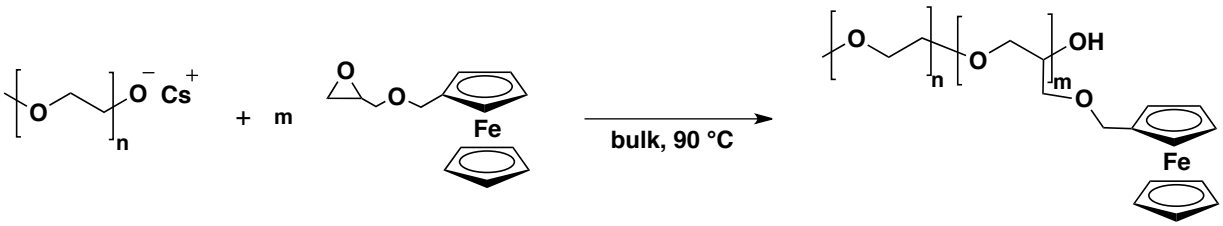

Scheme 2. Anionic ring-opening polymerization of fcGE for the preparation of amphiphilic PEG-*b*-PfcGE block copolymers.

The degree of polymerization of the PfcGE block was adjusted to be ca. 11 to ensure a completely water-soluble block copolymer, but also micellization of the system. Molecular weights were calculated by comparing the integrals of the resonances for the initial mPEG and fcGE. Starting from mPEG5000 (with a detected M_n of 5,500 g mol^{-1}) as the macroinitiator, molecular weights from 7,400 to 8,500 g mol^{-1} were achieved by varying the molar fraction of fcGE from 5.7 to 8.2% (**P1**-**P4**). The molecular weight dispersities ($Đ=M_w/M_n$) range from 1.05 to 1.10 indicating a living polymerization and are listed in Table 1, which are determined by size exclusion chromatography (Figure 1).

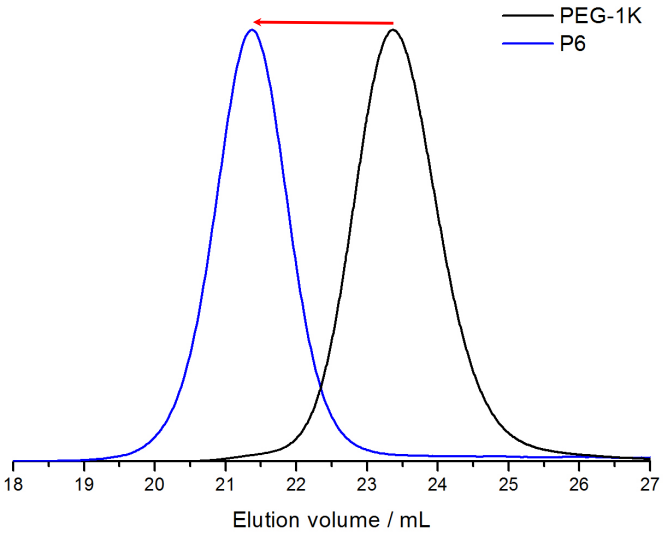

Figure 1. SEC traces of the macroinitiator PEG (1000 g/mol) and **P6** (DMF, 323 K, RI detection, 1 mL min^{-1}).

Molecular weights, which are determined via SEC are slightly underestimated compared to molecular weights determined from ^{1}H NMR spectroscopy.

In addition, $mPEG_{44}$ and $mPEG_{24}$ was used as a macroinitiator to generate block copolymers with higher fcGE fractions. Therefore, mPEG2000 led to a block copolymer with 11.7 mol% fcGE, a molecular weight of 3600 g mol^{-1} and a dispersity of 1.08 (**P5**). With mPEG1000 27.2 mol% fcGE were incorporated (**P6**).

Table 1. Characterization data for PEG-*b*-PfcGE block copolymers.

code	formula	fcGE (mol%)	M_n [a]	M_n [b]	$Đ$ [b]	*cmc* *[mmol/L]*	*HLB* [c]
P1	$mP(EG)_{124}$-*block*-$P(fcGE)_{7.5}$	5.7	7400	5100	1.05	n.d. [d]	14.9
P2	$mP(EG)_{124}$- *block* -$P(fcGE)_{9.8}$	7.3	7900	5900	1.10	0.053	13.9
P3	$mP(EG)_{124}$- *block* -$P(fcGE)_{11.1}$	8.2	8500	5700	1.06	n.d. [d]	12.9
P4	$mP(EG)_{124}$- *block* -$P(fcGE)_{10.4}$	7.7	8300	5700	1.07	n.d. [d]	13.3
P5	$mP(EG)_{45}$- *block* -$P(fcGE)_{5.7}$	11.7	3600	2600	1.08	n.d. [d]	11.1
P6	$mP(EG)_{24}$- *block* -$P(fcGE)_{9.1}$	27.2	3600	1900	1.05	0.034	5.6

a) M_n and molar ratio of fcGE (mol%) determined from ^{1}H NMR; b) M_n determined via SEC in DMF vs PEG standards, $Đ=M_w/M_n$; c) calculated by the method of Griffin;[248] d) not determined.

The block copolymer **P3** is further analyzed via DOSY ^{1}H NMR spectroscopy. Figure 2 displays the spectrum, whereby the x-axis shows the conventional ^{1}H NMR spectrum, and the y-axis gives the diffusion coefficient. From the 2D plot it is obvious that the resonances of ferrocene (4.36-4.00 ppm) and the PEG backbone (3.56-3.41 ppm) of the 1D ^{1}H NMR spectrum appear at the same diffusion coefficient, which indicates that a block copolymer rather than a homo polymer has formed.

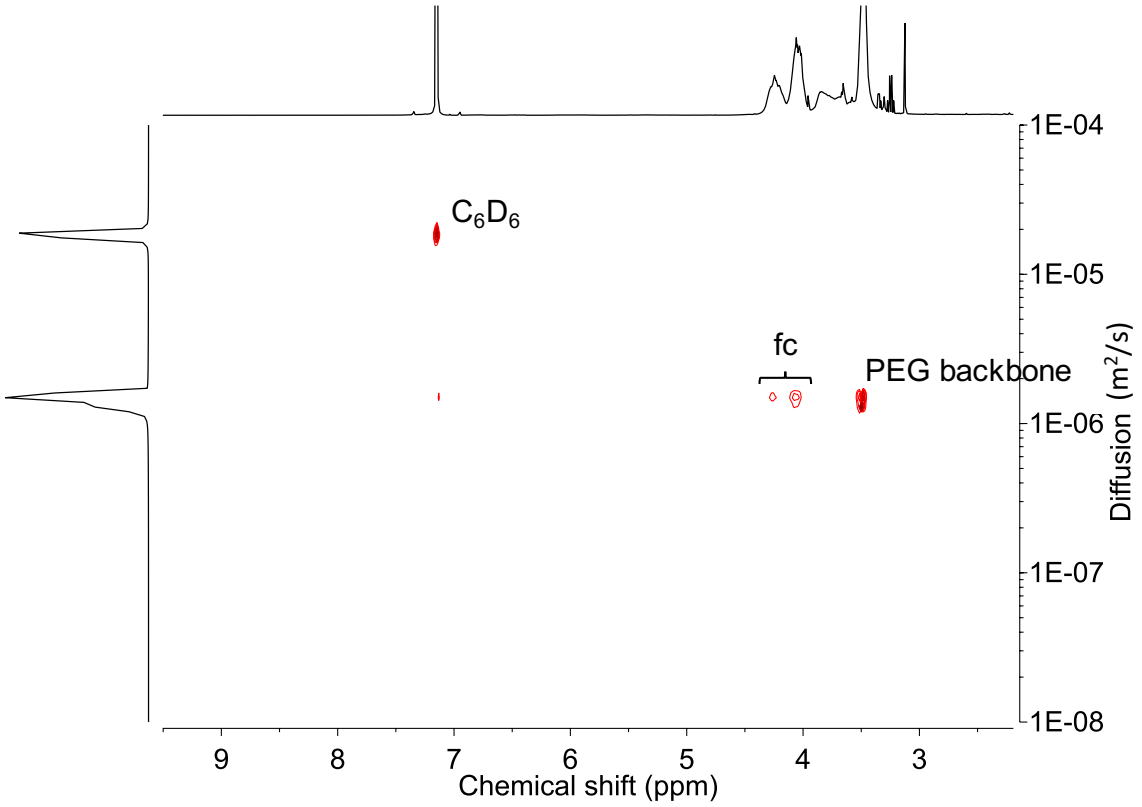

Figure 2. ^{1}H DOSY NMR spectrum of **P3** (benzene-d_6, 400 MHz, 298K).

To further confirm incorporation of fcGE into the block copolymer structure, matrix-assisted laser desorption/ionization time-of-flight mass spectrometry (MALDI-ToF MS) was performed. Figure 3 shows the MALDI-ToF mass spectrum of **P2**. The repeating units of EO and fcGE are clearly recognizable (and all distributions are marked with different colors). Each detected signal corresponds to the mass of a linear combination of both monomers in the copolymer. It also important to mention that different combinations can have very similar masses, which is why the respective peaks overlap in the spectrum.

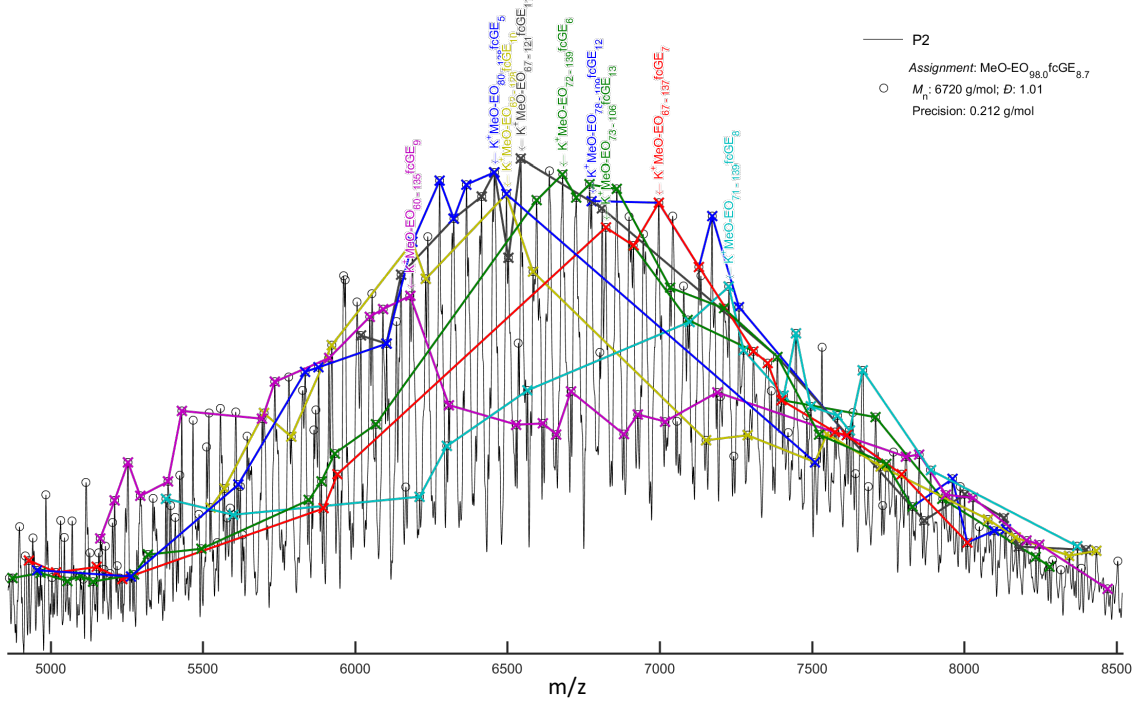

Figure 3. MALDI-ToF mass spectrum of mP(EG)$_{124}$-*b*-P(fcGE)$_{9.8}$ (**P2**).

The surface active properties of the block copolymers mP(EG)$_m$-*b*-P(fcGE)$_n$ are characterized numerically by their HLB (hydrophilic-lipophilic balance, Table 1).[248]

P2 exhibits a formal HLB value of 13.9, while **P6** exhibits the lowest HLB value of 5.6. As the fcGE block is not fully hydrophobic (as in conventional surfactants, e.g. alkyl chains), the HLB values calculated by the Griffin method should be regarded as a first indication of their surfactant properties only. The critical micelle concentrations (cmcs) of these block copolymers were determined by isothermal titration calorimetry, revealing cmcs in the range of 0.034 (**P6**) – 0.053 (**P2**) mmol/L (Table 1). As comparison the common non-ionic surfactant Lutensol AT 50 ($C_{16\text{-}18}$-alkyl-*block*-PEG$_{50}$, M_n ca. 2,500 g/mol exhibits a HLB value of 18 with a cmc below 0.01 mmol/L.[249] This further indicates that the fcGE segment cannot be compared with a very hydrophobic alkyl chain, but the detected cmcs of all fcGE containing block copolymers are in a low mmol regime.

The water-soluble block copolymers were studied as redox-active surfactants in oil-in-water (direct) miniemulsions. Thus, polystyrene nanoparticles were stabilized in a proof-of-

principle synthesis with **P2**, **P3** and **P6** (Table 2). As reference experiments, miniemulsion polymerizations of styrene stabilized with commercially available surfactants, Lutensol AT50 or SDS, were performed to evaluate the properties of the redox-active block copolymers. In all miniemulsion polymerizations an osmotic pressure agent (hexadecane) and AIBN as the initiator were dispersed together with styrene in the water phase including different concentrations of surfactants (Table 2).

Table 2. Results of generated PS-nanoparticles by direct miniemulsion polymerizations.

code	typ of surfactant	surfactant concentration [mg/mL]	water to monomer ration	d [nm][a]
ME1	P2	0.43	2:0.056	402
ME2	P3	0.42	2:0.056	319
ME3	P6	0.13	2:0.056	265
ME4	P6	0.26	2:0.056	215
ME5	P2	1.02	2:0.056	216
ME6	P3	1.04	2:0.056	245
ME7	P6	1.00	2:0.056	113
ME8	P2	1.50	2:0.056	178
ME9	Lutensol AT50	1.03	2:0.056	193
ME10	Lutensol AT 50	8.33	2:0.056	236
ME11	SDS	3.00	2:0.056	106

a) determined by Dynamic light scattering (DLS) analysis.

Stable nanoparticles were generated in all miniemulsion polymerizations, using Lutensol AT50, SDS and mP(EG)$_m$-*b*-P(fcGE)$_n$ block copolymers. The nanoparticle diameters can be varied with the amount of surfactant added to the polymerization mixture: the general trends for the commercially available and well known surfactants Lutensol AT50 and SDS are, that low surfactant concentrations lead to large nanoparticles with broad diameter distributions and high concentrations lead to small nanoparticles with more defined size distributions. This trend was also observed for the miniemulsion polymerizations performed with mP(EG)$_m$-*b*-P(fcGE)$_n$ block copolymers. Low concentrations of 0.42 (**P3**) mg mL^{-1} and

0.43 (**P2**) mg mL^{-1} lead to broadly distributed nanoparticle sizes (with mean diameters of 319 nm (**ME2**) to 402 nm (**ME1**); see Table 2 and Figure 4).

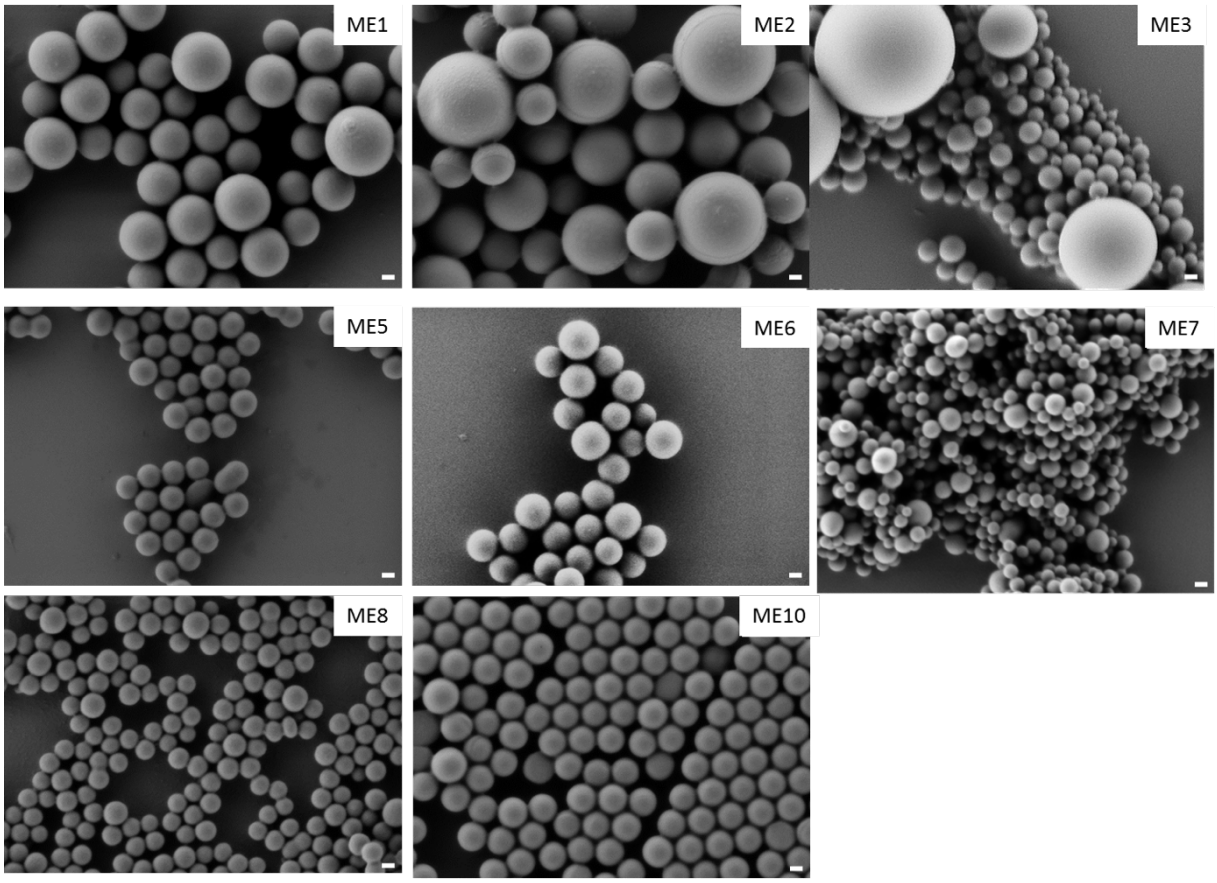

Figure 4. SEM pictures of PS nanoparticles generated by direct miniemulsion with **P2** (**ME1**, **ME5**, **ME8**), **P3** (**ME2**, **ME6**) / Lutensol AT50 (**ME10**) and **P6** (**ME3**, **ME4**, **ME7**) - scale bar = 100 nm.

P6 produced also broadly distributed nanoparticles at a concentration of 0.13 mg mL^{-1} with mean nanoparticle sizes of 265 nm and in addition, low amounts of bigger nanoparticles with sizes up to around 1 μm (**ME3**; Figure 4). Increasing the concentration of **P6** to 0.26 mg mL^{-1} leads to **ME4** with a decreased nanoparticle diameter and narrow size distribution. Increasing the concentrations of **P2**, **P3** and **P6** to 1 mg mL^{-1} yielded polystyrene nanoparticles with sizes of 216 nm for **ME5**, 245 nm for **ME6** and 113 nm for **ME7** (see Table 2 and Figure 4). Increasing the concentration of **P2** to 1.5 mg mL^{-1} (**ME8** in Table 2 and Figure 4) resulted in a further decrease of the nanoparticle diameters from 215 nm to 178 nm.

The influence of the PEG and PfcGE block lengths ratio (PEG:PfcGE varied from 93:7 to 73:27) can be analyzed by the comparison of samples **ME5**, **ME6** and **ME7**. The concentration of these four samples is almost same (ca. 1 mg ml^{-1}) and therefore the nanoparticle sizes can be compared and the differences can be considered as an impact of the block lengths ratio. Sample **P6** with the largest hydrophobic PfcGE block fraction (with 27.2 mol% fcGE) produces smaller PS nanoparticles (113 nm) as **P2** (216 nm) and **P3** (245 nm) (with 7.3 and 8.2 mol% fcGE). PS nanoparticles synthesized with Lutensol AT50 have mean diameters (193 nm for **ME9**) in the same order of magnitude. Also, nanoparticle sizes do not differ significantly at concentrations above 1 mg mL^{-1} for Lutensol AT50, which can be concluded comparing **ME9** (193 nm at 1.03 mg mL^{-1}) and **ME10** with 236 nm (at 8.33 mg mL^{-1}).

Besides the stabilization of a free radical polymerization in miniemulsion, the fc-containing surfactants were studied in the solvent evaporation miniemulsion.[250] The results for the samples **SE1**, **SE2** and **SE3** (Table 3 and Figure 5) show very polydisperse PS nanoparticles. Compared to the samples **ME1**, **ME2** and **ME3** – with similar surfactant concentrations the solvent evaporation process yielded much larger mean diameters of around 956 – 550 nm. Increasing the surfactant amount to 0.82 mg mL^{-1} for **SE4** and 0.73 mg mL^{-1} for **SE5** generated smaller nanoparticles compared to **SE1** and **SE2** as expected. In general, the PS nanoparticles synthesized by **solvent evaporation** miniemulsion are much bigger, than the nanoparticles synthesized by the miniemulsion polymerization, regardless of the utilized surfactant concentrations. The experiment **SE6** did not yield any nanoparticles, because the emulsion destabilized and phase separated during the solvent evaporation process. The hydrophobic character of **P6** seem to be prevailing and therefore **P6** not suitable for the application in solvent evaporation miniemulsions at higher surfactant concentrations.

Table 3. Results of generated PS-nanoparticles according to miniemulsion approach in combination with solvent evaporation.

code	typ of surfactant	surfactant concentration [mg/mL]	water to monomer ration	d [nm][a]
SE1	P2	0.42	5:0.03	956
SE2	P3	0.34	5:0.03	550
SE3	P6	0.13	5:0.03	874
SE4	P2	0.82	5:0.03	522
SE5	P3	0.73	5:0.03	512
SE6	P6	0.72	5:0.03	-

a) Determined by Dynamic light scattering (DLS) analysis. b) Under argon atmosphere.

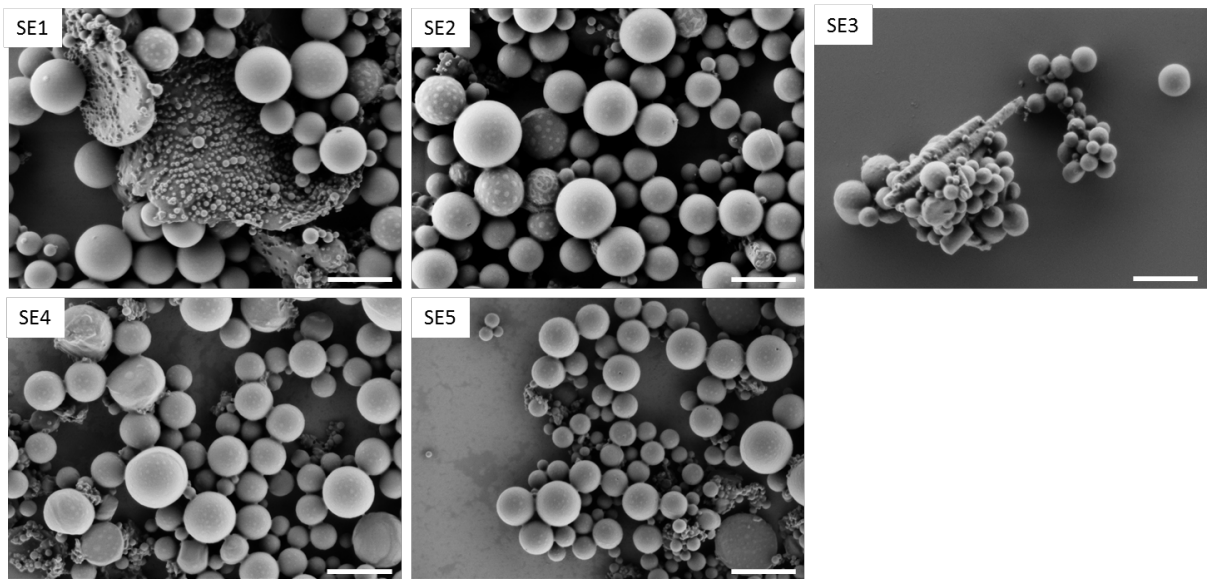

Figure 5. SEM pictures of PS nanoparticles generated by direct miniemulsion in combination with solvent evaporation **P2** (**SE1** and **SE4**), **P3** (**SE2** and **SE5**) and **P6** (**SE3**) – scale bar=1 μm.

Redox- and pH-triggered destabilization of the different miniemulsions were studied in details. Therefore, the emulsions were acidified to lower the pH values (pH = 1, 3, 5, 7) or oxidants (different concentrations of H_2O_2, $AgNO_3$ or $KMnO_4$) were added to oxidize ferrocene to the ferrocenium ion. After oxidation with acid or oxidant the hydrophilic-lipophilic balance (HLB) of the surfactant is altered and the nanoparticle dispersion should

be destabilized, resulting in the precipitation of the nanoparticles. Figure 6 summarized the destabilization behavior of miniemulsions stabilized with the redox-responsive surfactants **P2** and **P3** in comparison to the miniemulsions stabilized with Lutensol AT50, which is not redox- or pH- responsive. Destabilization of **ME1** and **ME2** with 36% H_2O_2 solution occurs after one day, whereas the destabilization after treatment with 18% and 8% H_2O_2 as well as HCl decreasing the pH to 1 and 3 occurs after three days. At pH 5 the destabilization behavior was slower than at pH 3 and proceeded over 5 days. In neutral pH solutions the miniemulsion remained stable over at least 2 weeks – as it is expected. The Lutensol-stabilized nanoparticles did not destabilize in any case as expected, since it does not include any redox- or pH-sensitive group.

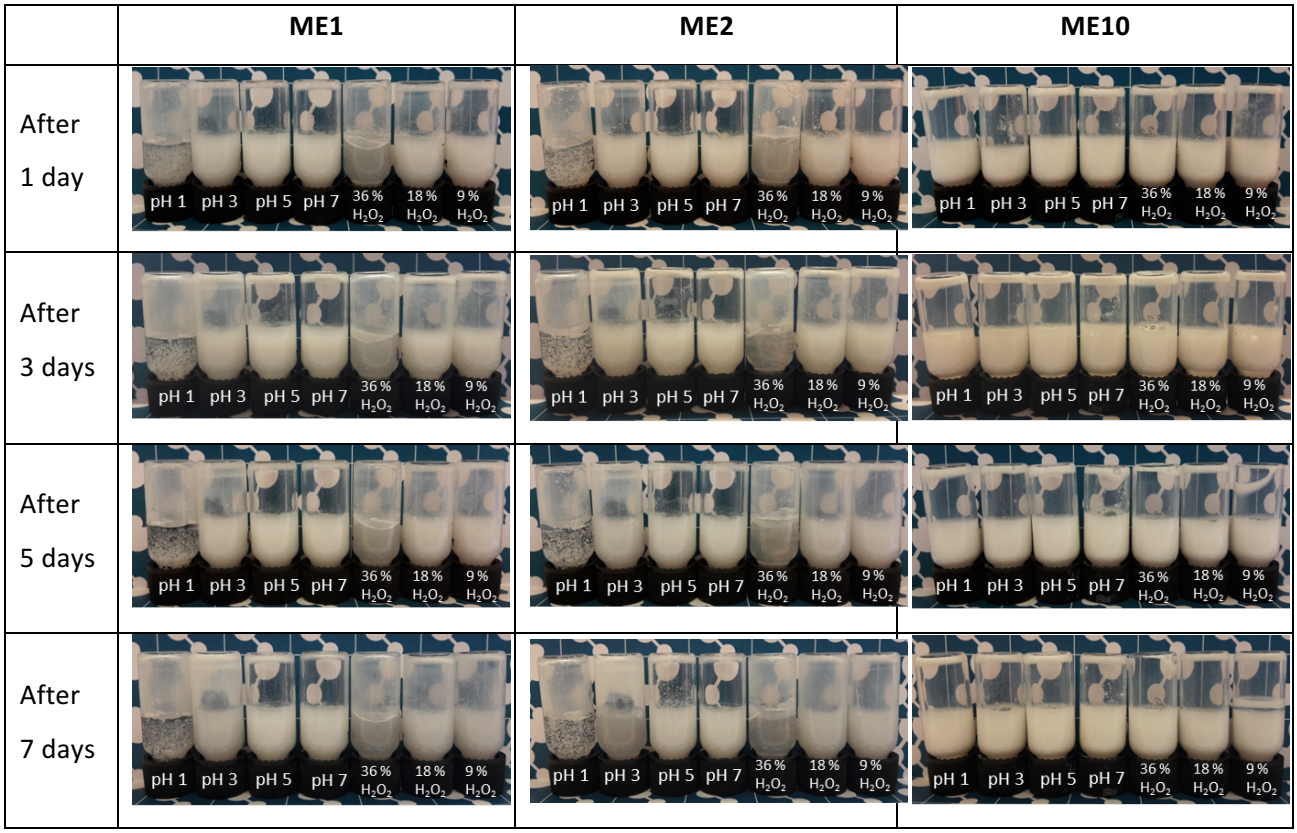

Figure 6. Destabilization of PS nanoparticles stabilized with **P2** and **P3** as well as Lutensol AT50 at pH = 1, 3, 5, 7 or 37%, 18% or 8% H_2O_2 detected over 1 week.

In addition, miniemulsions with different concentrations of **P2** and **P3** were analyzed under same conditions with same results, proving concentration independent destabilization

kinetics. Indeed, significant differences were determined for miniemulsions stabilized with **P6**, which showed faster destabilization probably because of a larger PfcGE block as in **P2** or **P3** including less ferrocene. For example, at pH 1 or with 36% H_2O_2 the destabilization of **P6** occurred immediately. Furthermore, solutions with other oxidants $AgNO_3$ and $KMnO_4$ instead of H_2O_2 were tested leading in flocculation of the nanoparticles after 1 day.

Conclusion

PEG-based ferrocene-containing amphiphilic block copolymers have been synthesized by anionic polymerization. PEG monomethyl ether was used as a macroinitiator for the polymerization of fcGE. The amphiphilic properties are characterized by calculation of the formal HLB values and the determination of the CMCs, which are similar compared to other polymeric nonionic surfactants, such as Lutensol AT50. The hydrophilic/lipophilic balance for the PEG-*b*-PfcGE was varied from 5.6 to 14.9 by varying the block ratios. The synthesized amphiphilic block copolymers were utilized for the oil-in-water miniemulsion process (miniemulsion polymerization and solvent evaporation protocol) to stabilize PS nanoparticles. The impact of different surfactant concentrations as well as the block lengths ratio of the polymers on the particle sizes were analyzed. Destabilization studies were performed under oxidative conditions using acids and oxidation agents. We hope that this new type of amphiphilic ferrocene block copolymers will find application as “smart” responsive surfactants.

3.1.1 Supporting Information

Experimental Section

Instrumentation. ^{1}H NMR spectra (300, 400 MHz) and ^{13}C NMR spectra (75.5 MHz) were recorded using a Bruker AC300 and a Bruker AMX400. All spectra were referenced internally to residual proton signals of the deuterated solvent. For SEC measurements in DMF (containing 0.25 g·L^{-1} of lithium bromide as an additive) an Agilent 1100 Series was used as an integrated instrument, including a PSS HEMA column (106/105/104 g·mol^{-1}), a UV detector (275 nm), and a RI detector at a flow rate of 1 mL·min^{-1} at 50 °C. Calibration was carried out using PEO standards provided by Polymer Standards Service. Matrix-assisted laser desorption/ionization time-of-flight (MALDI-ToF) measurements were performed using a Shimadzu Axima CFR MALDI-TOF mass spectrometer, employing dithranol (1,8-dihydroxy-9(10*H*)-anthracenone) as a matrix. Scanning electron microscopy (SEM) of the formed nanoparticles was operated at a Zeiss 1530 LEO Gemini microscope with a accelerating voltage of 0.2 kV and a working distance of ~3 mm. Therefore, the nanopartciles were diluted in water, dropped onto a silica wafer and dried under ambient conditions.

Dynamic light scattering was used to detect the hydrodynamic diameter of the nanoparticles by a Nicomp 380 Submicron particle Sizer (PSS-Nicomp) at a fixed scattering angle of 90 °C. 10 μL of the emulsion was diluted in 1000 μL distilled water. Critical micelle concentration was measured by isothermal titration calorimetry using a MicroCal VP-ITC (GE Healthcare, Piscataway, USA). Therefore, a stock solution of each polymer (concentration of **P2** 8 g/L, of **P6** 2 g/L) was added dropwise (2 μl in 25 steps) into an ITC chamber at 25 °C. During the measurement, the heat flow was detected, whereas an exothermic heat flow contributes from dilution of the surfactant solution, which decreases the surfactant concentration. Micelle formation below the cmc leads in an endothermic heat flow. The addition of both terms maintained a minimum of the heat flow at the cmc.

Reagents. Solvents and reagents were purchased from Acros Organics, Sigma-Aldrich or Fluka and used as received, unless otherwise stated. Chloroform-d_1 and benzene-d_6 were purchased from Deutero GmbH. fcGE was synthesized according to the published procedures.[85] fcGE and mPEG were dried by azeotropic distillation of benzene to remove traces of water. Styrene was purified by column chromatography over neutral Al_2O_3 and stored at 4 °C.

General Procedure for the polymerization of fcGE: (mPEG-b-PfcGE). The initiator, 800.0 mg (0.1600 mmol) mPEG, and 24.2 mg (0.1441 mmol, 0.9 eq.) of cesium hydroxide monohydrate were placed in a 100 mL Schlenk flask and suspended in 10 mL of benzene. The mixture was stirred at 60 °C under an argon atmosphere for 1 h and evacuated at 40 °C (10^{-2} mbar) for 12 h to remove benzene and the water formed (as an azeotrope with benzene) to generate the corresponding cesium alkoxide. The flask was filled with argon and cooled to room temperature, and then fcGE (824.4 mg (3.029 mmol) was added. The reaction mixture was heated up to 100 °C and stirred for 24 h before the living chain ends were terminated with methanol and the block copolymer was precipitated in cold diethyl ether to get rid of unreacted fcGE. The block copolymer was obtained as a yellow to orange solid. Yields: 70-85%. ^{1}H NMR (C_6D_6, 400 MHz): δ(ppm) = 4.40-4.15 (br, 4H, -O-CH_2-Cp(*2*, *5*)), 4.15-3.92 (br, 7H, -O-CH_2-Cp(*3*, *4*)-Fe-*Cp*), 3.60-3.38 (br, PEG-backbone), 3.13 (s, 3H, H_3C-O-).

General Procedure for polymerization of styrene by miniemulsion: PEO-*b*-PfcGE (for amount see Table 2) was dissolved in 2 mL water. After a solution of 56 μL styrene, 3.2 μl hexadecane and 0.5 mg AIBN was added, the dispersion was stirred for 1 h at 1000 rpm. The dispersion was treated by inverse ultrasonication at 70 % amplitude for 2 min and stirred for 24 h at 72 °C. Results are listed in Table 2.

General Procedure for solvent evaporation miniemulsion: 30 mg polystyrene (35 kDa) and PEO-*b*-PfcGE (for amount see Table 3) were dissolved in 1 g $CHCl_3$ and added to 5 mL water. After stirring for 1 h, the dispersion was treated with ultrasonication at ½ tip, 70 %

amplitude for 2 min with 30 sec puls and 10 sec pause. Then the emulsion as stirred with open cap at 35 °C over night. Results are listed in Table 3.

General Procedure for destabilization of polystyrene nanoparticles: 0.1 mL emulsion were added to 0.75 mL HCl solution with different pH values (pH = 1, 3, 5 7) or oxidant solutions (37 %, 18 % or 8 % H_2O_2, 4 mg/mL $KMnO_4$, 8 mg/mL $AgSO_3CF_3$). At the latest after 3 days the emulsions destabilized and the nanoparticles aggregated. As comparison also 0.1 mL polystyrene emulsion stabilized with SDS or Lutensol AT 50 was added to 0.75 mL HCl solutions with different pH values or hydrogen peroxide solution.

Chapter 4: Monomer Sequence Monitoring by Real-Time NMR Spectroscopy

4.1 Ferrocene-Containing Multifunctional Polyethers: Monomer Sequence Monitoring via Quantitative ^{13}C NMR Spectroscopy in Bulk

Published in *Macromolecules* **2014**, 47, 2242–2249. (Published by the American Chemical Society.)

Authors: *Arda Alkan,[+,§] Adrian Natalello,[+,‡] Manfred Wagner,[§] Holger Frey[+] and Frederik R. Wurm*[*,§]*

[+]Institute of Organic Chemistry, Johannes Gutenberg-Universität Mainz (JGU), Duesbergweg 10-14, 55099 Mainz, Germany.

[‡]Graduate School Materials Science in Mainz, Staudinger Weg 9, 55128 Mainz, Germany.

[§]Max Planck Institute for Polymer Research (MPIP), Ackermannweg 10, 55128 Mainz, Germany.

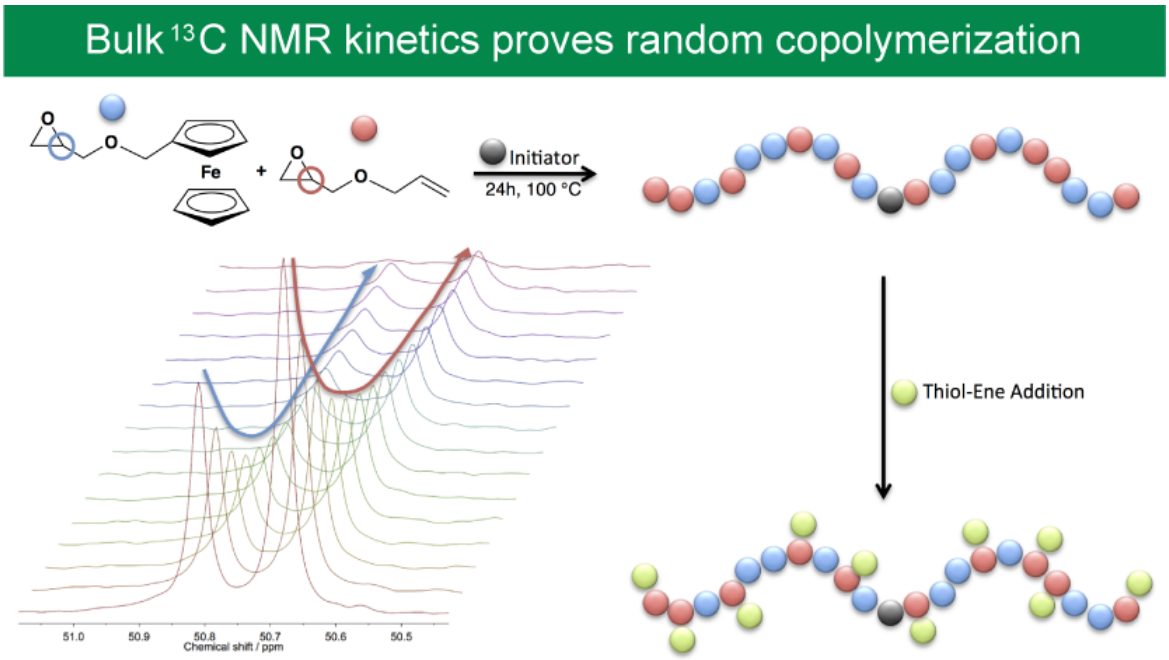

Abstract

Ferrocenyl glycidyl ether (fcGE) and allyl glycidyl ether (AGE) are copolymerized via living anionic ring-opening polymerization to generate polyfunctional copolymers with molecular weights up to 40 300 g/mol and low molecular weight dispersities (M_w/M_n <1.18). Copolymerizations were carried out in bulk at 100 °C and unexpectedly found to proceed without any isomerization of the allyl double bonds. The copolymerization behavior of fcGE and AGE was monitored by in-situ quantitative ^{13}C NMR kinetic measurements in bulk, evidencing the formation of random copolymers under these conditions, showing no gradient of comonomer incorporation. The redox-active behavior of the copolymers and homopolymers of fcGE was studied by cyclovoltammetry (CV). In order to demonstrate possible postmodification reactions, the random copolymers were modified with N-acetyl-L-cysteine methyl ester via a thiol-ene addition. All polymers have furthermore been characterized by ^{1}H NMR spectroscopy, DOSY ^{1}H NMR spectroscopy, size exclusion chromatography (SEC), and MALDI-ToF mass spectrometry.

Introduction

Metallocene-containing polymers, particularly materials based on ferrocene (fc), are unusual polymers due to their unique physical and chemical properties.[95,251] Ferrocene is thermally very stable (up to 454 °C)[252], and it can be oxidized reversibly to the ferrocenium ion, rendering it a highly interesting organometallic group for materials for various applications. For example, fc is used as electroactive material in amperometric glucose sensors[144] and as a catalyst[145-147] in fuel for the oxidation of soot.[148,253] Furthermore fc-containing materials are currently also discussed for biomedical applications, since ferrocene and its derivatives have proven to be active against cancer cells,[25,30,53,254] fungal infections,[37] malaria[38,255] and also the human immunodeficiency virus (HIV).[16,17,36,256,257]

Ferrocene (or other metallocenes)[251] can be introduced into polymeric structures via several approaches: (i) either fc-containing monomers are polymerized to generate structures with

fc in the main chain or as pendant groups, or (ii) fc-groups are attached to a multivalent, prefabricated polymer as side chains subsequent to polymerization. The latter strategy is often preferred, since special monomer syntheses can be circumvented;[258] however, in many cases the degree of functionalization is difficult to control. Such polymer modifications are often used to generate random copolymers (not necessarily with fc), especially in radical polymerization, where direct copolymerization of different monomers often results in gradient or block-like structures.[259]

Direct copolymerization needs to be applied to place fc in the polymer backbone, which can be achieved by ring-opening polymerization (ROP) of metallocenophanes[260,261] to obtain main-chain poly(metallocene)s,[262] while the polymerization of vinylferrocene or fc-acrylates attaches fc-groups to the polymers' side chains.[263,264]

The above-mentioned fc-containing polymers are usually hydrophobic. For many (and particularly) bio-applications, they have to be converted into water-soluble fc-containing materials via different post-polymerization modification strategies.[265] In a previous work we presented a general synthetic protocol to generate hydroxyl terminated poly(ferrocenyl-silane)s (PFS) for use as macroinitiators to prepare water-soluble PEG chains as a second block and thus to synthesize amphiphilic, water-soluble PFS-*b*-PEG.[68] In the context of fast access to water-soluble fc-containing polymers, we recently introduced ferrocene glycidyl ether (fcGE, **1**) as a novel epoxide monomer carrying a fc side chain.[85] Ferrocene glycidyl ether was utilized for living anionic ring-opening polymerization: **1** was homopolymerized as well as copolymerized with ethylene oxide (EO) leading to water-soluble fc-containing copolymers (with fcGE contents up to 10 mol%), which show a lower critical solution temperature (LCST) in water. The copolymerization was studied and found to be random in the case of EO and **1**. Interestingly, despite the bulky fc-side chain, no gradient copolymers were formed.

The current work aims at two separate objectives: on the one hand it expands the applications of fcGE to polyvalent materials and on the other hand it presents the first *in situ* microstructure analysis throughout a bulk copolymerization via quantitative ^{13}C NMR spectroscopy. Copolymerization of **1** was studied with a functional comonomer, namely allyl glycidyl ether (AGE; **2**). The anionic ROP was carried out in bulk aiming at novel, polyvalent

fc-containing polymers, i.e. poly[(ferrocenyl glycidyl ether)-*co*-(allyl glycidyl ether)] (P[fcGE-*co*-AGE]). The materials possess an adjustable number of redox-active ferrocenes and reactive double bonds, which can be addressed by further transformations (Scheme 1). Conventional characterization of the copolymers is presented in section A of the Results and Discussion part of this work. Thiol-ene addition was chosen as a proof-of-principle modification to confirm that all allyl double bonds are addressable.

As an unusual feature, we introduce in part B the *in situ* quantitative ^{13}C NMR kinetic measurements in bulk. This general method allows receiving integratable ^{13}C NMR spectra within minutes and permits to follow the polymerization until completion over a period of several hours to assess comonomer reactivity.

Scheme 1. Synthetic protocol for the anionic copolymerization of fcGE and AGE with subsequent thiol-ene modification.

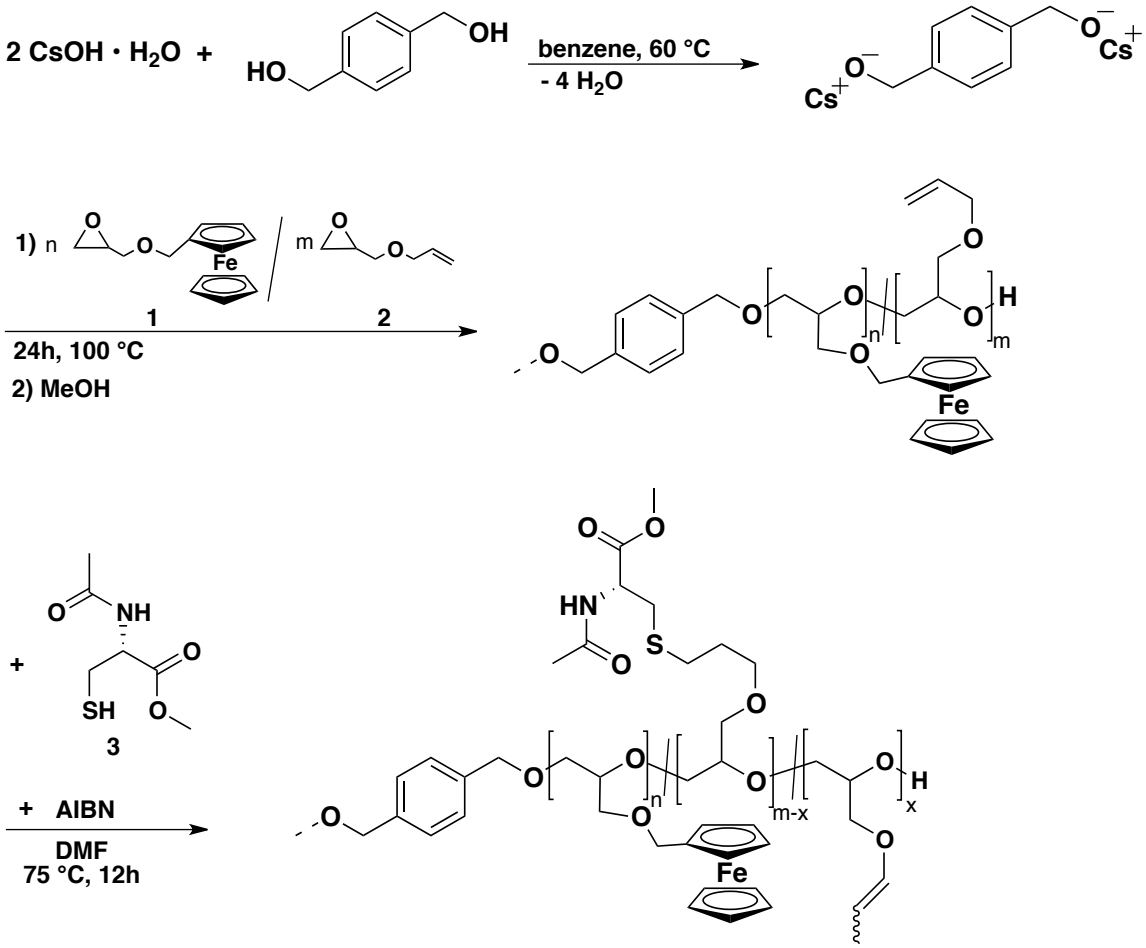

Results and Discussion

An important feature for any copolymerization is the resulting comonomer sequence,[266] i.e., the microstructure, of the polymer chain.[267,268] Ionic polymerization permits tailoring of the monomer sequence by several handles, such as the counter-ion or solvent. The averaged monomer sequence distribution can be investigated subsequent to polymerization via ^{13}C NMR spectroscopy, i.e. triad distribution. However, it is desirable to follow the monomer sequence throughout the polymerization process *in situ* in order to directly monitor gradient formation in the growing polymer chain. In previous works, *in situ* ^{1}H NMR spectroscopy was used to monitor the copolymerization behavior of two monomers in solution.[160,161] With this technique several carb- and oxyanionic comonomer pairs (usually with EO as a comonomer) have been investigated in unprecedented detail in recent years.

Polymer Synthesis and Characterization

Oxyanionic copolymerization of epoxides allows the synthesis of polyfunctional PEG-like materials.[158,180,269,270] In this study we developed novel copolymers that are based on a flexible polyether backbone and multiple functions: (i) ferrocene moieties that can be addressed by reversible redox chemistry which can be used in sensors or as drugs, and (ii) multiple double bonds that can be post-modified in several reactions to attach labels or targeting moieties which would not sustain an anionic polymerization.

For the copolymerization of **1** and **2**, the cesium salt of benzene-1,4-dimethanol was used as the respective initiator. All polymerizations were performed in the absence of solvent in bulk at 100 °C over a period of several hours until complete conversion was achieved. A copolymerization temperature of approximately 100 °C is required to achieve an adequate reaction rate, which is shown in Figure S1 where the temperature dependency is shown by SEC traces of polymer samples synthesized at different temperatures. After 24 h at 70°C or 80°C only incomplete conversion was detected via SEC. When the reaction temperature was raised to 100°C, after 24 h complete conversion and monomodal SEC traces were obtained. With the optimized reaction conditions, all (co-)polymers synthesized herein exhibit narrow

molecular weight distributions (M_w/M_n<1.18 and below 1.1 in most cases), and their molecular weight was controllable by the monomer initiator ratio as expected for a living polymerization.

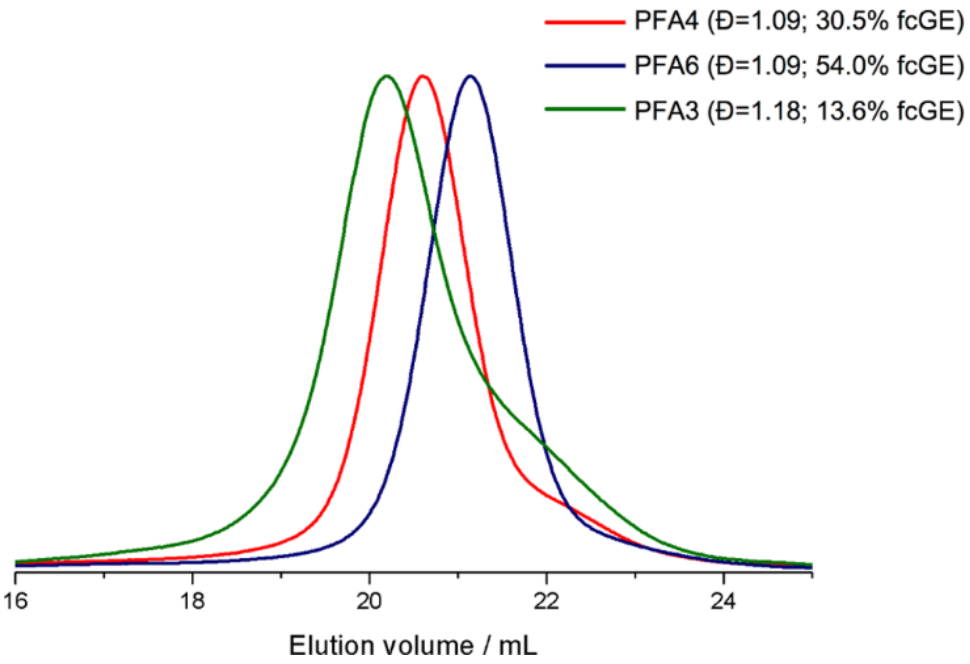

Figure 1. Typical SEC traces of three copolymers (DMF, RI detection, 1 mL/min, 40°C).

Figure 1 shows three SEC traces, which are representative of all polymers shown in Table 1. PFA4 and PFA6 exhibit low dispersities (*Đ*<1.10) and PFA3 shows a slightly broader molecular weight distribution (*Đ*=1.18), most probably due to increased viscosity during the generation of higher molecular weight material in the bulk polymerization or due to transfer reactions because of a high reaction temperature and bulk conditions. (Figures S2-S5 show additional SEC traces). Table 1 lists the molecular weights and composition data for the copolymers. The molecular weights of all (co-)polymers determined from SEC are underestimated compared to the molecular weights by end group analysis from the ^{1}H NMR spectra (Figures 2 and S6). As the molecular weight dispersity is low, a controlled polymerization mechanism appears to occur even in bulk, and the discrepancy between SEC and absolute molecular weight is related to the apparent molecular weights obtained from SEC with conventional calibration.

The molecular weights calculated from the ^{1}H NMR spectra are in good agreement with theoretical values. To calculate the M_n values, the resonances of the initiator at 7.34 ppm (aromatic protons) and 4.42 ppm (resonances of the benzyl protons) were integrated and compared to the protons of the allyl groups (4.96-6.03 ppm) and to the residual resonances of the backbone protons of the copolymer (3.26-4.34 ppm).

Table 1. Characterization data for P(fcGE-*co*-AGE) copolymers and homopolymers P(fcGE) and P(AGE).

no.	sum	fcGE/(fcGE +AGE) (%)	M_n[a] (g/mol)	M_n[b] (g/mol)	M_n[c] (g/mol)	$Đ$[c]	T_g[d] (°C)
PA1	$C_6H_4(CH_2O)_2$-[P(AGE_{117})]$_2$	0	30 000	26 700	5 600	1.12	-77
PFA1	$C_6H_4(CH_2O)_2$-[P($fcGE_{12}$-*co*-AGE_{138})]$_2$	8.0	49 000	38 200	3 500	1.17	-74
PFA2	$C_6H_4(CH_2O)_2$-[P($fcGE_{12}$-*co*-AGE_{114})]$_2$	9.0	26 000	32 400	2 200	1.08	-71
PFA3	$C_6H_4(CH_2O)_2$-[P($fcGE_{20}$-*co*-AGE_{128})]$_2$	13.6	52 000	40 300	3 200	1.18	-77
PFA4	$C_6H_4(CH_2O)_2$-[P($fcGE_{32}$-*co*-AGE_{73})]$_2$	30.5	32 000	34 300	2 200	1.09	-52
PFA5	$C_6H_4(CH_2O)_2$-[P($fcGE_5$-*co*-AGE_6)]$_2$	41.9	4 800	4 630	2 200	1.11	-58
PFA6	$C_6H_4(CH_2O)_2$-[P($fcGE_{50}$-*co*-AGE_{43})]$_2$	54.0	39 000	37 000	1 900	1.09	-38
PF1	$C_6H_4(CH_2O)_2$-[P($fcGE_{55}$)]$_2$	100	27 000	30 100	1 700	1.14	-8

a) Theoretical molecular weight according to initiator concentration (see Table S1 for details); b) M_n determined from ^{1}H NMR by end group analysis; c) M_n determined via SEC in DMF vs PEG standards, $Đ=M_w/M_n$. d) Determined from differential scanning calorimetry.

All copolymers were further characterized via DOSY ^{1}H NMR spectroscopy; Figure 2 displays the DOSY ^{1}H NMR spectrum of PFA2 as an example. The x-axis shows the conventional

^{1}H NMR spectrum (highly magnified to show the initiator's resonances), and the y-axis gives the diffusion coefficient. From the 2D plot it is obvious that all resonances of the 1D ^{1}H NMR spectrum (except for the solvent signal of benzene at 7.16 ppm) stem from the polymer plus the initiator, since they exhibit the same diffusion coefficient.

From the ^{1}H NMR spectra the allyl double bonds can be clearly detected and, in contrast to anionic ring-opening polymerization of AGE in previous works,[271] no isomerization of the terminal double bonds was detected under the reaction conditions chosen (bulk, 100°C, 24h). We assume that the strict absence of solvent and the use of cesium alkoxides in our case reduces isomerization compared to the respective potassium alkoxide propagating species prepared from potassium naphthalenide solution.

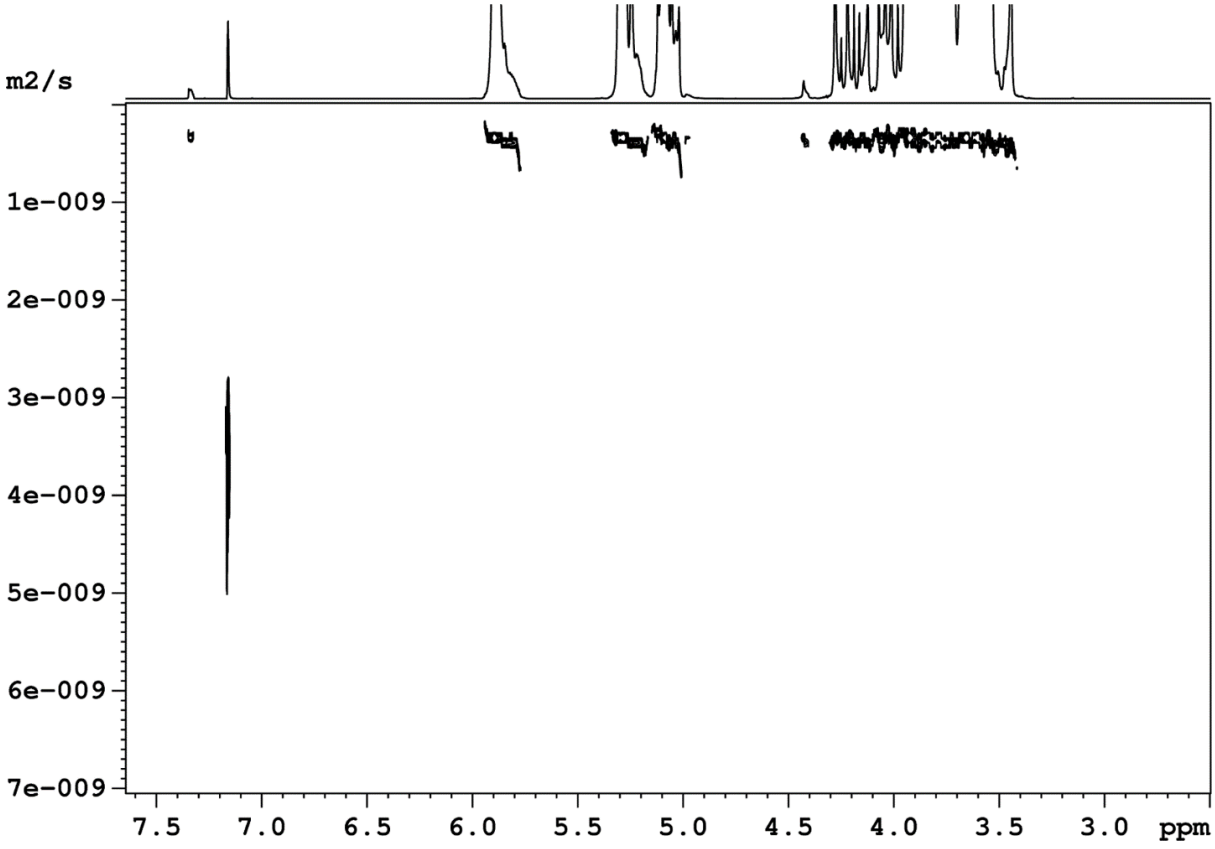

Figure 2. DOSY ^{1}H NMR spectrum of P(fcGE-*co*-AGE) (PFA2, C_6D_6, 500 MHz, 298 K).

To further confirm incorporation of both monomers and the initiator into the copolymer structure, matrix-assisted laser desorption/ionization time-of-flight mass spectrometry

(MALDI-ToF MS) was used. Figure 3 shows the MALDI-ToF mass spectrum of PFA5. The repeating units with 114 g/mol for AGE (blue) and 272 g/mol for fcGE (red) are clearly recognizable and marked with arrows. Each detected signal corresponds to the mass of a linear combination of both monomers in the copolymer (in Figure 3 two peaks are marked exemplarily, using silver cations as counter ions).

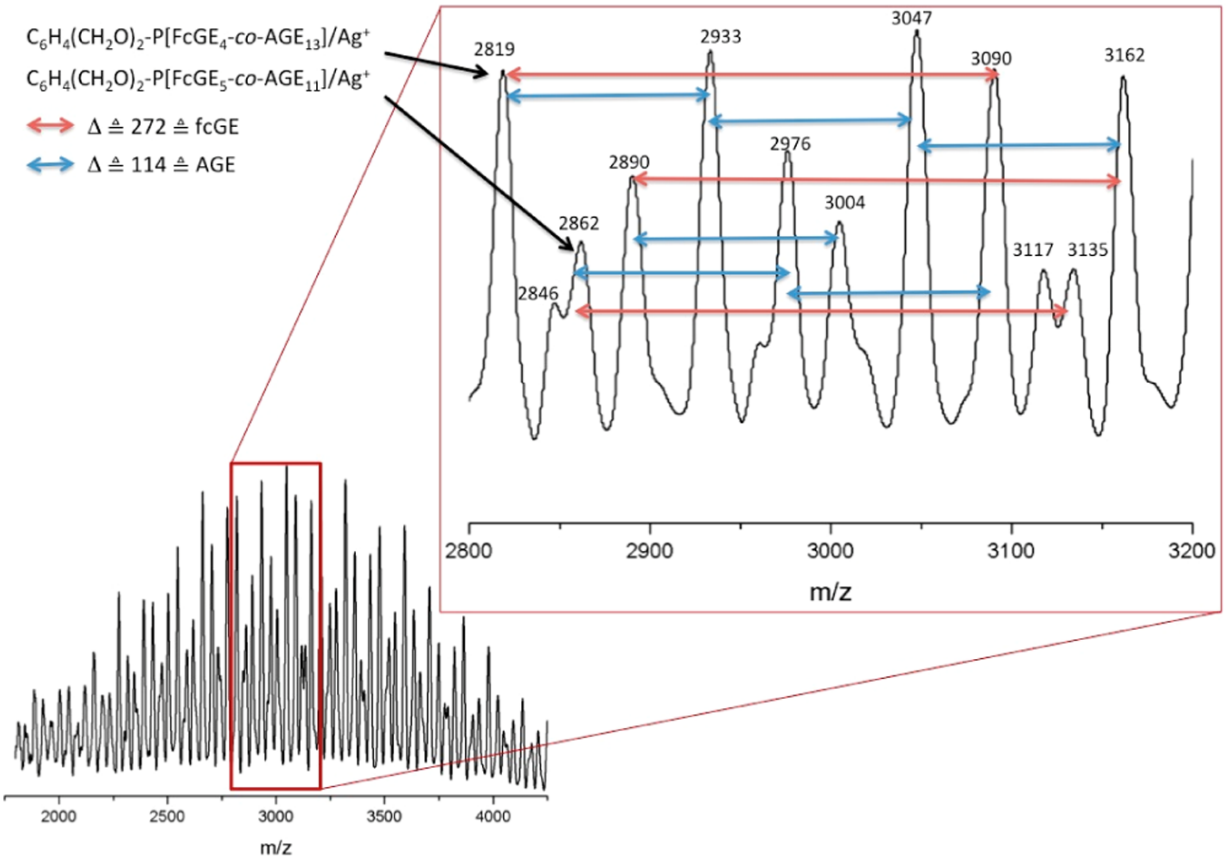

Figure 3. MALDI-ToF mass spectrum of P(fcGE-*co*-AGE) (PFA5).

In situ ^{13}C NMR Copolymerization Kinetics

Epoxide copolymerization in bulk, i.e., avoiding the addition of a solvent is attractive, since work-up procedures and scale-up are greatly facilitated. As the comonomer distribution is crucial for direct copolymerization, a robust method for in situ monitoring of the monomer consumption is necessary. A general quantitative, in situ monitoring method for bulk

(co)polymerizations based on ^{13}C NMR spectroscopy was developed. To the best of our knowledge, quantitative ^{13}C NMR spectroscopy has not been used to follow copolymerizations in situ. This is due to the low natural abundance of NMR-active ^{13}C isotopes, making quantitative measurement in a deuterated solvent time-consuming, i.e., too slow for a kinetic study. In this case ^{13}C-enriched compounds would be necessary. We recently used ^{1}H NMR to monitor anionic copolymerizations in situ (i.e. conducting the copolymerization directly in an NMR-tube in a deuterated solvent in the spectrometer), as it is a readily accessible and quantitative method to follow the consumption of both monomers.[158,161] In a previous work, we were able to prove by ^{1}H NMR kinetic studies that fcGE forms random copolymers with EO in solution (DMSO or DMSO/THF mixtures).[85]

Following ionic bulk (co)polymerizations via conventional NMR, the addition of any solvent would alter the polymerization behavior of the ionic propagating species and could influence comonomer incorporation. However, copolymerization of **1** and **2** was conducted without any solvent, thus conventional NMR becomes impossible. However, in a bulk polymerization the natural abundance of ^{13}C isotopes is sufficient to obtain a quantitative ^{13}C NMR spectrum within minutes. For the epoxide copolymerizations we found that ^{13}C NMR spectra can be measured *in situ* and in bulk as the viscosity is low enough to obtain quantitative spectra. This general protocol allows elucidating the microstructure of the growing polymer at any time point throughout the reaction (compare the Experimental Section for details). As here no solvent dilutes the ^{13}C-concentration of the monomers, the natural abundance suffices to obtain a quantitative, i.e.integratable, ^{13}C NMR spectrum within minutes. The reaction can be conducted in a conventional NMR spectrometer in a standard NMR tube. It is important that the viscosity of the reaction mixture allows the full relaxation of all carbon atoms that are monitored (for further details please refer to the Experimental Part). In an initial experiment traces of benzene were added to the reaction mixture as an internal standard which did not change its integral throughout the polymerization. Thus, the monomer consumption during the copolymerization in bulk can be monitored at any time point throughout the polymerization by integration of the epoxide carbon resonances of each comonomer (Figure 4 & Figures S7, S8).

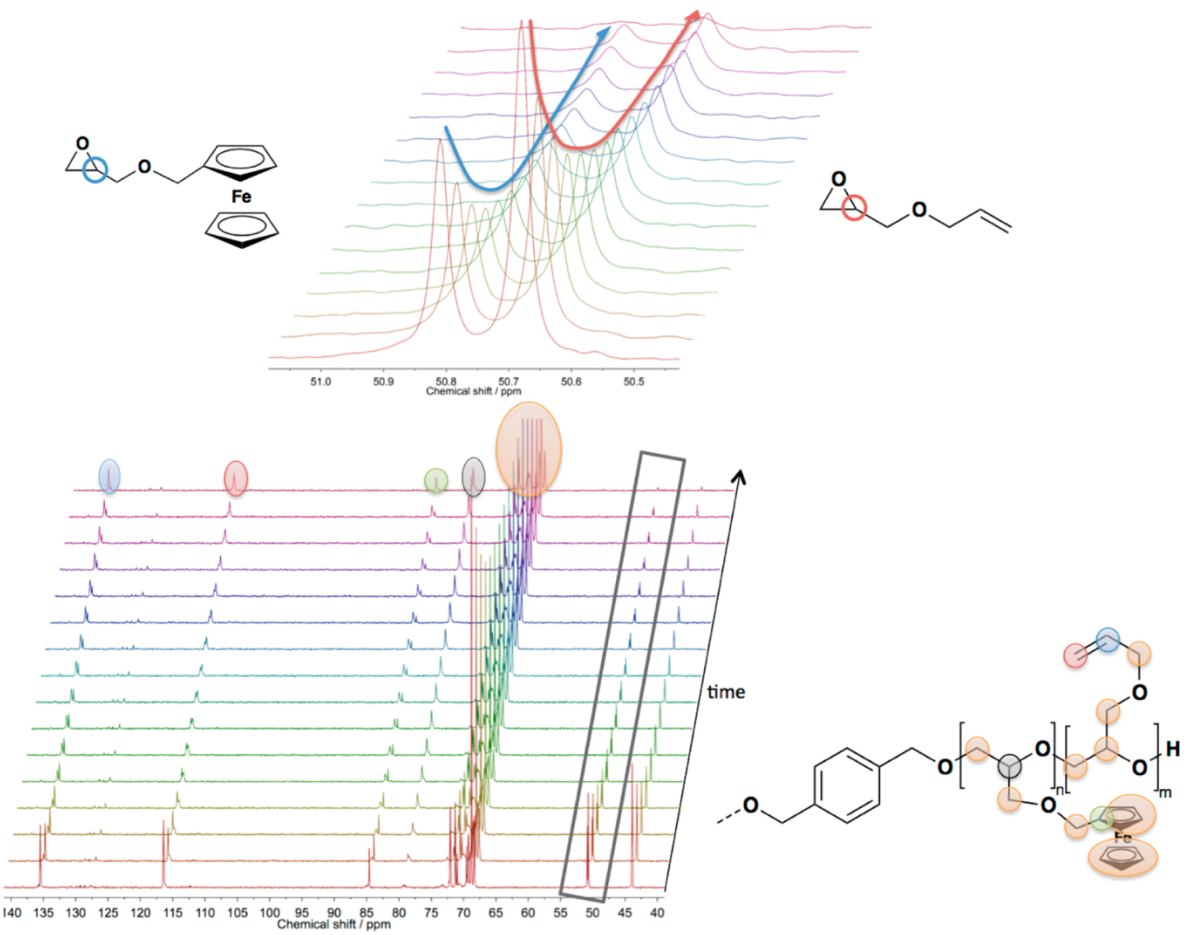

Figure 4. ^{13}C NMR *in situ* kinetics of the anionic ring-opening copolymerization of fcGE and AGE (monomer ratio 1:1.2) with a zoom into the methine carbons at ca. 50 ppm (no solvent, 126 MHz; 363 K).

In the case of **1** and **2** the resonances for the substituted carbons in both epoxides, i.e. the methine groups (at 50.65 and 50.8 ppm, compare Figure 4), were compared during the reaction to determine the comonomer consumption. The methylene resonances can also be used, however, the chemical shift difference is lower in this case. In both cases it was secured by internal standards (e.g. the double bonds of AGE, substituted carbon atom of ferrocene which remain unchanged during the measurement or addition of benzene). The growing polymer backbone is also visible in the spectra, but cannot be used for reliable integration due to its longer relaxation times. In Figure 5 (and Figure S9) the monomer concentrations for two different monomer ratios are plotted against the total conversion

(percentage, note: the monomer concentrations in the first ^{13}C NMR spectrum are set to 100%).

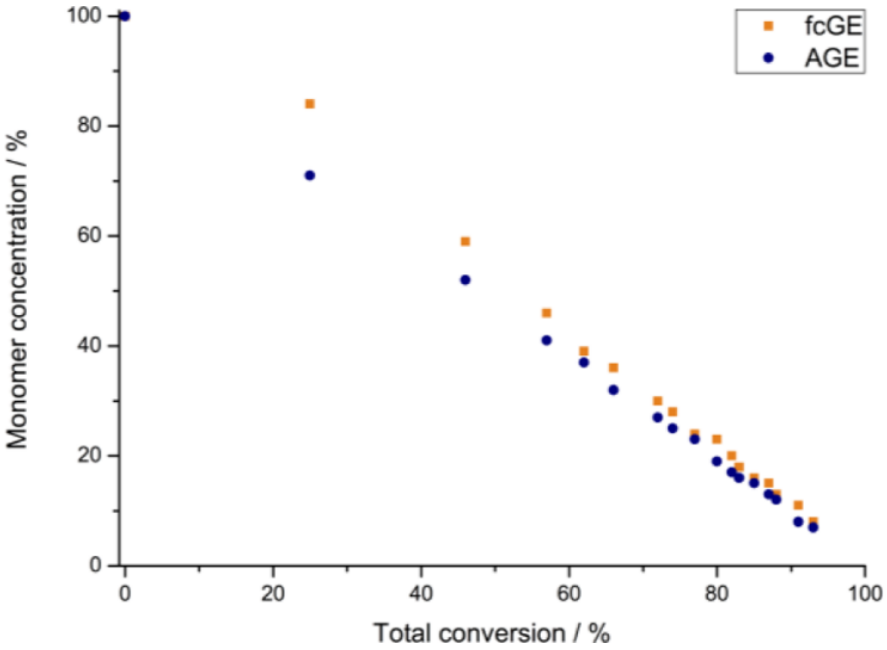

Figure 5. Percentage of monomer concentration vs. total conversion for copolymerization of fcGE and AGE (monomer ratio 1:1.2) determined from quantitative ^{13}C NMR kinetics in bulk.

For both comonomer ratios a random distribution of AGE and fcGE under these conditions (bulk, 100°C) was found. This is in good agreement with previous works showing random incorporation of several glycidyl ethers upon copolymerization with EO conducted in polar solvents (such as THF or DMSO).[158,161] Since the copolymerization of **1** and **2** is conducted in bulk, one cannot necessarily assume the same reactivity ratios for this system as in the case of copolymerization with EO studied in various solvents. However, also for the herein investigated comonomer pair, we were able to prove that both monomers are consistently incorporated at the same rate throughout the whole polymerization.

Properties of P(fcGE-*co*-AGE) Copolymers

Thermal Analysis. Thermal analysis of all copolymers was carried out using differential scanning calorimetry (DSC). The determined T_gs increase with increasing amount of **1** in the

copolymer structure from -77 °C for the PAGE homopolymer to -8 °C for the PfcGE homopolymer.

Due to the lack of tacticity and the sterically demanding side chains of allyl- and ferrocenyl-groups a fully amorphous polymer is obtained. The linear increase of the T_gs indicates an increase in the fcGE-content of the copolymers, which was proven before via ^{1}H NMR spectroscopy and can be also seen with the naked eye from the color of the samples (Figure S10). *Cyclic voltammetry measurements.* Fc can be oxidized reversibly by applying a cyclic potential, and this redox-active behavior can be studied by cyclic voltammetry. Two copolymers with different fc contents were studied with cyclic voltammetry. The copolymer samples PFA1 with 8% fcGE and PFA5 with 42% fcGE incorporated were dissolved in dichloromethane at a concentration of 5 g/L with 0.1 M conducting salt (tetrabutylammonium hexafluorophosphate). Figures 6, S11 and S12 show the cyclic volt-ammograms of both copolymers and in addition of a PfcGE homopolymer.

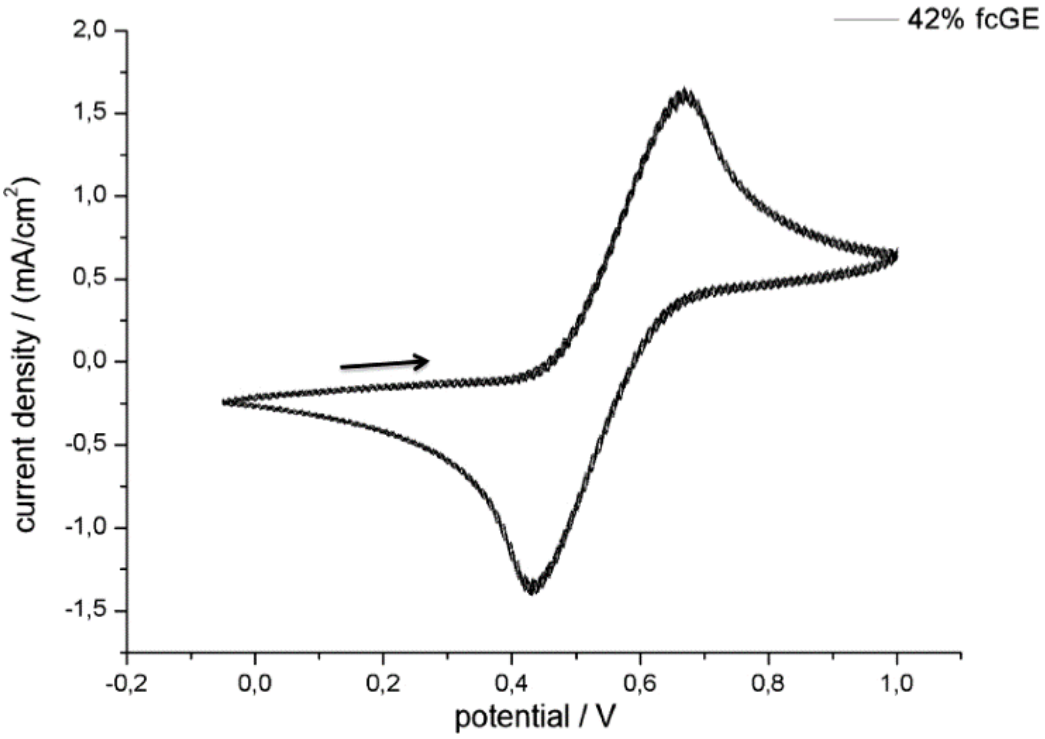

Figure 6. Cyclic voltammogram of copolymer PFA5 with 42% fcGE (10 cycles).

As known from P(fcGE-*co*-EO) copolymers the oxidation is a homogeneous process for polyethers based on fcGE.[85] Adjacent ferrocene units do not communicate with each other, and therefore only one reversible oxidation is observed. Each polymer was measured in 10 consecutive cycles without any decrease in current density, demonstrating excellent redox-stability of the ferrocene-containing polyethers. Furthermore, UV spectra of the copolymer PFA6 before and after oxidation was recorded and is shown in Figure 7. The absorption band is shifted from 440 to 630 nm after oxidation with silver triflate in agreement with expectation.

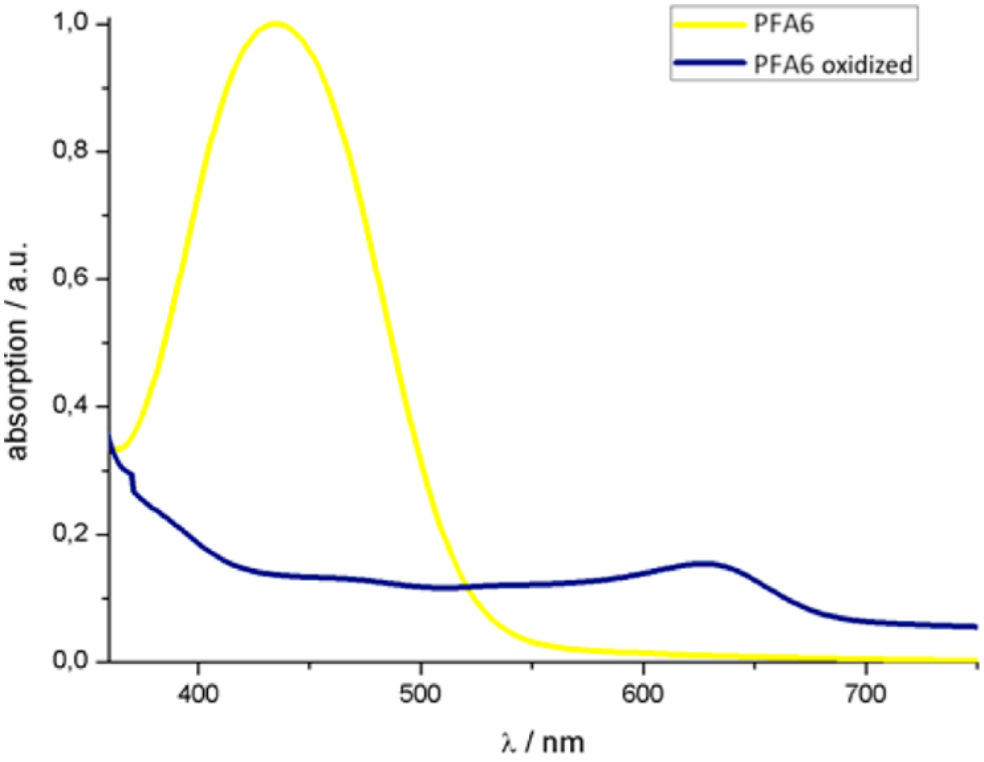

Figure 7. UV spectra of copolymer PFA6 (yellow) in THF and after oxidation (blue) in water.

Modification of the double bonds

Thiol-ene reactions are known to be very efficient and are often used for polymer post-modification reactions. Due to the random nature of the P(fcGE-*co*-AGE) copolymers they can be modified with many different side chains that are all placed in a random manner

along the polymer backbone together with ferrocene units and would not sustain the conditions of anionic polymerization. The P(fcGE-*co*-AGE) copolymers were post-modified via radical thiol-ene addition with *N*-acetyl-L-cysteine methyl ester as a model for a biomolecule or drug. The ^{1}H NMR spectra of the post-modified copolymers (PFA1 & PFA6) compared to the starting materials are shown in Figures 8 (and S14, S15) and display a high degree of functionalization up to 90%. Quantitative functionalization was not achieved under these conditions due to concurrent isomerization, as the reaction needs to be carried out in solution at elevated temperatures which favors isomerization of the allyl double bonds as mentioned above. The resulting cis- and trans-propenyl ether is much less reactive in thiol-ene reactions than the allyl ether group, since it is a disubstituted olefin.[43] The postpolymerization functionalization is also proven by SEC (Figure S13). The SEC curves of modified copolymers are shifted to lower elution volumes as the molecular weight increases. All allyl groups were available for thiol-ene addition reaction, since no isomerization had occurred during copolymerization in bulk at 100 °C. However, after thiol-ene addition conditions 7 to 10% isomerized allyl groups were observed. It is remarkable that the ferrocene moiety is stable in the presence of radicals.

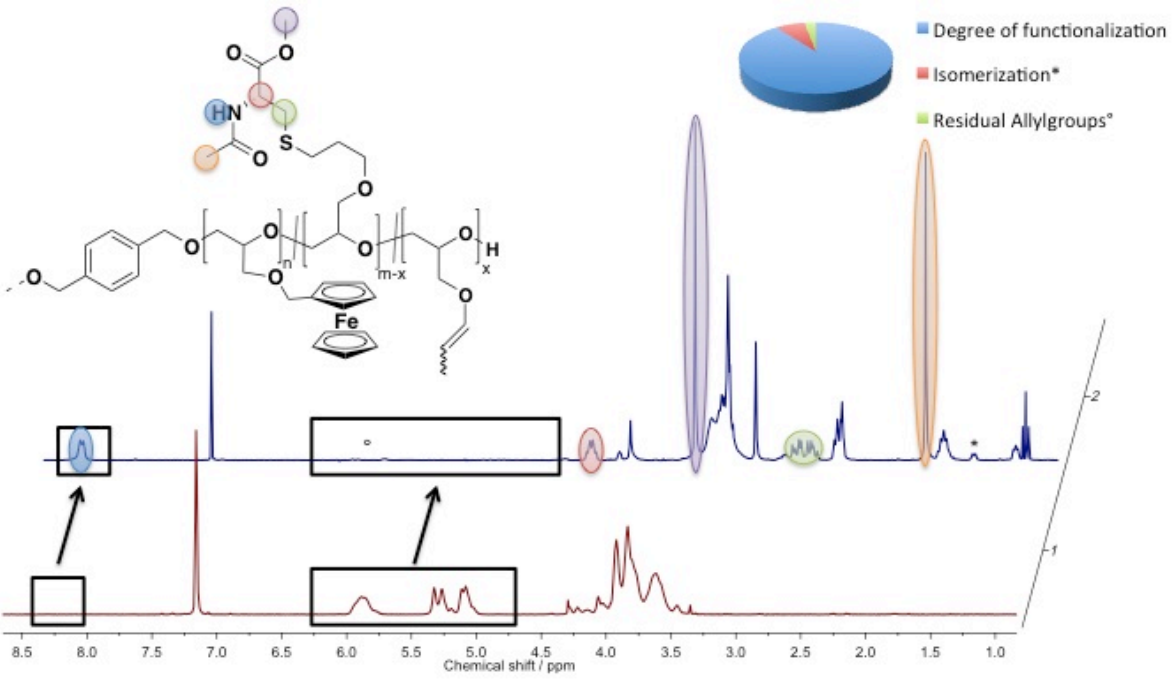

Figure 8. ^{1}H NMR spectra of PFA1 (300MHz, C_6D_6, 298K) and functionalized polymer after thiol-ene addition of *N*-acetyl-l-cysteine methyl ester.

Conclusion

We have demonstrated the synthesis of random copolymers of ferrocenyl glycidyl ether and allyl glycidyl ether (P[fcGE-*co*-AGE]) with varying comonomer ratios by living oxyanionic ring-opening copolymerization in bulk.

Quantitative *in situ* ^{13}C NMR spectroscopy has been used for the first time to study the copolymerization behavior of two monomers in bulk. By recording ^{13}C NMR spectra in bulk, quantitative information on the monomer consumption can be obtained at every time point throughout the reaction in order to determine the comonomer sequence. Due to the absence of any solvent, the natural abundance of ^{13}C isotopes is sufficiently high to record quantitative ^{13}C NMR spectra within minutes only, making this method very interesting and generally useful for many (slow) reactions in the melt. Notably, the method relies on a conventional NMR spectrometer.

Having confirmed the random structure of the copolymers, the allyl groups in the side chains were addressed by radical thiol-ene addition, resulting in randomly distributed cysteine and ferrocene units along the polyether backbone. The redox stability of the ferrocene moiety in the copolymers has been demonstrated by 10 consecutive cycles, showing no decrease in current density.

We believe that these functional materials expand the range of ferrocene-containing polymers, especially polyethers for manifold applications in materials science and biomedical areas.

Experimental Section

Instrumentation. ^{1}H NMR spectra (300, 400, 500 and 700 MHz) and ^{13}C NMR spectra (75.5 MHz) were recorded using a Bruker AC300, a Bruker AMX400, Bruker Avance 500 and Bruker Avance III. All spectra were referenced internally to residual proton signals of the deuterated solvent. For SEC measurements in DMF (containing 0.25 g·L^{-1} of lithium bromide as an additive) an Agilent 1100 Series was used as an integrated instrument, including a PSS HEMA column (106/105/104 g·mol^{-1}), a UV detector (275 nm), and a RI detector at a flow rate of 1 mL·min^{-1} at 50 °C. Calibration was carried out using PEO standards provided by Polymer Standards Service. DSC measurements were performed using a PerkinElmer 7 series thermal analysis system and a PerkinElmer thermal analysis controller TAC 7/DX in the temperature range from -95 to 80 °C. Heating rates of 20 K·min^{-1} were employed under nitrogen.

Matrix-assisted laser desorption/ionization time-of-flight (MALDI-ToF) measurements were performed using a Shimadzu Axima CFR MALDI-TOF mass spectrometer, employing dithranol (1,8-dihydroxy-9(10*H*)-anthracenone) as a matrix.

Cyclic voltammetry (CV) was carried out in a conventional three electrode cell using a µ-Autolab Type III potentiostat (Metrohm AG) and dichloromethane as a solvent under argon. The supporting electrolyte was tetrabutylammonium hexafluorophosphate ([0.1 M]). All experiments were performed at 25 °C. A glassy carbon disc served as working electrode

and a glassy carbon rod as counter electrode. As reference an Ag/AgCl electrode (silver wire in saturated LiCl/ethanol solution) was employed.

Reagents. Solvents and reagents were purchased from Acros Organics, TCI, Sigma-Aldrich or Fluka and used as received, unless otherwise stated. Chloroform-d_1, benzene-d_6, DMSO-d_6 were purchased from Deutero GmbH. fcGE was synthesized according to the published procedures.[85] fcGE was dried by azeotropic distillation of benzene to remove traces of water. AGE was dried over calcium hydride and freshly distilled before use.

General Procedure for the copolymerization of fcGE and AGE: (P(AGE-co-fcGE). The initiator, 5.0 mg (0.036 mmol) benzene-1,4-dimethanole, and 11.0 mg (0.0655 mmol, 1.8 eq.) of cesium hydroxide monohydrate were placed in a 100 mL Schlenk flask and suspended in 10 mL of benzene. The mixture was stirred at 60 °C under an argon atmosphere for 1 h and evacuated at 60 °C (10^{-2} mbar) for 12 h to remove benzene and the water formed (as an azeotrope with benzene) to generate the corresponding cesium dialkoxide. The flask was filled with argon and cooled to room temperature, and then a mixture of both comonomers (200 mg (0.735 mmol) fcGE and 953 mg (8.35 mmol) AGE (for a composition 1:11) was added. The reaction mixture was heated up to 100 °C and stirred for 24 h before the living chain ends were terminated with methanol and the copolymer was dialyzed against freshly distilled dichloromethane (MWCO 1,000 g·mol^{-1}). The copolymer was obtained as an orange to dark orange viscous liquid, the color strongly depending on fc content (Fig S1). Yields: 70-90%. ^{1}H NMR (C_6D_6, 700 MHz): δ(ppm) = 7.34 (s, 4H, aromatic protons of initiator), 6.03-5.73 (br, 1H, H_2C=C*H*-CH_2-O-), 5.42-4.96 (br, 2H, *H*$_2$C=CH-CH_2-O-), 4.42 (s, 4H, aliphatic signals of initiator), 4.34-4.10 (fc), 4.10-3.26 (residual protons: PEO backbone, R-C*H*$_2$-O- C*H*$_2$-backbone).

Polymer modification via thiol-ene addition. 50 mg of the respective copolymer were dissolved in 5 mL dimethylformamide and a 10-fold molar excess of *N*-acetyl-L-cysteine methyl ester and 19 mg (0.75 eq.) of azobis(isobutyronitrile) (AIBN) with respect to the absolute number of allyl groups, were added. After three freeze-pump-thaw cycles (to remove any oxygen from the system) the reaction mixture was heated to 75 °C and stirred for 12 h. The reaction mixture was dialyzed against methanol, using benzoylated tubings (MWCO 1,000 g/mol) over a period of 48 h. Yield: 95%-quantitative. ^{1}H NMR (DMSO-*d*$_6$, 300

MHz): δ(ppm) = 8.36 (d, J_1 = 7.72 Hz, N*H*), 4.43 (m, C*H*-NH), 4.25-4.08 (methylferrocenyl group), 3.63 (s, -COOC*H*$_3$), 3.58-3.23 (br, PEO backbone), 2.90-2.67 (m, -CH-C*H*$_2$-S-), 2.54 (t, J1 = 7.38 Hz, J2 = 7.38 Hz, -O-CH$_2$-CH$_2$-C*H*$_2$-S-), 1.86 (s, -NH-COC*H*$_3$), 1.72 (m, -O-CH$_2$-C*H*$_2$-CH$_2$-S-).

^{1}H DOSY NMR. The diffusion (DOSY, Diffusion Ordered Spectroscopy)[44,45] experiment was done with a 5 mm BBI z-gradient probe and a gradient strength of 5.350 [G/mm] on the 700 MHz NMR Avance III system. For the proton nucleus the used spectral width was 8400 Hz with 90° pulse of 9.0 µs. For the calibration of the gradient strength, a sample of ^2H_2O/^1H_2O was measured at a defined temperature and compared with the literature diffusion coefficient of ^2H_2O/^1H_2O.[46] The used temperature of 298.3 K was approved with a standard ^{1}H methanol NMR sample. The gradient strength was varied in 16 steps or 16 steps from 2% to 100%. The diffusion time d20 was optimised at 60 ms and the gradient length p30 of 1.8 ms. The optimization was realized by comparing the remaining intensity of the signals at 2% and 98% gradient strength, where the intensity loss of the echo was in the range of 90%. The 2D NMR sequences for measuring diffusion coefficient using echoes for convection compensation and longitudinal eddy current delays to store the magnetization in the z-axis, and only be dependent on T_1-relaxation. The evaluation of the diffusion value was automatically calculated with a mono exponential function:[47]

$$\ln\left(\frac{I(G)}{I(0)}\right) = -\gamma^2\delta^2G^2\left(\Delta - \frac{\delta}{3}\right)D$$

where I(G) and I(0) were the intensities of the signals with and without gradient, γ the gyromagnetic ratio of the nucleus (^{1}H in this measurements), G is the gradient strength, δ the duration of the pulse field gradient (PFG), D the diffusion value in m^2/s and Δ the "diffusion time" between the beginning of the two gradient pulses (d20). The relaxation delay between the scans was 2 s.

^{13}C NMR Kinetics. The initiator cesium benzene-1,4-dimethanolate and a mixture of AGE and fcGE were separately frozen under an argon atmosphere in a conventional NMR tube, which was subsequently sealed with a septum. The kinetic measurements were recorded on a 500

MHz Avance III system with a 5 mm z-gradient BBFO $^{1}H/X$ probe with z-gradient. ^{1}H and ^{13}C NMR spectra were measured without solvent. The accuracy of the temperature was controlled with an ethylene glycol NMR sample.[48] The spin lattice relation time (T_1) was measured with the inversion recovery method.[49] A standard kinetic ^{13}C NMR (176 MHz) experiment needed 32 transients for one experiment attained with a 13,2 µs 90° pulse, a spectral width of 297000 Hz and a recycling delay of 10 s. For one kinetic run 140 experiments were used over a time of 14 hours with an inverse gated decoupling experiment and a flip angle of 30°

4.1.1 Supporting Information

Experimental Details

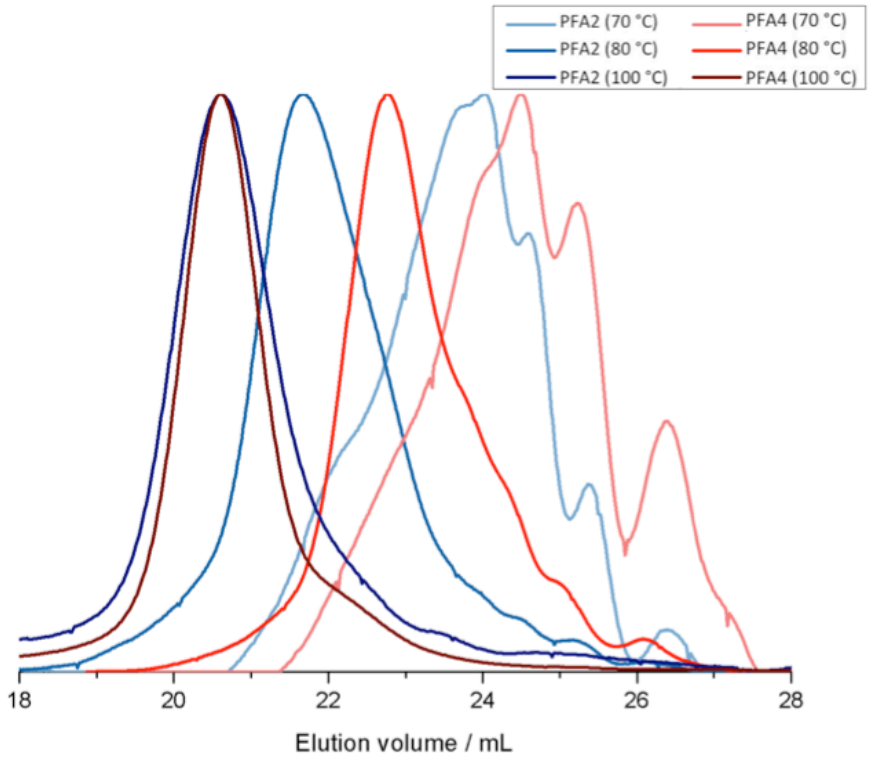

Figure S1. Temperature dependency of the copolymerization behavior after 24 h reaction time at each temperature. At 100°C full conversion and narrow molecular weight distributions are observed.

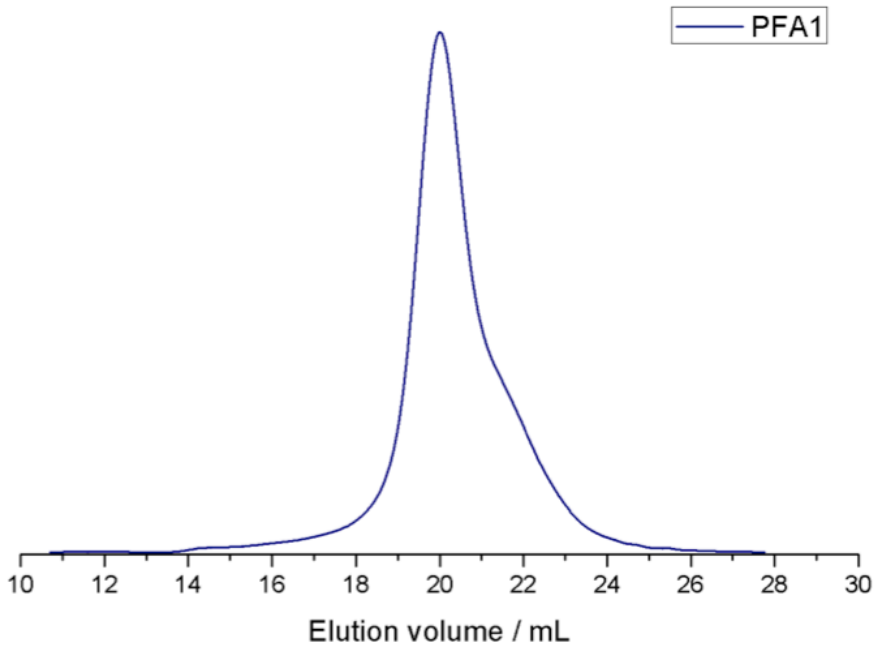

Figure S2. SEC trace of copolymer PFA1 (DMF, RI detection, 1 mL/min, 40 °C).

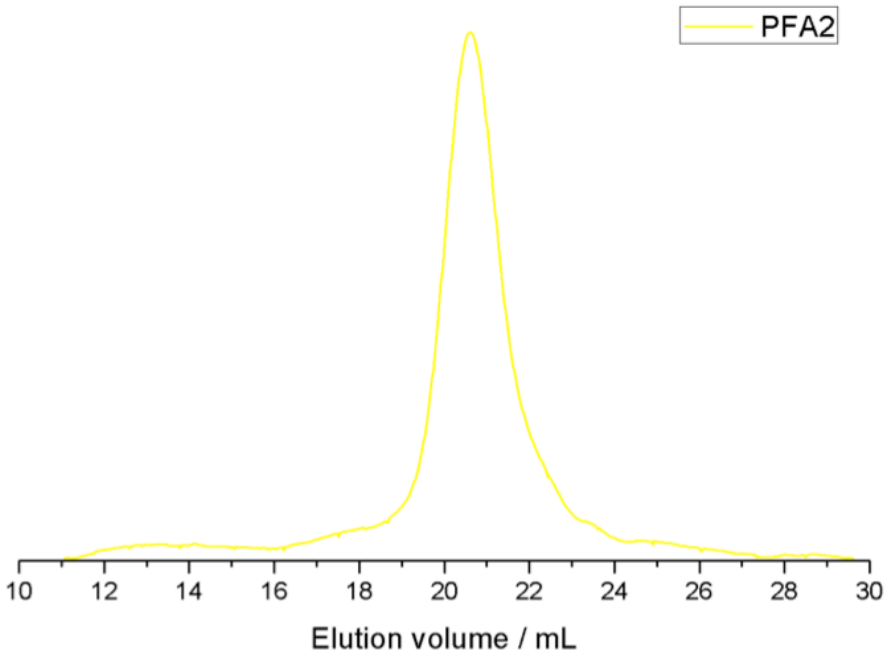

Figure S3. SEC trace of copolymer PFA2 (DMF, RI detection, 1 mL/min, 40 °C).

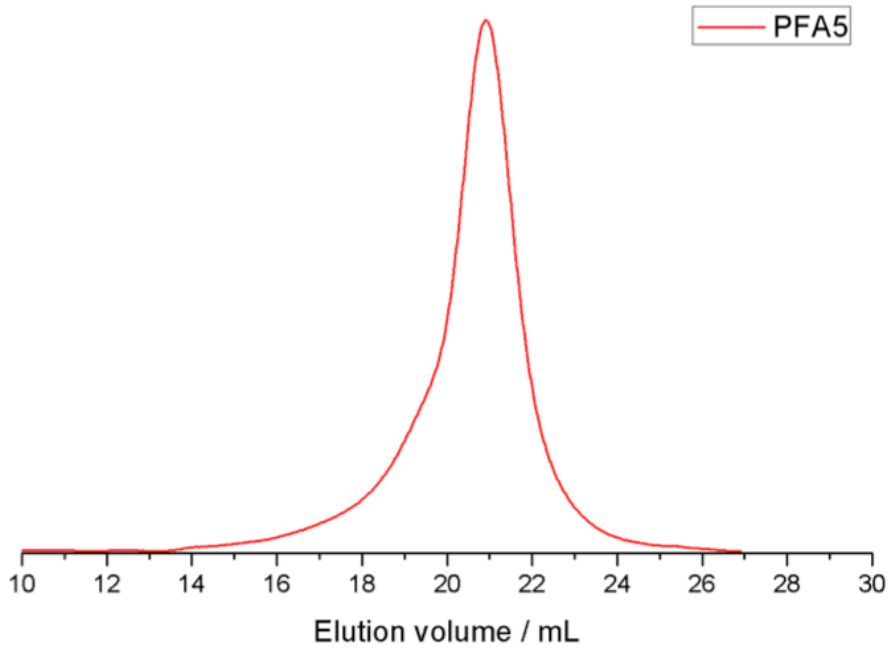

Figure S4. SEC trace of copolymer PFA5 (DMF, RI detection, 1 mL/min, 40 °C).

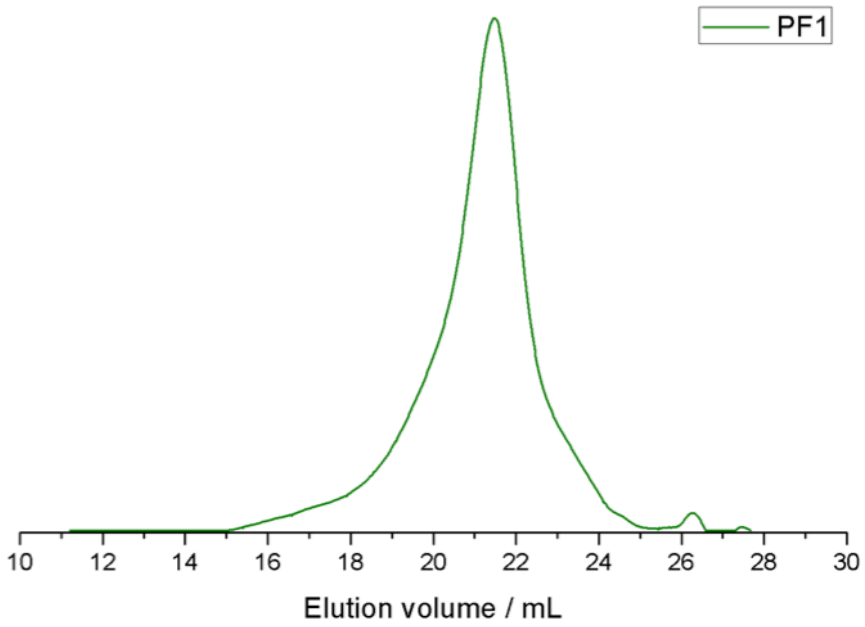

Figure S5. SEC trace of homopolymer PF1 (DMF, RI detection, 1 mL/min, 40 °C).

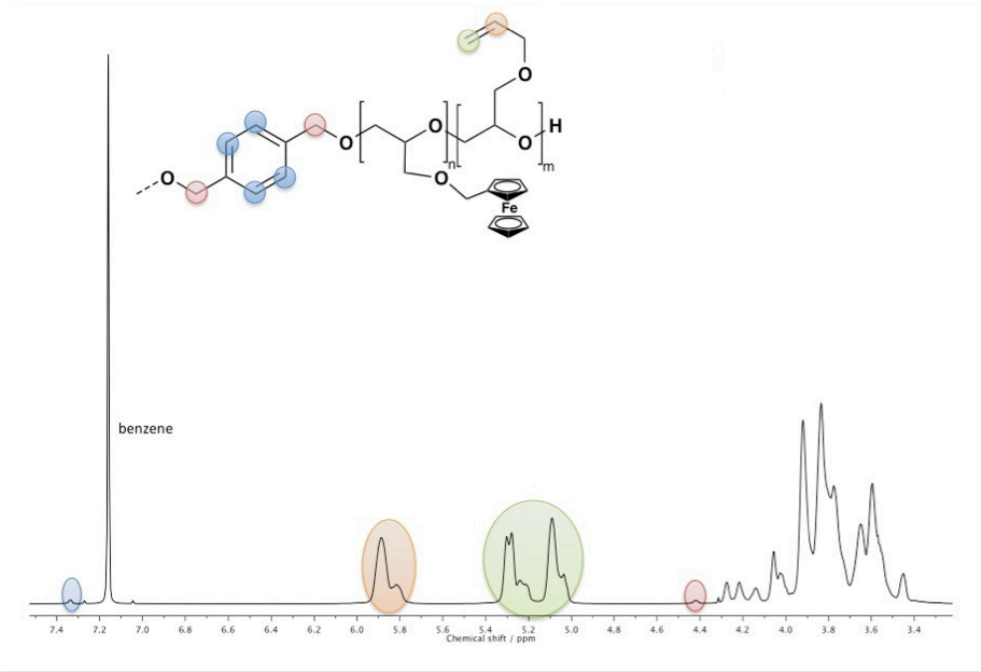

Figure S6. ^{1}H NMR spectrum of P(fcGE-*co*-AGE) (PFA2) (C_6D_6; 700 MHz, 298K).

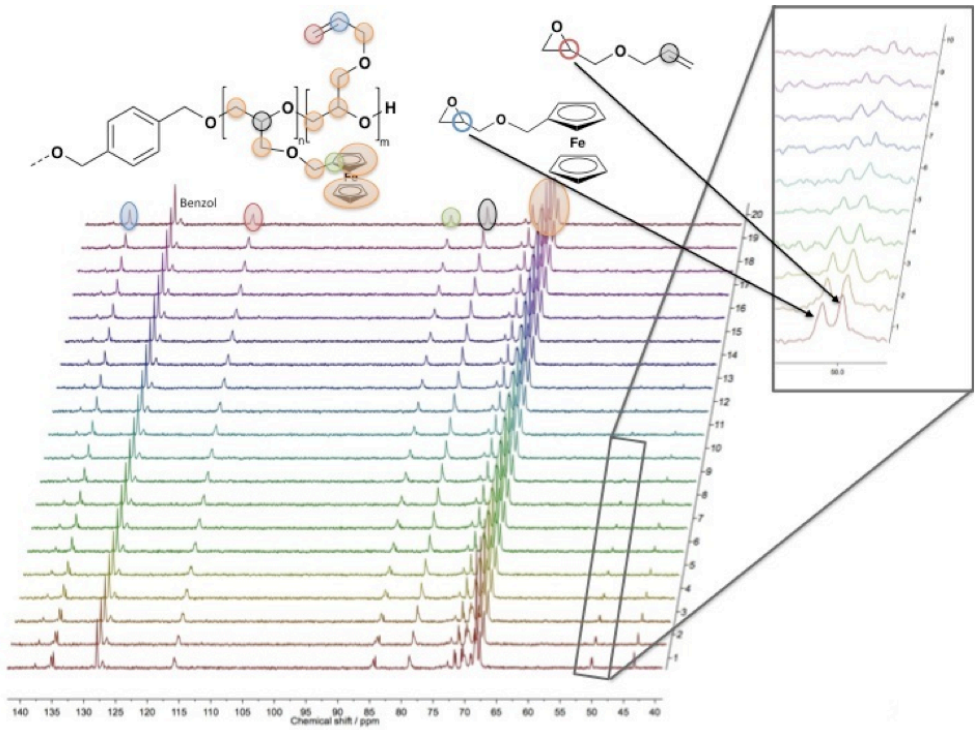

Figure S7. ^{13}C NMR *in situ* kinetics of anionic ring-opening copolymerization of 50% fcGE and 50% AGE with a zoom in at ca. 50 ppm (C_6D_6; 126 MHz; 373 K)

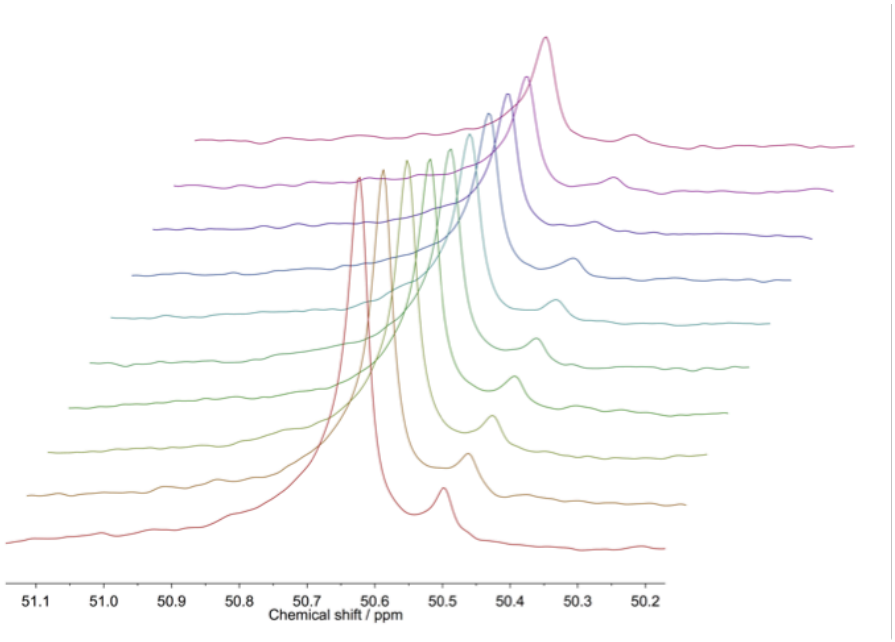

Figure S8. ^{13}C NMR *in situ* kinetics of anionic ring-opening copolymerization of 80% fcGE and 20% AGE with a zoom in at ca. 50 ppm (C_6D_6; 126 MHz; 363 K, spectra shown until ca. 25% total conversion).

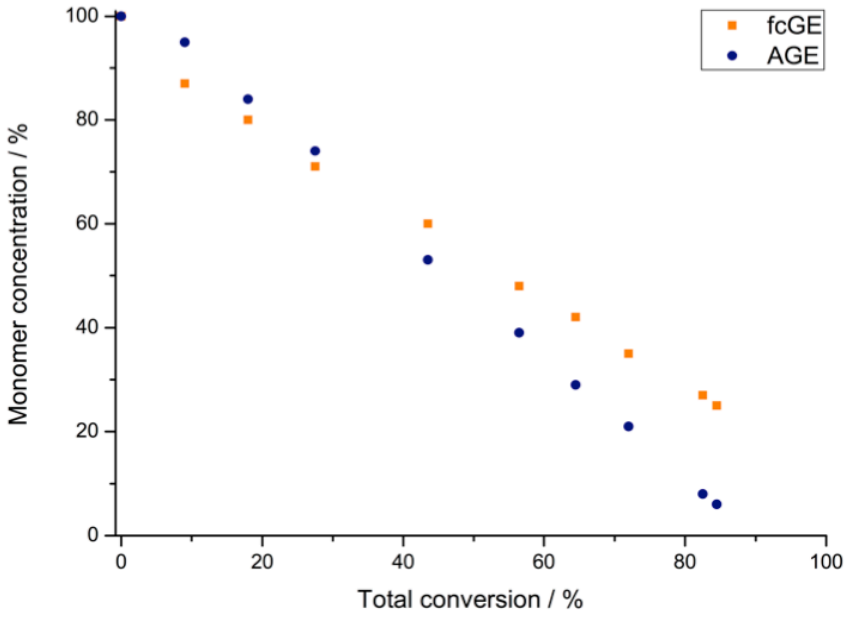

Figure S9. Percentage of monomer concentration versus total monomer conversion for the copolymerization of 80% fcGE and 20% AGE via ^{13}C NMR kinetics in bulk (Fig S16).

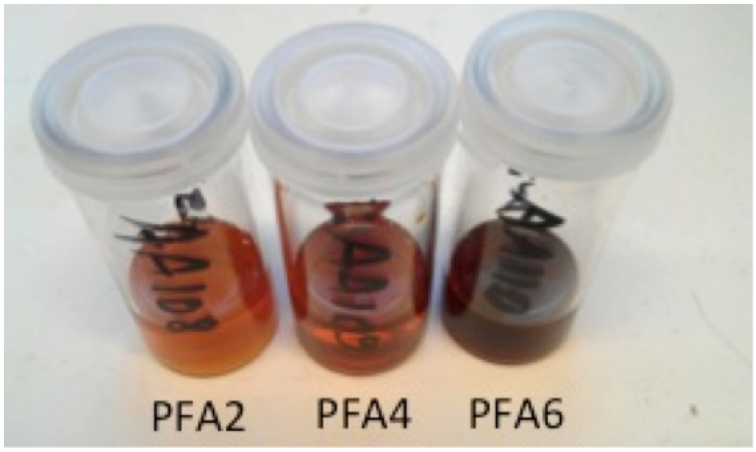

Figure S10. Amorphous polymer samples with 9.0% (PFA2), 30.5% (PFA4) and 54.0% (PFA6) fcGE.

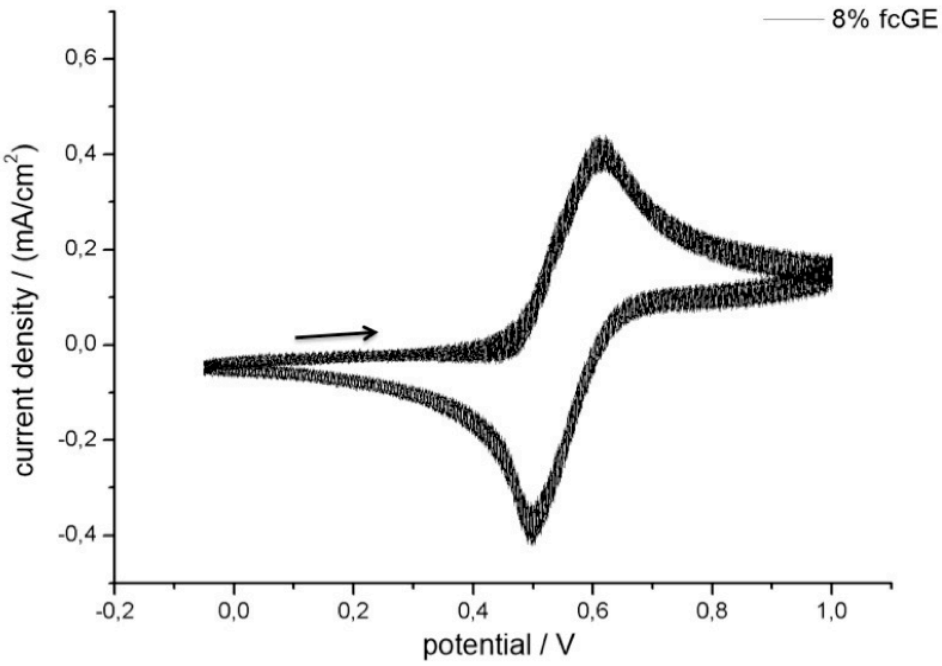

Figure S11. Cyclovoltammogram of copolymer PFA1 with 8% fcGE (10 cycles).

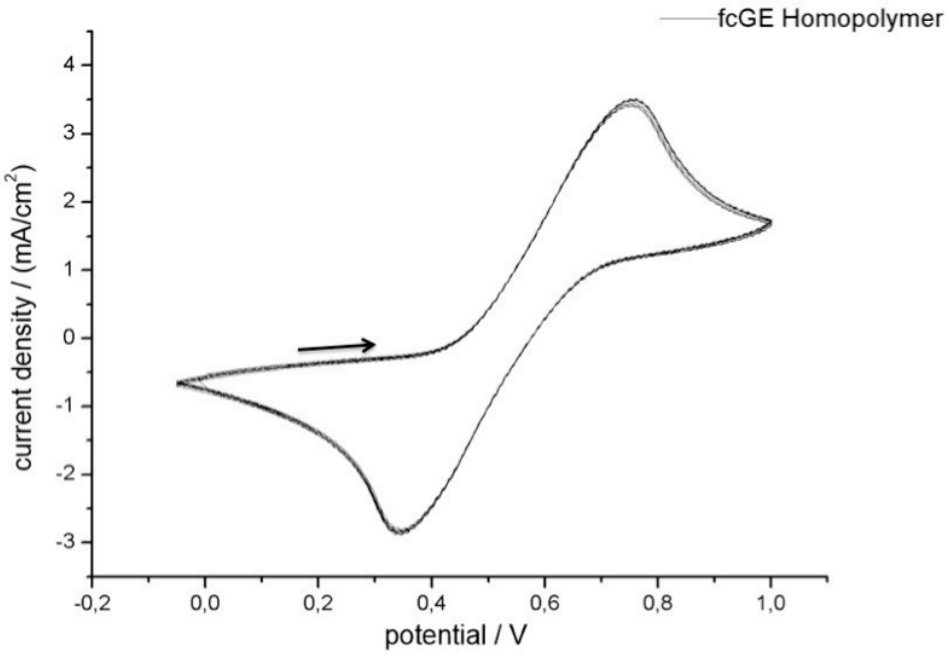

Figure S12. Cyclovoltammogram of fcGE (PF1) homopolymer (10 cycles).

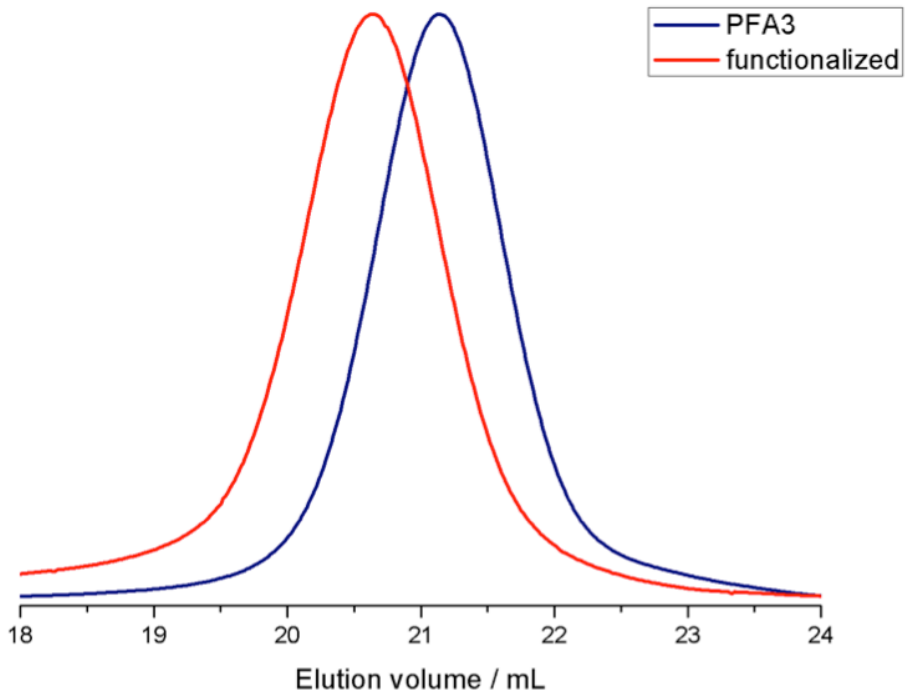

Figure S13. SEC traces of copolymer PFA3 (blue) and after functionalization of PFA3 (red) (DMF, RI detection, 1 mL/min, 40 °C).

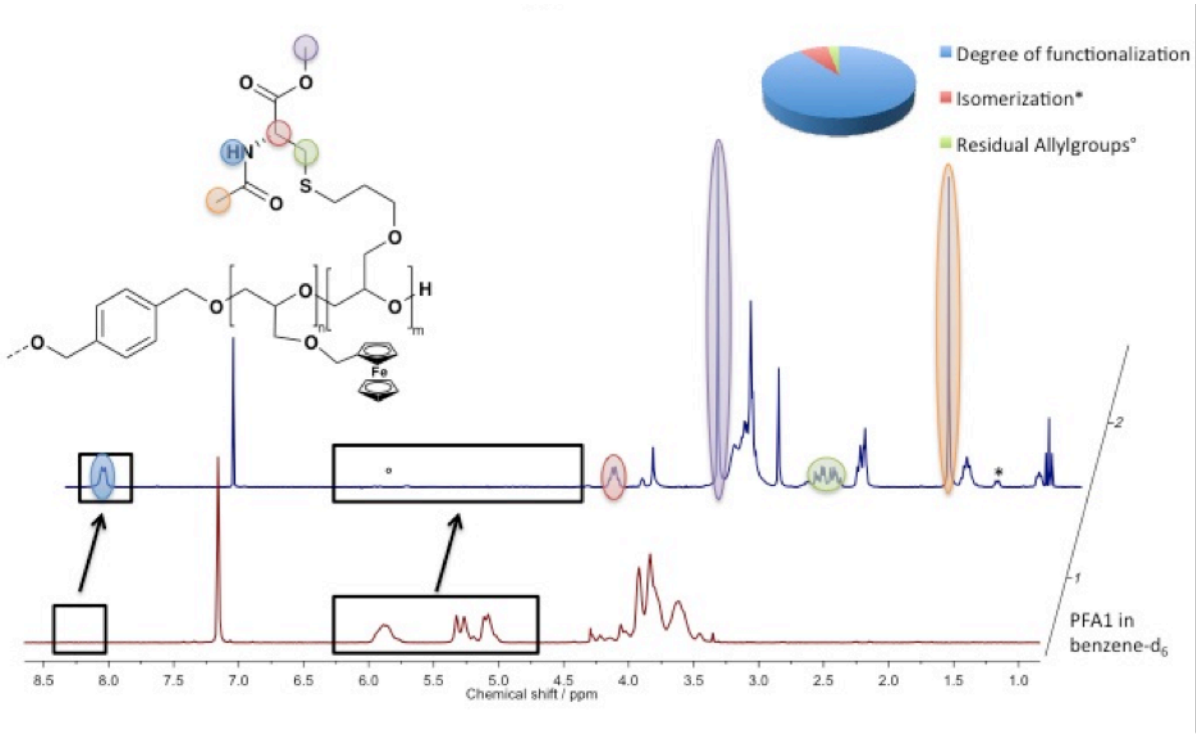

Figure S14. ^{1}H NMR spectra of PFA1 (300MHz, C_6D_6) and functionalized polymer by thiol-ene addition of *N*-Acetyl-L-cysteine methyl ester.

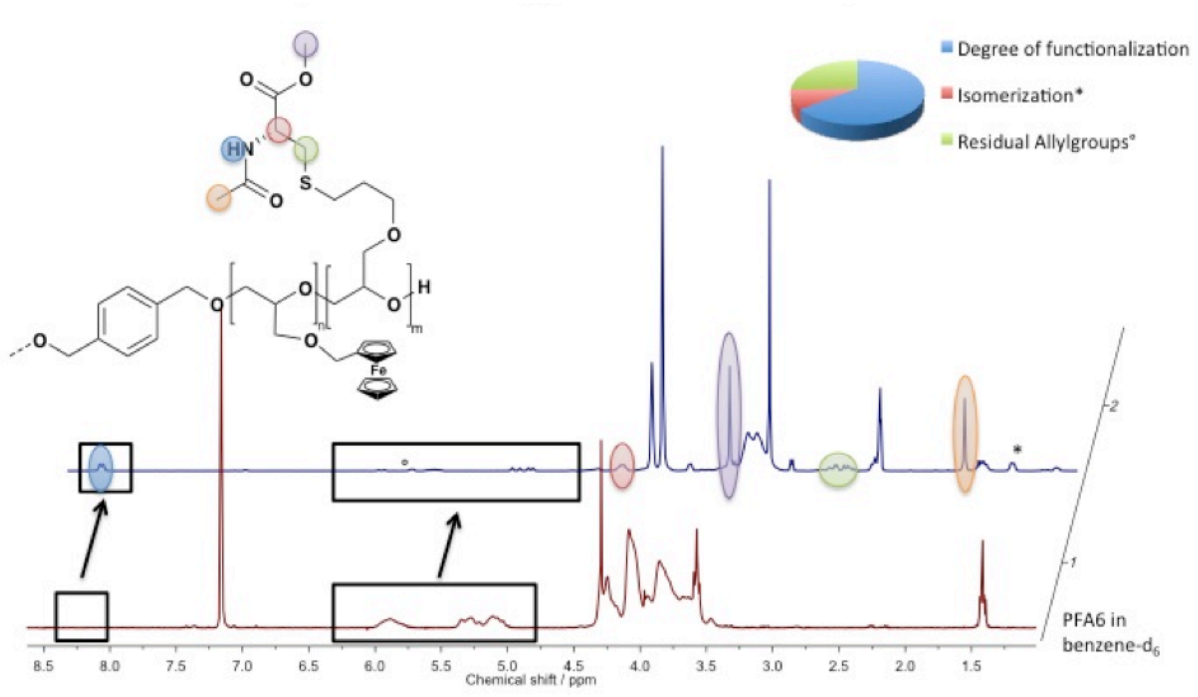

Figure S15. ^{1}H NMR spectra of PFA6 (300MHz, C_6D_6) and functionalized polymer by thiol-ene addition of *N*-Acetyl-L-cysteine methyl ester.

Table S1. Theoretical M_n and monomer ratio compared to the values determined from ^{1}H NMR for P(fcGE-*co*-AGE) copolymers.

no.	sum	fcGE/(fcGE+AGE)[a] (%)	fcGE/(fcGE+AGE)[b] (%)	M_n[c] (g/mol)	M_n[d] (g/mol)	M_n[e] (g/mol)
PA1	$C_6H_4(CH_2O)_2$-$[P(AGE_{117})]_2$	0	0	30 000	26 700	5 600
PFA1	$C_6H_4(CH_2O)_2$-$[P(fcGE_{12}$-*co*-$AGE_{138})]_2$	5.0	8.0	49 000	38 200	3 500
PFA2	$C_6H_4(CH_2O)_2$-$[P(fcGE_{12}$-*co*-$AGE_{114})]_2$	10.0	9.0	26 000	32 400	2 200
PFA3	$C_6H_4(CH_2O)_2$-$[P(fcGE_{20}$-*co*-$AGE_{128})]_2$	15.0	13.6	52 000	40 300	3 200
PFA4	$C_6H_4(CH_2O)_2$-$[P(fcGE_{32}$-*co*-$AGE_{73})]_2$	30.0	30.5	32 000	34 300	2 200
PFA5	$C_6H_4(CH_2O)_2$-$[P(fcGE_5$-*co*-$AGE_6)]_2$	40.0	41.9	4 800	4 630	2 200
PFA6	$C_6H_4(CH_2O)_2$-$[P(fcGE_{50}$-*co*-$AGE_{43})]_2$	50.0	54.0	39 000	37 000	1 900
PF1	$C_6H_4(CH_2O)_2$-$[P(fcGE_{55})]_2$	100	100	27 000	30 100	1 700

a) Theoretical amount of fcGE in percent according to the monomer ratio; b) a) Amount of fcGE in percent determined from ^{1}H NMR; c) Theoretical molecular weight according to initiator concentration (see Table S1 for details); d) M_n determined from ^{1}H NMR by end group analysis; e) M_n determined via SEC in DMF vs PEG standards, $Đ=M_w/M_n$.

References

(1) Miller, S.; Tebboth, J.; Tremaine, J. *J. Chem. Soc.* **1952**, 632–635.

(2) Kealy, T. J.; Pauson, P. L. *Nature* **1951**, *168*, 1039–1040.

(3) Wilkinson, G.; Rosenblum, M.; Whiting, M. C.; Woodward, R. B. *J. Am. Chem. Soc.* **1952**, *74*, 2125–2126.

(4) Fischer, E. O.; Pfab, W. *Z. Naturforsch. B* **1952**, *7*, 377–379.

(5) Geivanidis, S.; Pistikopoulos, P.; Samaras, Z. *Sci. Total Environ.* **2003**, *305*, 129–141.

(6) Fujimura, K.; Ouchi, M.; Sawamoto, M. *ACS Macro Lett.* **2012**, *1*, 321–323.

(7) Mülhaupt, R. *Macromol. Chem. Phys.* **2003**, *204*, 289–327.

(8) Ziegler, K.; Holzkamp, E.; Breil, H.; Martin, H. *Angew. Chem.* **1955**, *67*, 541–547.

(9) Ayranci, R.; Demirkol, D. O.; Ak, M.; Timur, S. *Sensors* **2015**, *15*, 1389–1403.

(10) Jiménez, A.; Armada, M. P. G.; Losada, J.; Villena, C.; Alonso, B.; Casado, C. M. *Sens. Actuators, B* **2014**, *190*, 111–119.

(11) Soganci, T.; Demirkol, D. O.; Ak, M.; Timur, S. *RSC Advances* **2014**, *4*, 46357–46362.

(12) Astruc, D. *New J. Chem.* **2011**, *35*, 764–772.

(13) Nagel, B.; Warsinke, A.; Katterle, M. *Langmuir* **2007**, *23*, 6807–6811.

(14) Tatsuma, T.; Saito, K.-I.; Oyama, N. *J. Chem. Soc., Chem. Commun.* **1994**, *0*, 1853–1854.

(15) Ornelas, C. *New J. Chem.* **2011**, *35*, 1973.

(16) Braga, S. S.; Silva, A. M. S. *Organometallics* **2013**, *32*, 5626–5639.

(17) Fouda, M. F. R.; Abd-Elzaher, M. M.; Abdelsamaia, R. A.; Labib, A. A. *Appl. Organometal. Chem.* **2007**, *21*, 613–625.

(18) Abd-El-Aziz, A. S.; Agatemor, C.; Etkin, N. *Macromol. Rapid Commun.* **2014**, *35*, 513–559.

(19) Hardy, C. G.; Zhang, J.; Yan, Y.; Ren, L.; Tang, C. *Prog. Polym. Sci.* **2014**, *39*, 1742-1796.

(20) Abd-El-Aziz, A. S.; Manners, I. *J. Inorg. Organomet. Polym.* **2005**, *15*, 157–195.

(21) Abd-El-Aziz, A. S.; Carraher, C. E.; Pittman, C. U.; Zeldin, M. *Inorganic and Organometallic Macromolecules*; Springer, 2007.

(22) Abd-El-Aziz, A. S.; Manners, I. *Frontiers in Transition Metal-Containing Polymers*; John Wiley & Sons, 2007.

(23) Hurvois, J. P.; Moinet, C. *J. Organomet. Chem.* **2005**, *690*, 1829–1839.

(24) Osella, D.; Ferrali, M.; Zanello, P.; Laschi, F.; Fontani, M.; Nervi, C.; Cavigiolio, G. *Inorg. Chim. Acta* **2000**, *306*, 42–48.

(25) Nguyen, A.; Vessières, A.; Hillard, E. A.; Top, S.; Pigeon, P.; Jaouen, G. *Chimia* **2007**, *61*, 716–724.

(26) Schatzschneider, U.; Metzler-Nolte, N. *Angew. Chem. Int. Ed. Engl.* **2006**, *45*, 1504–1507.

(27) Hamels, D.; Dansette, P. M.; Hillard, E. A.; Top, S.; Vessières, A.; Herson, P.; Jaouen, G.; Mansuy, D. *Angew. Chem. Int. Ed. Engl.* **2009**, *48*, 9124–9126.

(28) Riccardi, A.; Ferlini, C.; Meco, D.; Mastrangelo, R.; Scambia, G.; Riccardi, R. *Eur. J. Cancer* **1999**, *35*, 86–90.

(29) Hartinger, C. G.; Dyson, P. J. *Chem. Soc. Rev.* **2009**, *38*, 391–401.

(30) Allardyce, C. S.; Dorcier, A.; Scolaro, C.; Dyson, P. J. *Appl. Organometal. Chem.* **2005**, *19*, 1–10.

(31) Gasser, G.; Ott, I.; Metzler-Nolte, N. *J. Med. Chem.* **2011**, *54*, 3–25.

(32) Köpf-Maier, P.; Köpf, H.; Neuse, E. W. *Angew. Chem. Int. Ed. Engl.* **1984**, *23*, 456–457.

(33) Popova, L. V.; Babin, V. N.; Belousov, Y. A.; Nekrasov, Y. S.; Snegireva, A. E.; Borodina, N. P.; Shaposhnikova, G. M.; Bychenko, O. B.; Raevskii, P. M.; Morozova, N. B.; Iiyina, A. I.; Shitkov, K. G. *Appl. Organometal. Chem.* **1993**, *7*, 85–94.

(34) Vessières, A.; Top, S.; Pigeon, P.; Hillard, E.; Boubeker, L.; Spera, D.; Jaouen, G. *J. Med. Chem.* **2005**, *48*, 3937–3940.

(35) Fouda, M. F. R.; Abd-Elzaher, M. M.; Abdelsamaia, R. A.; Labib A. A. *Appl. Organometal. Chem.* **2007**, *21*, 613-625.

(36) van Staveren, D. R.; Metzler-Nolte, N. *Chem. Rev.* **2004**, *104*, 5931–5985.

(37) Biot, C.; François, N.; Maciejewski, L.; Brocard, J.; Poulain, D. *Bioorg. Med. Chem. Lett.* **2000**, *10*, 839–841.

(38) Biot, C.; Glorian, G.; Maciejewski, L. A.; Brocard, J. S.; Domarle, O.; Bamplain, G.; Millet, P.; Georges, A. J.; Abessolo, H.; Dive, D.; Lebibi, J. *J. Med. Chem.* **1997**, *40*, 3715–3718.

(39) Delhaes, L.; Biot, C.; Berry, L.; Maciejewski, L. A.; Camus, D.; Brocard, J. S.; Dive, D. *Bioorg. Med. Chem.* **2000**, *8*, 2739–2745.

(40) Pigeon, P.; Top, S.; Vessières, A.; Huché, M.; Görmen, M.; Arbi, El, M.; Plamont, M.-A.; McGlinchey, M. J.; Jaouen, G. *New J. Chem.* **2011**, *35*, 2212–2218.

(41) Hillard, E.; Vessières, A.; Thouin, L.; Jaouen, G.; Amatore, C. *Angew. Chem. Int. Ed. Engl.* **2005**, *45*, 285–290.

(42) Jaouen, G.; Top, S.; Vessières, A.; Leclercq, G.; Quivy, J.; Jin, L.; Croisy, A. *C. R. Acad. Sci., Ser. IIc: Chim.* **2000**, *3*, 89–93.

(43) Top, S.; Vessières, A.; Leclercq, G.; Quivy, J.; Tang, J.; Vaissermann, J.; Huché, M.; Jaouen, G. *Chemistry* **2003**, *9*, 5223–5236.

(44) Görmen, M.; Pigeon, P.; Top, S.; Vessières, A.; Plamont, M.-A.; Hillard, E. A.; Jaouen, G. *Med. Chem. Commun.* **2010**, *1*, 149–151.

(45) Vessières, A. *J. Organomet. Chem.* **2013**, *734*, 3–16.

(46) Top, S.; Vessières, A.; Cabestaing, C.; Laios, I.; Leclercq, G.; Provot, C.; Jaouen, G. *J. Organomet. Chem.* **2001**, *637-639*, 500–506.

(47) Ringsdorf, H. *J. polym. sci., C Polym. symp.* **1975**, *51*, 135–153.

(48) Bader, H.; Ringsdorf, H.; Schmidt, B. *Angew. Makromol. Chem.* **1984**, *123*, 457–485.

(49) Micha-Screttas, M.; Ringsdorf, H. *Curr. Top. Med. Chem.* **2008**, *8*, 1161–1164.

(50) Meirim, M. G.; Neuse, E. W.; Caldwell, G. A. *J. Inorg. Organomet. Polym.* **1997**, *7*, 71–91.

(51) Caldwell, G.; Meirim, M. G.; Neuse, E. W.; van Rensburg, C. E. J. *Appl. Organometal. Chem.* **1998**, *12*, 793–799.

(52) Neuse, E. W. *Macromol. Symp.* **2001**, *172*, 127–138.

(53) Neuse, E. W. *J. Inorg. Organomet. Polym.* **2005**, *15*, 3–31.

(54) Swarts, J. C.; Neuse, E. W.; Lamprecht, G. J. *J. Inorg. Organomet. Polym.* **1994**, *4*, 143–153.

(55) Johnson, M. T.; Kreft, E.; N'Da, D. D.; Neuse, E. W.; van Rensburg, C. E. J. *J. Inorg. Organomet. Polym.* **2003**, *13*, 255–267.

(56) Neuse, E. W.; Khan, F. B. D. *Macromolecules* **1986**, *19*, 269–272.

(57) Neuse, E. W.; Kanzawa, F. *Appl. Organometal. Chem.* **1990**, *4*, 19–26.

(58) Xue, C.; Chen, Z.; Luo, F.-T.; Palaniappan, K.; Chesney, D. J.; Liu, J.; Chen, J.; Liu, H. *Biomacromolecules* **2005**, *6*, 1810–1815.

(59) Podkoscielny, D.; Hooley, R. J.; Rebek, J., Jr.; Kaifer, A. E. *Org. Lett.* **2008**, *10*, 2865–2868.

(60) Duan, Q.; Cao, Y.; Li, Y.; Hu, X.; Xiao, T.; Lin, C.; Pan, Y.; Wang, L. *J. Am. Chem. Soc.* **2013**, *135*, 10542–10549.

(61) Wang, X. S.; Winnik, M. A.; Manners, I. *Macromol. Rapid Commun.* **2002**, *23*, 210–213.

(62) Massey, J. A.; Temple, K.; Cao, L.; Rharbi, Y.; Raez, J.; Winnik, M. A.; Manners, I. *J. Am. Chem. Soc.* **2000**, *122*, 11577–11584.

(63) Gädt, T.; Ieong, N. S.; Cambridge, G.; Winnik, M. A.; Manners, I. *Nat. Mater.* **2009**, *8*, 144–150.

(64) Gilroy, J. B.; Rupar, P. A.; Whittell, G. R.; Chabanne, L.; Terrill, N. J.; Winnik, M. A.; Manners, I.; Richardson, R. M. *J. Am. Chem. Soc.* **2011**, *133*, 17056–17062.

(65) Hudson, Z. M.; Lunn, D. J.; Winnik, M. A.; Manners, I. *Nat. Commun.* **2014**, *5*, 3372.

(66) Gohy, J. F.; Lohmeijer, B. G. G.; Alexeev, A.; Wang, X. S.; Manners, I.; Winnik, M. A.; Schubert, U. S. *Chemistry* **2004**, *10*, 4315–4323.

(67) Zhang, M.; Rupar, P. A.; Feng, C.; Lin, K.; Lunn, D. J.; Oliver, A.; Nunns, A.; Whittell, G. R.; Manners, I.; Winnik, M. A. *Macromolecules* **2013**, *46*, 1296–1304.

(68) Natalello, A.; Alkan, A.; Friedel, A.; Lieberwirth, I.; Frey, H.; Wurm, F. R. *ACS Macro Lett.* **2013**, *2*, 313–316.

(69) Schacher, F. H.; Elbert, J.; Patra, S. K.; Yusoff, S. F. M.; Winnik, M. A.; Manners, I. *Chem. Eur. J.* **2012**, *18*, 517–525.

(70) Resendes, R.; Massey, J.; Dorn, H.; Winnik, M. A.; Manners, I. *Chimia* **2000**, *33*, 8–10.

(71) Tonhauser, C.; Mazurowski, M.; Rehahn, M.; Gallei, M.; Frey, H. *Macromolecules* **2012**, *45*, 3409–3418.

(72) Gao, C.; Liu, C.; Zhou, H.; Wang, S.; Zhang, W. *J. Polym. Sci., Part A: Polym. Chem.* **2016**, *54*, 900–909.

(73) Xiao, Z.-P.; Cai, Z.-H.; Liang, H.; Lu, J. *J. Mater. Chem.* **2010**, *20*, 8375–8381.

(74) Hatozaki, O.; Anson, F. C. *J. Phys. Chem.* **1996**, *100*, 8448–8453.

(75) Hatozaki, O.; Anson, F. C. *J. Electroanal. Chem.* **1997**, *420*, 195–199.

(76) Power-Billard, K. N.; Peckham, T. J.; Butt, A.; Jäkle, F.; Manners, I. *J. Inorg. Organomet. Polym.* **2000**, *10*, 159–168.

(77) Hempenius, M. A.; Robins, N. S.; Lammertink, R. G. H.; Vancso, G. J. *Macromol. Rapid Commun.* **2001**, *22*, 30–33.

(78) Power-Billard, K. N.; Manners, I. *Macromol. Rapid Commun.* **2002**, *23*, 607–611.

(79) Hempenius, M. A.; Vancso, G. J. *Macromolecules* **2002**, *35*, 2445–2447.

(80) Wang, Z.; Lough, A.; Manners, I. *Macromolecules* **2002**, *35*, 7669–7677.

(81) Hempenius, M. A.; Péter, M.; Robins, N. S.; Kooij, E. S.; Vancso, G. J. *Langmuir* **2002**, *18*, 7629–7634.

(82) Jańczewski, D.; Song, J.; Vancso, G. J. *Eur. Polym. J.* **2014**, *54*, 87–94.

(83) Watson, K. J.; Nguyen, S. T.; Mirkin, C. A. *J. Organomet. Chem.* **2000**, *606*, 79–83.

(84) Le Floch, F.; Ho, H. A.; Harding-Lepage, P.; Bédard, M.; Neagu-Plesu, R.; Leclerc, M. *Adv. Mater.* **2005**, *17*, 1251–1254.

(85) Tonhauser, C.; Alkan, A.; Schömer, M.; Dingels, C.; Ritz, S.; Mailänder, V.; Frey, H.; Wurm, F. R. *Macromolecules* **2013**, *46*, 647–655.

(86) Alkan, A.; Klein, R.; Shylin, S. I.; Kemmer-Jonas, U.; Frey, H.; Wurm, F. R. *Polym. Chem.* **2015**, *6*, 7112–7118.

(87) Ashton, P. R.; Balzani, V.; Clemente-León, M.; Colonna, B.; Credi, A.; Jayaraman, N.; Raymo, F. M.; Stoddart, J. F.; Venturi, M. *Chemistry* **2002**, *8*, 673–684.

(88) Astruc, D.; Ornelas, C.; Ruiz, J. *Acc. Chem. Res.* **2008**, *41*, 841–856.

(89) Alkan, A.; Thomi, L.; Gleede, T.; Wurm, F. R. *Polym. Chem.* **2015**, *6*, 3617–3624.

(90) Alkan, A.; Steinmetz, C.; Landfester, K.; Wurm, F. R. *ACS Appl. Mater. Interfaces* **2015**, *7*, 26137-26144.

(91) Connelly, N. G.; Geiger, W. E. *Chem. Rev.* **1996**, *96*, 877–910.

(92) Mayer, U. F. J.; Charmant, J. P. H.; Rae, J.; Manners, I. *Organometallics* **2008**, *27*, 1524–1533.

(93) Mayer, U. F. J.; Gilroy, J. B.; O'Hare, D.; Manners, I. *J. Am. Chem. Soc.* **2009**, *131*,

10382–10383.

(94) Ren, L.; Hardy, C. G.; Tang, S.; Doxie, D. B.; Hamidi, N.; Tang, C. *Macromolecules* **2010**, *43*, 9304–9310.

(95) Zhang, J.; Ren, L.; Hardy, C. G.; Tang, C. *Macromolecules* **2012**, *45*, 6857–6863.

(96) Ren, L.; Zhang, J.; Hardy, C. G.; Doxie, D.; Fleming, B.; Tang, C. *Macromolecules* **2012**, *45*, 2267–2275.

(97) Ren, L.; Zhang, J.; Bai, X.; Hardy, C. G.; Shimizu, K. D.; Tang, C. *Chemical Science* **2012**, *3*, 580–583.

(98) Ren, L.; Hardy, C. G.; Tang, C. *J. Am. Chem. Soc.* **2010**, *132*, 8874–8875.

(99) González, B.; Casado, C. M.; Alonso, B.; Cuadrado, I.; Morán, M.; Wang, Y.; Kaifer, A. E. *Chem. Commun.* **1998**, *0*, 2569–2570.

(100) Zhang, J.; Yan, Y.; Chance, M. W.; Chen, J.; Hayat, J.; Ma, S.; Tang, C. *Angew. Chem. Int. Ed. Engl.* **2013**, *52*, 13387–13391.

(101) Zhang, J.; Yan, Y.; Chen, J.; Hayat, J.; Chance, M. W.; Gai, Z.; Tang, C. *Chem. Mater.* **2014**, *26*, 3185–3190.

(102) Zhang, J.; Chen, Y. P.; Miller, K. P.; Ganewatta, M. S.; Bam, M.; Yan, Y.; Nagarkatti, M.; Decho, A. W.; Tang, C. *J. Am. Chem. Soc.* **2014**, *136*, 4873–4876.

(103) Gu, H.; Ciganda, R.; Hernandez, R.; Castel, P.; Zhao, P.; Ruiz, J.; Astruc, D. *Macromol. Rapid Commun.* **2016**, *37*, 630-636.

(104) Gale, R. J.; Job, R. *Inorg. Chem.* **1981**, *20*, 42–45.

(105) Swarts, J. C.; Nafady, A.; Roudebush, J. H.; Trupia, S.; Geiger, W. E. *Inorg. Chem.* **2009**, *48*, 2156–2165.

(106) Yan, Y.; Zhang, J.; Qiao, Y.; Ganewatta, M.; Tang, C. *Macromolecules* **2013**, *46*, 8816–8823.

(107) Rider, D. A.; Manners, I. *Polymer Reviews* **2007**, *47*, 165–195.

(108) Ni, Y.; Rulkens, R.; Manners, I. *J. Am. Chem. Soc.* **1996**, *118*, 4102–4114.

(109) Arimoto, F. S.; Haven, A. C. *J. Am. Chem. Soc.* **1955**, *77*, 6295–6297.

(110) Lai, J. C.; Vanderpool, D. P.; Good, M.; Prado, R.; Pittman, C. U. *Macromolecules* **1970**, *3*, 746–754.

(111) Alkan, A.; Natalello, A.; Wagner, M.; Frey, H.; Wurm, F. R. *Macromolecules* **2014**,

47, 2242–2249.

(112) Wu, W.; Tang, R.; Li, Q.; Li, Z. *Chem. Soc. Rev.* **2015**, *44*, 3997–4022.

(113) Lhenry, S.; Jalkh, J.; Leroux, Y. R.; Ruiz, J.; Ciganda, R.; Astruc, D.; Hapiot, P. *J. Am. Chem. Soc.* **2014**, *136*, 17950–17953.

(114) Wurm, F.; Hilf, S.; Frey, H. *Chem. Eur. J.* **2009**, *15*, 9068–9077.

(115) Kong, J.; Schmalz, T.; Motz, G.; Müller, A. H. E. *Macromolecules* **2011**, *44*, 1280–1291.

(116) Tan, Q.; Wang, L.; Ma, L.; Yu, H.; Liu, Q.; Xiao, A. *Macromolecules* **2009**, *42*, 4500–4510.

(117) Shi, J.; Jim, C. J. W.; Mahtab, F.; Liu, J.; Lam, J. W. Y.; Sung, H. H. Y.; Williams, I. D.; Dong, Y.; Tang, B. Z. *Macromolecules* **2010**, *43*, 680–690.

(118) Kim, Y. H.; Webster, O. W. *J. Am. Chem. Soc.* **1990**, *112*, 4593–4594.

(119) Gao, C.; Yan, D. *Prog. Polym. Sci.* **2004**, *29*, 183–275.

(120) Voit, B. I.; Lederer, A. *Chem. Rev.* **2009**, *109*, 5924–5973.

(121) Vögtle, F.; Richardt, G.; Werner, N. *Dendrimer Chemistry*; Wiley-VCH Verlag GmbH & Co. KGaA: Weinheim, Germany, 2009.

(122) Wilms, D.; Stiriba, S.-E.; Frey, H. *Acc. Chem. Res.* **2010**, *43*, 129–141.

(123) Klein, R.; Wurm, F. R. *Macromol. Rapid Commun.* **2015**, *36*, 1147–1165.

(124) Kainthan, R. K.; Janzen, J.; Levin, E.; Devine, D. V.; Brooks, D. E. *Biomacromolecules* **2006**, *7*, 703–709.

(125) CalderÃ³n, M.; Quadir, M. A.; Sharma, S. K.; Haag, R. *Adv. Mater.* **2010**, *22*, 190–218.

(126) Sunder, A.; Hanselmann, R.; Frey, H.; Mülhaupt, R. *Macromolecules* **1999**, *32*, 4240–4246.

(127) Wilms, D.; Wurm, F.; Nieberle, J.; Böhm, P.; Kemmer-Jonas, U.; Frey, H. *Macromolecules* **2009**, *42*, 3230–3236.

(128) Sunder, A.; Türk, H.; Haag, R.; Frey, H. *Macromolecules* **2000**, *33*, 7682–7692.

(129) Schömer, M.; Seiwert, J.; Frey, H. *ACS Macro Lett.* **2012**, *1*, 888–891.

(130) Kojima, C.; Yoshimura, K.; Harada, A.; Sakanishi, Y.; Kono, K. *Bioconjugate Chem.* **2009**, *20*, 1054–1057.

(131) Kojima, C.; Yoshimura, K.; Harada, A.; Sakanishi, Y.; Kono, K. *J. Polym. Sci., Part A: Polym. Chem.* **2010**, *48*, 4047–4054.

(132) Sun, X.; Zhou, Y.; Yan, D. *Macromol. Chem. Phys.* **2010**, *211*, 1940–1946.

(133) Tonhauser, C.; Schüll, C.; Dingels, C.; Frey, H. *ACS Macro Lett.* **2012**, *1*, 1094–1097.

(134) Shenoi, R. A.; Narayanannair, J. K.; Hamilton, J. L.; Lai, B. F. L.; Horte, S.; Kainthan, R. K.; Varghese, J. P.; Rajeev, K. G.; Manoharan, M.; Kizhakkedathu, J. N. *J. Am. Chem. Soc.* **2012**, *134*, 14945–14957.

(135) Shenoi, R. A.; Lai, B. F. L.; ul-haq, M. I.; Brooks, D. E.; Kizhakkedathu, J. N. *Biomaterials* **2013**, *34*, 6068–6081.

(136) Son, S.; Shin, E.; Kim, B.-S. *Macromolecules* **2015**, *48*, 600–609.

(137) Lagarec, K.; Rancourt, D. G. *Nucl. Instrum. Methods Phys. Res., Sect. B* **1997**, *129*, 266–280.

(138) Schüll, C.; Gieshoff, T.; Frey, H. *Polym. Chem.* **2013**, *4*, 4730–4736.

(139) Lederer, A.; Burchard, W.; Khalyavina, A.; Lindner, P.; Schweins, R. *Angew. Chem. Int. Ed. Engl.* **2013**, *52*, 4659–4663.

(140) Hölter, D.; Burgath, A.; Frey, H. **1997**, *48*, 30–35.

(141) Frey, H.; Hölter, D. *Acta Polym.* **1999**, *50*, 67–76.

(142) Wertheim, G. K.; Herber, R. H. *J. Chem. Phys.* **1963**, *38*, 2106–2111.

(143) Rabiee Kenaree, A.; Berven, B. M.; Ragogna, P. J.; Gilroy, J. B. *Chem. Commun.* **2014**, *50*, 10714–10717.

(144) Hendry, S. P.; Cardosi, M. F.; Turner, A. P. F.; Neuse, E. W. *Anal. Chim. Acta* **1993**, *281*, 453–459.

(145) Togni, A.; Hayashi, T. *Organic Synthesis* **2015**.

(146) Wei, B.; Vajtai, R.; Choi, Y.; Ajayan, P.; Zhu, H.; Xu, C. *Nano Lett.* **2002**, *2*, 1105–1107.

(147) Zhang, X.; Cao, A.; Wei, B.; Li, Y.; Wei, J.; Xu, C.; Wu, D. *Chem. Phys. Lett.* **2002**, *362*, 285–290.

(148) Kasper, M.; Sattler, K.; Siegmann, K.; Matter, U. *J. Aerosol Sci.* **1999**, *30*, 217–225.

(149) Scheid, D.; Lederle, C.; Vowinkel, S.; Schäfer, C. G.; Stühn, B.; Gallei, M. *J. Mater. Chem. C* **2014**, *2*, 2583–2590.

(150) Hudson, Z. M.; Manners, I. *Science* **2014**, *344*, 482–483.

(151) Whittell, G. R.; Manners, I. *Adv. Mater.* **2007**, *19*, 3439–3468.

(152) Hardy, C. G.; Ren, L.; Tamboue, T. C.; Tang, C. *J. Polym. Sci., Part A: Polym. Chem.* **2011**, *49*, 1409–1420.

(153) Hirata, H.; Iwama, Y.; Kuroda, S.; Fukuda, T.; Hagiwara, T. *Reactive and Functional Polymers* **2009**, *69*, 170–175.

(154) Jing, F.; Hillmyer, M. A. *J. Am. Chem. Soc.* **2008**, *130*, 13826–13827.

(155) Kanoh, S.; Nishimura, T.; Tsuchida, T.; Senda, H.; Motoi, M.; Takani, M.; Matsuura, N. *Macromol. Chem. Phys.* **2001**, *202*, 2489–2503.

(156) Brocas, A.-L.; Mantzaridis, C.; Tunc, D.; Carlotti, S. *Prog. Polym. Sci.* **2013**, *38*, 845–873.

(157) Barry, K. P.; Nataro, C. *Inorg. Chim. Acta* **2009**, *362*, 2068–2070.

(158) Mangold, C.; Dingels, C.; Obermeier, B.; Frey, H.; Wurm, F. *Macromolecules* **2011**, *44*, 6326–6334.

(159) Wurm, F.; Nieberle, J.; Frey, H. *Macromolecules* **2008**, *41*, 1909–1911.

(160) Mangold, C.; Wurm, F.; Obermeier, B.; Frey, H. *Macromolecules* **2010**, *43*, 8511–8518.

(161) Obermeier, B.; Wurm, F.; Frey, H. *Macromolecules* **2010**, *43*, 2244–2251.

(162) Günay, K. A.; Theato, P.; Klok, H.-A. *J. Polym. Sci., Part A: Polym. Chem.* **2013**, *51*, 1–28.

(163) Jing, X.; Liu, Y.; Liu, Z.; Tan, H. *J. Appl. Polym. Sci.* **2014**, *131*, 40835.

(164) Landfester, K. *Angew. Chem. Int. Ed.* **2009**, *48*, 4488–4507.

(165) Staff, R. H.; Gallei, M.; Mazurowski, M.; Rehahn, M.; Berger, R.; Landfester, K.; Crespy, D. *ACS Nano* **2012**, *6*, 9042–9049.

(166) Yiamsawas, D.; Baier, G.; Thines, E.; Landfester, K.; Wurm, F. R. *RSC Adv.* **2014**, *4*, 11661–11663.

(167) Rudolph, T.; Nunns, A.; Schwenke, A. M.; Schacher, F. H. *Polym. Chem.* **2015**, *6*, 1604–1612.

(168) Schenning, A. P. H. J. *Angew. Chem. Int. Ed. Engl.* **2014**, *53*, 11130–11131.

(169) Chatani, S.; Wang, C.; Podgórski, M.; Bowman, C. N. *Macromolecules* **2014**, *47*,

4949–4954.

(170) Eloi, J.-C.; Rider, D. A.; Cambridge, G.; Whittell, G. R.; Winnik, M. A.; Manners, I. *J. Am. Chem. Soc.* **2011**, *133*, 8903–8913.

(171) Kelly, J. C.; Pepin, M.; Huber, D. L.; Bunker, B. C.; Roberts, M. E. *Adv. Mater.* **2012**, *24*, 886–889.

(172) Hudson, S. M.; Gil, E. S. *Prog. Polym. Sci.* **2004**, *29*, 1173–1222.

(173) Helmy, S.; Leibfarth, F. A.; Oh, S.; Poelma, J. E.; Hawker, C. J.; Read de Alaniz, J. *J. Am. Chem. Soc.* **2014**, *136*, 8169–8172.

(174) Ahmed, R.; Priimagi, A.; Faul, C. F. J.; Manners, I. *Adv. Mater.* **2012**, *24*, 926–931.

(175) Yang, Z.; Fan, X.; Tian, W.; Wang, D.; Zhang, H.; Bai, Y. *Langmuir* **2014**, *30*, 7319–7326.

(176) Sambe, L.; La Rosa, de, V. R.; Belal, K.; Stoffelbach, F.; Lyskawa, J.; Delattre, F.; Bria, M.; Cooke, G.; Hoogenboom, R.; Woisel, P. *Angew. Chem. Int. Ed. Engl.* **2014**, *53*, 5044–5048.

(177) Cheng, M.; Liu, Q.; Ju, G.; Zhang, Y.; Jiang, L.; Shi, F. *Adv. Mater.* **2014**, *26*, 306–310.

(178) Dou, Y.; Han, J.; Wang, T.; Wei, M.; Evans, D.; Duan, X. *Langmuir* **2012**, *28*, 9535–9542.

(179) Dai, F.; Sun, P.; Liu, Y.; Liu, W. *Biomaterials* **2010**, *31*, 559–569.

(180) Mangold, C.; Obermeier, B.; Wurm, F.; Frey, H. *Macromol. Rapid Commun.* **2011**, *32*, 1930–1934.

(181) Heskins, M.; Guillet, J. E. *J. Macromol. Sci.-Chem.* **1968**, *A2*, 1441–1455.

(182) Bae, Y. H.; Okano, T.; Hsu, R.; Kim, S. W. *Makromol. Chem., Rapid Commun.* **1987**, *8*, 481–485.

(183) Schild, H. G. *Prog. Polym. Sci.* **1992**, *17*, 163–249.

(184) Schattling, P.; Jochum, F. D.; Theato, P. *Polym. Chem.* **2014**, *5*, 25–36.

(185) Van Gough, D.; Bunker, B. C.; Roberts, M. E.; Huber, D. L.; Zarick, H. F.; Austin, M. J.; Wheeler, J. S.; Moore, D.; Spoerke, E. D. *ACS Appl. Mater. Interfaces* **2012**, *4*, 6247–6251.

(186) Sumaru, K.; Kameda, M.; Kanamori, T.; Shinbo, T. *Macromolecules* **2004**, *37*, 4949–4955.

(187) Tang, X.; Liang, X.; Gao, L.; Fan, X.; Zhou, Q. *J. Polym. Sci., Part A: Polym. Chem.* **2010**, *48*, 2564–2570.

(188) Zhang, J.; Liu, H.-J.; Yuan, Y.; Jiang, S.; Yao, Y.; Chen, Y. *ACS Macro Lett.* **2012**, *2*, 67–71.

(189) Schattling, P.; Jochum, F. D.; Theato, P. *Chem. Commun.* **2011**, *47*, 8859–8861.

(190) Zhan, Y.; Gonçalves, M.; Yi, P.; Capelo, D.; Zhang, Y.; Rodrigues, J.; Liu, C.; Tomás, H.; Li, Y.; He, P. *J. Mater. Chem.* **2015**, *3*, 4221–4230.

(191) Li, F.; Ito, T. *J. Am. Chem. Soc.* **2013**, *135*, 16260–16263.

(192) Park, K. S.; Schougaard, S. B.; Goodenough, J. B. *Adv. Mater.* **2007**, *19*, 848–851.

(193) Crulhas, B. R.; Ramos, N. P.; Basso, C. R.; Costa, V. E.; Castro, G. R.; Pedrosa, V. A. *Int. J. Electrochem. Sci.* **2014**, *9*, 7596–7604.

(194) Chen, M.; Diao, G. *Talanta* **2009**, *80*, 815–820.

(195) Lallana, E.; Tirelli, N. *Macromol. Chem. Phys.* **2013**, *214*, 143–158.

(196) Ma, Y.; Dong, W.-F.; Hempenius, M. A.; Möhwald, H.; Vancso, G. J. *Nat. Mater.* **2006**, *5*, 724–729.

(197) Yan, Y.; Zhang, J.; Wilbon, P.; Qiao, Y.; Tang, C. *Macromol. Rapid Commun.* **2014**, *35*, 1840–1845.

(198) Song, S.; Hu, N. *J. Phys. Chem. B* **2010**, *114*, 3648–3654.

(199) Yan, Y.-M.; Tel-Vered, R.; Yehezkeli, O.; Cheglakov, Z.; Willner, I. *Adv. Mater.* **2008**, *20*, 2365–2370.

(200) Foo, K.; Sella, E.; Thomé, I.; Eastgate, M. D.; Baran, P. S. *J. Am. Chem. Soc.* **2014**, *136*, 5279–5282.

(201) Prucker, O.; Naumann, C. A.; Rühe, J.; Knoll, W.; Frank, C. W. *J. Am. Chem. Soc.* **1999**, *121*, 8766–8770.

(202) Hoyle, C. E.; Bowman, C. N. *Angew. Chem. Int. Ed.* **2010**, *49*, 1540–1573.

(203) Eckert, W. G.; James, S. H. *Interpretation of Bloodstain Evidence at Crime Scenes, Second Edition*; CRC Press, 1998.

(204) Hurvois, J. P.; Moinet, C. *J. Organomet. Chem.* **2005**, *690*, 1829–1839.

(205) Eötvös, R. *Ann. Phys. (Berlin)* **1886**, *263*, 448–459.

(206) Almgren, M.; Edwards, K.; Karlsson, G. *Colloids Surf., A* **2000**, *174*, 3–21.

(207) Resch, G. P.; Goldie, K. N.; Krebs, A.; Hoenger, A.; Small, J. V. *J Cell Sci* **2002**, *115*, 1877–1882.

(208) Kuntsche, J.; Horst, J. C.; Bunjes, H. *International Journal of Pharmaceutics* **2011**, *417*, 120–137.

(209) De Carlo, S.; Harris, J. R. *Electron Microscopy* **2011**, *42*, 117–131.

(210) Adrian, M.; Dubochet, J.; Fuller, S. D.; Harris, J. R. *Micron* **1998**, *29*, 145–160.

(211) Bailon, P.; Berthold, W. *PSTT* **1998**, *1*, 352–356.

(212) Harris, J. M.; Chess, R. B. *Nat Rev Drug Discov* **2003**, *2*, 214–221.

(213) Allen, T. M.; Hansen, C.; Martin, F.; Redemann, C.; Yau-Young, A. *Biochim. Biophys. Acta* **1991**, *1066*, 29–36.

(214) Pattni, B. S.; Chupin, V. V.; Torchilin, V. P. *Chem. Rev.* **2015**, *115*, 10938–10966.

(215) Ingram, G.; Mueller-Westerhoff, U. T. *J. Organomet. Chem.* **1996**, *512*, 219–224.

(216) Barlow, S.; Cowley, A.; Green, J. C.; Brunker, T. J.; Hascall, T. *Chimia* **2001**, *20*, 5351–5359.

(217) Massing, U.; Cicko, S.; Ziroli, V. *J. Controlled Release* **2008**, *125*, 16–24.

(218) Hirsch, M.; Ziroli, V.; Helm, M.; Massing, U. *J. Controlled Release* **2009**, *135*, 80–88.

(219) Edwards, K.; Johnsson, M.; Karlsson, G.; Silvander, M. *Biophys. J.* **1997**, *73*, 258–266.

(220) Fritz, T.; Hirsch, M.; Richter, F. C.; Müller, S. S.; Hofmann, A. M.; Rusitzka, K. A. K.; Markl, J.; Massing, U.; Frey, H.; Helm, M. *Biomacromolecules* **2014**, *15*, 2440–2448.

(221) Rosslee, C.; Abbott, N. L. *Curr. Opin. Colloid Interface Sci.* **2000**, *5*, 81–87.

(222) Fameau, A.-L.; Carl, A.; Saint-Jalmes, A.; Klitzing, von, R. *Chemphyschem* **2015**, *16*, 66–75.

(223) Brown, P.; Butts, C. P.; Eastoe, J. *Soft Matter* **2013**, *9*, 2365–2374.

(224) Anton, P.; Heinze, J.; Laschewsky, A. *Langmuir* **1993**, *9*, 77–85.

(225) Saji, T.; Hoshino, K.; Aoyagui, S. *J. Chem. Soc., Chem. Commun.* **1985**, *0*, 865–866.

(226) Liu, X.; Abbott, N. L. *J Colloid Interface Sci* **2009**, *339*, 1–18.

(227) Jacob, C.; Yang, H.-T.; Hill, H. A. O. *J. Electroanal. Chem.* **1996**, *416*, 83–88.

(228) Aydogan, N.; Rosslee, C. A.; Abbott, N. L. *Colloids Surf., A* **2002**, *201*, 101–109.

(229) Datwani, S. S.; Truskett, V. N.; Rosslee, C. A.; Abbott, N. L.; Stebe, K. J. *Langmuir*

2003, *19*, 8292–8301.

(230) Tajima, K.; Huxur, T.; Imai, Y.; Motoyama, I.; Nakamura, A.; Koshinuma, M. *Colloids Surf., A* **1995**, *94*, 243–251.

(231) Gallardo, B. S.; Abbott, N. L. *Langmuir* **1997**, *13*, 203–208.

(232) Jewell, C. M.; Hays, M. E.; Kondo, Y.; Abbott, N. L.; Lynn, D. M. *J Control Release* **2006**, *112*, 129–138.

(233) Kakizawa, Y.; Sakai, H.; Nishiyama, K.; Abe, M.; Shoji, H.; Kondo, Y.; Yoshino, N. *Langmuir* **1996**, *12*, 921–924.

(234) Pizzey, C. L.; Jewell, C. M.; Hays, M. E.; Lynn, D. M.; Abbott, N. L.; Kondo, Y.; Golan, S.; Talmon, Y. *J. Phys. Chem. B* **2008**, *112*, 5849–5857.

(235) Wang, K.; Gokel, G. W. *J. Phys. Org. Chem.* **1997**, *10*, 323–334.

(236) Saji, T. *Chem. Lett.* **1988**, *4*, 693–696.

(237) Saji, T. *Bull. Chem. Soc. Jpn.* **1989**, *62*, 2992–2994.

(238) Saji, T.; Ishii, Y. *J. Electrochem. Soc.* **1989**, *136*, 2953–2956.

(239) Takei, T.; Sakai, H.; Kondo, Y.; Yoshino, N.; Abe, M. *Colloids Surf., A* **2001**, *183-185*, 757–765.

(240) Takeoka, Y.; Aoki, T.; Sanui, K.; Ogata, N.; Yokoyama, M.; Okano, T.; Sakurai, Y.; Watanabe, M. *J. Controlled Release* **1995**, *33*, 79–87.

(241) Cheng, Z.; Ren, B.; Gao, M.; Liu, X.; Tong, Z. *Macromolecules* **2007**, *40*, 7638–7643.

(242) Gallardo, B. S.; Hwa, M. J.; Abbott, N. L. *Langmuir* **1995**, *11*, 4209–4212.

(243) Gallardo, B. S.; Metcalfe, K. L.; Abbott, N. L. *Langmuir* **1996**, *12*, 4116–4124.

(244) Saji, T.; Hoshino, K.; Aoyagui, S. *J. Am. Chem. Soc.* **1985**, *107*, 6865–6868.

(245) Aydogan, N.; Abbott, N. L. *Langmuir* **2001**, *17*, 5703–5706.

(246) Shi, P.; Qu, Y.; Liu, C.; Khan, H.; Sun, P.; Zhang, W. *ACS Macro Lett.* **2015**, *5*, 88–93.

(247) Musyanovych, A.; Schmitz-Wienke, J.; Mailänder, V.; Walther, P.; Landfester, K. *Macromol. Biosci.* **2008**, *8*, 127–139.

(248) Griffin, W. C. *J. Soc. Cosmet. Chem.* **1949**, *1*, 311–326.

(249) Hecht, L. L.; Schoth, A.; Muñoz-Espí, R.; Javadi, A.; Köhler, K.; Miller, R.; Landfester, K.; Schuchmann, H. P. *Macromol. Chem. Phys.* **2013**, *214*, 812–823.

(250) Staff, R. H.; Landfester, K.; Crespy, D. In *Hierarchical Macromolecular Structures: 60*

Years after the Staudinger Nobel Prize II; Advances in Polymer Science; Springer International Publishing, 2013; Vol. 262, pp. 329–344.

(251) Cao, K.; Tsang, B.; Liu, Y.; Chelladural, D.; Power, W. P.; Wang, X. *Organometallics* **2014**, *33*, 531-539.

(252) Johns, I. B.; McElhill, E. A.; Smith, J. O. *J. Chem. Eng. Data* **1962**, *7*, 277–281.

(253) Braun, A.; Huggins, F. E.; Kelly, K. E.; Mun, B. S.; Ehrlich, S. N.; Huffman, G. P. *Carbon* **2006**, *44*, 2904–2911.

(254) Hillard, E. A.; Vessières, A.; Jaouen, G. *Medicinal Organometallic Chemistry*; Jaouen, G.; Metzler-Nolte, N., Eds.; Springer: Berlin, Heidelberg, 2010; Vol. 32, pp. 81–117.

(255) Itoh, T.; Shirakami, S.; Ishida, N.; Yamashita, Y.; Yoshida, T.; Kim, H. S.; Wataya, Y. *Bioorg. Med. Chem. Lett.* **2000**, *10*, 1657–1659.

(256) Kondapi, A. K.; Satyanarayana, N.; Saikrishna, A. D. *Arch. Biochem. Biophys.* **2006**, *450*, 123–132.

(257) Gasser, G.; Ott, I.; Metzler-Nolte, N. *J. Med. Chem.* **2011**, *54*, 3–25.

(258) Günay, K. A.; Theato, P.; Klok, H.-A. *J. Polym. Sci., Part A: Polym. Chem.* **2013**, *51*, 1–28.

(259) Zhao, H.; Gu, W.; Kakuchi, R.; Sun, Z.; Sterner, E.; Russell, T. P.; Coughlin, E. B.; Theato, P. *ACS Macro Lett.* **2013**, *2*, 966–969.

(260) Foucher, D.; Tang, B.; Manners, I. *J. Am. Chem. Soc.* **1992**, *114*, 6246–6248.

(261) Manners, I. *Can. J. Chem.* **1998**, *76*, 371–381.

(262) Nguyen, P.; Gómez-Elipe, P.; Manners, I. *Chem. Rev.* **1999**, *99*, 1515–1548.

(263) Du, V. A.; Manners, I. *Macromolecules* **2013**, *46*, 4742-4753.

(264) Elbert, J.; Mersini, J.; Vilbrandt, N.; Lederle, C.; Kraska, M.; Gallei, M.; Stühn, B.; Plenio, H.; Rehahn, M. *Macromolecules* **2013**, *46*, 4255–4267.

(265) Wang, Z.; Masson, G.; Peiris, F. C.; Ozin, G. A.; Manners, I. *Chem. Eur. J.* **2007**, *13*, 9372–9383.

(266) Li, J.; Rothstein, S. N.; Little, S. R.; Edenborn, H. M.; Meyer, T. Y. *J. Am. Chem. Soc.* **2012**, *134*, 16352–16359.

(267) Natalello, A.; Werre, M.; Alkan, A.; Frey, H. *Macromolecules* **2013**,

131101141738002.

(268) Lutz, J.-F.; Ouchi, M.; Liu, D. R.; Sawamoto, M. *Science* **2013**, *341*, 1238149.

(269) Obermeier, B.; Wurm, F.; Mangold, C.; Frey, H. *Angew. Chem. Int. Ed. Engl.* **2011**, *50*, 7988–7997.

(270) Obermeier, B.; Frey, H. *Bioconjugate Chem.* **2011**, *22*, 436–444.

(271) Lee, B. F.; Kade, M. J.; Chute, J. A.; Gupta, N.; Campos, L. M.; Fredrickson, G. H.; Kramer, E. J.; Lynd, N. A.; Hawker, C. J. *J. Polym. Sci., Part A: Polym. Chem.* **2011**, *49*, 4498–4504.

Appendix

A.1 Cooperation Projects

During my diploma and PhD thesis a number of cooperation project have been developed. Already published papers are presented in the following. Ongoing projects will not be presented herein. The publications are sorted in analogy to the main part of this thesis:

1. Water-Soluble Multi-Stimuli-Responsive Metallocene-Containing Copolymers

"Ferrocenyl Glycidyl Ether: A Versatile Ferrocene Monomer for Copolymerization with Ethylene Oxide to Water-Soluble, Thermoresponsive Copolymers"

C. Tonhauser, A. Alkan, M. Schömer, C. Dingels, S. Ritz, V. Mailänder, H. Frey, F. R. Wurm, *Macromolecules* **2013**, 46, 647–655.

2. Water-Soluble Ferrocene-Containing Block Copolymers

"Enlarging the Toolbox: Epoxide Termination of Polyferrocenylsilane (PFS) as a Key Step for the Synthesis of Amphiphilic PFS-Polyether Block Copolymers"

A. Natalello, A. Alkan, A. Friedel, I. Lieberwirth, H. Frey, F. R. Wurm, *ACS Macro Letters* **2013**, 2, 313-316.

3. Monomer Sequence Monitoring by Real-Time NMR Spectroscopy

"Sequence-Controlled Polymers via Simultaneous Living Anionic Copolymerization of Competing Monomers"

E. Rieger, A. Alkan, A. Manhart, M. Wagner, F. R. Wurm, *Macromol. Rapid Commun.* **2016**, DOI: 10.1002/marc.201600092.

“Functional Group Distribution and Gradient Structure Resulting from the Living Anionic Copolymerization of Styrene and para-But-3-enyl Styrene”

A. Natalello, A. Alkan, P. von Tiedemann, F. R. Wurm, H. Frey, *ACS Macro Letters* **2014**, 560–564.

“Monomer Sequence Distribution Monitoring in Living Carbanionic Copolymerization by Real-Time ^{1}H NMR Spectroscopy”

A. Natalello, M. Werre, A. Alkan, H. Frey, *Macromolecules* **2013**, 46, 8467–8471.

A.1.1 Water-Soluble Multi-Stimuli-Responsive Metallocene-Containing Copolymers

Macromolecules

Article

pubs.acs.org/Macromolecules

Ferrocenyl Glycidyl Ether: A Versatile Ferrocene Monomer for Copolymerization with Ethylene Oxide to Water-Soluble, Thermoresponsive Copolymers

Christine Tonhauser,[†,‡] Arda Alkan,[‡,§] Martina Schömer,[‡] Carsten Dingels,[‡] Sandra Ritz,[§] Volker Mailänder,[§] Holger Frey,[‡] and Frederik R. Wurm*[,§]

[†]Graduate School Materials Science in Mainz, Staudinger Weg 9, D-55128 Mainz, Germany

[‡]Institute of Organic Chemistry, Organic and Macromolecular Chemistry, Duesbergweg 10-14, Johannes Gutenberg-Universität Mainz (JGU), D-55128 Mainz, Germany

[§]Max-Planck Institute for Polymer Research (MPI-P), Ackermannweg 10, D-55128 Mainz, Germany

Supporting Information

ABSTRACT: The first ferrocene-containing epoxide monomer, ferrocenyl glycidyl ether (fcGE), is introduced. The monomer has been copolymerized with ethylene oxide (EO). This leads to electroactive, water-soluble, and thermoresponsive poly(ethylene glycol) (PEG) derived copolyethers. Anionic homo- and copolymerization of fcGE with EO was possible. Molecular weights could be varied from 2000 to 10 000 g mol^{-1}, resulting in polymers with narrow molecular weight distribution (M_w/M_n = 1.07−1.20). The ferrocene (fc) content was varied from 3 to 30 mol %, obtaining water-soluble materials up to 10 mol % incorporation of the apolar ferrocenyl comonomer. Despite the steric bulk of fcGE, random copolymers were obtained, as confirmed via detailed ^{1}H NMR kinetic measurements as well as ^{13}C NMR studies of the polymer microstructure, including detailed triad characterization. In addition, the poly(fcGE) homopolymer has been prepared. All water-soluble copolyethers with fc side chains exhibited a lower critical solution temperature (LCST) in the range 7.2−82.2 °C in aqueous solution, depending on the amount of fcGE incorporated. The LCST is further tunable by oxidation/reduction of ferrocene, as demonstrated by cyclic voltammetry. Investigation of the electrochemical properties by cyclovoltammetry revealed that the iron centers can be oxidized reversibly. Further, to evaluate the potential for biomedical application, cell viability tests of the fc-containing PEG copolymers were performed on a human cervical cancer cell line (HeLa), revealing good biocompatibility only in the case of low amounts of fcGE incorporated (below 5%). Significant cytotoxic behavior was observed with fcGE content exceeding 5%. The ferrocene-substituted copolyethers are promising for novel redox sensors and create new options for the field of organometallic (co)polymers in general.

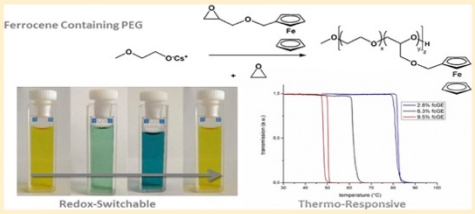

INTRODUCTION

Ferrocene (fc)-containing polymers[1] are interesting materials because of their unique physical and chemical properties such as redox-[2] and/or stimuli-responsive behavior.[3,4] Fc derivatives are used in (electro)catalysis[5] and in nonlinear optical polymers.[6] In addition, fc-containing materials may also become important for biomedical uses, since ferrocenyl moieties exhibit antineoplastic properties,[7,8] and the redox potential enables their utilization as amperometric glucose sensors.[9] Ferrocenyl groups can be incorporated into polymers either in the side chains or in the polymer backbone.[10−13] To date, the introduction of ferrocene units in polymers has relied mainly on two monomer structures, namely ferrocenophanes and vinylferrocene. Manners and co-workers introduced and intensively studied the controlled ring-opening polymerization of metallocenophanes[14,15] leading to poly(metallocenes) via different polymerization techniques and with variable bridging elements.[1] These elegant works rely on strict Schlenk techniques during monomer preparation, and the resulting polymers are usually not water-soluble. Therefore, they have to be converted into water-soluble derivatives via postpolymerization modification in most cases.[16]

The field of ferrocene side group polymers is currently dominated by monomers such as the above-mentioned vinylferrocene[12] but also ferrocenylmethyl (meth)acrylate.[13,17−19] Very recently, a series of (meth)acrylate (MA)-based monomers with varying spacers between fc and the MA unit have been introduced by Laschewsky and co-workers.[20] Other fruitful approaches to incorporate fc moieties in polymers are polymerization by hydrosilylation[21,22] or the

Received: October 29, 2012
Revised: December 5, 2012
Published: January 11, 2013

introduction of amide linkages subsequent to the polymerization.[23]

Most of the above-mentioned strategies result in organo-soluble materials. Water-soluble fc-containing polymers have been reported in very few publications only. These approaches rely on the synthesis of block copolymers carrying highly hydrophilic segments, such as poly(2-(*N*,*N*-dimethylamino)-ethyl methacrylate) (at pH 8)[24] or poly(ethylene glycol) (PEG) attached to the fc-containing block.[25−27] Another approach capitalizes on the polymerization of fc-containing monomers with hydrophilic side chains, such as oligo(ethylene glycol)[28] or poly(electrolytes),[29,30] which lead to aqueous solubility with decreased aggregation behavior.

A versatile, yet unexplored approach is the random (co)polymerization of designed fc-based monomers with a hydrophilic comonomer, resulting in water-soluble (random) copolymers. Herein we present the first ferrocene-containing epoxide monomer that can be copolymerized and incorporated into polyether structures that differ significantly from all other fc-containing polymers reported to date. In this context we also present water-soluble poly(ethylene glycol) (PEG)-based copolymers bearing ferrocenyl side chains randomly distributed at the polyether backbone. The synthesis is based on the anionic homo- and copolymerization of ferrocenyl glycidyl ether (fcGE, **1**). Copolymerization was carried out with ethylene oxide, since PEG is an important water-soluble polymer (Scheme 1).

Scheme 1. Synthesis of Poly(ferrocenyl glycidyl ether) and Poly(ethylene glycol-*co*-ferrocenyl glycidyl ether) Homo- and Copolymers by Anionic Ring-Opening Polymerization

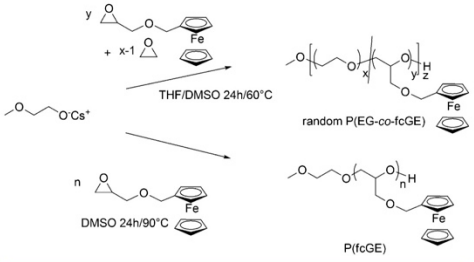

The polymers synthesized in this study have been investigated with respect to their properties, particularly aqueous solubility, thermoresponsive behavior,[31] and cytotoxicity as a function of the ferrocene content in the polyether. An interesting finding is that all water-soluble copolymers exhibit an LCST behavior. This LCST can be tailored by the fc content and further tuned by oxidation/reduction of the iron centers, resulting in multiresponsive structures.[32]

■ EXPERIMENTAL SECTION

Instrumentation. ^{1}H NMR spectra (300 and 400 MHz) and ^{13}C NMR spectra (75.5 MHz) were recorded using a Bruker AC300 or a Bruker AMX400. All spectra were referenced internally to residual proton signals of the deuterated solvent. For SEC measurements in DMF (containing 0.25 g/L of lithium bromide as an additive) an Agilent 1100 Series was used as an integrated instrument, including a PSS HEMA column ($10^6/10^5/10^4$ g/mol), a UV detector (275 nm), and a RI detector at a flow rate of 1 mL/min at 40 °C. Calibration was carried out using poly(ethylene oxide) standards provided by Polymer Standards Service. DSC measurements were performed using a PerkinElmer 7 series thermal analysis system and a PerkinElmer thermal analysis controller TAC 7/DX in the temperature range from −100 to 80 °C. Heating rates of 10 K min^{-1} were employed under nitrogen. Cloud points were determined in deionized water and observed by optical transmittance of a light beam (λ = 632 nm) through a 1 cm sample quartz cell. The measurements were performed in a Jasco V-630 photospectrometer with a Jasco ETC-717 Peltier element. The intensity of the transmitted light was recorded versus the temperature of the sample cell. The heating/cooling rate was 1 °C min^{-1}, and values were recorded every 0.1 °C. Cyclic voltammetry (CV) was performed using a BAS CV-50 W potentiostat using dichloromethane as a solvent under an inert atmosphere (N_2). The supporting electrolyte was tetrabutylammonium hexafluorophosphate (TBAH [0.1 M]). All experiments were performed at 25 °C in a conventional three-electrode cell, using a platinum working electrode (A 1/4 0.02 cm^2). All potentials are referred to a saturated calomel reference electrode (SCE). A coiled platinum wire was used as counter electrode.

Reagents. Solvents and reagents were purchased from Acros Organics, Sigma-Aldrich, or Fluka and used as received, unless otherwise stated. Chloroform-d_1, methanol-d_4, and DMSO-d_6 were purchased from Deutero GmbH. Ferrocenecarboxaldehyde and ferrocenemethanol were synthesized according to reported procedures.[33]

Synthesis. *Ferrocenyl Glycidyl Ether (fcGE, 1).* A synthesis pathway was developed relying on transformations known for other oxiranes.[34] In a typical reaction 5 g of ferrocenemethanol (23 mmol) was placed in a round-bottom flask, and 100 mL of benzene and 100 mL of a 50% NaOH solution were added. 1 g of tetrabutylammonium bromide (TBAB) was added as a phase transfer catalyst. To this mixture an excess of epichlorohydrin (4.3 g, 46 mmol) was added, while cooling the reaction mixture with ice. The solution was allowed to warm up to room temperature and rapidly stirred for 24 h. The progress of the reaction was followed by thin layer chromatography. The organic phase was washed with brine and $NaHCO_3$ solution, and the solvent was removed under vacuum. The crude product was purified by column chromatography using ethyl acetate and petroleum ether (3:7) as eluents. Besides the desired product (ferrocenyl glycidyl ether; R_f = 0.5), unreacted starting material (ferrocenemethanol; R_f = 0.2) was recovered and reused. The product was obtained as orange solid in typical yields of 70−80%. ^{1}H NMR (300 MHz, C_6D_6): δ (ppm) = 4.27−4.13 (m, 4 H, cp), 3.97 (d, 7 H, cp and CH_2-cp), 3.48−3.43 (dd, 1 H, CHCH*H*O), 3.20−3.14 (dd, 1 H, CHC*H*HO), 2.87 (q, 1 H, methine), 2.29−2.17 (m, 2 H, epoxide). The synthetic strategy is shown in Scheme 2. For a detailed assignment of the signals compare Figure 1 and Figures S1−S5 in the Supporting Information.

Scheme 2. Sequence for the Synthesis of the Novel Epoxide Monomer Ferrocenyl Glycidyl Ether (1, fcGE)

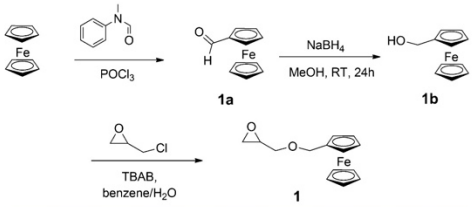

General Procedure for the Copolymerization of fcGE with EO: (P(EO-co-fcGE). Methoxyethanol and 0.9 equiv of cesium hydroxide monohydrate were placed in a 250 mL Schlenk flask, and benzene was added. The mixture was stirred at 60 °C under an argon atmosphere for 1 h and evacuated at 60 °C (10^{-2} mbar) for 12 h to remove benzene and water to generate the corresponding cesium alkoxide. Subsequently, ∼20 mL of dry THF was cryo-transferred into the

dx.doi.org/10.1021/ma302241w | *Macromolecules* 2013, 46, 647−655

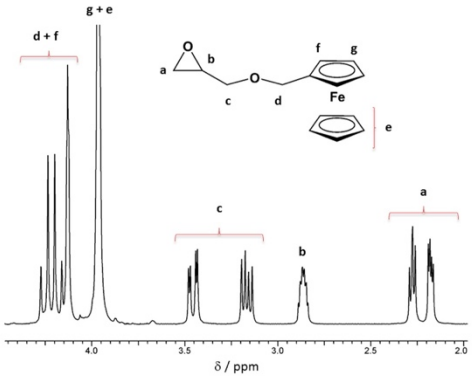

Figure 1. Detailed assignment of ^{1}H NMR resonances of ferrocenyl glycidyl ether (**1**) (measured in benzene-d_6).

Schlenk flask. EO was cryo-transferred to a graduated ampule and then cryo-transferred into the reaction flask containing the initiator in THF. Then, the second comonomer, fcGE, was added via syringe in a 50 wt % solution in anhydrous DMSO. The mixture was heated to 60 °C and stirred for at least 12−24 h. The copolymer solution was dried *in vacuo* and precipitated into cold diethyl ether to remove residual DMSO or dialyzed against deionized water (MWCO 1000 g/mol). The copolymer was obtained as an orange powder or viscous liquid depending on the fc content. Yields: 60−90%. ^{1}H NMR (300 MHz, DMSO-d_6): δ (ppm) = 4.24−4.16 (m, 4 H, cp), 4.07 (d, 7 H, cp and CH_2-cp), 3.68−3.45 (br, polyether backbone), 3.33 (s, 3 H, CH_3). For a detailed assignment compare Supporting Information Figure S6.

^{1}H NMR Kinetics. In a conventional NMR tube, a DMSO-d_6 solution of the initiator benzyl alcohol (deprotonated with 0.9 equiv of cesium hydroxide monohydrate) and a mixture of EO and fcGE in DMSO-d_6 were separately frozen under an argon atmosphere. High vacuum was applied, and the tube was flame-sealed while the solutions were kept frozen. To reduce the necessary time for locking and shimming of the polymerization mixture, a sample of the pure monomer mixture was measured in advance at the relevant temperature. Immediately after melting and mixing, the first spectrum was recorded. The temperature was kept at 40 °C. Sample spinning was turned off. Intervals between two measurements were 30 s (see also Figure S7).

Cell Viability Studies. The effect of fc-containing PEG copolymers on the viability of a human cervical cancer cell line (HeLa cells) was measured with a commercial luminescence assay CellTiter-Glo (Promega, Germany). The assay was based on the enzymatic reaction of luciferase transferring luciferin and ATP, supplied by the living cells, to oxyluciferin, resulting in luminescence. The luminescence is used as a measure of cell proliferation and cytotoxicity.

HeLa cells were cultured in Dulbeccós modified eagle medium (DMEM), supplemented with 10% FCS, 100 units penicillin, and 100 mg mL^{-1} streptomycin, 2 × 10^{-3} M L-glutamine (all from Invitrogen, Germany). Cells were grown in a humidified incubator at 37 °C and 5% CO_2. For determining the cell viability, HeLa cells were seeded at a density of 20 000 cells cm^{-2} (6 × 10^4 cells mL^{-1}) in 96-well plates (black, opaque-walled, Corning, Netherlands). FcGE copolymers (100 mg/mL) were dissolved in sterile water (Ampuwa , pH 7.4, Fresenius Kabi, Germany), and the indicated concentrations were produced by a serial dilution in cell culture medium (DMEM, 10% FCS). After 24 h, the culture medium was replaced by fcGE copolymer supplemented medium (200 μL, DMEM, 10% FCS) or medium without compound (DMEM, 10% FCS) as a specific control for 100% cell viability. The cells were treated for 24 or 48 h, and the number of viable cells was determined by the CellTiter-Glo assay following the manufacturer's instructions. Briefly, cell culture medium with compound was replaced by 100 μL CellTiter-Glo reagent. The 96-well plates were mixed for 2 min and incubated for 10 min at room temperature. During this time, the cytosolic ATP was released for the enzymatic reaction. The luminescence was detected with a plate reader (Infinite M1000, Tecan, Germany) using i-control software (Tecan, Germany). The values represent the mean ± SD of four replicates and were plotted relative to the untreated cells.

■ RESULTS AND DISCUSSION

A. Monomer and Polymer Synthesis. Water-soluble fc-containing (co)polymers with aliphatic polyether backbone are of interest for sensing, electrochemical, or potentially also biomedical fields and many other applications. The incorporation of fc into a water-soluble polymer backbone (viz. PEG) has been targeted by oxyanionic copolymerization of the newly designed monomer (**1**) with EO. The resulting copolymers were studied with respect to preservation of the metallocene during the anionic ring-opening polymerization of the oxirane. The monomer (fcGE, **1**) was synthesized in a three-step protocol (Scheme 2), starting with a Vilsmeier synthesis to generate ferrocenecarboxaldehyde (**1a**). The aldehyde was reduced into the corresponding alcohol (ferrocenemethanol (**1b**)) with $NaBH_4$, which was subsequently used in a phase-transfer-catalyzed nucleophilic substitution reaction with epichlorohydrin to yield fcGE similar to the synthetic protocols of other previously described glycidyl ethers (GEs)[34,35] (note: **1a** and **1b** are also commercially available). The monomer was obtained in overall good yields (up to 80%) and purified by column chromatography.

Figure 1 shows the ^{1}H NMR spectrum of **1** in benzene-d_6 (Figure S1 shows the ^{1}H NMR in DMSO-d_6). Unequivocal signal assignments were obtained using 2D NMR techniques (Figures S3−S5). ^{13}C NMR spectra with the respective assignments can also be found in the Supporting Information (Figure S2).

The (co)polymer synthesis was carried out similar to previous works on poly(ether) copolymers.[36−39] The cesium salt of methoxyethanol was used as the respective initiator, and a mixture of THF and DMSO as well as a reaction time of 12−24 h were found to represent the best suited polymerization conditions with respect to complete conversion. When exceeding an fc content of 10% incorporation into the PEG backbone, the copolymers were no longer soluble in water (at room temperature); therefore, the focus was placed on copolymers with limited fc content in the current work to obtain hydrophilic materials and to guarantee a certain degree of aqueous solubility. The homopolymer of fcGE is insoluble in water. All polymers synthesized in this study exhibited narrow molecular weight distributions (in the range of M_w/M_n = 1.07−1.20, compare Table 1) and monomodal SEC traces (compare Figure 2). This confirms that fc is stable toward the highly basic conditions applied during the anionic polymerization, and no undesired side reactions that would lead to cross-linking, occur. UV/vis spectra (Supporting Information) also prove the incorporation of fc with the characteristic absorption band at ca. 450 nm. The stability of fc during polymerization may be expected, since other fc-based monomers have also been used in (carb)anionic polymerizations in recent works.[12,27]

Molecular weights of the (co)polymers as well as the comonomer content were determined by ^{1}H NMR spectroscopy and are in agreement with theory. The methyl group of the initiator (at 3.28 ppm) can be used as a reference signal and

Table 1. Molecular Weight Data for the Ferrocene-Containing (Co)polymers Synthesized in This Study by Anionic ROP

no.	formula[a]	fcGE/(fcGE + EG) (%)	M_n[a] (g/mol)	M_n[b] (g/mol)	PDI[b]
P1	MeOP(EO_{99}-*co*-$fcGE_3$)	2.8	5200	4700	1.10
P2	MeOP(EO_{195}-*co*-$fcGE_6$)	2.9	10200	8100	1.20
P3	MeOP(EO_{64}-*co*-$fcGE_4$)	6.3	3900	2600	1.07
P4	MeOP(EO_{73}-*co*-$fcGE_6$)	7.1	4800	2200	1.14
P5	MeOP(EO_{36}-*co*-$fcGE_4$)	9.5	2500	2300	1.16
P6	MeOP(EO_{50}-*co*-$fcGE_6$)	10.6	3850	2100	1.10
P7	MeOP(EO_{28}-*co*-$fcGE_{11}$)	28	4200	2200	1.15
P8	MeOP$(fcGE)_{17}$	100	4800	1300	1.17

[a]Determined via end-group analysis from ^{1}H NMR spectroscopy in DMSO-d_6. [b]Determined from size exclusion chromatography in DMF vs PEG standards using the RI-signal detection.

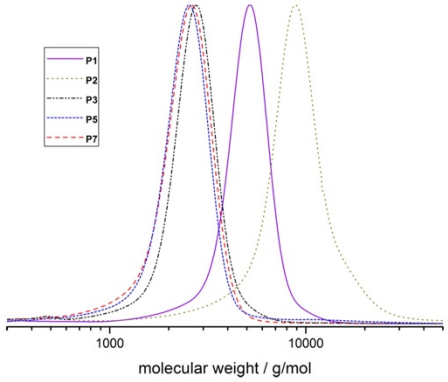

Figure 2. SEC traces (DMF, RI detection, 1 mL/min, 40 °C) of different P(EG-*co*-fcGE) copolymers, showing monomodal molecular weight distributions and low PDIs. Characterization data are summarized in Table 1.

is compared to the integral of the resonances of the polyether backbone between 3.68 and 3.45 ppm as well as the signals resulting from the cyclopentadienyl (cp) rings of fc at 4.24–4.16 and 4.07 ppm (Figure S6). The determined molecular weights correspond to the theoretical values based on the amount of initiator employed and are in good agreement with the conditions for a living anionic polymerization even with the sterically demanding fcGE.

The comonomer distribution and microstructure of the copolymer chains can be determined via the triad sequence distribution from ^{13}C NMR spectroscopy with different amounts of fcGE incorporated into the PEG backbone (Figure 3). For abbreviations, EO units are named "E", while the glycidyl ether signals of fcGE are named "G"; other carbon centers stemming from the cyclopentadienyl groups are marked with an "fc". The hompolymer of fcGE (100% in Figure 3, **P8**) allowed for the signal assignment of the GGG triad. For the copolymers, it can be clearly detected that the integral of the EEE triad decreases with increasing amount of fcGE incorporated (signal EEE, Figure 3). In addition, the resonance for the tertiary carbon of fcGE (b′) is detected at 78.3 ppm for the homopolymer (GGG), while the copolymers show additional signals, i.e., the EGE triad at ca. 77.7 ppm and with increasing amount of fcGE also the presence of GGE, EGG, and GGG triads. This effect is also visible for the substituted carbon at the cp ring (at ca. 85 ppm) that splits up for higher comonomer content (see Supporting Information). The triad sequence distribution indicates random incorporation of fcGE into the PEG backbone.

An overview of all polymer samples prepared is given in Table 1. A comparison of the molecular weights determined via end-group analysis from ^{1}H NMR spectroscopy and SEC measurements shows a considerable difference of the two values. This can be ascribed to the high molecular weight of the fc side chains changing the hydrodynamic radii during the SEC experiment only slightly compared to PEG. Thus, calibration vs linear PEG standards underestimates the molecular weights. In most of the cases an increasing content of fcGE in the copolymer leads to an increasing deviation during the SEC experiment. This effect was already observed for other P(EG-*co*-glycidyl ether) copolymers.[40] SEC equipped with a UV detector also confirms the incorporation of fc, as all polymers exhibit a strong absorption and are yellow to orange materials.

MALDI ToF mass spectrometry gives further insight into the copolymer microstructure. The MALDI ToF spectrum of the fcGE homopolymer shows a single distribution with a distance of 272 Da for the monomer (see Figure S15). For the copolymers, MALDI ToF mass spectrometry reveals the incorporation of both monomers into the polymer (Figure 4). A linear combination of the molecular weights of both monomers can be detected throughout the whole apparent molecular weight distribution (also compare Figure S8), as expected for a copolymer (M(EO) = 44 Da, M(fcGE) = 272 Da), supporting the incorporation of the two monomers into the polymer backbone.

Copolymerization Kinetics via ^{1}H NMR Spectroscopy. To confirm the random nature of the copolymerization of EO and fcGE in the anionic polymerization, ^{13}C NMR triad statistics has been determined (see above), and further detailed characterization of the evolution of the copolymer structure during the reaction was carried out, following the polymerization kinetics via *in situ* ^{1}H NMR spectroscopy. An experimental procedure[36] recently developed in our group was adapted for the comonomer pair EO/fcGE. Briefly, a DMSO-d_6 solution of the initiator and a mixture of fcGE (10 mol %) and EO (90 mol %) in DMSO-d_6 were separately transferred into a NMR tube under an argon atmosphere and quickly frozen with liquid nitrogen cooling. The cold NMR tube was evacuated and flame-sealed, and the polymerization was subsequently initiated by warming the tube to 40 °C in the NMR spectrometer. The growth of the polymer backbone as well as the consumption of both monomers was followed *in situ* by the decrease of the epoxide signals located at 2.61 ppm for the methylene protons of EO and at 3.07 ppm for the methine proton of fcGE, respectively (compare Figure S7). All signals are normalized to the 11 protons of the ferrocenyl methyl moiety (d–g) that remain constant during the reaction. Because of the overlap of the EO proton signal with the fcGE proton a (cf. Figures S1 and S7) and the residual DMSO signal, the value has to be corrected with the corresponding peak intensities. The intensity of the DMSO peak was determined from the last spectra recorded in which all EO and fcGE had reacted, and therefore no superposition of the mentioned peaks was observed, allowing the determination of the absolute value for the DMSO integral.

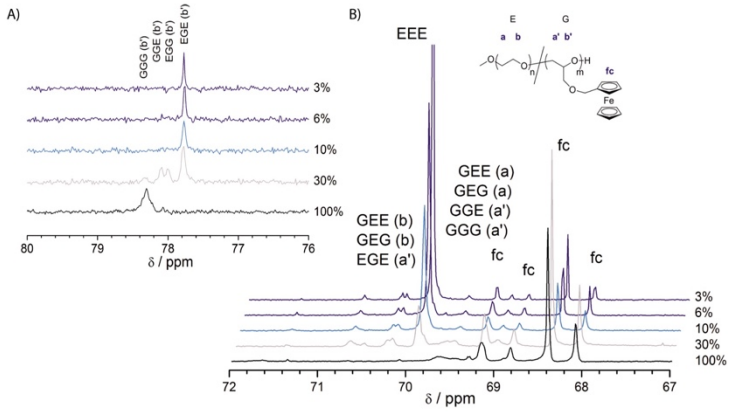

Figure 3. Zoom into typical ^{13}C NMR spectra of several copolymers of ethylene oxide and ferrocenyl glycidyl ether and the homopolymer of ferrocenyl glycidyl ether (in DMSO-d_6). The triad signals are highlighted, indicating a random distribution of ferrocenyl glycidyl ether units at the PEG backbone. (The percentages represent the amount of fcGE incorporated into the (co)polymer.)

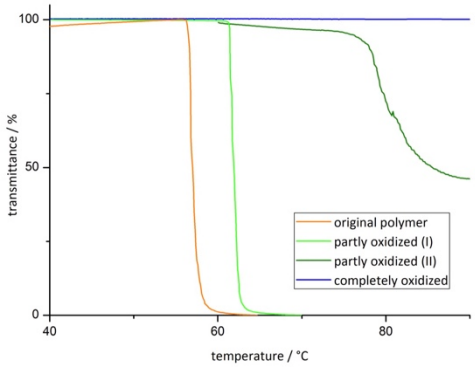

Figure 4. Zoom-in of the MALDI-ToF mass spectrum of sample **P7** showing linear combinations of the molecular masses of both comonomers (ethylene oxide M = 44 Da and ferrocenyl glycidyl ether M = 272 Da) proving that both are incorporated into the copolymer.

Figure 5a shows a representative example for the monomer conversion in the course of the polymerization with comonomer content of 10% fcGE. The copolymerization at 40 °C requires ~8 h to completion. From earlier copolymerization studies it is known that the relative reactivity of the comonomers is independent of the temperature.[35,36]

Figure 5b illustrates the evolution of monomer feed composition during polymerization, revealing concurrent incorporation of fcGE and EO into the growing polymer chain during the whole reaction time. Throughout the polymerization, the molar ratio of fcGE and EO units in the polymer chain remains constant, and there is no deviation from the initial ratio of the comonomer feed. Unexpectedly, the sterically demanding fc moiety does not lower the reactivity of the glycidyl ether structure. This evidence unambiguously the formation of random copolymers of EO and fcGE by anionic

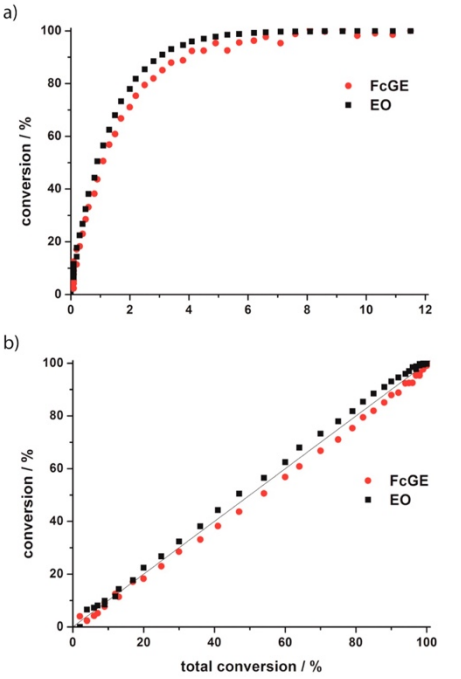

Figure 5. (a) Monomer conversion versus time plot for copolymerization of EO with fcGE ether (10%) at 40 °C measured via ^1H NMR kinetics in DMSO-d_6. (b) Percentage of monomer conversion of EO and fcGE versus total monomer conversion for copolymerization at 40 °C measured via ^1H NMR kinetics in DMSO-d_6.

dx.doi.org/10.1021/ma302241w | *Macromolecules* 2013, 46, 647−655

copolymerization under the copolymerization conditions studied and is in line with the results of the microstructure characterization, i.e., the triad analysis described before.

B. Materials Properties of the PEG-*co*-PfcGE Copolymers. *Thermal Analysis.* Thermal analysis of all copolymers was carried out using differential scanning calorimetry (DSC). The copolymers prepared in this study show variable molecular weight which has to be taken into account when analyzing the results. Most of the samples, however, have a molecular weight (as determined by NMR) of around 5000 g/mol, making a comparison possible and also the other samples with different molecular weight and chain length still follow the expected trends (the results are summarized in Table 2): (1) The glass transition temperatures (T_g) for most copolymers determined are close to the value of PEG (−56 °C) because these copolymers consist of a major fraction of PEG. Only in the case of copolymers **P6** and **P7**, a slight increase of the T_g can be observed (which could be also attributed to a different chain length and molecular weight). These rather low T_g's, however, can be attributed to the aliphatic polyether backbone structure with its high flexibility, resulting in amorphous, low-T_g materials, even with a high fc content. (2) Considering the melting behavior of the copolymers, a clear trend is observed. PEG is a crystalline material with a melting temperature of 65 °C.[41] The degree of crystallization of the copolymers is gradually lowered with increasing incorporation of the comonomer, since the fc side chains disturb the crystallization of the PEG domains. This is also visible with the naked eye, as the copolymers are either obtained as orange powders for low fc content or deep orange, sticky solids for higher amounts of fcGE or the poly(fcGE) homopolymer. In a previous work it was estimated that ∼13 adjacent EO units are needed (i.e., PEG with a molecular weight of 600 g/mol)[35,42] to observe crystallization in random PEG copolymer structures, which is still the case for copolymer **P5** (with an average of ca. 10 adjacent EO units) but not observable for copolymer **P7**. An incorporation of 28% of comonomer is required to completely suppress the crystallization of the PEG chains. The gradual change of the thermal behavior of the copolymers mirrors the random comonomer distribution in the polymer backbone in addition to the NMR kinetics and the triad abundance observed in ^{13}C NMR spectra.

Table 2. Thermal Data of the Copolymers Synthesized in This Study As Determined via Differential Scanning Calorimetry (DSC)

no.	formula	fcGE/(fcGE + EO) (%)	T_g[a] (°C)	T_m[b] (°C)	ΔH[c] (J/g)
P1	MeOP(EO_{99}-*co*-fcGE_3)	2.8	−56	43	82
P2	MeOP(EO_{195}-*co*-fcGE_6)	2.9	−54	42	72
P3	MeOP(EO_{64}-*co*-fcGE_4)	6.3	−56	27	48
P4	MeOP(EO_{73}-*co*-fcGE_6)	7.1	−58	16	27
P5	MeOP(EO_{36}-*co*-fcGE_4)	9.5	−59	14	40
P6	MeOP(EO_{50}-*co*-fcGE_6)	10.6	−51	8	6
P7	MeOP(EO_{28}-*co*-fcGE_{11})	28	−49		

[a]Glass transition temperature T_g. [b]Melting temperature T_m. [c]Melting enthalpy determined by integration of the melting peak.

Lower Critical Solution Temperature (LCST) Behavior. Very recently, we have been able to demonstrate that different copolymers based on EO and varied concentration of hydrophobic glycidyl ether comonomers exhibit tunable thermoresponsive behavior over a broad temperature range.[31] It was demonstrated that the LCST can be varied by two different parameters, the first (i) being the comonomer hydrophobicity and the second (ii) the comonomer content. With increasing content of hydrophobic comonomer and with increasing hydrophobicity of the comonomer the LCST is lowered gradually, as it is expected. Also for the herein reported fcGE copolymers an LCST behavior was detected. All polymers were investigated at a concentration of 5 g/L, and the results are summarized in Table 3. The cloud points of the aqueous polymer solutions have been measured by monitoring the transmittance of a light beam (wavelength 632 nm) through a 1 cm quartz sample cell at a heating (cooling) rate of 1 °C min^{-1}. The cloud point temperatures of the very sharp transitions from translucent to opaque solutions were defined as the value measured at 50% transmittance. The respective graphs of the turbidimetry measurements can be found in the Supporting Information (Figure S9).

Table 3. Lower Critical Solution Temperature Values of Different P(EO-*co*-fcGE) Copolymers Determined by Turbidity Measurements

no.	formula[a]	fcGE/(fcGE + EO)[a] (%)	LCST[b] (°C)
P1	MeOP(EO_{99}-*co*-fcGE_3)	2.8	82.2
P2	MeOP(EO_{195}-*co*-fcGE_6)	2.9	69.1
P3	MeOP(EO_{64}-*co*-fcGE_4)	6.3	61.8
P4	MeOP(EO_{73}-*co*-fcGE_6)	7.1	37.7
P5	MeOP(EO_{36}-*co*-fcGE_4)	9.5	50.0
P6	MeOP(EO_{50}-*co*-fcGE_6)	10.6	7.2
P7	MeOP(EO_{28}-*co*-fcGE_{11})	28	
P8	MeOP(fcG$E)_{17}$	100	

[a]Obtained from ^1H NMR spectroscopy. [b]For a 5 mg mL^{-1} solution of the copolymer in deionized water.

The LCST values of different copolymers with similar molecular weights have been plotted against the comonomer content. A linear relationship between comonomer content and cloud point is observed. A comparison of the slope of the fitted line with the values from the literature[31] indicates the degree of hydrophobicity of fcGE compared to other glycidyl ethers. It was found that the slope of the line and therefore the hydrophobicity of ferrocenyl glycidyl ether are situated between ethoxy vinyl glycidyl ether[35] and dibenzylamino gycidol.[31,36] Furthermore, it was found that in the case of perfectly random copolymers the interception with the *y*-axis is situated at around 100 °C, as it is also present in PEG homopolymers (Figure S10). For the fcGE-containing copolymers the interception was found to be at 94 ± 6 °C, which again suggests a random distribution of fcGE units in the chain, as proven by NMR studies (see above). The LCST for the P(EO-*co*-fcGE) copolymers could be varied from 82.2 °C for 2.8% fcGE to 7.2 °C for 10.6% incorporation (at similar molecular weights). It has to be kept in mind that the LCST of a polymer also depends on the molecular weight.[43] This effect is also detectable in the investigated copolymer library. For example, for polymers **P1** and **P2** the fcGE content is almost the same; however the LCST of **P3** (M_n(NMR) = 10 200 g/mol) is with 69.1 °C much lower than for **P1** with 82.2 °C having ca. half of the molecular weight (M_n (NMR) = 5200 g/mol).

In contrast to all other PEG copolymers investigated before, fc-containing PEGs offer a further possibility to tune the cloud points of a given polymer by an external stimulus. This was

demonstrated with two different experiments: First, fine-tuning of the LCST was achieved by supramolecular complexation and, second, by using the redox properties of fc.

It is well-known from the literature that β-cyclodextrin (β-CD)[43] forms inclusion complexes with fc which should be also generated upon the addition of β-CD to the herein presented copolymers. The addition of β-CD led to a shift of the respective LCST to slightly higher values due to the presence of the hydrophilic β-CD. For **P3**, for example, an increase of the LCST from 61.8 to ca. 68 °C was observed. This unexpected small influence on the cloud point (increase by ca. 5 °C) can most probably be ascribed to the temperature dependence of this host−guest complex[44] as well as to steric reasons (experimental results in the Supporting Information, Figure S11).[45] However, the host−guest complexation without a significant influence on the LCST could be used to tailor micellization or to attach dyes or labels in a noncovalent manner; this is currently under further investigation.

In a second approach, the influence of the oxidation of the fc moieties on the LCST was investigated. A strong influence on the LCST was observed after the oxidation to the poly(ferrocenium)-PEGs with silver(I) triflate ($AgCF_3SO_3$). Upon addition of the oxidizing agent, the yellow color vanished and a greenish to blue solution resulted, depending on the amount of oxidizing agent (compare Figure S12) and the formation of silver(0). After filtration from the precipitate, the clear solutions were measured in turbidimetry experiments. With increasing fc-oxidation level, higher LCST values were detected, until finally a fully water-soluble polymer without LCST behavior was obtained (compare Figure 6). Finally, this effect is reversible by

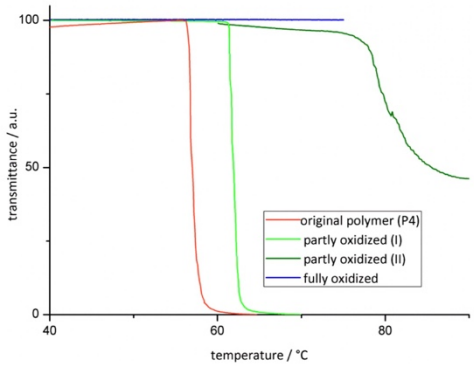

Figure 6. Turbidity measurements of **P5** upon oxidation. By the addition of oxidizing agents the LCST of the starting polymer (P5, red) can be altered (green) until finally the thermoresponsive behavior disappears (blue).

the reduction of the iron center using sodium thiosulfate ($Na_2S_2O_3$). The LCST values obtained after reduction reached similar values as for the pristine solutions, although it is important to mention that the salt concentration may have an influence on the absolute LCST ("salting out effect").[46] Intense studies on the direct correlation of the oxidation state and the LCST behavior are currently under way.

Cyclic Voltammetry Measurements. Fc can be oxidized reversibly by applying a cyclic potential, and this redox-active behavior can be studied by cyclic voltammetry.[47] We investigated two copolymers with different fc content with cyclic voltammetry. The copolymer samples **P1** and **P7** with the lowest and the highest amount of fc incorporated have been dissolved in dichloromethane with 0.1 M conducting salt (tetrabutylammonium hexafluorophosphate) at a concentration of 5 g/L. Figure 7 shows the cyclic voltammogram of both

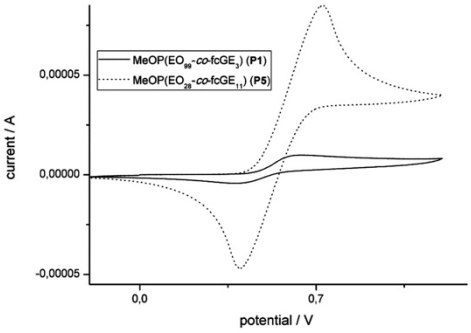

Figure 7. Cyclic voltammogram of **P1** and **P7** at a scan rate of 0.5 V/s.

polymers at a scan rate of 0.5 V/s. It can be seen that at a similar weight fraction (targeted: 5 mg/mL) different maximum currents can be detected. For **P1**, 5 g/L correspond to 2.9×10^{-6} mol of fc units/mL, while for **P7** 5 g/L correspond to 1.31×10^{-5} mol of fc units/mL, which is in accordance with the different maximum currents observed. Another important information that can be obtained from the cyclic voltammogram is that in this case oxidation is a homogeneous process, and no stepwise oxidation is observed, as for example reported for poly(ferrocenylsilane)s; i.e., the fc units are separated and do not communicate.[48]

C. Cell Viability Studies. Cell viability of the PEG copolymers represents an important feature of the materials properties with respect to potential applications in the biomedical field. PEG is used in many biomedical applications due to its low toxicity and immunogenicity. Further, it was shown recently that many P(EO-*co*-GE)s exhibit similarly low toxicity as PEG.[49] In this context we were interested in the effect of the fc moieties at the PEG backbone on the cytotoxicity of these materials, since ferrocenium salts are known to be cytostatic and have recently been investigated with respect to their potential use in anticancer therapy.[50,51]

The toxicity of the P(EO-*co*-fcGE) copolymers was investigated against a human cervical cancer cell line (HeLa) from a concentration range of 1−1000 μg mL^{-1} by measuring the ATP content of viable cells in relation to untreated cells. The results are displayed in Figure 8. While the two copolymers with less than 5 mol % fcGE units showed good biocompatibility comparable to the PEG homopolymer, the two copolymers with higher fcGE incorporation (6.3 and 9.5%) are clearly cytotoxic for concentrations exceeding 10 μg mL^{-1}.

With respect to biomedical applications these novel water-soluble polymers might be interesting for PEGylation[52]-like applications, enabling tracking of the polymer molecules due to the fc moieties, provided polymers with low iron content and low toxicity are used. In contrast, copolyethers with high ferrocene content might be interesting for applications as

dx.doi.org/10.1021/ma302241w | *Macromolecules* 2013, 46, 647−655

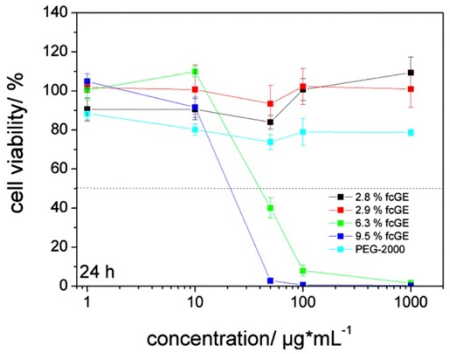

Figure 8. Cell viability of HeLa cells treated with fc-containing PEG copolymers after 24 h of incubation. Untreated cells were set to 100%. The experiment was carried out as four independent replicates.

polymeric cytotoxic agents. Further studies of this issue are in progress and will be reported soon.

CONCLUSION

A new ferrocene-containing epoxide monomer, namely ferrocenyl glycidyl ether, has been prepared, and its homo- and copolymerization behavior with ethylene oxide have been studied. This represents the first synthesis ferrocene-containing polyether structures via anionic polymerization and of water-soluble polyether-based ferrocene containing polymer with a PEG-like structure. Homopolymerization of the sterically demanding fcGE was accomplished, and also anionic *co*-ROP of EO and the fcGE monomer, affording random copolymers with narrow molecular weight distributions, have been established. The random microstructure of the materials is supported by detailed kinetic characterization data of the polymerization with *in situ* ^{1}H NMR spectroscopy and further triad sequence analyses via ^{13}C NMR. The novel monomer fcGE broadens the field of ferrocene-containing monomers and polymers toward polyethers and may be viewed as the first epoxide analogue of vinylferrocene. Further, the thermal properties also support random incorporation of fcGE into the PEG backbone. As expected, the degree of crystallization is reduced with increasing fcGE content. The homopolymer of fcGE is an amorphous material. The copolymers exhibit thermoresponsive behavior in water with tunable LCSTs in the range 82.2 to 7.2 °C. The LCST can be further tailored either by the addition of β-cyclodextrin to form inclusion complexes or by oxidation/reduction of the fc moieties.

The cytotoxicity of these materials has been investigated against HeLa cells. It was found that for a low amount of fc moieties (ca. 3%) the polymers are comparable to PEG in their toxicity, while higher fc concentrations lead to strongly cytotoxic behavior. We believe that these PEG-derived copolymers with pending ferrocene units possess intriguing potential for application in various fields, e.g., for sensing, detection, and as potential polymer therapeutics, as one can easily detect the iron centers of the ferrocene unit.

ASSOCIATED CONTENT

Supporting Information

Figures S1−S15. This material is available free of charge via the Internet at http://pubs.acs.org.

AUTHOR INFORMATION

Corresponding Author

*E-mail wurm@mpip-mainz.mpg.de, Ph 0049 6131 379 502, Fax 0049 6131 370 330.

Notes

The authors declare no competing financial interest.

ACKNOWLEDGMENTS

C.T. is recipient of a fellowship through funding of the German Excellence Initiative (DFG/GSC 266). M.S. and C.D. are grateful to the Max Planck Graduate Center with the Johannes Gutenberg-Universität Mainz (MPGC) for fellowships and financial support. H.F. acknowledges the Fonds der Chemischen Industrie and the SFB 625 for support. F.W. thanks the Alexander-von-Humboldt foundation for a fellowship.

REFERENCES

(1) Nguyen, P.; Gomez-Elipe, P.; Manners, I. *Chem. Rev.* **1999**, *99* (6), 1515−1548.
(2) Frede, M.; Steckhan, E. *Tetrahedron Lett.* **1991**, *32* (38), 5063−5066.
(3) Arimoto, F. S.; Haven, A. C. *J. Am. Chem. Soc.* **1955**, *77* (23), 6295−6297.
(4) Eloi, J.-C.; Rider, D. A.; Cambridge, G.; Whittell, G. R.; Winnik, M. A.; Manners, I. *J. Am. Chem. Soc.* **2011**, *133* (23), 8903−8913.
(5) Durkee, D. A.; Eitouni, H. B.; Gomez, E. D.; Ellsworth, M. W.; Bell, A. T.; Balsara, N. P. *Adv. Mater.* **2005**, *17* (16), 2003−2006.
(6) Wright, M. E.; Toplikar, E. G.; Kubin, R. F.; Seltzer, M. D. *Macromolecules* **1992**, *25* (6), 1838−1839.
(7) Top, S.; Dauer, B. n. d.; Vaissermann, J.; Jaouen, G. R. *J. Organomet. Chem.* **1997**, *541* (1−2), 355−361.
(8) Top, S.; Vessières, A.; Leclercq, G.; Quivy, J.; Tang, J.; Vaissermann, J.; Huché, M.; Jaouen, G. *Chem.—Eur. J.* **2003**, *9* (21), 5223−5236.
(9) Foulds, N. C.; Lowe, C. R. *Anal. Chem.* **1988**, *60* (22), 2473−2478.
(10) Rehahn, M. Organic-Inorganic Hybrid Polymers. In *Synthesis of Polymers*; Schlüter, A.-D., Ed.; Wiley-VCH: Weinheim, Germany, 1999; p 319.
(11) Gallei, M.; Schmidt, B. V. K. J.; Klein, R.; Rehahn, M. *Macromol. Rapid Commun.* **2009**, *30* (17), 1463−1469.
(12) Gallei, M.; Klein, R.; Rehahn, M. *Macromolecules* **2010**, *43* (4), 1844−1854.
(13) Gallei, M.; Tockner, S.; Klein, R.; Rehahn, M. *Macromol. Rapid Commun.* **2010**, *31* (9−10), 889−896.
(14) Foucher, D. A.; Tang, B. Z.; Manners, I. *J. Am. Chem. Soc.* **1992**, *114* (15), 6246−6248.
(15) Manners, I. *Can. J. Chem.* **1998**, *76* (4), 371−381.
(16) Wang, Z.; Masson, G.; Peiris, F. C.; Ozin, G. A.; Manners, I. *Chem.—Eur. J.* **2007**, *13* (33), 9372−9383.
(17) Pittman, C. U.; Lai, J. C.; Vanderpool, D. P. *Macromolecules* **1970**, *3* (1), 105−107.
(18) Pittman, C. U.; Hirao, A. *J. Polym. Sci., Polym. Chem. Ed.* **1977**, *15* (7), 1677−1686.
(19) Pittman, C. U.; Hirao, A. *J. Polym. Sci., Polym. Chem. Ed.* **1978**, *16* (6), 1197−1209.
(20) Herfurth, C.; Voll, D.; Buller, J.; Weiss, J.; Barner-Kowollik, C.; Laschewsky, A. *J. Polym. Sci., Part A: Polym. Chem.* **2012**, *50* (1), 108−118.
(21) Wurm, F.; Villanueva, F. J. L.; Frey, H. *J. Polym. Sci., Part A: Polym. Chem.* **2009**, *47* (10), 2518−2528.

(22) Hale, P. D.; Boguslavsky, L. I.; Inagaki, T.; Lee, H. S.; Skotheim, T. A.; Karan, H. I.; Okamoto, Y. *Mol. Cryst. Liq. Cryst.* **1990**, *190* (1), 251−258.
(23) Swarts, J. C. *Macromol. Symp.* **2002**, *186* (1), 123−128.
(24) Wang, X.-S.; Winnik, M. A.; Manners, I. *Macromol. Rapid Commun.* **2002**, *23* (3), 210−213.
(25) Gohy, J.-F.; Lohmeijer, B. G. G.; Alexeev, A.; Wang, X.-S.; Manners, I.; Winnik, M. A.; Schubert, U. S. *Chem.—Eur. J.* **2004**, *10* (17), 4315−4323.
(26) Resendes, R.; Massey, J.; Dorn, H.; Winnik, M. A.; Manners, I. *Macromolecules* **2000**, *33* (1), 8−10.
(27) Tonhauser, C.; Mazurowski, M.; Rehahn, M.; Gallei, M.; Frey, H. *Macromolecules* **2012**, *45* (8), 3409−3418.
(28) Power-Billard, K. N.; Manners, I. *Macromolecules* **1999**, *33* (1), 26−31.
(29) Power-Billard, K. N.; Spontak, R. J.; Manners, I. *Angew. Chem., Int. Ed.* **2004**, *43* (10), 1260−1264.
(30) Yang, W.; Zhou, H.; Sun, C. *Macromol. Rapid Commun.* **2007**, *28* (3), 265−270.
(31) Mangold, C.; Obermeier, B.; Wurm, F.; Frey, H. *Macromol. Rapid Commun.* **2011**, *32* (23), 1930−1934.
(32) Schattling, P.; Jochum, F. D.; Theato, P. *Chem. Commun.* **2011**, *47*, 31.
(33) Broadhead, G. D.; Osgerby, J. M.; Pauson, P. L. *J. Chem. Soc.* **1958**, 650−656.
(34) Wurm, F.; Nieberle, J.; Frey, H. *Macromolecules* **2008**, *41* (6), 1909−1911.
(35) Mangold, C.; Dingels, C.; Obermeier, B.; Frey, H.; Wurm, F. *Macromolecules* **2011**, *44* (16), 6326−6334.
(36) Obermeier, B.; Wurm, F.; Frey, H. *Macromolecules* **2010**, *43* (5), 2244−2251.
(37) Mangold, C.; Wurm, F.; Obermeier, B.; Frey, H. *Macromolecules* **2010**, *43* (20), 8511−8518.
(38) Mangold, C.; Wurm, F.; Obermeier, B.; Frey, H. *Macromol. Rapid Commun.* **2010**, *31* (3), 258−264.
(39) Obermeier, B.; Frey, H. *Bioconjugate Chem.* **2011**, *22* (3), 436−444.
(40) Obermeier, B.; Wurm, F.; Mangold, C.; Frey, H. *Angew. Chem., Int. Ed.* **2011**, *50* (35), 7988−7997.
(41) Fuller, C. S. *Chem. Rev.* **1940**, *26* (2), 143−167.
(42) Henning, T. *SOFW J.* **2001**, *127*, 28−35.
(43) Zhang, Y.; Furyk, S.; Sagle, L. B.; Cho, Y.; Bergbreiter, D. E.; Cremer, P. S. *J. Phys. Chem. C* **2007**, *111* (25), 8916−8924.
(44) Rekharsky, M. V.; Inoue, Y. *Chem. Rev.* **1998**, *98* (5), 1875−1918.
(45) Giannotti, M.; Lv, H.; Ma, Y.; Steenvoorden, M.; Overweg, A.; Roerdink, M.; Hempenius, M.; Vancso, G. J. *J. Inorg. Organomet. Polym. Mater.* **2005**, *15* (4), 527−540.
(46) Zhang, Y.; Furyk, S.; Bergbreiter, D. E.; Cremer, P. S. *J. Am. Chem. Soc.* **2005**, *127* (41), 14505−14510.
(47) Rulkens, R.; Lough, A. J.; Manners, I.; Lovelace, S. R.; Grant, C.; Geiger, W. E. *J. Am. Chem. Soc.* **1996**, *118* (50), 12683−12695.
(48) Whittell, G. R.; Manners, I. *Adv. Mater.* **2007**, *19* (21), 3439−3468.
(49) Mangold, C.; Richard, O.; Frey, H.; Wurm, F. M.; Wurm, F. Submitted, 2012.
(50) Wasczcak, M. D.; Lee, C. C.; Hall, I. H.; Carroll, P. J.; Sneddon, L. G. *Angew. Chem.* **1997**, *109* (20), 2300−2302.
(51) Köpf-Maier, P.; Köpf, H.; Neuse, E. W.; Köpf, H. *Angew. Chem.* **1984**, *96* (6), 446−447.
(52) Abuchowski, A.; McCoy, J. R.; Palczuk, N. C.; van Es, T.; Davis, F. F. *J. Biol. Chem.* **1977**, *252* (11), 3582−3586.

Supporting Information for

Ferrocenyl Glycidyl Ether: A Versatile Ferrocene Monomer for Copolymerization with Ethylene Oxide to Water-Soluble, Thermo-Responsive Copolymers

Christine Tonhauser,[1,2] Arda Alkan,[2,3] Martina Schömer,[2] Carsten Dingels,[2] Sandra Ritz,[3] Volker Mailänder,[3] Holger Frey,[2] Frederik R. Wurm[3]*

[1]Graduate School Materials Science in Mainz, Staudinger Weg 9, D-55128 Mainz, Germany

[2]Institute of Organic Chemistry, Organic and Macromolecular Chemistry, Duesbergweg 10-14, Johannes Gutenberg-Universität Mainz (JGU), D-55128 Mainz, Germany

[3] Max-Planck Institute for Polymer Research (MPI-P), Ackermannweg 10, D-55128 Mainz, Germany

Contact address: wurm@mpip-mainz.mpg.de, phone: 0049 6131 379 502, fax: 0049 6131 370 330.

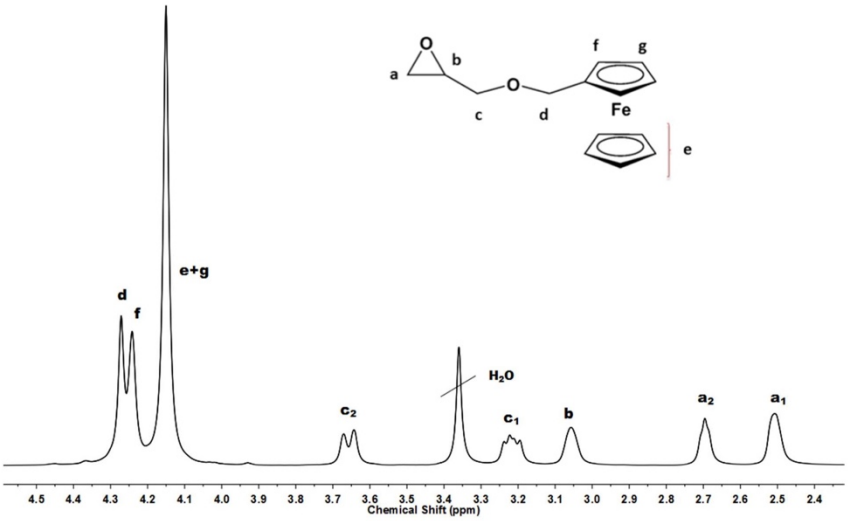

Figure S1: ^{1}H NMR (400 MHz, DMSO-d_6) of fcGE (**1**).

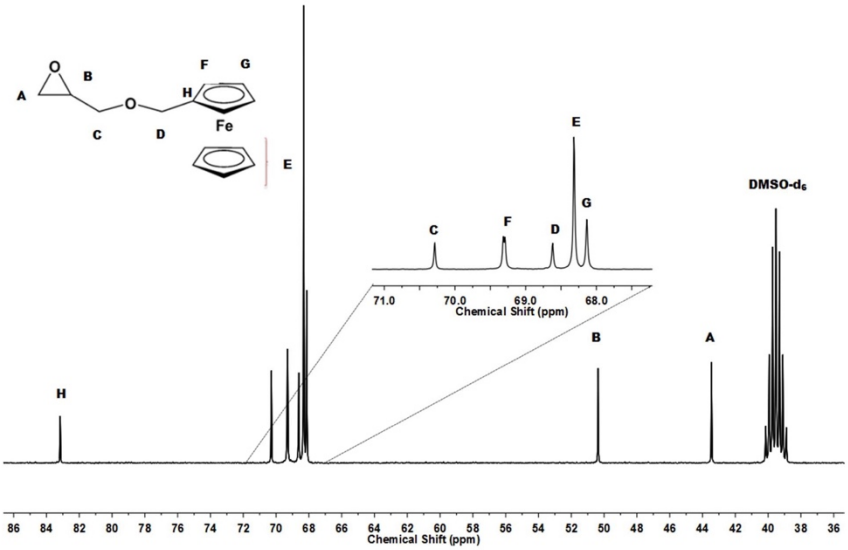

Figure S2: ^{13}C NMR (400 MHz, DMSO-d_6) of fcGE.

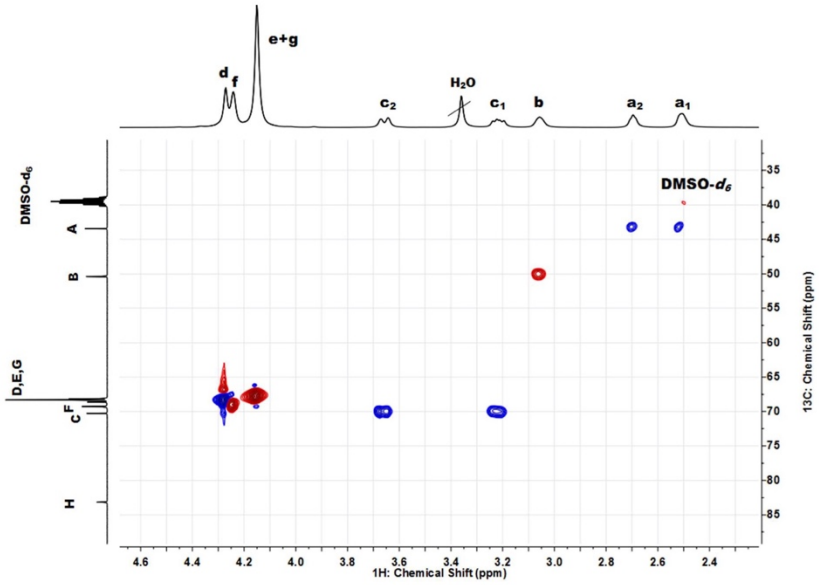

Figure S3: HSQC NMR (400 MHz, DMSO-d_6) of fcGE.

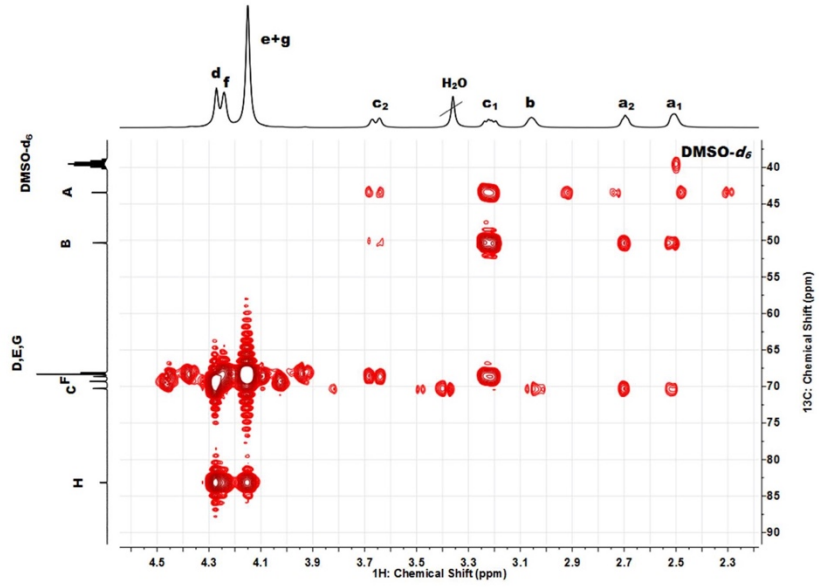

Figure S4: HMBC NMR (400 MHz, DMSO-d_6) of fcGE.

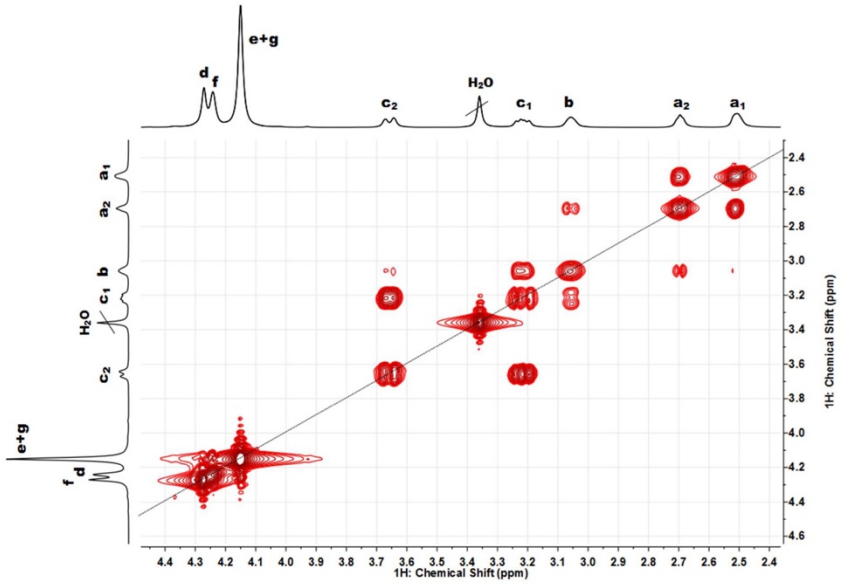

Figure S5: COSY NMR (400 MHz, DMSO-d_6) of fcGE.

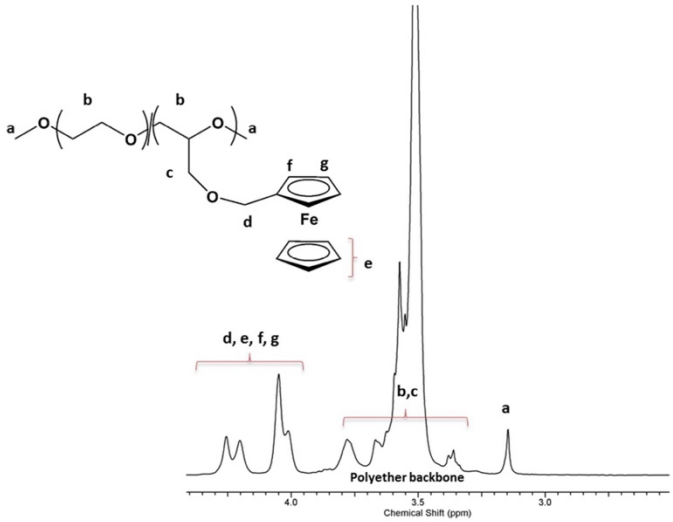

Figure S6. Peak assigment of P(EO-*co*-fcGE)/sample **P3** in ^{1}H NMR.

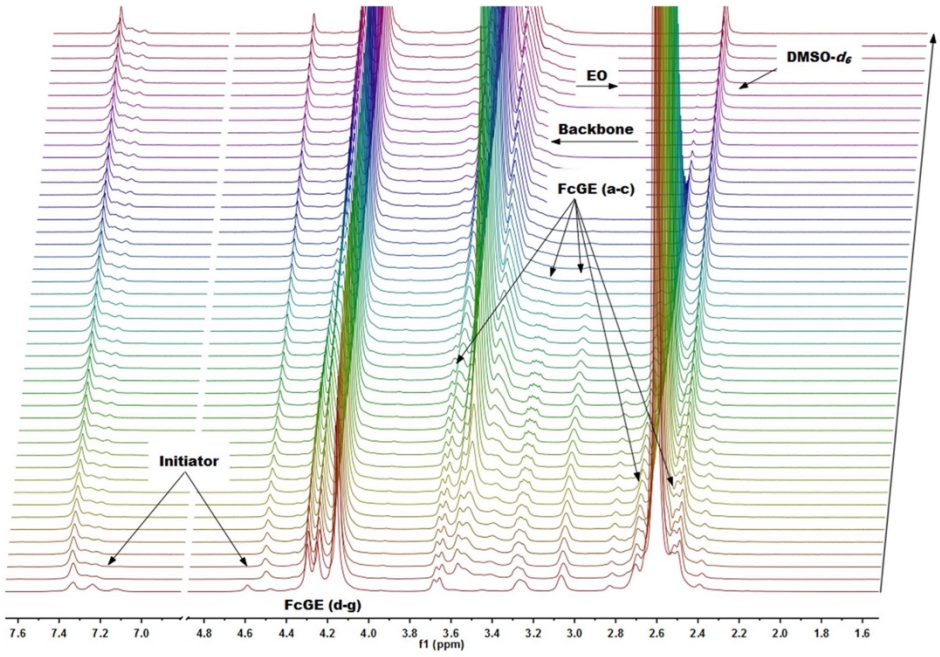

Figure S7: ^{1}H NMR (400 MHz, DMSO-d_6) kinetics of the copolymerization of EO and fcGE at 40 °C with benzyl alcohol as initiator.

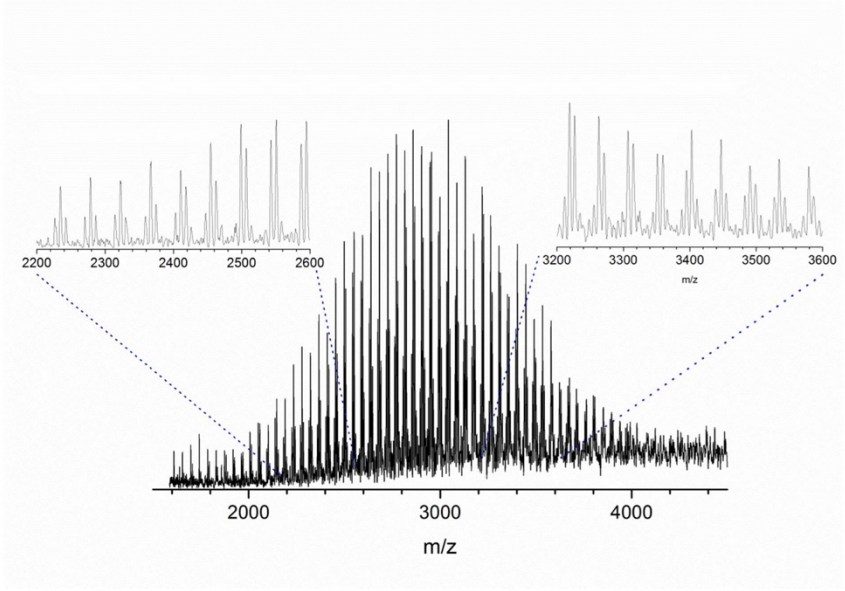

Figure S8: MALDI ToF mass spectrum of P(EO-*co*-fcGE)/sample **P5**.

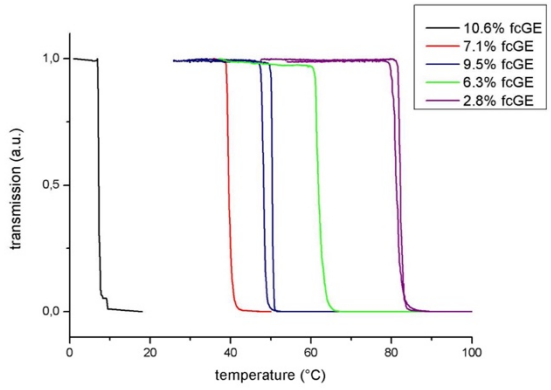

Figure S9. Cloud point measurements exhibit reversible LCST behavior.

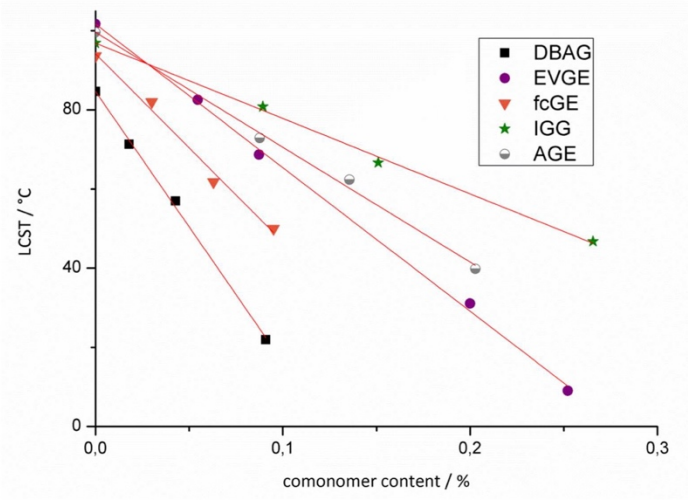

Figure S10. LCST temperature versus comonomer content of P(EO-*co*-fcGE) copolymer and other previously described copolyethers.[30]

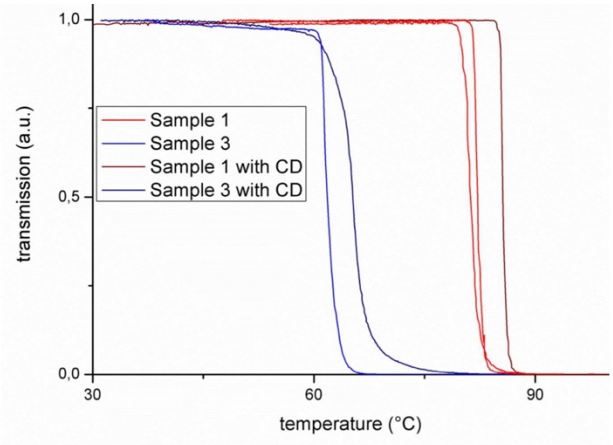

Figure S11. Cloud point measurements before and after treatment with β-cyclodextrin.

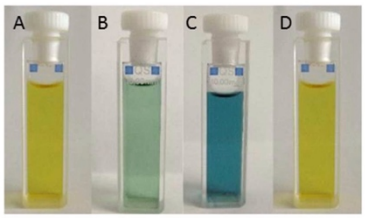

Figure S12. P2 in aqueous solution (A). **P2** in aqueous solution after partly oxidation (B) and complete oxidation (C) with silver(I)triflate. Oxidized **P2** reduced with sodium thiosulfate (D).

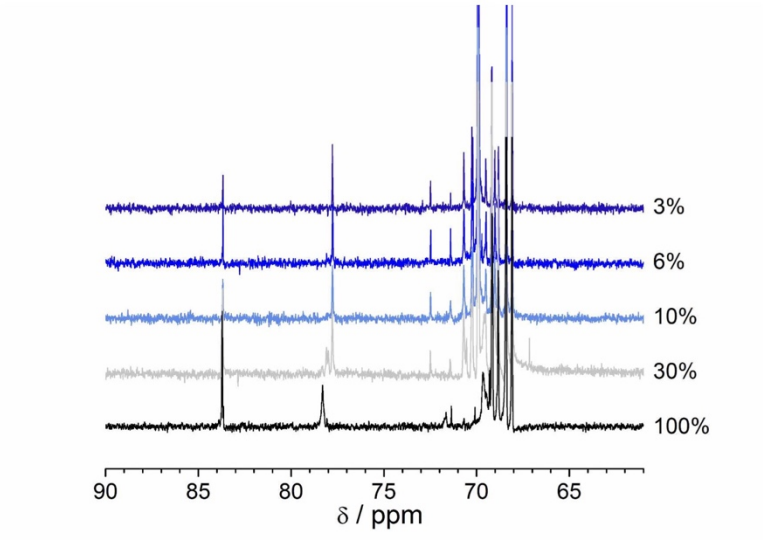

Figure S13. A) Complete ^{13}C NMR spectra of the (co)polymers synthesized in this study and B) zoom on carbon H showing splitting of the signals with increasing amount of fcGE into the copolymers.

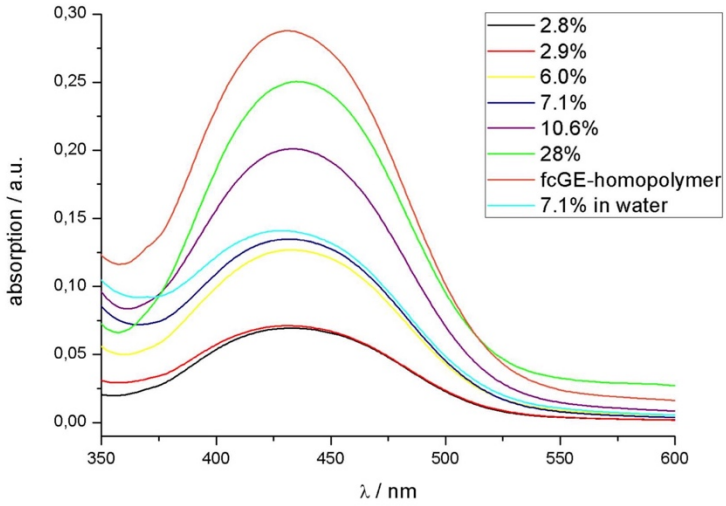

Figure S14. UV spectra of (co)polymers in THF (1 g/L) and of **P4** in water.

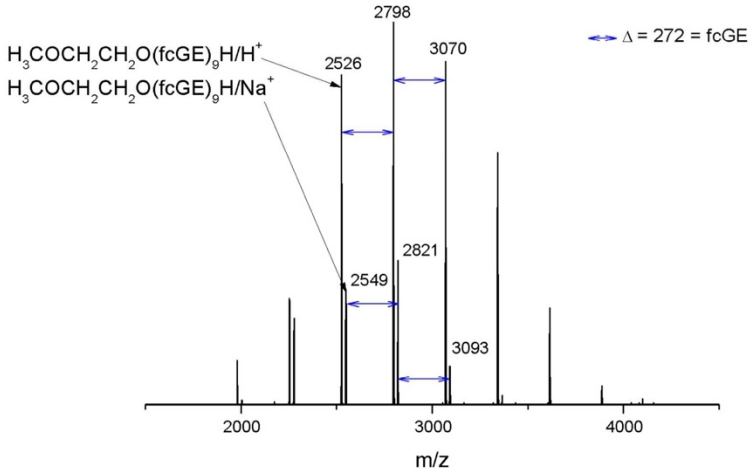

Figure S15. MALDI ToF of a fcGE-homopolymer (**P8**).

A.1.2 Water-Soluble Ferrocene-Containing Block Copolymers

ACS Macro Letters

Letter

pubs.acs.org/macroletters

Enlarging the Toolbox: Epoxide Termination of Polyferrocenylsilane (PFS) as a Key Step for the Synthesis of Amphiphilic PFS–Polyether Block Copolymers

Adrian Natalello,[†,‡] Arda Alkan,[†,§] Andreas Friedel,[†] Ingo Lieberwirth,[§] Holger Frey,[†] and Frederik R. Wurm*[,§]

[†]Institute of Organic Chemistry, Johannes Gutenberg-University (JGU), Duesbergweg 10-14, 55099 Mainz, Germany

[‡]Graduate School Materials Science in Mainz, Staudinger Weg 9, D-55128 Mainz, Germany

[§]Max Planck Institut für Polymerforschung, Ackermannweg 10, 55128 Mainz, Germany

Supporting Information

ABSTRACT: Epoxide termination and functionalization of living poly(ferrocenyldimethylsilane) (PFDMS) is introduced by precapping the living PFDMS with a 4/2 molar mixture of 1,1-diphenylethylene and 1,1-dimethylsilacyclobutane acting as a "carbanion pump" system. Subsequent addition of allyl glycidyl ether (AGE) leads to quantitatively functionalized PFDMS–AGE polymers with molecular weights between 1500 and 15 400 g mol^{-1} and polydispersity indices ≤1.10, carrying one hydroxyl group and an additional allylic double bond. PFDMS–AGE was then applied as a macroinitiator for the living anionic ring-opening polymerization of ethylene oxide (EO) to generate amphiphilic and water-soluble poly(ferrocenyldimethylsilane-*b*-ethylene oxide) block copolymers with a low polydispersity index. All polymers have been characterized by ^{1}H NMR spectroscopy, DOSY ^{1}H NMR spectroscopy, size exclusion chromatography (SEC), and MALDI-ToF mass spectrometry. In addition, for the characterization of the morphology of the PFDMS-*b*-PEO block copolymers transmission electron microscopy (TEM) was performed in methanol, confirming the formation of cylindrical micelles with an organometallic core and polyether corona.

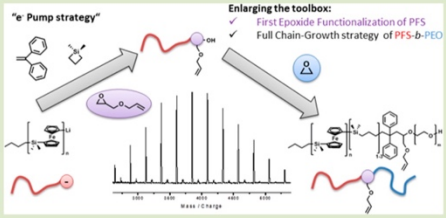

Metals are often the determining component of materials with magnetic, conductive, redox-active, and catalytic properties. Modern polymer science allows the precise synthesis of "soft materials" with metals incorporated in the structure. As early as 1955 at the DuPont company, poly(vinyl ferrocene) (PVfc) was synthesized to combine the advantages of polymers and inorganic solids. This opened the field of metal-containing polymers.[1] However, for a long time no well-defined polymers with high molecular weights could be achieved, due to low solubility, side reactions, or stability problems.[2−6] With the discovery of the ring-opening polymerization (ROP) of the ansa-metallocenophanes by Manners and co-workers, ferrocene-based (fc) polymers turned out to be no longer an academic curiosity.[7] Nowadays fc-containing polymers represent key materials in this research area, and fc-units can be incorporated in the polymer backbone or in the side chains for sensing, catalytic, or biomedical applications.[8−10]

Main-chain fc-containing polymers are of special interest due to their electrochemical properties and ability to control aggregation phenomena in bulk and solution.[11,12]

In 2007, Wang et al. discovered the first cylindrical block comicelles with narrow size distribution in analogy to a living chain growth polymerization mechanism by adding subsequently different poly(ferrocenyldimethylsilane) (PFDMS) block copolymers to a nonsolvent for PFDMS, leading to an epitaxial growth of the micelle due to crystallization of the PFDMS segment.[13] Recently, this modular system was expanded to the unidirectional growth of cylindrical micelles.[14] All these constructs, however, are currently only possible in organic (and mostly nonpolar) solvents.

To date, only few reports deal with the preparation of water-soluble fc-containing polymers. These approaches often rely on the introduction of hydrophilic segments or side chains.[15−17] The combination of fc-based polymers with epoxide-based monomers was not reported until recently. Our group introduced an fc-containing epoxide monomer, i.e., ferrocenyl glycidyl ether (fcGE), and copolymerized it with ethylene oxide (EO) to generate poly(ethylene oxide)s (PEO) carrying fc in the side chains. A variety of different molar ratios have been synthesized, leading to electroactive, thermoresponsive, and also water-soluble (up to 10 mol % incorporation of fcGE) polymers.[18] However, it has not been possible to combine PFDMS as a main-chain fc-containing polymer with the

Received: February 19, 2013
Accepted: March 25, 2013

modular and well-established anionic ring-opening polymerization of epoxides.

Manners and co-workers devised different synthetic strategies to obtain PFDMS-*b*-PEO block copolymers. The first approach utilizes a Si−H end-functionalized methoxy-PEO as a macroinitiator for the Pt(0) (Karstedt's catalyst)-catalyzed ROP of dimethylsila[1]-ferrocenophane (FDMS), leading to—unlike most other PFDMS copolymers—spherical micelles in an aqueous solution.[19] By using a four-arm Si−H-functionalized PEO star polymer, Schacher et al. recently synthesized [(PEO-*b*-PFDMS)]$_4$ star-block copolymers and studied their self-assembly behavior.[20] A different strategy relies on polymer coupling reaction, i.e., the combination of two functionalized homopolymers of PEO and PFDMS via a bis(terpyridine)-ruthenium(II) complex. In contrast to the previously observed spherical micelles, these authors found rod-like structures.[21] Very recently, Manners, Winnik, and co-workers enlarged the coupling methods by synthesizing terminal alkyne-functionalized PFDMS. Via copper-catalyzed "click" chemistry, a variety of block copolymers are accessible.[22]

Gallei and Frey et al. developed a strategy for the synthesis of PVFc-*b*-PEO block copolymers and PVFc-(PEO)$_2$ miktoarm star polymers. Living anionic polymerization of VFc allowed quantitative termination functionalization with benzyl glycidyl ether (BGE), generating one free hydroxyl group and a second protected one. Subsequent ROP of EO leads to the block copolymer (prior to hydrogenolysis) or to miktoarm star polymers after hydrogenation.[23]

The current work describes the first quantitative end functionalization of PFDMS generated by living anionic polymerization with an epoxide, namely, allyl glycidyl ether (AGE). Direct epoxide termination of living PFDMS is not possible (Scheme 1, **3**) because the living PFDMS species is not capable of ring opening the epoxide. As detailed studies have shown, only protonated PFDMS is obtained after workup (see Supporting Information, Figure S 5). To overcome this problem and further activate the living PFDMS chain end, the so-called "carbanion pump" system was introduced prior to AGE termination.[24,25] 1,1-Dimethylsilacyclobutane (DMSB) can be easily attacked by molecules with limited nucleophilicity, such as living PFDMS, generating a very reactive terminal organolithium species. To prevent the living chain end from being proton terminated, the reactivity has to be adjusted by the introduction of 1,1-diphenyl ethylene (DPE). Furthermore, the living DPE-capped polymer chain cannot react with the remaining DMSB due to the sterical hindrance, but still with epoxide derivatives.

This termination strategy allows the introduction of two orthogonal functional groups at the PFDMS chain end and, more importantly, to combine carb- and oxyanionic polymerization to generate PFDMS−polyether block copolymers for the first time in a complete and living chain growth manner (Scheme 1).

A series of AGE-terminated PFDMS homopolymers have been prepared by living anionic polymerization of FDMS, using a subsequent "quenching" sequence (Scheme 1). All polymerizations of FDMS were carried out in THF at room temperature in a nitrogen-filled glovebox. After full conversion of FDMS was reached, the living PFDMS was reacted simultaneously with a mixture of DPE and DMSB (Scheme 1, **3**).[25] A change of color from light orange to deep red indicates complete formation of the precapped PFDMS. The subsequent addition of the epoxide changed the color of the reaction solution to orange, again indicative of the desired termination reaction. The end-functional series of homopolymers prepared exhibited molecular weights in the range of 1500−15 000 g mol^{-1}, with polydispersity indices (PDI) below 1.10 (see Table 1, further characterization data can be found in the Supporting Information).

Scheme 1. Synthetic Strategy for PFDMS−AGE and Amphiphilic PFDMS−PEO Block Copolymers

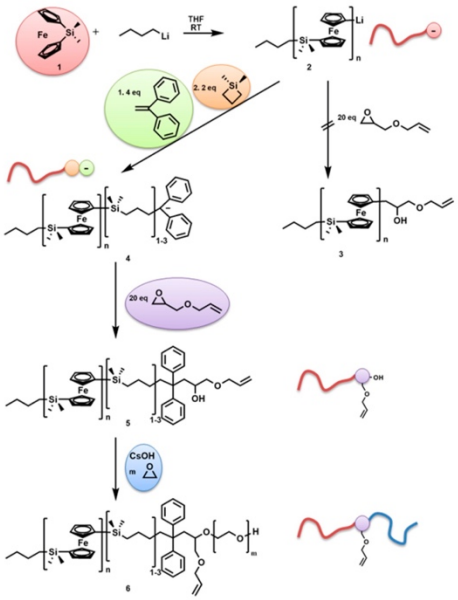

Table 1. Characterization Data for Homo- and Block Copolymers

no.	polymer[a]	M_n[a]	Mn[b]	PDI[b]
1	PFDMS$_6$−AGE	1500	1600	1.08
2	PFDMS$_{14}$−AGE	3400	3700	1.10
3	PFDMS$_{28}$−AGE	6800	9100	1.08
4	PFDMS$_{64}$−AGE	15400	16900	1.07
5	PFDMS$_{14}$−AGE-*b*-PEO$_{186}$	11600	6500[c]	1.10[c]

[a]Molecular weight in g mol^{-1}, calculated from ^{1}H NMR via end group analysis. [b]Number average and polydispersity index determined via size exclusion chromatography (SEC) in THF (vs PS standard). [c]Determined via SEC in DMF (vs PS standards).

To verify quantitative functionalization, different characterization methods were utilized. A very efficient tool for end group determination is high-resolution NMR spectroscopy, especially with a diffusion probe head. With this technique end group and polymer resonances can be distinguished with respect to the diffusion coefficient and integrated to calculate the degree of functionalization (Figure 1 shows the diffusion-ordered (DOSY) ^{1}H NMR spectrum). The horizontal axis displays the ^{1}H NMR spectrum (in benzene-d_6), while the vertical axis allows for determination of the diffusion coefficient. As a consequence of the terminal functionalization sequence

dx.doi.org/10.1021/mz400080s | ACS Macro Lett. 2013, 2, 313−316

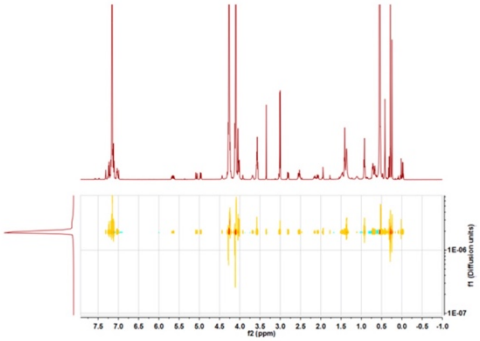

Figure 1. DOSY ^{1}H NMR spectrum (benzene-d_6, 700 MHz) of AGE-functionalized PFDMS (PFDMS–AGE #2), demonstrating that every signal belongs to the end-functional polymer.

several additional resonances can be distinguished in the ^{1}H NMR spectra in comparison to a proton-terminated PFDMS homopolymer (fc signals at 4.1 and 4.3 ppm)—most importantly, the signals of the terminal allyl group at 5.0 and 5.7 ppm. All ^{1}H NMR resonances can be assigned to the same diffusion signal at 1.93×10^{-6} m^2/s proving that the end group is attached to the PFDMS with the same molecular weight. Full signal assignment was achieved by the combination of the ^{1}H with the ^{13}C-HSQC NMR spectrum (Figure S 3, Supporting Information).

Conclusive evidence for quantitative termination of the functionalized PFDMS–AGE polymer samples (#1–4, Table 1) is gained by matrix-assisted laser desorption/ionization time-of-flight mass spectrometry (MALDI-ToF MS). Each signal of the resulting spectrum can be assigned to AGE-terminated polymer chains.

Figure 2 shows the MALDI-ToF mass spectrum of polymer sample #2. The main distribution marked in red can be

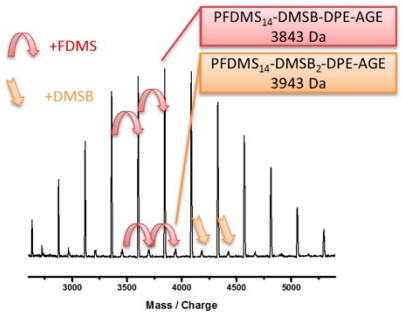

Figure 2. MALDI ToF MS spectrum of quantitative functionalized PFDMS–AGE (#2).

attributed to the quantitatively functionalized polymer with 14 repeating units of the FDMS monomer (respective mass 3843 Da). The peaks of the small subdistribution have an increased molecular weight compared to the main distribution of 100 Da, which can be assigned to the AGE-functionalized polymer with two DMSB repeating units.

The quantitative end functionalization of PFDMS opens a new field for PFDMS chemistry in general. First of all, termination with any epoxide leads inevitably to a terminal hydroxyl group. Earlier, deprotection steps were necessary to generate terminal hydroxyl groups, which could be harmful to the PFDMS backbone, as reported before.[26] The generated hydroxyl group can be used for subsequent post modification or initiation of anionic or other, e.g., controlled radical polymerizations to generate PFDMS-based copolymers in a subsequent polymerization step. Furthermore, the use of functionalized glycidyl ethers offers a new access to multi- and heterofunctional PFDMS polymers, as demonstrated by the functionalization with AGE. As mentioned before, to demonstrate one possible application, the AGE-functionalized PFDMS has been used as a macroinitiator for the anionic ROP of EO. The hydroxyl group of PFDMS–AGE (#2, Table 1) was deprotonated with cesium hydroxide, and subsequent addition of EO leads to the formation of water-soluble, redox-active PFDMS–AGE-*b*-PEO block copolymer (#5, Table 1), still carrying an additional double bond at the block junction. The PFDMS–AGE-*b*-PEO block copolymer has been characterized by ^{1}H NMR, DOSY ^{1}H NMR, SEC, and transmission electron microscopy (TEM).

The increase in molecular weight detected by SEC and the appearance of the polyether resonances in the ^{1}H NMR spectrum (at 3.5 ppm) indicate successful formation of the targeted block copolymer. Conclusive evidence is gained from the DOSY ^{1}H NMR spectrum (shown in Figure 3). Clearly, the

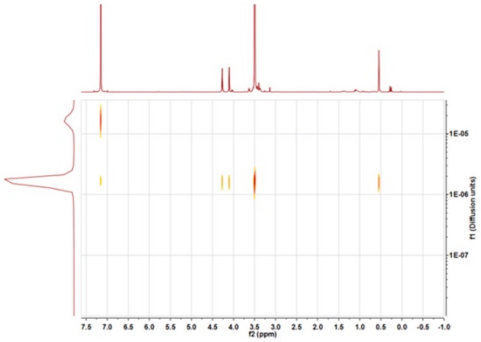

Figure 3. DOSY ^{1}H NMR spectrum (benzene-d_6, 500 MHz) of the PFDMS$_{14}$–AGE-*b*-PEO$_{186}$ block copolymer, verifying block formation.

resonances of the fc groups at 4.3 and 4.1 ppm as well as the signals of the PEO backbone at 3.5 ppm can be detected at the same diffusion coefficient at 1.30×10^{-6} m^2/s, verifying complete block copolymer formation and the absence of any homopolymer (note that the second signal on the vertical axis belongs to the NMR solvent, benzene-d_6).

Furthermore, preliminary studies on the self-assembly of the amphiphilic PFDMS–AGE-*b*-PEO block copolymers were accomplished via TEM (by drop-cast from an aqueous or a methanol solution). To this end, the respective block copolymer was directly dissolved in water or methanol ($c \approx 1$ g L^{-1}), and one drop of the solution was deposited on a carbon-coated copper TEM grid. The prepared TEM grid was dried under high vacuum overnight before recording the TEM

dx.doi.org/10.1021/mz400080s | ACS Macro Lett. 2013, 2, 313–316

images. Typical TEM images are shown in Figure 4. With the highly crystalline PFDMS-block forming the inner part of the

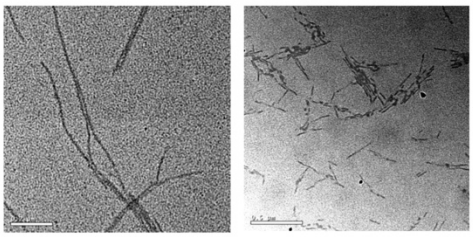

Figure 4. TEM images of the amphiphilic PFDMS-*b*-PEO block copolymer (#5, Table 1), prepared by drop-casting of an aqueous solution (left, $c \approx 1$ g L^{-1}) and of a methanol solution (right, $c \approx 1$ g L^{-1}); scale bar: 0.5 μm.

aggregates, exclusively cylindrical micelles are obtained with a length in the range of approximately 400 nm for the aggregates from methanol and longer aggregates from water which are currently under further investigation.

In summary, epoxide termination of PFDMS has been established as a key step for the preparation of well-defined and orthogonally functionalized PFDMS with low PDI by living carbanionic polymerization. Compared to the well-studied terminal functionalization of conventional vinyl monomers with different epoxide derivatives, direct termination is not possible for living PFDMS and leads to the coexistence of living PFDMS and unreacted epoxide.[27,28] To transfer the epoxide termination chemistry to living PFDMS the "electron pump" system established by Rehahn et al.[6,25] had to be introduced prior to termination, leading to quantitative end functionalization. Use of AGE as the termination agent introduces two different terminal functionalities, an allylic double bond and a hydroxyl group. This robust synthetic protocol allows for a large variety of further post modifications, some of which are currently under investigation. In addition, the AGE-functionalized PFDMS has been used as a macroinitiator for the living anionic ROP of ethylene oxide to generate a well-defined, water-soluble PFDMS-*b*-PEO block copolymer. Further studies on other functionalization sequences as well as the aggregation behavior of PFDMS-*b*-PEO with different block ratios in combination with other PFDMS block copolymers are in progress.

■ ASSOCIATED CONTENT

Supporting Information

Detailed experimental procedures as well as analytical and spectral characterization data. This material is available free of charge via the Internet at http://pubs.acs.org.

■ AUTHOR INFORMATION

Corresponding Author

*E-mail: wurm@mpip-mainz.mpg.de. Phone: 0049 6131 379 723. Fax: 0049 6131 370 330.

Notes

The authors declare no competing financial interest.

■ ACKNOWLEDGMENTS

A.N. thanks the Graduate School of Excellence MAINZ for financial support. F.W. thanks the Alexander von Humboldt Foundation for support. We thank Kevin Tritschler for technical assistance.

■ REFERENCES

(1) Arimoto, F. S.; Haven, A. C. *J. Am. Chem. Soc.* **1955**, *77* (23), 6295−6297.
(2) Neuse, E. W.; Rosenberg, H. *J. Macromol. Sci., Part C: Polym. Rev.* **1970**, *4* (1), 1−145.
(3) Neuse, E. W. *J. Macromol. Sci., Part A: Chem.* **1981**, *16* (1), 3−72.
(4) Withers, H. P.; Seyferth, D.; Fellmann, J. D.; Garrou, P. E.; Martin, S. *Organometallics* **1982**, *1* (10), 1283−1288.
(5) Walter, S. *Russ. Chem. Rev.* **1991**, *60* (7), 784.
(6) Bellas, V.; Rehahn, M. *Angew. Chem., Int. Ed.* **2007**, *46* (27), 5082−5104.
(7) Foucher, D. A.; Tang, B. Z.; Manners, I. *J. Am. Chem. Soc.* **1992**, *114* (15), 6246−6248.
(8) Foulds, N. C.; Lowe, C. R. *Anal. Chem.* **1988**, *60* (22), 2473−2478.
(9) Top, S.; Dauer, B.; Vaissermann, J.; Jaouen, G. *J. Organomet. Chem.* **1997**, *541* (1−2), 355−361.
(10) Top, S.; Vessières, A.; Leclercq, G.; Quivy, J.; Tang, J.; Vaissermann, J.; Huché, M.; Jaouen, G. *Chem.—Eur. J.* **2003**, *9* (21), 5223−5236.
(11) Ma, Y.; Dong, W.-F.; Hempenius, M. A.; Möhwald, H.; Julius Vancso, G. *Nat. Mater.* **2006**, *5* (9), 724−729.
(12) Wurm, F.; Hilf, S.; Frey, H. *Chem.—Eur. J.* **2009**, *15* (36), 9068−9077.
(13) Wang, X.; Guerin, G.; Wang, H.; Wang, Y.; Manners, I.; Winnik, M. A. *Science* **2007**, *317* (5838), 644−647.
(14) Rupar, P. A.; Chabanne, L.; Winnik, M. A.; Manners, I. *Science* **2012**, *337* (6094), 559−562.
(15) Wang, X.-S.; Winnik, M. A.; Manners, I. *Macromol. Rapid Commun.* **2002**, *23* (3), 210−213.
(16) Power-Billard, K. N.; Spontak, R. J.; Manners, I. *Angew. Chem., Int. Ed.* **2004**, *43* (10), 1260−1264.
(17) Yang, W.; Zhou, H.; Sun, C. *Macromol. Rapid Commun.* **2007**, *28* (3), 265−270.
(18) Tonhauser, C.; Alkan, A.; Schömer, M.; Dingels, C.; Ritz, S.; Mailänder, V.; Frey, H.; Wurm, F. R. *Macromolecules* **2013**, *46*, 647−655.
(19) Resendes, R.; Massey, J.; Dorn, H.; Winnik, M. A.; Manners, I. *Macromolecules* **2000**, *33* (1), 8−10.
(20) Schacher, F. H.; Elbert, J.; Patra, S. K.; Mohd Yusoff, S. F.; Winnik, M. A.; Manners, I. *Chem.—Eur. J.* **2012**, *18* (2), 517−525.
(21) Gohy, J.-F.; Lohmeijer, B. G. G.; Alexeev, A.; Wang, X.-S.; Manners, I.; Winnik, M. A.; Schubert, U. S. *Chem.—Eur. J.* **2004**, *10* (17), 4315−4323.
(22) Zhang, M.; Rupar, P. A.; Feng, C.; Lin, K.; Lunn, D. J.; Oliver, A.; Nunns, A.; Whittell, G. R.; Manners, I.; Winnik, M. A. *Macromolecules* **2013**, *46*, 1296−1304.
(23) Tonhauser, C.; Mazurowski, M.; Rehahn, M.; Gallei, M.; Frey, H. *Macromolecules* **2012**, *45* (8), 3409−3418.
(24) Sheikh, M. R. K.; Imae, I.; Tharanikkarasu, K.; LeStrat, V.-J.; Kawakami, Y. *Polym. J.* **2000**, *32* (6), 527−530.
(25) Kloninger, C.; Rehahn, M. *Macromolecules* **2004**, *37* (5), 1720−1727.
(26) Korczagin, I.; Hempenius, M. A.; Vancso, G. J. *Macromolecules* **2004**, *37* (5), 1686−1690.
(27) Tonhauser, C.; Frey, H. *Macromol. Rapid Commun.* **2010**, *31* (22), 1938−1947.
(28) Natalello, A.; Tonhauser, C.; Berger-Nicoletti, E.; Frey, H. *Macromolecules* **2011**, *44* (24), 9887−9890.

Supporting Information

for

Enlarging the Toolbox: Epoxide Termination of Polyferrocenylsilane (PFS) as a Key Step for the Synthesis of Amphiphilic PFS-Polyether Block Copolymers

Adrian Natalello,[†,‡] Arda Alkan,[†] Andreas Friedel,[†] Ingo Lieberwirth,[§] Holger Frey[†] and Frederik R. Wurm[§]*

[†]Institute of Organic Chemistry, Johannes Gutenberg-University (JGU), Duesbergweg 10-14, 55099 Mainz, Germany

[‡]Graduate School Materials Science in Mainz, Staudinger Weg 9, D-55128 Mainz, Germany

[§]Max Planck Institut für Polymerforschung, Ackermannweg 10, 55128 Mainz, wurm@mpip-mainz.mpg.de

Experimental details

Reagents. All solvents and reagents were purchased from Acros Organics or Sigma Aldrich and used as received unless otherwise stated. Tetrahydrofuran (THF) was distilled from sodium/benzophenone under reduced pressure into a liquid nitrogen cooled reaction vessel (cryo-transfer). Ferrocene (98%) was purified by recrystallization from hexane. *N,N,N',N'*-Tetramethylethylenediamine (TMEDA) (≥ 99.5%), dichlorodimethylsilane (≥ 99.5%), allyl glycidyl ether (AGE) (≥ 99%), 1,1-diphenylethylene (DPE) (Acros, 99%) and 1,1-

Dimethylsilacyclobutane (DMSB, ≥ 97%) were dried over CaH_2 and cryo-transferred prior to use.

Instrumentation. ^{1}H NMR spectra were recorded at 294 K on a Bruker Avance III 700 (16,4 T) with a 5 mm z-gradient BBI invers ^{1}H/X probe (700 MHz spectra). Spectra recorded on the 700 MHz spectrometer were regulated by a standard ^{1}H methanol NMR sample using the topspin 3.0 software (Bruker). The spectra were referenced the residual HDO (^{1}H) = 4,80 ppm. All 1D spectra were processed with MestReNova 6.1.1-6384 software. The diffusion (DOSY, Diffusion Ordered Spectroscopy) experiments were recorded with a 5 mm BBI ^{1}H/X z-gradient probe and a gradient strength of 5.516 [G/mm] on the 700 MHz spectrometer using double stimulated echo for convection compensation. The relaxation time was 2 s, the diffusion delay was kept at 90 ms and the gradient pulse with a length of 1600 µs. For the calibration of the gradient strength, a sample of $^2H_2O/^1H_2O$ was measured at a defined temperature and compared with the literature diffusion coefficient of $^2H_2O/^1H_2O$.[1, 2] 2D spectra were processed with Topspin 3.0. Size exclusion chromatography (SEC) measurements were carried out in THF and DMF. For SEC measurements in THF an instrument consisting of a Waters 717 plus autosampler, a TSP Spectra Series P 100 pump, a set of three PSS SDV columns (104/500/50 A°), and RI and UV (275 nm) detectors was used. For SEC measurements in DMF (containing 0.25 g/L of lithium bromide as an additive) an Agilent 1100 Series have been used as an integrated instrument, including a PSS HEMA column (106/105/104 g/mol), a UV (275 nm) and a RI detector. All SEC elugrams show the RI detector signal, and the molecular weight refers to linear polystyrene (PS) standards provided by Polymer Standards Service (PSS). The morphology of the PFDMS-*b*-PEO block copolymers in solution was studied by TEM using a FEI Tecnai F20 transmission electron microscope . 4µL of the diluted polymer solution (1 g/L) of methanol was deposited on a carbon-coated copper grid and excess solution was blotted off with a filter paper before the specimen was dried in air.

Matrix-assisted laser desorption/ionization time-of-flight (MALDI-ToF) measurements were performed using a Shimadzu Axima CFR MALDI-TOF mass spectrometer, employing dithranol (1,8,9-trishydroxy-anthracene) as a matrix.

Dimethylsila[1]-ferrocenophane (FDMS)

The two-step monomer synthesis of FDMS was carried out as described in literature before.[3-5]

Synthesis of PFDMS-AGE (#1-4)

Exemplary Synthesis Procedure for PFDMS$_6$-AGE (#1). FDMS was sublimed prior use at 10^{-3} mbar at 40 °C. After cryo-transferring DPE, AGE, DMSB and THF the reagents were deposed in the glovebox. 0.5 g (2.06 mmol) of FDMS was dissolved in 7 mL of THF. To the vigorously stirred reaction mixture 132 µL (0.33 mmol) *n*-BuLi (2,5 M) was added as initiator via syringe. After 45 min the reaction was terminated by adding first a 4/2 molar mixture of of 1,1-diphenylethylene (230 µL, 1.32 mmol) and 1,1-dimethylsilacyclobutane (85 µL, 0.66 mmol) and after additional five minutes allyl glycidyl ether (0.75 mL, 6.35 mmol). The crude polymerization mixture was purified by precipitation into methanol and dried under high vacuum. Yield 80%

^{1}H NMR (700 MHz, C_6D_6, δ in ppm): 7.09-7,00 (m, 10H, aromatic system of DPE), 5.71-5.61 (m, 1H, allyl group), 5.12-4.93 (dd, J = 52.6, 13.5 Hz, 2H, terminal CH_2 of the allyl group), 4.49-3.90 (m, cyclopentadienyl group of the PFDMS backbone), 3.74-3.66 (m, O-CH_2- of the allyl end group), 2.81 (dd, J = 9.0, 3.8 Hz, O-CH_2- of AGE unit), 2.59-2.49 (m, -CH- of AGE unit), 2.21-2.01 (dd, J = 39.8, 12.3 Hz, -CH_2- unit of AGE next to DPE), 1.78 (s, 1H, OH of the AGE unit), 1.40-1.32 (m, 4H, -CH_2- of the initiator), 0.93 (t, J = 6.9 Hz, CH_3- of the initiator), 0.55 (s, (CH_3-)$_2$Si of PFDMS backbone), 0.29 (s, 6H, (CH_3-)$_2$Si of DMSB).

Synthesis of PFDMS-*b*-PEO (#5)

PFDMS$_{14}$-AGE (#2) was utilized as a macroinitiator for the anionic ring opening polymerization of EO. Under argon atmosphere 200 mg (58,8 µmol) of PFDMS$_{14}$-AGE and 4,9 mg (29.4 µmol) cesium hydroxide were added in a 100 mL Schlenk flask. In order to dry

the reaction mixture 20 mL of dry benzene were added and evaporated after dissolving the reaction mixture to generate the cesium alkoxide by azeotropical removal of water. This procedure was repeated three times. After cryo-transferring 20 mL of THF into the reaction mixture, the monomer EO (0.5 mL, 0.49 g, 11.12 mmol) was cryo-transferred first into a graduated ampoule and subsequently into the reaction flask at approximately -80 °C. The reaction mixture was directly heated up to 60 °C and the polymerization was kept at this temperature for 24 h. The polymer was precipitated in cold diethyl ether (T = -25 °C) and dried under high vacuum (Yield 72%).

^{1}H NMR (500 MHz, C_6D_6, δ in ppm): 7.09-7,00 (m, 10H, aromatic system of DPE), 5.86-5.71 (m, 1H, allyl group), 5.25-4.98 (dd, J = 85.4, 14.0 Hz, 2H, terminal CH_2 of the allyl group), 4.29-3.90 (m, cyclopentadienyl group of the PFDMS backbone), 3.50 (s, PEO backbone), 2.70-2.00 (m, signals of the AGE unit), 1.40-1.35 (m, 4H, -CH_2- of the initiator), 0.93 (t, J = 6.9 Hz, CH_3- of the initiator), 0.55 (s, $(CH_3\text{-})_2Si$ of PFDMS backbone), 0.29 (s, 6H, $(CH_3\text{-})_2Si$ of DMSB).

Additional characteriazation data

Table S1. Characterization data for homo- and block copolymers.

no.	polymer[a]	Mn[a]	Mn[b]	PDI[b]
1	$PFDMS_6$-AGE	1 500	1 600	1,08
2	$PFDMS_{14}$-AGE	3 400	3 700	1,10
3	$PFDMS_{28}$-AGE	6 800	9 100	1,08
4	$PFDMS_{64}$-AGE	15 400	16 900	1,07
5	$PFDMS_{14}$-AGE-*b*-PEO_{186}	11 600	6 500[c]	1,10[c]

[a]Molecular weight in g mol^{-1}, calculated from ^1H NMR via end group analysis. [b]Number average and polydispersity index determined via SEC in THF (vs. PS standard). [c]Determined via SEC in DMF(vs. PS standards).

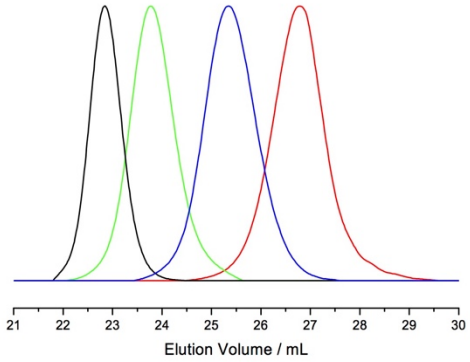

Fig S 1. SEC traces of PFDMS-AGE homo-polymers (#1, #2, #3 and #4) measured in THF.

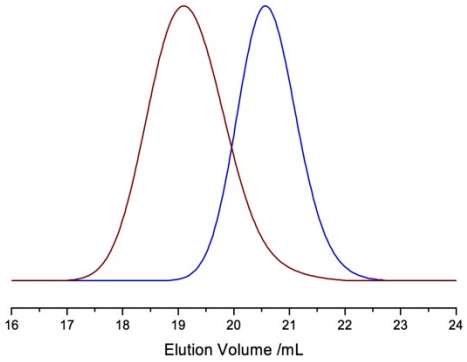

Fig S 2. SEC traces of $PFDMS_{14}$-AGE precursor and $PFDMS_{14}$-AGE-*b*-PEO_{186} block copolymer measured in DMF

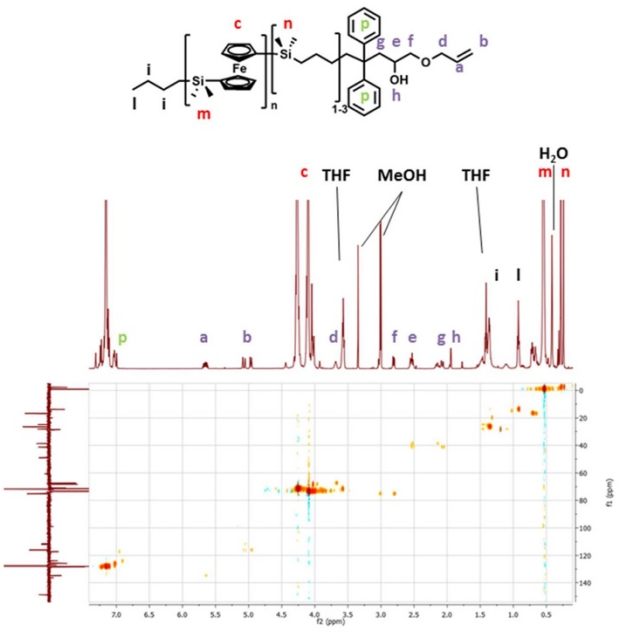

Fig. S 3. ^{1}H ^{13}C-HSQC NMR measured in benzene-d_6 of polymer #2 with detailed assignment of the signals.

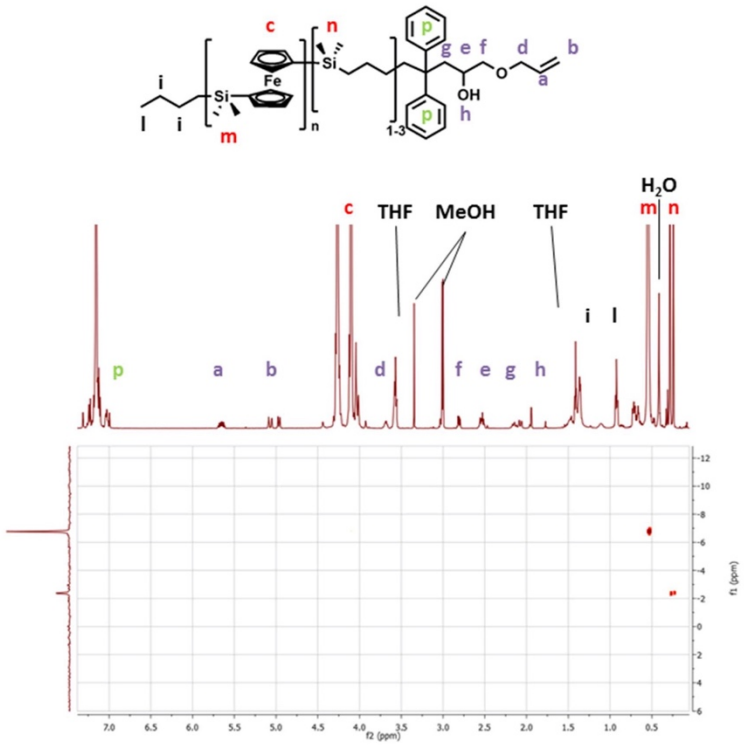

Fig. S 4. ^{1}H ^{29}Si-HSQC NMR measured in benzene-d_6 of polymer #2 with detailed assignment of the signals.

Attempted synthesis protocol for direct AGE terminated PFDMS.

The synthesis was accomplished in analogy to the synthesis protocol of polymer #1-4 (see above), but without the "carbanion pump" system (DMSB and DPE). From literature it is known that quantitative functionalization of living PFDMS with the more reactive (compared to epoxides) DPE cannot be reached at room temperature after 1.5 d (max. 80%).[5] By increasing the temperature up to 50°C the end capping reaction can be accelerated (4.5 h), but trough out the reaction a significant amount (38%) of proton terminated PFDMS arises.[6] Figure S4. shows the MALDI ToF mass spectrum of the synthesized polymer after direct

termination with AGE. The spectrum containing one distribution, which belongs to proton terminated PFDMS. This demonstrates, that living PFDMS is not reactive enough to ring open epoxides directly.

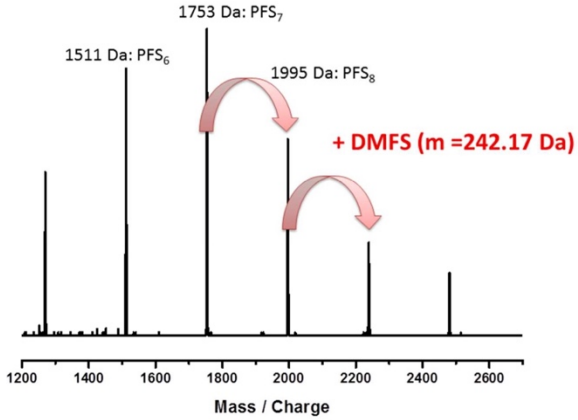

Fig. S 5. MALDI ToF mass spectrum of a PFDMS terminated with AGE directly. Only, protonated species are found. (m_{peak} = *m*(*n*-butyl) + n x m(FDMS) + m(H) = 57.11 g/mol + n x 242.17 g/mol + 1.01 g/mol).

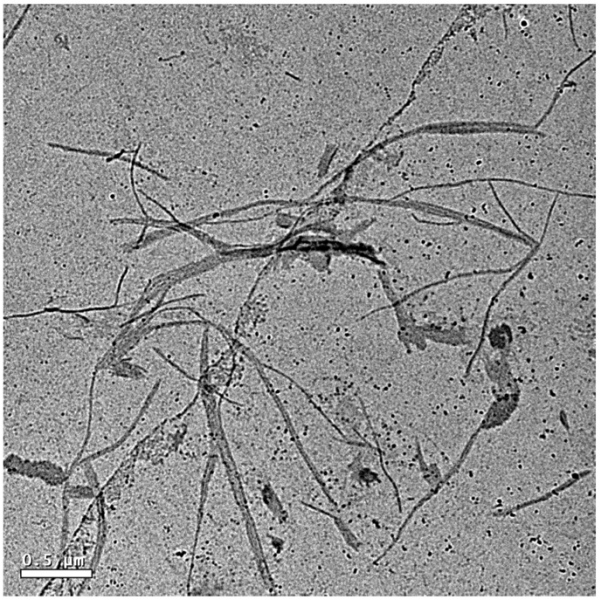
0.5 µm

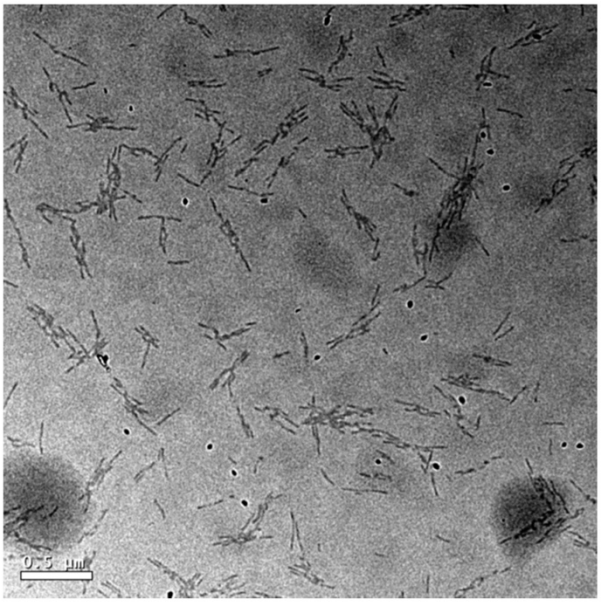
0.5 µm

Fig. S.6. TEM images of the amphiphilic PFDMS-*b*-PEO block copolymer (#5, Table 1.), prepared by drop-cast method of an aqueous solution (top, $c \approx 1\ g\ L^{-1}$) and of a methanol solution (bottom, $c \approx 1\ g\ L^{-1}$); scale bar: 0.5 μm.

REFERENCES

1. Jerschow, A.; Müller, N. *Journal of Magnetic Resonance, Series A* **1996,** 123, (2), 222-225.
2. Jerschow, A.; Müller, N. *Journal of Magnetic Resonance* **1997,** 125, (2), 372-375.
3. Wrighton, M. S.; Palazzotto, M. C.; Bocarsly, A. B.; Bolts, J. M.; Fischer, A. B.; Nadjo, L. *J. Am. Chem. Soc.* **1978,** 100, (23), 7264-7271.
4. Ni, Y.; Rulkens, R.; Manners, I. *J. Am. Chem. Soc.* **1996,** 118, (17), 4102-4114.
5. Kloninger, C.; Rehahn, M. *Macromolecules* **2004,** 37, (5), 1720-1727.
6. Vanderark, L.; Januszewski, E.; Gwyther, J.; Manners, I. *Eur. Polym. J.* **2011,** 47, (4), 823-826.

A.1.3 Monomer Sequence Monitoring by Real-Time NMR Spectroscopy

Communication

Macromolecular Journals

Macromolecular Rapid Communications

Sequence-Controlled Polymers via Simultaneous Living Anionic Copolymerization of Competing Monomers

Elisabeth Rieger, Arda Alkan, Angelika Manhart, Manfred Wagner, Frederik R. Wurm*

Dedicated to the 60th anniversary of the discovery of the "living" anionic polymerization by Michael M. Szwarc.

Natural macromolecules, i.e., sequence-controlled polymers, build the basis for life. In synthetic macromolecular chemistry, reliable tools for the formation of sequence-controlled macromolecules are rare. A robust and efficient chain-growth approach based on the simultaneous living anionic polymerization of sulfonamide-activated aziridines for sequence control of up to five competing monomers resulting in gradient copolymers is presented. The simultaneous azaanionic copolymerization is monitored by real-time ^{1}H NMR spectroscopy for each monomer at any time during the reaction. The monomer sequence can be adjusted by the monomer reactivity, depending on the electron-withdrawing effect by the sulfonamide (nosyl-, brosyl-, tosyl-, mesyl-, busyl) groups. This method offers unique opportunities for sequence control by competing copolymerization: a step forward to well-engineered synthetic polymers with defined microstructures.

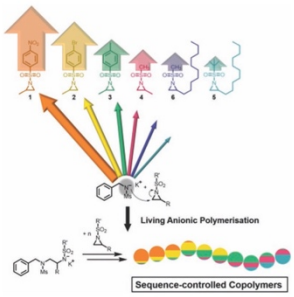

Complex macromolecules are the basis for life: the genetic information is stored in exactly coded polyesters, i.e., DNA and RNA. In polymer science, synthetic macromolecules—far from their perfectly structured natural counterparts—have been created by men to fulfill certain scientific and industrial properties. All these synthetic macromolecules, however, rely on rather simple sequences, i.e., mainly homopolymers, statistical, or diblock copolymers. The design of sequence-controlled macromolecules is a current challenge to achieve a new breakthrough for synthetic polymers. Meaningful applications in information storage, nanotechnology, biomaterials, and catalysis are envisaged.[1,2]

Current strategies to generate sequence-controlled macromolecules rely on the sequential addition of monomers or solid-phase syntheses.[3–6] These strategies are perfect for the generation of well-defined model compounds on small scale (typically several hundred milligrams); however, they are not suitable for large-scale production and cannot be combined with established techniques. Achieving control over monomer sequence with classical monomers and/or polymerization techniques would be very attractive, as it allows transfer to industrial application and the use of a plethora of available monomers.[7] After all, macroscopic properties, such as crystallinity or glass transition, can be tuned by the monomer sequence.[8]

Only living anionic polymerization brings polymer chemistry close to natures' precision of generating macromolecules with a single molecular weight and complex architecture.[9,10] Handling of different building blocks is well-established, e.g., basic vinyl monomers (styrenes and acrylates) or epoxides, with high control in the university-lab as well as industrially on a ton scale to generate block copolymers and other structures, which are commodities today.[10] The competing, sequence-controlled (ionic) copolymerization of several monomers to high

E. Rieger, A. Alkan, A. Manhart, Dr. M. Wagner, Dr. F. R. Wurm
Max-Planck-Institut für Polymerforschung
Ackermannweg 10, D-55128 Mainz, Germany
E-mail: wurm@mpip-mainz.mpg.de

Macromol. Rapid Commun. **2016**, DOI: 10.1002/marc.201600092

molecular (multi)block copolymers is rarely reported. Simultaneous copolymerization of different monomers by anionic polymerization is difficult, as in most cases control over monomer incorporation is lost, mainly due to the different nucleophilicities of the propagating species[11] and had only limited success;[7,12–17] the terpolymerization of styrene with diphenylethylene (DPE) derivatives was reported to exhibit sequence-controlled behavior by tuning of the DPE reactivity.[18]

Herein, the simultaneous, sequence-controlled copolymerization of up to five different *N*-sulfonyl-aziridines, **1–5** (Figure 1), in a one-step, one-pot reaction is presented, i.e., omitting sequential monomer addition.

Activated aziridines differing in their side-chains (methyl or decyl) and their activating groups (mesyl, busyl, tosyl, brosyl, or nosyl) have been developed. In contrast to styrene or acrylate-derivatives, the different sulfonamide derivatives allow—due to the different electron-withdrawing strength—adjusting the reactivities of the growing chain end and the monomer. Ter-, quarter-, and quinto-copolymers have been prepared by simultaneous anionic ring-opening polymerization (AROP) for the first time with M_w/M_n = 1.1–1.2 and control over monomer sequence along the polymer backbone.

N-sulfonyl aziridines represent a rather new monomer class for the AROP,[19–21] with a direct access to poly(ethylene imine)-derivatives. With a comparable ring strain of ≈111 kJ mol^{-1} for ethylene imine[22] and 114 kJ mol^{-1} for ethylene oxide,[23] aziridines can undergo ring-opening reactions and are typically polymerized by an uncontrolled cationic mechanism.[22,24] Since nitrogen is trivalent, branched polymers with broad molecular weight distributions are obtained. The acidic proton needs to be altered to allow the anionic ring-opening of an aziridine.[22] This is an ideal handle to control the monomer reactivity by the nature of the activating group and to generate sequence-controlled polymers. We have chosen different sulfonamides as activating groups to control the kinetics of the nucleophilic ring-opening. The amide resonance contributes to the stability of the aziridine itself and the resulting amide anion after ring-opening. These monomers are prepared in high yield reactions, are convenient to handle, often crystalline, and can be combined with the current setup for anionic polymerization.

To date only very few reports use in situ techniques to follow the individual monomer incorporation rates during co-polymerizations. Infrared or UV spectroscopy was applied to monitor cationic polymerizations at low temperatures[16,17] and the copolymerization of styrene and isoprene.[25,26] Real-time ^{1}H and/or ^{13}C nuclear magnetic resonance (NMR) spectroscopy was used for the anionic copolymerization of oxiranes[12,27] and styrenes.[14,15]

All aziridine monomers prepared herein can be distinguished in their ^{1}H (either the ring methylenes or methines) and ^{15}N NMR resonances (Supporting Information), which indicates their different electron densities in the rings, similar to the β-^{13}C NMR shift for styrenes.[11] Thus, we expected different polymerization rate constants for all monomers. As the AROP of tosyl- and mesyl-substituted aziridines has been reported to follow a living polymerization mechanism,[19,21] real-time ^{1}H NMR spectroscopy is the ideal tool to monitor monomer incorporation. For all monomers, their homopolymerization rate constants have been determined and chain extension experiments have proven a living polymerization mechanism (cf. Supporting Information). In homopolymerizations the reaction rates followed directly the electron withdrawing effects of the sulfonamides with nosyl-substituted monomers being the most reactive, followed by brosyl > tosyl > mesyl. Thus, when two aziridines with different activating groups are simultaneously copolymerized, copolymers with a gradient depending on the difference in reaction kinetics are expected. In the case of brosyl- and mesyl-activated aziridines (2-methyl-*N*-brosylaziridine (BsMAz, **2**) and 2-methyl-*N*-mesylaziridine (MsMAz, **4**)) copolymers with two separate glass transition temperatures (T_g) were obtained (poly(BsMAz-*co*-MsMAz) (T_g(1) = 142 °C and T_g(2) = 175 °C; Figure S33, Supporting Information) indicating a block-like structure. Copolymers of two monomers with the same activating groups show a single T_g (Figure S33,

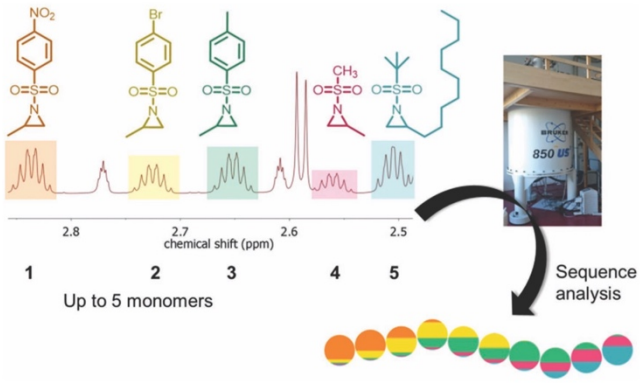

Figure 1. Real-time NMR allows following the sequence distribution. Monomer chemistry determines the monomer reactivity and the sequential incorporation which is monitored by ^{1}H NMR spectroscopy.

Macromolecular Journals
Macromol. Rapid Commun. **2016**, DOI: 10.1002/marc.201600092

Early View Publication; these are NOT the final page numbers, use DOI for citation !!

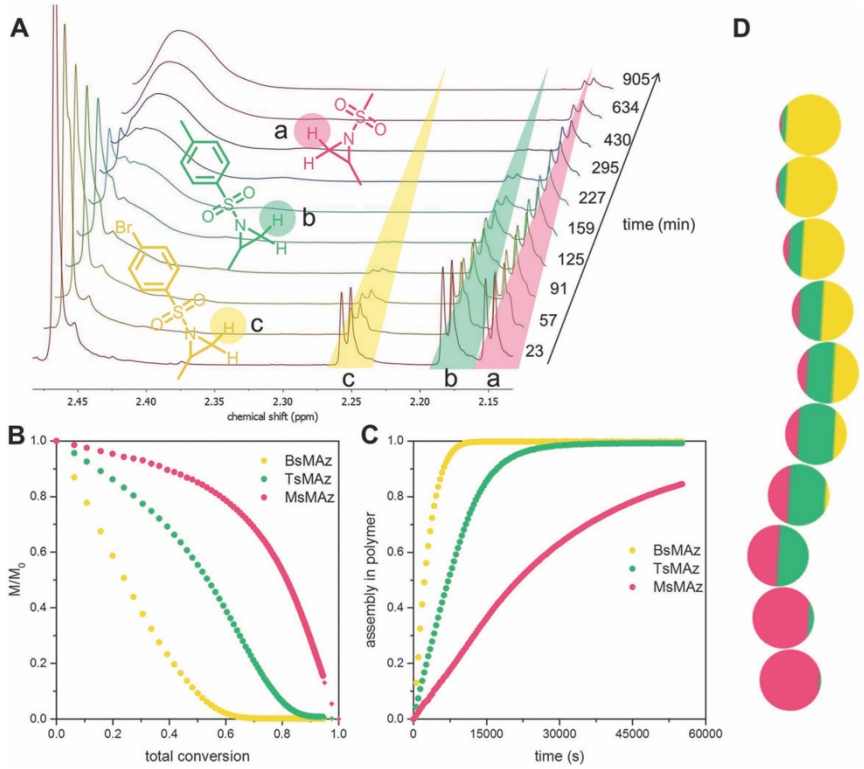

Figure 2. Simultaneous copolymerization of BsMAz, TsMAz, and MsMAz. A) Zoom into the real-time ^{1}H NMR spectra of the terpolymerization, showing the consumption of the monomers. (BsMAz (yellow), TsMAz (green), and MsMAz (red)). B) Normalized monomer concentrations in the reaction versus total conversion. C) Assembly of each monomer in the polymer versus reaction time. D) Visualization of a single chain for poly(BsMAz-*co*-TsMAz-*co*-MsMAz)—each sphere stands for 10% conversion.

Supporting Information). Motivated by these initial findings, the simultaneous copolymerization of up to five different aziridines has been studied. By simple electronic consideration we expected the propagation rates to decrease in the following order regarding the activation groups nosyl > brosyl > tosyl > mesyl ≥ busyl due to electronic effects. In addition, the effect of the pendant side chain (methyl or decyl) was analyzed.

Terpolymerization: The simultaneous copolymerization of BsMAz, 2-methyl-*N*-tosylaziridine (TsMAz), and MsMAz was studied after initiation at 50 °C by the addition of the potassium salt of *N*-benzyl-sulfonamide (BnNKMs). From the recorded real-time ^{1}H NMR spectra, the fast incorporation of the brosylated aziridine (BsMAz) is obvious from the fast disappearance of the doublet of the ring methylenes of BsMAz at 2.25 ppm (Figure 2A, yellow). The distinct doublets at 2.18 and 2.15 ppm for the ring methylenes of the two other monomers, i.e., TsMAz and MsMAz respectively, disappear subsequently regarding their propagation rate constants (Ts > Ms), while simultaneously the broad resonance of the polymer backbone emerges at ≈4.64–3.01 ppm. By integration of the well-separated monomer resonances over time (Figure 2A: signals a, b, and c) and normalization to the amount of unreacted monomer, plotting of the assembly of each monomer in the growing polymer chain versus the reaction time or total conversion is possible (Figure 2). By fitting these values, the probability of comonomer incorporation (which is mathematically the mole fraction of the incorporated comonomer), and thus the monomer sequence distribution over the final polymer was calculated and is shown schematically with every sphere summarizing 10% of monomer conversion (the color code and proportions display the incorporation probability of each comonomer in the respective polymer segment, Figure 2D).

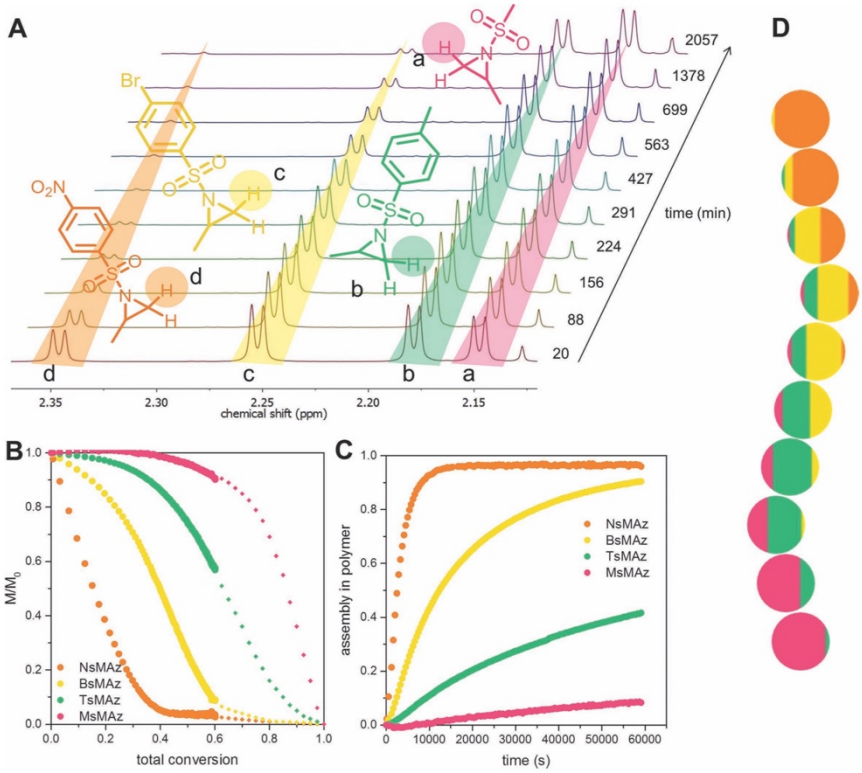

Figure 3. Simultaneous copolymerization of NsMAz, BsMAz, TsMAz, and MsMAz. A) Zoom into the real-time ^{1}H NMR measurement (NsMAz (orange), BsMAz (yellow), TsMAz (green), and MsMAz (red)). B) Normalized monomer concentrations in the reaction versus total conversion (diamonds: extrapolated). C) Assembly of each monomer in the polymer versus reaction time. D) Visualization of a single chain for poly(NsMAz-*co*-BsMAz-*co*-TsMAz-*co*-MsMAz).

Figure 2C reveals that BsMAz is fully consumed within the first 3 h, while at that time only 50% of TsMAz have reacted. For full consumption of TsMAz, additional 5 h are required, whereas MsMAz needs more than 17 h to reach full conversion, i.e., the monomer incorporation follows the trend of the homopolymerization rate constants (cf. Table S1, Supporting Information, i.e., BsMAz > TsMAz > MsMAz). These plots clearly show the formation of copolymers with very sharp gradients between the three segments; however overlapping areas cannot be prevented, as expected for a chain-growth copolymerization compared to sequential monomer addition. This simultaneous terpolymerization allows the generation of sequence-controlled terpolymers by AROP. There is a single report on the simultaneous AROP of three lactones for the synthesis of terpolymers, but monomer incorporation rates were not investigated.[28]

Quarterpolymerization: When 2-**m**ethyl-*N*-**n**osyla**z**iridine (NsMAz) carrying a nosyl activating group was additionally added to the polymerization mixture, a copolymer with four segments was expected. Figure 3 shows the copolymerization behavior of the copolymerization of NsMAz (orange), BsMAz (yellow), TsMAz (green), and MsMAz (red). The influence of the four different sulfonamides on the incorporation rate of the monomers in the polymer chain follows their individual rate constants. NsMAz with the highest polymerization rate constant was incorporated into the polymer chain as twice the rate as BsMAz. From the real-time ^{1}H NMR spectra, the resonances of the methylene group of NsMAz at 2.35 ppm (Figure 3A) are consumed quickly followed by the other three monomers sequentially and according to their relative homopolymerization rate constants. Thus, the incorporation rate follows the same general trends, i.e., the more

Macromolecular Journals
Macromol. Rapid Commun. **2016**, DOI: 10.1002/marc.201600092

Materials Views
www.MaterialsViews.com
Early View Publication; these are NOT the final page numbers, use DOI for citation !!

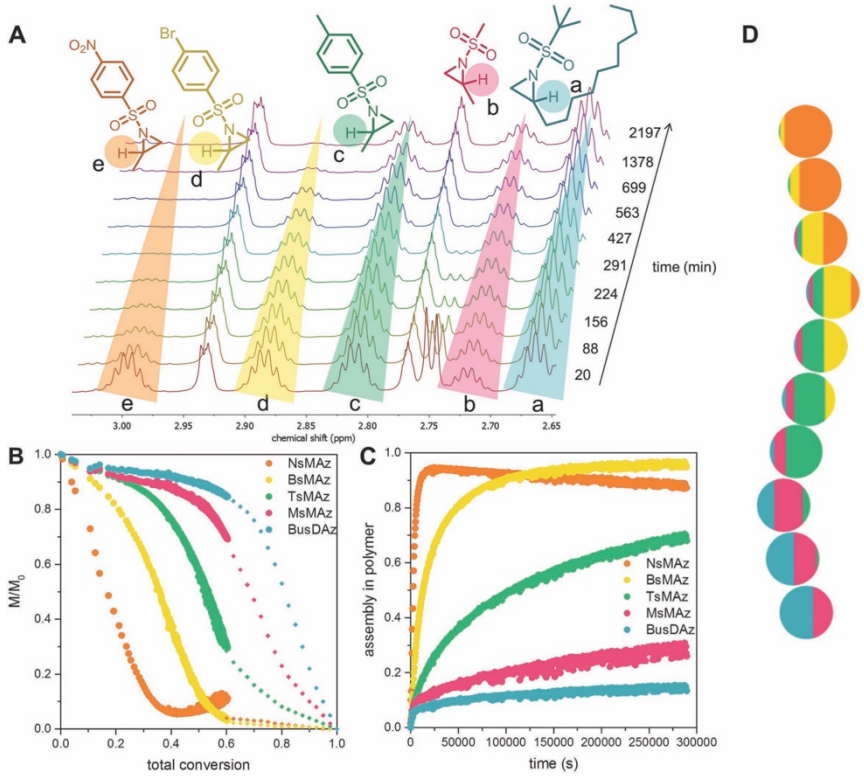

Figure 4. Simultaneous copolymerization of NsMAz, BsMAz, TsMAz, MsMAz, and BusDAz. A) Zoom into the real-time ^{1}H NMR measurement (NsMAz, (orange), BsMAz (yellow), TsMAz (green), MsMAz (red), and BusDAz (cyan)). B) Normalized monomer concentrations in the solution versus total conversion (diamonds: extrapolated). C) Assembly of monomer in the polymer versus time. D) Visualization of a single chain for poly(NsMAz-*co*-BsMAz-*co*-TsMAz-*co*-MsMAz-*co*-BusDAz).

electron-withdrawing the *N*-sulfonyl-group, the faster its incorporation rate; this results in a segmented copolymer with gradient structure nosyl > brosyl > tosyl > mesyl (poly(NsMAz-*co*-BsMAz-*co*-TsMAz-*co*-MsMAz), Figure 3). The size exclusion chromatogram (SEC) after the reaction under conventional conditions proves full conversion of all monomers and M_w/M_n of 1.16 (Figure S30, Supporting Information: SEC; Figure S22, Supporting Information: ^{1}H NMR of the final copolymer).

In the following, the steric effect of the side chains with the same activating groups was investigated. Following the above-mentioned trends, a copolymer from NsMAz, BsMAz, MsMAz, and 2-decyl-*N*-mesylaziridine (MsDAz) was synthesized (compare Figure S1-II, Supporting Information). In this mixture two monomers carry the same sulfonamide chain, i.e., mesyl, but the side chain differs (methyl vs decyl). Figure S1-II (Supporting Information) summarizes the results: both mesyl-monomers show lower polymerization rates compared to the nosylated and brosylated monomers in the mixture and are not fully consumed during the real-time NMR measurement. Interestingly, the sterically demanding decyl-side chain has only a slight impact on the polymerization rates, thus resulting in a copolymer with three segments, while the third segment has almost random distribution of MsMAz and MsDAz (poly(NsMAz-*co*-BsMAz-*co*-(MsMAz-*co*-MsDAz)).

Quintopolymerization: To the best of our knowledge, a simultaneous polymerization of five different monomers has not been conducted to date by any ionic polymerization strategy; only sequential monomer addition has been used to prepare pentablock quintopolymers.[29,30] The simultaneous copolymerization of five different activated aziridines can be monitored via ^{1}H NMR spectroscopy. As an additional handle, a new monomer was

synthesized, i.e., 2-decyl-*N*-*tert*-butylsulfonylaziridine (BusDAz) carrying a busyl activating group. All monomers can be distinguished by their ^{1}H NMR resonances of their ring methines in this case (Figure 4: multiplets at 3.01–2.97 ppm (NsMAz: orange), 2.90–2.86 ppm (BsMAz: yellow), 2.83–2.79 ppm (TsMAz: green), 2.73–2.70 ppm (MsMAz: red), and 2.68–2.64 ppm (BusDAz: cyan)). Also for the competing copolymerization of five comonomers the trends of monomer incorporation follow the trends of the homopolymerization rate constants of the individual monomers. NsMAz is incorporated as the fastest monomer into the living polymer (note: the slight decreasing in Figure 4C is due to partial overlapping to the polymer backbone, as in this case the methine resonances of the monomers had to be used). The incorporation of NsMAz is followed by BsMAz > TsMAz > MsMAz. The additional BusDAz shows the slowest incorporation, probably caused by the less negative inductive effect of the *tert*-butyl-group of the busyl group versus the methyl-group in the mesylate due to the additional methyl-groups and additional steric hindrance (separate polymerization, however, proves their living nature and full conversion). Thus the different polymerization rate constants of these five monomers allow the synthesis of copolymer with a sequenced gradient poly(NsMAz-*co*-BsMAz-*co*-TsMAz-*co*-MsMAz-*co*-BusDAz).

In summary, the anionic copolymerization of a series of competing N-sulfonyl aziridines allowed for the first time to synthesize gradient copolymers with up to five different monomers. Control over monomer incorporation brings classical polymerization methods closer to natures' perfection and allows the production of advanced polymers for various applications in materials science. As the polymerization follows a living polymerization mechanism (without termination/transfer), simultaneous copolymerization of aziridines is possible and due to excellent signal separation, the polymerization can be monitored by real-time ^{1}H NMR spectroscopy. The monomers were designed to exhibit distinctively different polymerization rate constants due to the electronic nature of the activating group (NsMAz > BsMAz > TsMAz > MsMAz ≥ MsDAz ≥ BusDAz). This allows the synthesis of copolymers with sharp gradients in a competing copolymerization affording polymers typically with $M_w/M_n < 1.2$. We believe that this platform is a new efficient way to design polyamides with a controlled gradient structure and well-defined polyamines (after removal of the activating groups). Furthermore the combination with other anionic polymerization techniques such as epoxides or vinyl monomers is worth to be investigated. This allows for the first time the combination of aziridine-based polymers with commodity monomers. The toolbox of monomers presented in this study will open the way for the establishment of aziridines as a new monomer class for anionic polymerization.

Supporting Information

Supporting Information is available from the Wiley Online Library or from the author.

Acknowledgements: The authors thank Prof. Katharina Landfester for continuous support. E.R. thanks the BMBF/MPG network MaxSynBio. The authors thank the Deutsche Forschungsgemeinschaft (DFG WU/750 7-1) for support.

Received: February 11, 2016; Revised: February 27, 2016; Published online: ; DOI: 10.1002/marc.201600092

Keywords: anionic polymerization; aziridines; copolymerization; ring-opening polymerization; sequence-controlled polymers

[1] J.-F. Lutz, M. Ouchi, D. R. Liu, M. Sawamoto, *Science* **2013**, *341*, 1238149.
[2] H. Mutlu, J.-F. Lutz, *Angew. Chem. Int. Ed.* **2014**, *53*, 13010.
[3] F. Alsubaie, A. Anastasaki, P. Wilson, D. M. Haddleton, *Polym. Chem.* **2015**, *6*, 406.
[4] N. Ten Brummelhuis, *Polym. Chem.* **2015**, *6*, 654.
[5] M. Porel, C. A. Alabi, *J. Am. Chem. Soc.* **2014**, *136*, 13162.
[6] G. Gody, T. Maschmeyer, P. B. Zetterlund, S. Perrier, *Nat. Commun.* **2013**, *4* 2505.
[7] L. R. Hutchings, P. P. Brooks, D. Parker, J. A. Mosely, S. Sevinc, *Macromolecules* **2015**, *48*, 610.
[8] S. Srichan, N. Kayunkid, L. Oswald, B. Lotz, J.-F. Lutz, *Macromolecules* **2014**, *47*, 1570.
[9] N. Hadjichristidis, M. Pitsikalis, S. Pispas, H. Iatrou, *Chem. Rev.* **2001**, *101*, 3747.
[10] D. Baskaran, A. H. E. Müller, *Controlled and Living Polymerizations*, Wiley-VCH Verlag, Weinhem, Germany **2010**, p. 1.
[11] A. Hirao, K. Takenaka, in *Anionic Polymerization* (Eds: N. Hadjichristidis, A. Hirao), Springer, Japan **2015**, p. 61.
[12] A. Alkan, A. Natalello, M. Wagner, H. Frey, F. R. Wurm, *Macromolecules* **2014**, *47*, 2242.
[13] P. P. Brooks, A. Natalello, J. N. Hall, E. A. L. Eccles, S. M. Kimani, K. Bley, L. R. Hutchings, *Macromol. Symp.* **2013**, *323*, 42.
[14] A. Natalello, A. Alkan, P. von Tiedemann, F. R. Wurm, H. Frey, *ACS Macro Lett.* **2014**, *3*, 560.
[15] A. Natalello, M. Werre, A. Alkan, H. Frey, *Macromolecules* **2013**, *46*, 8467.
[16] J. E. Puskas, K. B. McAuley, S. W. P. Chan, *Macromol. Symp.* **2006**, *243*, 46.
[17] S. Shaikh, J. E. Puskas, G. Kaszas, *J. Polym. Sci., Part A: Polym. Chem.* **2004**, *42*, 4084.
[18] A. Natalello, J. N. Hall, E. A. L. Eccles, S. M. Kimani, L. R. Hutchings, *Macromol. Rapid Commun.* **2011**, *32*, 233.
[19] I. C. Stewart, C. C. Lee, R. G. Bergman, F. D. Toste, *J. Am. Chem. Soc.* **2005**, *127*, 17616.
[20] L. Thomi, F. R. Wurm, *Macromol. Rapid Commun.* **2014**, *35*, 585.
[21] L. Thomi, F. R. Wurm, *Macromol. Symp.* **2015**, *349*, 51.

[22] J. B. Sweeney, *Chem. Soc. Rev.* **2002**, *31*, 247.
[23] M. Bednarek, P. Kubisa, S. Penczek, *Macromolecules* **1999**, *32*, 5257.
[24] R. Tanaka, I. Ueoka, Y. Takaki, K. Kataoka, S. Saito, *Macromolecules* **1983**, *16*, 849.
[25] S. Quinebèche, C. Navarro, Y. Gnanou, M. Fontanille, *Polymer* **2009**, *50*, 1351.
[26] T. E. Long, H. Y. Liu, B. A. Schell, D. M. Teegarden, D. S. Uerz, *Macromolecules* **1993**, *26*, 6237.
[27] C. Tonhauser, A. Alkan, M. Schömer, C. Dingels, S. Ritz, V. Mailänder, H. Frey, F. R. Wurm, *Macromolecules* **2013**, *46*, 647.
[28] C. Barbaud, F. Faÿ, F. Abdillah, S. Randriamahefa, P. Guérin, *Macromol. Chem. Phys.* **2004**, *205*, 199.
[29] P. Fragouli, H. Iatrou, D. J. Lohse, N. Hadjichristidis, *J. Polym. Sci., Part A: Polym. Chem.* **2008**, *46*, 3938.
[30] N. Ekizoglou, N. Hadjichristidis, *J. Polym. Sci., Part A: Polym. Chem.* **2002**, *40*, 2166.

Supporting Information

for *Macromol. Rapid Commun.*, DOI: 10.1002/marc.201600092

Sequence-Controlled Polymers via Simultaneous Living Anionic Copolymerization of Competing Monomers

Elisabeth Rieger, Arda Alkan, Angelika Manhart, Manfred Wagner, and Frederik R. Wurm*

Supporting Information

for

Sequence-Controlled Polymers via Simultaneous Living Anionic Copolymerization of Competing Monomers

*Elisabeth Rieger[1], Arda Alkan[1], Angelika Manhart[1], Manfred Wagner[1], Frederik R. Wurm[1]**

[1]Max Planck Institute for Polymer Research (MPI-P), Ackermannweg 10, 55128 Mainz, Germany.

**e-mail: wurm@mpip-mainz.mpg.de*

Table of Contents

Section A. Synthetic Protocols – Small molecules 3

Monomers derived from methylaziridine. 3

Monomers derived from olefins. 8

Initiator 13

Section B. Synthetic Protocols – Polymers. 14

Homo- and Copolymers 16

Copolymers for living polymerizations. 20

Copolymers for kinetic measurements. 22

Section C. Spectroscopic Characterization 25

Small molecules 25

Polymers 35

Section D. Representative SECs of several homo and copolymers. 39

Section E. Thermal Characterization 43

Section F. k-values 44

Section G. References 44

Section A. Synthetic Protocols – Small molecules

Chemicals. All solvents and reagents were purchased from Sigma-Aldrich, Acros Organics or Fluka and used as received unless otherwise mentioned. Deuterated N,N-dimethylformamide (DMF-d7) was purchased from Deutero GmbH and was distilled from CaH2 and stored in a glovebox prior to use. All monomers and the initiator were dried extensively by azeotropic distillation with benzene prior to polymerization.

Methods.

NMR. 1H NMR, 13C NMR and 15N NMR spectra were recorded using a Bruker Avance III 250, a Bruker Avance 300, a Bruker Avance III 500, a Bruker Avance III 700 and a Bruker Avance III 850. All spectra were referenced internally to residual proton signals of the deuterated solvent.

SEC. For size exclusion chromatography measurements in DMF (containing 0.25 g/L of lithium bromide as an additive) an Agilent 1100 Series was used as an integrated instrument, including a PSS HEMA column (106/105/104 g/mol), a UV detector (275 nm), and a RI detector at a flow rate of 1 mL/min at 50 °C. Calibration was carried out using PEO standards provided by Polymer Standards Service.

DSC. Differential scanning calorimetry measurements were performed using a Mettler Toledo DSC 823 calorimeter. Three scanning cycles of heating-cooling were performed in the temperature range from –140 to 250 °C. Heating rates of 10 °C/min were employed under nitrogen (30 mL/min).

IR. The monomers were pressed with KBr to form a pellet and the absorption between 4,000 and 400 cm−1 was recorded in a Spectrum BX spectrometer from PerkinElmer.

Elemental analyses were determined with a Elementar Vario EL.

HRMS. High resolution mass spectroscopy spectra were recorded on a Q-ToF-Ultima 3 instrument (Waters, Milford, Massachusetts) with LockSprayTM interface and a suitable external calibrant.

Monomers derived from methylaziridine.

2-Methyl-N-mesylaziridine (MsMAz).

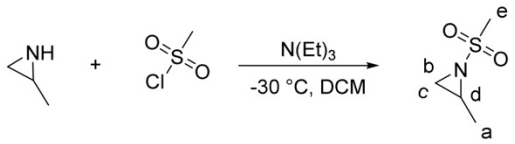

Scheme 1. Synthesis of **2-Methyl-*N*-mesylaziridine**

The compound was synthesized according to literature procedure[1]. Briefly, ca. 15 mL 2-methylaziridine were cryo transferred for purification. 2-Methylaziridine (10.7 g, 187 mmol) and triethylamine (37.4 mL, 281 mmol) were dissolved in anhydrous dichloromethane (DCM) (200 mL). The solution was cooled to -30 °C and mesylchloride (16.7 mL, 215 mmol) was added dropwise over a period of 20 minutes. Afterwards, the reaction mixture was stirred at -30 °C for one hour. Saturated aqueous sodium bicarbonate (200 mL) was added and the mixture was allowed to reach room temperature. After washing with brine, the organic phases were combined, dried over magnesium sulfate and concentrated at reduced pressure. The product was purified via chromatography over silica gel (petroleum ether/ethyl acetate 1:1) and sublimation at 35 °C at 0.05 mbar. The yield of the colorless needles were 11.68 g, 86 mmol, 46%. ^{1}H NMR (300 MHz, 295 K, Chloroform-*d*): δ 3.05 (s, 3H, e), 2.85–2.76 (m, 1H, d), 2.60 (d, *J* = 7.0 Hz, 1H, c), 2.07 (d, *J* = 4.6 Hz, 1H, b), 1.34 (d, *J* = 5.6 Hz, 3H, a). ^{13}C NMR (176 MHz, 298 K, Chloroform-*d*): δ 39.67, 35.25, 34.32, 16.90. ^{15}N NMR (71 MHz, 298 K, Chloroform-*d*): δ 78.27. HRMS (*m/z*): $[M]^+$ calcd. for $C_4H_{10}NO_2S$, 136.0432; found, 136.0442. Analysis (calcd., found for $C_4H_{10}NO_2S$): C (33.58, 33.67), H (7.15, 7.02), N

(10.06, 9.90), S (12.15, 12.29). IR: $\tilde{\nu}$: 3090 (w), 3022 (w), 2989 (w), 2936 (w), 1454 (s), 1399 (w), 1302 (b), 1236 (m), 1187 (m), 1141 (s), 794 (s), 665 (s) cm^{-1}.

2-Methyl-N-tosylaziridine (TsMAz).

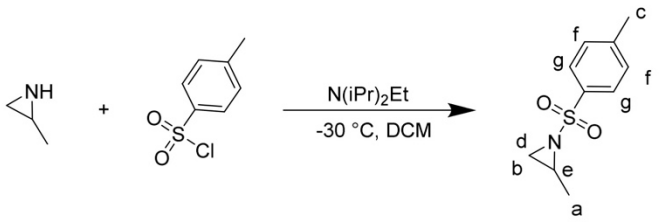

Scheme 2. Synthesis of **2-Methyl-*N*-tosylaziridine**

5 mL 2-methylaziridine were cryo transferred for purification. 2-Methylaziridine (4.36 g, 76 mmol) and *N,N*-diisopropylethylamine (19.4 mL, 115 mmol) were dissolved in anhydrous DCM (100 mL). The solution was cooled to -30 °C and tosylchloride (17.96 g, 94 mmol) in anhydrous DCM (50 mL) was added over a period of 25 minutes. Afterwards the reaction mixture was stirred at -30 °C for 1.5 hour. Saturated aqueous sodium bicarbonate (150 mL) was added and the mixture was allowed to reach room temperature and stirred overnight. After washing with saturated aqueous sodium bicarbonate and brine, the organic phases were combined, dried over magnesium sulfate and concentrated at reduced pressure. Chromatography over silica gel (petroleum ether/ethyl acetate 5:1) yielded the product as a colorless solid (12.04 g, 57 mmol, 75%). ^{1}H NMR (300 MHz, 295 K, Chloroform-*d*): δ 7.89-7.71 (m, 2H, g), 7.37–7.28 (m, 2H, f), 2.92–2.74 (m, 1H, e), 2.59 (d, J = 7.0 Hz, 1H, d), 2.42 (s, 3H, c), 2.00 (d, J = 4.6 Hz, 1H, b), 1.23 (d, J = 5.6 Hz, 3H, a). ^{13}C NMR (176 MHz, 298 K, Chloroform-*d*): δ 144.47, 135.41, 129.75, 127.85, 35.92, 34.79, 21.68, 16.84. ^{15}N NMR (71 MHz, 298 K, Chloroform-*d*): δ 80.45. HRMS (*m/z*): $[M]^+$ calcd. for $C_{10}H_{14}NO_2S$, 212.0745; found, 212.0749. Analysis (calcd., found for $C_{10}H_{14}NO_2S$): C (55.96, 56.12), H (5.95, 5.83), N (6.99, 7.19), S (15.19, 15.39). IR: $\tilde{\nu}$: 3066 (w), 2976 (w), 2929 (w), 1597 (s), 1447 (s), 1402

(m), 1320 (b), 1238 (s), 1154 (s), 1098 (m), 1034 (m), 848 (s), 769 (s), 714 (s), 687 (s), 659 (s) cm^{-1}.

2-Methyl-N-brosylaziridine (BsMAz).

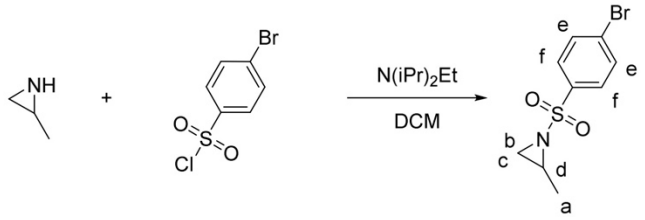

Scheme 3. Synthesis of **2-Methyl-*N*-brosylaziridine**

Prior to the reaction 2 mL 2-methylaziridine were cryo transferred for purification. 2-Methylaziridine (1.60 g, 28 mmol) and *N,N*-diisopropylethylamine (7.2 mL, 42 mmol) were dissolved in anhydrous DCM (60 mL). The solution was cooled to -30 °C and brosylchloride (8.18 g, 32 mmol) in anhydrous DCM (10 mL) was added over a period of 30 minutes. Afterwards the reaction mixture was stirred at -30 °C for half an hour and then allowed to reach room temperature. The mixture was washed with deionized water, hydrochloric acid (2%), saturated aqueous sodium bicarbonate and brine, the organic phases were combined, dried over magnesium sulfate and concentrated at reduced pressure. Chromatography over silica gel (hexanes/ethyl acetate 10:1) yielded the product as a colorless solid (1.55 g, 5.6 mmol, 20%, yield not optimized). ^{1}H NMR (300 MHz, 295 K, Chloroform-*d*): δ 7.80–7.69 (m, 2H, f), 7.68–7.56 (m, 2H, e), 2.86-2.78 (m, 1H, d), 2.57 (d, *J* = 7.0 Hz, 1H, c), 1.99 (d, *J* = 4.7 Hz, 1H, b), 1.20 (d, *J* = 5.6 Hz, 3H, a). ^{13}C NMR (176 MHz, 298 K, Chloro- form-*d*): δ 137.69, 132.55, 129.41, 128.70, 50.27, 49.47, 36.39, 35.17, 19.21, 16.90. ^{15}N NMR (71 MHz, 298 K, Chloroform-*d*): δ 80.13. HRMS (*m/z*): $[M]^+$ calcd. for $C_9H_{11}NO_2SBr$, 275.9694; found, 275.9697. Analysis (calcd., found for $C_9H_{11}NO_2SBr$): C (38.18), H (4.88), N (4.85), S (10.42). IR: $\tilde{\nu}$: 3301 (w), 3088 (w), 2970 (w), 1573 (s), 1429 (s), 1391 (s), 1330 (ss), 1275 (m), 1238

(m), 1162 (ss), 1069 (s), 1038 (s), 848 (s), 825 (s), 772 (s), 742 (s), 708 (s), 676 (s), 610 (s), 559 (s) cm^{-1}.

2-Methyl-N-nosylaziridine (NsMAz).

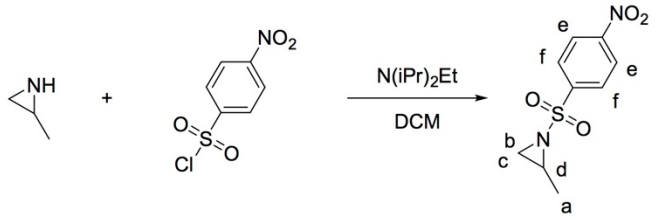

Scheme 4. Synthesis of **2-Methyl-*N*-nosylaziridine**

Prior to the reaction 2 mL 2-methylaziridine were cryo transferred for purification. 2-Methylaziridine (2.50 g, 44 mmol) and *N,N*-diisopropylethylamine (7.5 mL, 44 mmol) were dissolved in anhydrous DCM (90 mL). The solution was cooled to -30 °C and nosylchloride (11.16 g, 50 mmol) in anhydrous DCM (20 mL) was added over a period of 30 minutes. Afterwards the reaction mixture was stirred at -30 °C for half an hour and then allowed to reach room temperature. The mixture was washed with deionized water, hydrochloric acid (2%) and brine, the organic phases were combined, dried over magnesium sulfate and concentrated at reduced pressure. Recristallisation from Methyl *tert*-butyl ether (TBME) yielded the product as a slightly yellow solid (4.00 g, 46.5 mmol, 38%). ^{1}H NMR (250 MHz, 297 K, Chloroform-*d*): δ 8.48–8.31 (m, 2H, f), 8.24–8.03 (m, 2H, e), 3.05–2.81 (m, 1H, d), 2.70 (d, *J* = 7.1 Hz, 1H, c), 2.13 (d, *J* = 4.7 Hz, 1H, b), 1.26 (d, *J* = 5.6 Hz, 3H, a). ^{13}C NMR (176 MHz, 298 K, Chloro-form-*d*): δ 150.70, 144.41, 129.22, 124.42, 36.96, 35.64, 16.91. ^{15}N NMR (71 MHz, 298 K, Chloroform-*d*): δ 80.03. HRMS (*m/z*): $[M]^+$ calcd. for $C_9H_{11}N_2O_4S$, 243.0440; found, 243.0439. Analysis (calcd., found for $C_9H_{11}N_2O_4S$): C (43.93, 43.75), H (4.42, 4.30), N (10.17, 10.17), S (13.16, 12.91). IR: $\tilde{\nu}$: 3107 (w), 3068 (w), 2977 (w), 2936 (w), 1607 (s), 1529 (ss), 1449 (s), 1401 (s), 1351 (s), 1328 (s), 1240 (s), 1161 (ss), 1099 (s), 1033 (s), 849 (s), 768 (s), 692 (s), 615 (s) cm^{-1}.

Monomers derived from olefins.

2-Decyl-N-tosylaziridine (TsDAz).

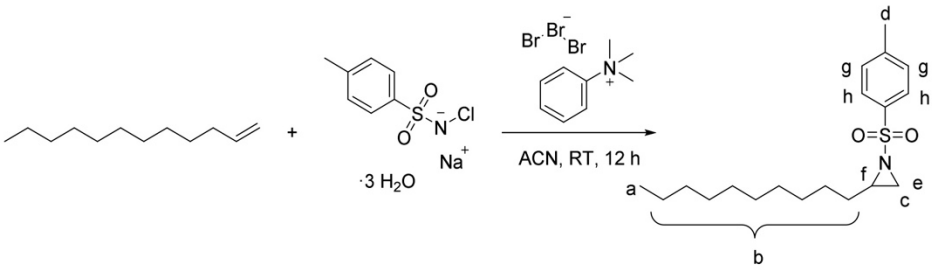

Scheme 5. Synthesis of **2-Decyl-*N*-tosylaziridine**

The compound was synthesized according to literature procedures.[2] Chloramine-T (13.99 g, 50 mmol) was dried azeotropically with benzene *in vacuo* for 6 h and at 90 °C for additional 8 h to remove the water. The anhydrous chloramine-T and 1-dodecene (10 mL, 45 mmol) were dissolved in anhydrous acetonitrile (ACN) (200 mL). Phenyltrimethylammonium tribromide (PTAB) (1.70 g, 4.5 mmol), dissolved in ACN (100 mL) was added and the mixture was stirred at room temperature for 16 hours. Ethyl acetate (40 mL) and deionized water (40 mL) were added. After washing with brine, the organic phases were combined, dried over magnesium sulfate and concentrated at reduced pressure. Chromatography over silica gel (hexanes/ethyl acetate 10:1 to 9:1) yielded the product as a yellowish oily liquid (7.12 g, 21 mmol, 47%). ^{1}H NMR (300 MHz, 295 K, Chloroform-*d*): δ 7.83 (d, *J* = 8.1 Hz, 2H, h), 7.33 (d, *J* = 8.1 Hz, 2H, g), 2.74–2.67 (m, 1H, f), 2.63 (d, *J* = 7.0 Hz, 1H, e), 2.44 (s, 3H, d), 2.05 (d, *J* = 4.5 Hz, 1H, c), 1.37–1.07 (m, 18H, b), 0.94–0.82 (m, 3H, a). ^{13}C NMR (176 MHz, 298 K, Chloroform-*d*): δ 144.44, 135.30, 129.66, 128.05, 40.55, 33.82, 31.96, 31.37, 29.50, 29.08, 26.82, 22.74, 21.66, 14.17. ^{15}N NMR (71 MHz, 298 K, Chloroform-*d*): δ 79.82. HRMS (*m/z*): $[M]^+$ calcd. for $C_{19}H_{32}NO_2S$, 338.2154; found, 338.2151. Analysis (calcd., found for $C_{19}H_{32}NO_2S$): C (67.16), H (6.66), N (6.00), S (10.78). IR: $\tilde{\nu}$: 3446 (w), 2926 (ss), 2855 (s), 1598 (s), 1461 (s), 1327 (ss), 1333 (s), 1162 (ss), 1193 (s), 816 (s), 715 (s), 694 (s), 662 (w) cm^{-1}.

2-Decyl-N-mesylaziridine (MsDAz).

Tert-butyl hypochlorite (tBuOCl).

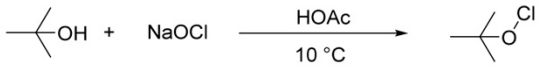

Scheme 6. Synthesis of ***Tert*-butyl hypochlorite**

The complete procedure was carried out in the absence of light. In an Erlenmeyer-flask a solution (372.26 g, 500 mmol) of sodium hypochlorite (14%) was cooled down to 10 °C and stirred rigorously. *Tert*-butanol (66 mL, 500 mmol) and acetic acid (40 mL, 500 mmol) were added in small portions. The mixture was stirred for another 5 minutes. The aqueous phase was separated. The organic phase was washed with aqueous sodium bicarbonate (10%) and deionized water and yielded the product as a yellow liquid with a pungent odor, which was used without further purification (39.48 g, 364 mmol, 73%).

Sodium chloro(methylsulfonyl)amide (Chloramine-M).

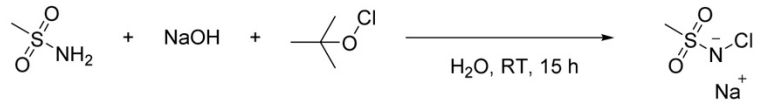

Scheme 7. Synthesis of **Sodium chloro(methylsulfonyl)amide**

Methanesulfonamide (13.32 g, 140 mmol) was solved in 120 mL deionized water and sodium hydroxide (5.60 g, 140 mmol) was added. 16 mL of the freshly prepared *tert*-butyl hypochlorite were added and the mixture instantly turned colorless and heated up slightly. The solution was stirred at room temperature for three days. The solvent was removed at reduced pressure and the crude was washed with acetone. The solid was dried *in vacuo* for several days and yielded the product as a colorless solid (18.87 g, 135 mmol, 89%) and was used without further purification.

2-Decyl-N-mesylaziridine (MsDAz).

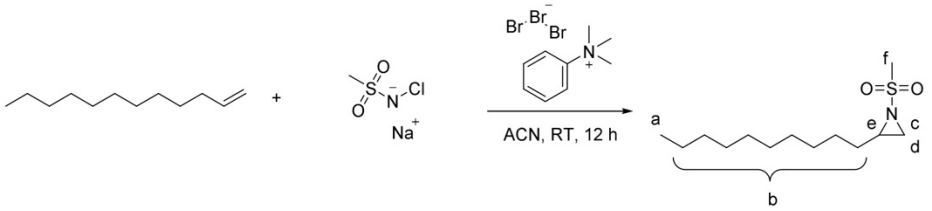

Scheme 8. Synthesis of **2-Decyl-*N*-mesylaziridine**

Chloramine-M (6.77 g, 44.70 mmol) was dried from benzene three times *in vacuo* for eight hours. Chloramine-M and 1-dodecene (9 mL, 40.64 mmol) were dissolved in anhydrous acetonitrile (ACN) (200 mL), phenyltrimethylammonium tribromide (PTAB) (1.53 g, 4.06 mmol) was added and the mixture was stirred at room temperature for 26 h. Ethyl acetate (40 mL) and deionized water (40 mL) were added and the phases were separated. After washing with brine, the organic phases were combined, dried over magnesium sulfate and concentrated at reduced pressure. Chromatography over silica gel by gradient (starting with 100% petroleum ether to petroleum ether/ethyl acetate 15:1 stepwise to 8:1) yielded the product as a yellowish oily liquid (5.28 g, 20 mmol, 49%). ^{1}H NMR (300 MHz, 295 K, Chloroform-*d*): δ 3.05 (s, 3H, f), 2.77-2.68 (m, 1H, e), 2.59 (d, *J* = 7.0 Hz, 1H, d), 2.10 (d, *J* = 4.6 Hz, 1H, c), 1.50–1.23 (m, 18H, b), 0.91–0.87 (m, 3H, a). ^{13}C NMR (176 MHz, 298 K, Chloroform-*d*): δ 40.02–39.37, 33.45, 31.94, 31.41, 29.97–28.90, 26.92, 22.73, 14.16. ^{15}N NMR (71 MHz, 298 K, Chloroform-*d*): δ 78.81. HRMS (*m/z*): $[M]^+$ calcd. for $C_{13}H_{28}NO_2S$, 262.1841; found, 262.1841. Analysis (calcd., found for $C_{13}H_{28}NO_2S$): C (59.67, 59.76), H (10.10, 10.31), N (6.07, 6.21), S (12.15, 12.29). IR: $\tilde{\nu}$: 3437 (w), 2926 (ss), 2856 (s), 1462 (s), 1372 (w), 1319 (ss), 1235 (w), 1153 (ss), 792 (m), 672 (w) cm^{-1}.

2-Decyl-N-busylaziridine (BusDAz).

Sodium chloro(tert-butylsulfonyl)amide (Chloramine-Bus).

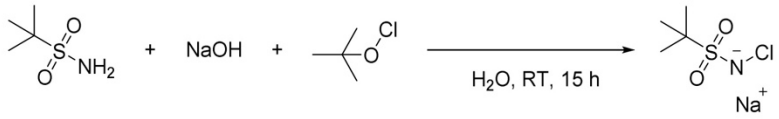

Scheme 9. Synthesis of **Sodium chloro(*tert*-butylsulfonyl)amide**

Tert-butylsulfonyl-amide (5 g, 35 mmol) was solved in 30 mL deionized water and sodium hydroxide (1.39 g, 35 mmol) was added. 3.3 mL of the freshly prepared *tert*-butyl hypochlorite were added and the mixture instantly turned colorless and heated up slightly. The solution was stirred at room temperature for three days. The solvent was removed at reduced pressure and the crude was washed with acetone. The solid was dried *in vacuo* from benzene for several days and yielded the product as a colorless solid (6.6 g, 35 mmol, 99%) and was used without further purification.

2-Decyl-N-busylaziridine (BusDAz).

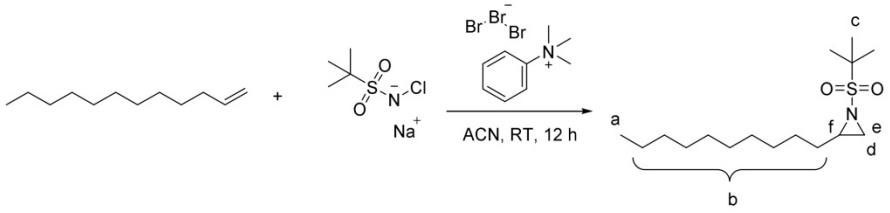

Scheme 10. Synthesis of **2-Decyl-*N*-busylaziridine**

Chloramine-Bus (2.58 g, 12.4 mmol) was dried from benzene three times *in vacuo* for eight hours. Chloramine-Bus and 1-dodecene (1.9 g, 11.3 mmol) were dissolved in anhydrous acetonitrile (ACN) (55 mL), phenyltrimethylammonium tribromide (PTAB) (420 mg, 1.13 mmol) was added and the mixture was stirred at room temperature for 48 h. Ethyl acetate (40 mL) and deionized water (40 mL) were added and the phases were separated. After washing with brine, the organic phases were combined, dried over magnesium sulfate

and concentrated at reduced pressure. Chromatography over silica gel (petroleum ether/ethyl acetate 20:3) yielded the product as a colorless oily liquid (1.4 g, 6 mmol, 50%). ^{1}H NMR (250 MHz, 297 K, Chloroform-*d*): δ 2.76-2.65 (m, 1H, f), 2.57 (d, *J* = 6.9 Hz, 1H, e), 2.05 (d, *J* = 4.6 Hz, 1H, d), 1.48 (s, 9H, c), 1.45-1.11 (m, 18H, b), 0.95–0.80 (m, 3H, a). ^{13}C NMR (176 MHz, 298 K, Chloroform-*d*): δ 59.34, 38.89, 34.04, 32.03, 31.46, 29.95–28.95, 26.44, 24.36, 22.81, 14.25. ^{15}N NMR (71 MHz, 298 K, Chloroform-*d*): δ 66.39. HRMS (*m/z*): [M + Na]$^{+}$ calcd. for $C_{16}H_{33}NO_2SNa$, 326.2130; found, 326.2124. Analysis (calcd., found for $C_{16}H_{33}NO_2S$): C (63.34, 63.15), H (11.97, 12.15), N (5.44, 5.64), S (10.99, 11.19). IR: $\tilde{\nu}$: 2926 (ss), 2855 (s), 1462 (s), 1398 (w), 1368 (w), 1310 (ss), 1132 (s), 711 (m), 658 (w) cm^{-1}.

Initiator

N-benzyl-sulfonamide (BnNHMs).

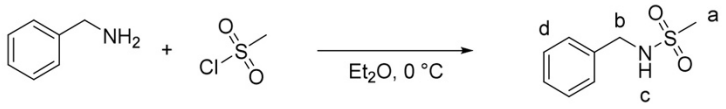

Scheme 11. Synthesis of ***N*-benzyl-mesylamide**

The compound was synthesized according to literature procedures[3]. A solution of benzylamine (15.3 mL, 139 mmol) in dry diethylether (360 mL) was cooled to 0 °C. Mesylchloride (5.2 mL, 66 mmol) was added dropwise. The reaction mixture was stirred overnight at room temperature. The precipitate was filtered and washed with diethylether. The organic phase was washed with 2 M hydrochloric acid and brine, dried over sodium sulfate and concentrated at reduced pressure. The resulting crude product was dissolved in THF (80 mL) and stirred for three hours at room temperature with a solution of 10% MeOH/ $NaHCO_3$ (40 mL). The mixture was concentrated at reduced pressure, the obtained syrup was dissolved in DCM. The organic phase was washed with water, dried over magnesium sulfate and concentrated at reduced pressure. The product was obtained as a colorless solid (7.83 g, 42 mmol, 30%). ^{1}H NMR (300 MHz, 295 K, Chloroform-*d*): δ 7.37–7.26 (m, 5H, d), 4.93 (s, 1H, c), 4.30 (d, 2H, J = 5.6 Hz, b), 2.84 (s, 3H, a).

Section B. Synthetic Protocols – Polymers.

All glassware was dried by *in vacuo* for at least three times. All reactants (except potassium bis(trimethylsilyl)amide (KHMDS)) were dried from benzene *in vacuo* for at least 6 h. The monomers and the BnNHMs-initiator were dissolved in 2 and 1 mL respectively anhydrous *N,N*-dimethylformamide (DMF). KHMDS was added very fast as a solid in argon-counter flow to the BnNHMs-solution and the sample boat was rinsed with another 1 mL DMF. The initiator-solution was transferred via syringe to the monomer-solution. For kinetic studies and syntheses of longer polymer chains due to the smaller amount, a stock solution of the initiator system was prepared and only the appropriate volume extracted and added to the monomer solution. The mixture was stirred at 55 °C for at least 18 h. To terminate the polymers, 0.5 mL degassed methanol were added and the reaction mixture was precipitated in ca. 30 mL methanol. The colorless solids were collected by centrifugation and dried at 70 °C *in vacuo.*

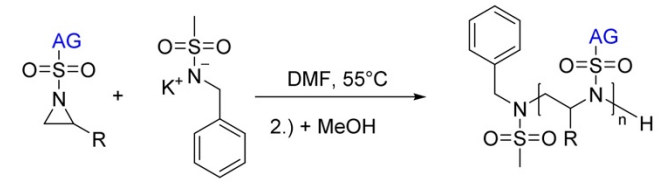

AG = Ns, Bs, Ts, Ms, Bus

Scheme 12. Azanionic polymerization of activated aziridines

Monitoring (co)polymerizations by real-time 1H NMR. All (co)polymerizations were carried out in analogy to the conventional procedure in a Schlenk-flask (compare Supp. Info.). Inside of a glove box under nitrogen the respective monomers were dissolved as a ca. 10 wt% solution in a total volume of 1 mL DMF-d7. The initiator solution in 1 mL DMF-d7 was prepared separately (exemplarily for the terpolymerization that is TsMAz (30.0 mg), MsMAz (19.2 mg), BsMAz (39.2 mg) and the initiator-system: BnNHMs (1.3 mg), Potassium bis(trimethylsilyl)-amide (KHMDS) (1.4 mg)). A conventional NMR-tube was filled with the reaction mixture and sealed with a rubber-septum. Prior to initiation, the pure monomer-solvent mixture was measured at 50 °C. From the stock solution of the initiator 100 μL were added to the monomer mixture, mixed quickly and inserted into the spectrometer. 1H NMR kinetics were recorded using a Bruker Avance III 700 and a Bruker Avance III 850. All spectra were referenced internally to residual proton signals of the deuterated solvent dimethylformamide at 8.03 ppm. The □/2-pulse for the proton measurements varied between 9.3 and 11 μs for the different frequency. The spectra of the polymerizations and terpolymerization were recorded at 700 MHz with 32 number of scans (equal to 404 s), a relaxation time of 2 s after every pulse over a period of at least 15 h. Quaterpolymerizations and the quinterpolymerization were recorded at 850 MHz with 64 number of scans (equal to 413 s) and a relaxation time of 2 s over a period of at least 17 h. No B-field optimizing routine was used over the kinetic measurement time. The relaxation rate (T1) of the protons was measured before the kinetic run with the inversion recovery method.[4]

Homo- and Copolymers

Poly(2-methyl-N-mesylaziridine) - P(MsMAz).

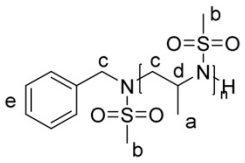

Scheme 13. Synthesis of **Poly(MsMAz)**

PMsMAz$_{124}$: [MsMAz (300.0 mg, 2.22 mmol), BnNHMs (9.3 mg, 50 μmol), KHMDS (10.1 mg, 50 μmol)]. ^{1}H NMR (300 MHz, 295 K, Methylene Chloride-d_2): δ 7.50–7.28 (m, e), 4.21–3.76 (m, d), 3.60–3.10 (m, c), 3.08–2.84 (m, b), 1.45–1.24 (m, a). M_n (SEC) = 4900 g/mol, $Đ$ = 1.08, M_n (NMR) = 16000 g/mol.

PMsMAz$_{168}$: [MsMAz (507.0 mg, 3.75 mmol), BnNHMs (2.8 mg, 15 μmol), KHMDS (3.0 mg, 15 μmol)]. ^{1}H NMR (300 MHz, 295 K, Methylene Chloride-d_2): δ 7.48–7.28 (m, e), 4.25–3.72 (m, d), 3.66–3.07 (m, c), 3.07–2.83 (m, b), 1.48–1.12 (m, 511H, a). M_n (SEC) = 11900 g/mol, $Đ$ = 1.15, M_n (NMR) = 22700 g/mol.

Poly(2-decyl-N-tosylaziridine) - (PTsDAz).

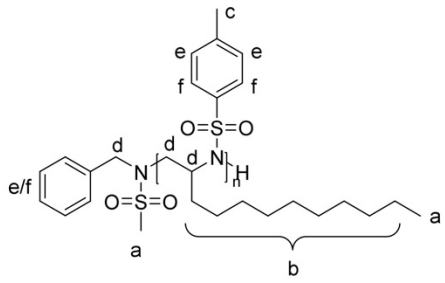

Scheme 14. Synthesis of **Poly(TsDAz)**

PTsDAz$_{26(theo)}$: [TsDAz (450.0 mg, 1.33 mmol), BnNHMs (9.3 mg, 50 μmol), KHMDS (10.1 mg, 50 μmol)]. ^{1}H NMR (300 MHz, 295 K, Methylene Chloride-d_2): δ 8.17–7.66 (m, f), 7.50–7.13 (m, e), 4.42–2.91 (m, d), 2.52–2.24 (m, c), 1.43–0.89 (m, b), 0.90–0.80 (m, a). M_n (SEC) = 4400 g/mol, $Đ$ = 1.10.

Poly(2-methyl-N-brosylaziridine) (PBsMAz)

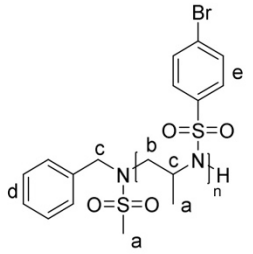

Scheme 15. Synthesis of **Poly(BsMAz)**

PBsMAz$_{22}$: [BsMAz (200.0 mg, 724 μmol), BnNHMs (6.7 mg, 36 μmol), KHMDS (7.2 mg, 36 μmol)]. ^{1}H NMR (300 MHz, 295 K, Methylene Chloride-d_2): δ 8.01–7.52 (m, e), 7.52-7.35 (m, d), 4.43–3.75 (m, c), 3.75–2.96 (m, b), 1.23–0.82 (m, a). M_n (SEC) = 3100 g/mol, $Đ$ = 1.10, M_n (NMR) = 6100 g/mol.

Poly(TsMAz-co-TsDAz).

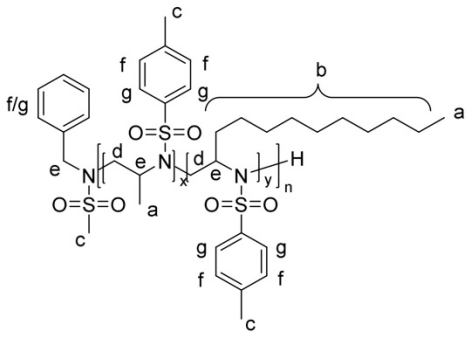

Scheme 16. Synthesis of **Poly(TsMAz-*co*-TsDAz)**

Poly(TsMAz$_{25(theo)}$-*co*-TsDAz$_{25(theo)}$): [TsMAz (211.3 mg, 1.0 mmol), TsDAz (337.5 mg, 1.0 mmol), BnNHMs (7.4 mg, 40 μmol), KHMDS (8.0 mg, 40 μmol)]. ^{1}H NMR (300 MHz, 295 K, Methylene Chloride-d_2): δ 8.01–7.52 (m, g), 7.41–6.99 (m, f), 4.42–3.63 (m, e), 3.61–2.55 (m, d), 2.49–2.13 (m, c), 1.31–0.86 (m, b), 0.84–0.69 (m, a). M_n (SEC) = 5200 g/mol, $Đ$ = 1.09.

Poly(BsMAz-co-MsMAz)

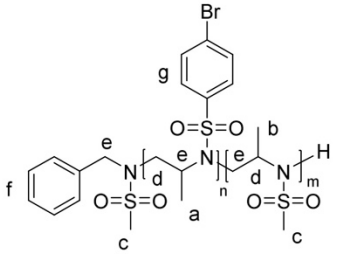

Scheme 17. Synthesis of **Poly(BsMAz-*co*-MsMAz)**

Poly(BsMAz$_{53}$-*co*-MsMAz$_{24}$): [BsMAz (306 mg, 1.1 mmol), MsMAz (150 mg, 1.1 mmol), BnNHMs (4.1 mg, 22 μmol), KHMDS (4.4 mg, 22 μmol)]. ^{1}H NMR (500 MHz, 298 K, Methylene Chloride-d_2): δ 7.97–7.55 (m, g), 7.52–7.36 (m, f), 4.48–3.76 (m, e), 3.76–3.07 (m,

d), 3.07-2.81 (m, c), 1.56–1.27 (m, b), 1.20–0.69 (m, a). M_n (SEC) = 3900 g/mol, $Đ$ = 1.14, M_n (NMR) = 17800 g/mol.

a) Poly(NsMAz-co-BsMAz-co-TsMAz-co-MsMAz).

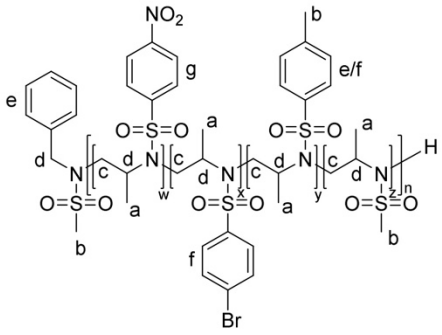

Scheme 18. Synthesis of **Poly(NsMAz-*co*-BsMAz-*co*-TsMAz-*co*-MsMAz)**

Poly(NsMAz$_{20(theo)}$-*co*-BsMAz$_{20(theo)}$-*co*-TsMAz$_{20(theo)}$-*co*-MsMAz$_{20(theo)}$): [MsMAz (75.0 mg, 555 μmol), TsMAz (117.2 mg, 555 μmol), BsMAz (153.2 mg, 555 μmol), NsMAz (134.4 mg, 555 μmol), BnNHMs (5.1 mg, 27.7 μmol), KHMDS (5.5 mg, 27.7 μmol)]. ^{1}H NMR (250 MHz, 297 K, Chloroform-*d*): δ 8.53–7.99 (m, g), 7.99–7.53 (m, f), 7.41–7.20 (m, e), 4.63–3.78 (m, d), 3.78–2.87 (m, c), 2.51–2.26 (m, b), 1.44–0.64 (m, a). M_n (SEC) = 4600 g/mol, $Đ$ = 1.16.

Copolymers for living polymerizations.

All copolymerizations were carried out in analogy to the conventional procedure. The first monomer and the BnNHMs-initiator were dissolved in 1 mL anhydrous *N,N*-dimethylformamide (DMF). KHMDS was added very fast as a solid in argon-counter flow to the BnNHMs-solution and the sample boat was rinsed with another 1 mL DMF. The initiator-solution was transferred via syringe to the monomer-solution. After stirring the mixture for 18 h at 55 °C, the second monomer was added and stirred for further 24 h at 55 °C.

Poly(NsMAz-block-TsMAz)

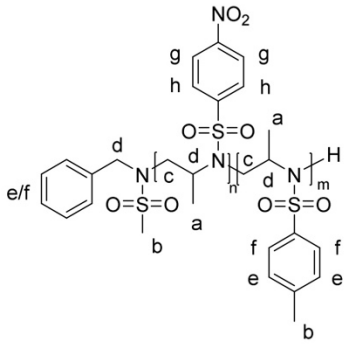

Scheme 19. Synthesis of **Poly(NsMAz-*block*-TsMAz)**

Poly(NsMAz$_{30(theo)}$-*block*-TsMAz$_{30(theo)}$): [1. NsMAz (115 mg, 473 μmol), 2. TsMAz (100 mg, 473 μmol), BnNHMs (2.9 mg, 16 μmol), KHMDS (3.2 mg, 16 μmol)]. ^{1}H NMR (250 MHz, 297 K, DMSO-d_6): δ 8.56–8.22 (m, h), 8.21–7.91 (m, g), 7.91–7.53 (m, f), 7.53–7.21 (m, e), 4.34–3.65 (m, d), 3.65–2.94 (m, c), 2.52–2.17 (m, b), 1.43–0.58 (m, a). M_n (SEC) = 7000 g/mol, $Đ$ = 1.20.

Poly(BsMAz-co-TsMAz)

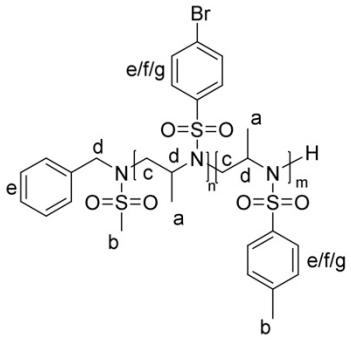

Scheme 20. Synthesis of **Poly(BsMAz-*block*-TsMAz)**

Poly(BsMAz$_{30(theo)}$-*block*-TsMAz$_{30(theo)}$): [1. BsMAz (131 mg, 473 μmol), 2. TsMAz (100 mg, 473 μmol), BnNHMs (2.9 mg, 16 μmol), KHMDS (3.2 mg, 16 μmol)]. ^{1}H NMR (250 MHz, 297 K, Chloroform-*d*): δ 7.97–7.74 (m, g), 7.74–7.49 (m, f), 7.39–7.17 (m, e), 4.54–3.82 (m, d), 3.82–2.99 (m, c), 2.49–2.22 (m, b), 1.22–0.70 (m, a). M_n (SEC) = 6100 g/mol, $Đ$ = 1.15.

Copolymers for kinetic measurements.

Poly(BsMAz-co-TsMAz-co-MsMAz).

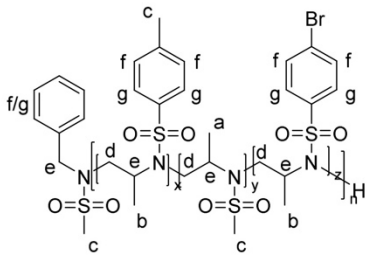

Scheme 21. Synthesis of **Poly(BsMAz-*co*-TsMAz-*co*-MsMAz)**

Poly(BsMAz$_{20(theo)}$-*co*-TsMAz$_{20(theo)}$-*co*-MsMAz$_{20(theo)}$): [TsMAz (30.0 mg, 142 μmol), MsMAz (19.2 mg, 142 μmol), BsMAz (39.2 mg, 142 μmol), BnNHMs (1.3 mg, 7.1 μmol), KHMDS (1.4 mg, 7.1 μmol)]. ^{1}H NMR (700 MHz, 323 K, *N,N*-dimethylformamide-d_7): δ 8.01–7.69 (m, g), 7.54-7.34 (m, f), 4.64–3.91 (m, e), 3.90–3.01 (m, d), 2.52–2.30 (m, c), 1.58–1.47 (m, b), 1.24–0.94 (m, a).

Poly(NsMAz-co-BsMAz-co-MsMAz-co-MsDAz).

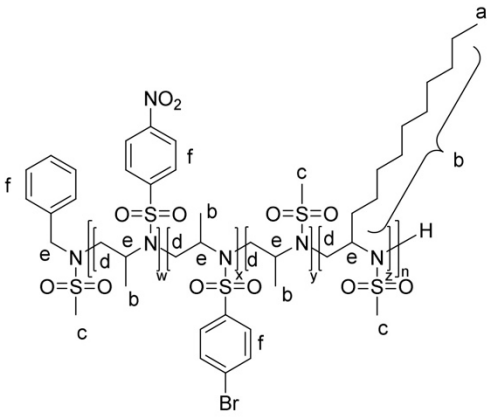

Scheme 22. Synthesis of **Poly(BsMAz-*co*-TsMAz-*co*-MsMAz-*co*-MsDAz)**

Poly(NsMAz$_{20(theo)}$-*co*-BsMAz$_{20(theo)}$-*co*-MsMAz$_{20(theo)}$-*co*-MsDAz$_{20(theo)}$): [MsMAz (15.0 mg, 111 μmol), MsDAz (29.0 mg, 111 μmol), BsMAz (30.6 mg, 111 μmol), NsMAz (26.9 mg, 111 μmol), BnNHMs (1.0 mg, 5.6 μmol), KHMDS (1.1 mg, 5.6 μmol)]. ^{1}H NMR (850 MHz, 323 K, *N,N*-dimethylformamide-d_7): δ 8.57–7.66 (m, f), 4.57–3.98 (m, e), 3.98–3.25 (m, d), 3.18–3.12 (m, c), 1.65–1.26 (m, b), 0.94–0.85 (m, a).

Poly(NsMAz-co-BsMAz-co-TsMAz-co-MsMAz).

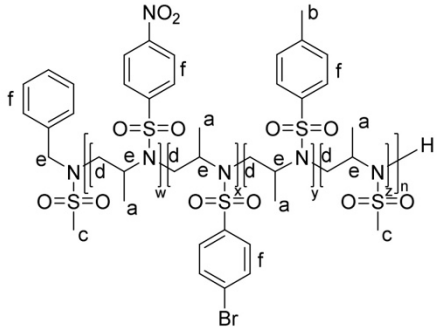

Scheme 23. Synthesis of **Poly(NsMAz-*co*-BsMAz-*co*-TsMAz-*co*-MsMAz)**

Poly(NsMAz$_{20(theo)}$-*co*-BsMAz$_{20(theo)}$-*co*-TsMAz$_{20(theo)}$-*co*-MsMAz$_{20(theo)}$): [MsMAz (15.0 mg, 111 μmol), TsMAz (23.4 mg, 111 μmol), BsMAz (30.6 mg, 111 μmol), NsMAz (26.9 mg, 111 μmol), BnNHMs (1.0 mg, 5.6 μmol), KHMDS (1.1 mg, 5.6 μmol)]. ^{1}H NMR (850 MHz, 323 K, *N,N*-dimethylformamide-d_7): δ 8.57–7.65 (m, f), 4.55–3.94 (m, e), 3.94–3.18 (m, d), 3.16–3.12 (m, c), 2.49–2.40 (m, b), 1.39–0.94 (m, a).

Poly(NsMAz-co-BsMAz-co-TsMAz-co-MsMAz-co-BusDAz).

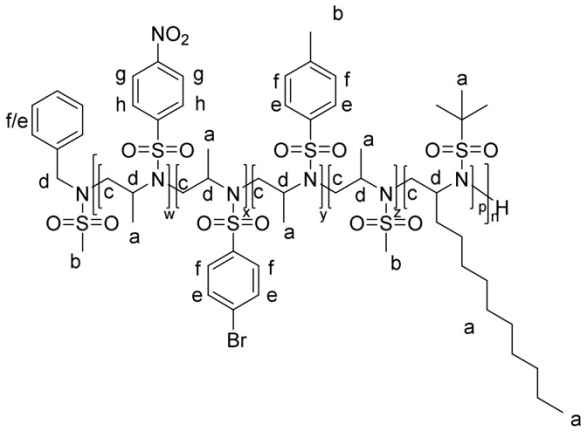

Scheme 24. Synthesis of **Poly(NsMAz-*co*-BsMAz-*co*-TsMAz-*co*-MsMAz-*co*-BusDAz)**

Poly(NsMAz$_{20(theo)}$-*co*-BsMAz$_{20(theo)}$-*co*-TsMAz$_{20(theo)}$-*co*-MsMAz$_{20(theo)}$-*co*-BusDAz$_{20(theo)}$): [MsMAz (13.0 mg, 96 μmol), BusDAz (29.2 mg, 96 mmol), TsMAz (20.3 mg, 96 μmol), BsMAz (26.6 mg, 96 μmol), NsMAz (23.3 mg, 96 μmol), BnNHMs (0.9 mg, 4.8 μmol), KHMDS (1.0 mg, 4.8 μmol)]. ^{1}H NMR (850 MHz, 323 K, *N,N*-dimethylformamide-d_7): δ 8.64–8.38 (m, h), 8.38–8.18 (m, g), 8.02–7.74 (m, f), 7.62–7.33 (m, e), 4.56–3.86 (m, d), 3.86–3.19 (m, c), 2.54–2.37 (m, b), 1.68–0.93 (m, a).

Section C. Spectroscopic Characterization

Small molecules

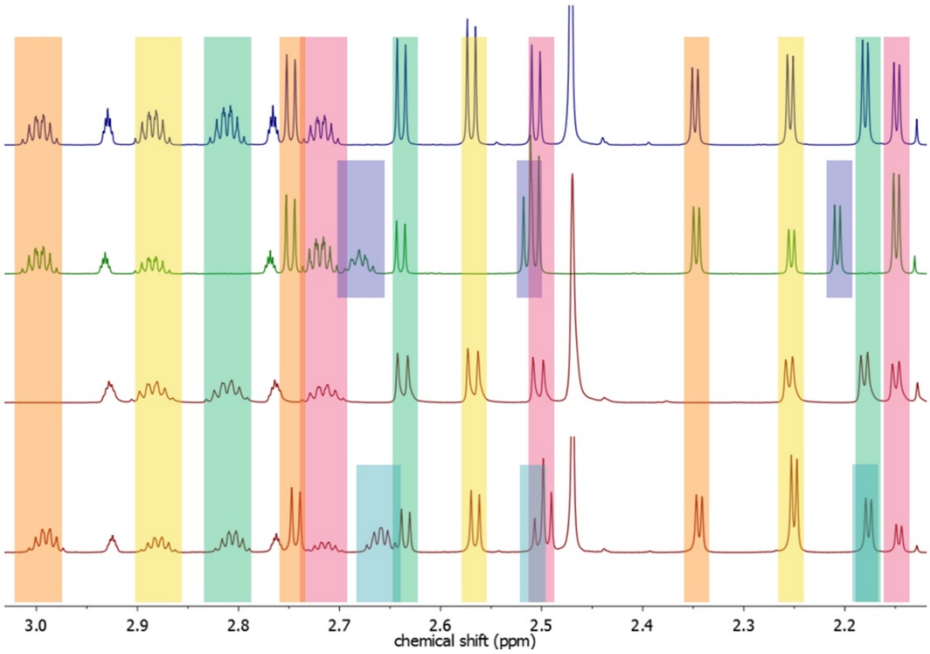

Supplementary Figure 1-I. Overlay of the ^{1}H NMR spectra of monomer mixtures showing no signal overlap for all monomer combinations. Color codes of the monomers: NsMAz (orange), BsMAz (yellow), TsMAz (green), MsMAz (red), MsDAz (blue) and BusDAz (cyan).

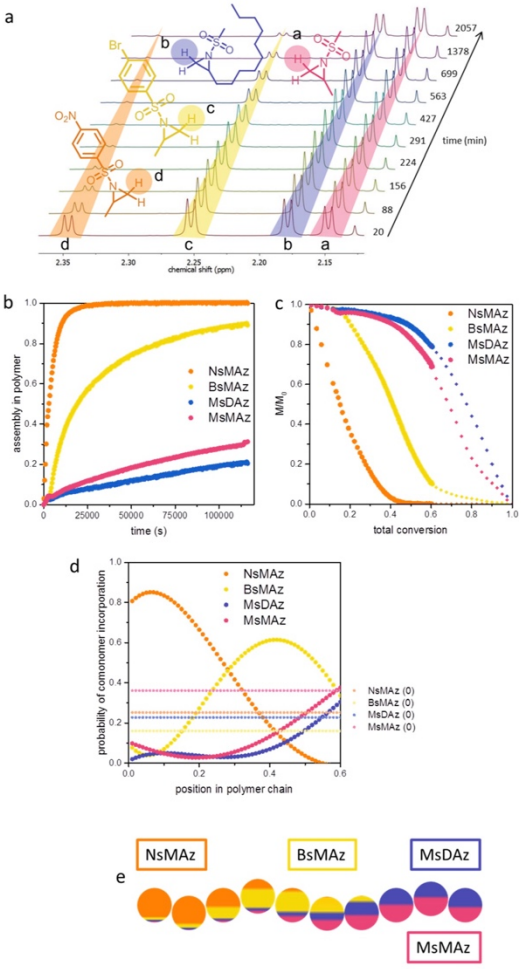

Supplementary **Figure 1-II.** One-pot synthesis of an AB(CD)-quasi-terblock copolymer of NsMAz, BsMAz, MsMAz and MsDAz. (a) Zoom into the real-time ^{1}H NMR spectra of the quaterpolymerization showing the consumption of the monomers. NsMAz, (orange), BsMAz (yellow), MsMAz (red) and MsDAz (blue). (b) Assembly of monomer in the polymer over time. (c) Normalized monomer concentrations in the solution *vs.* total conversion (diamonds: extrapolated data). (d) Probability of comonomer incorporation *vs.* relative position in the polymer chains and theoretical incorporation in case of an ideal random copolymerization (straight, bright lines (0)). (e) Visualization of a single chain for poly(NsMAz-*co*-BsMAz-*co*-(MsMAz-*co*-MsDAz)).

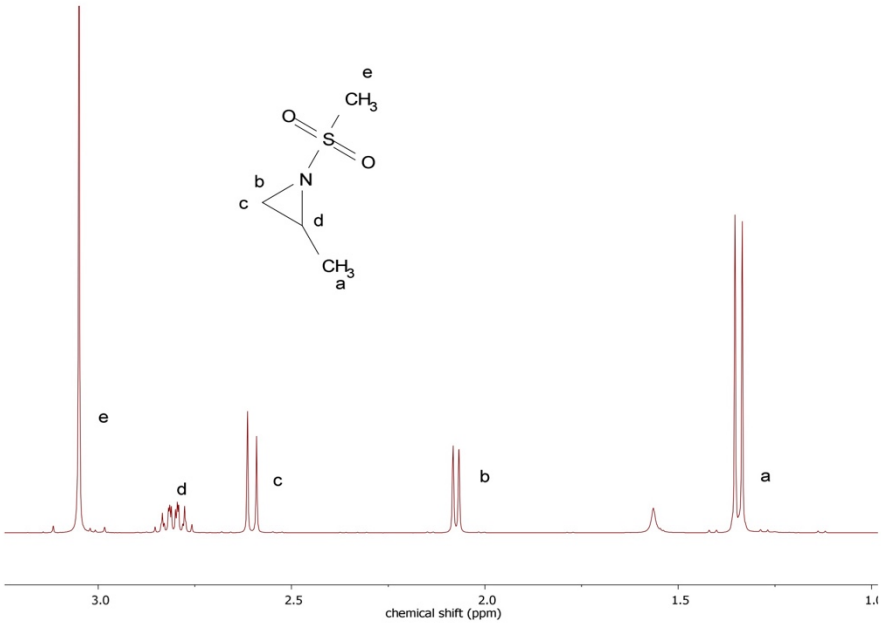

Supplementary Figure 2. ^{1}H NMR (300 MHz, 295 K, Chloroform-*d*) of 2-Methyl-*N*-mesylaziridine (MsMAz).

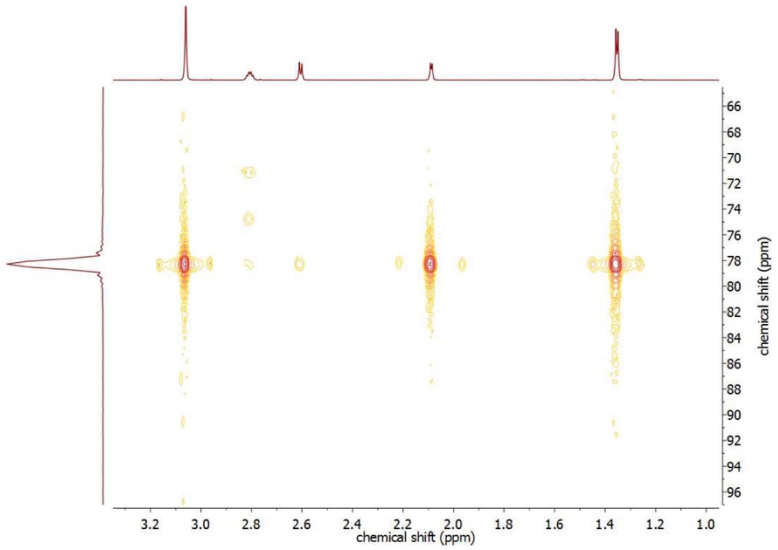

Supplementary Figure 3. $^{1}H^{15}N$, HMBC-^{15}N-spectrum (71 MHz, 298 K, Chloroform-*d*) of 2-Methyl-*N*-mesylaziridine (MsMAz).

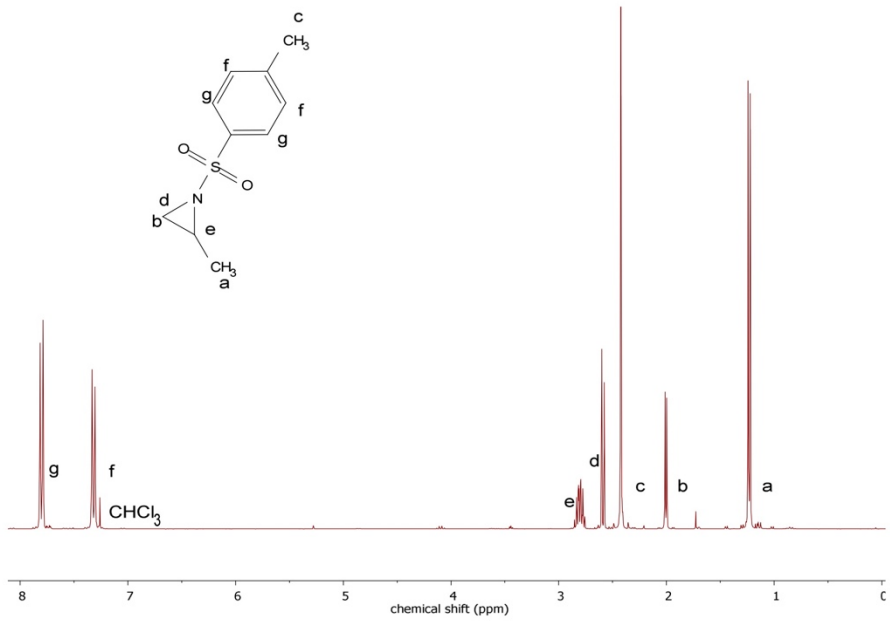

Supplementary Figure 4. ^{1}H NMR (300 MHz, 295 K, Chloroform-*d*) of 2-Methyl-*N*-tosylaziridine (TsMAz).

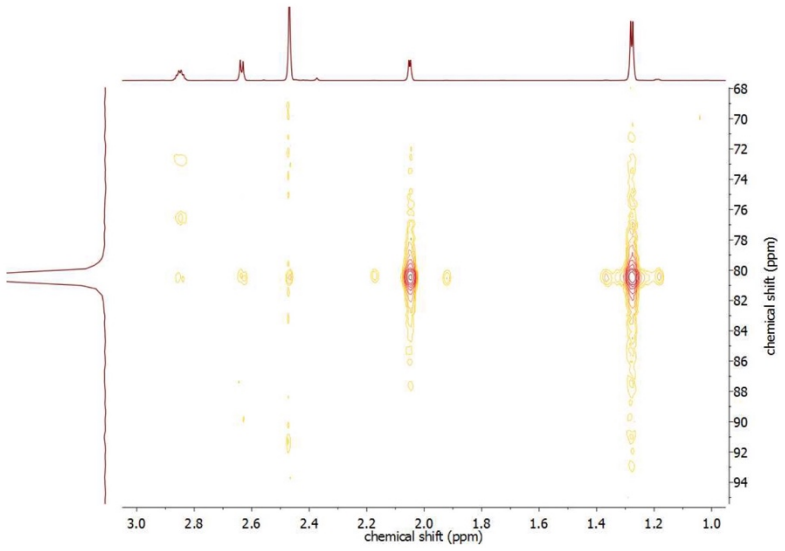

Supplementary Figure 5. ^{1}H^{15}N, HMBC-^{15}N-spectrum (71 MHz, 298 K, Chloroform-*d*) of 2-Methyl-*N*-tosylaziridine (TsMAz).

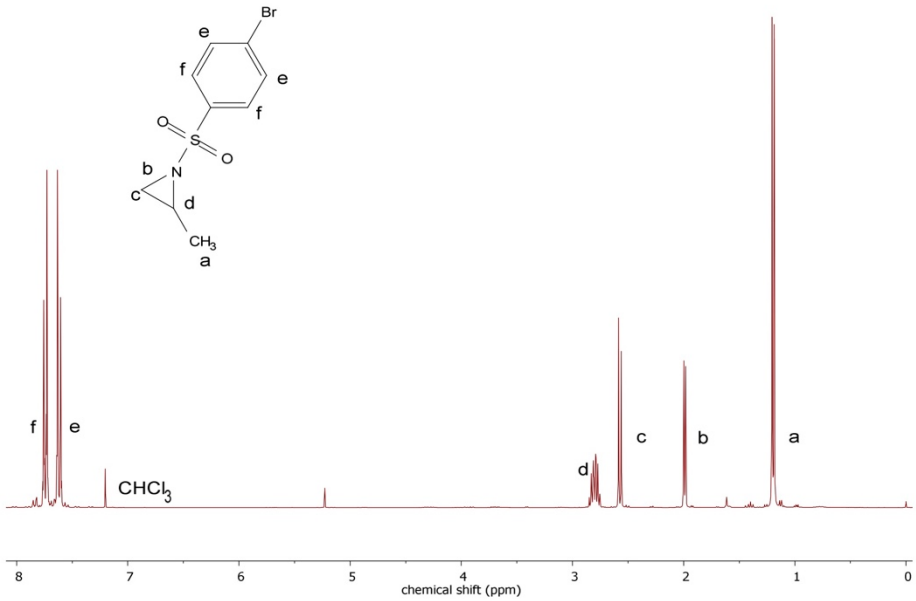

Supplementary Figure 6. ^{1}H NMR (300 MHz, 295 K, Chloroform-*d*) of 2-Methyl-*N*-brosylaziridine (BsMAz).

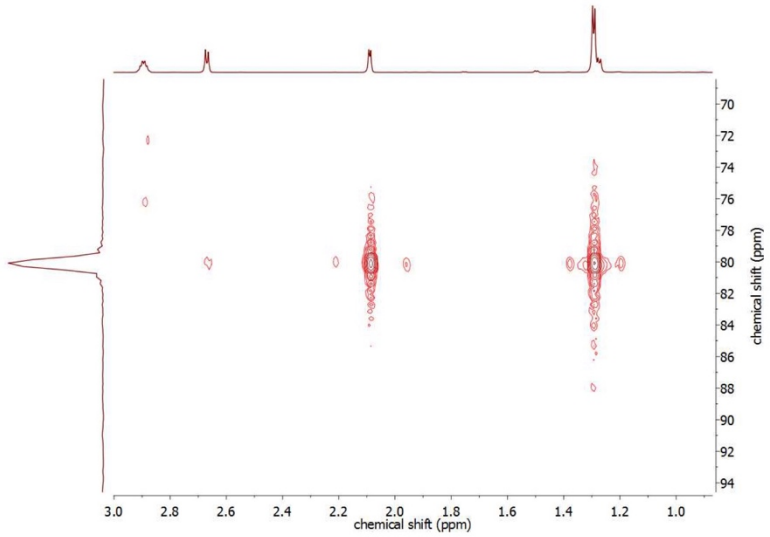

Supplementary Figure 7. $^{1}H^{15}N$, HMBC-^{15}N-spectrum (71 MHz, 298 K, Chloroform-*d*) of 2-Methyl-*N*-brosylaziridine (BsMAz).

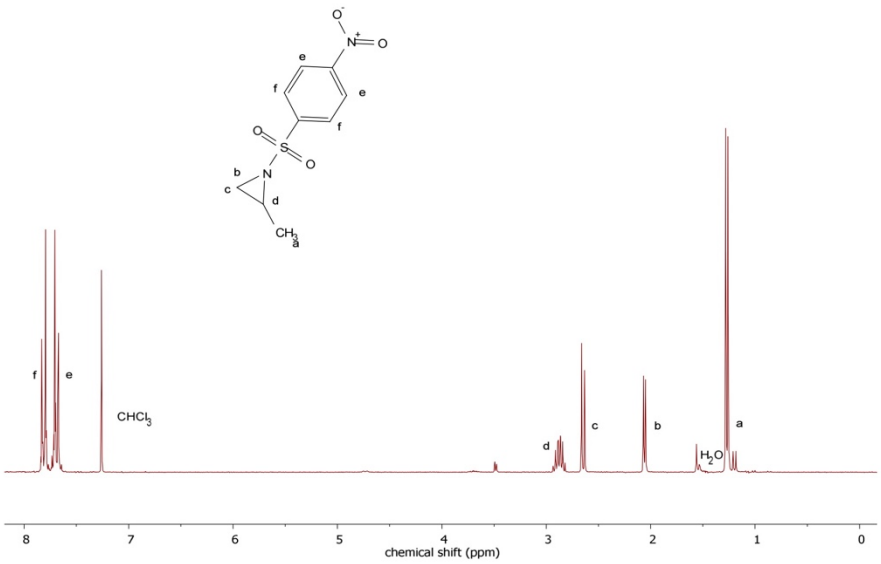

Supplementary Figure 8. ^{1}H NMR (250 MHz, 297 K, Chloroform-*d*) of 2-Methyl-*N*-nosylaziridine (NsMAz).

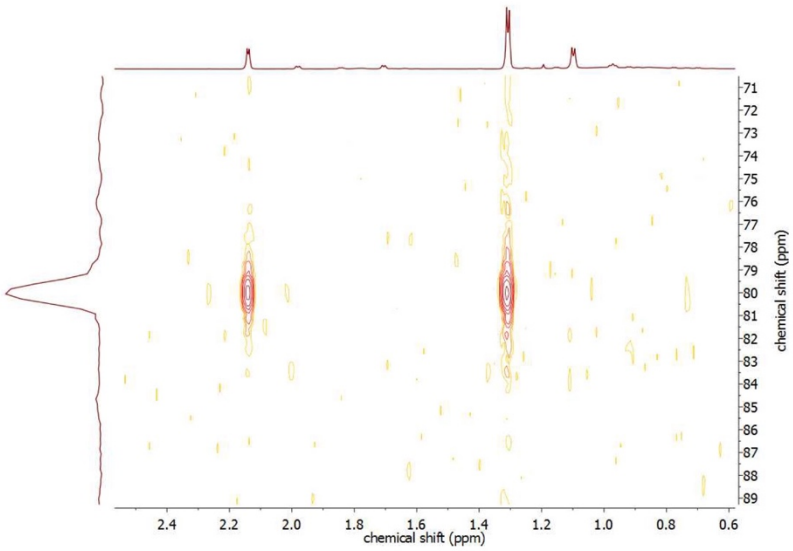

Supplementary Figure 9. ^{1}H^{15}N, HMBC-^{15}N-spectrum (71 MHz, 298 K, Chloroform-*d*) of 2-Methyl-*N*-nosylaziridine (NsMAz).

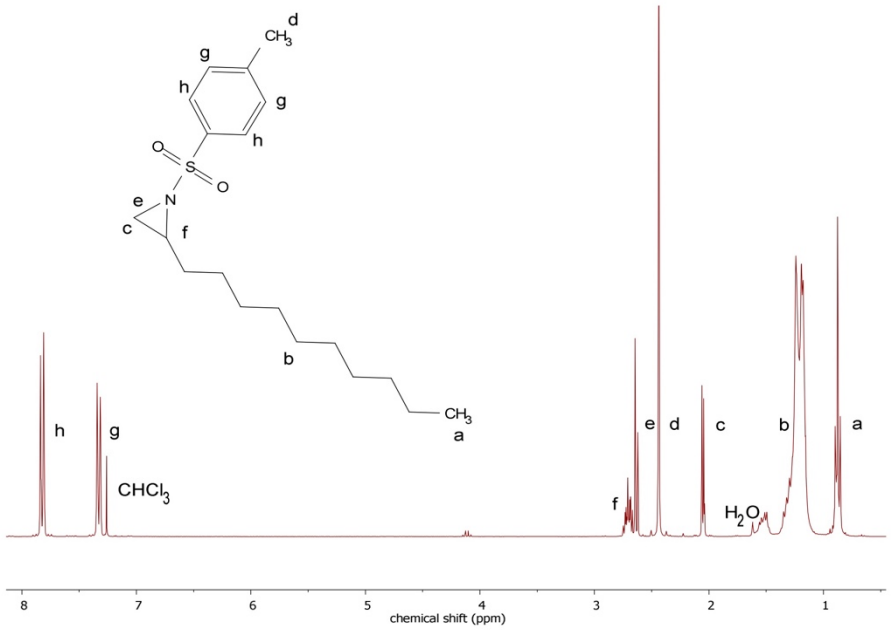

Supplementary Figure 10. ^{1}H NMR (300 MHz, 295 K, Chloroform-*d*) of 2-Decyl-*N*-tosylaziridine (TsDAz).

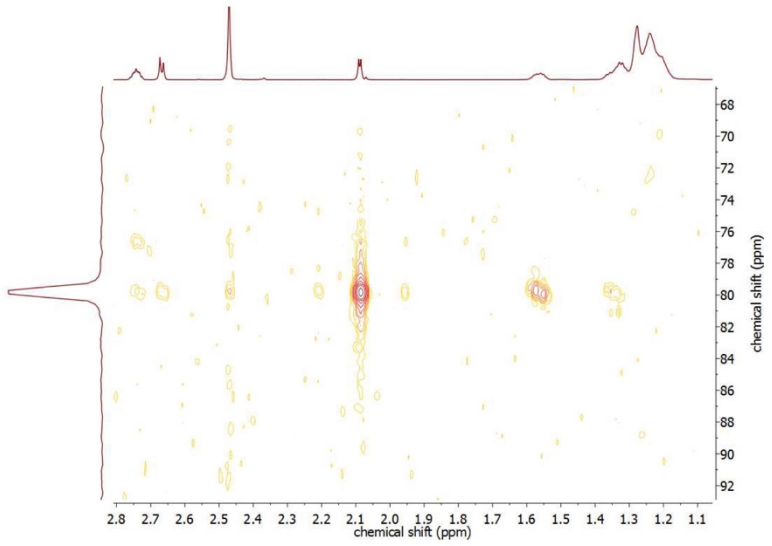

Supplementary Figure 11. ^{1}H^{15}N, HMBC-^{15}N-spectrum (71 MHz, 298 K, Chloroform-*d*) of 2-Decyl-*N*-tosylaziridine (TsDAz).

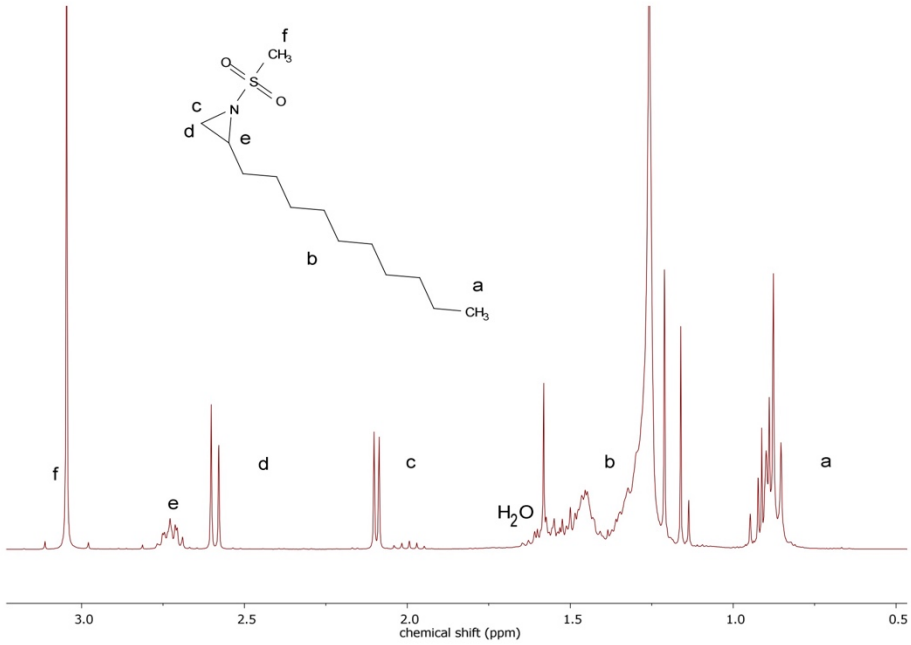

Supplementary Figure 12. ^{1}H NMR (300 MHz, 295 K, Chloroform-*d*) of 2-Decyl-*N*-mesylaziridine (MsDAz).

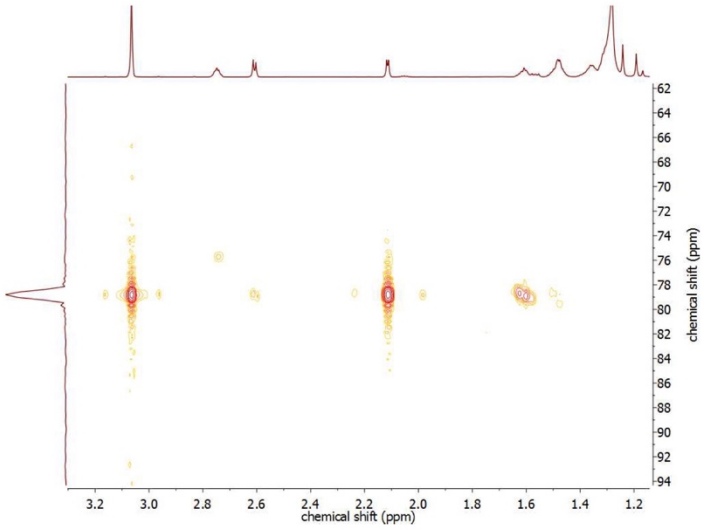

Supplementary Figure 13. ^{1}H^{15}N, HMBC-^{15}N-spectrum (71 MHz, 298 K, Chloroform-*d*) of 2-Decyl-*N*-mesylaziridine (MsDAz).

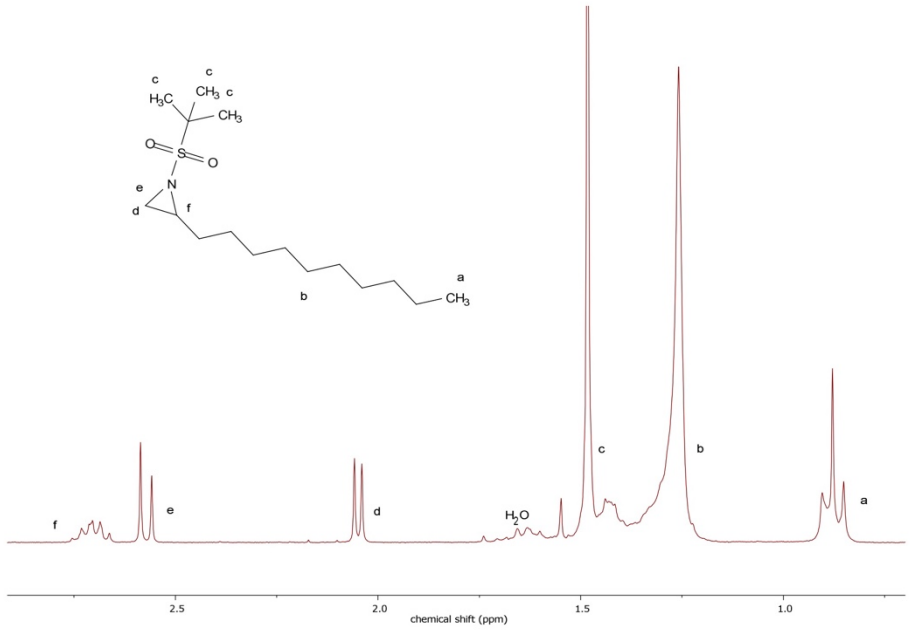

Supplementary Figure 14. ^{1}H NMR (250 MHz, 297 K, Chloroform-*d*) of 2-Decyl-*N*-busylaziridine (BusDAz).

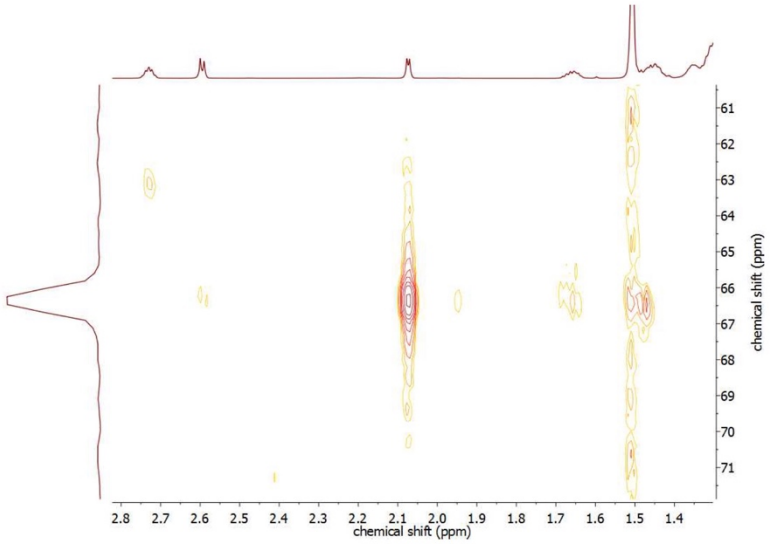

Supplementary Figure 15. ^{1}H^{15}N, HMBC-^{15}N-spectrum (71 MHz, 298 K, Chloroform-*d*) of 2-Decyl-*N*-busylaziridine (BusDAz).

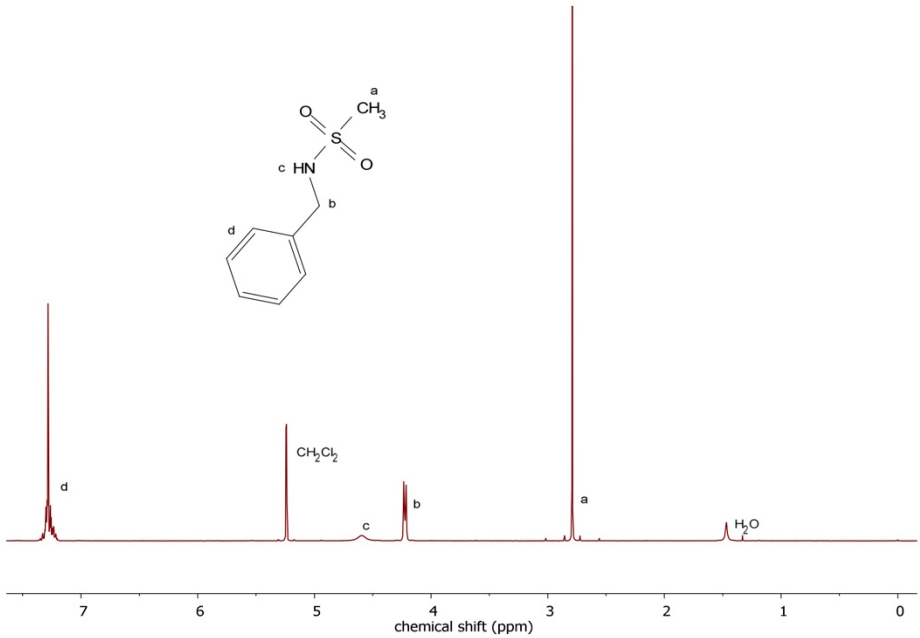

Supplementary Figure 16. ^{1}H NMR (300 MHz, 295 K, Chloroform-*d*) of *N*-benzyl-mesylamide (BnNHMs).

Polymers

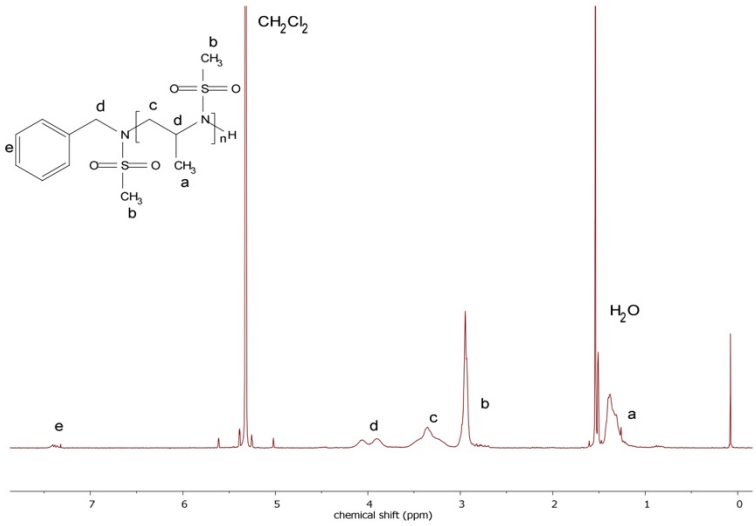

Supplementary Figure 17. ^{1}H NMR (300 MHz, 295 K, Methylene Chloride-d_2) of Poly(2-methyl-*N*-mesylaziridine) - P(MsMAz).

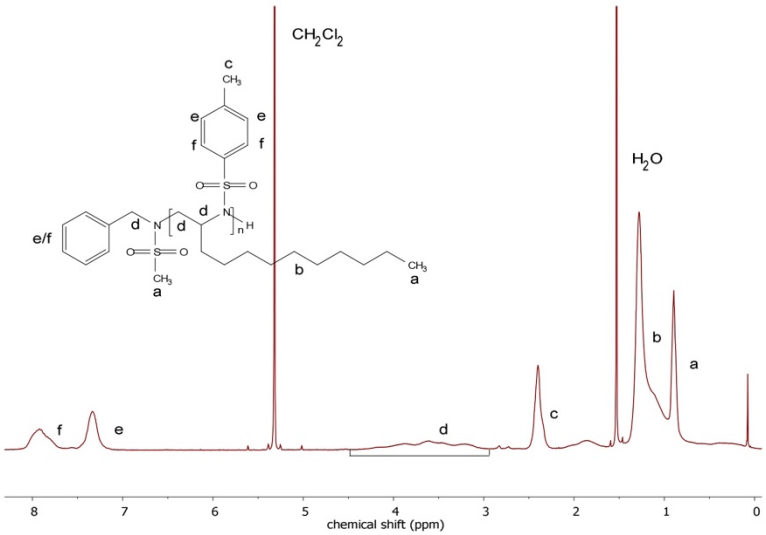

Supplementary Figure 18. ^{1}H NMR (300 MHz, 295 K, Methylene Chloride-d_2) of Poly(2-decyl-*N*-tosylaziridine) - P(TsDAz).

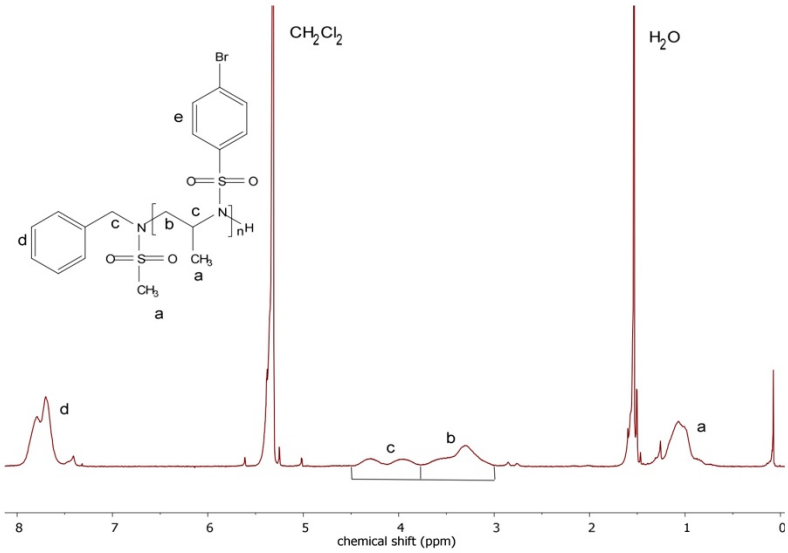

Supplementary Figure 19. ^{1}H NMR (300 MHz, 295 K, Methylene Chloride-d_2) of Poly(2-methyl-*N*-brosylaziridine) - P(BsMAz).

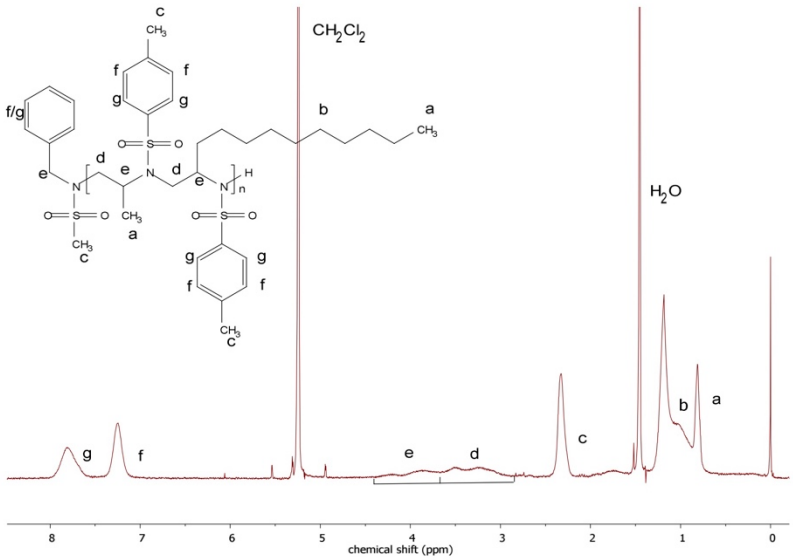

Supplementary Figure 20. ^{1}H NMR (300 MHz, 295 K, Methylene Chloride-d_2) of Poly(2-methyl-*N*-tosylaziridine)-*co*-(2-decyl-*N*-tosylaziridine) - P(TsMAz-*co*-TsDAz).

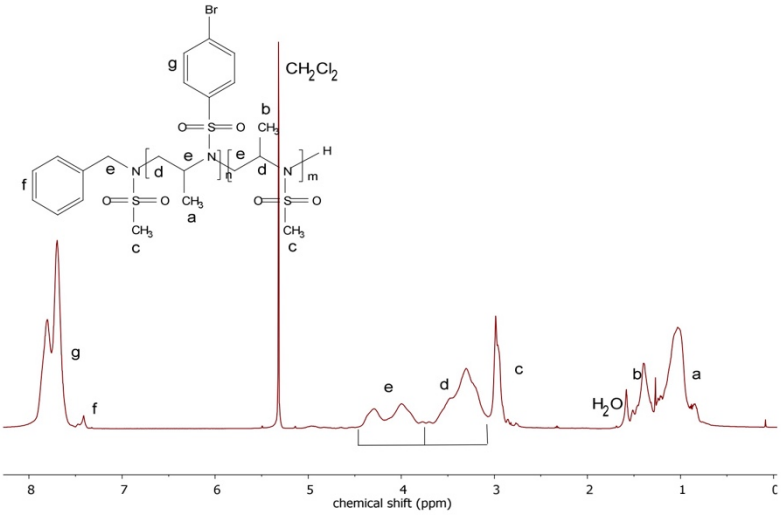

Supplementary Figure 21. ^{1}H NMR (500 MHz, 298 K, Methylene Chloride-d_2) of Poly(2-methyl-*N*-brosylaziridine)-*co*-(2-methyl-*N*-mesylaziridine) - P(BsMAz-*co*-MsMAz).

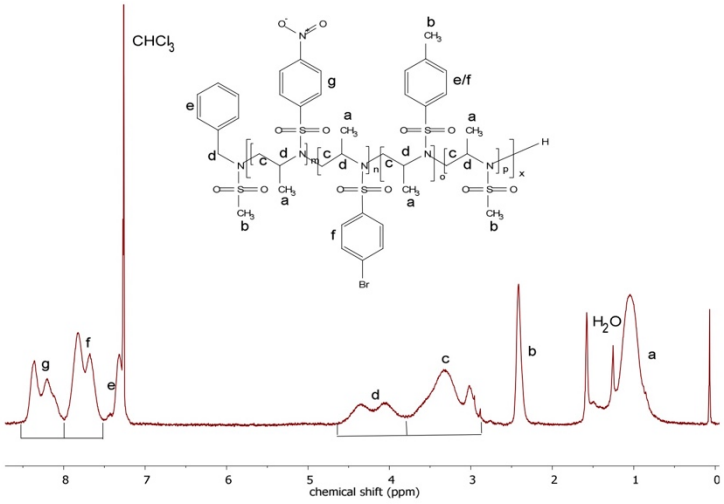

Supplementary Figure 22. ^{1}H NMR (250 MHz, 297 K, Chloroform-*d*) of Poly(2-methyl-*N*-nosylaziridine-*co*-2-methyl-*N*-brosylaziridine-*co*-2-methyl-*N*-tosylaziridine-*co*-2-methyl-*N*-mesylaziridine) - P(NsMAz-*co*-BsMAz-*co*-TsMAz-*co*-MsMAz).

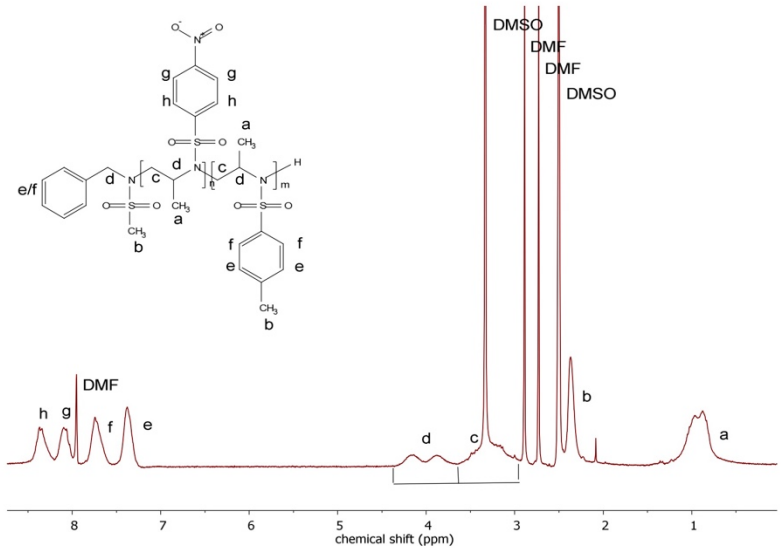

Supplementary Figure 23. ^{1}H NMR (250 MHz, 297 K, Dimethyl sulfoxide-d_6) of Poly(2-methyl-*N*-nosylaziridine)-*block*-(2-methyl-*N*-tosylaziridine) - P(NsMAz-*block*-TsMAz).

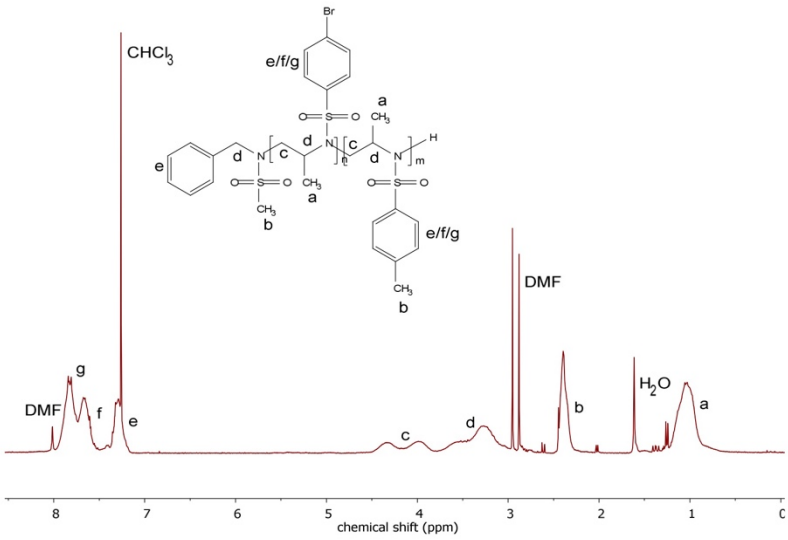

Supplementary Figure 24. ^{1}H NMR (250 MHz, 297 K, Chloroform-*d*) of Poly(2-methyl-*N*-brosylaziridine)-*block*-(2-methyl-*N*-tosylaziridine) - P(BsMAz-*block*-TsMAz).

Section D. Representative SECs of several homo and copolymers.

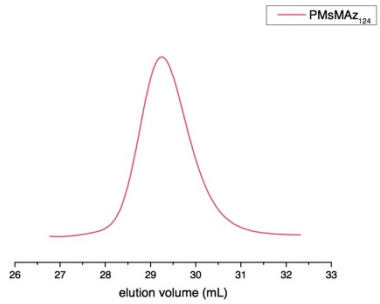

Supplementary Figure 25. SEC traces of Poly(2-methyl-*N*-mesylaziridine) - P(MsMAz) in DMF (RI signal).

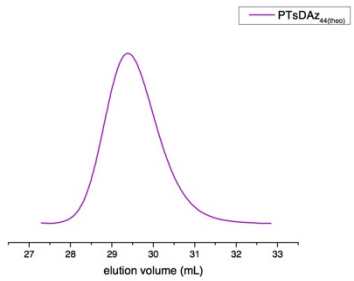

Supplementary Figure 26. SEC traces of Poly(2-decyl-*N*-tosylaziridine) - P(TsDAz) in DMF (RI signal).

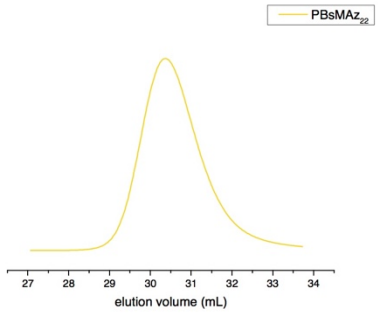

Supplementary Figure 27. SEC traces of Poly(2-methyl-*N*-brosylaziridine) - P(BsMAz) in DMF (RI signal).

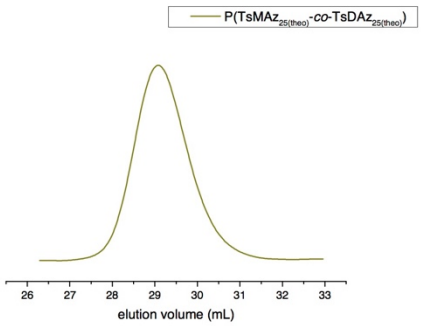

Supplementary Figure 28. SEC traces of Poly(2-methyl-*N*-tosylaziridine)-*co*-(2-decyl-*N*-tosylaziridine) - P(TsMAz-*co*-TsDAz) in DMF (RI signal).

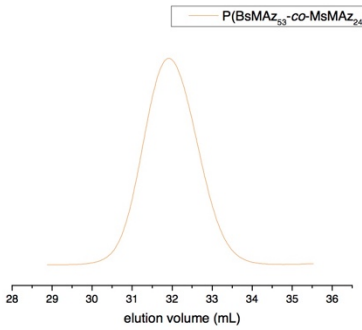

Supplementary Figure 29. SEC traces of Poly(2-methyl-*N*-brosylaziridine)-*co*-(2-methyl-*N*-mesylaziridine) - P(BsMAz-*co*-MsMAz) in DMF (RI signal).

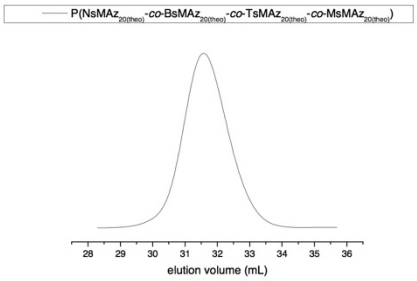

Supplementary Figure 30. SEC traces of Poly(2-methyl-*N*-nosylaziridine-*co*-2-methyl-*N*-brosylaziridine-*co*-2-methyl-*N*-tosylaziridine-*co*-2-methyl-*N*-mesylaziridine) - P(NsMAz-*co*-BsMAz-*co*-TsMAz-*co*-MsMAz) in DMF (RI signal).

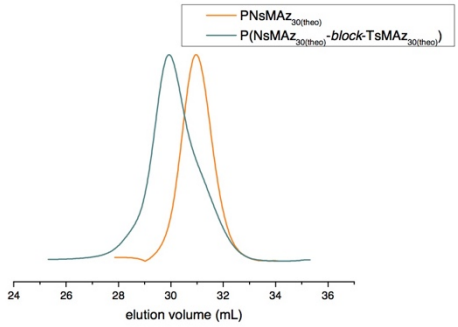

Supplementary Figure 31. SEC traces of Poly(2-methyl-*N*-nosylaziridine) and Poly(2-methyl-*N*-nosylaziridine)-*block*-(2-methyl-*N*-tosylaziridine) after sequential addition of TsMAz - P(NsMAz-*block*-TsMAz) in DMF (RI signal).

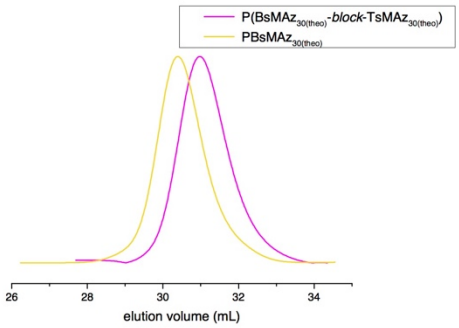

Supplementary Figure 32. SEC traces of Poly(2-methyl-*N*-brosylaziridine) and Poly(2-methyl-*N*-brosylaziridine)-*block*-(2-methyl-*N*-tosylaziridine) after sequential addition of TsMAz - P(BsMAz-*block*-TsMAz) in DMF (RI signal).

Section E. Thermal Characterization

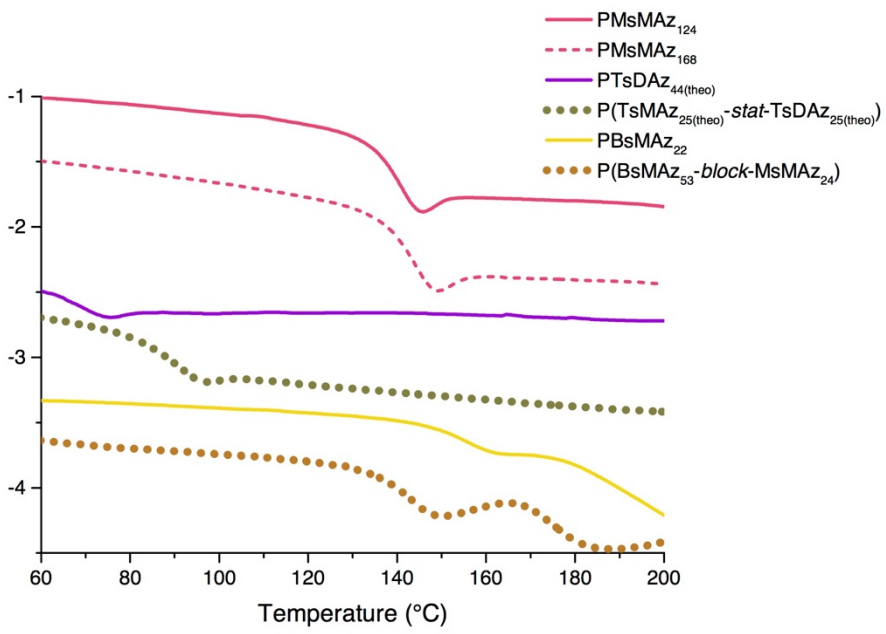

Supplementary Figure 33. DSC curves (3rd run (heating)) of representative poly(aziridine)s – homopolymers, random copolymers, diblock copolymers.

Section F. k-values

Table 1. Propagation rate constants (k-values) calculated from kinetic ^{1}H NMR measurements from homopolymerizations, using $\ln(M_0/M_t) = kt$.

	NsMAz	BsMAz	TsMAz	MsMAz	BusDAz
k / 1ms^{-1}	97	71	41	15	5

Section G. References

[1] I. C. Stewart, C. C. Lee, R. G. Bergman, F. D. Toste, *Journal of the American Chemical Society* **2005**, *127*, 17616-17617.

[2] J. U. Jeong, B. Tao, I. Sagasser, H. Henniges, K. B. Sharpless, *Journal of the American Chemical Society* **1998**, *120*, 6844-6845.

[3] D. C. Johnson, T. S. Widlanski, *J. Org. Chem.* **2003**, *68*, 5300-5309.

[4] R. Freeman, H. D. W. Hill, R. Kaptein, *J. Magn. Reson.* **1972**, *7*, 327-329.

ACS Macro Letters

Letter

pubs.acs.org/macroletters

Functional Group Distribution and Gradient Structure Resulting from the Living Anionic Copolymerization of Styrene and *para*-But-3-enyl Styrene

Adrian Natalello,[†,‡] Arda Alkan,[†,§] Philipp von Tiedemann,[†] Frederik R. Wurm,*[,§] and Holger Frey*[,†]

[†]Institute of Organic Chemistry, Johannes Gutenberg-University (JGU), Duesbergweg 10-14, 55128 Mainz, Germany

[‡]Graduate School Materials Science in Mainz, Staudinger Weg 9, D-55128 Mainz, Germany

[§]Max Planck Institute for Polymer Research (MPI-P), Ackermannweg 10, D-55128 Mainz, Germany

Supporting Information

ABSTRACT: The functional group distribution along the polymer backbone resulting from the living anionic copolymerization of styrene (S) and *para*-but-3-enyl styrene (*p*BuS) was investigated in cyclohexane at room temperature. A variety of copolymers with different comonomer contents $x(S) = 0-0.84$ have been synthesized with molecular weight dispersities $M_w/M_n \leq 1.12$. All polymers have been characterized in detail by ^{1}H NMR spectroscopy, size exclusion chromatography (SEC), and differential scanning calorimetry (DSC). A detailed understanding of the monomer sequence distribution during the copolymerization was achieved by real-time ^{1}H NMR spectroscopy. This technique permits us to determine the changing monomer concentration of each monomer in stock throughout the reaction. Consequently, monomer incorporation and thus the probability of incorporation can be determined at any time of the copolymerization, and a precise determination of the functional group density along the polymer chain is possible. To demonstrate accessibility of the olefin side chains of the copolymer for transformations, quantitative thiol−ene addition of a cysteine derivative has been studied.

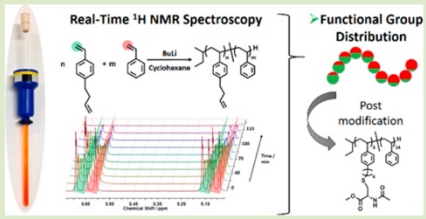

Living anionic polymerization (LAP) was discovered 60 years ago by Michael Szwarc and still represents the key technique in terms of high molecular weight (MW) polymers, narrow molecular weight distributions (MWDs), block copolymers, terminal functionalized polymers, and complex polymer architectures.[1−7] Even if functional groups are limited in carbanionic polymerizations, the control of MW without the use of a heavy metal catalyst or additional ligands makes this technique superior to many other controlled polymerization techniques. However, in contrast to radical polymerization, simultaneous copolymerization (often called "random copolymerization") of different monomers by living (carb)anionic polymerization is a rather neglected field, although a detailed understanding and control of the monomer sequence distribution during a copolymerization are of growing interest.[8−11] First attempts to tailor the monomer sequence distribution in LAP were made 50 years ago. For example, knowing that diphenylethylene (DPE) does not self-propagate, Okamoto and co-workers synthesized alternating copolymers of DPE with styrene (S), isoprene (I), or butadiene.[12−14] Recently, Hutchings and co-workers enlarged this concept investigating the simultaneous terpolymerization of S, DPE, and functionalized DPE derivatives. Due to different electron densities of the double bonds in pure DPE and the functionalized analogues, an enhanced degree of monomer sequence control has been achieved.[15,16]

In contrast, direct oxyanionic copolymerizations of epoxide derivatives which are usually more tolerant to impurities but, above all, much slower have been investigated in several reports. Relying on the rather slow propagation of living oxyanionic copolymerizations our group investigated the monomer sequence distribution during the polymerization via real-time ^{1}H NMR or ^{13}C NMR spectroscopy.[17,18] This technique allows us to follow the consumption of each monomer, respectively, and the growth of the polymer backbone at any point of the polymerization.[19−21] Very recently, we studied carbanionic copolymerizations by real-time ^{1}H NMR spectroscopy of two different comonomer pairs: Although the vinyl bonds of the protected *p*-hydroxystyrene (*p*HS) derivatives, *p*-(1-ethoxy ethoxy)styrene (*p*EES) and 4-*tert*-butoxystyrene (*t*BuOS), appear to be chemically very similar, it was found that *t*BuOS was incorporated preferentially. As expected, the copolymerization of the chemically more different comonomers S and *p*EES leads to a pronounced gradient polymer structure.[22]

Surprisingly, to date only very few reports use in situ techniques to follow living copolymerizations.[23−25] In 1993 Long and co-workers investigated the copolymerization of S

Received: April 28, 2014
Accepted: May 27, 2014

and I by near-infrared spectroscopy.[26] Fontanille, Gnanou et al. further expanded this work by combining mid-infrared and UV−visible spectroscopy.[27]

In 1999 Ruckenstein introduced the nonprotected bifunctional monomer 4-(vinylphenyl)-1-butene and investigated the living anionic homo- and copolymerization with S.[28,29] We prefer to handle this compound as *para*-but-3-enyl styrene (*p*BuS) to clarify the relation to S. This monomer is interesting as it allows the direct introduction of olefins via carbanionic polymerization (without protective groups). A different reactivity of *p*BuS and S is expected due to the inductive effects of the substituent. Herein, we use the real-time ^{1}H NMR spectrometric tool to investigate the living anionic copolymerization behavior of S with *p*BuS in cyclohexane at room temperature. To the best of our knowledge this is the first report on the sequence distribution monitoring of a copolymerization via real-time ^{1}H NMR spectroscopy using a nonprotected bifunctional comonomer. Monomer sequence distribution is the key for many applications and to mimic control of biological molecules. Achieving this knowledge is of high importance and would be desirable to gain with classical monomers and polymerization techniques.

We chose *p*BuS as a bifunctional monomer that is suitable for carbanionic polymerization and reinvestigate the copolymerization with S with respect to monomer sequence distribution.[28,29] To monitor the monomer sequence in situ, we first investigated the homopolymerization of *p*BuS in cyclohexane to restrict the reaction kinetics. From the data shown in the Supporting Information (SI) (Table S1 and Figure S2 SEC), it is obvious that prolonged reaction times lead to bimodal MWDs due to branching side reactions with the pendant double bonds. However, for reaction times not exceeding 2.5 h, narrow and monomodal molecular weight distributions are obtained, and no side reactions are observed in the ^{13}C NMR spectrum (Figure S3, SI). However, to guarantee quantitative monomer conversion, no polymers with molecular weights higher than 6700 g·mol^{-1} have been synthesized (see Table 1). Well-defined copolymers with high MW are accessible only in polar solvent mixtures (of toluene and THF (2:1 by volume) at −40 °C) resulting in strongly reduced reaction times which are undesirable for the in situ kinetics studied herein.[29] All synthesized polymers have been characterized by SEC, ^{1}H NMR spectroscopy, and differential scanning calorimetry (DSC).

Table 1. Characterization Data for Homo- and Copolymers Based on *para*-But-3-enyl Styrene (*p*BuS) and Styrene (S)

#	polymer[a]	x(S)[b]	M_n[a]	M_n[c]	$Đ$[c]	T_g/°C[d]
1	P*p*BuS$_{42}$	0	6700	7900	1.12	−13
2	P*p*BuS$_{33}$-*co*-PS$_{6.5}$	0.18	6000	6600	1.11	22
3	P*p*BuS$_{14}$-*co*-PS$_{14}$	0.50	3700	4500	1.12	35
4	P*p*BuS$_3$-*co*-PS$_{14}$	0.79	2000	2100	1.09	40
5	P*p*BuS$_4$-*co*-PS$_{33}$	0.90	4100	4100	1.08	45
6	(P*p*BuS-Cys)$_3$-*co*-PS$_{14}$	0.79	2500	2500	1.10	n.d.

[a]Number-average molecular weight (in g·mol^{-1}), calculated from ^{1}H NMR spectra. [b]Mole fraction styrene. [c]Number-average molecular weight and molecular weight dispersity $Đ$ determined via SEC in DMF (vs PS standards). [d]Glass transition temperature (T_g) determined via DSC.

In contrast to PS (M_n = 4000 g·mol^{-1}) with a glass transition temperature (T_g) of ca. 80 °C,[30] P*p*BuS (#1, M_n = 6 700 g·mol^{-1}) exhibits a rather low T_g of −13 °C, which is clearly a consequence of the flexible butenyl side chains. With increasing amount of S within the copolymers, P*p*BuS-*co*-PS (#2−5, at similar molecular weight), the T_g values also increase, reflecting the (co)polymer composition (Scheme 1).

Scheme 1. Synthetic Strategy for the Synthesis of P*p*BuS-*co*-PS and Subsequent Cysteine Functionalization

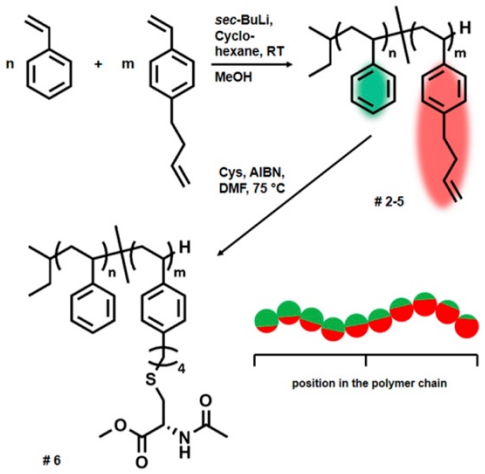

Also NMR spectra of the final copolymers allow determining the copolymer composition; however, for investigating the monomer sequence distribution within the copolymer chains, real-time ^{1}H NMR spectroscopy was employed. The carbanionic copolymerization was carried out in a conventional NMR tube in analogy to the batch procedure. The reaction mixture was prepared inside an argon-filled glovebox, and the tube was sealed with a rubber septum. Prior to the initiation of the polymerization, an ^{1}H NMR spectrum of the reaction mixture was recorded to calibrate the equipment and to determine the exact comonomer ratios in the comonomer mixture at t = 0 s (x(*p*BuS) = 0.55) by comparing the integrals of the styrenic vinyl double bonds of *p*BuS (δ = 5.58 ppm, dd, J = 15.4, 1.1 Hz and δ = 5.06 ppm, dd, J = 10.9, 1.1 Hz) and S (δ = 5.63 ppm, dd, J = 15.4, 1.1 Hz and δ = 5.11 ppm, dd, J = 10.9, 1.0 Hz). Subsequently, the reaction was initiated by the addition of *sec*-BuLi and the progress of the copolymerization monitored by real-time ^{1}H NMR spectroscopy over a period of 2.5 h. Every spectrum was recorded with four scans and a relaxation time of 1 s between the individual scans. The time between two measurements ranged from 0 to 42 s with increasing reaction time.

Figure 1 shows a selection of the ^{1}H NMR spectra measured during the copolymerization. With increasing time of the reaction the sharp signals of the monomers disappear, and simultaneously broad polymer resonances become more intense. In particular, the zoom-in clearly shows the decreasing intensity of the vinyl double bonds from both monomers (*p*BuS highlighted in red and S highlighted in green), indicating the consumption of the monomers and formation of the copolymer (note that the olefin resonances of the side chains (at 6.04–

dx.doi.org/10.1021/mz500255h | ACS Macro Lett. 2014, 3, 560−564

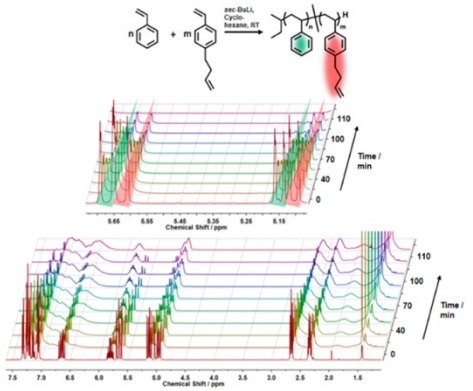

Figure 1. Real-time ^{1}H NMR copolymerization kinetics. Bottom: Overlay of spectra of the real-time ^{1}H NMR kinetics study. Top: Zoom-in, showing the consumption of *p*BuS (vinyl signals highlighted in red) and S (vinyl signals highlighted in green).

5.78 ppm and 5.20−4.88 ppm) remain unchanged after complete monomer consumption).

Figure 2a visualizes the normalized amount of unreacted monomer in stock vs the total conversion. From the measured values a fit curve was prepared. From these graphs it is clear that S (green) is incorporated into the copolymer faster than *p*BuS at the beginning of the polymerization, due to the lower electron density of the reactive vinyl double bond. Since in carbanionic polymerizations all polymer chains are initiated at the same time and there are no side reactions, the total conversion represents the average position of a single polymer chain. Thus, the probability of comonomer incorporation can be calculated for every point in the copolymer chains, which is visualized in Figure 2b. For an ideal random copolymerization the probability of incorporation for each monomer does not change during polymerization and therefore only depends on the initial concentration, resulting in a straight line in the diagram (dashed lines in Figure 2b). In the copolymer system, in the initial stages of the copolymerization the incorporation of S is preferred, although the molar ratio in stock is x(*p*BuS) = 0.55. Consequently with ongoing reaction time the concentration of S decreases. At 42% total conversion, equivalent to a mole fraction of x(*p*BuS) = 0.67 in stock, both monomers are incorporated equally (crossover point in Figure 2b). Figure 2c illustrates the results from Figure 2b schematically: each sphere represents 10% conversion, and the filling level represents the probability of the respective comonomer incorporation at this point.

Due to the different reactivity of both comonomers the relative monomer concentration in the stock changes steadily during the polymerization. Consequently the copolymerization, i.e., reactivity ratios, can also be determined by the classical Fineman−Ross formalism from the fitting curves (equation S1, SI).[31] Since the first measuring point was taken at 16% total conversion and the integrals of the monomers in stock above 80% total conversion become considerably small, we have taken the values in between into account to minimize the error of the calculated reactivity ratios. The results are shown in Figure 3. The slope of the straight line corresponds to r_1 = 3.07, indicating a preferred homopolymerization of S versus cross

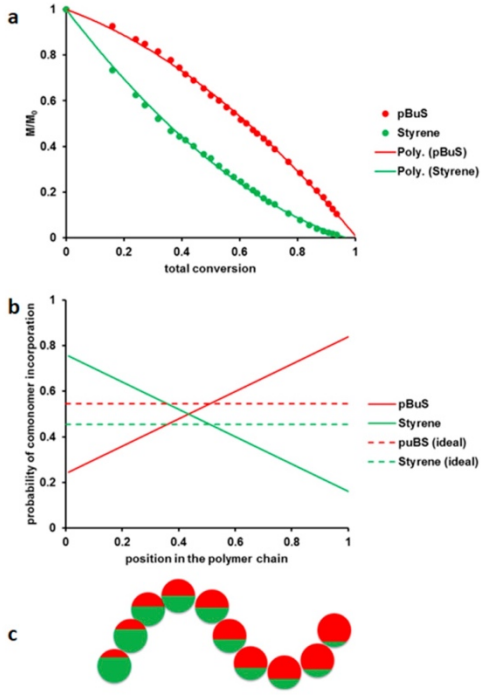

Figure 2. (a) Normalized monomer concentrations in the reaction mixture vs total conversion, (b) probability of comonomer incorporation vs relative position in the polymer chains (straight line) and theoretical incorporation in the case of an ideal random copolymerization (dashed line), and (c) corresponding visualization of the polymer chain for the P*p*BuS-*co*-PS copolymers.

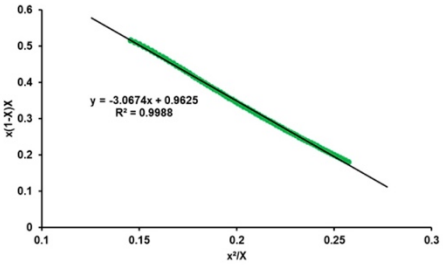

Figure 3. Determination of the reactivity ratios by the Fineman−Ross formalism for the system S/*p*BuS in cyclohexane at 23 °C. Counterion: lithium.

propagation (equation S2, SI). The *y*-axis section represents r_2 having a value of 0.96, which describes an almost equal ratio of homopolymerization of *p*BuS versus cross propagation.

Functional copolymers are useful for many potential fields of application. The average functional group distance is a relevant parameter for the postpolymerization functionalization to generate tailored structures, e.g., by the introduction of polar groups, labels, dyes, etc.[32] The polyvalent P*p*BuS-*co*-PS

dx.doi.org/10.1021/mz500255h | *ACS Macro Lett.* 2014, 3, 560−564

copolymers exhibit a gradient profile of the pendant double bonds which has to be taken into account for postfunctionalization. As a model reaction, we used the thiol−ene reaction with a protected cysteine derivative (Cys) to demonstrate the formation of conjugates. The reaction was initiated with azobis(isobutyronitrile) (AIBN) in dimethylformamide (DMF) at 75 °C. After work-up the resonances of the butenyl double bonds at 5.89 and 5.01 ppm have disappeared, and the corresponding signals of Cys appear at 8.39 and 4.48 ppm (Figure 4 displays the ^{1}H NMR spectra prior to (#4) and after (#6) functionalization), indicating quantitative functionalization.

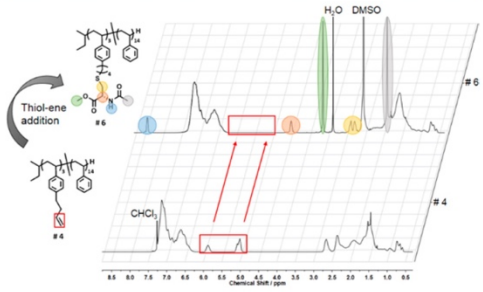

Figure 4. ^{1}H NMR spectra of the functionalization of PS_{14}-*co*-P*p*BuS$_3$ (#4) by the radical thiol−ene reaction PS_{14}-*co*-(P*p*BuS-Cys)$_3$ (#6).

In summary, we have investigated the synthesis of polyvalent P*p*BuS-*co*-PS with different molar fractions x(S) = 0−0.84 by LAP in cyclohexane at room temperature. The focus of this study was the determination of the functional group distribution. By limitation of the reaction time to 2.5 h, side reactions were suppressed, and copolymers with a narrow molecular weight distribution were obtained. A detailed understanding of the copolymerization behavior was achieved by real-time ^{1}H NMR spectroscopy. Due to the chemical similarity, classical methods such as the study of triad abundances cannot be employed for styrene and styrene derivatives to determine the comonomer distribution in detail. By real-time ^{1}H NMR spectroscopy the monomer content can be distinguished at every point of the copolymerization. Since in living anionic polymerizations all polymer chains are initiated at the same time, the probability of comonomer incorporation can be determined at every point of the copolymerization synonymously with every position of the polymer chain (Figure 2c). The chemically different monomers *p*BuS and S lead to a gradient polymer structure where S is incorporated preferably. Finally, we demonstrate the addressability of the butenyl double bonds of *p*BuS in the PS-*co*-P*p*BuS copolymer by performing a thiol−ene reaction with protected Cys. Further postmodifications such as hydrosilylation,[29] Diels−Alder, or cross-linking reactions demonstrate the versatile opportunities of this copolymer.

■ ASSOCIATED CONTENT

Supporting Information

Detailed experimental procedures as well as analytical and spectral characterization data. This material is available free of charge via the Internet at http://pubs.acs.org.

■ AUTHOR INFORMATION

Corresponding Authors

*E-mail: wurm@mpip-mainz.mpg.de (F.R.W.)
*E-mail: hfrey@uni-mainz.de (H.F.).

Notes

The authors declare no competing financial interest.

■ ACKNOWLEDGMENTS

A.N. thanks the Graduate School of Excellence MAINZ for financial support. F.R.W. thanks the Max Planck Graduate Center (MPGC) for support. We thank Prof. Axel H. E. Müller (JGU Mainz) and Markus Pauly (JGU Mainz) for valuable discussions as well as Kevin Tritschler for technical assistance.

■ REFERENCES

(1) Szwarc, M. *Nature* **1956**, *178*, 1168−1169.
(2) Hirao, A.; Goseki, R.; Ishizone, T. *Macromolecules* **2014**, *47*, 1883−1905.
(3) Baskaran, D.; Müller, Axel H. E. *Prog. Polym. Sci.* **2007**, *32*, 173−219.
(4) Quirk, R. P.; Hsieh, H. L. In *Anionic Polymerization: Principles And Practical Applications*; Hudgin, D. E., Ed.; Marcel Dekker Inc: New York, 1996; pp 261−306.
(5) Ito, S.; Goseki, R.; Ishizone, T.; Senda, S.; Hirao, A. *Macromolecules* **2013**, *46*, 819−827.
(6) Natalello, A.; Alkan, A.; Friedel, A.; Lieberwirth, I.; Frey, H.; Wurm, F. R. *ACS Macro Lett.* **2013**, *2*, 313−316.
(7) Carlotti, S.; Desbois, P.; Warzelhan, V.; Deffieux, A. *Polymer* **2009**, *50*, 3057−3067.
(8) Lutz, J.-F.; Ouchi, M.; Liu, D. R.; Sawamoto, M. *Science* **2013**, *341*, 1238149.
(9) Lutz, J.-F. *Acc. Chem. Res.* **2013**, *46*, 2696−2705.
(10) Ouchi, M.; Badi, N.; Lutz, J.-F.; Sawamoto, M. *Nat. Chem.* **2011**, *3*, 917−924.
(11) Brown, J. R.; Sides, S. W.; Hall, L. M. *ACS Macro Lett.* **2013**, 1105−1109.
(12) Yuki, H.; Hotta, J.; Okamoto, Y.; Murahashi, S. *Bull. Chem. Soc. Jpn.* **1967**, *40*, 2659−2663.
(13) Yuki, H.; Okamoto, Y. *Bull. Chem. Soc. Jpn.* **1969**, *42*, 1644−1649.
(14) Yuki, H.; Okamoto, Y. *Bull. Chem. Soc. Jpn.* **1970**, *43*, 148−151.
(15) Natalello, A.; Hall, J. N.; Eccles, E.; Alex, L.; Kimani, S. M.; Hutchings, L. R. *Macromol. Rapid Commun.* **2011**, *32*, 233−237.
(16) Brooks, P. P.; Natalello, A.; Hall, J. N.; Eccles, E.; Alex, L.; Kimani, S. M.; Bley, K.; Hutchings, L. R. *Macromol. Symp.* **2013**, *323*, 42−50.
(17) Obermeier, B.; Wurm, F.; Frey, H. *Macromolecules* **2010**, *43*, 2244−2251.
(18) Alkan, A.; Natalello, A.; Wagner, M.; Frey, H.; Wurm, F. R. *Macromolecules* **2014**, *47*, 2242−2249.
(19) Mangold, C.; Wurm, F.; Frey, H. *Polym. Chem.* **2012**, *3*, 1714−1721.
(20) Reuss, V. S.; Obermeier, B.; Dingels, C.; Frey, H. *Macromolecules* **2012**, *45*, 4581−4589.
(21) Tonhauser, C.; Alkan, A.; Schömer, M.; Dingels, C.; Ritz, S.; Mailänder, V.; Frey, H.; Wurm, F. R. *Macromolecules* **2013**, *46*, 647−655.
(22) Natalello, A.; Werre, M.; Alkan, A.; Frey, H. *Macromolecules* **2013**, *46*, 8467−8471.
(23) Williamson, D. T.; Buchanan, T. D.; Elkins, C. L.; Long, T. E. *Macromolecules* **2004**, *37*, 4505−4511.
(24) Storey, R. F.; Donnalley, A. B.; Maggio, T. L. *Macromolecules* **1998**, *31*, 1523−1526.
(25) Michel, A. J.; Puskas, J. E.; Brister, L. B. *Macromolecules* **2000**, *33*, 3518−3524.
(26) Long, T. E.; Liu, H. Y.; Schell, B. A.; Teegarden, D. M.; Uerz, D. S. *Macromolecules* **1993**, *26*, 6237−6242.

(27) Quinebèche, S.; Navarro, C.; Gnanou, Y.; Fontanille, M. *Polymer* **2009**, *50*, 1351−1357.
(28) Zhang, H.; Ruckenstein, E. *Macromolecules* **1999**, *32*, 5495−5500.
(29) Ruckenstein, E.; Zhang, H. *Macromolecules* **1999**, *32*, 6082−6087.
(30) Claudy, P.; Létoffé, J. M.; Camberlain, Y.; Pascault, J. P. *Polym. Bull.* **1983**, *9*−*9*, 208−215.
(31) Fineman, M.; Ross, S. D. *J. Polym. Sci.* **1950**, *5*, 259−262.
(32) Gauthier, M. A.; Gibson, M. I.; Klok, H.-A. *Angew. Chem., Int. Ed.* **2009**, *48*, 48−58.

Supporting Information

for

Functional Group Distribution and Gradient Structure Resulting from the Living Anionic Copolymerization of Styrene and *para*-But-3-enyl Styrene

Adrian Natalello,[†,‡] Arda Alkan,[†,§] Philipp von Tiedemann,[†] Frederik R. Wurm[§] and Holger Frey*[†]*

[†]Institute of Organic Chemistry, Johannes Gutenberg-University (JGU), Duesbergweg 10-14, 55128 Mainz, Germany

[‡]Graduate School Materials Science in Mainz, Staudinger Weg 9, D-55128 Mainz, Germany

[§]Max Planck Institute for Polymer Research (MPI-P), Ackermannweg 10, D-55128 Mainz, Germany

Experimental Details

Reagents. All solvents and reagents were purchased from Acros Organics or Sigma Aldrich and used as received unless otherwise mentioned. *para*-But-3-enyl styrene (*p*BuS) was synthesized as described previously.[1] Chloroform-d_1, DMSO-d_6 and cyclohexane-d_{12} were purchased from Deutero GmbH.

Cyclohexane was distilled from sodium/benzophenone under reduced pressure into a liquid nitrogen-cooled reaction vessel (cryo-transfer). Styrene (S), *p*BuS and cyclohexane-d_{12} were dried over calcium hydride (CaH_2) and cryo-transferred prior to use. *sec*-Butyllithium (*sec*-BuLi, 1,3 M, Acros) was used as received.

Instrumentation. 1H NMR spectra (400 MHz) and ^{13}C NMR (100 MHz) were recorded on a Bruker AMX400 spectrometer and were referenced internally to the residual proton signals of the deuterated solvent. For size exclusion chromatography (SEC) measurements in DMF (containing 0.25 g/L of lithium bromide as an additive) an Agilent 1100 Series was used as an integrated instrument, including a PSS HEMA column (300/100/40 g/mol), a UV detector (operating at 275 nm) and a RI detector. All molecular weights and molecular weight distributions determined by SEC were referenced to linear polystyrene (PS) standards provided by Polymer Standards Service (PSS). DSC curves were recorded on a Perkin-Elmer DSC 8500 in the temperature range from -100 to 100°C at heating rates of 10 K min^{-1} under nitrogen.

Poly(*p*-but-3-enyl styrene) (P*p*BuS, #1)

0.75 mL (3.89 mmol) of *p*BuS and 6.75 mL Cyclohexane were freshly purified and mixed inside an argon-filled glove box. To the vigorously stirred system 0.08 mL (0.10 mmol) *sec*-BuLi was

added via syringe at room temperature, and immediately the typical orange color of the living carbanions was observed. After 2.5 h the reaction was terminated with degassed methanol via syringe. The resulting polymer was precipitated in methanol at - 25 °C and dried under high vacuum (yield = 87%). ^{1}H NMR (400 MHz, $CDCl_3$, δ in ppm): 7.25-6.29 (m, aromatic resonances P*p*BuS), 6.05-5.78 (s, -C*H*=CH_2), 5.19-4.89 (m, -CH=CH_2), 2.90-2.52 (Ar-CH_2), 2.52-0.87 (CH_2 group of the butenyl group, CH_2 CH initiator, P*p*BuS backbone), 0.86-0.53 (m, 6H, initiator). ^{13}C NMR, see Figure S2.

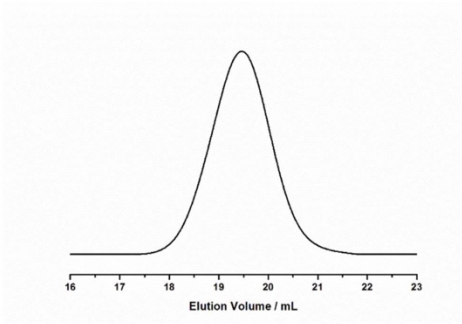

Figure S1. SEC elugram (DMF) of P*p*BuS (#1)

Branching side reaction during the homo polymerization of *para*-but-3-enyl styrene

trace	reaction time / h
Black	2.5
Red	24
Yellow	48
Green	120
Blue	336

Table S1. Different reaction times for the polymerization of *p*BuS.

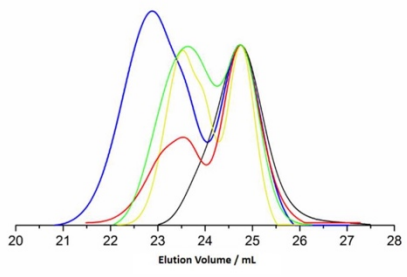

Figure S2. Overlay of several SEC elugrams (DMF) of the polymerization of *p*BuS after different reaction times (black: 2.5h, red: 24 h, yellow: 48 h, green 120 h, blue: 336 h)

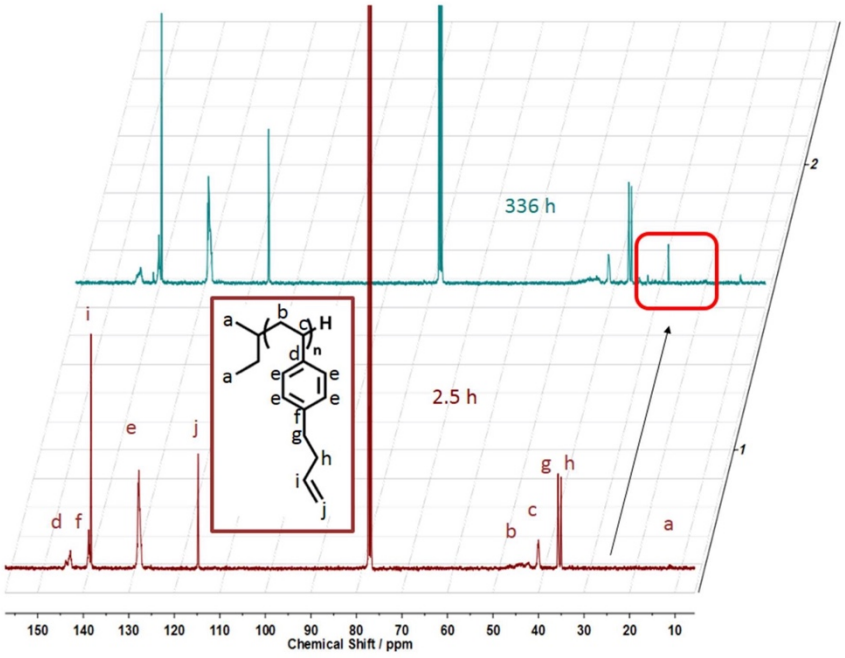

Figure S3. ^{13}C NMR (100 MHz) spectra of P*p*BuS obtained after 2.5 h and 336 h reaction time.

Poly(*p*-but-3-enyl styrene)-*co*-poly(styrene) (P*p*BuS-*co*-PS, #2-5)

Exemplary Synthesis Procedure for PpBuS$_{33}$-co-PS$_{6.5}$ (#2). The polymerization of polymer #2 was carried out in analogy to the synthesis P*p*BuS (#1). 0.5 mL (2.59 mmol) *p*BuS, 0.06 mL (0.052 mmol) S and 5.6 mL of cyclohexane were mixed in an NMR tube. Subsequently the reaction was initiated by the addition of 0.06 mL (0.08 mmol) *sec*-BuLi at room temperature. After 2.5 h reaction time the polymerization was terminated with degassed methanol. The polymer was precipitated in cold (T = -25 °C) methanol (yield: 90%).

^{1}H NMR (400 MHz, $CDCl_3$, δ in ppm): 7.24-6.21 (m, aromatic resonances of P*p*BuS and S), 5.99-5.72 (s, -C*H*=CH_2), 5.16-4.89 (m, -CH=CH_2), 2.85-2.46 (Ar-CH_2), 2.52-0.81 (CH_2 resonances of the butenyl group, CH_2 CH initiator, P*p*BuS and S backbone), 0.81-0.53 (m, 6H, initiator).

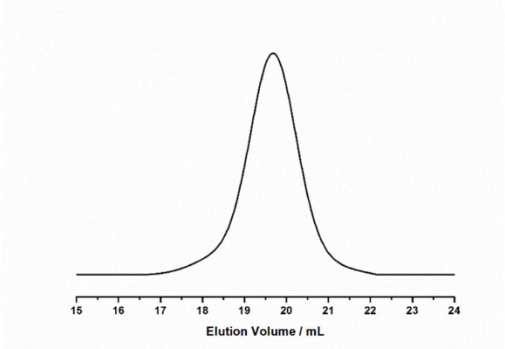

Figure S4. SEC elugram (DMF) of P*p*BuS-*co*-PS (#2)

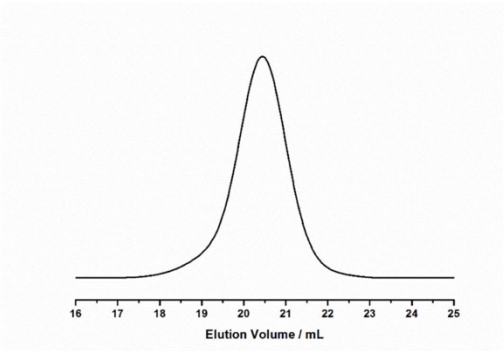

Figure S5. SEC elugram of P*p*BuS-*co*-PS (#3)

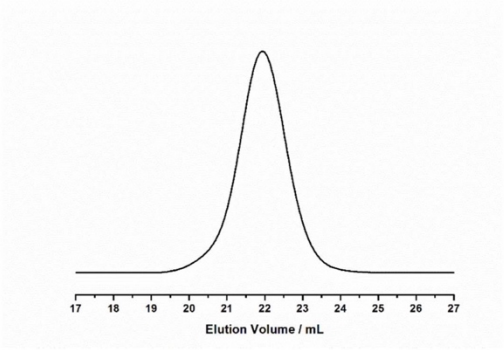

Figure S6. SEC elugram of P*p*BuS-*co*-PS (#4)

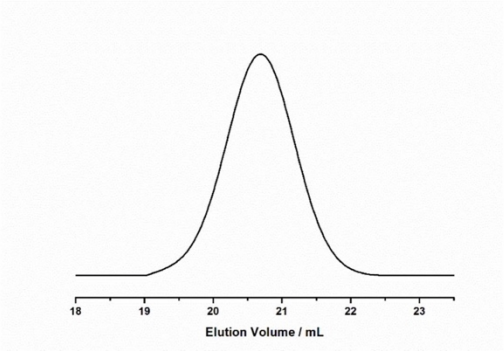

Figure S7. SEC elugram of P*p*BuS-*co*-PS (#5)

Thiol-ene addition of PS_{14}-*co*-P*p*BuS_3 (#4) with protected cysteine (PS_{14}-*co*-(P*p*BuS-Cys)$_3$, #6)

100 mg of polymer #4 (50.25 µmol) and 0.52 g of *N*-acetal-*L*-cysteine methyl ester (Cys) were dissolved in 2 mL of DMF. Oxygen was removed from the reaction mixture by three freeze-pump-thaw cycles and flushed with argon. Subsequently 0.172 g (0.001 mol) AIBN were added under a flow of argon and the reaction mixture was heated up to 75 °C for 24 h. The functionalized polymer was purified by dialysis (MWCO 1000 g/mol) against THF for 24 h (Yield: 56%).

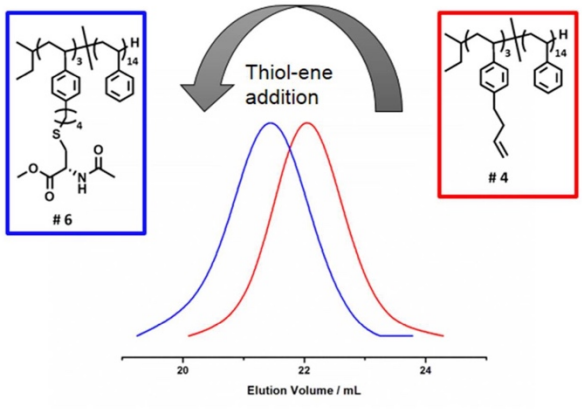

Figure S8. SEC elugrams of thiol-ene addition.

^{1}H NMR Kinetics. A monomer solvent mixture (10 wt%) was prepared inside an argon-filled glove-box (for purification established procedures were used previously). Then a conventional NMR tube was filled with the reaction mixture and sealed with a septum. The monomer mixture was measured separately in NMR to set all parameters (locking/ shimming procedures). Then

sec-BuLi was added to the mixture and the kinetic measurement was started with 4 scans per spectrum, a relaxation time of 1 s between the individual scans and increasing time intervals between two measurements ranging from 0 s to 42 s with increasing reaction time.

Additional equations: Copolymerization:

$$P_1^- + M_1 \xrightarrow{k_{11}} P_1M_1^-$$

$$P_1^- + M_2 \xrightarrow{k_{12}} P_1M_2^-$$

$$P_2^- + M_1 \xrightarrow{k_{21}} P_2M_1^-$$

$$P_2^- + M_2 \xrightarrow{k_{22}} P_2M_2^-$$

P_i: active chain end

M_i: monomer

k_{ii}: reactivity constant

Fineman Ross equation:

$$x \cdot \frac{1-X}{X} = -\frac{x^2}{X} r_1 + r_2$$

Equation S1: Fineman Ross equation

x: mol fraction of the stock

X: mol fraction of the Polymer at certain mole fraction of the stock

r_1: reactivity ratio

$$r_1 = \frac{k_{11}}{k_{12}}$$

Equation S2: Reactivity ratio r_1

r_2: reactivity ratio

$$r_2 = \frac{k_{22}}{k_{21}}$$

Equation S3: Reactivity ratio r_1

Determination of the probability of comonomer incorporation vs. relative position in the polymer chains (Figure 2).

The theoretical comonomer probability for an ideally random copolymerization is independent of the comonomer feed (dashed lines in Figure 2b). For the system pBuS and S it was calculated as follows: From the ^{1}H NMR kinetics for each position in the polymer chain the respective comonomer concentrations can be calculated (as plotted in Figure 2a). The probability of the respective comonomer incorporation is calculated from the fit function of these values by the mol-fraction of incorporation (using the concentration between two consecutive concentrations).

REFERENCES

(1) Zhang, H.; Ruckenstein, E. *Macromolecules*. **1999,** *32* (17), 5495–5500.

Macromolecules

Article

pubs.acs.org/Macromolecules

Monomer Sequence Distribution Monitoring in Living Carbanionic Copolymerization by Real-Time ^{1}H NMR Spectroscopy

Adrian Natalello,[†,‡] Mathias Werre,[†,‡] Arda Alkan,[†,§] and Holger Frey*[,†]

[†]Institute of Organic Chemistry, Johannes Gutenberg-University (JGU), Duesbergweg 10-14, 55128 Mainz, Germany

[‡]Graduate School Materials Science in Mainz, Staudinger Weg 9, 55128 Mainz, Germany

[§]Max Planck Institute for Polymer Research (MPI-P), Ackermannweg 10, 55128 Mainz, Germany

Supporting Information

ABSTRACT: Detailed understanding of the monomer sequence distribution in carbanionic copolymerization was achieved by direct online monitoring of copolymerizations in an NMR tube. Obtaining detailed knowledge of the changing monomer concentration in stock during the reaction, this technique permits to determine the incorporation probability for each monomer at every position of the polymer chain. An in situ kinetic study of two different carbanionic copolymerizations has been carried out. On the one hand, the copolymerization of the structurally similar, protected hydroxystyrene derivatives, *p*-(1-ethoxy ethoxy)styrene (*p*EES) and 4-*tert*-butoxystyrene (*t*BuOS), and on the other hand the copolymerization of the chemically different monomers, styrene (S) and *p*EES, have been studied. Whereas in the first case a slight deviation from an ideal random copolymerization was observed, the latter copolymerization leads to gradient copolymers. Real-time ^{1}H NMR spectroscopy gave detailed insight into the reaction behavior at every stage of the copolymerization and leads to precise understanding of the resulting gradient structures.

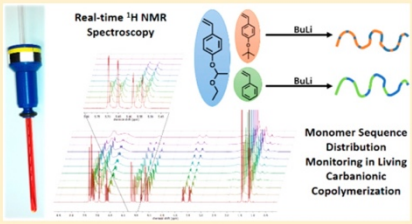

INTRODUCTION

In recent decades, important progress has been made in the field of controlled polymerization techniques. Controlled radical polymerization strategies have been introduced, allowing the tailoring of molecular weight with narrow molecular weight distributions (MWD) and permitting the use of an immense variety of different functional monomers.[1−3] However, despite the success of controlled radical polymerization, living anionic polymerization remains an important methodology, especially in terms of high molecular weight polymers, block copolymers, end-functionalized polymers, and complex polymer architectures, particularly with respect to actual commercial application.[4−9] Nevertheless, carbanionic random copolymerization represents an almost neglected field in recent decades.

Detailed understanding and control of the monomer sequences within polymer chains is of growing interest with respect to monomer sequence control.[10] In a recent feature article, monomer sequence control has been hailed as one of the "holy grails" of modern polymer science.[11] In the late 1960s, pioneering works demonstrated the possibility of synthesizing alternating copolymers by carbanionic copolymerization. The respective works made use of the fact that diphenylethylene (DPE) does not undergo self-propagation and consequently copolymerized DPE with styrene (S), isoprene (I), or butadiene (B).[12−14] Recently, Hutchings and co-workers further developed this strategy by performing a kinetically controlled terpolymerization of S, DPE, and a DPE derivative with electron donating groups, obtaining an improved degree of monomer sequence control and multiple functional groups in the polymer.[15] A related approach has been investigated by Lutz and co-workers for atom transfer radical copolymerizations (ATRP) of styrene and a series of N-substituted maleimides (MI). To a certain extent MI represents the DPE-analogue for radical polymerizations, showing very low tendency for homopolymerization and a strongly favored cross-propagation with S.[16]

In 2010, our group developed the direct monitoring of living oxyanionic copolymerizations by real-time ^{1}H NMR spectroscopy.[17] To date this technique has been employed for a variety of different epoxides and epoxide derivative combinations to follow the incorporation of the different monomer units in the polymer backbone during the copolymerization process.[18−21]

Because of the high sensitivity of carbanions and their irreversible termination, direct monitoring of the copolymerization by carrying out the respective copolymerization in an NMR tube is considerably more difficult than for the case of oxyanionic polymerization. In a single work, Niu and co-workers studied the aggregation behavior during the carbanionic homopolymerization of butadiene in heptane by combining in situ small angle neutron scattering and ^{1}H NMR spectroscopy.[22] Generally, in a few reports in situ techniques have been employed to follow living polymerizations.[23−25] For

Received: September 4, 2013
Revised: October 16, 2013
Published: November 1, 2013

example in 2009 Gnanou and Fontanille et al. studied the copolymerization of styrene and isoprene in great detail by combining in situ mid-IR and UV−visible spectroscopy.[26]

However, to the best of our knowledge no other example for the study of a carbanionic polymerization followed by real-time ^{1}H NMR has been reported to date. In addition, the direct in situ study of carbanionic copolymerization via NMR techniques has not been reported.

Here we describe the in situ monitoring of the carbanionic copolymerization of protected *p*-hydroxystyrene (*p*HS) derivatives, which gives access to a variety of polymer architectures (Scheme 1).[27−29] At present, usually poly(4-*tert*-butoxystyrene) (P*t*BuOS) is utilized as a protected precursor for the synthesis of P*p*HS by carbanionic or living radical polymerization techniques.[30−32] As an alternative to 4-*tert*-butoxy styrene (*t*BuOS) our group investigated the living anionic polymerization of *p*-(1-ethoxy ethoxy)styrene (*p*EES).[33] Compared with P*t*BuOS the experimental effort for the cleavage of the acetal protecting group of P*p*EES is considerably reduced, and full removal is achieved within minutes at room temperature.[34]

Scheme 1. Copolymerization of *p*EES and *t*BuOS and *p*EES and S, Respectively, Monitored by Real-Time ^{1}H NMR Spectroscopy in an NMR Tube

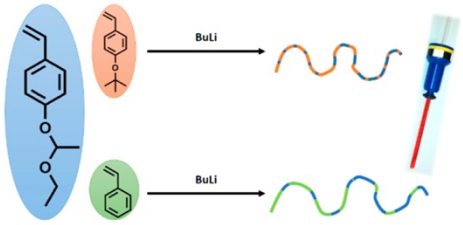

Classical methods for microstructure investigation, such as NMR characterization of triad abundances cannot be employed for styrene and styrene derivatives to monitor the comonomer distribution in detail, because of their chemical similarity. Besides, these methods only afford global information, but do not permit to obtain direct information for (local) monomer gradients within the chains formed. Consequently in situ ^{1}H NMR spectroscopic monitoring of the chemically similar monomers, *p*EES and *t*BuOS, and chemically different monomers, S and *p*EES, is explored in this work. It is an intriguing issue, how these comonomer pairs behave during carbanionic copolymerization and whether random monomer incorporation is possible under the chosen conditions.

EXPERIMENTAL SECTION

Reagents. All solvents and reagents were purchased from Sigma-Aldrich or Acros Organics and used as received unless otherwise mentioned. *p*EES was provided by TOSOH Organic Chemical Co., Ltd. Cyclohexane-d_{12} was purchased from Deutero GmbH. Cyclohexane-d_{12}, styrene, *t*BuOS and *p*EES were dried over calcium hydride (CaH_2) and distilled under reduced pressure into a liquid nitrogen-cooled reaction vessel (cryo-transfer) or distilled in the case of *t*BuOS and *p*EES prior to use. *sec*-Butyllithium (*sec*-BuLi, 1,3 m, Acros) was used as received.

Instrumentation. NMR spectra were recorded at 400 MHz on a Bruker AMX400 spectrometer, and are referenced internally to residual proton signals of the deuterated solvent. The DOSY NMR spectrum (DOSY, diffusion ordered spectroscopy) was recorded at

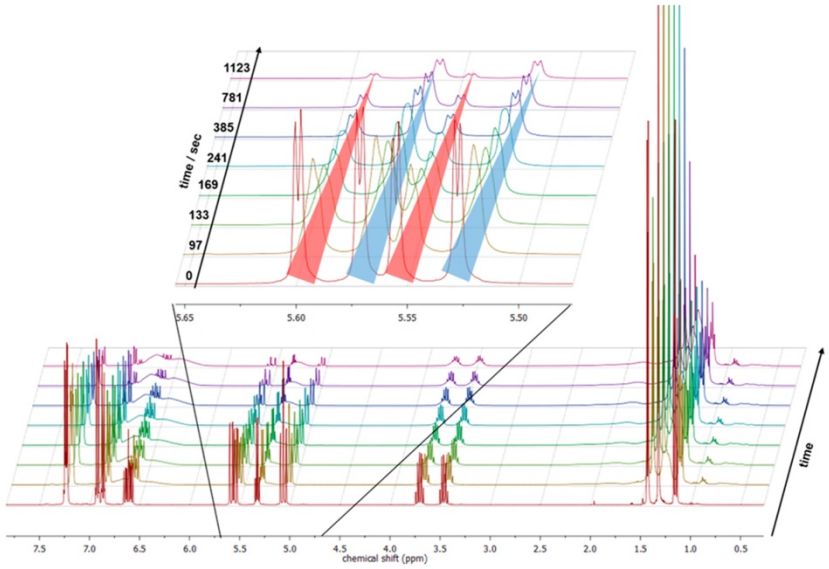

Figure 1. Real-time ^{1}H NMR spectra overlay, showing the consumption of the *p*EES monomer (signals highlighted in blue) and the *t*BuOS (signals highlighted in red) monomer in the zoom-in.

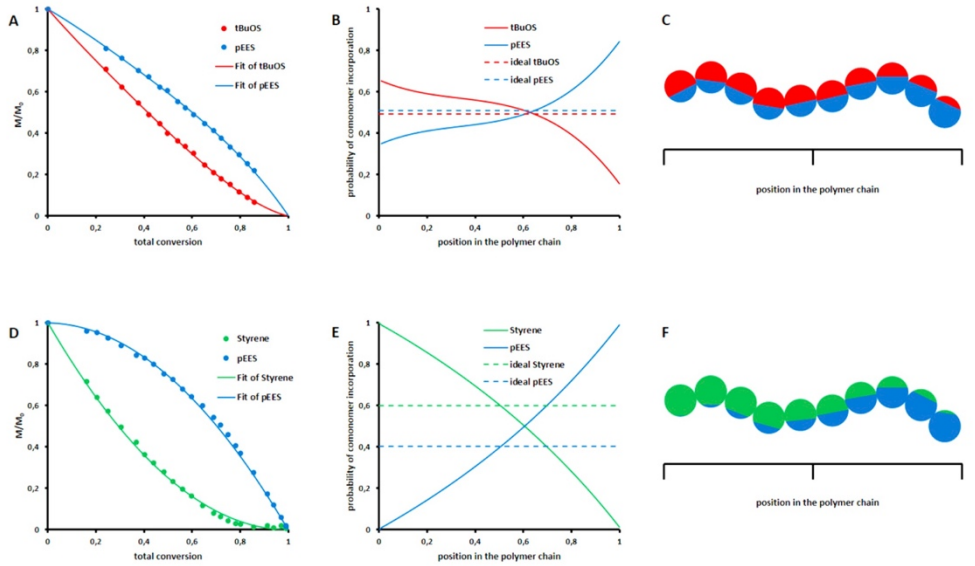

Figure 2. (a) Residual monomer concentrations in the reaction solution vs total conversion, (b) probability of comonomer incorporation vs relative position in the polymer chains (straight line) and theoretical incorporation in case of an ideal random copolymerization (dashed line) and (c) corresponding visualization of the polymer chain for the P*t*BuOS-*co*-P*p*EES copolymers and respectively, parts d–f, for the PS-*co*-P*p*EES copolymers.

ambient temperature on a digital Bruker Avance DRX 400 MHz spectrometer with B_0 field corresponding to ^{1}H resonance frequency of 400.31 MHz. The spectrometer was equipped with a commercial Bruker 5 mm inverse probe head. All polymers were synthesized by living anionic polymerization carried out under argon atmosphere with purified reagents.

^{1}H NMR Kinetics. All monomer solvent mixtures (10 wt %) were prepared inside a glovebox subsequent to their purification and established drying procedures. Then a conventional NMR tube was filled with the reaction mixture. Prior to initiation with *sec*-BuLi, the pure monomer–solvent mixture was measured at 13 °C. To reduce the time after initiation, we skipped repeated shimming and locking of the polymerization mixture. All spectra were recorded at 400 MHz with 4 scans, a relaxation time of 1 s between the scans and increasing time intervals between two measurements ranging from 0 to 882 s with increasing reaction time.

■ RESULTS AND DISCUSSION

We aim at a study of the carbanionic copolymerization of two different monomer combinations using real-time ^{1}H NMR spectroscopy (Scheme 1). First the copolymerization of chemically similar protected P*p*HS derivatives has been studied. P*t*BuOS is a well-known styrene derivative and has been frequently used to generate functional polystyrene. Compared to the recently introduced P*p*EES,[34] *t*BuOS shows a different property profile. The glass transition temperature (T_g) of P*p*EES (T_g = 9 °C, M_n = 4000 g·mol^{-1})[33] is considerably lower and differs by 64 °C from the T_g of P*t*BuOS (T_g = 73 °C, M_n = 4000 g·mol^{-1}),[31] leading to a highly viscous sample at room temperature. More importantly, the cleavage of the acetal protecting group can be achieved within minutes in acidic dioxane at room temperature. In contrast, the deprotection of P*t*BuOS is carried out at 60 °C and with much longer reaction time.[31] To follow the polymerization kinetics an in situ ^{1}H NMR monitoring strategy was developed. The results are compared to the carbanionic copolymerization of styrene (S) and *p*EES (Scheme 1, bottom), a system of chemically different monomers.

Real-Time ^{1}H NMR Copolymerization Kinetics. Using real-time ^{1}H NMR spectroscopy to directly follow monomer incorporation, the consumption of each monomer at any time can be determined and used to calculate the total conversion, which is equivalent to the relative position in the polymer backbone chain, since there are no termination or transfer processes. The carbanionic copolymerization in the NMR tube was carried out in analogy to the conventional procedure in batch. All monomers and the deuterated solvent (C_6D_{12}) were purified and mixed inside the glovebox. Subsequently, the NMR tube was sealed with a septum. Prior to initiation of the reaction, a ^{1}H NMR spectrum was recorded to determine the precise monomer ratio at the beginning of the reaction. For this purpose the signals of the double bonds of (δ = 5.60–5.54 ppm, dd, J = 17.6, 0.9 Hz) and *t*BuOS (δ = 5.61–5.57 ppm, dd, J = 17.6, 1.0 Hz) were compared. After initiation of the reaction mixture with *sec*-BuLi via syringe the copolymerization was monitored by ^{1}H NMR spectroscopy. All spectra were recorded at 400 MHz. The intervals between two measurements were adjusted with the progress of the reaction, ranging from 0 to 882 s with regard to the decreasing propagation rate of the living copolymerization.

Figure 1 shows a typical series of ^{1}H NMR spectra for the copolymerization of *p*EES and *t*BuOS, which demonstrate the consumption of both monomers (pEES highlighted in blue and tBuOS highlighted in red) and at the same time the formation of the polymer (backbone in the spectral region of 0.90–2.3

ppm). Consequently, monomer incorporation can be determined at any time of the copolymerization. This is visualized in Figure 2a. The normalized amount of unreacted monomer is plotted vs total conversion. As can be seen, *t*BuOS is incorporated slightly faster compared to *p*EES, indicated by a more rapid decrease of monomer concentration in the reaction mixture. A perfectly random copolymerization would yield a straight line in between the measured values. Additionally, using the measured values a fit curve describing the monomer consumption has been created. Since in carbanionic copolymerization every polymer chain is initiated at the same time and there are no termination or transfer steps, the total conversion of the copolymerization corresponds to the average position in a single polymer chain. As a result, the probability for incorporation of each monomer can be calculated from the fitting curve at every point of the polymer chain (Figure 2b). The incorporation probability for the case of an ideally random copolymerization is shown in Figure 2b (dashed lines) as well. In this case the initially used monomer concentration ratio would not change with the progress of the reaction, and the probability of the monomer consumption at every point of the copolymerization would remain unchanged. Although the structures of *p*EES and *t*BuOS appear to be similar at first glimpse, incorporation of *t*BuOS is favored compared to *p*EES, resulting in a slightly tapered polymer structure, characterized by 65% tBuOS incorporation at the beginning of the polymerization to 16% at the end of the polymer chain (Figure 2c). Starting with a molar ratio of approximately one to one of both monomers, equal incorporation is reached at 63% total conversion, equivalent to a monomer fraction of x(*t*BuOS) = 0.36 in the reaction mixture. To gain additional evidence for the successful copolymerization, a diffusion-ordered ^{1}H NMR spectrum has been measured. As expected, all ^{1}H NMR resonances of the polymer can be correlated to the same diffusion signal at 2.14 × 10^{-6} cm^2/s (Figure S1, Supporting Information).

To underline the benefits of this approach for direct observation of copolymer composition, we applied the online ^{1}H NMR spectroscopy technique to another monomer system, namely styrene (S) and *p*EES (Figure S4) having a starting mole fraction of x(S) = 0.60 in the feed. As expected, in this case the reactivities of the two monomers differ significantly. As can be seen in Figure 2d, S is incorporated considerably faster than *p*EES. This translates to a significantly higher probability for reaction of the living chain end with S over a long period of the reaction. At 61% total conversion synonymous with a mole fraction of x(S) = 0.27 in the reaction mixture, both monomers are incorporated to the same degree. Because of the different reactivity and the accompanying changes in the monomer concentration as well as the probability of incorporation during the copolymerization, the r parameters for this copolymerization conditions could be distinguished using the Fineman−Ross formalism.[35] To minimize the error of the calculated r-parameters from the fitting curves the monomer consumption between 10% and 90% was considered, due to the high number of measuring points after 10% total conversion respectively only small integrals of the monomers in stock after 90% (Figure 2d). Figure 3 displays the result of the Fineman−Ross formalism. On the basis of the slope of the straight line r_1, indicating the reactivity of S for homo propagation divided by cross propagation, can be determined with a value of 1.34. The parameter r_2 exhibits a value of 0.47 and was determined from the y-axis section, representing the preferred cross propagation

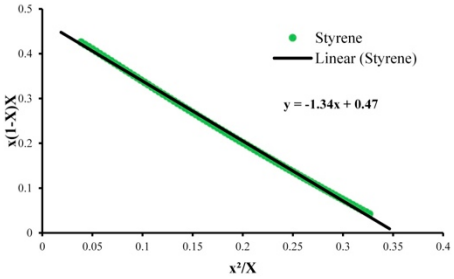

Figure 3. Determination of the r-parameters by the Fineman−Ross equation for the system S/*p*EES.

of living *p*EES chain ends compared over self-propagation. In general, the r parameters for copolymerization of *p*EES (r_2 = 0.56) and *t*BuOS (r_1 = 0.72) were determined by the same procedure (Figure S3).

Taking into account the small difference in reactivity between both monomers for the *p*EES/*t*BuOS system and the associated small variations of the monomer concentrations in the feed during the reaction, the calculated r-parameters are affected by small errors. Nevertheless, the resulting r-parameters fit well with the observed results of the measurement (Figure 2a−c).

■ CONCLUSION

It is current textbook knowledge that monomer sequences in copolymers can be determined by NMR-spectroscopy via quantification of monomer triads. In this work, direct in situ monitoring of the living carbanionic copolymerization has been established as a key method to study the evolution of the comonomer sequence in great detail. The use of real-time ^{1}H NMR spectroscopy in selected apolar solvents permits to calculate the incorporation of each monomer at every point of the polymer chain and detailed sequence studies. Two different comonomer pairs have been investigated, (i) the chemically related, protected poly(*p*-hydroxystyrene) (P*p*HS) derivatives, *p*-(1-ethoxy ethoxy)styrene (*p*EES) and 4-*tert*-butoxystyrene (*t*BuOS) as well as (ii) styrene (S) and *p*EES, which differ in their reactivity to a greater extent.

Although the reactive double bonds of *p*EES and *t*BuOS appear to be chemically equal, especially with regard to the carbanionic polymerization technique, preferential incorporation of *t*BuOS was observed in the initial stages of the copolymerization. For the S/*p*EES copolymer system a pronounced gradient structure was obtained, due to the higher reactivity of styrene. The use of real-time ^{1}H NMR spectroscopy permitted detailed incorporation studies according to the change of the monomer concentration during the copolymer formation.

To conclude, the in situ ^{1}H NMR kinetic study of carbanionic copolymerization in an NMR tube represents merely a step toward the initially mentioned "holy grail" of monomer sequence control.[11] However, the in situ NMR technique can considerably improve the understanding of monomer sequence distributions in living anionic random copolymerization, which can be considered to be a rather neglected technique. We emphasize the general applicability of

the method for carbanionic copolymerization in apolar solvents, particularly for styrene derivatives.

■ ASSOCIATED CONTENT

Supporting Information

Detailed experimental procedures as well as analytical and spectral characterization data. This material is available free of charge via the Internet at http://pubs.acs.org.

■ AUTHOR INFORMATION

Corresponding Author

*E-mail: (H.F.) hfrey@uni-mainz.de.

Notes

The authors declare no competing financial interest.

■ ACKNOWLEDGMENTS

We thank Frederik Wurm (MPI-P Mainz) and Markus Pauly (JGU Mainz) for fruitful discussions as well as Kevin Tritschler for technical assistance and TOSOH Organic Chemical Co., Ltd., for providing *p*-(1-ethoxy ethoxy)styrene. A.N. and M.W. thank the Graduate School of Excellence Mainz for financial support.

■ REFERENCES

(1) di Lena, F.; Matyjaszewski, K. *Prog. Polym. Sci.* **2010**, *35* (8), 959−1021.
(2) Ouchi, M.; Terashima, T.; Sawamoto, M. *Chem. Rev.* **2009**, *109* (11), 4963−5050.
(3) Moad, G.; Rizzardo, E.; Thang, S. H. *Polymer* **2008**, *49* (5), 1079−1131.
(4) Hsieh, H. L.; Quirk, R. P. *Anionic Polymerization: Principles And Practical Applications*; Marcel Dekker Inc: New York, 1996.
(5) Baskaran, D.; Müller, A. H. E. *Prog. Polym. Sci.* **2007**, *32* (2), 173−219.
(6) Higashihara, T.; Hayashi, M.; Hirao, A. *Prog. Polym. Sci.* **2011**, *36* (3), 323−375.
(7) Tonhauser, C.; Frey, H. *Macromol. Rapid Commun.* **2010**, *31* (22), 1938−1947.
(8) Natalello, A.; Tonhauser, C.; Berger-Nicoletti, E.; Frey, H. *Macromolecules* **2011**, *44* (24), 9887−9890.
(9) Natalello, A.; Alkan, A.; Friedel, A.; Lieberwirth, I.; Frey, H.; Wurm, F. R. *ACS Macro Lett.* **2013**, *2* (4), 313−316.
(10) Ouchi, M.; Badi, N.; Lutz, J.-F.; Sawamoto, M. *Nature Chem.* **2011**, *3* (12), 917−924.
(11) Lutz, J.-F. *Polym. Chem.* **2010**, *1* (1), 55−62.
(12) Yuki, H.; Hotta, J.; Okamoto, Y.; Murahashi, S. *Bull. Chem. Soc. Jpn.* **1967**, *40* (11), 2659−2663.
(13) Yuki, H.; Okamoto, Y. *Bull. Chem. Soc. Jpn.* **1969**, *42* (6), 1644−1649.
(14) Yuki, H.; Okamoto, Y. *Bull. Chem. Soc. Jpn.* **1970**, *43* (1), 148−151.
(15) Natalello, A.; Hall, J. N.; Eccles, E. A. L.; Kimani, S. M.; Hutchings, L. R. *Macromol. Rapid Commun.* **2011**, *32* (2), 233−237.
(16) Pfeifer, S.; Lutz, J.-F. *J. Am. Chem. Soc.* **2007**, *129* (31), 9542−9543.
(17) Obermeier, B.; Wurm, F.; Frey, H. *Macromolecules* **2010**, *43* (5), 2244−2251.
(18) Mangold, C.; Wurm, F.; Frey, H. *Polym. Chem.* **2012**, *3* (7), 1714−1721.
(19) Reuss, V. S.; Obermeier, B.; Dingels, C.; Frey, H. *Macromolecules* **2012**, *45* (11), 4581−4589.
(20) Tonhauser, C.; Alkan, A.; Schömer, M.; Dingels, C.; Ritz, S.; Mailänder, V.; Frey, H.; Wurm, F. R. *Macromolecules* **2013**, *46* (3), 647−655.
(21) Zhang, W.; Allgaier, J.; Zorn, R.; Willbold, S. *Macromolecules* **2013**, *46* (10), 3931−3938.
(22) Niu, A. Z.; Stellbrink, J.; Allgaier, J.; Willner, L.; Richter, D.; Radulescu, A.; Koenig, B. W.; Gondorf, M.; Willbold, S.; Fetters, L. J. *Physica B: Condensed Matter* **2004**, *350* (1−3, Supplement), E921−E925.
(23) Williamson, D. T.; Buchanan, T. D.; Elkins, C. L.; Long, T. E. *Macromolecules* **2004**, *37* (12), 4505−4511.
(24) Storey, R. F.; Donnalley, A. B.; Maggio, T. L. *Macromolecules* **1998**, *31* (5), 1523−1526.
(25) Michel, A. J.; Puskas, J. E.; Brister, L. B. *Macromolecules* **2000**, *33* (10), 3518−3524.
(26) Quinebèche, S.; Navarro, C.; Gnanou, Y.; Fontanille, M. *Polymer* **2009**, *50* (6), 1351−1357.
(27) Grayson, S. M.; Fréchet, J. M. J. *Macromolecules* **2001**, *34* (19), 6542−6544.
(28) Laurent, B. A.; Grayson, S. M. *J. Am. Chem. Soc.* **2011**, *133* (34), 13421−13429.
(29) Hirao, A.; Loykulnant, S.; Ishizone, T. *Prog. Polym. Sci.* **2002**, *27* (8), 1399−1471.
(30) Conlon, D. A.; Crivello, J. V.; Lee, J. L.; O'Brien, M. J. *Macromolecules* **1989**, *22* (2), 509−516.
(31) Rahman, S. S. A.; Kawaguchi, D.; Matsushita, Y. *Polymer* **2011**, *52* (1), 164−171.
(32) Schüll, C.; Frey, H. *ACS Macro Lett.* **2012**, *1* (4), 461−464.
(33) Natalello, A.; Tonhauser, C.; Frey, H. *ACS Macro Lett.* **2013**, *2*, 409−413.
(34) Ishikawa, T.; Morino, K.; Sudo, A.; Endo, T. *J. Polym. Sci., Part A: Polym. Chem.* **2011**, *49* (21), 4714−4720.
(35) Fineman, M.; Ross, S. D. *J. Polym. Sci.* **1950**, *5* (2), 259−262.

Supporting Information

for

Monomer Sequence Distribution Monitoring in Living Carbanionic Copolymerization by Real-Time ^{1}H NMR Spectroscopy

Adrian Natalello,[†,‡] Mathias Werre,[†,‡] Arda Alkan[†,§] and Holger Frey[†]*

[†]*Institute of Organic Chemistry, Johannes Gutenberg-University (JGU), Duesbergweg 10-14, 55099 Mainz, Germany*

[‡]*Graduate School Materials Science in Mainz, Staudinger Weg 9, D-55128 Mainz, Germany*

[§]*Max Planck Institut für Polymerforschung, Ackermannweg 10, 55128 Mainz*

Experimental details

Copolymerization:

$$P_1^- + M_1 \xrightarrow{k_{11}} P_1M_1^-$$

$$P_1^- + M_2 \xrightarrow{k_{12}} P_1M_2^-$$

$$P_2^- + M_1 \xrightarrow{k_{21}} P_2M_1^-$$

$$P_2^- + M_2 \xrightarrow{k_{22}} P_2M_2^-$$

P: active chain end

M: Monomer

k: reactivity constant

Fineman Ross equation:

$$x \cdot \frac{1-X}{X} = -\frac{x^2}{X} r_1 + r_2$$

eq S 1: Fineman Ross equation

x: mole fraction of the stock

X: mole fraction of the Polymer at certain mole fraction of the stock

r_1: reactivity ratio

$$r_1 = \frac{k_{11}}{k_{12}}$$

r_2: reactivity ratio

$$r_2 = \frac{k_{22}}{k_{21}}$$

Additional characteriazation data

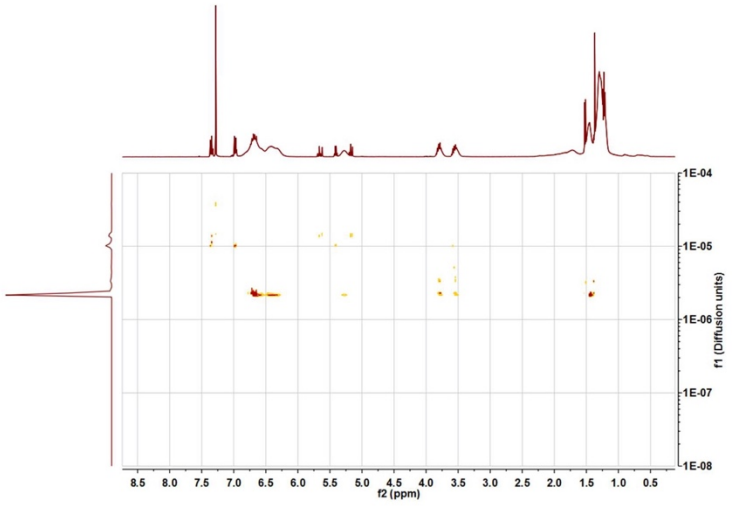

Fig S 1. DOSY ^{1}H NMR spectrum (benzene-d_6, 400 MHz) of P*t*BuOS-P*p*EES after termination.

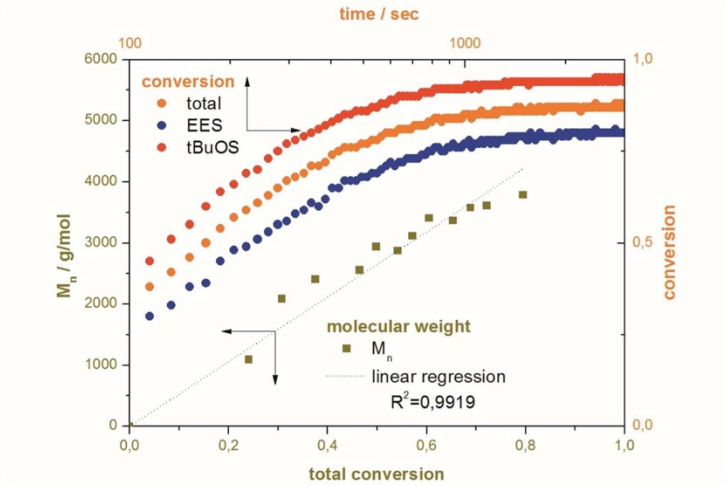

Fig S 2. Conversion vs time (orange) and molecular weight vs total conversion (dark yellow) for the *t*BuOS-*p*EES system

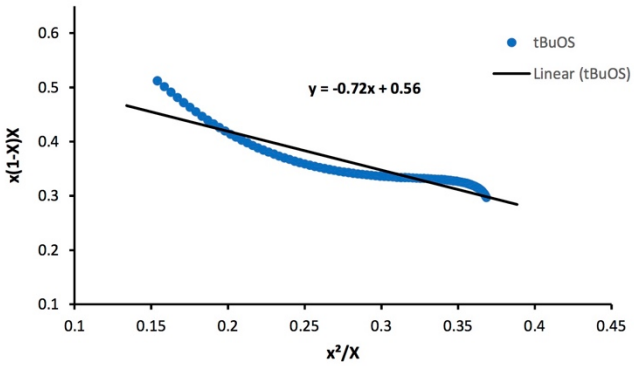

Fig S 3. Determination of the r-parameters by the Fineman-Ross equation for the system *t*BuOS/*p*EES

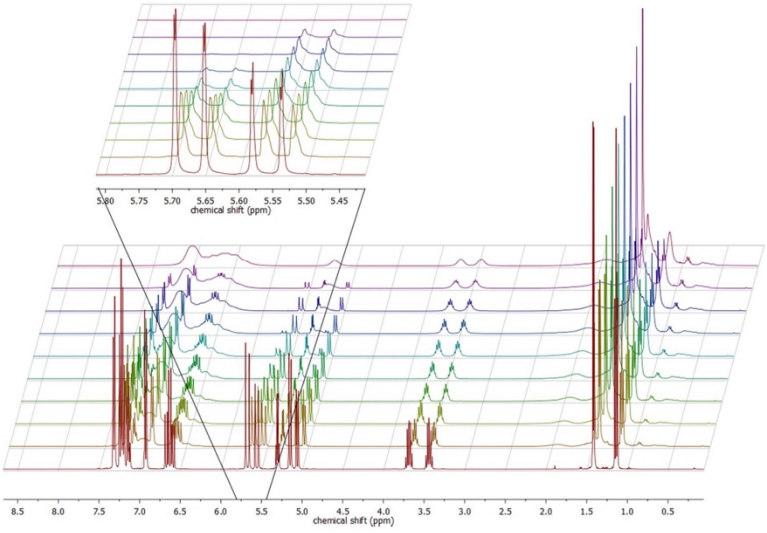

Fig S 4. Real-time ^{1}H NMR spectra overlay showing the consumption of the S (δ = 5.70 – 5.66 ppm) and the *p*EES (δ = 5.58 – 5.54 ppm) monomers in the zoom-in.

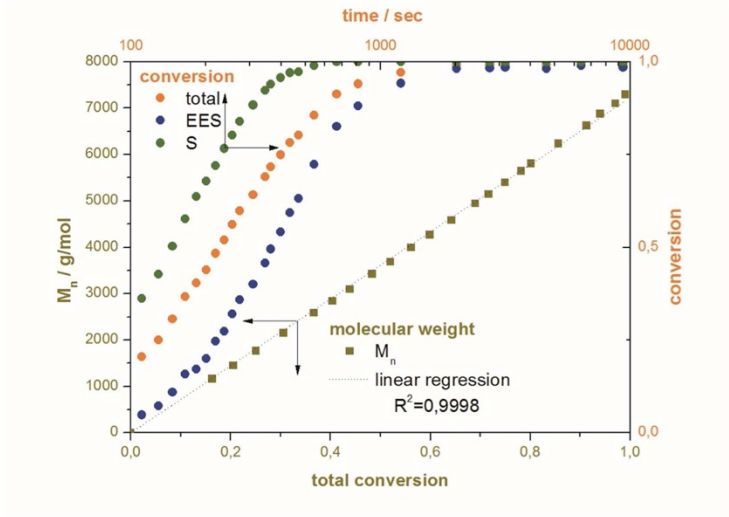

Fig S 5. Conversion vs time (orange) and molecular weight vs total conversion (dark yellow) for the Styrene-*p*EES copolymerization

A.2 List of Publications

A.2.1 Journal Articles

[1] Water-Soluble Metallocene-Containing Polymers
Alkan, F. R. Wurm, *submitted*

[2] PEG-Staining for Electron Microscopy with Ruthenocenyl Glycidyl Ether
A. Alkan, T. Fritz, M. Worm, K. Landfester, F. R. Wurm, *in preparation*

[3] Amphiphilic Ferrocene-Containing PEG Block Copolymers for Miniemulsion Process and Cell Uptake
A. Alkan, S. Wald, F. R. Wurm, *in preparation*

[4] Sequence-Controlled Polymers via Simultaneous Living Anionic Copolymerization of Competing Monomers
E. Rieger, A. Alkan, A. Manhart, M. Wagner, F. R. Wurm *Macromol. Rapid. Commun.* **2016**, DOI: 10.1002/marc.201600092.

[5] Triple-Stimuli Responsive Ferrocene-Containing PEGs in Water and on Surface
A. Alkan, C. Steinmetz, K. Landfester, F. R. Wurm, *ACS Appl. Mater. Interfaces* **2015**, 7, 26137-26144

[6] Water-Soluble and Redox-Responsive Hyperbranched Polyether Copolymers Based on Ferrocenyl Glycidyl Ether
A. Alkan, R. Klein, S. I. Shylin, U. Kemmer-Jonas, H. Frey, F. R. Wurm, *Polymer Chemistry* **2015**, 6, 7112–7118

[7] Vinyl Ferrocenyl Glycidyl Ether: An Unprotected Orthogonal Ferrocene Monomer for Anionic and Radical Polymerization
A. Alkan, L. Thomi, T. Gleede, F. R. Wurm, *Polymer Chemistry* **2015**, 6, 3617–3624

[8] Ferrocene-Containing Multifunctional Polyethers: Monomer Sequence Monitoring via Quantitative ^{13}C NMR Spectroscopy in Bulk
A. Alkan, A. Natalello, M. Wagner, H. Frey, F. R. Wurm, *Macromolecules* **2014**, 47, 2242–2249

[9] Functional Group Distribution and Gradient Structure Resulting from the Living Anionic Copolymerization of Styrene and para-But-3-enyl Styrene A. Natalello, A. Alkan, P. von Tiedemann, F. R. Wurm, H. Frey, *ACS Macro Letters* **2014**, 560–564

[10] Living Anionic Polymerization in Continuous Flow: Facilitated Synthesis of High-Molecular Weight Poly(2-vinylpyridine) and Polystyrene
A. Natalello, J. Morsbach, A. Friedel, A. Alkan, C. Tonhauser, A. H. E. Müller, H. Frey, *Organic Process Research & Development* **2014**, 18, 1408–1412

[11] Ferrocenyl Glycidyl Ether: A Versatile Ferrocene Monomer for Copolymerization with Ethylene Oxide to Water-Soluble, Thermoresponsive Copolymers
C. Tonhauser, A. Alkan, M. Schömer, C. Dingels, S. Ritz, V. Mailänder, H. Frey, F. R. Wurm, *Macromolecules* **2013**, 46, 647–655

[12] Enlarging the Toolbox: Epoxide Termination of Polyferrocenylsilane (PFS) as a Key Step for the Synthesis of Amphiphilic PFS-Polyether Block Copolymers
A. Natalello, A. Alkan, A. Friedel, I. Lieberwirth, H. Frey, F. R. Wurm, *ACS Macro Letters* **2013**, 2, 313-316

[13] Monomer Sequence Distribution Monitoring in Living Carbanionic Copolymerization by Real-Time ^{1}H NMR Spectroscopy
A. Natalello, M. Werre, A. Alkan, H. Frey, *Macromolecules* **2013**, 46, 8467–8471

A.2.2 Conference Contributions

Poster – 12/2015	PACIFICHEM 2015 in Honolulu, USA "Triple-Stimuli-Responsive Ferrocene-Containing Polyethers for Smart Surfaces and Catalysis in Water"
Oral - 07/2015	International Symposium on Ionic Polymerization (IP15) in Bordeaux, Frankreich *"Poly(Vinyl Ferrocenyl Glycidyl Ether): Water-Soluble Multi Stimuli Responsive Materials with Tuneable Electrochemistry"*
Oral - 04/2014	Europolymer Conference 2014 (EUPOC) in Gargnano, Italien *"In-Situ Monomer Sequence Monitoring in Living Anionic Copolymerization by Real-Time NMR Spectroscopy"*
Poster - 03/2014	247th ACS National Meeting & Exposition in Dallas, USA *"Ferrocene-Containing Polyethers: Monomer Sequence Monitoring via Quantitative ^{1}H and ^{13}C NMR Spectroscopy"*